ANL-7055

ANL-7055

Argonne National Laboratory

CHEMICAL ENGINEERING DIVISION SEMIANNUAL REPORT

January-June 1965

LEGAL NOTICE

This report was prepared as an account of Government sponsored work. Neither the United States, nor the Commission, nor any person acting on behalf of the Commission:

A. Makes any warranty or representation, expressed or implied, with respect to the accuracy, completeness, or usefulness of the information contained in this report, or that the use of any information, apparatus, method, or process disclosed in this report may not infringe privately owned rights; or

B. Assumes any liabilities with respect to the use of, or for damages resulting from the use of any information, apparatus, method, or process disclosed in this report.

As used in the above, "person acting on behalf of the Commission" includes any employee or contractor of the Commission, or employee of such contractor, to the extent that such employee or contractor of the Commission, or employee of such contractor prepares, disseminates, or provides access to, any information pursuant to his employment or contract with the Commission, or his employment with such contractor.

Printed in USA. Price $6.00. Available from the Clearinghouse for Federal Scientific and Technical Information, National Bureau of Standards, U. S. Department of Commerce, Springfield, Virginia

ANL-7055
Chemical Separations Processes
for Plutonium and Uranium
(TID-4500, 47th Ed.)
AEC Research and
Development Report

Argonne National Laboratory
9700 South Cass Avenue
Argonne, Illinois 60440

CHEMICAL ENGINEERING DIVISION SEMIANNUAL REPORT

January-June, 1965

R. C. Vogel, Division Director
Milton Levenson, Associate Division Director
F. R. Masten, Assistant Division Director

October, 1965

Preceding Semiannual Reports:

ANL-6800	July-December, 1963
ANL-6900	January-June, 1964
ANL-6925	July-December, 1964

Operated by The University of Chicago
under
Contract W-31-109-eng-38
with the
U.S. Atomic Energy Commission

Table of Contents

SUMMARY 1

I. COMPACT PYROCHEMICAL PROCESSES 21

A. Compact Pyrochemical Process Development 21
1. Melt Refining 21
2. Processes Employing Liquid Metal Solvents 29
B. Fuel Processing Facilities for EBR-II 56
1. Technical Assistance and Service Equipment Development 56
2. Process Equipment Development 59
C. EBR-II Fuel Cycle Facility Operations 72
1. Operations with Equipment for Recovery of Irradiated Fuel 72
2. Operations with Equipment for Fuel Fabrication 75
3. Fuel Surveillance Program 77
4. Performance of Process Auxiliaries 78
D. Chemistry of Liquid Metals 80
1. Fundamental Studies 80
2. Liquid Sodium Chemistry: Behavior of Carbon 83
E. Preparation of Fuels for Fast Reactors 87
1. Solid Refractory Fuels 87
2. Studies of Mobile Blanket Fuels for Fast Reactors 94

II. FUEL CYCLE APPLICATIONS OF VOLATILITY AND FLUIDIZATION TECHNIQUES 99

A. Laboratory Investigations 102
1. Fluid-Bed Fluorination of U_3O_8 Mixtures in a 1½-inch Diameter Reactor 102
2. Fluorination of UO_2-PuO_2 (and F.P.) Pellets in a 2-inch Diameter Fluidized-Bed Reactor 105
3. Reactions of Bromine Pentafluoride 114
4. Chemistry of Neptunium Hexafluoride 122
5. Solid-Liquid Equilibria 127
B. Engineering-Scale Investigations of Fluid-Bed Fluoride Volatility Processes 134
1. The Engineering-Scale Alpha Facility 134
2. Decladding and Fluorination of Uranium Dioxide Fuels 142
3. Cleanup of Cell Exhaust Air Contaminated with Plutonium Hexafluoride 145
4. Process Studies on the Recovery of Uranium from Highly Enriched Uranium Alloy Fuels 147
5. Basic Studies of Fluidized-Bed Behavior Related to Process Operations 159

III. HIGH TEMPERATURE REACTOR MATERIALS DEVELOPMENT 163

A. Phase Diagram Studies 163
1. The Uranium-Urania System 163
2. Hypostoichiometric Phase Boundary of Urania: Isopiestic Measurements 164
3. The Uranium-Urania-Tungsten System 165
B. Vapor Pressure Studies 165
1. Transpiration Studies of the Total Vapor Pressure of Uranium-Bearing Species over Urania 165
2. Effusion Studies of the Total Vapor Pressure of Uranium-Bearing Species over the Uranium-Urania Two-Phase System 166
3. Mass Spectrometric-Effusion Studies of the Partial Pressures of Uranium-Bearing Species over the Uranium-Urania Two-Phase System 166

IV. CALORIMETRY 167

A. The Enthalpies of Formation of the Hexafluorides of Sulfur, Selenium, and Tellurium 167
B. The Enthalpies of Formation of the Trifluorides of Aluminum, Yttrium, Gadolinium, and Holmium 170
C. Combustion of Silicon Carbide in Fluorine 171
D. Combustion of Boron in Fluorine 172
E. Fluorine Flow Calorimeter 174
F. 1500°C Drop Calorimeter 174
G. 2500°C Calorimeter System 175

V. REACTOR SAFETY 177

A. Metal-Water Reactions 177
1. Isothermal Studies of the Aluminum-Steam Reaction by the High Pressure Furnace Method 177
2. Studies of Metal-Water Reactions by the Laser Heating Method 181
3. Short-Period Transient Irradiation 183
4. In-Pile Studies of Metal-Water Reactions in TREAT 190
5. Calculation of the Extent of Metal-Water Reaction During a Loss-of-Coolant Accident 199

B. Fast Reactor Safety Studies 199
1. Fuel-Coolant and Cladding-Coolant Interaction Studies 199
2. Transient Heat Transfer Studies: Measurement of Heat Flux from a Heated Metal Sphere Moving Through Water 206
3. Sodium-Air Reaction Calculations 208
4. Other Fast Reactor Safety Studies 212

VI. ENERGY CONVERSION 213

A. Regenerative Emf Cells—Physical-Chemical Laboratory Studies 213
1. Lithium Hydride Cell Studies 213
2. Voltammetric Studies of the Lithium Hydride Cell 216
3. Intermetallic Systems 218
4. Liquid-Vapor Equilibria in the Sodium-Bismuth Regenerative Cell 221

B. Regenerative Emf Cells—Engineering Studies 225
1. Physical Properties of Electrolytes and Bimetallic Mixtures 225
2. Experimental Sodium-Bismuth Bimetallic Cell 226
3. Experimental Sodium-Cathode Metal Thermal Regenerator 227
4. Corrosion Studies 228

VII. NUCLEAR CONSTANTS 230

A. Radiative Capture 230
B. Capture-to-Fission Ratios in EBR-II 232
C. Neutron Inelastic Scattering 232

SUMMARY

Chemical Engineering Division Semiannual Report

I. Compact Pyrochemical Processes (pages 21 to 98)

Melt refining is being used currently to reprocess fuel discharged from the first core loading of EBR-II. Although development work on the melt refining process has been completed, a modification of melt refining that involves the use of a chloride flux (halide slagging) has been investigated further. In the halide slagging process, the lanthanons and other electropositive fission products are extracted from molten fuel alloy into an overlying $CaCl_2$ flux containing a small amount of $MgCl_2$ which serves as an oxidant. Plutonium is then extracted from the molten alloy by a second $CaCl_2$ flux containing UCl_3 as the oxidant. To provide supporting chemical data for the latter procedure, equilibrium constants have been determined for the reaction

$$UCl_3\,(CaCl_2) + Pu\,(U) \rightleftarrows PuCl_3\,(CaCl_2) + U$$

The measurements were made with initial UCl_3:Pu ratios of about 1 to 18, and initial plutonium concentrations of 0.2 to 4.2% in the uranium alloy. The minimum time required to reach equilibrium was about 30 min. Values for the equilibrium constant were about 200 at 1150 and 1200°C. This value is sufficiently high so that satisfactory separation of plutonium from uranium should be achievable with one equilibrium stage. The corresponding free energy change for the reaction at 1200°C is 15.2 kcal/mole. The rate of reaction ($\sim$150 $\mu g/cm^2$ in 45 min) of the molten alloy, with the beryllia containment crucibles was roughly an order of magnitude greater in the current experiments with a flux present than in earlier work with the alloy alone.

Materials, principally the borides, carbides and nitrides of the 4th, 5th, and 6th metallic groups of the periodic table, are being investigated for containing uranium and uranium alloys at temperatures from near the melting points to several hundred degrees above the melting points. The investigation consists of partially submerging the test samples in molten uranium for 24 hr at elevated temperatures and examination of the samples by various methods at the completion of a run. From data obtained at temperatures up to 1365°C, the stability of the intermetallic compounds tested decreased in the following order: nitrides, borides, and carbides. The nitrides were unattacked at 1365°C, the borides were only slightly attacked, and the carbides more severely attacked. Because of the good resistance of many of the materials, particularly nitrides, the tests will be extended to higher temperatures.

"Vitreous" carbon a proprietary product of Société le Carbone, France, was tested as a containment material for molten uranium, After molten uranium was held in this material at 1400°C for 1 hr at a pressure of 10^{-4} to 10^{-6} torr, is was found by X-ray diffraction techniques that a substantial portion of the uranium had been converted to uranium carbide. It is therefore concluded that vitreous carbon is not suitable for use as a container material for solutions containing high concentrations of uranium.

The possible detrimental effect of the argon-5% nitrogen atmosphere in the Argon Cell of the EBR-II Fuel Cycle Facility on alloys which may see service in the facility has been investigated. These alloys are limited to nickel-rich alloys, since they are about the only easily available materials with sufficient structural strength to permit use in process applications, for example, the skull reclamation furnace, which require temperatures of 900°C. Consequently, a series of nickel-bearing alloys (Inconel 600, Inconel 800, Hastelloy C, Hastelloy X, and types 304 and 316 stainless steel and tungsten and molybdenum-30 w/o tungsten were exposed to argon-5% nitrogen for 450, 1000 and 2000 hr at 900°C. After 2000 hr, tungsten, molybdenum-30 w/o tungsten, and types 304 and 316 stainless steels were affected very little except for the formation of slight nitride surface layers. It is doubtful that nitridation will present a serious problem in the EBR-II Argon Cell because high-nickel alloys will be at temperatures above 650°C for limited periods.

Work was continued on the removal of nitrogen from argon by gettering the nitrogen on hot titanium

sponge. Although this method has general utility for purifying argon for such applications as glovebox atmospheres, the major incentive for its development is a possible need to remove nitrogen from the atmosphere in the Argon Cell of the EBR-II Fuel Cycle Facility. The kinetics of the nitrogen-titanium sponge reaction at 900°C have now been determined at nitrogen concentrations of 100, 300, 1000, 5000 and 50,000 ppm in argon. Correlations of these data are now in progress. Operation of a 10-cfm pilot plant for the removal of nitrogen from argon was discontinued after a total of 1800 hr of continuous operation. It is felt that this loop has performed its design function by adequately demonstrating the feasibility and economy of using titanium sponge for the removal of nitrogen impurity from large volumes of argon.

Work was continued on an EBR-II fuel recovery process which supplements melt refining. Known as the skull reclamation process, it effects recovery and purification of the uranium contained in melt refining crucible residues. These residues are first converted by controlled oxidation to oxide powders which are poured from the crucible. Reduction of the oxide and purification of the uranium is then accomplished in a series of process steps conducted in molten metal (zinc-magnesium systems) and molten halide salt media. These latter steps are being conducted on a pilot plant scale of about 2 kg of skull oxide per process batch, which compares to a plant batch size of 5.8 kg of skull oxide. During the last 7 runs, the pilot plant equipment has been operated in a closed glovebox containing a dry (150 ppm H_2O) nitrogen-argon atmosphere.

The operation of the pilot plant equipment has been improved steadily through the course of the runs. The flux foaming problem has been solved in recent runs by the magnesium pretreatment technique described in the previous semiannual report. Molybdenum-30 w/o tungsten transfer lines have operated satisfactorily, and transfer efficiencies uniformly have reached or exceeded the desired goal of 90% for certain transfers and have reached that goal for other transfers.

A problem of fuming in skull reclamation runs still exists, inasmuch as the use of calcium metal turnings to react with the vaporized flux is not possible because the temperature in the basket which contains the turnings exceeds the melting point of calcium; however, Molecular Sieves appear to be effective in trapping the fumes.

Emphasis was placed in the last series of skull reclamation runs on the development of techniques, especially phase transfers of metal and salt solutions, which would minimize uranium losses in the waste streams. In two experiments total uranium losses in the waste streams were reduced to 2.0 and 3.0% of the uranium charged. These losses are low in view of the solubility and equilibrium losses of 2% inherent in the process and are well within the overall allowable processing loss of 5%. This reduction in uranium losses was mainly accomplished by producing a well-settled precipitate bed before transfer of the supernatant solution from the intermetallic precipitation step, and by the installation of strainer-weirs over the ends of the transfer tubes.

With the exception of zirconium, fission product removals have been satisfactory. Cerium removals have ranged between 87 and 95%, ruthenium removals between 73 and 99%, and molybdenum removals between 60 and 86%. A 60% removal of the latter two elements would be satisfactory. Zirconium removals have been low, varying from 49 to 78%. Since removal of at least 85% of the zirconium is desired in this process, methods for increasing zirconium removal are being sought.

Efforts are being made to secure more satisfactory containment crucibles for the skull reclamation process. Although pressed and sintered tungsten crucibles have given excellent service during the 25 engineering-scale demonstration runs made to date, a fabrication method which results in a lighter, less unwieldy crucible is being sought. Alternative methods of fabrication include (1) plasma-spraying on a removable mandrel, (2) shear forming, (3) vapor depositing, and (4) welding. Tungsten and beryllia are under consideration for use in the final or retorting step of the skull reclamation process.

The EBR-II blanket process entails the use of a 50 w/o Mg-50 w/o Zn alloy as a solvent in a uranium-plutonium separation step. Solution stability tests showed that a solution of uranium and plutonium in this alloy can be contained in type 405 stainless steel at 730°C for 100 hr without significant plutonium losses. Although there were indications of some interaction of the uranium with the container material, this effect appears to be of little process importance since the uranium is present as precipitated metal in this step.

Development work has continued on compact pyrochemical processes for the recovery of uranium and plutonium from fast breeder reactor fuels. The basic separations in present process concepts for oxide, carbide and metal core and blanket material are effected by solvent extraction in liquid metal and molten salt solvents.

A vanadium-20 w/o titanium alloy is under consideration as a cladding material for metallic fuels. It has been found that both U-fissium alloy and U-Pu-fissium alloy enclosed in V-20 w/o Ti tubing with crimped ends can be hydrided by exposure to 2 atm

hydrogen pressure at 250–300°C for about 6 hr. The cladding is disintegrated into fragments, while the fuel forms a hydride powder. Addition of molten cadmium to the mixture results in a fuel-cladding separation, since the cladding fragments float on the surface of the cadmium, whereas the uranium and plutonium settle to the bottom. However, for oxide and carbide fuels, and possibly metallic fuels, alternate oxidation and reduction to convert the fuel to a mixed oxide powder appears to be an attractive method of separating the fuel from the cladding.

The codistribution behavior of uranium, plutonium, and praseodymium between 50 m/o $MgCl_2$-30 m/o NaCl-20 m/o KCl and Cu-Mg alloys has been investigated. Praseodymium favors the salt phase at low magnesium concentrations, while plutonium distributes to the metal phase. Uranium distributes to the metal phase more strongly than the plutonium. Decreasing the temperature from 800°C to 600°C causes the praseodymium distribution coefficient to increase by a factor of two, while that for uranium decreases by nearly a factor of two, and that for plutonium remains essentially constant. At 20 w/o magnesium in the Cu-Mg alloy and a temperature of 800°C, the uranium-praseodymium separation factor is about 5,600. The maximum praseodymium-plutonium separation factor observed in this experiment was 205 at 9 w/o magnesium and 800°C. The solubility of uranium in Cu-Mg alloys at 800°C was found to decrease from about 3 w/o in Cu-10 w/o Mg to about 0.03 w/o in Cu-70 w/o Mg.

The extraction of lanthanon fission products from molten chlorides by Al-Mg alloy is being investigated as a technique that would permit the purification of recycled salt and consolidation of the fission products in a metallic ingot. The distribution coefficients for yttrium, lanthanum, cerium, and praseodymium between 50 m/o $MgCl_2$-30 m/o NaCl-20 m/o KCl and Al-20 w/o Mg alloy and their solubilities in this alloy were determined. For all lanthanons tested, the distribution coefficients are sufficiently low to permit a single-stage extraction and the solubilities are large enough to allow high concentrations of these elements in the Al-Mg ingot.

Two conceptual processes for the recovery of uranium and plutonium from irradiated fuels are presented. One process, which utilizes Cd-Mg alloys as a liquid metal solvent, is designed primarily for metallic fuels. The other process employs Cu-Mg alloys as the principal liquid metal solvent, and is aimed at oxide, carbide, or metallic fuel.

In the liquid cadmium-based process, a portion of the cadmium from the retorting step used for recovery of the product is recycled and chlorinated to form $CdCl_2$, which is used as an oxidant in the first stages of the process. Laboratory experiments showed that cadmium metal can be chlorinated satisfactorily in the presence of molten 50 m/o $MgCl_2$-30 m/o NaCl-20 m/o KCl, but that sufficient means for heat removal must be provided. In the use of the resulting $CdCl_2$-bearing salt as an oxidizing agent, it was shown that UCl_3 concentrations up to 30 or 35 m/o can be accommodated by the 50 m/o $MgCl_2$-30 m/o NaCl-20 m/o KCl process salt at 600°C.

Work was continued on a program to develop the engineering technology required for the separation of plutonium and uranium from fission products by multistage extractions between molten metal and molten salt phases. The mass transfer rates of uranium and cerium from a cadmium solution to a chloride salt in a packed column have been estimated. The overall mass transfer coefficient for the transfer of uranium from the metal to the salt phase has been measured to be 0.0076 sec^{-1}. If this value applies to plutonium and rare earths, the calculated height of a theoretical stage in which plutonium is separated from rare earths is 2.3 ft. In a similar experiment made with cerium it was found that somewhat more than one equilibrium stage was provided by a 12.5-in. packed column. The rates determined for both cerium and uranium transfer indicate that the transfer kinetics in a packed countercurrent extraction column are in a useful range.

Batch mass transfer rates have also been determined in mixer-settlers. The results indicate mixer-settlers are feasible for liquid metal-liquid salt extractions. Such units would require modest agitation and a residence time of several minutes. However, since the system is limited to a separation equivalent to one equilibrium stage, mixer-settlers are attractive only in extractions involving very high separation factors.

An engineering test loop facility, constructed for the purpose of testing components for eventual use in a metal-salt extraction pilot plant, has undergone initial tests with a 50 m/o $MgCl_2$-30 m/o NaCl-20 m/o KCl salt stream. These tests revealed that the threaded and compression fittings used throughout the loop were unreliable for the containment of the salt. The facility is presently being converted to a completely welded unit. Improved methods of heating and insulating, in order to minimize temperature variations around the loop, are being sought.

An eddy-current induction probe which measures the level of metal in a tank and detects the location of the metal-salt interface in extraction devices has proved to be reliable over long periods of operation; to be easy to use, maintain, and calibrate; and to be accurate to within ⅛ in. of depth in cadmium, zinc, bismuth, and sodium. The response signal-metal depth

curves were similar, although with slightly different slopes, for all four metals which had widely varying specific resistivities. It was found that the material of construction of the containment well had a marked effect on the signal output; materials with low specific resistivity, such as tungsten and molybdenum, are not suitable container materials for the high frequency eddy-current probe. After about 1000 hr of operation, it is necessary to redetermine the zero point because of drifting caused by aging of the electronic components. The probe is now considered operational, and no further development work is planned.

Various materials of construction are being investigated for use in the processes under development for advanced reactor fuels. In one of the processes which utilizes cadmium-base solvent metals, initial screening tests indicated excellent resistance of this alloy to low (under 10 w/o) zinc alloys. Therefore, the tests were extended to test the corrosion resistance of type 405 stainless steel in an 81.4 w/o Cd-5.4 w/o Mg-10.9 w/o Zn-2.3 w/o U metal phase and a 50 m/o $MgCl_2$-30 m/o NaCl-20 m/o KCl salt phase at 650°C for 200 hr. The apparatus was arranged so that a type 405 test coupon would be at each of four locations—in the metal phase, at the metal-salt interface, in the salt phase, and in the vapor phase. The results indicate that type 405 stainless steel has excellent resistance to corrosion provided that the salt is dried. Other steel alloys will be tested under similar conditions to determine if a less expensive or more fabricable alloy also possesses adequate corrosion resistance to this system.

The critical temperatures of the alkali metals, cesium, rubidium, sodium, and potassium, have been estimated from their densities, which were determined by a radioactive counting technique. Alkali metal thermodynamic properties, many of which can be predicted from a knowledge of the critical constants, are of particular interest because of the use of these materials as heat-exchange media in nuclear reactors. For rubidium the estimated critical temperature is 1820 ± 30°C; for cesium the estimated critical temperature is 1850 ± 50°C; for sodium, 2300 ± 100°C; and for potassium, 2050 ± 250°C. These values are in general agreement with the available estimates of others.

The Chemical Engineering Division at Argonne, Illinois, continues to provide technical assistance for problems arising in the operation of the EBR-II Fuel Cycle Facility in Idaho.

In collaboration with Fuel Cycle Facility personnel, measurements were carried out (in January 1965) of in-cell illumination and of light transmittance of the 31 shielding windows installed in the shielding walls of the Air Cell and Argon Cell. One-thousand watt mercury vapor lamps in wall-mounted luminaires are used for the in-cell lighting of the two cells. The lamps have proved to be very satisfactory; only one lamp has burned out in the 30 months (as of January 1965) that they have been in use. During this time, the illumination along the center-line of the working area in the Argon Cell has decreased to about 90 ft-candles, which is about one-half of the value at the time of installation. Preparations are underway to start replacing lamps on a regular schedule in order to minimize the possibility of several lamps simultaneously burning out.

All of the shielding windows in the Air Cell and Argon Cell have been subjected to irradiation exposure. At the time of the most recent light transmittance tests, the windows of the Air Cell had been exposed to irradiation during disassembly of the first discharged EBR-II subassemblies from the core (about 0.1 a/o burnup) and from the inner blanket; the windows of the Argon Cell had received their irradiation during the processing of the core subassembly through melt refining and injection casting. The results of the transmittance tests were compared with those obtained when the windows were accepted from the manufacturer in August 1962. No significant change in the average light transmittance was shown. Additional light transmittance measurements are planned after the shielding windows have been subjected to substantially greater irradiation exposure.

The 64-pin connector insert on the top end of the manipulator feed cable is being replaced on all Argon Cell manipulators because of failures attributed to arcing between adjacent conductor pins. The new inserts will have an increased spacing between conductors (⅛-in. spacing) and a higher voltage rating (600-volt rating). The increased spacing, which should prevent arcing, was achieved by using a connector with 22 pins. The 54 wires in the cable (there are three or more wires for each of 17 circuit sides) will be consolidated into 18 conductors, and the 18 conductors will be soldered to the new connector.

A bridge-drive lifting tool was designed and fabricated to carry out the remote removal and reinstallation of a bridge-drive motor from a crane bridge in the Argon Cell. Although the drive motor is difficult to reach and the operations must be viewed with a periscope, the lifting tool was successfully used to perform these operations. This was the first time that a bridge-drive motor was remotely removed and installed in this Facility.

With the installation of a large inert atmosphere enclosure, the construction of an argon-atmosphere environment system in the Chemical Engineering Division is complete. The system now consists of two

gloveboxes, the large inert atmosphere enclosure, and the associated argon gas purification system. The gloveboxes are being used for the development of equipment and for testing of component parts. The large enclosure contains an atmosphere equivalent to that of the EBR-II Argon Cell and is being used for the testing and evaluation of skull reclamation process equipment designed for use in the Argon Cell. Plant-scale[1] equipment has been installed in the large enclosure. These items include (1) a skull oxide reduction and purification (M-2) furnace and associated auxiliary equipment and (2) retorting apparatus. For preparing unirradiated uranium oxide charges for the M-2 furnace, a skull oxidation furnace is available in the large enclosure.

The effect of heat transfer on the ability to separate metal and flux phases in the M-2 skull reduction and purification furnace has been studied. In the noble metal extraction step of the skull reclamation process, the skull oxide is suspended in molten flux, and the noble metal fission products in the skull oxide are selectively reduced by and extracted into molten zinc at 800°C. The two phases are separated by allowing the flux to solidify (melting range 560 to 600°C) and then pressure-siphoning the zinc phase (m.p. 420°C). An earlier (1961) heat transfer study indicated that fission product heating would not prevent solidification of the flux at the end of the noble metal extraction step. Since that study was made, the process and the furnace have undergone substantial changes. New calculations have been made which show that fission product heating is sufficiently great that the flux cannot solidify while the zinc is still molten. Therefore, removal of the zinc from beneath molten flux is required. Separation of the two molten phases will still be carried out by a pressure-siphoning technique; the transfer operation will be terminated when the required weight of zinc has been transferred and before any molten flux enters the transfer line. This technique has been successfully demonstrated in semiworks runs.

The final material transferred from the M-2 furnace consists of about 4 kg of uranium in approximately 36 kg (~8 liters) of Zn-12 w/o Mg-12 w/o U. Development work is being conducted on recovering the uranium from this solution in a form suitable for use as make-up feed material for the melt refining process.

Retorting equipment is under development to recover the uranium by distilling the volatile zinc-magnesium. In recent retorting runs, pressed-and-sintered tungsten crucibles were used. Tungsten is being considered for the retorting crucible as an alternative to beryllia, which was used in earlier small-scale tests. Beryllia crucibles are subject to cracking and are not yet available in plant-scale sizes.

After the retorting step of the flowsheet, the uranium is consolidated by melting. This operation was successfully carried out in beryllia; beryllia is not wetted by molten uranium. However, when this consolidation step was performed in a tungsten crucible, the uranium product adhered to and reacted with the crucible. Previously reported experiments have shown that the adhering uranium product can be hydrided to form a free-flowing, easily removable powder.

Several small-scale retorting and uranium hydriding runs have been conducted in a modified melt refining furnace which is located in an inert-atmosphere glovebox. In these runs, zinc and magnesium were distilled from an alloy having a nominal composition of Zn-12 w/o Mg-10 w/o U. The uranium remaining in the crucible was then sucessfully hydrided and removed.

Hydrided uranium prepared in these runs has been used successfully as make-up material in the feed charge (unirradiated uranium-5 w/o fissium) to a melt refining run. The use of this material did not appear to affect the pouring yield and the quality of the ingot. Additional runs are planned to verify the suitability of hydrided uranium in this application.

Although hydriding of the retorted product would permit the use of tungsten crucibles, it would be desirable to avoid this additional processing step. Consequently, BeO crucibles continue to be considered for use in the retorting operation. A plant-sized thixotropically cast BeO crucible has been obtained and a plant-sized isopressed BeO crucible of improved quality has been ordered for testing.

Retorting runs made with charges simulating a poor transfer of process flux in the uranium reduction step have shown poor removal of zinc and magnesium in the presence of excessive flux. Thus, it will be necessary to remove any visible flux from the zinc-magnesium-uranium ingot before the ingot is retorted.

Preliminary retorting tests were carried out using the prototype retorting equipment prior to its installation in the large argon-atmosphere enclosure. The retorting equipment was operated in air; the atmosphere within the retort was argon. Charges of Zn-Mg (no uranium) were distilled from a graphite crucible. Distillation rates as high as 97 g/min were achieved with a 30-kg charge of Zn-14 w/o Mg at an argon pressure of 10 torr and at a temperature of about 950°C. (A 100 g/min distillation rate has been tentatively selected for plant operation in the EBR-II Fuel Cycle Facility.) Following these preliminary tests, the retorting equipment was installed in the

[1] The equipment to be used in the EBR-II Fuel Cycle Facility is sized for operation with a batch size of about 5.8 kg of skull oxide (~5 kg of uranium oxide).

large inert-atmosphere enclosure. Tests of the induction heating system are being conducted.

The use of the Fuel Element Removal Machine (FERM), an attachment to the subassembly dismantler, has reduced the time required to remove irradiated fuel elements from the lower subassembly grid plates. This device removes fuel elements in rows rather than singly as formerly accomplished with master-slave manipulators.

Difficulties encountered in jamming of fuel pins in the decanner scrap separator tube, attributed in part to sticking by the sodium bond, appear to have been overcome by heating the tube.

Additional irradiated subassemblies have been received from the EBR-II Reactor and are now being processed. Pouring yields in melt refining irradiated fuel average 94 w/o. These subassemblies have been irradiated to a maximum total atom percent burnup of between 0.25 and 0.50.

The crucible used in the melt refining of 0.50 maximum a/o burnup fuel exhibited a glowing ring at the level of the melt within the crucible after oxidation. This glow was still present after the skull was dumped from the crucible. Thermocouple measurements indicate that the glow is not a temperature effect; it is assumed to be a radiation effect.

An improvement in the readout system of the eddy-current porosity detection system of the pin processing equipment has resulted in significantly increasing the sensitivity and simplifying the interpretation of the detection signal. Both phase angle and current are observed; a distinction between surface and central defects is apparent.

The reliability of fuel element welding has been increased by construction of a machine which accepts only one element at a time rather than a magazine of 20 elements. Alignment difficulties are minimized.

The first subassembly made from irradiated fuel processed and refabricated in the Fuel Cycle Facility has been returned to the EBR-II reactor and is now undergoing additional irradiation.

Examination of surveillance elements from subassemblies which have attained up to 0.75 maximum a/o burnup indicates an increase in fuel volume as evidenced by the increase in sodium level within the fuel can.

In the Argon Cell of the Fuel Cycle Facility, the atmosphere control system continues to maintain satisfactory operation, although one bearing on a cell atmosphere circulation fan became overheated and was replaced.

Activities of potassium in liquid sodium-potassium solutions were measured using an atomic absorption spectrophotometric method. Positive deviations from ideal solution behavior were observed; the observed potassium activities are in excellent agreement with values calculated by the Gibbs-Duhem relation from previously measured sodium activities.

Standard free energies of formation were measured by the Knudsen effusion method for eight 1:1 lanthanon-cadmium compounds, LnCd, with Ln = La, Nd, Sm, Gd, Tb, Ho, Tm, and Lu. The negative free energies of formation at 500°C between LaCd and LuCd increase to a maximum value at GdCd, the middle of the series.

An ultrasonic absorption method is proposed to search for intermetallic complexes in liquid metal solutions. The value of this method as a spectroscopic tool arises largely from the fact that metal solutions are not opaque to sound.

Magnetic susceptibilities of uranium monosulfide-thorium monosulfide solid solutions were measured to obtain information on the electronic configuration of uranium in uranium monosulfide. Dilution with thorium monosulfide was found to remove effectively the ferromagnetic ordering in uranium monosulfide.

The nature of carbon in liquid sodium is under study. Black particles, 20 to 200 microns in size and presumably amorphous carbon, were formed when sodium was dissolved in water. These particles may account for 70% or more of the carbon originally present. Centrifugation of liquid sodium at 2000 rpm and 200°C did not result in significant segregation of its carbon content. Partial removal of carbon was achieved by filtration of sodum through a variety of filter media, thereby indicating the particulate nature of part of the carbon content of sodium. The vapors over heated specimens of sodium were examined in a mass spectrometer. The results indicate that volatile, high molecular weight, presumably organic compounds can persist for extended periods of time in liquid sodium at about 300°C. However, such compounds are not necessarily present in sodium which is contaminated with carbon.

Refractory compounds of uranium and plutonium, such as carbides, nitrides, and sulfides, show promise as fast reactor fuels capable of withstanding high temperatures and high burnup. Methods are being sought for preparation of these fuels which would be superior to current techniques in producing a high quality product at moderate expense by means that could be easily incorporated into reprocessing schemes. At the present time, efforts are being directed at developing both a fluidized-bed process for preparation of uranium-plutonium monocarbide fuels and a paste blanket fuel consisting of uranium mononitride powder in a sodium vehicle.

In the fluidized-bed method for preparation of

(U-Pu)C, particles of U-Pu alloy, prepared by hydriding are reacted with hydrocarbon gas at 600 to 750°C to form the monocarbide. A thermodynamic study of the reactions of hydrocarbon gases with uranium and uranium carbides indicates that the solid phase in equilibrium with the gas may be UC, UC_2, or free carbon, depending on the hydrogen-to-carbon ratio in the gas. Fluidized-bed experiments on the preparation of UC and thermobalance experiments on the preparation of (U-20% Pu)C tended to confirm the thermodynamic analysis. However, reaction kinetics seem to favor the formation of UC rather than that of UC_2 for gas compositions which would form UC_2 or free carbon at equilibrium.

Most of the fluidized-bed experiments on the preparation of UC were conducted at hydrogen-to-carbon ratios for which the solid phase in equilibrium with the gas was free carbon; however, the product formed was usually UC. Future efforts will be directed at reducing the oxygen contents of the products which were usually about 1 w/o in these fluidized-bed experiments.

In the thermobalance experiments, the weight change was recorded as a sample of (U-20% Pu) hydride, suspended in a furnace from a balance pan, reacted with a flowing stream of propane and hydrogen. In runs with pure propane, the weight gain was larger than that calculated for formation of (U-Pu)C and the specimens contained free carbon. At hydrogen-to-carbon ratios for which the solid phase in equilibrium with the gas would be expected to be the monocarbide, no higher carbides formed as evidenced by the weight gains during the run, the carbon analyses and X-ray lattice parameters of the products, and the monophasic structure of the pressed and sintered products.

Studies are continuing on the preparation and testing of a uranium mononitride-sodium paste blanket fuel. Uranium mononitride powder was prepared by reaction of nitrogen with uranium shot at 800 to 1350°C and subsequent grinding of the product. By conducting the major portion of the nitriding operation at a temperature of 1250 to 1350°C, a dense product resulted which was in the form of the original uranium shot. The bulk densities of the products after grinding ranged from 3.0 to 8.2 g/cc. Low bulk density resulted if moderate oxidation of the product took place (0.5 to 1.0 w/o increase) during grinding. In one grinding operation in which the increase in oxygen concentration was small (from 0.04 to 0.23 w/o oxygen), the product had a high bulk density of 8.2 g/cc. A paste of UN in sodium was prepared using this high bulk density powder. The UN powder was easily wetted at 300°C after about ½ hr of stirring. (Other wetting experiments gave similar results.) The resulting paste, which was quite viscous, contained 49 v/o solids (6.6 g of uranium/cc) and a calculated gas volume of 8%.

II. Fuel Cycle Applications of Volatility and Fluidization Techniques (pages 99 to 162)

Laboratory-scale fluid-bed fluorinations of mixtures of uranium, plutonium, and fission product element oxides are being performed in support of the fluid-bed fluoride volatility process. This laboratory work is being performed to determine the optimum reaction conditions under which the retention of plutonium in the inert fluid bed material (alumina) is minimized, and to obtain general information applicable to the operation of the fluid-bed fluoride volatility pilot plant.

The distribution of iron and chromium was determined for typical fluid-bed fluorination experiments. In these experiments a mixture of plutonium and uranium oxides, fission product oxides, alumina, and stainless steel decladding product (prepared by the HF-promoted oxidation of type 304 stainless steel) was fluorinated for a total of 20 hr over the temperature range 450 to 550°C. The material balance showed that essentially all of the iron had stayed in the fluid-bed reactor but that only 30 to 40% of the chromium had remained in the reactor. These data indicate that a substantial fraction of the chromium originally present in the reactor system will be transferred along with the volatile UF_6 and PuF_6 during the fluorination step.

The distribution of zirconium (as a representative fission product) between coarse and fine particle fractions of an alumina bed was measured to determine if a significant segregation of fission products occurs during the fluorination step. If a substantial portion of the fission products appears in the fine particle fraction of the bed, the removal of that fraction would allow the alumina bed to be reused a greater number of times because of the reduction of fission product heating and improvement of the fluidizing quality of the alumina. The results showed a 4:1 ratio between the zirconium concentrations in the fine and coarse particle fractions. If it is assumed that the fine particle fraction including the decladding product represents as much as 10 w/o of the alumina bed, then as much as 50 w/o of the fission products would be present in the fine particle fraction. Under these conditions, separation of the fine particle fraction from the bulk of the alumina would be advantageous.

A preliminary study was made to determine the efficiency of removal of the small amount of plutonium retained on fluid-bed alumina by leaching the plutonium with nitric acid. Recovery of plutonium by acid leaching of the alumina is not expected to be a process operation but was investigated only as a backup procedure in the event that some malfunction should prevent removal of plutonium by the fluorination method. Alumina beds containing plutonium from previous fluorination experiments were used in the leaching tests. In each test, 50 g of alumina bed material was slurried with 100 ml of a leaching solution containing 6*N* nitric acid and 0.1*M* aluminum nitrate. After a leaching period of 5 hr at 100°C, between 80 and 90% of the plutonium originally present on the alumina was leached from the solid. Uranium recovery was essentially complete. Also recovered in the leaching solution was 80 to 90% of the chromium and iron originally present on the alumina.

A two-inch diameter fluidized bed reactor is being used to determine fluorination conditions for UO_2-PuO_2 pellets which insure a minimum retention of uranium and plutonium by the fluidized bed of alumina. The reactor has been equipped to study: (a) the fluorination of pellets by the two-zone oxidation and fluorination technique and (b) the fluorination of fine particles of uranium and plutonium oxides and fluorides which are produced by the pulverization of either clad or bare pellets with hydrogen fluoride-oxygen mixtures.

Prior to studies with plutonium, several runs were performed in the 2-in. reactor which involved the demonstration of the pulverization of UO_2 pellet beds with HF-O_2 mixtures followed by fluorination of the fines, and the demonstration of the two-zone oxidation-fluorination cycle with UO_2 fuel. When 2-in. deep beds of UO_2 pellets were reacted with 40 v/o HF in oxygen at both 400 and 550°C, some caking of the pellet bed was generally encountered. In run Sure-5, caking in the pellet bed was alleviated by continued reaction with a mixture of hydrogen fluoride and oxygen, and the reaction cycle was completed by fluorination of the uranium fines in the alumina bed and subsequent recycle-fluorination periods at 450, 500, and 550°C.

Satisfactory pulverization of the pellets, as determined by the absence of caking of the pellet bed, was demonstrated when the pellets were contained in open nickel baskets, 9/16-in. dia. by 8 in. long, in order to represent the orientation of the pellets in the fiud bed under actual decladding conditions. In these runs, Sure-3 and Sure-4, the pellets were pulverized by a reaction mixture of approximately 40 v/o HF in oxygen at 550°C. Several runs (Sure-9, Sure-10 and Sure-11) were completed to study further the effects of reactant concentration and reaction temperature during pulverization of 2-in. deep beds of pellets with HF-oxygen. Satisfactory pulverization of the bed of pellets was demonstrated at 450°C using 20 v/o HF-30 v/o oxygen in nitrogen.

In two experiments, runs Sure-6 and Sure-8, 2-in. deep beds of UO_2 pellets were fluorinated by the two-zone oxidation and fluorination technique, one run at 450 and the other at 500°C. No operational difficulties were encountered.

Three runs (Pure-1, Pure-2, and Pure-3) have been completed with UO_2-PuO_2 pellets containing 19 nonradioactive fission product oxides. In each of the runs, 2-in. deep beds of pellets (0.5-in. dia. by 0.5 in. long right cylinders) were reacted in a sequence consisting of two-zone oxidation-fluorination, single-zone fluorination, and recycle-fluorination. Total processing time varied from 20 hr in run Pure-1 to 24 hr in runs Pure-2 and Pure-3.

The final uranium and plutonium concentrations in the fluidized beds of alumina were about 0.004 w/o and 0.007 w/o, respectively. In each run, the uranium removal was virtually complete (>99.99%) and the plutonium removal was 97% complete, for a single use of the alumina bed. These results are in good agreement with the results of previous experiments with U_3O_8-PuO_2-fission product oxide feed mixtures in a 1.5-in. dia. fluidized bed reactor. In the present experiments, the final uranium and plutonium concentrations in the alumina beds were apparently independent of variations in the operating conditions among the runs. Changes in fluorine concentration (80–95%), filter blowback frequency (once every 5 min per filter to once every hour per filter), and superficial gas velocity (0.3–0.7 ft per sec) in the fluidized bed during recycle-fluorination had no significant effects nor did the type of alumina used as the fluid-bed material (i.e., Alcoa T-61 tabular alumina or Norton RR Alundum).

It was observed, from chemical analysis of alumina bed samples taken at intervals during recycle-fluorination, that the overall recycle-fluorination time may be longer than necessary and could probably be reduced without affecting the final retention of plutonium on the alumina.

An experimental program has been started to evaluate the fluorinating ability of BrF_5 for mixtures of uranium and plutonium compounds. It is postulated that the reaction between BrF_5 and mixtures of uranium and plutonium compounds will result in the conversion of the uranium compounds to volatile UF_6 while converting the plutonium to nonvolatile PuF_4. Such a reaction procedure would result in the separation of uranium and plutonium in a single fluorinat-

ing step; the plutonium would be converted to PuF_6 in a subsequent fluorination step using elemental fluorine. This reaction procedure is being considered as a possible step in the fluid-bed fluoride volatility process now being developed at Argonne.

The experimental work covered in this report involves the reactions of BrF_5 with various uranium compounds and with mixtures of uranium compounds, alumina, and fission product oxides. The reactions were carried out using a horizontal tubular reactor. In all of the experiments, the BrF_5 flow rate was about 0.5 g/min in a gas phase containing 20 v/o BrF_5 and 80 v/o nitrogen. The total gas flow rate was 250 ml/min, corresponding to a linear velocity of about 0.04 ft/sec in the reactor at a temperature of 300°C.

Experimental results are reported for the following investigations: (1) the reaction of BrF_5 with soda lime to develop a procedure for BrF_5 disposal; (2) determination of the kinetics of the UF_4-BrF_5 reaction and the UO_2F_2-BrF_5 reaction; (3) determination of the reaction rates for the reaction between BrF_5 and mixtures containing UF_4, UO_2F_2, alumina, and fission product oxides; (4) determination of the extent of uranium removal at 300°C for reaction periods of 1 hr from a mixture as described in (3) above and such mixtures together with Zircaloy or stainless steel decladding product; and (5) determination of the comparative reactivity of BrF_5 and fluorine toward reaction with UF_4, UO_2F_2 and mixtures of the type described in (3) above.

In the experiments to determine the effectiveness of activated alumina and soda lime as solid disposal agents for BrF_5, activated alumina was found not suitable for this purpose. Although the fluoride component of the BrF_5 reacted with activated alumina (apparently forming AlF_3), the bromine component did not react but was absorbed on the alumina. Both components of BrF_5 reacted with the soda lime, however. The experiments showed that about 4.3 g of soda lime is required in order to react with 1 g of BrF_5. Further, the experiments indicated that the portion of the soda lime reacting with bromine had to be at least 100°C for efficient reaction to occur.

Kinetic data were obtained for the UF_4-BrF_5 reaction over the temperature range 175 to 275°C, and for the UO_2F_2-BrF_5 reaction over the temperature range 175 to 300°C. The data were treated using the diminishing sphere model, in which the fraction reacted, F, is related to a rate constant, k', and the reaction time, t, by the expression $(1 - F)^{1/3} = A - k't$. Determination of the value of the rate constant at each temperature was accomplished by a least squares fit of the equation to the experimental data. Values of k' for the UF_4-BrF_5 reaction varied from 0.0005 to 0.0331 min^{-1}. A fit, by least squares, of the integrated form of the Arrhenius equation to the rate constants resulted in the following equation:

$$\log k' = 5.71942 - 3948.3/T \qquad (1)$$

Using the appropriate constant of Equation 1, a value for the apparent activation energy of 18.1 kcal/mole was calculated. Values of k' for the UO_2F_2-BrF_5 reaction varied from 0.0040 to 0.0276 min^{-1}. The least squares fit for this data of the Arrhenius equation resulted in the following equation:

$$\log k' = 1.49312 - 1747.1/T \qquad (2)$$

Using the appropriate constant of Equation 2, a value for the apparent activation energy of 8.0 kcal/mole was calculated.

A series of experiments was performed, each of which used a solid reaction mixture containing 10 g of alumina, 4.2 g of UO_2F_2, 2.2 g of UF_4, and 0.07 g of fission product mixture VI.[2] In these solid mixtures, the alumina to uranium and the UO_2F_2 to UF_4 weight ratios were each 2:1. The temperature range studied was 175 to 250°C, and the reaction time was 30 min in each experiment. Values of the fraction of uranium reacted varied from 0.3 to 0.9, and calculated rate constants, k', varied from 0.0038 to 0.017 $min.^{-1}$ A least squares fit of the Arrhenius equation to these rate data resulted in the following equation:

$$\log k' = 2.01969 - 1970.3/T \qquad (3)$$

Comparison of these rate data with values calculated for a ⅔ UO_2F_2-⅓ UF_4 mixture using the data obtained for UO_2F_2 and UF_4 alone showed reasonably good agreement. The rate data for the mixtures containing UO_2F_2, UF_4, alumina, and fission product oxides were about 20% greater than those calculated for the ⅔ UO_2F_2-⅓ UF_4 mixture. An apparent activation energy calculated from the appropriate constant of Equation 3 is 9.0 kcal/mole, while that calculated for the ⅔ UO_2F_2-⅓ UF_4 mixture is 10.0 kcal/mole.

Extrapolation to 300°C of the rate data presented above indicates that a reaction time of about 30 min at that temperature would be adequate to convert the uranium contained in the solid reaction mixture completely to UF_6. An experiment with a mixture of Al_2O_3, UO_2F_2, UF_4, and fission product oxides was performed at 300°C for a reaction period of 60 min. This experiment resulted in conversion of 99.8% of the uranium contained in the solid to UF_6. Two additional experiments were performed using the same

[2] For the composition of fission product mixture VI, see Table II-10, this report.

reaction conditions with the solid reaction mixture also containing Zircaloy or stainless steel decladding product prepared by the HF-promoted oxidation reaction. Over 99% of the uranium was converted to UF_6 in both experiments, indicating that the presence of decladding products does not affect removal of uranium.

Experiments were performed to determine the comparative reactivities of BrF_5 and fluorine. Fluorinations were made using as the solid reactant UO_2F_2 or UF_4 or mixtures containing UF_4, UO_2F_2, alumina, and fission product oxides. The experimental results showed that the reaction rates for reactions with fluorine are an order of magnitude lower than comparable reactions using BrF_5.

Neptunium hexafluoride was prepared by fluorination of neptunium dioxide with elemental fluorine at 500°C. The reaction of NpO_2 with fluorine proceeds at reasonable rates—greater than 2 g NpO_2/hr at this temperature. The absorption spectrum of gaseous NpF_6 was determined in the ultraviolet, visible, and near-infrared region. Molar absorptivities were determined for all principal peaks as well as for other parts of the spectrum observed. Peak separations have been correlated with the known vibrational spectrum of NpF_6. Beer's law plots, determined for absorption at 2210 Å and 12970 Å, showed no significant deviations from linearity.

Temperature halts in UF_6-MoF_6 mixtures have been measured to obtain a temperature-composition diagram. The system is a simple eutectic with the eutectic point at 13.7 ± 0.3°C and a composition of 20 m/o UF_6. The solid transition in pure MoF_6 creates an isothermal boundary line extending across the entire diagram at −8.7 ± 0.4°C. Additional temperature halts were observed for the solid mixtures at temperatures which increase with increasing concentration of UF_6, creating a boundary extending from the temperature of the solid transition of pure MoF_6 to the eutectic temperature at a UF_6 composition of about 23 m/o. The molecular or crystalline processes which give rise to this boundary are not presently understood.

The solubility of UF_6 in the UF_6-MoF_6 mixtures has been compared with values calculated for an ideal solution and also for a regular solution. The activity coefficient of UF_6 in UF_6-saturated solutions increases from 1.0 in pure UF_6 to about 1.5 in the eutectic mixture at 20 m/o UF_6. Activity coefficients calculated on the basis of regular solution theory increase from 1.000 to 1.001 over the same range.

Engineering-scale development work is in progress on a fluid-bed fluoride volatility process for the recovery of uranium and plutonium from spent uranium dioxide fuels. The process scheme under current investigation includes the following steps: decladding, fluorination of the UO_2-PuO_2 fuel to the corresponding hexafluorides, distillation of UF_6-PuF_6 mixtures, and conversion of the mixed hexafluorides to dense particles of UO_2-PuO_2. In addition, thermal decomposition of PuF_6 to PuF_4 provides a means of separating the plutonium from the uranium. Process steps are to be demonstrated with nonirradiated uranium-plutonium materials in three pilot-scale units—a fluorinator, a distillation column, and a converter—installed in an engineering-scale alpha facility. The facility comprises two large alpha boxes; the larger box contains the main process equipment, and the smaller box houses auxiliary equipment.

The fluorinator and converter systems have been installed in the facility and are undergoing shakedown tests with uranium materials. The distillation column was recently fabricated and has been erected in a mock-up area for preliminary testing. The unit will be installed in the large alpha box upon completion of the tests. Meanwhile, work has continued on the facility itself in preparation for operations with plutonium.

A full batch of UO_2 pellets (8.8 kg, about 12-in. bed depth) was successfully processed to UF_6 in a shakedown test for the fluorinator process equipment. The two-zone oxidation-fluorination method was used for the bulk UF_6 recovery period and was followed by a cleanup fluorination period in which the fluorine was recycled. The reactions were conducted in a fluidized bed of alumina (24-in. static depth, 6.04 kg, Alcoa Tabular 61, nominal 48 to 100 mesh).

In the two-zone portion of the run, oxygen with a concentration of about 11 v/o (in nitrogen) was fed to the bottom of the reactor to effect the oxidation of the UO_2 to U_3O_8 fines; fluorine in the concentration range 6 to 12 v/o was fed to the zone above the UO_2 pellets. With these conditions, the reaction was 95% complete in an 11.5-hr period (average UF_6 production rate 1.0 kg/hr). Peak UF_6 rates of 2.2 kg/hr were attained. The remainder of the charge was reacted during a final 7-hr period in which the unconsumed fluorine was recycled through the reactor through a bottom inlet; fluorine concentrations were in the range 30 to 75 v/o. Less than 0.1 w/o of the uranium from the initial charge was associated with the alumina bed after the fluorination. About 98% of the UF_6 was collected in the first cold trap, about 1.3% in the second cold trap, and about 0.7% in a NaF trap downstream of the second cold trap.

Succeeding shakedown experiments will be made under simulated alpha conditions—with all windows, gloves, and bags in place and with the required ven-

tilation flow. Plutonium work will start upon successful completion of the equipment testing period.

The first hexafluoride conversion experiment ($UF_6 + H_2 + 2H_2O \rightarrow UO_2 + 6HF$) was successfully carried out in the 2-in. dia. fluid-bed converter using conditions established earlier in a 3-in. dia. unit. The processing conditions included: bed temperature of 650°C, 30-min feed periods alternated with 30-min periods of fluoride cleanup, UF_6 feed rates of 12 and 16 g/min, and a starting bed of 2.5 kg of UO_2 (static bed height, 9 in.). Approximately 1.3 kg of UF_6 was processed. Product density remained constant throughout the run at about 8.4 g/cc. The converter unit is being readied for operation under alpha conditions.

Development work on the decladding and fluorination of uranium dioxide fuels has continued. The objective of this work is to optimize the processing conditions for the fluid bed fluoride volatility process for the recovery of fissionable values from spent PuO_2-UO_2 fuels by conducting experiments with non-plutonium fuels.

Additional work on the processing of UO_2-SS cermet fuels in a bench-scale fluid-bed reactor indicated that >99% of the uranium in the charge can be recovered. The processing procedure involves destructive oxidation of the cermet in 40 v/o HF-40 v/o oxygen-20 v/o nitrogen at 550°C, followed by fluorination at 250 to 550°C with fluorine.

In other work, a simulated fuel bundle, comprising six 2-ft long Zircaloy-2 tubes packed with cylindrical UO_2 pellets (0.43 by 0.43 in.), was destructively oxidized in a fluidized bed of alumina. The decladding reaction proceeds by the conversion of the zirconium alloy to ZrO_2 and/or $ZrOF_2$ flakes and the UO_2 pellets to UO_2F_2 and UF_4 powder. The reaction products were contacted with 17 to 90 v/o fluorine in nitrogen at 300 to 600°C. High UF_6 production rates [50 lb/(hr)(sq ft)] were achieved during the initial 2 hr of fluorination, wherein 56% of the uranium was recovered as UF_6. Further development work on this method of processing Zircaloy-clad UO_2 fuels is being conducted at other laboratories as an alternative to the currently accepted method of processing: decladding of zirconium by reaction with hydrogen chloride to produce volatile $ZrCl_4$ followed by treatment of the UO_2 pellets using the two-zone oxidation-fluorination technique.

The feasibility of pulverizing the UO_2 pellets with gas mixtures of HF and oxygen and fluorinating the resultant uranium fines was explored in several bench-scale and pilot-scale tests. Operation of both the steps was satisfactory. Further work on this method of processing is being done at other laboratories. The development program of this Division includes the evaluation of a processing scheme involving the use of oxygen as the pulverizing agent followed by the conversion of the uranium oxides to the fluorides.

Investigation of the cleanup of cell exhaust air contaminated with plutonium hexafluoride was continued. Additional experiments on the hydrolysis and filtration of dilute PuF_6 confirmed the previous observation that its hydrolysis rates are no more than twice those of dilute UF_6. Experiments made with an approximately equimolar mixture of PuF_6 and UF_6 diluted with nitrogen indicate that: (a) the PuF_6 hydrolysis rates were uniformly higher than those of the UF_6 in the mixture, (b) the hydrolysis rates of PuF_6 in the mixture were higher than the rates obtained when diluted PuF_6 alone was contacted with air of low moisture content, and (c) the UF_6 hydrolysis rates were lower than those obtained with dilute UF_6 alone.

Development studies on a fluid-bed fluoride volatility process for the recovery of uranium from highly enriched uranium-alloy fuels were continued. The process cycle includes hydrochlorination and fluorination steps; the fuel charge is reacted while immersed in a fluid bed of alumina which serves as a heat-transfer medium. During the current period, the final series of pilot-plant demonstration experiments were completed with unirradiated normal uranium fuel subassemblies. Studies with irradiated fuel materials were continued on a bench-scale level in a 1½-in. dia. fluid-bed reactor.

The final pilot-scale work included three experiments each with uranium-Zircaloy (U-Zr) subassemblies and uranium-aluminum (U-Al) subassemblies. The overall concentrations of uranium in these two materials were about 0.8 w/o and 4.5 w/o, respectively. Individual batch charges weighed about 12 to 20 kg for uranium-Zircaloy fuel and about 6 kg for uranium-aluminum fuel.

Results of the pilot-scale experiments showed that reuse of the alumina bed material for several process cycles effected an overall reduction in the fraction of uranium processed which was retained on the alumina bed material at completion of the final process cycle (a nonrecoverable loss). Uranium retention levels on the halogenation reactor alumina equivalent to 1.9 and 0.8 w/o of the uranium in the charge were obtained in two successive uranium-Zircaloy experiments. The three experiments with uranium-aluminum subassemblies also gave successive overall reductions in uranium loss with reuse of the halogenation reactor alumina bed; the final uranium levels in the three experiments corresponded to 0.13, 0.08, and 0.03% of the uranium in the charge.

A multicharge technique for achieving improved processing (hydrochlorination) rates and HCl utiliza-

tion, demonstrated earlier with uranium-aluminum subassemblies, proved beneficial for uranium-Zircaloy subassemblies. In this procedure, additional fuel elements are charged after the bulk (60 to 80%) of the previous element has been reacted to the point at which the reaction rate starts to diminish with a corresponding decrease in HCl utilization. The uranium which has accumulated in the bed during the multicharging step is subsequently recovered as UF_6 in a single fluorination step. In the multicharge uranium-Zircaloy run, the HCl utilization was about 35%, as compared with 25% when a single fuel subassembly was processed; a corresponding improvement in average reaction rate was also achieved.

The processing of both types of alloy fuels proceeded satisfactorily except for caking of the packed-bed filter under specific conditions of temperature during the hydrochlorination of uranium-aluminum subassemblies. The caking was related to the presence of iron in the charged alloy (0.7 w/o Fe); the iron condensed as $FeCl_3$ or as an iron-aluminum-chloride complex. The problem was complicated by the fact that high uranium losses through the packed-bed filter occurred under those conditions which precluded condensation of iron chloride species. Means for avoiding the caked layer by minor changes in operating conditions and equipment design have been considered.

High recoveries (99%) of the uranium in both alloy fuels were achieved under a wide variety of process operating conditions. Recommended operating conditions for processing both fuel types are:

Bed Material: Fluid bed: sufficient quantity of fused or sintered alumina (40 to 200 mesh) to cover the fuel subassembly (a multiplate assembly).
Packed-bed filter: coarse (−14 +48 mesh) alumina, >12 in. deep.

Hydrochlorination: Temperature of fluid bed: 350 to 450°C for uranium-Zircaloy fuel and as low as 200°C for uranium-aluminum fuel.
Temperature of packed-bed filter: 330 to 350°C for uranium-Zircaloy fuel and 180 to 200°C for uranium-aluminum fuel.
Gas Velocity: 0.4 to 0.6 ft/sec in the fluid bed.
Concentration of HCl: 80 v/o.
Total time: 6 to 10 hr for typical pilot-plant charges.

Fluorination: Gradual increase in temperature of the fluid bed and packed-bed filter from 250°C to 500°C while fluidizing with 1 to 5 v/o fluorine in nitrogen, followed by a gradual increase in fluorine concentration to 60 to 80 v/o; the alumina particulate material may be maintained static during the later period.
Total time: about 4 to 9.5 hr, depending on the quantity of fuel charged.

A hydrofluorination step of <1-hr duration at 350°C using gaseous HF at a concentration of about 25 v/o may be employed immediately following the hydrochlorination step to remove the bulk of the chloride before fluorine is introduced.

In-plant corrosion studies indicated that nickel is suitable as a material of construction for the halogenation reactor for the fluid-bed fluoride volatility process. Welded and unwelded corrosion coupons of nickel-200 and -201 showed corrosion rates of 0.08 to 0.12 mil/day for the fluid bed zone, and 0.03 to 0.09 mil/day for the region above the bed. Average corrosion rates of 0.04 mil/day were observed for stainless steel and Inconel coupons in the pyrohydrolysis reactor, indicating that either of these materials should be satisfactory for this application.

This pilot plant demonstration program has made evident certain advantages of the fluid-bed fluoride volatility process. These advantages are: a small volume of solid radioactive wastes is produced; process operations are few and employ simple, compact equipment; and the UF_6 product is directly amenable to isotope separation or conversion to other uranium compounds for fuel fabrication.

A program involving fluid-bed volatility process studies with irradiated fuel materials is being carried out on a bench-scale (1½-in. dia. reactor) level. Eight experiments with fuels of the highly enriched uranium-alloy type (uranium-Zircaloy and uranium-aluminum) and the low enriched ceramic uranium oxide type have been completed. Analytical results for the first two experiments performed with 5-yr-cooled uranium-Zircaloy-2 alloy fuel show:

(1) On the basis of results of tests performed with irradiated and unirradiated fuel materials, it appears that the presence of fission products from irradiated fuel had no marked effect on uranium recovery or loss.
(2) Decontamination factors for uranium, calculated from activities in the sodium fluoride trap

used for the collection of the UF_6 product, ranged from about 3×10^4 for gross gamma, gross beta, and ^{137}Cs, to about 1×10^4 for ^{125}Sb and ^{106}Ru.

Preliminary data from subsequent runs show that additional decontamination is achieved in desorbing the UF_6 product from the sodium fluoride traps and collecting it in cold traps.

Basic studies on fluidized-bed processing of fine particles were continued. Current work was aimed at the determination of the optimum size distribution of coarse particles which, when mixed with fine particles, would produce a maximum residence time and a uniform distribution of the fine particles in the fluidized bed. Tests were made with sintered alumina, median diameter 165μ, as the coarse particles, and with uranium oxide powder or nickel metal powder as the fine materials.

Several qualitative observations have been made in these studies on the behavior of fine particles in a fluidized bed. The elutriation rates of nickel fines from a fluidized bed of alumina particles decreased with an increase in the concentration of the nickel fines in the bed. The concentration of uranium fines in the fluidized bed varied longitudinally with no distinct separation of fine and coarse particles. The incipient fluidization velocity decreased from 0.18 to 0.06 ft/sec with the addition of 50 w/o uranium fines to the alumina. Fluidization of these mixtures was fairly uniform with the bed expanding almost linearly with increase in the gas velocity above the minimum fluidization velocity. These results indicated that beds containing large quantities of fines could be processed with a high rate of heat transfer and freedom from caking. Further tests are planned with smaller size alumina.

III. High Temperature Reactor Materials Development (pages 163 to 166)

A program directed toward the development of reactor materials for use at high temperatures (1500 to 3000°C) is under way, the objective being to build up a reservoir of basic data which may be used for screening and evaluation. The study will be concerned with the chemical stability of potential high temperature fuels, i.e., uranium oxides, phosphides, sulfides, arsenides, nitrides, and their solid solutions; and with the reactions of these fuels with hydrogen, its contaminants, and refractory structural materials such as tungsten, rhenium, molybdenum, tantalum, and certain alloys. These studies will be done quantitatively to yield thermodynamic and phase-diagram information. Selected systems are to be investigated in an integrated way using several methods which are mutually supporting. Progress in the application of these methods to the uranium-urania system follows.

Phase Diagram Studies. Additional data have been obtained in order to delineate certain features of the uranium-urania phase diagram. At the monotectic temperature, 2500 ± 30°C, the compositions in O/U atom ratio units of the three condensed phases in mutual equilibrium are: liquid uranium, 0.06 ± 0.02; monotectic liquid, 1.30 ± 0.10; hypostoichiometric urania solid, 1.64 ± 0.02. Compositions on the hypostoichiometric urania phase boundary between 1600 and 2300°C can be expressed by the equation, $\log x = 1.854 - 6066/T$, where x is the oxygen deficiency in the formula UO_{2-x}, and T is temperature in °K. The changes in the phase diagram brought about by the addition of tungsten are also being examined.

Vapor Pressure Studies: Transpiration Method. Transpiration measurements using inert carrier gases have been carried out to determine the total vapor pressure of the uranium-bearing species over nearly stoichiometric uranium dioxide between 1850 and 2600°C. The prime purpose of these preliminary measurements was to check the reliability of the experimental apparatus and procedures. A comparison of the results with those from effusion measurements reported in the literature indicates that reliable results are being obtained.

Vapor Pressure Studies: Effusion Method. Effusion measurements to determine the total vapor pressure of uranium-bearing species over the uranium-urania two-phase system between 1300 and 2000°C are complete. An ANL topical report on this work is being prepared. In a future study, the transpiration method will be used to extend the measurements up to 2500°C.

Vapor Pressure Studies: Mass Spectrometric-Effusion Method. Five sets of mass spectrometric effusion measurements of the partial pressures of uranium-bearing species over the uranium-urania two-phase system have been carried out between 1650 and 2050°C. Agreement among the several sets, however, is not yet satisfactory probably owing to temperature gradients in the effusion cells. Improvements in the spectrometer furnace to eliminate the uneven heating are being studied.

IV. Calorimetry (pages 167 to 176)

A technique previously developed for the combustion of phosphorus in fluorine has been used for com-

bustions of sulfur, selenium, and tellurium. The enthalpies of formation of SF_6, SeF_6, and TeF_6 were found to be approximately 10 percent more negative than the values determined by Yost and Claussen 30 years ago. The new data are an order of magnitude more precise and are believed to be more accurate.

Techniques have been developed for combustion in fluorine of metals that form nonvolatile fluorides. Calorimetric results have been calculated for magnesium, aluminum, yttrium, gadolinium, and holmium.

The enthalpy of formation of β-silicon carbide, as determined by fluorine bomb calorimetry, was given in the last report. Similar measurements with α-silicon carbide gave discordant results. Since then, combustions in fluorine of a more finely divided specimen of α-silicon carbide have been carried out with satisfactory results. The enthalpy of formation of the α-form is 0.4 kcal. mole^{-1} less negative than the β-form.

Suspicion of a low bias in our previous determination of the enthalpy of formation of boron trifluoride by fluorine bomb calorimetry has led to a redetermination using a purer specimen of boron. Combustions were carried out in both single-chambered and two-chambered systems to investigate the possibility of systematic errors. The new value obtained for the enthalpy of formation of boron trifluoride is indeed more negative. The previous low result is attributed to the presence of unsuspected impurities in the original boron specimen.

A fluorine flow calorimetric system is being constructed for the combustion of substances that react spontaneously with fluorine. This system is expected to have advantages over the two-chambered system now used for such substances. Its first application will be to uranium compounds.

The 1500°C drop calorimeter is being tested by measuring the enthalpy increments of a standard sample of synthetic sapphire over a range of temperatures. Much of the work during this report period has been involved with familiarizing and training personnel in the use of the equipment. Plans are being made to measure the high-temperature enthalpy increments of uranium monophosphide.

Work has been resumed on the procurement of parts, assembly, and component testing of a calorimeter for measuring enthalpy increments up to 2500°C. The 2500°C calorimeter differs from the 1500°C calorimeter principally in the method of furnace heating (electron bombardment instead of resistance windings) and in the method of sample transfer to the calorimeter proper (pneumatic pressure instead of gravity).

V. Reactor Safety (pages 177 to 212)

The experimental program to determine rates of reaction of molten fuels and cladding metals with water is continuing. In general, it has been necessary to study the reaction of each metal of interest by several methods. One of these techniques utilizes a high pressure furnace which was designed especially for isothermal studies of the reaction of steam with aluminum and with stainless steel. The initial series of isothermal experiments has been performed with high-purity aluminum at 1200 and 1300°C. Pressures ranged from 1 to 8 atm in the preliminary experiments. The results of the experiments showed a reaction rate which increased with increasing pressure as judged by the amount of hydrogen evolved during the aluminum-steam reaction. Appearance of reacted samples also indicated greater oxide formation with increasing pressure and temperature.

One of the experimental techniques used to study metal-water reactions was designed to observe the reactions of small particles. This method uses energy from a pulsed ruby laser to heat single particles of metal submerged in water. The method was designed to study not only the chemical reaction of particles with water, but also to study the transient energy exchange and hydrodynamic effects. In recent work, experimental studies of the aluminum-water reaction were completed. The aluminum samples were squares of 1-mil foil which formed spheres when fully melted by the laser pulse. The extent of reaction was determined by hydrogen analysis of the reaction cell contents. Previous experiments had shown that aluminum particles, 360μ nominal diameter, reacted about 8% in 25°C water over a range of laser energy from 10 to 50 joules. In 100°C water, there was no reaction with laser energies ranging from 16 to 40 joules; with laser energies above 45 joules, virtually complete reaction occurred. Recent experiments were performed in 25°C water with a 1-atm overpressure of argon added to the reaction cell. In these experiments, gas analyses were performed by gas chromatography. The extent of reaction was found to be less than 4% for four experiments over a range of laser energies from 24 to 45 joules. These results suggested that it is the water vapor pressure (water temperature) which is important in controlling the reaction and not the total pressure. The effect of increased steam overpressure was also studied. A metal reaction cell was constructed in which the aluminum-water reaction was studied at 1 and 10 atm of steam overpressure (100 and 181°C water). Although the value of the threshold laser beam energy changed from that found in the quartz reaction cell, there was no apparent additional effect

of pressure between 1 and 10 atm on the reaction. X-ray diffraction analyses of reacted particles from the laser studies indicated that the oxide product was α-Al_2O_3 (corundum) in all cases.

Another general method of studying metal-water reactions involves nuclear heating of typical reactor fuel materials submerged in water. Previous studies in this program have been performed in TREAT. The destructive test of the Kiwi-TNT reactor (conducted on Jan. 12, 1965) offered a unique opportunity to obtain data on metal-water reactions of typical fuel materials during a short-period (0.6 msec) transient. The Kiwi-TNT transient allowed fission heating of the fuel material under conditions more closely approximating those achieved during a short-period nuclear reactor excursion. Prior to the test, twenty-four stainless steel autoclaves containing fuel samples in water were placed at distances of from 8 in. to 12 ft from the Kiwi-TNT reactor vessel. The autoclaves were contained within an outer steel capsule and enclosed a flux-monitor wire in additional to the fuel sample. Six samples of each of the following enriched fuel materials were used: (1) uranium alloy (5 w/o Zr, 1.5 w/o Nb) pin, unclad; (2) UO_2-core, Zircaloy-2-clad pin; (3) UO_2-core, 304 stainless steel-clad pin; and (4) aluminum alloy (17 w/o U, 2 w/o Ni) plate, unclad.

Twenty-three of the autoclaves were recovered intact although all were damaged to some degree. The nuclear energy input to each sample was calculated from the data obtained by counting the 1.6 Mev barium-lanthanum-140 photopeak from the natural uranium flux monitor wires. From the energy, the adiabatic temperatures of each fuel sample were computed and ranged from 1133 to 3800°C for the uranium alloy pins, from 700 to 3300°C for both types of the clad UO_2 pins, and from 100 to 660°C for the aluminum alloy plates. In all cases, the samples reaching the highest temperatures were extensively fragmented. The extent of metal-water reaction could not, in general, be obtained from hydrogen analyses because damage to the autoclaves resulted in loss of hydrogen; for these the extent of reaction will be obtained by chemical analyses of the residues. Particle size analyses for the uranium alloy fuel samples showed that fragmentation began at a lower energy threshold and was more extensive than in previous TREAT experiments at equal energy input values. This finding was consistent with the shorter period of the excursion.

Studies of metal-water reactions in TREAT are continuing. Experimental work is progressing in three areas. Four scale-up experiments are in progress in which 9-pin assemblies of Zircaloy-2-clad and 304 stainless steel-clad, UO_2 pellet fuel are subjected to a neutron burst in TREAT. A series of 8 experiments using individual samples of High Flux Isotope Reactor (HFIR) fuel are in progress. HFIR fuel contains a 0.030-in. thick core of 41 w/o U_3O_8 (93% enriched)-aluminum cermet which is clad on each face with 0.010 in. of 6061 aluminum. The results of the experiments with HFIR fuel will be compared with previous results with aluminum-uranium alloy fuel. Attempts to obtain high speed motion pictures of meltdowns of aluminum-base fuel in TREAT are being made. Principal differences between present photographic experiments and previous studies by other investigators are the need for a high intensity light source within the capsule and the presence of water surrounding the specimen. It is expected that the nature and the time of failure of submerged fuel will be determined.

The calculational study to demonstrate the application of metal-water reaction data to the analysis of a reactor loss-of-coolant accident was continued. A previous analysis was made for the proposed Loss of Flow Test (LOFT) reactor as a model using a 25-mil Zircaloy-clad core for the calculations rather than the 15-mil stainless steel-clad core proposed in the LOFT design. In the previous analysis the assumption was made that the reactor core was cooled uniformly to 285°C during the 10 sec blowdown which followed the pipe rupture. The present analysis has been made on the basis that none of the energy stored in the UO_2 fuel during full-power operation was lost to the coolant during the blowdown. In this case, the initial fuel and cladding temperatures range from 337°C in the lowest power section of the reactor to 1289°C in the highest. The elevated core temperatures following blowdown result in the elimination of the 200 sec delay in the start of significant zirconium-water reaction. The reaction begins immediately after blowdown; however, the subsequent reaction rates for the overall core are about the same as those calculated for the case where the stored energy in the fuel had been dissipated during blowdown.

The program of studies of potential problems in the field of fast reactor safety has continued. As part of this program, studies are being made of the interaction of fuel and cladding materials with molten sodium. The method consists of levitating and heating samples (about 0.3 cc in volume) to maximum temeratures between 2100 and 2400°C and then dropping them into a beaker of liquid sodium maintained at 250°C. The refractory metals niobium, molybdenum, tantalum, and niobium-1 w/o zirconium were dropped

as solid pellets; the experiments indicated that there was no chemical interaction with the sodium. Stainless steel, mild steel, zirconium, nickel, and vanadium samples were dropped as molten pellets. Although there was no indication of chemical interaction with any of the metals tested, there were violent physical interactions. Type 304 stainless steel, at an initial temperature of 2400°C, fragmented violently upon entering the sodium. Considerable sodium was expelled from the beaker and was found as small droplets on the walls of the glovebox, a distance of 4 ft from the beaker. A sodium vapor cloud was observed immediately following the contact. While fragmentation occurred with the other molten metals at the highest temperatures studied, the degree of fragmentation was less and the interactions were correspondingly less violent.

Studies of transient boiling heat transfer are continuing. The research is directed toward obtaining the information necessary to predict the magnitude of explosive pressures generated when hot fuel materials are suddenly dispersed into liquid coolant. Both water and molten sodium coolants are of interest, although the initial work has been limited to water systems. The initial experiments have been performed with a swinging arm apparatus in which a heated nickel ball is passed rapidly through a pool of water. The temperature difference of the ball before and after immersion yields subcooled boiling heat transfer rates at a definite velocity of travel through the water. Preliminary experiments have indicated that a ¼-in. dia. nickel ball with a velocity of about 10 ft/sec loses heat to subcooled water at rates ranging from 80 cal/(cm^2)(sec) for an initial ball temperature of 300°C to between 150 and 210 cal/(cm^2)(sec) for an initial ball temperature of 1000°C.

A series of calculations have been performed of the maximum adiabatic temperatures and pressures produced when molten sodium is sprayed into an air-filled enclosure. In the calculations, the air was assumed to be initially at 12.2 psia and 25°C and the sodium at 427°C. The thermodynamic equilibrium compositions, temperatures, and pressures were calculated for sodium-to-oxygen molar ratios of 1 to 9. The maximum temperature calculated was 1950°C for a mixture consisting of 5 gram atoms Na/mole O_2 whereas the maximum pressure calculated was 102 psig for a mixture of 7 gram atoms Na/mole O_2. The maximum temperature was far below previous values given in the literature for calculations that ignored the thermal decomposition of the oxide, which becomes appreciable at 2000°K (1727°C).

Two other research programs concerning fast reactor safety are underway. One, currently in the apparatus development stage, is the determination of the extent of fuel migration and segregation in mixed uranium-plutonium fuels. A significant degree of segregation could seriously inhibit the effectiveness of Doppler broadening as a shutdown mechanism in an operating reactor. The other program concerns the determination of the high temperature physical properties of various fast reactor materials. The specific heat of molten UO_2 has been selected for initial study.

VI. Energy Conversion (pages 213 to 229)

Investigations on regenerative emf cells for the conversion of heat into electrical energy were continued. Two types of cells are being studied, bimetallic concentration cells and a lithium hydride cell.

The emf-temperature relationships obtained in previous studies of the lithium hydride cells have been shown to be inconsistent with certain thermodynamic requirements. This was especially apparent when cells containing electrolyte saturated with lithium hydride were compared with cells containing electrolytes unsaturated with lithium hydride. The difficulty is associated with the increasing solubility of lithium metal from the anode in the electrolyte with both increasing temperature and mole fraction of lithium hydride in the fused-salt electrolyte. The dissolved lithium metal in the electrolyte polarizes the cell by reaction at the cathode to form lithium hydride. Electronic conduction in the electrolyte is not believed to be appreciable. The lithium metal-saturated electrolyte was isolated to a small region inside an enclosed anode, and diffusion potentials between the lithium metal anodes in saturated and unsaturated electrolytes were measured as a function of temperature. These diffusion potentials were then used to correct the emf-temperature plots of the lithium hydride cell. Diffusion potentials ranged from 1 mv at 520°C to 22 mv at 600°C for the lithium chloride-saturated lithium hydride binary electrolyte.

The lithium hydride cell has been studied by the method of solid-electrode voltammetry. Uninsulated microelectrodes, necessary as a consequence of the chemical reactivity of liquid lithium metal and lithium hydride toward all known insulating materials except the frozen lithium halides, were shown to be practical. The cell $Li^o(\ell)$/LiCl-KCl, LiH/H_2(g), Fe was studied at 375°C. The voltammetric curves obtained for the lithium hydride-hydrogen electrode were interpreted

on the basis of a simple two-step electrochemical reaction mechanism:

$$LiH \rightleftarrows Li^+ + H(adsorbed) + e^-$$
$$2H(adsorbed) \rightleftarrows H_2(g).$$

An unusual peak observed in the voltammetric curves of cells unsaturated with respect to lithium hydride was explained on the basis of concentration changes in the immediate vicinity of the microelectrode due to the electrochemical production or removal of lithium hydride.

The solubilities of sodium-bismuth intermetallic species from a 55 a/o sodium-bismuth alloy in the fused salt ternary eutectic mixture 53.2 m/o NaI-31.6 m/o NaCl-15.2 m/o NaF have been measured over the temperature range from 550 to 750°C. The solubility of bismuth ranged from 0.7 m/o at 550°C to 1.0 m/o at 750°C. The observed sodium-bismuth ratio was 2.71 ± 0.19 up to 600°C and 2.89 ± 0.41 above 600°C. This solubility level of sodium-bismuth intermetallics in the ternary eutectic would not be expected to be a problem at cell operation temperatures.

Previously reported absorption spectra of the alkali tellurides in fused cesium chloride were in error owing to impurities in the cesium chloride. This difficulty has since been resolved and the following are the corrected data. Cs_2Te solutions in fused cesium chloride exhibit a single peak at 555 mμ in addition to a charge transfer band. The spectrum of tellurium dissolved in molten cesium chloride (1.28×10^{-2} w/o Te) exhibits peaks at 645 and 470 mμ with a minor peak at 1050 mμ and a charge transfer band. A solution of tellurium in fused lithium chloride (less than 5×10^{-4} w/o Te) was not colored and yielded no absorption spectrum. Dilute solutions of Cs_2Te and Li_2Te in the lithium and cesium chloride reciprocal systems give spectra identical with those obtained in solutions of Cs_2Te and Li_2Te in their common ion halides. The identical spectra indicate complete metathetical reaction of the alkali metal associated with the tellurium and the alkali ion in the melt.

Temperature-pressure-composition relationships in the liquid-vapor equilibria involved in the regeneration portion of the sodium-bismuth cell are being determined. Total pressure measurements and transpiration experiments to determine total atom content of the vapor phase are supplying the necessary data. The Rodebush-Dixon technique is being developed to obtain total pressure data below 50 mm, which is the lower pressure limit of operation of the ebulliometer.

Mathematically, the two measurements, total pressure and transpiration (atom content of vapor), may be combined to yield thermodynamic information (activities) for the components of the liquid phase. This is possible for a two-component system if the vapor species are monomers and dimers only, as is essentially the case for the sodium-bismuth system.

Ebulliometric data have been obtained for the systems 10, 15, 18.75 and 20 a/o bismuth in sodium. In addition, results utilizing a transpiration apparatus have been obtained for the 60 and 80 a/o bismuth in sodium systems. At 902°C the vapor composition changes from 40.4 to 4.90 a/o bismuth as the liquid composition changes from 80 to 60 a/o bismuth. A tentative conclusion is that the sodium-rich systems (about 10 to 20 a/o bismuth) exhibit positive deviations from ideality, whereas on the bismuth-rich side the deviations are negative.

Work on the engineering development of thermally regenerative emf cell systems of the bimetallic and hydride types has been continued.

Measurements of the densities, viscosities, and surface tensions of electrolyte and bimetallic mixtures, which are needed for engineering design of cell and regenerator apparatus, have been initiated.

An experimental sodium-bismuth bimetallic closed cell apparatus without a thermal regenerator has been operated as a battery by charging and discharging it electrically. The cell has a frozen electrolyte-silicone rubber combination electrical insulator and pressure seal. It has been at an operating temperature of from 535 to 650°C for over 200 days (as of June 30, 1965).

An experimental bimetallic regenerator for continuously regenerating sodium from lead by thermal distillation has been constructed. To date 28 test runs under various operating conditions, for a total operating time of 91 hr, have been made with this device.

Corrosion studies of materials of construction of the cell components by liquid cathode metals (bismuth and tin) are in progress. Both static and dynamic tests are being conducted. These tests have indicated that mild or stainless steel may be suitable for the cell portions of the system (operating temperature about 550°C). However, refractory metals will undoubtedly be required for the regenerator (operating temperature near 1000°C).

VII. Nuclear Constants (pages 230 to 233)

Measurements of neutron cross sections of materials important to the fast reactor program are being con-

tinued. Radiative capture cross sections of ^{185}Re and ^{187}Re have been measured for monoenergetic neutrons between 4 keV and 2.6 MeV and of ^{141}Pr between 0.2 and 2.5 MeV. Samples of uranium and plutonium isotopes have been inserted into EBR-II in experiments designed to measure the ratio of the capture and fission cross sections of these isotopes. The neutron inelastic scattering cross sections leading to four excited states of ^{93}Nb have been measured as a function of neutron energy.

ARGONNE NATIONAL LABORATORY

Chemical Engineering Division Semiannual Report

January - June, 1965

SEMIANNUAL REPORT

I

Compact Pyrochemical Processes[1]

Compact pyrochemical processes are nonaqueous processes which utilize liquid metal and molten salt solvent media for the recovery and purification of partially burned reactor fuels. The metal solvent systems consist principally of various alloys of zinc, cadmium, magnesium, and copper. The salt systems are halide salts of alkali and alkaline earth metals. Metallic fuels are sometimes processed directly, i.e., without dissolution in any solvent media, as in melt refining.

Hitherto, these processes have been called "pyrometallurgical" processes. The processes have been renamed "compact pyrochemical" processes in order to emphasize their utility for recovery of ceramic fuels (for example, oxides and carbides) as well as metallic fuels, and their suitability for use in small plants serving as few as one reactor.

Compact pyrochemical processes have continued to be intensively developed for recovery and purification of fuel materials discharged from power reactors. Because inorganic, radiation-stable materials are employed in these processes, they can accommodate short-cooled, high-burnup fuels, thus permitting rapid recycle of fuel. The resulting reduction of fuel inventories outside the reactor is one of the major economic incentives for the development of pyrochemical processes. This is an especially important factor for fast reactor fuels which contain a high concentration of valuable fissionable isotopes. Other advantages of these processes, which also have economic merit, are the avoidance or simplification of chemical conversions, small process volumes (and, hence, compact processing equipment), direct production of solid wastes, decrease in criticality problems because of the absence of aqueous solutions, and, in some of these processes, the retention of valuable alloying elements. Because of the above characteristics, particularly the advantage of compact processing equipment, pyrochemical processes are suited for use in small plants located on or near a reactor site.

A. COMPACT PYROCHEMICAL PROCESS DEVELOPMENT (L. Burris, R. K. Steunenberg, R. D. Pierce)

1. Melt Refining

The concept of on-site recovery and recycle of discharged reactor fuel materials is being evaluated in Argonne's EBR-II reactor complex, which includes the EBR-II reactor and a spent-fuel processing and refabrication plant known as the EBR-II Fuel Cycle Facility. During the past year, the Facility was placed in operation and several batches of fuel material, consisting of approximately 50% enriched uranium alloyed with about 5 w/o noble metal fission product elements (fissium) were discharged from the reactor, successfully processed by melt refining,[2] fabricated into a fuel subassembly,[3] and transferred back to the reactor. The successful operation of the present melt refining process precluded the need for additional development work on this process during the last reporting period. However, a modification of this process (halide slagging) which shows promise for the processing of uranium-plutonium alloy fuels is being investigated. This process involves the use of a halide flux.

a. EXTRACTION OF PLUTONIUM FROM URANIUM-PLUTONIUM ALLOYS WITH URANIUM TRICHLORIDE (N. R. Chellew, J. T. Feeney)

In the development of refining processes for metallic fuels and blanket elements from fast breeder reactors, the use of chloride salt systems for the extraction of

[1] A summary of this section is given on pages 1 to 7.

[2] A complete description of the melt refining process is given in ANL-6605, pp. 61–73.

[3] There are 91 fuel elements in each subassembly.

highly electropositive fission products and plutonium from the metal is of interest. Bennett *et al*[4] have shown that when uranium-plutonium-fissium alloys were melted in contact with chloride fluxes containing $MgCl_2$ as an oxidant, selective removal of cerium from uranium and plutonium could be accomplished by controlling the amount of oxidant present in the flux. Other work carried out by McKenzie *et al*[5] indicated that more than 90% of the plutonium present in irradiated uranium could be extracted from plutonium-containing fuel heated at temperatures exceeding 1150°C when large excesses of either undiluted UCl_3 or $MgCl_2$ were used as oxidant salts. This investigation also presented evidence that UCl_3 and $MgCl_2$ behave similarly in that with $MgCl_2$ the following reactions occur at elevated temperatures:

$$3MgCl_2 + 2U \rightarrow 2UCl_3 + 3Mg \uparrow$$

$$3MgCl_2 + 2Pu \rightarrow 2PuCl_3 + 3Mg \uparrow$$

$$UCl_3 + Pu \rightleftarrows PuCl_3 + U$$

For the reaction of UCl_3 with tracer level plutonium (250 ppm) in uranium at 1200°C, an equilibrium constant of 189 was reported[5] (solution ideality in both phases was assumed).

During the present report period a series of experiments was carried out to investigate the uranium trichloride-plutonium reaction with higher initial concentrations of plutonium in uranium (>2000 ppm) and with $CaCl_2$ added as a salt diluent for the uranium trichloride:

$$UCl_3\ (CaCl_2) + Pu\ (U_{soln.}) \rightleftarrows PuCl_3\ (CaCl_2) + U\ (U_{soln.})$$

A primary objective of the work was to obtain equilibrium data for this reaction under various conditions which would approximate those considered for the halide slagging of discharged EBR-II fuel. Such data are of interest in the development of conceptual process flowsheets. Information was also obtained on the interaction of the charges with the beryllia containment crucibles and on the loss of plutonium by vaporization of $PuCl_3$.

Calculations of equilibrium constants for the reaction of UCl_3 with plutonium at temperatures of process interest were made. However, the uncertainties in the calculations were of such a magnitude that reliable values could not be obtained. The calculations were based on data obtained by Benz *et al*,[6,7] Egan *et al*,[8] and Fuger *et al.*[9] Using these data, I. Johnson[10] derived mathematical relationships for the estimation of free energies of formation at the temperature of interest, 1200°C. At this temperature, the calculated free energies of formation for UCl_3 and $PuCl_3$ were about −127 and −147 kcal/mole, respectively, with an uncertainty of as much as 4 kcal for $PuCl_3$ at this temperature. Assuming the same uncertainty for UCl_3, the free energy change for the reaction could vary from −12 to −28 kcal.

(1) Experimental

Uranium-4.21 w/o plutonium alloy pins (dia. of 0.144 in.) were prepared by melting the constituent metals in an yttria-coated graphite crucible and injection-casting the melt into yttria-coated Vycor tubes. This metal contained about 300 ppm of carbon. The initial concentration of plutonium in the charges was varied, when desired, by the addition of oxide-free uranium pins to the charge. Uranium trichloride was prepared by passing anhydrous HCl gas through a bed of UH_3 which was heated to about 300°C.[11] For this preparation a weight comparison of the uranium used with the salt product formed indicated that the conversion of metal to the trichloride was 100 ± 0.5%. Anhydrous $CaCl_2$, used as a UCl_3 diluent salt in the experimental work to achieve a more efficient salt-metal separation, was prepared by passing anhydrous HCl through $CaCl_2 \cdot 2H_2O$ while the salt was heated to 830°C and subsequently sparging the molten salt with helium to remove dissolved HCl. Analysis of the oxygen content of the purified salt by a neutron activation method showed that the level of this impurity was about 200 ppm. For three separate preparations the average chlorine content was 63.2 w/o as compared with 63.9 w/o in pure $CaCl_2$. All salts were stored and handled in dry helium or nitrogen atmospheres.

Beryllia was selected as the container material for

[4] Bennett, G. A., Burris, L., and Vogel, R. C., Halide Slagging of Uranium-Plutonium Alloys, ANL-6918 (1964).

[5] McKenzie, D. E., Elsdon, W. L., and Fletcher, J. W., The Extraction of Plutonium from Neutron-Irradiated Uranium by Uranium Trichloride and Magnesium Chloride, Can. J. Chem., **36**, 1233 (1958).

[6] Benz, R., Some Thermodynamic Properties of the System $PuCl_3$-KCl from Electromotive Force Data, J. Phys. Chem. **65**, 81 (1961).

[7] Benz, R., and Leary, J. A., Some Thermodynamic Properties of the System $PuCl_3$-NaCl from Electromotive Force Data, J. Phys. Chem. **65**, 1056 (1961).

[8] Egan, J. J., McCoy, W., and Bracker, J., The Standard Molar-Free Energy of Formation of Some Solid Chlorides of Mg, Ce, U, and Th by Solid-State EMF Techniques, "Proceedings of the Symposium on Thermodynamics of Nuclear Materials," IAEA, Vienna, 163, 1962.

[9] Fuger, J. and Cunningham, B. B., J. Inorg. and Nucl. Chem. **25**, 1429 (1963).

[10] Johnson, I., Argonne National Laboratory, private communication, 1965.

[11] Katz, J. J. and Rabinowitch, E., The Chemistry of Uranium, Part I, McGraw-Hill Book Co., Inc., New York, p. 451, 1951.

the charges because, based on the experience of Bennett *et al*,[4] it was believed to be one of the more stable refractories of those commercially available with respect to a combination of liquid uranium and molten chloride fluxes. Slip-cast crucibles[12] having reported densities of 2.7+ g/cc (density of pure BeO, 3.008 g/cc) and purities of 99+ % were used. Prior to each experiment the crucibles were subjected to a high-temperature outgassing treatment at pressures of less than 1 μ.

Equilibration of metal and salt were carried out in a resistance-heated furnace assembly which is shown in Figure I-1. The crucible and charge were positioned in a Mullite tube (OD, 1⅝ in.; length, 19 in.) as shown in Figure I-1. Charge temperatures were monitored with a Pt/Pt-10% Rh thermocouple which was sheathed with tantalum and located above the mouth of the crucible. Preliminary furnace heating tests to determine the relationship between the temperatures measured with this reference thermocouple and one located at the bottom of the crucible showed the temperature differential between these two furnace zones to be within 3°C, when the crucible was heated to constant temperatures between 1150 and 1250°C. The charge temperatures reported herein are considered to be accurate to ±5°C.

For each experiment, accurately weighed amounts of salt, uranium, and/or uranium-plutonium alloy were loaded into the beryllia crucible and degassed in vacuum (~0.01μ) at a maximum temperature of 150°C. The system was pressurized to about one atmosphere with purified helium, and the charges were heated to the selected equilibrium temperature (1150 or 1200°C), held at this temperature for a predetermined time, then rapidly quenched by withdrawing the molten charge to a water-cooled zone of the furnace.

In the preparation of analytical samples, the salt phase was washed from the metal phase and crucible surface with 1.5*N* acetic acid.[13] The ingot was then physically separated from the crucible and completely dissolved in aqua regia. During the course of the experiments a thin, grey reaction layer formed over the area of the crucible that was in contact with the molten charge. Analytical solutions of this crucible-charge reaction product, which largely adhered to the crucible wall during physical separation of the ingot, were obtained by treatment of the material with aqua regia. For each experiment, samples of alloy rod adjacent to that used as charge material were dissolved for use as reference material.

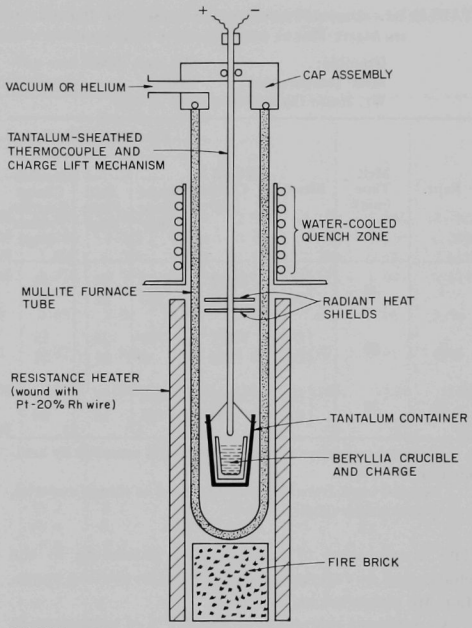

108-8896

FIG. I-1. Apparatus for Study of Plutonium Extraction from Uranium-Plutonium Alloy.

Analyses of the solutions were by standard techniques. The crucible-charge reaction product and the salt phase were analyzed for uranium and plutonium; the metal phase and control samples were analyzed for plutonium. The accepted precisions of the analyses were: uranium, ±5% (relative), and plutonium, ±2% (relative). Weights of plutonium in metal fractions (charge and ingot) were calculated from the alpha activity present in the sample and the specific alpha activity of the plutonium metal employed in the experimental work. The uranium content of metal fractions was based on the weight of metal, corrected for analyzed plutonium content.

(2) Results

Three blank experiments were carried out in which uranium-plutonium alloy was melted at 1200°C under $CaCl_2$ without the addition of UCl_3 oxidant. The purpose of these experiments was to gain insight into any processes that might affect removal of plutonium from the alloy. The weight ratio of $CaCl_2$ to total metal in the experimental charges was similar to that used in later experiments employing UCl_3 oxidant (see below).

[12] Product of National Beryllia Corp., Haskell, N. J.

[13] Separate tests in which uranium-4.2 w/o plutonium was treated with 1.5*N* acetic acid indicated that the rate of plutonium dissolution was 0.06%/(hr)(cm² of metal contacted). For the experiments reported herein, the total metal ingot areas varied from 1.7 to 5.5 cm² and the time of exposure to the dilute acid was typically 30 min. Therefore, the maximum amount of plutonium dissolved from the metal phase by the acetic acid washing operation is believed to have been less than 0.2% of that present in the metal after equilibration.

TABLE I-1. DISTRIBUTION OF URANIUM AND PLUTONIUM IN ALLOY MELTS WITH CALCIUM CHLORIDE

Crucible: Slip-cast BeO
Melt Temperature: 1200°C
Wt. Ratio $CaCl_2$:Metal: 0.17 ± 0.02

Expt.	Melt Time (min)	Element	Weight in Charge (mg)	Element Distribution		
				Metal Phase (mg)	Salt Phase (mg)	Crucible-Charge Reaction Product (mg)
1	30	U	15199	15171	12	14
		Pu	299	270	21	17
5	50	U	13371	736[a]	24	18
		Pu	254	8[a]	21	21
6	30	U	12593[b]	12546	27	~8[c]
		Pu	204[b]	163	15	26

[a] Material in surface skin of ingot; metal removed by acid-etching technique.
[b] Skinned ingot from Experiment 5 used as charge material.
[c] Questionable value.

The distributions of uranium and plutonium in the charge and in various fractions after the melting operation are presented in Table I-1.

An apparent extraction of about 7 % of plutonium to the salt phase cannot be explained on the basis of reaction of $CaCl_2$ with plutonium since the calculated equilibrium constant for the reaction is extremely low (from 10^{-8} to 10^{-10} at 1200°C depending on the $\Delta F°$ data used for $CaCl_2$ and $PuCl_3$). To determine if this apparent extraction was related to insoluble impurities which had moved to the surface during liquation, the ingot produced in experiment 5 was skinned by acid etching and employed as charge metal in experiment 6. The similar fraction of plutonium in the salt phase in experiments 1 and 5, which utilized untreated alloy, and in experiment 6, in which previously liquated and skinned alloy was employed, suggests that the incorporation of plutonium in the salt phase was probably not caused by impurities in the charged alloy. On the other hand, the ratios of uranium to plutonium in the salt phases and in the crucible-charge reaction products were roughly similar. It is thought that the plutonium found in the salt phase might have been transferred as a part of the crucible-charge reaction product during the separation of the salt phase by acetic acid leaching.

The plutonium and uranium distribution data and conditions for ten experiments conducted with UCl_3 oxidant in the flux are shown in Table I-2. The transfer of plutonium to the reaction layer formed between the melt and the crucible varied widely (from 0.6 to 12.5 %) whereas the transfer of uranium, with one exception (experiment 11), showed much less variation. These large variations in plutonium transfer made it difficult to assess the amount of salt or metal contamination by the crucible reaction product during phase separation procedures. Therefore, in treatment of the experimental data it was assumed that the competing side reaction with the crucible did not disturb the equilibration of metal and salt phases and that $CaCl_2$ behaved as an inert diluent for the UCl_3 oxidant.

Good material balances were obtained during the experiments. As indicated in Table I-2, recoveries were >94 % for plutonium and >99.2 % for uranium. Comparison of the total weight of the crucible and charge prior to and after each experiment showed that the overall material recovery was >99.7 %.

A major variable in experiments 2, 3, and 4 was the time during which the phases were contacted at 1200°C. Mole ratios of UCl_3 to plutonium in the charge were similar (1.01 to 1.26). Calculated equilibrium constants from the resulting data, by a method described in a subsequent paragraph, showed that the 15-min experiment had an apparent equilibrium constant value which was at least 40 % lower than those calculated for the 30- and 90-min experiments. In additional experiments the salt and metal phases were contacted for a minimum time of 45 min.

A cylindrical furnace tube liner fabricated from tantalum was used in experiment 3 to collect material volatilized during the 30-min equilibration of charge materials at 1200°C. The loss of plutonium through vaporization was 1.1 % of that originally charged. Only 0.006 % of the calcium and 0.4 % of the uranium originally present in the salt phase were vaporized. The small amount of volatilization of these elements would have little effect on results obtained in the equilibrium experiments.

If the thermodynamic activity of reactants and products is assumed to be equal to solute concentration in the reaction:

$$UCl_3\ (CaCl_2) + Pu\ (U_{soln}) \rightleftarrows PuCl_3\ (CaCl_2) + U\ (U_{soln})$$

the equilibrium can be expressed in terms of moles, i.e.,

$$K_e = \frac{n_{PuCl_3} \cdot n_U}{n_{UCl_3} \cdot n_{Pu}}$$

where n_{PuCl_3} and n_{UCl_3} are moles of $PuCl_3$ and UCl_3 in the salt phase, and n_U and n_{Pu} are moles of uranium and plutonium in the metal phase.

In the calculation of equilibrium constants from the available analytical data, n_{PuCl_3} and n_{Pu} values were based on the fraction of plutonium in these phases determined by analysis. The n_U value was determined

TABLE I-2. Distribution of Plutonium and Uranium in Halide Slagging Experiments Conducted with Uranium Trichloride

Crucible: Slip-cast BeO
Melt Atmosphere: Helium

	Experiment No.									
	2	3	4	7	8	10	9	11	12	15
Charge Material										
Uranium (g)	13.931	2.644	13.756	13.569	13.365	13.777	12.902	13.178	13.445	13.762
Plutonium (g)	0.268	0.055	0.256	0.266	0.245	0.034	0.568	0.246	0.263	0.269
$CaCl_2$ (g)	2.198	0.356	2.199	1.999	2.000	2.004	1.997	1.999	2.010	2.012
UCl_3 (g)	0.461	0.080	0.465	1.371	0.862	0.860	0.861	0.571	1.009	0.874
Initial Mole Ratio UCl_3:Pu	1.19	1.01	1.26	3.58	2.44	17.89	1.05	1.61	2.66	2.26
Crucible-Metal Contact Area (cm^2)	4.39	1.41	4.00	3.97	4.06	4.40	3.88	3.87	3.91	4.04
Melt Temperature (°C)	1200	1200	1200	1200	1200	1200	1200	1150	1150	1150
Melt Time (min)	15	30	90	45	45	45	45	60	60	60
Plutonium Distribution (% of original in charge)										
Metal Phase	36.3	26.2	28.7	10.2	21.7	8.3	25.3	16.8	12.6	12.6
Salt Phase	49.0	59.0	59.5	88.9	69.0	87.4	68.0	80.1	85.7	77.4
Crucible-Charge Reaction Product[a]	11.4	12.5	5.8	0.6	9.2	4.8	3.8	1.1[c]	1.2	11.0
Volatilized[b]	—	1.1	—	—	—	—	—	—	—	—
Plutonium Recovery (%)	96.7	98.8	94.0	99.7	99.9	100.5	97.1	98.0	99.5	101.0
Uranium Distribution (% of original in charge)										
Metal Phase	98.4	98.7	98.2	94.9	96.2	94.8	97.4	97.3	95.2	95.3
Salt Phase	1.1	0.9	0.9	4.9	2.6	3.4	1.8	1.9	4.0	3.5
Crucible-Charge Reaction Product[a]	0.5	0.3	0.8	0.7	0.7	1.0	0.6	0.02[c]	0.6	0.7
Volatilized[b]	—	0.009	—	—	—	—	—	—	—	—
Uranium Recovery (%)	100.0	99.9	99.9	100.5	99.5	99.2	99.8	99.2	99.8	99.5

[a] Material adhering to inner surface of crucible after physical removal of ingot.
[b] Tantalum condenser employed to collect material volatilized during experiment 3; assembly not used in other experiments.
[c] Transfer of a portion of the crucible-charge reaction product to the salt phase and/or to the metal phase is suspected.

from the weight of the metal ingot produced corrected for its analyzed plutonium content, and the n_{UCl_3} value was obtained by difference between n_{UCl_3} initially present and n_{PuCl_3} formed in the salt phase. Standard free energies for the reaction were then calculated from the equilibrium constants using the equation

$$\Delta F^o = -RT \ln K_e$$

Values of K_e and ΔF^o are presented in Table I-3 for those experiments in which the salt and uranium were contacted for 30 min or more and contamination of metal and/or salt phases was not indicated during preparation of analytical samples. Average calculated values for the equilibrium constant, 187 at 1200°C and 203 at 1150°C, were in the direction that would be predicted from thermodynamic considerations. The calculated standard free energy changes were 15.1 kcal at 1150°C and 15.2 kcal at 1200°C. The latter value is in good agreement with an estimate of 15.3 kcal at 1200°C previously reported by McKenzie *et al.*[5]

Although the data in Table I-3 indicate appreciable uncertainty for the equilibrium constant at 1200°C, they do suggest that K_e does not grossly change as the mole ratios of UCl_3 to plutonium vary from about 1 to 17 and the concentration of plutonium in uranium varies from about 0.2 to 4.2%. The large variations in K_e are believed to be related mainly to problems associated with the separation of salt and metal phases from reaction products formed at the crucible-charge interface. The average experimental equilibrium constant of about 200 at temperatures of 1150 to 1200°C is believed to be sufficiently large to allow application of

TABLE I-3. THERMODYNAMIC VALUES FOR THE REACTION $UCl_3\,(CaCl_2) + Pu\,(U_{soln}) \rightleftarrows PuCl_3\,(CaCl_2) + U\,(U_{soln})$

Experiment No.	Mole Ratio, UCl_3:Pu	Per cent Plutonium in Alloy Charge	Temperature (°C)	K_e	$-\Delta F°$ (kcal)
3	1.01	2.04	1200	264	16.3
9	1.05	4.21	1200	168	15.0
4	1.26	1.83	1200	169	15.0
8	2.44	1.80	1200	100	13.5
7	3.58	1.92	1200	168	15.0
10	17.89	0.24	1200	254	16.2
				Av. 187	15.2
12	2.66	1.92	1150	194	14.9
15	2.26	1.91	1150	212	15.2
				Av. 203	15.1

halide slagging to processing of uranium breeder blanket material.

b. EVALUATION OF BERYLLIA CRUCIBLES FOR HALIDE SLAGGING (N. R. CHELLEW, J. T. FEENEY)

In the development of halide slagging processes for the extraction of plutonium and fission products from fast breeder reactor blanket material, the interaction of charges through reaction with container materials is important. Data offered in the previous section have shown that when uranium is melted under a $CaCl_2$ or UCl_3-$CaCl_2$ flux in a beryllia crucible, a reaction layer covering the area of the crucible in contact with the charge was formed. Although factors contributing to the corrosion reaction were not established, evidence of the degree of contamination of processed metal by beryllium was obtained from spectrographic analyses of the ingot material.

Table I-4 is a summary of the beryllium contamination in seven ingots resulting from the halide slagging operations. Contamination is expressed as micrograms of beryllium/cm² of metal area in contact with the crucible. The results for metal processed at 1200°C show a greater contamination of the metal as liquation times were increased; however, the data are insufficient to determine the manner in which the corrosion proceeds with time. Within the limits of the precision of the beryllium analysis (±10%), the corrosion behavior did not appear to be affected by the initial concentrations of plutonium in the charge (0.2 to 4.2 w/o). In a separate study[14] in which uranium was melted without flux for 120 min at 1200°C, an ingot contamination value of 13 μg Be/cm² of contact area was reported. A comparison of this value with those given in Table I-4 suggests that the presence of flux accelerates the reaction with the crucible by at least one order of magnitude.

TABLE I-4. CONTAMINATION OF URANIUM-PLUTONIUM ALLOY BY BERYLLIA CRUCIBLES USED IN HALIDE SLAGGING EXPERIMENTS

Crucible: Slip-cast BeO[a]
Conditions: Alloy (~14 g) melted under flux (~2.9 g) in helium atmosphere

Experiment No.	Charge Composition		Equilibrium Temp. (°C)	Time at Equilibrium Temp.[b] (min)	Crucible-Metal Contact Area (cm²)	Alloy Contamination[c] (μg Be/cm² of crucible contacted)	
	Alloy	Flux					
2	U-1.9 w/o Pu	$CaCl_2$-17 w/o UCl_3	1200	15	4.39	71	
7	U-1.9 w/o Pu	$CaCl_2$-41 w/o UCl_3	1200	45	3.97	146	147 (av.)
8	U-1.8 w/o Pu	$CaCl_2$-30 w/o UCl_3	1200	45	4.06	134	
9	U-4.2 w/o Pu	$CaCl_2$-30 w/o UCl_3	1200	45	3.88	149	
10	U-0.2 w/o Pu	$CaCl_2$-30 w/o UCl_3	1200	45	4.40	157	
4	U-1.8 w/o Pu	$CaCl_2$-17 w/o UCl_3	1200	90	4.00	186	
11	U-1.8 w/o Pu	$CaCl_2$-22 w/o UCl_3	1150	60	3.87	97	

[a] Product of National Beryllia Corp.; reported purity, 99+%; reported minimum density of body, 90% of theoretical.
[b] Does not include period (8 min) during which the charge was molten but at a lower temperature than the equilibrium temperature indicated.
[c] Accuracy of beryllium analyses, ±10% (relative).

The average beryllium pickup by charges melted for 45 min at 1200°C (experiments 7–10) was 44 ppm. Assuming that the beryllium contamination for similar melt time and temperature is proportional to the crucible area contacted, the beryllium pickup in a plant-scale blanket processing operation would likely be decreased to about 3 ppm for a 50-kg charge. This low concentra-

[14] Feder, H. M. et al, Interaction of Uranium and Its Alloys with Ceramic Oxides, ANL-5765, 1957, p. 18.

tion of beryllium should not have a deleterious effect on the fuel.

c. MATERIALS FOR CONTAINMENT OF MOLTEN URANIUM AND ITS ALLOYS (G. A. Bennett, W. Spicer)

Materials are being investigated for containing uranium and uranium alloys at temperatures from near their melting points to several hundred degrees above their melting points. The container materials being tested consist primarily of the borides, carbides, and nitrides of some of the 4th, 5th, and 6th metallic groups of the periodic table. The work of Brewer[15, 16] is being used as a guide in selecting materials for testing.

The experimental procedure consists in partially submerging 1-in. dia. by 1-in. long rods by means of a boron nitride holder into a bath of molten uranium for a given period of time. Materials are initially tested at 1165°C for 24 hr. Those materials which survive this test are then tested at 1365°C and then at increasingly higher temperatures until the approximate temperature limit of each material has been found.

At the conclusion of a run the test rod is examined visually for wetting and corrosion. After the rod is photographed, it is sectioned and photographs of the sections are then taken. To date, these photographs have been sufficient to evaluate the material being tested; however, other means of evaluation, such as the use of metallographs, autoradiographs, and electron probe analyses are available if they are needed. In addition, any changes in dimensions or weight of the sample material are carefully noted.

Up to the present time the following materials have been tested by the method described:

Nitrides: niobium, titanium, zirconium
Carbides: titanium, hafnium, niobium, tantalum
Borides: chromium, zirconium, titanium

The results, although preliminary and possibly subject to modification as the tests become more severe, lead to the following tentative conclusions concerning the stability of these materials in molten uranium:

(1) The nonmetallic component of the compound has a much greater effect than the metallic component.

(2) The stability of the compounds tested decreases in the following order: nitrides, borides, and carbides.

Thus, the three nitrides tested appear to possess greatest inertness to molten uranium. The borides, although wetted to a much greater extent than the nitrides, likewise show some promise. Further tests will be made on the most promising nitrides and borides already tested and on other similar materials.

d. PURIFICATION OF ARGON FROM NITROGEN WITH TITANIUM SPONGE (M. L. Kyle, J. Arntzen)

A method for removing nitrogen from argon by gettering the nitrogen on hot titanium sponge is being investigated. Although this method has general utility for purifying argon for such applications as glovebox atmospheres, the major incentive for its development is a possible future need to remove nitrogen from the atmosphere in the Argon Cell of the EBR-II Fuel Cycle Facility.

Two sets of experimental equipment were constructed for the nitrogen-removal study: (1) equipment for determining the kinetics of nitrogen removal from argon on hot titanium sponge and (2) a pilot plant for obtaining overall process performance data and information on component reliability. Studies were conducted with argon containing nitrogen concentrations between 100 and 50,000 ppm.

(1) Kinetics of Nitrogen Removal from Argon with Titanium Sponge

A gas-circulating loop was built for a study of the kinetics of nitridation of titanium sponge by argon-nitrogen mixtures. Operating principles of the loop were described in detail in ANL-6800, pp. 54–56. In this loop an argon-nitrogen mixture of carefully controlled composition is continuously circulated (by a diaphragm pump) through a series of eight small test beds each containing 0.7 to 2 g of titanium sponge. The circulation rate (100 to 800 liters/hr) is such that only a small fraction (ideally less than 5%) of the nitrogen reacts with the titanium sponge in a single pass through the series of beds. By this technique, all beds in the stack are exposed to approximately the same nitrogen concentration in the reacting gas and no correction is required for a decreasing nitrogen concentration as the gas moves from bed to bed. The extent of reaction of the titanium sponge metal is determined at time intervals by successively and permanently removing the topmost titanium bed and determining the amount of nitrogen reacted by a modified Kjeldahl analysis.

Data have now been obtained at nitrogen concen-

[15] Brewer, L., and Haraldsen, H., The Thermodynamic Stability of Refractory Borides, J. Electrochem. Soc. **102**, No. 7, 399 (July 1955).

[16] Brewer, L., Sawyer, D. L., Templeton, D. H., and Daufen, O. H., A Study of the Refractory Borides, J. Amer. Ceramic Soc. **34**, No. 6, 173 (June 1951).

TABLE 1-5. Surface Area Measurements of Titanium Sponge Sieve Fractions

Sieve Size	Surface Area[a] (cm^2/g)	% of Sponge
+¼ −½ in.	623	55.4
−¼ in. +8 mesh	1289	30.1
−8 +10 mesh	792	5.3
−10 +12 mesh	672	3.5
−12 mesh	746	5.7

[a] Average of two measurements.

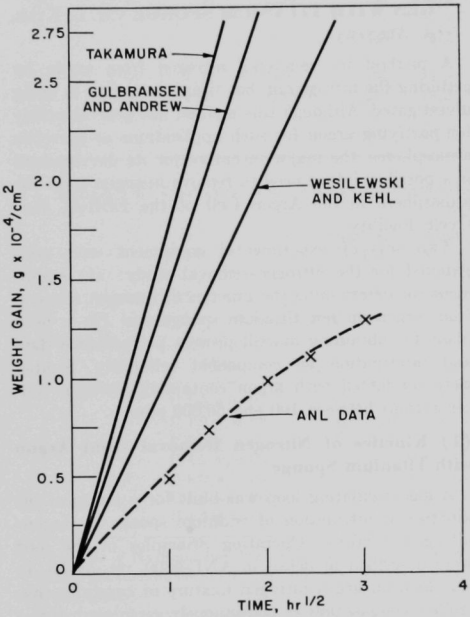

108-8885

Fig. I-2. Comparison of Rate of Nitridation of Titanium. Temperature: 900°C.

Takamura, A., Nitriding of Titanium, J. Japan Inst. Metals, **24**, 565 (1960).

Gulbransen, E. A., and Andrew, K. F., Kinetics of the Reaction of Titanium with O_2, N_2 and H_2, Trans. AIME, **185**, 741 (1949).

Wesilewski, R. J. and Kehl, G. L., Diffusion of Oxygen and Nitrogen in Titanium, J. Inst. Metals, **83**, 94 (1954–55).

trations of approximately 100, 300, 1000, 5000, and 50,000 ppm in argon. Preliminary reaction rate curves at a temperature of 900°C were presented in ANL-6925, p. 23. Experimental work on this project has been completed except for data which might be required to clarify experimental results already obtained. Chemical analyses on most runs have now been received and efforts to correlate the data are in progress. The results of these correlations will be presented in the next semiannual report.

Surface area measurements of sieve fractions of as-received titanium metal sponge have been made by krypton gas adsorption and are reported in Table I-5. Screen analyses of as-received titanium sponge are presented to indicate the relative quantity of material of each sieve fraction. Several analyses of this kind have been made. The percentages of material in the various sieve fractions did not vary by more than 20% from the values given in Table I-5.

The reason for the high value of the surface area for the −¼ in. +8 mesh fraction is not known. Visually this material appears similar to the other size fractions tested. No further attempts to determine if this difference is real or merely the result of a nonrepresentative sample will be made at this time, since this particular sieve fraction was not used in obtaining experimental data. However, since titanium sponge of a specific size fraction can be purchased at little additional cost, purchase of a fraction which has a larger surface area may be of great benefit in a full-scale facility.

A literature survey was made to obtain results of any previous investigations[17] of the titanium-nitrogen reaction. No reference was found pertaining to the nitridation of titanium sponge nor to titanium-nitrogen reactions employing a carrier gas. All references found dealt with titanium metal sheet in nitrogen or air atmospheres; a lower nitridation rate would be expected for the Argonne data, which were obtained with a nitrogen partial pressure about 5% of that used in the other experiments. This occurred, as is shown in Figure I-2. It is also probable that based on equal surface areas titanium sponge did not react as rapidly as sheet because of the geometries involved. Some areas of the sponge are probably less reactive because of the difficulty of transporting nitrogen to the reacting surface. However, on a volume or weight basis, there is a larger effective surface for sponge than for sheet material.

It is concluded that titanium sponge is more useful than sheet as a gettering material because the increased surface area more than offsets the somewhat less reactive surface.

(2) Pilot Plant for the Removal of Nitrogen in Argon

The pilot plant loop designed to obtain overall process performance data for the continuous removal

[17] Data from journal articles on the nitriding of titanium are plotted in Fig. I-2.

of nitrogen from argon has not been in operation since the failure of the system blower after approximately 1800 hr of loop operation.[18] It is felt that this loop performed its design function by adequately demonstrating the feasibility and economy of using titanium metal sponge for the removal of nitrogen impurity from large volumes of argon. The failure of the system blower was not caused by failure of the titanium gettering system but was a result of the blower's inability to circulate dry inert gas without introducing either air or lubricant into the circulating gas stream. Except for large, expensive diaphragm pumps, no commercial pump capable of circulating dry gas at several psi pressure drop is available for the 10 cfm range. Since the circulation of dry inert gas is a problem at this and many similar laboratories, it is planned to use the existing loop to test any alternate blowers which show promise for this application.

2. Processes Employing Liquid Metal Solvents

Several processes are being developed which employ liquid metals and salts as processing media. The skull reclamation process is under development for recovery of the fissionable material remaining in the crucible residue (skull) after a melt refining operation. Skull reclamation runs are now being conducted in a pilot plant which has a capacity of about one-third that proposed for the EBR-II plant equipment.

a. DEVELOPMENT OF THE SKULL RECLAMATION PROCESS (I. O. Winsch, T. F. Cannon, P. Mack, K. L. Nishio, K. R. Tobias, W. H. Spicer, L. Kirkel[19])

The skull reclamation process is an adjunct to the melt refining process in the EBR-II fuel cycle and has been developed to recover uranium from melt refining crucible[20] residues for return to the main fuel stream. These residues, also known as skulls, consist principally of unpoured metal, some oxidized uranium, and oxidized rare earth and alkaline earth fission products that are concentrated in the skull material during melt refining. The recovery process must effect a separation of uranium from the rare earth and alkaline earth metals and also from noble and refractory metal fission products (Zr, Mo, Ru, Pd, Nb, and Tc) that are not removed in melt refining. The removal of these elements in the skull reclamation process offsets their generation by fission of uranium in the reactor and serves to maintain their concentrations at nearly constant values in recycled fuel. Since the residual skull left in the melt refining crucible is expected to contain between 5 and 10% of the uranium charged to melt refining, a uranium recovery of 95% in the skull reclamation process should be adequate.

Operation of a pilot plant for study and demonstration of the skull reclamation process on an engineering scale was continued during the period of this semiannual report. During this time there has been a steady evolution of techniques and equipment. About 2 kg of skull oxide (containing about 75% uranium) is processed in each run. (In full-scale operations in the EBR-II Fuel Cycle Facility, 5.8 kg of skull oxide will be processed in each run.) Seven skull reclamation process demonstration runs were started during the past period (six were completed), making a total of 24 demonstration runs that have been completed to date in the pilot plant. The current series of runs is expected to demonstrate the reliability of the process and will terminate this phase of the development.

(1) Flowsheet

The skull reclamation process flowsheet presently in use has been described in detail in Fig. I-3 of ANL-6925, and is reproduced as Fig. I-3 of this report. This flowsheet incorporates two process modifications from the earlier flowsheet shown in Fig. 2 of ANL-6818. The first modification involves delaying the transfer of waste flux until after the uranium precipitation step, and the second substitutes a tungsten crucible for the beryllia crucible in the retorting step of the ANL-6818 flowsheet. Delaying the removal of the waste flux transfer allowed the transfer line (an inverted U-tube) to be kept in a fixed position throughout the process. In the latest runs this transfer has been made somewhat earlier, i.e., after the intermetallic compound precipitation step, to augment zirconium removal (see subsection (3) of this report section for details). The substitution of a tungsten crucible for the beryllia crucible is necessitated by the present inability of fabricators to supply a satisfactory full-scale beryllia crucible (see Section IA2c of this report). This change of the retorting crucible material prohibits melting of the recovered uranium in the retort after solvent evaporation because tungsten is slightly soluble in molten uranium (~1%). The use of a tungsten crucible at this point increases the likelihood that product ura-

[18] After one period of 100 hr of continuous operation, followed by a second period of 1000 hr of continuous operation, the loop was shut down because of the failure of two shaft seals (see ANL-6925, p. 23). The blower was repaired by replacing the seals that had failed and increasing the seal lubrication, but seal failure again occurred after an additional 150 hr of operation.

[19] CEN Machine Shop.

[20] Lime-stabilized zirconia crucibles.

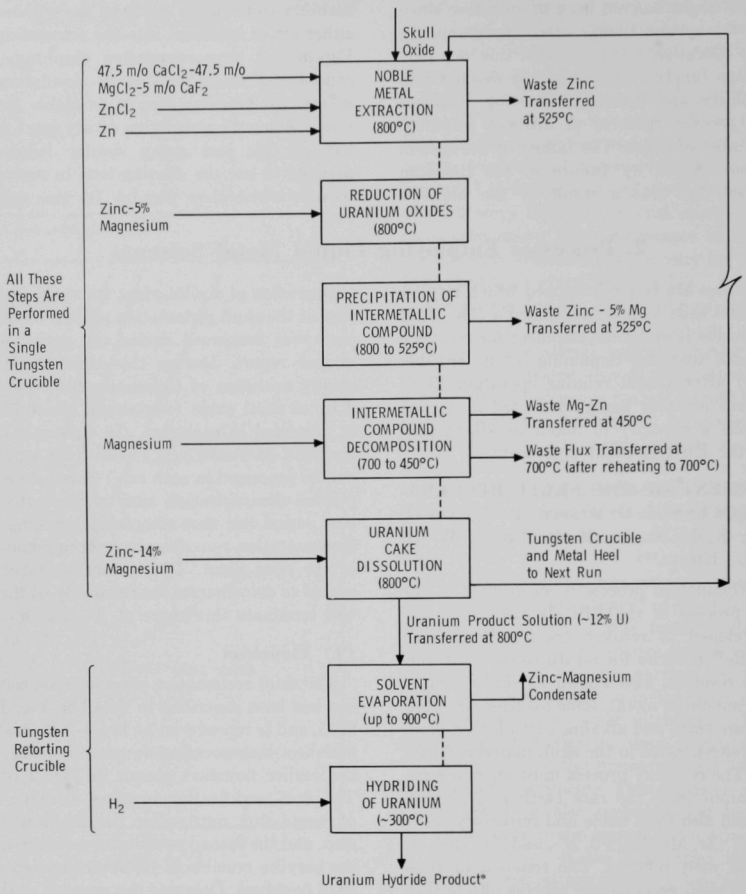

*The uranium hydride product may be decomposed and consolidated into a metal button in a beryllia crucible for return to melt refining, or it may be returned directly to melt refining.

108-8567

FIG. I-3. Flowsheet for Skull Reclamation Process.

nium will adhere to the crucible walls; however, adherence is decreased if the retorting temperature is kept low (~800°C). Should adherence of uranium become a problem, a hydriding step (currently under investigation) may be used to convert the uranium to a hydride powder.

(2) Equipment Performance

All process steps up to the retorting (solvent evaporation) step are performed in a 9½-in. ID tungsten crucible. The crucible is inductively heated in a bell jar furnace which is part of the pilot plant described in ANL-6687, p. 37. The bell jar allows performance of the process steps in an inert atmosphere and permits pressurization of the system for transfer of molten metals or salts through a transfer line to a container outside the bell jar.

During the last seven runs, the equipment has been operated in a closed glovebox containing a dry (about 150 ppm H_2O) nitrogen-argon atmosphere. This proce-

dure virtually eliminates the severe problem of moisture pickup which occurs when the furnace is open between runs, exposing to the atmosphere flux which has vaporized and condensed on surfaces of the equipment.

Phase Transfer. Waste and product streams are removed from the process crucible by pressure transfer through a single molybdenum-30 w/o tungsten transfer line. Changes in the method of fabrication, and the installation of external resistance heaters, have resulted in sufficient improvement that the operation of the line is now completely reliable (see ANL-6900, p. 59 and ANL-6925, p. 26).

Since the percentage of fission products removed is limited by the transfer efficiency of the waste phases, transfers of about 90% are desired. In the most recent runs the percent of total phase transfer uniformly exceeded 90% for the waste zinc transfer of the noble leach step and 95% for the final waste flux transfer. The efficiencies of the waste transfers after the intermetallic precipitation step and after the intermetallic decomposition step have had a wider range than desired (from about 80 to 93%, and from 79 to 90%, respectively). Transfer efficiencies ranging from 81 to 95% have been experienced with the uranium product solutions; these transfer efficiencies are limited as a result of the small total volume of product solution as compared to the large volumes of the waste flux and metal phases. That portion of a product solution which is not transferred is recycled through the next run.

In several of the process steps, a liquid metal phase is pressure-transferred from beneath a frozen flux. In order to provide a path through the flux for the pressurizing gas, the agitator is operated during the time the flux is freezing. A hexagonal agitator shaft has proved highly satisfactory for insuring an adequate opening through the frozen flux.

Flux Foaming. A flux foaming problem attributable to water of hydration in the flux has been solved by the magnesium pretreatment technique described in the preceding semiannual report (ANL-6925, p. 26). Flux foaming has not been observed in any of the last seven skull reclamation process demonstration runs.

Fuming. Some vaporization of flux and metal phases or "fuming" occurs in the skull reclamation process runs, and a light deposit of flux containing a small amount of metal is found on the inside of the bell jar wall at the conclusion of each run. The use of a perforated metal basket (ANL-6925, p. 26) containing calcium metal turnings to react with the vaporized flux appeared to be an effective means of trapping vaporized metal and flux. However, in the present equipment it has not been possible to use calcium because the region in which the trap is required is adjacent to the reduction furnace susceptor which reaches temperatures above the melting point of calcium (851°C). Consequently, carbon wool and Molecular Sieves have been used in the fume traps. Molecular Sieves have proved to be more effective than carbon wool in trapping the fumes.

Tungsten Crucible. As described in Section IA2c below, the welded tungsten crucible cracked after use in three process demonstration runs. A new pressed-and-sintered tungsten crucible, shown in Fig. I-4, has been put into service and used in all seven of the subsequent skull reclamation process runs.

Resampling of transferred supernatant waste solutions has been carried out in a repaired pressed-and-

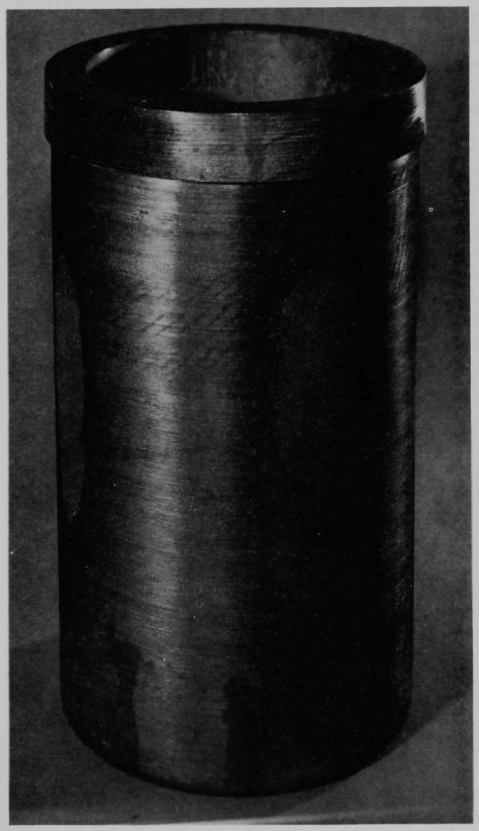

108-8121

Fig. I-4. Pressed-and-Sintered Tungsten Crucible. 12-in. OD by 20 in. high by 1-in. wall.

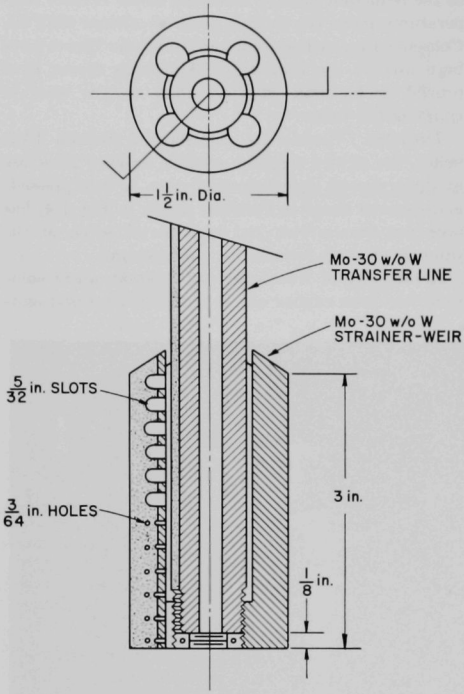

108-8897
FIG. I-5. Strainer-Weir Attached to End of Transfer Line.

sintered tungsten crucible (ANL-6925, p. 32) which was originally a manufacturer's reject. This crucible, which was also used in a number of earlier skull reclamation process demonstration runs, has performed well. It is concluded that pressed-and-sintered tungsten crucibles are satisfactory for use in the skull reclamation process, providing precautions are taken to prevent flux-metal freezing during the process. When a frozen flux-metal charge is remelted, the stresses on the crucible may be sufficiently high to cause crucible failure (see ANL-6900, pp. 60–61). (See Section IA2c of this report for further discussion of the procurement and testing of crucibles for the skull reclamation process.)

(3) Process Results

The behavior of uranium in the pilot plant runs through Run SKR-17 was previously discussed (ANL-6925, p. 29). The results for subsequent runs through SKR-26 are now available and are reported below.

Uranium Recovery. The uranium material balances for the last seven runs range from 94 to 111%. These fluctuations are reasonable in view of probable sampling and analytical deviations. In repetitive operations, adequate overall uranium recovery is achieved by processing the heel of the product solution of any particular run in the succeeding run. This was done in three repetitive runs. Zinc chloride was used successfully to oxidize the uranium and magnesium being recycled. Analyses of the reduction solution (Fig. I-3) have shown 100% of the uranium charged in skull oxide and product solution heel to be in the solution.

Uranium in Waste Streams. In the last series of runs emphasis was placed on the development of techniques, especially improvement of the techniques for transferring metal and salt solutions, which would minimize uranium losses in the waste streams. This involved continual changing of various operating parameters.

Specifically, in the skull reclamation process (Fig. I-3), four waste streams are transferred as follows: (1) waste zinc after the noble metal extraction step, (2) supernatant solution after the intermetallic precipitation step, (3) supernatant solution after the intermetallic compound decomposition step, and (4) waste flux.

Transfer of the waste zinc after noble metal extraction has given no problems. In all but one case, which is believed to be attributable to cross-contamination of the sample, the uranium losses were 0.5% or less. Losses in the most recent runs have been less than 0.1%.

Uranium losses in the supernatant from the intermetallic precipitation step have been a serious problem. At the transfer temperature of 525°C uranium losses due to solubility should run about 0.5%, but the losses have ranged from 1 to 27%. In the last five runs different techniques were tried in the intermetallic precipitation step in an attempt to reduce uranium entrainment. These techniques were aimed at producing a well-settled precipitate bed. In the intermetallic precipitation step, it is necessary to backflush with argon until the temperature is lowered to 650°C (to prevent crystallization of the intermetallic in the transfer line) and to agitate the metal-flux charge until the temperature is lowered to 540°C (to provide a route through the frozen flux for pressurizing gas). Periods of 15 to 30 min were allowed for settling of the uranium-zinc intermetallic crystals prior to the phase transfer. These techniques, plus the installation of strainer weirs (shown in Fig. I-5) which fit over the end of the transfer tubes, were successful, in one case, in reducing the uranium losses in this step to as little as 0.6% of the uranium charged; in several other cases these losses were ~1%. The strainer weirs were added to permit increased speed of transfer while

maintaining a minimum amount of uranium entrainment.

Uranium losses in the waste streams from the intermetallic decomposition step will be a minimum of about 0.8% based on the solubility of uranium in the 50 w/o Mg-Zn supernatant at 450°C. In almost no case has a uranium loss in excess of this value been experienced.

Uranium losses in the waste flux phase, as in previous runs, ranged from 0.5 to 1.2%. There appears to be no problem with this transfer.

During the development program, total uranium losses in the waste streams were reduced to 2.0 to 3.0% of the uranium charged. These losses are low in view of solubility and equilibrium losses of 2% inherent in the process and indicate that the process goal of 95% recovery of the uranium can be realized.[21]

Fission Product Removal. Cerium removals have been good, ranging between 87 and 95%. A recently developed method of cerium analysis has been used to analyze samples. Overall material balances of 96 and 95% were obtained in the two most recent runs.

In the latest runs, zirconium removals have been low, ranging from 49 to 78 percent. Zirconium removals of at least 85% are desired in this process. A method for possibly increasing the zirconium removal has been shown to be practical from an operating standpoint. Instead of transferring the waste flux at 700°C after the intermetallic decomposition step as indicated in the flowsheet of Fig. I-3, the waste flux transfer can be made at 600–625°C following the transfer of the 5 w/o Mg-Zn supernatant prior to the intermetallic compound decomposition step. This modification offers the possibility of removing unreduced ZrO_2 with the flux to improve zirconium removal from the process. Delaying the removal of the flux until after the intermetallic decomposition step (as shown in the flowsheet) had provided additional opportunity for further reduction of the zirconium in the flux phase and had resulted in coprecipitation of the zirconium with the uranium product. Early flux removal has been tried in one run; however, analytical results are not yet available.

The possibility of removing significant amounts of zirconium from melts in the reduction step, Fig. I-3, by contacting the solution with carbon to form zirconium carbide has been investigated. A block of porous CS type graphite was immersed in a Zn-4 w/o Mg-4 w/o U-0.14 w/o Zr-0.06 w/o Pu solution for a period of 2.5 hr at 800°C. The solution was agitated vigorously and sampled periodically. Analytical results from these samples show that no measurable amount of uranium or zirconium carbides was formed. The use of carbide slagging in this process does not appear promising.

At the phase transfer temperature of 525°C, ruthenium and molybdenum are insoluble in the zinc-noble metal extract which is the waste phase from the noble metal extraction step. An agitation rate of 400 rpm is used to keep the molybdenum and ruthenium in suspension in the zinc during the transfer. Ruthenium removals of 73 to 99% and molybdenum removals of 60 to 86%[22] have been experienced. Removal of approximately 60% of these elements is satisfactory for the process.

Status. The only aspect of the skull reclamation process still requiring demonstration is adequate zirconium removal. After the necessary operating techniques for accomplishing this have been established in the pilot plant unit, further development work will be carried out in the full-scale, prototype plant unit (see Section IB2 of this report).

b. DEVELOPMENT OF THE BLANKET PROCESS (I. O. Winsch, H. O. Smith[23])

The blanket process (see ANL-6605, p. 122) is being developed for the isolation of plutonium from EBR-II blanket material. Plutonium at an initial level of about 1 w/o is to be concentrated to a value of at least 40 w/o in uranium. Separation of plutonium from uranium is based on the high solubility of plutonium in magnesium-rich solutions and the contrasting low solubility of uranium in such solutions. The process involves dissolution of the blanket metal in a 12 w/o magnesium-zinc solution to a uranium concentration of about 14 w/o, addition of magnesium to about a 50 w/o concentration to precipitate most of the uranium away from the plutonium, separation of phases, and retorting the individual phases for recovery of plutonium and uranium. No experimental work has been done on the blanket process during this reporting period. However, preliminary designs have been prepared and evaluated for a tantalum-lined retorting unit.

c. PROCUREMENT AND TESTING OF CRUCIBLES FOR THE SKULL RECLAMATION PROCESS (M. L. Kyle, G. A. Bennett, W. Spicer)

Two pressed-and-sintered tungsten crucibles are presently being employed in the EBR-II skull rec-

[21] In addition to the 2 to 3% uranium loss occurring in the skull reclamation process, a loss of ~2% occurs during the skull oxidation step required to remove residual uranium from the melt refining crucible.

[22] In one run, molybdenum removal was 50%. This low removal has been traced to insufficient agitation.

[23] Central Shop Drafting Group assigned to Chemical Engineering Division.

lamation process. One crucible of relatively large size (15-in. ID by 30 in. high) is used for the bulk of the process steps, i.e., those steps between the oxidation of melt refining crucible skulls and the retorting of the uranium-magnesium-zinc solution to recover uranium metal product; the other crucible, of smaller size (7½-in. ID by 17 in. high), is used for the retorting step. Tungsten-lined crucibles are also under consideration for use in the bulk of the process steps, and beryllia or beryllia-lined crucibles are being considered for the retorting step.

(1) Tungsten Crucibles

Five fabrication procedures are currently being investigated for the production of tungsten crucibles: (1) pressing and sintering, (2) plasma spraying, (3) shear forming, (4) welding, and (5) vapor depositing.

Pressed and Sintered Crucibles. The pressed-and-sintered tungsten crucibles used to date have given good performance. Four small (4½-in. ID by 12 in. high) crucibles have been in service for about 3 yr for miscellaneous process operations and all are still in excellent condition. Twenty-five engineering-scale (1.5 kg of uranium charge) demonstration runs of the skull reclamation process have been performed in three larger crucibles (10-in. ID by 20 in. high by 1-in. wall).

One of the three larger crucibles failed after 10 runs by cracking under the expansion stresses imposed during remelting of a full metal and flux charge. Inspection of this crucible after rupture showed no evidence of corrosion. In subsequent runs, precautions have been taken to insure that no occasions arise that require freezing and remelting of metal charges.

The second large crucible, which was a manufacturer's reject because of high porosity of the walls and the presence of several cracks in the walls, was repaired by plasma spraying the outside of the crucible with tungsten. The tungsten coating sealed the cracks and eliminated seepage of molten metals through the walls. This crucible has now been used a total of 518 hr at elevated temperatures up to 800°C.

The third large crucible is still in satisfactory condition. A still larger pressed-and-sintered crucible (14-in. ID by 25¾ in. high by 0.75-in. wall) has been obtained and will be tested in process applications.

Thus, from a process standpoint, pressing and sintering is considered an entirely satisfactory procedure for the fabrication of skull reclamation process crucibles. However, because the method of fabrication results in crucibles with thick walls, the crucibles are heavy and unwieldy. Alternative methods of fabrication, which might overcome the disadvantages of pressed-and-sintered tungsten crucibles, are therefore being examined.

Tungsten Crucible Formed by Plasma-Spraying. Tungsten crucibles of nearly any size or shape can be produced by a plasma-spraying technique. In this procedure tungsten powder is sprayed on a suitable mandrel, the mandrel removed, and the tungsten shape fired in hydrogen to increase its density. It has been found that a sintering temperature of 2500°C maintained for 1 hr is required to increase the "green" density sufficiently (from about 75% to 87% of theoretical) to prevent salt leakage from the crucible. This technique was used in the repair of the manufacturer's reject crucible discussed in the previous section.

A small crucible (4-in. OD by 6 in. high by $^3/_{16}$-in. wall) fabricated by this technique has been obtained and tested under process conditions for a total exposure time of about 200 hr at temperatures around 800°C. No corrosion, salt leakage, or visual deterioration of the crucible has been seen. Attempts to obtain a larger crucible fabricated by this technique are in progress.

Shear Formed Tungsten Crucible. Shear forming offers the advantages of producing a light, strong, thin-walled crucible of nearly theoretical density. Such a crucible would be relatively easy to handle and, with a lower heat capacity than the heavier pressed-and-sintered crucibles, would permit faster heating and cooling cycles. At the present time, the size of the crucible which can be fabricated by this method is limited. However, because of the excellent performance of a small (4-in. OD by 6 in. high) shear-formed tungsten crucible (ANL-6900, p. 62), an order has been placed to secure a larger (10⅝-in. OD by 18⅝ in. high by 0.18-in. wall) engineering-scale crucible.

Heliarc Welded Tungsten Crucible. A welded tungsten crucible would have several advantages over a pressed-and-sintered tungsten crucible. Specifically, such a crucible would be relatively light in weight (~80 lb) as compared with a pressed and sintered crucible (~500 lb). It would also not be limited in size.

A welded tungsten crucible (10-in. OD by 21 in. high by 0.18-in. wall) fabricated by spinning and welding of tungsten sheet failed after exposure in three pilot plant skull reclamation runs (see ANL-6925, p. 33). Fig. I-6 shows the crack that developed around approximately one-third of the bottom circumferential weld (see Fig. I-5, ANL-6925, p. 32 for view of the complete crucible). Closer inspection revealed that the crucible had failed in the coarse grain area of the heat-affected zone of the weld. Several cracks were also

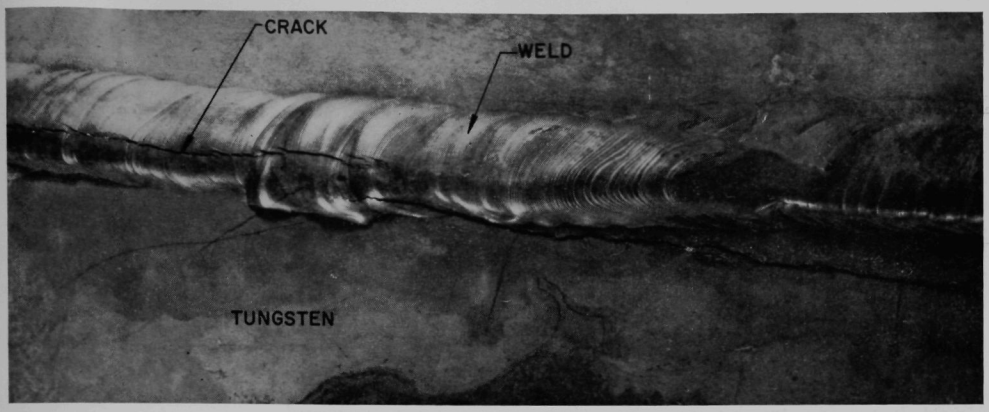

108-8118A

FIG. I-6. Weld Failure of Heliarc-Welded Tungsten Crucible.

evident in the spun crucible bottom. X-ray examination of the weld area disclosed poor penetration of the base metal by the weld. It is postulated that a combination of poor weld penetration, highly localized stresses, and too rapid heating of the crucible in the brittle temperature region (up to 400°C) induced failure by thermal shock.

Inherent problems are present in obtaining a sound weld on tungsten sheet. These problems arise from the high melting point of the metal and the difficulty of properly stress-relieving tungsten after the welding operation. Complete weld penetration of large welded crucibles is also difficult at the present state of the art, because of the limited availability of very high amperage welding machines. It is not planned to order additional welded crucibles until techniques for the welding of tungsten have been improved.

Vapor Deposited Tungsten Crucibles. The fabrication of tungsten crucibles by the deposition of tungsten vapor on a suitable base material would have the advantage of producing a light-weight crucible which would not be limited in size. The tungsten may be deposited on a base material that is removable (for example, by acid dissolution) and the resultant crucible densified by hydrogen sintering, or the tungsten vapor may be deposited on a permanent substrate material, such as a molybdenum crucible. Two fabricators believe the latter technique to be feasible. Both of these approaches are being investigated.

(2) Tungsten-Lined Crucibles

A silicon carbide crucible with a 0.03-in. thick coating of tungsten deposited by plasma spraying was tested for porosity. This crucible proved to be porous to both acetone and water at room temperature. The areas of porosity were widespread and not limited to any specific area. The major reason for the porosity of this crucible is the inability to sinter the crucible at a high temperature after the coating has been applied. The silicon carbide substrate would not withstand the 1350°C temperature required for adequate sintering of the tungsten coating. For this reason, the use of a silicon carbide substrate for a plasma-formed crucible is not considered feasible at this time.

Since the thermal coefficients of expansion of tungsten and the substrate material must match closely to insure adherence of the tungsten to the substrate during thermal cycling, the number of possible substrate materials is limited. An attempt is being made to obtain a suitable graphite substrate.

(3) Beryllia Crucibles

In a previous flowsheet, the retorting step in the skull reclamation process was to be performed in a beryllia crucible. In this step the product uranium was to be separated from the Mg-Zn solvent by heating the mixture to 1200°C and evaporating the solvent metals from the molten uranium. Beryllia crucibles have desirable characteristics for use in this step, since they do not react significantly with the solvent metals or with molten uranium. However, to date, fabricators have been unable to produce a structurally sound plant-size crucible (see ANL-6925, p. 32). Consequently, attention has been turned to the investigation of tungsten crucibles (see preceding sections of this

report) for use in this step of the skull reclamation process.

(4) Beryllia-lined Crucibles

Previous tests (ANL-6725, p. 75) have shown that beryllia, deposited by flame-spraying, appears to adhere well to silicon carbide and to alundum. Either of these would be a suitable substrate material for beryllia-lined crucibles since they are inexpensive and easily fabricated.

The concept of a beryllia-lined crucible was explored in a run (halide slagging) in which a uranium-plutonium-fissium alloy (420 g) was melted together with a 75 m/o $BaCl_2$-25 m/o $CaCl_2$ flux (120 g) in a beryllia-coated alundum crucible (4¼-in. OD by 4¼ in. high) and held at 1150°C for 1 hr. At the conclusion of the run, the crucible contents were poured into a mold. It was apparent that the molten salt had soaked into the crucible walls. A similar run in which salt alone was charged to a beryllia-coated silicon carbide crucible likewise resulted in penetration of the salt into the crucible walls.

Since flame spraying does not produce the dense lining that would be required to contain salt, no further work is planned on the containment of fluxes in beryllia-lined crucibles. However, beryllia-lined crucibles may still be satisfactory for the containment of metal solutions.

d. PROCESSES FOR FAST BREEDER REACTOR FUELS (L. Burris, R. K. Steunenberg)

Compact pyrochemical processes which employ liquid metal and molten salt solvents are being developed for the recovery of plutonium and uranium from future EBR-II fuels and from fast breeder reactor fuels in general. Although the development effort has been oriented primarily toward metallic fuels, the processes currently under investigation are also adaptable to ceramic fuels such as carbides, oxides, and possibly nitrides, sulfides, and phosphides. Metallic core fuels are expected to consist primarily of uranium alloyed with about 10 to 20 w/o plutonium, and stabilizing additives such as fissium, titanium, or zirconium. Blanket elements will probably consist of unalloyed natural or depleted uranium. At the present time, refractory metal alloys, e.g., an alloy of titanium and vanadium, are receiving serious consideration as cladding materials for both core and blanket elements. Because the development of high-performance fuels for fast breeder reactors is still in an early stage, the emphasis in fuel reprocessing studies has been placed on basic separations that can be used in a variety of process flowsheets.

The objectives of pyrochemical processing are to remove the bulk of the fission products, to extract bred plutonium from the blanket, to re-enrich the core with plutonium, and to repair irradiation damage. To achieve these objectives, separations of cladding material, uranium, plutonium and fission products from one another are required. Remote operation of all steps will probably be a necessity because even if complete fission product removal were achieved, the concentrations of radioactive isotopes of uranium and plutonium would increase during long irradiations.

(1) Chemical Decladding (D. A. Wenz)

A vanadium-20 w/o titanium alloy is being considered as a cladding material for future fast breeder reactor fuels. Since mechanical methods for the removal of cladding from high-burnup fuels may prove to be unsatisfactory, chemical decladding techniques are being investigated.

It was reported previously (ANL-6925, p. 34) that uranium-fissium alloy enclosed in V-Ti tubing with the ends crimped shut can be hydrided directly with simultaneous disintegration of the V-Ti alloy. A subsequent experiment was performed in which a U-20 w/o Pu-10 w/o fissium rod (0.14-in. dia.) was placed inside V-20 w/o Ti tubing having an ID of 0.17 in. after which the ends of the tubing were crimped. This specimen was then exposed to 2 atm hydrogen pressure at a temperature of 250 to 300°C for about 6 hr. The resulting mixture was held overnight under the hydrogen atmosphere at room temperature, dehydrided under vacuum by raising the temperature to about 400°C, and finally contacted with liquid Cd-15 a/o Zn-15 a/o Mg alloy at 600°C. Analysis of a sample of the liquid metal showed 96% of the plutonium and 55% of the uranium to be in solution. The solubility of vanadium and titanium from the cladding alloy in the liquid metal was less than 0.01 w/o.

The possibility of separating the fragments of cladding material from uranium and plutonium through differences in their densities was investigated briefly.

The V-Ti alloy floats on molten cadmium, while uranium and plutonium in excess of their solubilities settle to the bottom. At 400°C, a ratio of about 20 g of cadmium to 1 g of uranium and 0.2 g of the cladding alloy was required to effect a separation. Under these conditions, the uranium is precipitated as the intermetallic compound, UCd_{11}. A much smaller amount of cadmium would probably be required at 475 to 500°C, since the uranium is precipitated as the element at temperatures above 472°C.

For the separation of oxide and carbide fuels from metallic cladding materials, alternate oxidation and reduction to convert the fuel to a free-flowing powder appears to be an attractive procedure. It is possible

that this technique could also be applied to metallic fuels.

(2) Distribution of Elements between Liquid Metals and Molten Salts

In the pyrochemical processes currently under study, the basic separations of uranium, plutonium and fission products are effected by differences in the distribution behavior of these elements between liquid metals and molten salts. Pertinent distribution coefficient measurements are therefore essential to the process development effort.

Distribution of Uranium, Plutonium, and Praseodymium Between 50 m/o $MgCl_2$-30 m/o NaCl-20 m/o KCl and Cu-Mg Alloy (J. B. Knighton, J. W. Walsh)

Individual distribution coefficient determinations for plutonium and praseodymium between 50 m/o $MgCl_2$-30 m/o NaCl-20 m/o KCl and Cu-Mg alloys had indicated plutonium-praseodymium separation factors nearly an order of magnitude greater than those obtained when Mg-Zn or Cd-Mg-Zn alloys were used as the metal phase (ANL-6925, p. 37). This result prompted a subsequent experiment to determine simultaneously the distribution coefficients of uranium, plutonium and praseodymium between 50 m/o $MgCl_2$-30 m/o NaCl-20 m/o KCl and Cu-Mg alloy. The resulting data are presented in Fig. I-7. These data show praseodymium distributing strongly to the salt phrase at low magnesium concentrations in the Cu-Mg alloy. Plutonium favors the metal phase, with distribution coefficients ranging from 0.680 to 0.275 at a temperature of 800°C and at magnesium concentrations from 9.0 to 70.9 w/o. Uranium favors the metal phase more strongly than does the plutonium, with a minimum distribution coefficient of 0.015 at about 17 w/o magnesium.

Fig. I-8 shows the effect of temperature on the distribution coefficients with a magnesium concentration of 40 w/o in the Cu-Mg alloy. Decreasing the temperature from 800°C to 600°C causes the distribution coefficient of praseodymium to increase by a factor of two, while that for uranium is decreased by nearly a factor of two. The plutonium distribution coefficient, however, shows no significant temperature dependence. The plutonium and praseodymium codistribution results obtained in this experiment for a temperature of 600°C and a magnesium concentration of 40 w/o in the Cu-Mg alloy are in excellent agreement with the data obtained earlier for the individual elements (ANL-6925, p. 37).

In this experiment sufficient uranium was present so that the Cu-Mg alloy was saturated with uranium

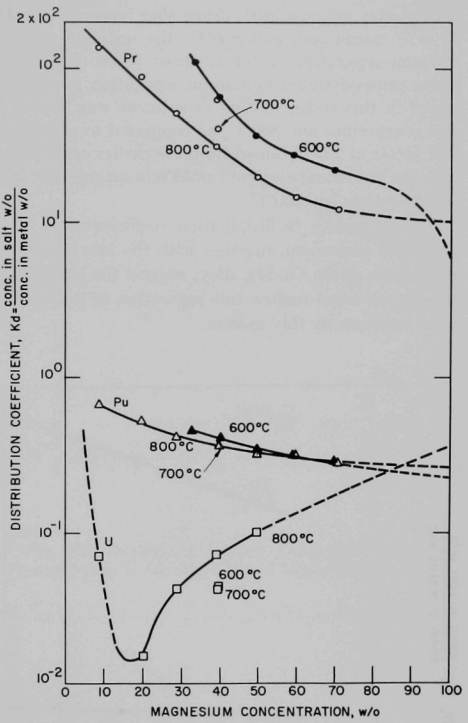

108-8887

Fig. I-7. Distribution of Praseodymium, Plutonium, and Uranium between 30 m/o NaCl-20 m/o KCl-50 m/o $MgCl_2$ and Copper-Magnesium Alloy.

at all magnesium concentrations. Thus the uranium content of the liquid metal samples should represent the solubility of uranium in Cu-Mg alloy. These data are shown in Fig. I-9. The solubility curve extrapolates nicely to the solubility of uranium in magnesium at 800°C obtained by Chiotti and Shoemaker.[24] Plutonium and praseodymium remained in solution in the Cu-Mg alloy and did not coprecipitate with the uranium as the magnesium concentration in the Cu-Mg alloy was increased.

Separation factors calculated from these data and from the earlier results of experiments with the individual elements at 600°C are shown in Fig. I-10. A decided maximum in each of the three separation factors appears to occur at magnesium concentrations of 10 to 20 w/o in the Cu-Mg alloy. The separation

[24] Chiotti, P. and Shoemaker, H. E., Ind. Eng. Chem. **50**, 137–140 (1958).

factors also increase with decreasing temperature. At 20 w/o magnesium and 800°C, the uranium-praseodymium separation factor is about 5,600. The maximum praseodymium-plutonium separation factor obtained in this codistribution experiment was 205 at 9 w/o magnesium and 800°C, as compared to a separation factor of 239 obtained from the earlier experiment with the individual elements at 33 w/o magnesium and a temperature of 600°C.

The differences in distribution coefficients for uranium and plutonium, together with the low solubility of uranium in the Cu-Mg alloy, suggest the possibility of a liquid metal-molten salt separation of plutonium from uranium in this system.

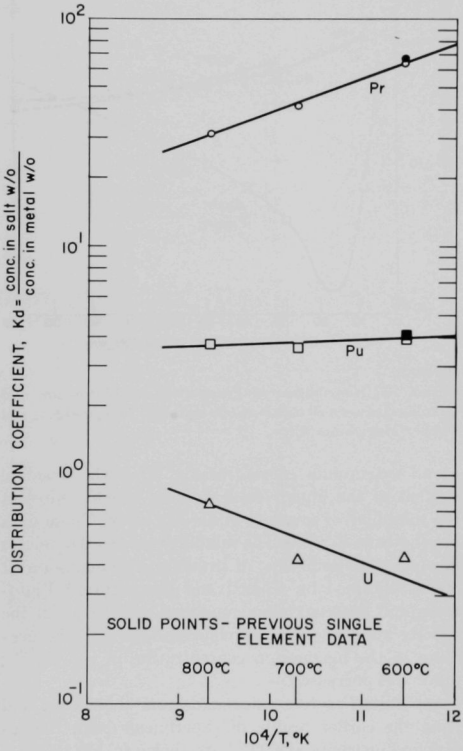

108-8881

FIG. I-8. Effect of Temperature on Praseodymium, Plutonium, and Uranium Distribution between 30 m/o NaCl-20 m/o KCl-50 m/o $MgCl_2$ Salt and Copper-40 w/o Magnesium Alloy.

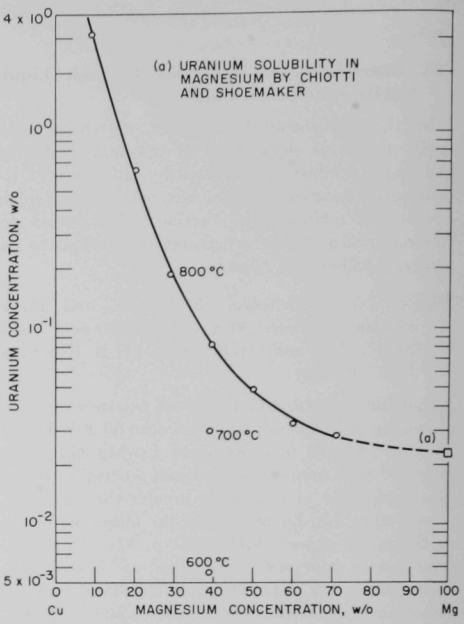

108-8892

FIG. I-9. Solubility of Uranium in Copper-Magnesium Alloy.

Distribution of Rare Earth Elements Between 50 m/o $MgCl_2$-30 m/o NaCl-20 m/o KCl and Al-Mg Alloys (J. B. KNIGHTON, R. A. MANCINI[25])

The extraction of rare earth fission product elements from molten chlorides by liquid Al-Mg alloy is being investigated as a salt purification technique that would permit recycle of the process salt and consolidation of the rare earths in a metallic ingot. This procedure would minimize or eliminate a salt waste stream from the rare earth-plutonium separation in a liquid metal-molten salt process. Previously reported survey experiments (ANL-6925, p. 36) showed the Al-Mg alloy system to be the most effective liquid metal medium studied thus far for the purification of this salt.

Additional experiments have been performed to determine the distribution coefficients of yttrium, lanthanum, cerium, and praseodymium between 50 m/o $MgCl_2$-30 m/o NaCl-20 m/o KCl and Al-Mg alloys and their solubilities in these alloys. Nominal magnesium concentrations of 13, 20 and 30 w/o in the Al-Mg alloy were selected, and the temperature was varied from 550°C to 900°C. The solubilities of

[25] Co-op Student, University of Detroit.

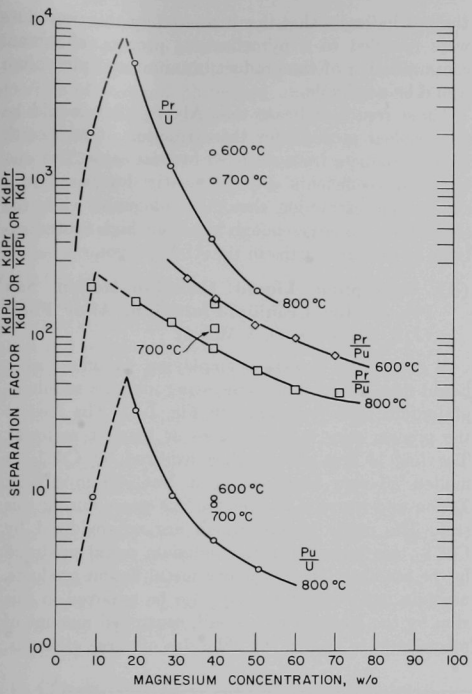

108-8888

FIG. I-10. Separation Factors for Praseodymium, Plutonium, and Uranium Distributing between 30 m/o NaCl-20 m/o KCl-50 m/o $MgCl_2$ Salt and Copper-Magnesium Alloy.

yttrium, lanthanum, cerium, and praseodymium in Al-20 w/o Mg alloy and their distribution coefficients between 50 m/o $MgCl_2$-30 m/o NaCl-20 m/o KCl and Al-20 w/o Mg alloy are presented in Figures I-11 and I-12, respectively. In the experiments with the Al-20 w/o Mg alloy, the temperature was varied from 550°C to 800°C.

Each of the elements investigated showed retrograde solubility at temperatures above about 700°C. The maximum solubility values fell in the range of about 7 to 10 w/o. Increasing magnesium concentration in the Al-Mg alloy between about 11 and 35 w/o magnesium resulted in a decrease in solubilities of the rare earth elements (Figure I-13).

The distribution coefficient measurements show that praseodymium distributes more strongly to the metal phase than yttrium, lanthanum, and cerium. This behavior was expected from earlier experiments in which $MgCl_2$ was used as the salt phase and Zn-Mg alloys as the metal phase (ANL-6569, p. 40). The data also show, as expected, that the distribution coefficients decrease as the temperature is lowered.

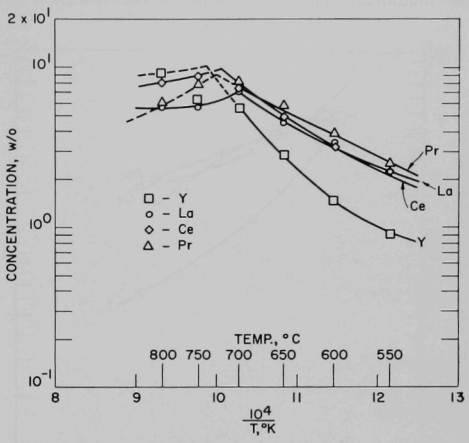

108-8878

FIG. I-11. Solubility of Yttrium, Lanthanum, Cerium, and Praseodymium in Aluminum-20 w/o Magnesium Alloy.

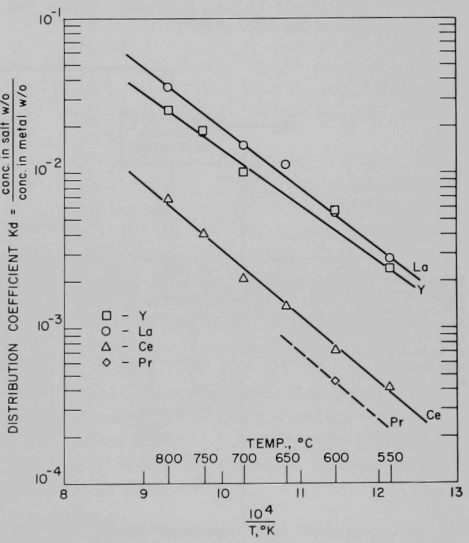

108-8890

FIG. I-12. Distribution of Yttrium, Lanthanum, Cerium, and Praseodymium between 30 m/o NaCl-20 m/o KCl-50 m/o $MgCl_2$ Salt and Aluminum-20 w/o Magnesium Alloy.

Analysis of the molten salt samples showed a very low aluminum concentration, 2.8×10^{-3} w/o, and a corresponding distribution coefficient of 3.4×10^{-5} for aluminum. This low aluminum concentration in the salt indicates that if salt treated by this procedure were recycled to a pyrochemical process, aluminum contamination of the product uranium and plutonium would be negligible.

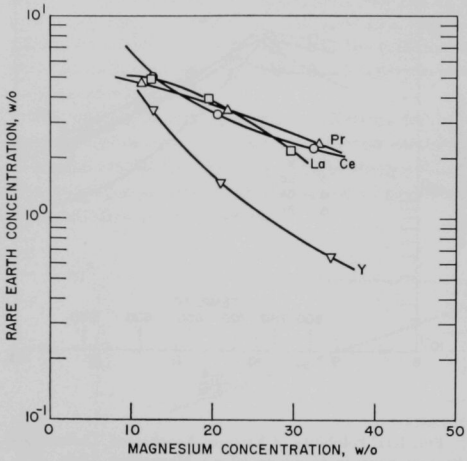

108-8883

FIG. I-13. Solubility of Yttrium, Lanthanum, Cerium, and Praseodymium in Al-Mg Alloy at 600°C.

These results indicate that Al-Mg alloy would be an excellent medium for the extraction of rare earth fission products from recycled process salts. The distribution coefficients are sufficiently low so that a single-stage extraction should be adequate, while the solubilities are large enough to permit high concentrations of the rare earths in the Al-Mg ingot.

(3) Conceptual Liquid Cadmium-Molten Salt Process for Uranium-Plutonium Alloy Fuels

(J. B. KNIGHTON, D. A. WENZ)

A conceptual flowsheet employing cadmium as a liquid metal solvent for processing metallic uranium-plutonium fuels is outlined in Fig. I-14. The feed to the process may be either core or blanket material. The fuel is first declad, then oxidized by $CdCl_2$ in molten 50 m/o $MgCl_2$-30 m/o NaCl-20 m/o KCl. Xenon and krypton are released as gases during this step. The noble metals, which are not oxidized by $CdCl_2$, are collected in the cadmium metal produced in the reaction. The refractory metal fission products, niobium and zirconium, may also be removed in this step by the addition of a small, controlled amount of magnesium to reduce the chlorides of these elements.

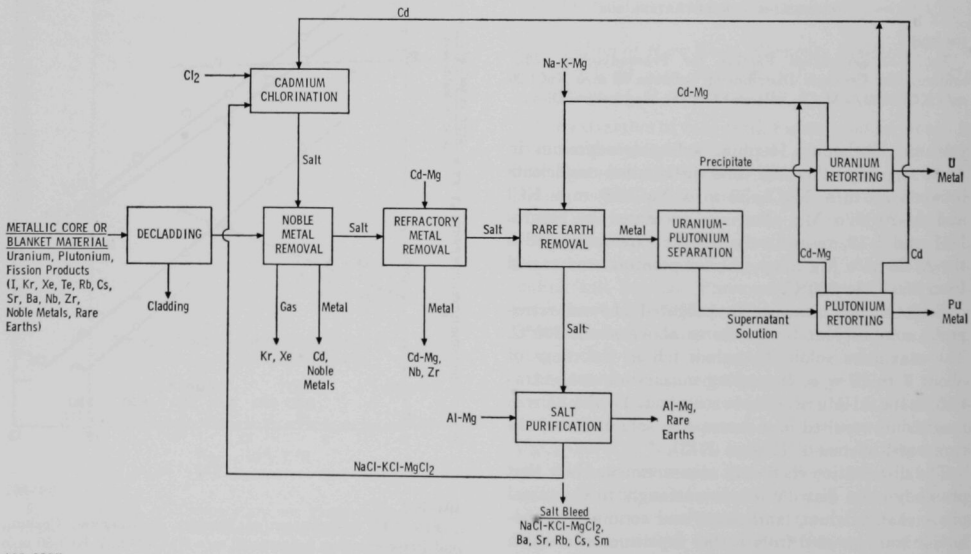

108-8895

FIG. I-14. Conceptual Liquid Cadmium-Molten Salt Process for Uranium-Plutonium Alloy Fuels.

(This operation is shown as a separate step in Fig. I-14 for the purpose of clarity.)

The $MgCl_2$-NaCl-KCl salt containing dissolved chlorides of uranium, plutonium, and the more electropositive fission products is then contacted with a Cd-Mg alloy containing sodium and potassium in the proper proportions so that after reduction of uranium and plutonium chlorides the salt has the proportions of $MgCl_2$, NaCl, and KCl required for rare earth removal. The metallic uranium and plutonium produced by the reduction are collected in the Cd-Mg phase, while the rare earths and other fission products remain in the salt. Multistage contacting is required for an adequate separation of the fission products from uranium and plutonium. Prior to recycle the salt is purified by contacting it with Al-Mg alloy to remove the rare earth fission products (see preceding section).

Uranium is precipitated as the metal from the liquid metal solution obtained in the uranium-plutonium reduction step, and the plutonium remains in solution. Metallic uranium and plutonium products are recovered separately by retorting the precipitated uranium phase and the supernatant solution to remove cadmium and magnesium. Part of the cadmium is recycled and chlorinated to regenerate $CdCl_2$ for the noble metal removal step. Experimental work demonstrating the feasibility of each separation has been completed.

(4) Chlorination of Cadmium in the Presence of Molten Salt (D. A. Wenz)

In the conceptual process shown in Fig. I-14, a portion of the cadmium from the retorting steps is recycled to a chlorination step in which $CdCl_2$ is regenerated for use as an oxidant. This procedure provides a convenient method for regenerating $CdCl_2$ and avoids disposal of large amounts of cadmium. To test this procedure, several experiments were performed, using a small-scale quartz apparatus in which cadmium was chlorinated in the presence of 50 m/o $MgCl_2$-30 m/o NaCl-20 m/o KCl. The cadmium and the salt were placed on a sintered quartz disk in a tube, melted, and sparged with chlorine at atmospheric pressure at a temperature of about 500°C. The chlorine gas entered the apparatus through a side arm below the sintered disk.

The results are listed in Table I-6. In all three experiments, chlorination of the cadmium was complete in less than 1 hr. The first two experiments proceeded smoothly with no unusual occurrences. In the third experiment, however, there were flashes of light from bubbles in the reacting materials, followed by a temperature excursion of about 150°C that caused the whole mixture to glow. Particularly in the last experiment, the salt was dark red to orange while cadmium metal was present but became colorless when all of the cadmium had been converted to $CdCl_2$. This color is attributed to the subchloride, Cd_2Cl_2.

TABLE I-6. Chlorination of Cadmium in Contact with the Ternary Salt, 50 m/o $MgCl_2$-30 m/o NaCl-20 m/o KCl

Chlorination with 100% Cl_2 at atmospheric pressure. Reaction time, less than one hour

Experiment	Starting Materials	Temp (°C)	Approx. Composition of Final Mixture	Appr. m.p. (°C)
1	15 g ternary salt 9.2 g Cd	450–500	30 m/o $CdCl_2$ 70 m/o ternary salt	450
2	10.5 g ternary salt 12 g Cd	500	45 m/o $CdCl_2$ 55 m/o ternary salt	475
3	7 g ternary salt 14 g Cd	500[a]	60 m/o $CdCl_2$ 40 m/o ternary salt	500

[a] A temperature excursion of about 150°C occurred during the reaction (see text).

In general, the reaction appears to proceed satisfactorily provided the reaction rate is kept within the heat removal capability of the system. By using a sufficiently large ratio of salt to cadmium initially, and by controlling the chlorine addition rate or diluting the chlorine with inert gas, satisfactory control of the reaction rate should be possible. The approximate melting points of the final salt mixtures, shown in Table I-6, indicate that any of them would be suitable for process use.

The salt solutions from Experiments 2 and 3 were used to oxidize metallic uranium so as to determine the approximate melting points of the resulting UCl_3-$MgCl_2$-NaCl-KCl mixtures, and thereby establish the UCl_3 concentrations which would be practical for process use. The oxidation procedure consisted of contacting the salts, which contained about 45 m/o and 60 m/o $CdCl_2$, respectively, with uranium rod at 600°C for about 3 or 4 hr. The resulting salt mixtures contained 43 m/o UCl_3 and 2.5 m/o $CdCl_2$ (m.p., ~625°C), and 33 m/o UCl_3 and 4 m/o $CdCl_2$ (m.p., 500–525°C). Since the proposed operating temperature for the process is 600°C, it appears that a UCl_3 concentration up to 30 or 35 m/o in the $MgCl_2$-NaCl-KCl salt would be acceptable.

(5) Stability of Uranium and Plutonium in 50 w/o Zn-50 w/o Mg Solution Toward Type 405 Stainless Steel (J. B. Knighton, J. D. Schilb)

In processes employing liquid metal solvents, it is necessary to determine whether the solutes, as well

as the solvents, undergo reactions with the container materials. An experiment was performed to determine the stability of a 50 w/o Mg-50 w/o Zn solution of uranium and plutonium contained in a type 405 stainless steel crucible for a period of 100 hr at 730°C. The purpose of the experiment was to provide information essential to the choice of material for equipment to be used in the retorting step of the present EBR-II blanket process (see Section IA2b).

Samples of the solution were taken at zero time and at 100 hr and analyzed to obtain evidence of any reactions between uranium or plutonium and the stainless steel constituents. Although 1 w/o uranium was added to the alloy initially in this experiment, the uranium concentration did not approach the solubility limit of 0.36 w/o at any time. The uranium concentration in the solution decreased with each successive sample, reaching a final value of 3×10^{-3} w/o at 100 hr. Although the plutonium concentration in samples taken at the beginning of the experiment was somewhat below the theoretical value of 0.991 w/o, the 100-hr sample showed the theoretical plutonium content.

These data indicate that uranium interacts with the container. Since nearly all of the uranium is present as a precipitated solid in this step of the EBR-II blanket process, this reaction appears to be of little consequence, provided the container attack is not excessive. Although the initially low plutonium concentrations are as yet unexplained, the 100-hr results indicate that type 405 stainless steel is a satisfactory material from the standpoint of plutonium solution stability.

(6) Conceptual Liquid Metal-Molten Salt Process for Oxide, Carbide, and Metal Fuels (J. B. Knighton)

In the development of compact pyrochemical processes for core and blanket fuel from fast breeder reactors, emphasis has been placed on process concepts that would be applicable to oxides and carbides, as well as metal fuels. A conceptual flowsheet for a process capable of handling oxide, carbide, and metallic core and blanket materials is presented in Fig. I-15.

The core or blanket elements are chopped, and the fuel is separated from the cladding by cyclic oxidation with air or oxygen and reduction with hydrogen. This procedure results in a free-flowing, finely divided mixture of U_3O_8, PuO_2, and fission product oxides that can be separated mechanically from the cladding material. Liquid Cu-Mg alloy (see Section IA2d) in the presence of a suitable molten salt (e.g., $MgCl_2$-CaF_2-$CaCl_2$-NaCl) is used to reduce the uranium and plutonium oxides, and the metal and salt phases are then separated. Oxides of the fission products in Groups I, II, and III of the Periodic Table are not reduced, and are therefore removed in the waste salt. The noble metal and refractory metal oxides are reduced, and these fission products appear with the uranium and plutonium in the Cu-Mg alloy.

The plutonium is then separated from the uranium and the remaining fission products by selective extraction from the Cu-Mg alloy through a $MgCl_2$-NaCl-KCl salt phase and into a Zn-Mg alloy, which is subsequently retorted for plutonium recovery. The uranium can then be extracted from the Cu-Mg alloy (which retains the fission products) through the salt and into a second Zn-Mg alloy of high magnesium content. This alloy is then retorted for uranium recovery. Both the plutonium extraction and the uranium extraction are performed with the two liquid metal alloys in mutual contact with the molten salt.

The metallic uranium and plutonium products are recombined in the desired proportions by melting. For the preparation of an oxide fuel, the metallic alloy would be oxidized by a procedure similar to the skull oxidation step of the EBR-II skull reclamation process, then reduced with hydrogen to form a UO_2-PuO_2 mixture. Several possible procedures for preparing a UC-PuC mixture are as follows: by carbothermic reduction of UO_2-PuO_2, by arc-melting the U-Pu alloy with carbon, or by hydriding and converting the hydrides to carbides by treatment with a hydrogen-propane mixture in a fluid bed (see Section IE1 of this report).

e. DEVELOPMENT OF ENGINEERING EQUIPMENT AND PROCEDURES (L. Burris, R. D. Pierce)

Large fast reactors will require high-capacity fuel processing plants capable of recovering plutonium as well as uranium. Investigations are being directed toward equipment and procedures for continuous pyrochemical processes that are capable of high processing rates and that can recover both plutonium and uranium.

Continuous processes generally require less space and less direct manipulation than batch processes. These advantages may be especially important in shielded facilities where space is expensive and any handling of the equipment must be done remotely. Because the advanced flowsheets are not clearly defined at this time, the objective of the engineering program is to develop equipment which is generally applicable to pyrochemical processes. The initial objective is the demonstration of countercurrent, liquid-liquid extraction between a liquid cadmium-base

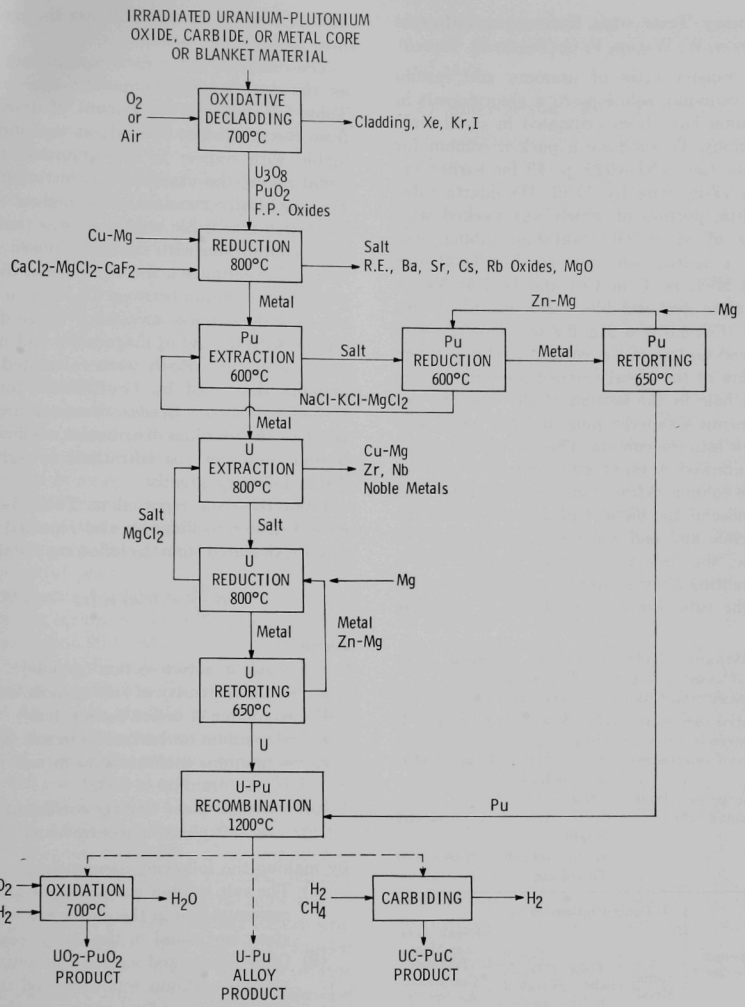

108-8694T

FIG. I-15. Conceptual Liquid Metal-Molten Salt Process for Oxide, Carbide, and Metallic Core and Blanket Materials.

metal and a liquid chloride salt. This unit operation is proposed in many advanced core processes to separate plutonium and uranium from rare earths and to extract rare earths from a liquid salt into a liquid metal solution for long-term storage.

Before the demonstration extraction unit is built, several support studies are being made. These include estimation of the mass transfer rates of actinides and rare earths between a liquid metal and a liquid salt; an investigation of components (such as valves, flow meters, liquid level detectors) for high-temperature service; and an investigation of the corrosion resistance of promising materials of construction toward the process solutions.

(1) Preliminary Tests with Extraction Columns

(T. Johnson, W. Walsh, F. G. Teats, K. Tobias)

The mass transfer rates of uranium and cerium from various cadmium solutions to a chloride salt in a packed column have been estimated in small-scale transient columns. To simulate a packed column for the latest tests (see ANL-6925, p. 45 for earlier experiments), a 17-in. long by ⅞-in. ID quartz tube, the middle 6-in. portion of which was packed with ¼-in. lengths of ¼-in. OD tantalum tubing, was charged with a molten salt (50 m/o $MgCl_2$-30 m/o NaCl-20 m/o KCl; no U or Ce) and held at 550 to 600°C. A stainless steel crucible, which was filled with a metal alloy (Cd, 3.6 w/o Mg, 0.2 w/o U or 2.5 w/o Ce), was placed on top of the column packing. When the temperature of the metal reached the temperature of the salt, a hole in the bottom of the crucible was opened by raising a tapered plug and the metal was allowed to flow into the column. The use of this charging crucible allowed a rapid and controlled flow of metal into the column. After about one minute, during which time most of the metal had drained out of the charging crucible and had collected in the bottom of the glass tube, the tube was lowered quickly into a bath of low-melting alloy at 100°C to freeze the metal and salt in the tube within one minute to minimize further transfer of solute across the metal-salt interface at the tube bottom.

TABLE I-7. Dynamic Extractions of Uranium from Molten Cadmium Alloy to Chloride Salt—Experimental Conditions and Results

Metal Alloy	Initial composition:	Cd-3.6 w/o Mg-0.2 w/o U
	Charge to column:	210 g
Salt	Initial composition:	50 m/o $MgCl_2$-30 m/o NaCl-20 m/o KCl
	Charge to column:	100 g
Column	(quartz tube):	⅞-in. ID, 6 in. packed height
Packing:		¼-in. length, ¼-in. OD Ta tubing

Temp (°C)	Contact Time (sec)[a]	U Concentrations (w/o)			Overall Average Mass Transfer Coefficient, $k_s a$ (sec^{-1})
		Initial Metal[b]	Final Salt[c] ($x_f \times 10^2$)	Salt at Equil. (calculated) ($x_e \times 10^2$)	
490	<300[d]	0.240	0.49	0.64	>0.005
610	60	0.244	0.92	2.6	0.0074
560	110	0.206	0.82	1.4	0.0079

[a] Time from start of metal flow to start of salt freezing.

[b] Final uranium concentration approximately equal to initial concentration.

[c] Assuming uranium transferred to salt only in packed section.

[d] Crucible leaked. Contact time uncertain.

The results of three such experiments with uranium as the transferring component are summarized in Table I-7. Because the amount of uranium extracted from the metal into the salt at equilibrium was negligible with respect to the uranium charged in the metal phase, the uranium concentration in the metal was essentially constant. The highest uranium concentration attainable in the salt was that which would be in equilibrium with the metal phase. In a separate series of experiments, the equilibrium distribution coefficient of uranium between Cd-3.6 w/o Mg alloy and the chloride salt was measured. These data were correlated with the aid of magnesium and uranium metal phase activities, which were calculated from an expression developed by G. Brown[26] for the ternary system Cd-Mg-U. Because temperature has a large effect on the uranium distribution coefficient, the equilibrium uranium concentrations in salt reported in Table I-7 vary greatly.

From the data reported in Table I-7, the overall mass transfer coefficients, also reported in Table I-7, can be calculated from the following equation:

$$S \frac{dx}{dt} = [k_s a]\, \rho_s\, [x_e - x]\, V$$

where

S = salt in active section (g-mole)
ρ_s = molar density of salt (g-mole/cm^3)
V = volume of active section (cm^3)
x = uranium concentration in salt (mole fraction)
x_e = uranium concentration in salt in equilibrium with uranium in metal
$k_s a$ = overall mass transfer coefficient (sec^{-1}) (based on salt phase concentrations)

by making the following assumptions:

(1) The salt column was stagnant and the uranium concentration in the metal was everywhere constant and equal to the initial concentration.
(2) Only the packed section was active for transfer and no uranium was extracted into the salt in the lower unpacked section of the tube. (There are qualitative indications from the column tests with cerium reported in this section and from the mixer-settler tests reported below that suggest that mass transfer in an unagitated zone is extremely slow.)
(3) The time the metal took to pass through the column was short compared to the total time

[26] Brown, G., Argonne National Laboratory, personal communication.

of the experiment. Thus the uranium content of the salt in the active section was uniform and a function of time only. Because of these assumptions, the time for the transfer of uranium was the total time that metal was flowing through the columns and not the residence time of metal in the column.

With the assumptions stated above, the expression for the mass transfer coefficient can be integrated over the total time, T (sec) of the experiment when the final uranium concentration in the salt in the active section is x_f.

$$[k_s a]_{\text{av.}} = \left(\frac{S}{\rho_s V}\right)\left(\frac{1}{T}\right)\ln\left(\frac{1}{1 - x_f/x_e}\right)$$

The average mass transfer coefficient of the second and third runs is 0.0076 sec^{-1}. If this value holds for plutonium and rare earths, the calculated height of a theoretical stage in which plutonium would be separated from rare earths is 2.3 ft. Higher coefficients would be expected in an operating countercurrent column because of the greater degree of turbulence due to the movement of the salt phase and because the more efficient column packing would result in a larger holdup of the metal phase.

Similar experiments have been made in a stainless steel column using cerium as the distributing element. It was calculated that 80 to 85% of the cerium would be in the salt phase at the end of these runs if the salt and metal were at equilibrium. In the first test, 58 g of Cd-11 w/o Zn-5 w/o Mg-2.56 w/o Ce alloy was passed through a stainless steel column packed with ¼-in. lengths of ¼-in. OD tantalum tubing and containing about 180 g of chloride salt (50 m/o $MgCl_2$-30 m/o NaCl-20 m/o KCl) at 550°C. The packed section was 12.5 in. long. After the alloy passed through the column, it was determined that 88% of the cerium had been removed from the alloy. A material balance could not be made because the salt phase could not be recovered completely. In a second similar experiment, the temperature was 600°C and the salt-to-metal weight ratio was about 20% lower. Analysis of the metal product indicated that 95% of the cerium had been removed.

The amount of cerium transferred from the metal in both runs indicated that somewhat more than one equilibrium stage had been provided in the 12.5-in. column. Comparing the kinetics of cerium and uranium transfer, the cerium appears to have transferred at a significantly higher rate than the uranium. The reasons for this difference are being sought.

The rates determined for both cerium and uranium transfer indicate that the transfer kinetics in a packed countercurrent extraction column are in a useful range for the partitioning of solutes between liquid metals and salts.

(2) Mixer-Settler Tests (W. J. Walsh, K. R. Tobias)

In addition to the various tests performed with extraction columns, three mixer-settler extraction experiments were made. Batch tests were conducted to determine the residence time and degree of agitation necessary to achieve a good separation in a mixer-settler unit.

The results of the mixer-settler simulation tests are given in Fig. I-16. Each run was made with 5 kg of Cd-11 w/o Zn-5 w/o Mg-3 w/o Ce in contact with 1.9 kg of purified 50 m/o $MgCl_2$-30 m/o NaCl-20 m/o KCl salt in a 4½-in. ID test crucible at 600°C. The first test was made for the case of gentle stirring (60 rpm) at the interface in an unbaffled crucible using a 3-in. by 3/32-in. flat paddle. The mass transfer was found to be extremely slow and, in this experiment, was limited by the low rate of diffusion of cerium in the metal phase from crystals which had precipitated prior to heating of the melt. Less than 50% of the equilibrium amount of cerium was extracted into the salt in 500 min. The second mixer-settler simulation run was conducted using a 2-in. by ¼-in. flat paddle at 350 rpm in a well-baffled crucible. The mass transfer proceeded much more rapidly in this case, with the extraction being 90% complete after 55 min of agitation. The third run was made using the 2-in. by ¼-in. flat paddle at 700 rpm in the baffled crucible. In this test, the extraction was 98% complete after 5 min of agitation.

These experimental results indicate that mixer-settlers are feasible for liquid metal-liquid salt extractions. Such units would require modest agitation and a residence time of several minutes. However, since the system is limited to a separation equivalent to one equilibrium stage, mixer-settlers are attractive only for extractions involving very high separation factors.

(3) Engineering Test Loop (W. J. Walsh, T. R. Johnson, L. F. Dorsey)

A test loop facility (Fig. I-12, ANL-6925) was constructed for the purpose of testing components for eventual use in a metal-salt extraction pilot plant. Initial tests with flowing liquid salt streams (50 m/o $MgCl_2$-30 m/o NaCl-20 m/o KCl) revealed that the threaded and compression fittings used throughout the loop are unreliable for containment of the salt. The facility is presently being converted to a completely welded unit.

The initial tests involved (1) the intermittent circu-

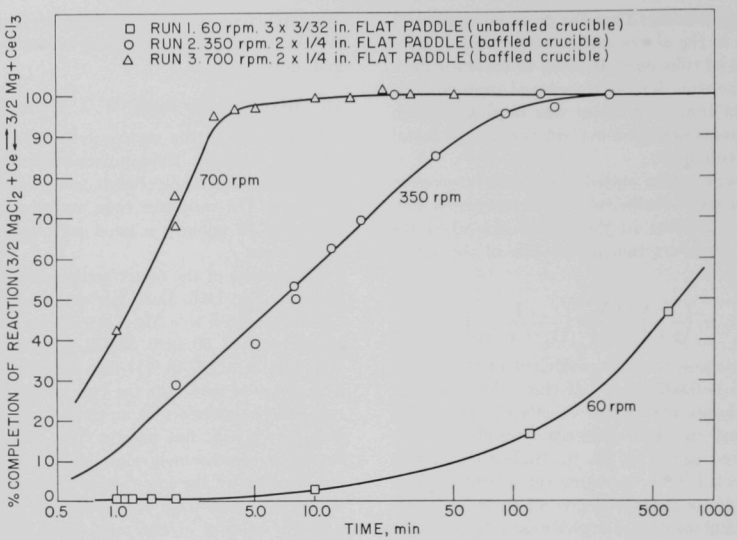

108-8916

FIG. I-16. Extraction of Cerium From Cd-11 w/o Zn-5 w/o Mg-3 w/o Ce into 50 m/o $MgCl_2$-30 m/o NaCl-20 m/o KCl by the Use of Mixer-Settlers. (600°C; 4½-in. ID Crucible.)

lation of liquid salt and (2) heating and cooling through several thermal cycles (the salt within the lines being frozen and remelted). No evidence of corrosive attack was found on the interior of the type 304 stainless steel tubing after over 200 hr of contact with liquid salt. However, severe local corrosion occurred on the outside of the tubing wherever salt leaked from the loop and was exposed to the atmosphere (see Section IA2f of this report).

The temperature distribution around the loop was found to vary by as much as ±95°C under stagnant conditions. Small-scale heating tests (8-ft heated section) are underway to determine improved methods of heating and insulating which will minimize the temperature variations around the loop.

(4) Eddy Current Induction Probe for Liquid Level Measurements (T. R. JOHNSON, F. G. TEATS)

Several types of instruments will be required for continuous processes, including devices to measure liquid flow rates, liquid levels, and pressures. Some of the instruments required for continuous processes will also be used for the batch processes currently being developed for the EBR-II fuel cycle. The first of these instruments to be developed is an eddy-current induction probe (see Fig. I-13, ANL-6925) which measures the level of metal in a tank and detects the location of the metal-salt interface in extraction devices. The probe consists of a bifilar winding of nichrome wire placed around an alumina form and encased in a corrosion-resistant well which extends into the liquid. When a high-frequency voltage is applied to one coil, the voltage induced in the second coil is sensitive to the presence of an electrical conductor in the medium surrounding the coil and, therefore, to the depth of immersion of the coil in a liquid metal. The induced voltage is decreased as a result of eddy currents induced in the liquid metal. This probe has proved to be reliable over long periods of operation, is easy to use, maintain, and calibrate, and is accurate to within ⅛ in. of depth in the liquid metals being considered for process solvents or for coolants in nuclear reactors. These include cadmium, zinc, bismuth and sodium.

Results of the calibration of the instrument in liquid cadmium were reported in ANL-6925, p. 43. The probe has now been calibrated in other liquid metals having different electrical resistivities in order to investigate the effect of this property on the output voltage of the probe (Fig. I-17).[27] Bismuth, which has the highest

[27] At lower temperatures, 150 to 300°C, sodium would not drain uniformly from the containment well as the liquid level was lowered. Consequently, one calibration curve was found for a falling liquid level, and a different curve was found for a

resistivity of the common liquid metals (147 μohm-cm at 525°C), produced a single response curve similar to that of cadmium, but with a slightly flatter slope. The effect of temperature on the determination of melt depth in liquid bismuth was the same as the effect of temperature with liquid cadmium and could be conveniently compensated for by changing the bias voltage (see Fig. I-15, ANL-6925, p. 45). Sodium, which has a lower resistivity (26 μohm-cm at 550°C),[28] showed a signal curve slope that was slightly greater than the slope with cadmium at the same temperature.

The slope of the signal output curve for zinc, which has a resistivity very close to that of cadmium, would be expected to be nearly the same as that for cadmium. Since stainless steel is rapidly attacked by zinc, a tantalum containment well was used for the zinc experiments instead of the stainless steel well used with cadmium. However, tantalum has a resistivity of 30 μohm-cm at 550°C as compared with 100 μohm-cm for stainless steel. Consequently, the signal response of the probe in a tantalum well does not vary enough to discern a small (0.5-in.) change in liquid depth of either cadmium or zinc. For cadmium, for example, a change in liquid level of 3.3 in. is required to produce a change in signal response of 0.25 mv when the probe is operated in a tantalum well as compared with a change of ~5.0 mv for the same change in liquid depth when it is operated in a stainless steel well. For zinc, results comparable to the cadmium data were obtained by using an alumina well. The results of the tests in zinc using the tantalum and ceramic wells are compared in Figure I-18 with the cadmium calibration curve obtained with the probe in a stainless steel well. Because the OD of the ceramic well was larger than that of the stainless steel well (¾ in. vs. ½ in.), no direct comparison can be made of the two signal output curves.

Since the material of construction of the containment well showed a marked effect on the signal output, comparative tests of signal outputs were made over a range of frequencies with the probe in air, in a stainless steel well, and in a tantalum well. The results are shown in Figure I-19. As the resistivity of the surrounding medium decreased, the signal output decreased. It can be concluded that materials with low resistivity, such as tungsten and molybdenum, are

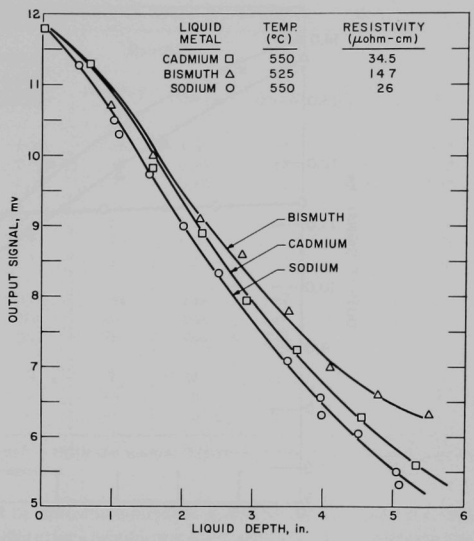

108-8889

FIG. I-17. Output Voltage of Eddy Current Induction Probe vs. Metal Depth for Several Liquid Metals.

Input frequency:	50,000 cps
Oscillator voltage:	7.0 volts
Bias voltage:	Adjusted to make S(O) coincide
Well:	304 SS, 0.032-in. wall by ½-in. OD
Crucible:	304 SS, 10-in. high by 5⅝-in. ID
Length of winding:	5⅛-in.

not suitable containment materials for the high-frequency eddy-current probe.

Two probes having the same physical dimensions and d-c resistances showed different calibration curves and required different amounts of bias voltage to produce the same zero point. It is thought that the use of fixed capacitors to match the impedence of the probes to the oscillator was the cause of these differences. This indicates that each probe needs to be calibrated individually.

Experience has shown that the calibration curve of a single probe is stable over a long period of operation. However, aging of the electronic components causes the zero point to drift. After approximately 1000 hr of operation, it has been necessary to redetermine the zero point by recalibrating the probe at a known liquid level.

Since the probe is now operational and has demonstrated a capacity for measuring the depth of solvent metals of process interest with the required accuracy and reliability for continuous processes, no further development is planned.

rising level. In addition, the signal change with falling liquid level was less than expected because of the rather thick layer of conducting liquid which adhered to the containment well. These effects were not found at temperatures above 350°C.

[28] Extrapolated from data of C. B. Jackson and J. W. Mausteller presented in *Modern Materials: Advances in Development and Applications*, Henry H. Hausner, Ed., Vol. 3, Academic Press, New York, 1962.

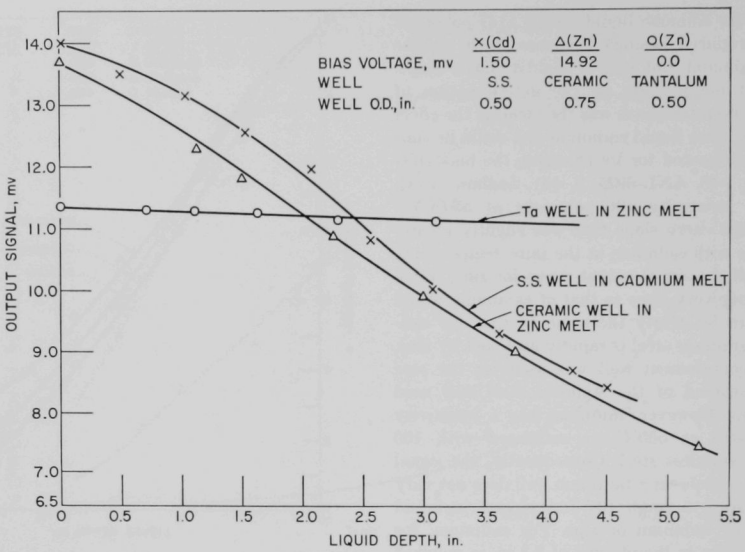

108-8880

FIG. I-18. Effect of Well Material on Output Signal of Eddy Current Liquid Level Probe. (Input frequency: 50,000 cps; Oscillator voltage: 7.0 volts.)

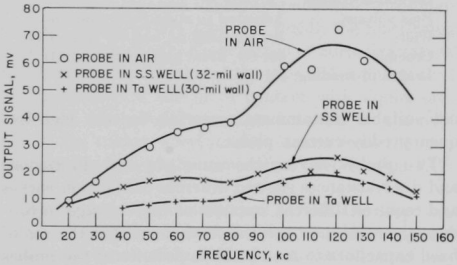

108-8891

FIG. I-19. Effect of Frequency and Well Material on Output Signal of Eddy Current Liquid Level Probe.

Probe length:	6 in.
Frequency:	varied
Bias voltage:	0.0 mv.
Oscillator output:	7 volts
Temperature:	30°C

f. CORROSION TESTING (M. KYLE, J. ARNTZEN, W. PEHL, A. SANDERS)

(1) Corrosion of Nickel, Molybdenum, and Tungsten Alloys by High-Temperature Argon-5% Nitrogen Atmospheres

The possible detrimental effect of the argon-5% nitrogen atmosphere present in the Argon Cell of the EBR-II Fuel Cycle Facility on alloys which may see service in the Facility has been investigated. Brunhouse and Titus[29] of Aerojet-General Nucleonics report that Inconel 600 and Hastelloy "X" alloys react with high-purity nitrogen at temperatures above about 650°C, causing embrittlement of the alloys. The reaction appears to result in the formation of a complex nitride phase and is probably common to most nickel-rich alloys. The effect appears to be enhanced in alloys which also contain molybdenum. Since the reaction is not noticed when these alloys are exposed to air, it is believed that oxygen inhibits the reaction.

The use of nickel-rich alloys in the Argon Cell is required, since these alloys are about the only easily available materials with sufficient structural strength to permit use in applications which require temperatures of 900°C. A specific application of these alloys is for the construction of the skull reclamation furnace, the exterior surfaces of which are expected to reach 900°C at times during an operating cycle.[30] Con-

[29] J. S. Brunhouse and G. W. Titus, Corrosion of Nickel-Based Alloys in High Temperature Nitrogen Environments, Corrosion, **17**, 203 (1961).

[30] Under steady state conditions of fuel flow, it should be necessary to operate the skull reclamation furnace about twice a month. Under unusual conditions, operation should be no more frequent than about once a week. Each run will last about

TABLE I-8. EXPOSURE OF NICKEL AND TUNGSTEN ALLOY COUPONS TO ARGON-5% NITROGEN AT 900°C

Exposure Time (hr)	Measured Effect	Material							
		Inconel 600	Inconel 800	Hastelloy C	Hastelloy X	304 SS	316 SS	Mo-30 w/o W	W
450	Wt. Increase, mg/cm²	0.25	1.99	1.30	0.94	0.40	0.62	—	0.012
1000		0.68	3.14	2.10	1.87	0.73	2.60	0.16	0.33
2000		0.67	3.15	2.11	1.32	2.16	3.15	0.18	0.31
450	Penetration of Nitride Phase, mils	1	1	1	1	0.5	0.5	—	<0.5
1000		1	1	2	2	1.5	1	<0.5	<0.5
2000		2	1	2	2	2	3	<0.5	<0.5
450	"2T" Bend Possible[a]	Yes	Yes	Yes	Yes	Yes	Yes	—	—
1000		Yes	No	No	No	Yes	Yes	—	—
2000		Yes	No	No	No	Yes	Yes	—	—
450	Number of 90° Flections before Failure	10	6	3	2	10	12	—	—
1000		5	—	—	—	9	4	—	—
2000		7	—	—	—	5	5	—	—

[a] In the "2T" bend test, the sample is bent 180° over a radius equal to twice the sample thickness. All coupons except tungsten and Mo-30 w/o tungsten would pass the "2T" bend test prior to exposure.

sequently, a program was initiated to study the possible detrimental effect of argon-5% nitrogen on various materials which may see service in the Argon Cell. These alloys included tungsten and molybdenum-30% tungsten, as well as the nickel-bearing alloys, Inconel 600, Inconel 800, Hastelloy C, Hastelloy X, and types 304 and 316 stainless steel.

Exposure tests of these alloys for 450, 1000, and 2000 hr at 900°C have now been completed (see results in Table I-8). After 1000 hr exposure to argon-5% nitrogen, Hastelloy C, Hastelloy X, and Inconel 800 coupons (2 in. by ½ in. by 0.60 in. thick) became embrittled to the extent that they could not be bent 180° on a radius equal to approximately twice the specimen thickness without cracking. They were not so brittle, however, that reasonable physical shock would cause cracking. Inconel 600 still possessed some ductility and passed the bend test. Metallographic examination revealed the existence of the complex nitride phase in both Hastelloy and both Inconel alloys. This phase extended from the surface exposed to nitrogen, along the grain boundaries, and into the matrix, probably causing embrittlement of the alloys. Tungsten, molybdenum-30% tungsten alloy, and types 304 and 316 stainless steel were affected very little except for the formation of slight nitride surface layers.

Exposure for an additional 1000 hr (total exposure time, 2000 hr) had little additional effect on the materials, and the same general conclusions are applicable. It is assumed that a reaction of this type would be diffusion-controlled and that consequently the rate of attack would probably decrease with increasing exposure time. The increased exposure time did increase the penetration of the nitride phase on the 300 series steels. Nevertheless, these alloys were still ductile after 2000 hr exposure.

It is doubtful that nitridation will present a serious problem in the EBR-II Argon Cell because high-nickel alloys will be at temperatures above 650°C for limited periods. It is possible, however, that the nitridation effect will limit the useful lifetime of these alloys in the cell atmosphere. Should this problem develop, protection methods such as oxide scaling or diffusion-bonded coatings of these alloys will be used.

(2) Corrosion of Type 405 Stainless Steels by Cadmium Base/Salt Systems

One of the processes currently under development for advanced reactor fuels utilizes cadmium as the solvent metal to which small amounts of magnesium and zinc are added with halide salts as the oxidant. Results of the initial screening tests of type 405 stainless steel indicate excellent corrosion resistance to low-zinc (under 10 w/o) alloy of this liquid metal system (see ANL-6925, p. 41).

These tests were extended to measurements of corrosion in two-phase, salt-metal systems. Results of four tests conducted at 650°C for 200 to 225 hr in a 81.4 w/o Cd-5.4 w/o Mg-10.9 w/o Zn-2.3 w/o U metal phase and a salt phase of 50 m/o $MgCl_2$-30 m/o NaCl-20 m/o KCl contained in an alumina crucible are presented in Table I-9. The testing procedure was

18 hr and the furnace will be above 650°C for about 12 hr and at 900°C for about 4 hr.

TABLE I-9. CORROSION OF TYPE 405 STAINLESS STEEL IN Cd-Mg-Zn-U/HALIDE SALT SYSTEMS

Temperature: 650°C
Metal Phase: 81.4 w/o Cd
5.4 w/o Mg
10.9 w/o Zn
2.3 w/o U
Salt Phase: 50 m/o $MgCl_2$-30 m/o NaCl-20 m/o KCl
Rotation speed: 30 rpm

Run	Length of Run (hr)	Method of Salt Drying	Approximate Length of Air Exposure of Salt (min)	Approximate Depth of Corrosion in Phase (mils)			
				Metal	Interface	Salt	Vapor
1	200	Melting under Argon Purge	30 to 40	1	2	2	5[a]
2	200	Contact with Cd-Mg Alloy[b,c]	3 to 5	<1	<1	<1	<1
3	225	Contact with Cd-Mg Alloy[b,d]	3 to 5	<0.5	<0.5	<0.5	<0.5
4	200	Contact with Cd-Mg Alloy[d]	3 to 5	<0.5[e]	<0.5	<0.5	<0.5

[a] Sample severely embrittled.
[b] Vapor phase purged with argon during run to remove HCl and H_2 vapors.
[c] Salt phase contained 0.2 w/o oxygen after purification.
[d] Salt phase contained <0.02 w/o oxygen after purification.
[e] Evidence of carbon migration out of outer 1.0 mil of sample surface.

the same as that previously described (ANL-6925, p. 42), i.e., the test coupons (2-in. by ½-in. by 0.060 in. thick) were mounted as four agitator blades on a single shaft, one blade at each of four positions: in the Cd-Zn-Mg-U metal phase, at the metal-salt interface, in the $MgCl_2$-NaCl-KCl salt phase, and in the vapor phase above the salt. Rotation speed was 30 rpm. These results indicate that type 405 stainless steel possesses excellent corrosion resistance to the system, providing the salt phase has been adequately dried. The procedure of melting the salt, contacting it with a cadmium-magnesium alloy, and filtering (ANL-6925, p. 41) seems adequate for salt drying. It also appears desirable to limit the air contact time of the dried hygroscopic salt. The vapor phase purge used in two runs to sweep away any HCl or hydrogen vapors produced during the run does not appear necessary when dried salts are used.

In Run 4 the sample exposed to the metal phase showed a definite carbon migration out of the outer 1.0 mil of the sample surface. Since the carbon concentration in these steels is low (0.08 w/o), this loss amounts to a very small quantity of carbon which probably dissolved in the liquid metal phase. Since the rate of carbon migration is diffusion-controlled, more extended service should not greatly reduce the amount of carbon in the steel. Samples exposed to the salt and vapor phases did not exhibit this carbon migration.

Other steel alloys will be tested under similar conditions to determine if there is a less expensive or more easily fabricated alloy which possesses adequate corrosion resistance to this system.

(3) Corrosion of Type 304 Stainless Steel from the Engineering Test Loop (M. KYLE, F. G. TEATS)

Samples from five locations in the vicinity of a leak in the Engineering Test Loop were examined in an effort to determine the nature and extent of halide flux[31] corrosion (see Section IA2e of this report) on the type 304 stainless steel (⅜ in. tubing of about 35-mil wall thickness). Samples were taken near a suspected leaky compression fitting, and from the tubing above and below the suspected failure. During dismantling of the loop to inspect the fitting, a second area of tubing failure was found below the fitting. This failure appeared to be a longitudinal crack about ¼ in. long. Metallographic examination of the samples indicated no detectable corrosion (less than 0.5 mil) of the interior of the tubing; however, external corrosion had proceeded to a depth of about 25 mils in this area. Examination of the tubing taken from the failed section of the line in the vicinity of the compression fitting revealed severe intergranular corrosion through the entire cross section of the tube wall. The appearance of the failure indicated that the corrosion had proceeded from the outside of the tube wall. Frozen salt had been remelted in this section of the loop; the pressure exerted on the tube as a result of the volume increase on melting was sufficient to rupture the weakened tubing. Portions of the tubing taken from below the point of the leaky compression fitting showed varying external corrosion depths of from 0 to 25 mils. It is believed that this corrosion resulted from contact

[31] 50 m/o $MgCl_2$-30 m/o NaCl-20 m/o KCl.

with the salt leaking down from the compression fitting, with the extent of corrosion dependent on the time of contact of the salt with the tube wall which in this case was a maximum of about 30 min.

It is concluded that the salt initially charged to the engineering test loop is not corrosive to 304 stainless steel. However, exposure of this salt to air or moisture renders the salt highly corrosive to this alloy.

(4) Corrosion of Vitreous Carbon by Uranium and Mg-Zn-U/Salt Systems (M. L. Kyle, J. Arntzen)

A small (1⅜-in. OD by 1⅜ in. tall by 0.1-in. wall) crucible fabricated from "vitreous" carbon[32] was obtained for testing as a containment material for Mg-Zn-U/halide salt systems. The vitreous carbon is a relatively new material which has the general characteristics of glass, i.e., it is fragile, microscopically sealed, and impervious to gases. Its thermal shock resistance is good because of its good thermal conductivity. This carbon is obtained by a proprietary process involving thermal decomposition of organic materials having strong transverse molecular bonds.

The sample crucible was exposed to a Zn-Mg-10% U/salt[33] solution for 24 hr at 800°C. Inspection of the crucible indicated that neither the flux nor the metal phase had wetted the crucible.

Because of these encouraging results, a much more severe test was performed to determine if metallic uranium could be melted in this crucible. In this test the uranium was melted by heating to about 1400°C and was maintained at this temperature for 1 hr at a pressure of 10^{-4} to 10^{-6} torr. Examination of the sample, after melting, by X-ray diffraction techniques indicated that a substantial portion of the uranium had been converted to uranium carbide. It is therefore concluded that vitreous carbon is not suitable for use as a container material for solutions containing high concentrations of uranium. Further testing of this material as a containment material for liquid metal/salt solutions is planned.

(5) Corrosion of Zirconium Diboride Coating on Niobium by Mg-Zn-U/Salt Systems

Niobium coated with zirconium diboride was tested for use as a process thermowell in the skull reclamation process because of recent success in the use of ZrB_2 crucibles for containing molten uranium (ANL-6900, p. 48). In a single test this material was exposed at 800°C to a Zn-5 w/o Mg-8 w/o U/salt[34] system. Catastrophic failure of the well occurred after about 7 hr of exposure. Although the reason for the failure is not known, it is suspected that the coating of ZrB_2 was not sufficiently dense to prevent the process solution from coming in contact with the niobium substrate.

(6) Corrosion of Copper and Steel Wools by Process Vapors

Two types of metallic wool, copper and steel, have been tested for use as a packing material to aid heat transfer between the tungsten crucible and the furnace wall of the plant prototype skull reclamation furnace. Use of such a packing would increase the rate of both heating and cooling of the crucible and its contents during the process. These wools were exposed under simulated process conditions to vapors emanating from the metal-flux system that is present in the reduction step of the skull reclamation process. During the test the crucible and its contents were heated to 800°C and held for 20 hr.

Examination of the copper wool after the test indicated the formation of brass (Cu-Zn alloy) in about the top 1 in. of the copper wool around the crucible. It is feared that continued exposure under these conditions would result in the formation of brasses which would be molten under process conditions.

Steel wool exposed to identical conditions showed no adverse effects after 20 hr of exposure. The phase diagram of this system also indicates the possibility of a low-melting compound forming at a high zinc concentration in the steel packing, but the amount of zinc required and the apparent kinetics of the reaction led to the conclusion that this would not occur under process conditions. Therefore, steel wool is being recommended for use in the plant skull reclamation furnace.

g. SUPPORTING ENGINEERING STUDIES

During the past reporting period, supporting engineering studies were conducted in two areas: (1) determination of the critical constants of alkali metals and (2) examination of the mechanism of liquid metal boiling and entrainment.

(1) Determination of the Critical Constants of Alkali Metals (I. G. Dillon,[35] P. A. Nelson[36])

Study of the nature of liquid metals indicates that their critical behavior may be expected to be considerably different from that of the so-called "normal" liquid used as a basis for the theorem of corresponding states. Knowledge of the critical behavior of a liquid metal, in particular, of the critical constants, permits

[32] A product of Société le Carbone, France.

[33] 38 m/o $MgCl_2$-38 m/o $CaCl_2$-4 m/o CaF_2-20 m/o MgO.

[34] 47½ m/o $MgCl_2$-47½ m/o $CaCl_2$-5 m/o CaF_2 .

[35] Ph.D. Candidate, Illinois Institute of Technology.

[36] Fast Reactors Fuel Group.

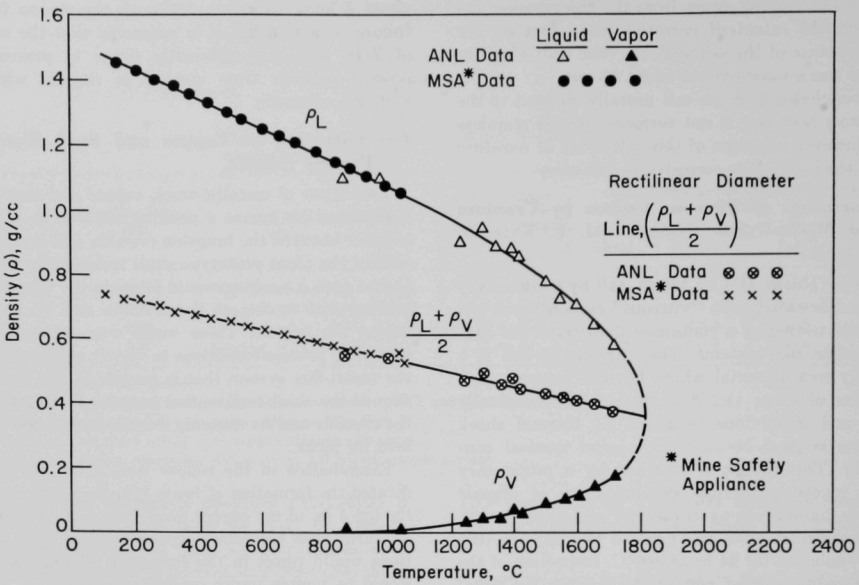

108-8893

FIG. I-20. Density and Rectilinear Diameter Plot for Rubidium. (Estimated Critical Constants: $\rho_c = 0.35$ g/cc, $T_c = 1820$°C.)

calculation of many thermodynamics and physical properties over the entire range of temperatures from the boiling point to the critical point. Thermodynamic properties of alkali metals are of particular interest because of their use as heat-exchange media in nuclear reactors. For most alkali metals, vapor pressures and liquid and vapor densities are generally known up to the vicinity of the boiling point. While many estimates have been made of the critical constants of the alkali metals, no actual measurements of the critical constants, or of vapor pressure, vapor density, and liquid density are known which cover the entire range of temperature from the boiling point to the critical point. To supply these missing data, measurements of the vapor and liquid densities of rubidium, cesium, sodium, and potassium are being made from room temperature up to as near as possible to the critical point. Densities are being determined by simultaneous measurement of gamma radiation emanating from the liquid phase and the vapor phase of irradiated tracer-containing alkali metal held in a capsule within a high-pressure cell. As the critical point is approached, the densities of the two phases and therefore the gamma activities emanating from the vapor and liquid phase regions approach each other.

Installation of Equipment. The revised high-pressure cell described previously (see Fig. I-18, ANL-6925, p. 50) has been received and has proved highly satisfactory. Capsules have been heated up to 1950°C and then have been successfully removed from the furnace.

Experimental Results. Data on vapor and liquid density have been obtained for rubidium, cesium, sodium, and potassium. From these data, density-temperature plots are presented in Figs. I-20 to I-23. Critical temperature estimates were made from assumptions of a straight rectilinear diameter line combined with various correlation methods. These include the Kordes[37] plot of

$$\ln \frac{4\,\rho_V\,\rho_L}{(\rho_L + \rho_V)^2} \text{ vs. } \ln T$$

which for a large number of substances has been found to be a straight line intercepting 1.0 on the ordinate at $T = T_c$,

where

ρ_V = vapor density, g/cc
ρ_L = liquid density, g/cc
T = temperature, °C
T_c = critical temperature, °C

[37] Kordes, E., Z. Electrochem. **57**, 731–738 (1953).

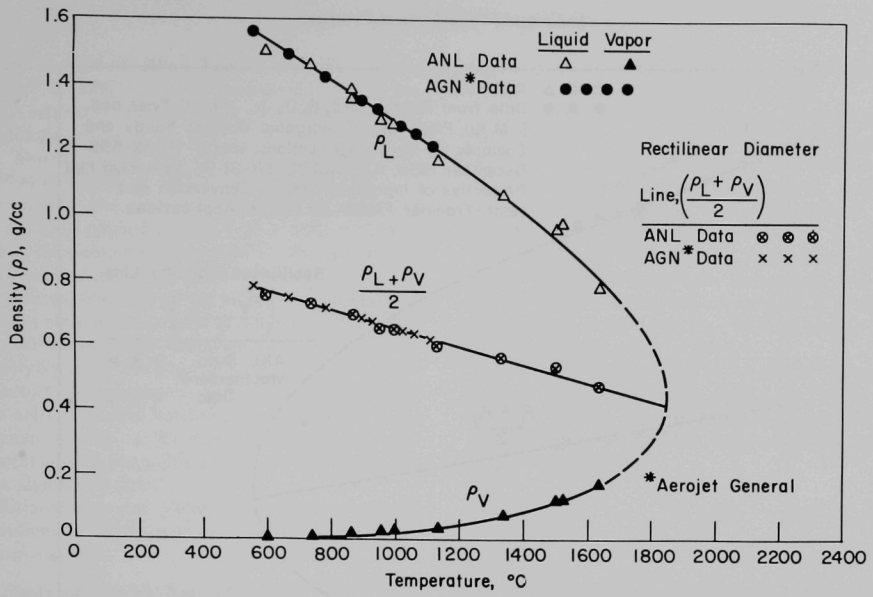

108-8894

FIG. I-21. Density and Rectilinear Diameter Plot for Cesium. (Estimated Critical Constants: ρ_c = 0.41 g/cc, T_c = 1850°C.)

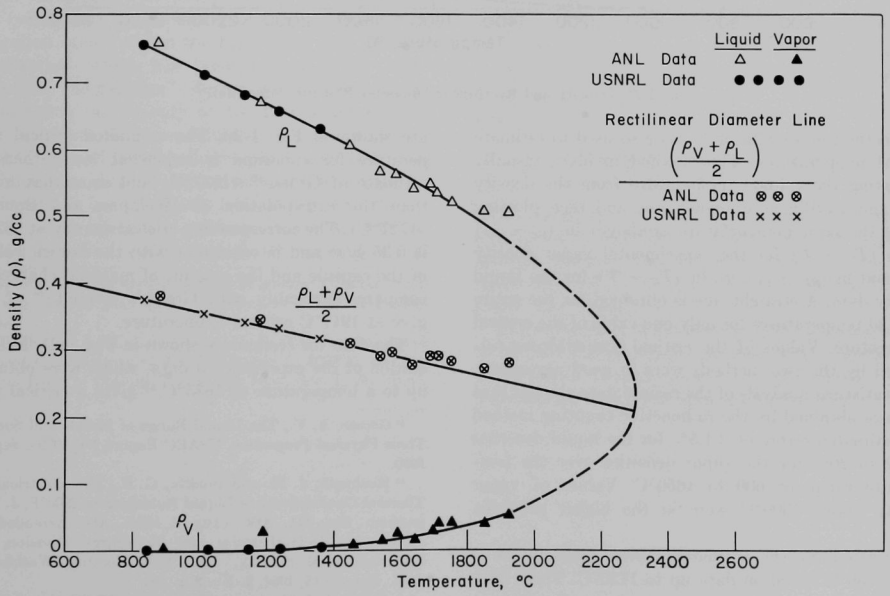

108-8879

FIG. I-22. Density and Rectilinear Diameter Plot for Sodium. (Estimated Critical Constants: ρ_c = 0.21 g/cc, T_c = 2300°C, P_c = 350 atm.)

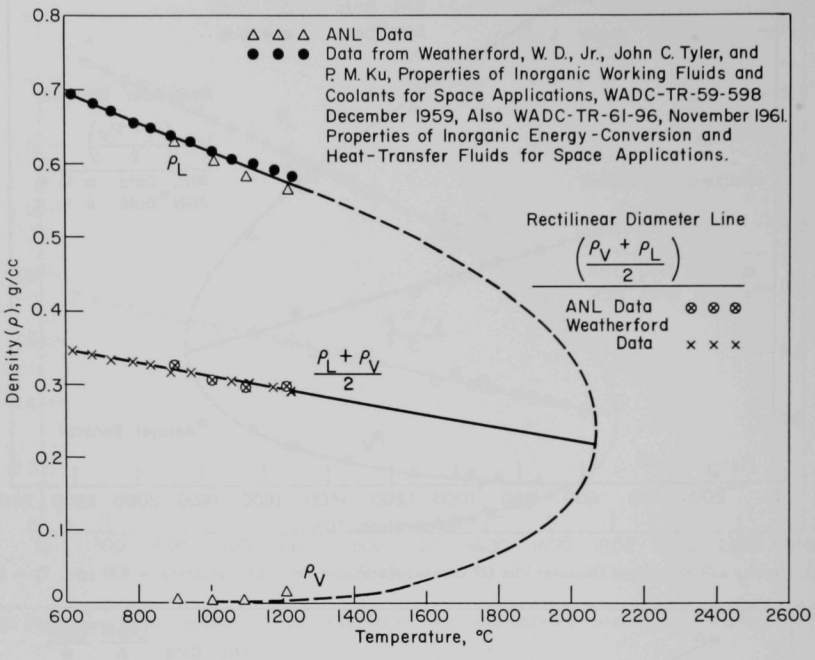

8-8884

FIG. I-23. Density and Rectilinear Diameter Plot for Potassium.

The method of Rowlinson[38] was also used to estimate critical temperatures. This method involves visually estimating the critical temperature from the density data and rectilinear diameter line and then plotting (using the same nomenclature as above) ln $(\rho_c - \rho_V)$ *vs.* ln $(T_c - T)$ for the experimental vapor density data and ln $(\rho_L - \rho_C)$ *vs.* ln $(T_C - T)$ for the liquid density data. A straight line is obtained for the entire range of temperatures for only one value of the critical temperature. Values of the critical temperatures calculated by the two methods were in good agreement.

A statistical analysis of the cesium data showed that densities obtained by the radioactive counting method had estimated errors of ±1.5% for the liquid densities and 2 to 20% for the vapor densities over the temperature range of 600 to 1650°C. Values of vapor density above 1300°C were in the higher precision range.

For rubidium, the estimated critical temperature is 1820 ± 30°C based on data up to 1720°C. These data are shown in Fig. I-20. The estimated critical temperature for rubidium is somewhat lower than the estimate of Grosse[39] (1917°C) and somewhat higher than the extrapolation of Hochman and Bonilla[40] (1727°C). The corresponding critical density at 1820°C is 0.35 g/cc and is consistent with the known volume of the capsule and the amount of material charged. It compares favorably with Grosse's estimate[39] of 0.32 g/cc at 1917°C critical temperature.

The data for cesium are shown in Fig. I-21. Extrapolation of the experimental data, which were obtained up to a temperature of 1635°C,[41] gives a critical tem-

[38] Rowlinson, J. S., Liquids and Liquid Mixtures, Academic Press, Inc., New York, 1959, p. 92.

[39] Grosse, A. V., The Liquid Range of Metals and Some of Their Physical Properties, USAEC Report NP-10795, Sept. 5, 1960.

[40] Hochman, J. M. and Bonilla, C. F., The Electrical and Thermal Conductivity of Liquid Rubidium to 2900°F, J. Electrochem. Soc. **111**, 200C (August 1964). Also Extended Abstracts of Electrothermics and Metallurgy Division, The Electrochemical Society, Inc., Fall Meeting, Washington, D.C., Oct. 11–15, 1964, **2**, No. 2, p. 58.

[41] Although data were obtained up to 1770°C, data between 1635°C and 1770°C were not used in estimating the critical temperature because for this temperature region the capsule con-

perature of 1850 ± 50°C. This is close to Grosse's estimate[39] of 1887°C, but is considerably above the 1783°C estimated by Hochman and Bonilla.[42] The corresponding density at 1850°C is 0.41 g/cc. This value also compares favorably with Grosse's estimate[39] of 0.42 g/cc at 1887°C critical temperature.

For sodium, the critical temperature as estimated from the data plotted on Fig. I-22 is 2300 ± 100°C, based on data obtained up to 1928°C. The corresponding critical density is 0.21 g/cc.

The critical temperature for potassium, as estimated from data obtained up to 1202°C is 2050 ± 250°C (Fig. I-23). With the present container materials (tungsten and molybdenum), the gamma counting method is unsatisfactory for potassium since high induced container activities make handling very difficult, and the potassium activity at the maximum possible irradiation attainable is not sufficiently above background to obtain significant data.

Additional runs are planned on rubidium, cesium, and sodium to obtain more data in the higher temperature regions.

(2) Study of Mechanisms of Liquid Metal Boiling and Entrainment (J. Wolkoff)

The vaporization of pure mercury during convective boiling has been under study. No vapor bubble nucleation occurs within the liquid with this mode of vaporization, which has been referred to as "nonturbulent vaporization" during the present study. Vaporization occurs only at the free liquid surface. Since there are no vapor bubbles, there are no liquid droplets formed at the liquid-vapor interface and, consequently, there is no entrainment of liquid by the vapors. It has previously been shown that vaporization rates equivalent to heat fluxes as high as 115,000 Btu/(hr)(sq ft) through the vaporizing surface could be attained under vacuum when good liquid mixing was provided (ANL-6687, p. 58).

The measurement of the surface temperature of the mercury during vaporization was difficult experimentally since a large temperature gradient combined with temperature fluctuations, existed within the liquid near the surface (ANL-6800, p. 133; ANL-6900, p. 93). A surface temperature probe consisting of a fine wire which penetrated the vaporizing surface from above to form a thermocouple with the liquid metal was developed to measure the surface temperature. A mathematical analysis of the probe has been discussed (ANL-6925, p. 51; ANL-6900, p. 95).

For the usual case of a constant temperature gradient at the vaporizing surface, it can be shown that the infinite series solution previously presented (ANL-6925, p. 51) can be reduced to the following simple approximation:

$$\frac{e}{g} \leq K_w R$$

where

e = error in reading the surface temperature, °C
g = surface temperature gradient, °C/in.
R = radius of the thermocouple wire, in.

and K_w is a parameter having the following values:

(1) $K_w = 0.9\, W^{0.6}$ when $3 \times 10^{-1} < W \leq 10^5$
(2) $K_w = 0.3 + 0.6\, W$ when $10^{-2} \leq W \leq 3 \times 10^{-1}$
(3) $K_w = 0.3$ when $W < 10^{-2}$

where

$$W = \frac{\text{electrical resistivity of the liquid metal}}{\text{electrical resistivity of the wire}}.$$

These relations are valid in the region where the measurement error is low, generally the region of greatest interest. The W dependence was not computed above $W = 10^5$ but can be assumed to be valid above this value.

The upper limit of the error is therefore proportional to the wire radius and the gradient, and is independent of the depth of submergence. Its independence of the submergence depth has been shown previously.

tained more than the critical amount of cesium. Thus the vapor hole was covered with liquid, resulting in erroneous density values.

[42] Hochman, J. M. and Bonilla, C. F., The Electrical and Thermal Conductivity of Liquid Cesium to 3000°F, and the Critical Point of Cesium, Trans. Am. Nucl. Soc. **1**, 101 (June, 1964).

B. FUEL PROCESSING FACILITIES FOR EBR-II

(J. H. Schraidt, M. Levenson, L. F. Coleman)

A direct-cycle fuel reprocessing plant (Fuel Cycle Facility) based on pyrochemical procedures was designed and constructed as part of the Experimental Breeder Reactor No. II (EBR-II) Project. Melt refining, liquid metal extraction, and processes involving fractional crystallization from liquid metal systems are methods being examined for the recovery and purification of EBR-II fuels. Based on these studies, process equipment is being designed and tested. The development of process equipment for the Fuel Cycle Facility has been a joint effort of the Central Shops Department, Reactor Engineering Division, Metallurgy Division, Remote Control Division, and Chemical Engineering Division. Actual installation of equipment items in the Air Cell and Argon Cell of the Fuel Cycle Facility is performed by members of the Idaho Division.

This section (I-B) of the report describes the efforts of the Chemical Engineering Division in providing technical assistance for problems arising in the operation of the Fuel Cycle Facility and in developing equipment for pyrochemical processes which will be subsequently operated in the Fuel Cycle Facility. The results of operations being carried out in the Fuel Cycle Facility are presented in Section I-C of this report.

1. Technical Assistance and Service Equipment Development

a. IN-CELL LIGHTING OF AIR CELL AND ARGON CELL (T. Eckels)

One thousand-watt mercury vapor lamps with white phosphor-coated soft-glass envelopes are being used for in-cell lighting of the Air Cell and Argon Cell (ANL-6596, pp. 99–101). The lamps are installed in wall-mounted luminaires that were designed by the Chemical Engineering Division. There are a total of 96 lamps in the two cells. This form of lighting has proved to be very satisfactory. In the 30 months (as of January 1965) that they have been in use, only one lamp has burned out. Most lamps have given about 17,000 hr of service. In the Argon Cell, which has 72 lamps, the illumination along the center-line of the cell working area has decreased from an initial value of 180 ft-candles in August 1962 to a value estimated (in January 1965) to be about one-half of the initial value. (In February 1963, this illumination value was 125 ft-candles.) Preparations are being made to start replacing lamps on a regular schedule in order to minimize the possibility of several lamps simultaneously burning out.

b. LIGHT TRANSMITTANCE MEASUREMENTS OF SHIELDING WINDOWS (T. Eckels)

Operations within the Fuel Cycle Facility Air Cell and Argon Cell are normally viewed through one of the 31 shielding windows installed in the 5-ft thick, heavy concrete shielding walls. (For a description of the shielding windows, see ANL-6605, pp. 30–31 and ANL-7020, p. 8.) When the windows were accepted from the manufacturer in August 1962, the measured light transmittance for all windows ranged from 15 to 17%, with an average value of 16.1%. Since these tests were made, glass cover plates[43] have been installed on the cell side of the window, and all shielding windows have been subjected to irradiation exposure. The shielding windows of the Air Cell were exposed to irradiation while the first radioactive core subassembly (about 0.1 a/o burnup) and an inner blanket subassembly from the EBR-II reactor were being disassembled; the shielding windows of the Argon Cell were subjected to irradiation exposure while the core subassembly was being processed through the melt refining and injection casting steps (see ANL-6925, pp. 72–75 and 85–86).

In collaboration with Fuel Cycle Facility operating personnel, the light transmittance of all windows was again measured (in January 1965) to determine if there was any reduction in the transmittance. The results of the second transmittance test showed that the average measured value for the light transmittance through the shielding windows plus the glass cover plates was 14.5%. The average calculated light transmittance through the shielding windows only (no glass cover plates) was found to be 15.7% or about 98% of the initial transmittance value. Additional light transmittance measurements of the shielding windows are planned after they have been subjected to substantially greater gamma irradiation.

Periodically, the clear mineral oil in the tank unit assemblies of each of the windows has been sampled and analyzed for changes in acid number, hydrogen

[43] The ¼-in. thick glass cover plate serves to protect the "Al" slab from any accidental blow which could bruise its glass surface and initiate the discharge of a gamma-induced electrical charge. This discharge produces tree-like patterns within a glass which destroy its viewing qualities (see ANL-6900, pp. 109–110).

peroxide content, and surface tension. No significant changes in these properties have been noted.

c. SHORT-CIRCUIT FAILURE OF CONNECTOR FOR MANIPULATOR CABLE (L. F. Coleman)

Manipulator No. 4, which is in the Argon Cell, became inoperative because of a short circuit in the 64-pin connector on the top end of the manipulator feed cable. This connector is in an argon atmosphere. Examination of the connector showed that a portion of the insulating material was severely carbonized, presumably as a result of arcing between adjacent conductor pins. This arcing is attributed to the poor dielectric strength of argon. A similar failure occurred previously (April, 1964) on an identical connector for Argon Cell manipulator No. 2 (see ANL-6900, p. 109).

The insert in this connector has a National Electric Code (NEC) rating of 250 volts a-c or d-c. The maximum voltage of any single circuit for the manipulator is 140 volts d-c, with higher voltages occurring as a result of switching transients. The nominal spacing between conductors in the insert is $\frac{1}{16}$ in. and this spacing is apparently not adequate for application in an argon atmosphere.

To eliminate the connector failures, the connector inserts will be replaced on all six manipulator cables for the Argon Cell. The new inserts will have a spacing between conductors of $\frac{1}{8}$ in. and a NEC rating of 600 volts. The revised connectors will have only 22-pin conductors. The 54 wires in the cable (there are three or more wires for each of 17 circuit sides) will be consolidated into 18 conductors, and the 18 conductors will be soldered to the new connector. The increased spacing in the new inserts should prevent arcing.

d. REMOTE HANDLING OF ARGON CELL BRIDGE-DRIVE MOTOR (J. Graae)

One of the more difficult remote maintenance operations in the Argon Cell is the remote removal of a bridge-drive motor from a crane bridge. (The design of a remotely removable and replaceable crane-bridge drive unit for the Fuel Cycle Facility is described in ANL-6966.) The drive motor is difficult to reach, and the removal operation must be viewed with a periscope in the cell. To carry out the remote removal step, a bridge-drive lifting tool was designed and fabricated for use with the crane-and-manipulator removal tool. The design of the lifting tool permits the operator to see whether or not the drive motor has been properly engaged by the lifting-tool hooks. The lifting tool has been successfully used to remove a bridge drive motor from a crane bridge in the Argon Cell and to reinstall it. No difficulties were encountered in these operations. This was the first time that a bridge drive motor has been remotely removed and installed in this Facility.

e. SHIELDING WINDOW DESIGN FOR FARET CELL (T. Eckels, R. Kush[44])

A modification of the Fuel Cycle Facility shielding window is being developed for the design of the shielding window for the cell of the Fast Reactor Test (FARET) Facility.[45] The window design is being carried out as a cooperative effort of the Reactor Engineering Division and the Chemical Engineering Division.

The FARET cell shielding windows are to meet rather stringent requirements. In addition to furnishing necessary biological radiation shielding, they form an integral part of the facility containment structure. The windows will be required to withstand (1) a transient pressure rise to 30 psig, (2) a transient temperature excursion of the cell gas to perhaps 1900°F, and (3) possible impact from a variety of missile fragments which may be released in a reactor incident without violation to the containment structure. In addition, normal cell operations require the total window inleakage rate to be less than 0.01 cu ft/day at a pressure of minus 4 in. of water.

The shielding windows (see Figure I-24) will have a total thickness of 60 in. and will consist of nine heavy slabs of glass, of which five are designed to be successive barriers to an internal cell pressure of 30 psig. The maximum bending stresses from this cell pressure were calculated for various slabs using thin-plate equations[46] and were found to be as follows:

Slab	Thickness (in.)	Width (in.)	Height (in.)	Maximum Stress (psi)
A-2	8	38	45	261
B-1	6	34	36	318
B-2	6	33	36	316
T-1	4	24	30.5	459
T-6	4	28	32	542

These maximum stresses are well within the design limits (800 psi) customarily used for plate glass. However, since there are no experimental data on the use of thick glass slabs for pressure containment, 8½-in. thick glass slabs (29 in. by 44 in.) were procured, and a steel test fixture was built for a hydrostatic test. This test was to verify the feasibility of the window

[44] Central Shops.

[45] This facility will be located at the National Reactor Testing Station, Idaho. FARET will be an experimental, sodium-cooled fast reactor and will be used for reactor physics and engineering studies associated with the development of large fast breeder power reactors.

[46] S. Timoshenko, *Theory of Plates and Shells*, McGraw-Hill Book Company, Inc., N. Y., 1940, pp. 116, 129 and 130.

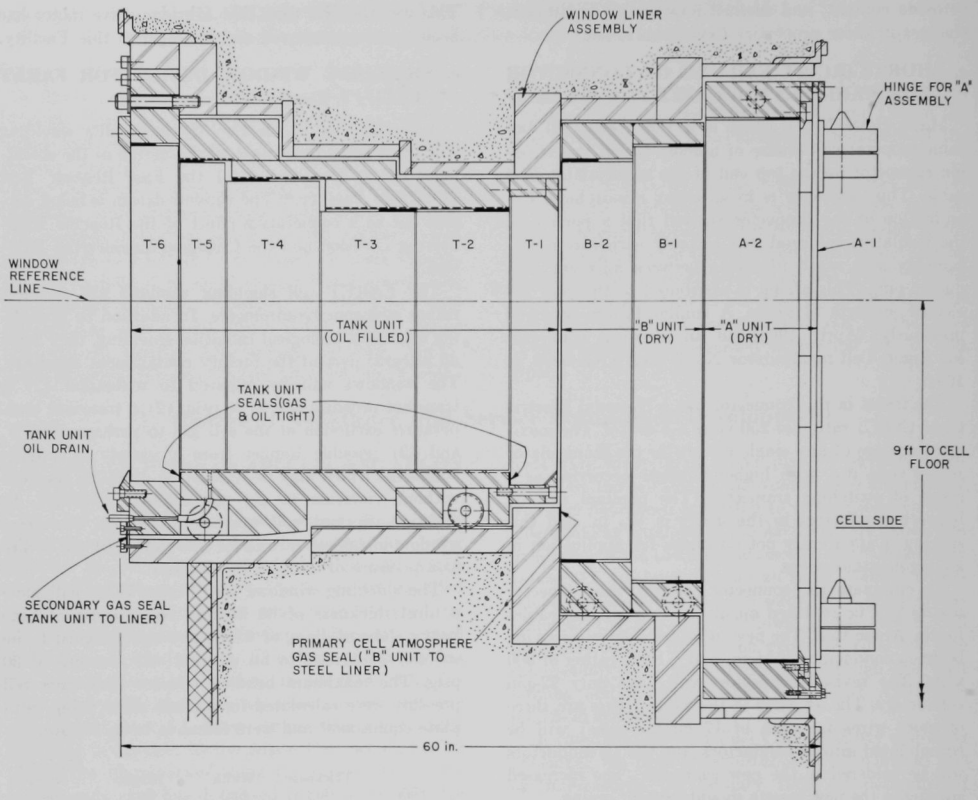

108-9096

FIG. I-24. Vertical Section through FARET Cell Shielding Window.

and gasket designs and the method of restraining glass slabs B-1 and B-2. For the last purpose, the frame exerted pressure on only two opposite edges of one face of the glass slab to effect a seal between the opposite face of the slab and a gasket around its outer perimeter.

The steel test fixture was designed to withstand a 200 psig pressure with a deflection of <0.002 in. of the machined gasketing surface. The gasket surface had a maximum deviation from flatness of <0.003 in. and the glass surface was flat within 0.005 in.

After installation of the glass slab, the test fixture was pressurized to 12 in. Hg with compressed air for a leak test. No appreciable loss of pressure was noted over a five-day period. The fixture was then filled with water and hydraulically pressurized to 160 psig. (The maximum stress in this 8½-in. test slab at 160 psig is equivalent to that in the 6-in. B-2 window slab at 80 psig.) No liquid leak or loss of pressure was observed over a 45-min period. Strain-gage data for determining maximum bending stress were obtained by monitoring fourteen electrical strain gages installed at various locations on the exposed glass surface and two strain gages on the steel structure during an initial pressure cycle to 60 psig and two test cycles to 160 psig. Using the strain-gage data, the maximum bending stress was calculated to be about 880 psi. Using the thin-plate equations,[46] this maximum bending stress was calculated to be 960 psi.

Following the release of pressure and drainage of water, the fixture was pressurized to 12 in. Hg with helium. At the end of 12½ days the pressure had dropped to 8 in. Hg, indicating a leak rate of 0.03 scf/day.

It is concluded that the heavy slabs of glass proposed for the window design will be satisfactory for sealing against the 30 psig pressure specified for FARET and that the use of simple flat Koroseal gaskets, ⅛ in. thick by 1 in. wide, will be feasible. Flatness tolerances on the steel structure need be no closer than 0.005 in. No machined recess or groove for gasket retention will be necessary.

2. Process Equipment Development

a. SERVICE EQUIPMENT (L. F. Coleman, J. O. Ludlow, W. E. Miller)

Operation of equipment in the EBR-II Fuel Cycle Facility Argon Cell and in argon atmosphere gloveboxes has disclosed a number of process and equipment problems uniquely attributed to operation in a dry argon environment. The lubricating and wetting properties of certain materials are changed markedly when their environment is changed from air to dry argon. Heat transfer rates for natural or forced convection, under otherwise identical conditions, are less in argon than in air. The dielectric strength of argon is much less than that of air.

To investigate these effects, the Chemical Engineering Division, Argonne, has designed and constructed an argon-atmosphere environment system (Figure I-25). The system, whose construction is now complete, consists of two gloveboxes, a large inert-atmosphere enclosure and an associated argon gas purification system (see ANL-6900, pp. 115–116, and ANL-6925, pp. 56–58). The gloveboxes are being used for the development of equipment and for testing of component parts. The large enclosure is being used for the operation and testing of pyrochemical equipment and processes designed for use in the Fuel Cycle Facility Argon Cell or similar cells with an argon atmosphere. The purification system is very similar to that used for the Argon Cell[47] and utilizes prototype equipment which was used in the development of the Argon Cell purification system.

(1) Glovebox Tests of Vanes for Rotary Blower (G. J. Bernstein, D. Grosvenor)

A vane-type rotary blower is being considered for recirculating and purging the argon atmosphere within the skull oxide reduction and purification (M-2) furnace now installed in the large inert-atmosphere enclosure. In order to determine if the performance of the blower vanes is affected by the low concentrations of oxygen and water vapor in the furnace atmosphere, testing was carried out with vanes fabricated of various materials. Blower vanes of graphite or graphite-impregnated Teflon were operationally tested in one of the gloveboxes of the argon atmosphere enclosure system. The concentrations of oxygen and water in the glovebox argon atmosphere were each less than 20 ppm. Of the materials tested, the graphite vanes proved unsatisfactory because of excessive wear. The graphite-impregnated Teflon vanes showed only nominal wear; the weight losses after 16 and 104 hr of continuous operation were 2% and 2.4%, respectively. A substantial part of the initial weight loss was apparently due to the wearing-in of the vanes. The rotary blower with graphite-impregnated Teflon vanes has been installed in the large enclosure for use with the M-2 furnace. The radiation stability of graphite-impregnated Teflon is being determined. Samples of this material are being irradiated in the EBR-II Argon Cell.

(2) Large Inert-Atmosphere Enclosure (J. H. Schraidt, L. F. Coleman, J. O. Ludlow, W. Miller, M. A. Slawecki, R. Malecha[43])

The construction of the large inert-atmosphere enclosure has been completed. Figure I-26 shows an interior view of the enclosure. The enclosure is about 24 ft long, 12 ft wide, and 14 ft high. Manipulations are performed with a remotely controlled 1-ton crane and through glove ports mounted in the windows in the cell walls. Power for the crane is supplied from a variable-frequency generator to permit continuously variable speed control over a range of about 5 to 1. Three 3-ton capacity refrigerated cooling units are provided for heat removal. Two vacuum transfer locks are available for the transfer of items into and out of the enclosure. One lock, a 35-in. ID by 69 in. high cylinder (Figure I-25) is capable of handling large-sized objects and the other lock, 7¾-in. ID by 28½ in. long, is for routine handling of small-sized objects. A removable section of the roof, 7½ ft wide and 11½ ft long, allows the introduction of very large pieces of experimental apparatus, including new crane bridges and trolleys.

As a safety measure, a pressure relief bubbler was designed, fabricated, and connected to the enclosure. The relief bubbler furnishes a means of venting the large enclosure in the event the cooling system fails at the instant that the maximum heat load is introduced. This maximum heat load occurs when the

[47] J. H. Schraidt, L. F. Coleman, W. F. Holcomb, M. Levenson, and J. O. Ludlow, Establishing and Maintaining a High Purity Atmosphere in EBR-II Fuel Cycle Facility Argon Cell, *Proceedings of the Eleventh Hot Laboratories and Equipment Conference, New York, Nov. 18–21, 1963*, pp. 181–190.

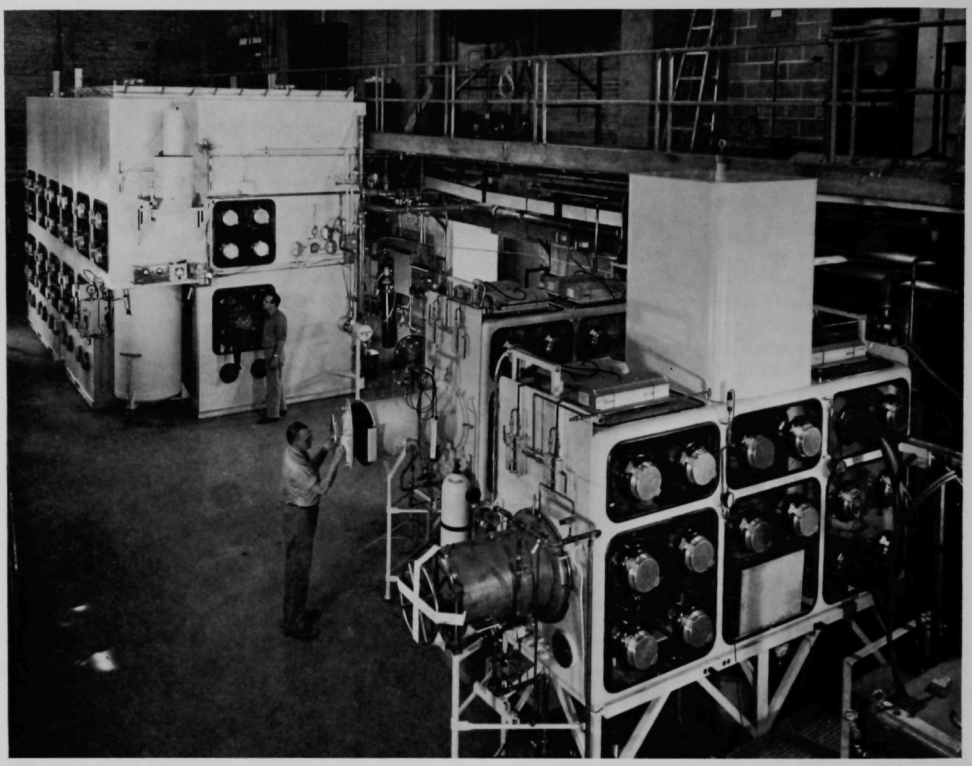

108-8726

FIG. I-25. View Showing Argon-Atmosphere Environment System.

The environment system consists of three primary components:

(1) Two gloveboxes (lower right foreground) which are used for equipment component testing and process development. The glovebox having a top blister (right foreground) contains distillation apparatus used in small-scale zinc-magnesium distillation tests.

(2) A large enclosure (left background), 24 ft long, 12 ft wide, and 14 ft high, which is utilized for operating prototype process and auxiliary equipment designed for use in the EBR-II Fuel Cycle Facility Argon Cell. The vertical cylinder in the corner niche of the large enclosure is a vacuum transfer lock for the transfer of large items into and out of the enclosure. A small transfer lock is also available for routine transfer of small-sized objects.

(3) An argon purification system (not shown).

heaters for the skull oxide reduction and purification (M-2) furnace are opened after a heating cycle. Opening the heaters exposes the furnace body (at about 800°C) which, during the cooling cycle, would radiate heat to and heat up the gas atmosphere in the enclosure. The bubbler is designed for pressure relief at plus two inches of water and for vacuum relief at minus four inches of water. The enclosure is maintained at a plus pressure of about 0.8 in. of water; thus, any leakage is outward. Argon gas is automatically added to or removed from the enclosure to maintain the gas inventory required.

Argon gas has been introduced into the large (4000 cu ft) enclosure. Approximately 7100 cu ft of argon gas from liquid argon cylinders was used to displace the air in the enclosure. This resulted in the displacement of about 94% of the air originally present in the enclosure. Following the air displacement step, purification of the enclosure atmosphere was carried out. A general description of the purification system is as

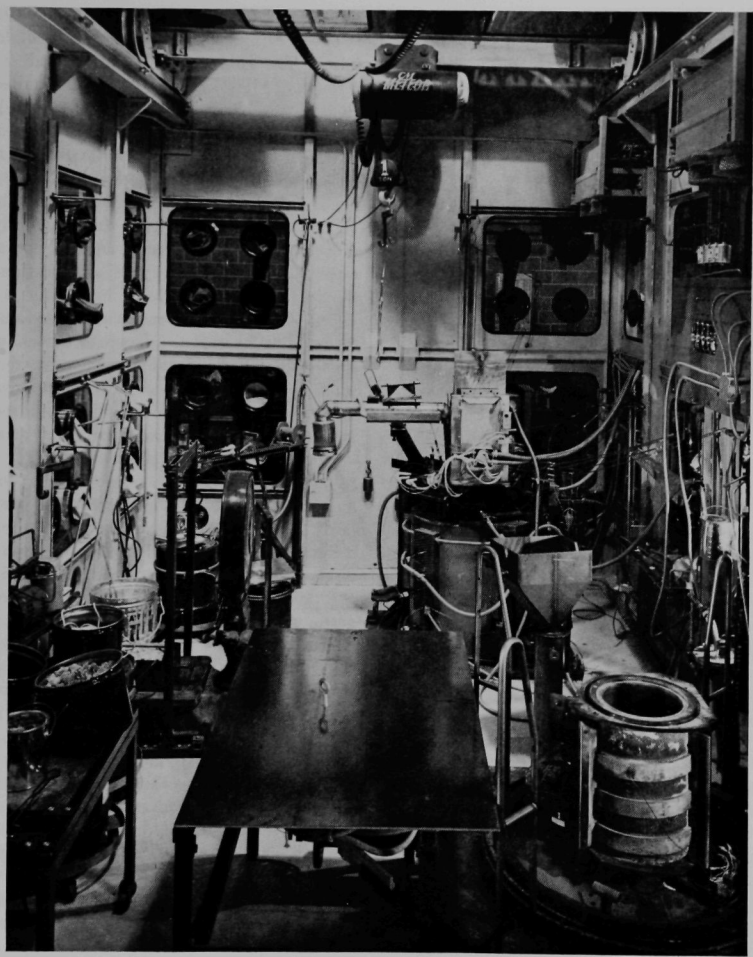

108-8728

FIG. I-26. Interior View of Large Argon-Atmosphere Enclosure.

Equipment for pyrochemical processes (skull reclamation) will be operated in an argon atmosphere in a large enclosure (24 ft long, 12 ft wide, and 14 ft high) to determine environmental effects on equipment performance. Manipulations are performed with a crane or through gloves mounted in 29 windows in the cell walls. Services for the equipment are provided through service ports located below the windows in the cell walls. Fluorescent fixtures (not shown) are mounted above three of the ten roof windows to provide lighting. Three 3-ton capacity refrigerated cooling units are provided for heat removal; two are shown above windows in the right-hand wall. A skull oxide reduction and purification (M-2) furnace is seen at the right rear with agitator and transfer line installed. A scale for weighing process waste materials and product solutions transferred from the M-2 furnace is at the left middle. Temporary transfer receiver equipment is being used for initial M-2 furnace tests. Pails containing fresh flux are shown on the table in the left foreground. A charging chute for the M-2 furnace is at the middle right. The induction heater portion of the zinc-magnesium distillation apparatus of the retorting furnace is shown on a base plate in the right foreground. A skull oxidation furnace (not shown) is used to prepare unirradiated uranium or fissium oxides for tests of the skull reclamation process.

follows: the oxygen in the enclosure atmosphere is reacted with hydrogen on a palladium catalyst bed; the product water and the water vapor initially present are removed by means of a Molecular Sieve[48] dryer. The concentrations of impurities in the enclosure atmosphere are being maintained at the same concentrations as in the Fuel Cycle Facility Argon Cell. These concentrations are as follows: nitrogen, about 5 v/o; oxygen or water, between 20 and 60 ppm each.[49] Nitrogen will be periodically added to the system (enclosure plus purification system) to maintain the desired concentration.[50]

A preliminary test indicates that the oxygen is entering the system at a low rate, 55 ml/hr. If the oxygen inleakage (plus diffusion) rate remains low, the system can be maintained at the desired oxygen concentration by adding hydrogen to the flowing stream for only a few minutes near the end of each day. After the water concentration in the enclosure has been reduced to 20 ppm, the water concentration can be prevented from going below the desired value by limiting the flow of gas circulated from the enclosure to the purification system.

An analysis of the results of the air displacement step and the enclosure-atmosphere purification step indicates that the enclosure contained 14 to 20 cu ft of oxygen in excess of that attributed to residual and leaked air. The source of this oxygen is not known, but may have been the cylinders which contained the argon used to displace the air. The composition of the argon used in future additions of the gas will be analyzed.

The trolley motor on the 1-ton hoist failed and was removed from the carriage and from the enclosure without affecting the purity of the enclosure atmosphere. Since the motor failure occurred after the enclosure had been filled with argon, its operation in the argon atmosphere is thought to be the cause of failure. Examination of the burned section of end windings in the motor gave no definite indication as to the direct cause of the failure, except that the insulation had burned as a result of overheating with a resultant grounding of a coil. The hoist had been in operation for approximately 3 months in air and for about 1½ weeks in argon before failure. Actual running time of the trolley motor is not known, but it is estimated at about ½ to 1 hour. The most plausible cause of failure is overheating[51] which resulted in breakdown of insulation. The hoist had been purchased as a standard 1-ton unit; however, actual loads handled in the enclosure were limited to a maximum of ½ ton. This method of de-rating, however, is applicable only to the hoist motor and not to the trolley motor which operates at or nearly at its full load rating whether or not the hoist is loaded. In addition, the motor, under variable frequency control, draws slightly more current at the high frequency range of operation than it would at a standard 60 cycles of operation. As a result, the trolley motor may have, in fact, been operating at higher than rated current. The burned-out motor was rewound with a higher temperature insulation wire and was re-installed on the carriage by remote means. Measurements of the trolley motor current will be taken, both with and without loads, to see if any difference in the trolley motor current exists for these two cases. The hoist manufacturer will be contacted to see if a larger capacity trolley motor, with the same mounting configuration, can be purchased for the hoist. Meanwhile, in order to lower the motor current, a limitation has been placed on the upper frequency used for control of motor speeds. It is planned to install running time meters in order to record actual accumulated running times.

The plant-scale apparatus[52] for the skull reclamation process is to be tested in the large enclosure. The status of this apparatus is as follows:

1. A skull oxidation furnace has been installed and is operational.
2. A skull oxide reduction and purification (M-2) furnace and associated auxiliary equipment have been installed and are being operationally tested, with and without process reagents, for checkout of equipment and controls and for training of personnel.
3. Retorting apparatus has been installed, and preliminary testing of the induction heating system carried out.

b. SKULL OXIDE PROCESSING EQUIPMENT

(L. Coleman, G. Bernstein, T. Eckels, D. Grosvenor, J. Ludlow, W. Miller, M. Slawecki, E. Johnston, P. Kelsheimer, R. Malecha[44])

At the conclusion of the EBR-II fuel melt refining operation, a residue (skull) remains in the processing

[48] A product of Linde Air Products Co., New York.

[49] The argon purification system for the Fuel Cycle Facility Argon Cell is capable of achieving much lower concentrations of oxygen and water. However, oxygen and water are being purposely maintained at these higher levels to reduce wear in graphite bearings and motor brushes and to improve the operation of equipment having metal parts wetted by sodium.

[50] For a detailed description of the argon purification system and a discussion of its operation, see previous semiannual reports, ANL-6900, pp. 116–117 and ANL-6925, pp. 56–58.

[51] Because of the poor heat-transfer properties of argon compared with air, the demand on a motor that is operated in argon should be limited to 70% of the rated capacity of the motor.

[52] The equipment to be used in the EBR-II Fuel Cycle Facility is sized for operation with a batch size of about 5.8 kg of skull oxide (~5 kg of uranium oxide).

crucible. A skull reclamation process is being developed for recovering the fuel material from the skull and removing fission products from the recovered fuel material (see ANL-6818 and ANL-7020, p. 17). The skull reclamation process includes the following basic steps: (1) oxidation of the skull, (2) extraction of noble metal fission products from the skull oxide, (3) reduction of the uranium oxide, (4) precipitation of a uranium-zinc intermetallic compound, (5) decomposition of the intermetallic compound, (6) dissolution of the uranium cake formed from the decomposition step, and (7) retorting of the uranium solution to yield a uranium ingot. A skull oxidation furnace for converting the skull to a free-flowing oxide powder (step 1) has been built and is being operated in the Fuel Cycle Facility (see ANL-6900, pp. 116–120). Equipment for processing skull oxides in the Fuel Cycle Facility is being built and tested by the Chemical Engineering Division at Argonne (see ANL-6925, pp. 58–62). The equipment to be used in the Fuel Cycle Facility is sized for operation on about 5.8 kg of skull oxide (~5 kg of uranium oxide).

The primary components of the skull oxide processing equipment are a skull oxide reduction and purification (M-2) furnace, a transfer line, transfer receiver equipment, and a retorting furnace for recovery of the uranium product. These components are briefly described below.

The reduction of uranium oxide to uranium metal and the gross separation of the uranium metal from fission products are to be carried out in the M-2 furnace (see Figure I-27). Process reactions will be performed in a tungsten crucible. For tests of the Fuel Cycle Facility plant equipment, a full-sized, pressed-and-sintered tungsten crucible (14-in. ID by 23¾ in. deep) has been procured.

The operations to be conducted in the M-2 furnace require several heating and cooling steps. To reduce the effects of fission product heating and the time necessary for cooling the crucible, the furnace was designed to enhance the rate of heat dissipation. The furnace body is a Hastelloy C[53] open-top cylinder which fits closely around the tungsten crucible. Heating of the furnace body is accomplished by a close-fitting 20-kw resistance heater in the form of a vertically split cylinder. Each heater half is rated at 10 kw and is divided horizontally into three independent heater sections to permit close control of the furnace body wall temperature. The cylinder halves are externally insulated and are held closed around the furnace during heating cycles (see Figure I-28a). When the furnace is to be cooled, the cylinder halves are opened by gas-operated, double-action cylinders to expose the furnace body (see Figure I-28b).

Skull oxide contained in zinc storage cans will be charged to the furnace through a charging chute. The charging chute consists of an assembly of four Mo-30 w/o W rods which protect the agitator and transfer line from damage during additions of the storage cans. One of the rods is hollow and serves as a thermocouple protection tube. Other process reagents (granular forms of zinc, magnesium, and flux) will be charged through a removable hopper which is placed into the charging chute for this purpose. The process reagents in the crucible will be mixed by means of a four-bladed Mo-30 w/o W agitator (see ANL-6925, pp. 58–61). The molten metals and flux will be transferred from the crucible through a heated transfer line (see Figure I-29) fabricated of Mo-30 w/o W. The transfer will be accomplished by pressurizing (14 to 15 psig argon) the furnace. (Fabrication details are described in ANL-6925, p. 61.) The transfer line is connected between the M-2 furnace and the transfer receiver equipment (see Figure I-30). The transfer receiver will provide for purging the transfer line, collecting and weighing the transferred material, and collecting furnace fumes which accompany the material. Materials transferred from the M-2 furnace will include: (1) metal and flux wastes which will be collected in 8-gal steel pails, and (2) uranium-zinc-magnesium product solution which will be cast into a mold. Operation of the transfer receiver is described in ANL-6925, pp. 61–62. The final material transferred from the M-2 furnace will consist of about 4 kg of uranium in approximately 36 kg (~8 liters) of Zn-12 w/o Mg-12 w/o U (nominal composition). Plant-scale distillation apparatus (Figure I-31) has been built to recover the uranium by distilling off the volatile zinc-magnesium (see ANL-6925, pp. 62–65).

Except for the transfer receiver equipment, all equipment items have been installed in the large inert-atmosphere enclosure. Temporary transfer receiver equipment has been installed for tests of the M-2 furnace.

Effect of Fission Product Heat on the Operation of the M-2 Furnace. The skull reclamation process involves a number of heating and cooling operations. These operations are designed to separate uranium from fission products in a series of process steps in which liquid metals and salt fluxes are employed. These steps require heating and cooling the processing media between temperatures of approximately 800°C and 425°C.

In the noble metal extraction step (see ANL-6818, p. 10), the skull oxide is suspended in molten flux and the noble metal fission products in the skull oxide are

[53] A product of the Haynes Stellite Company.

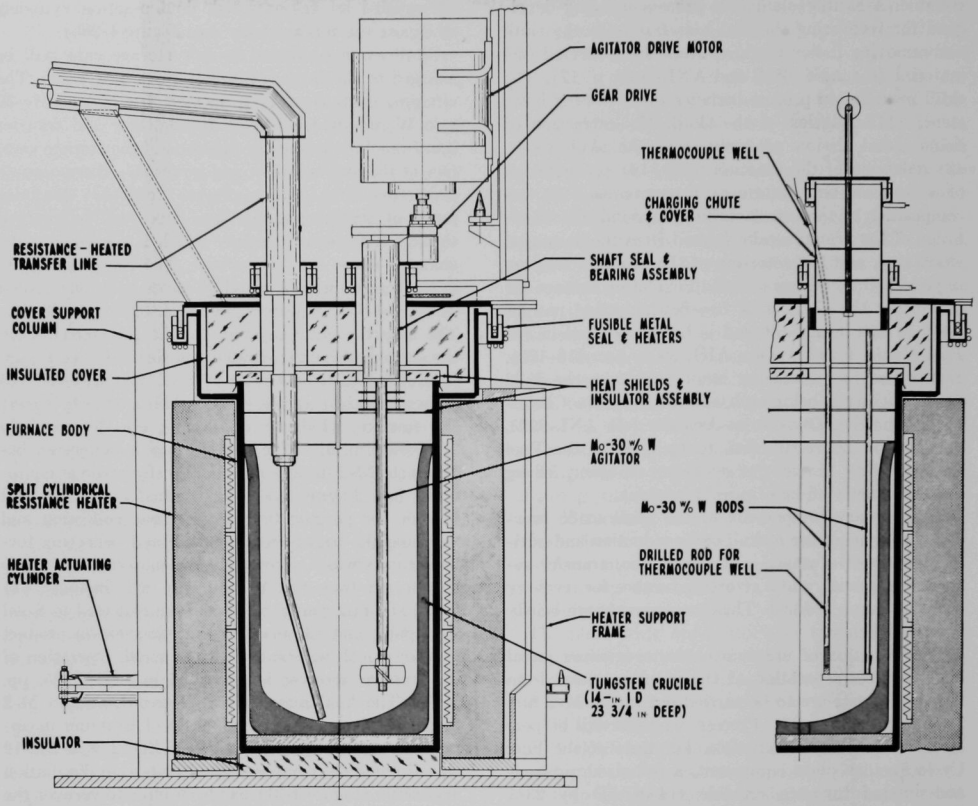

108-8540 Rev.

FIG. I-27. Skull Oxide Reduction and Purification (M-2) Furnace (Vertical Sections).

The drawing at the left shows the large tungsten crucible inside the furnace body. The drawing at right shows the charging chute, which is an assembly of four Mo-30 w/o W rods that protect the agitator and transfer line from damage by materials charged to the furnace.

selectively reduced by and extracted into molten zinc at 800°C. The process provides for separation of these two phases by freezing the flux (melting range 560 to 600°C) and pressure-siphoning the zinc phase (m.p. 420°C).

The scale of operation planned for the skull reclamation process in the EBR-II Fuel Cycle Facility will treat skull oxides from five melt refining skulls (approximately 5.8 kg of skull oxide). On such a scale, the heat output of fission products in the skull oxide charge is estimated to be about 3.6 kw (see ANL-6605, pp. 21 and 71).

The furnace must provide for adequate removal of the fission product decay heat as well as sensible heat (800°C to 425°C) in order to permit the above phase separation to take place. A cooling test was performed on the M-2 furnace which contained an empty, plant-scale pressed-and-sintered tungsten crucible. This test showed that at the start of the cooling cycle (when the crucible is at 800°C), the heat loss rate is about 12 kw. The rate drops to about 6 kw at a crucible temperature of 425°C. Thus, the loss of heat from the crucible would overcome the effects of fission product heating under process conditions. Calculations based upon this cooling test showed that the crucible and its contents under process conditions will cool from 800°C to 425°C in about 2½ hr.

However, at the end of the noble metal extraction

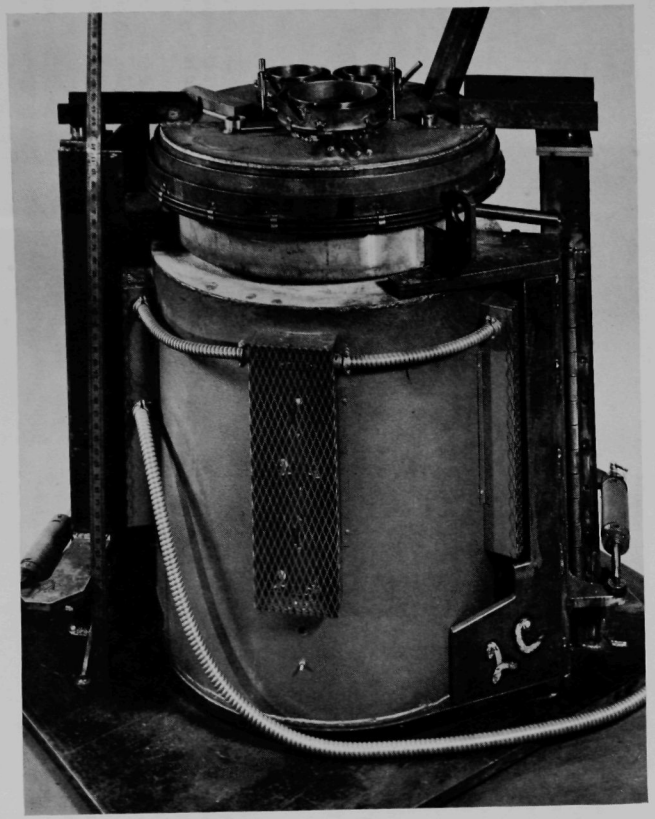

108-8138

a

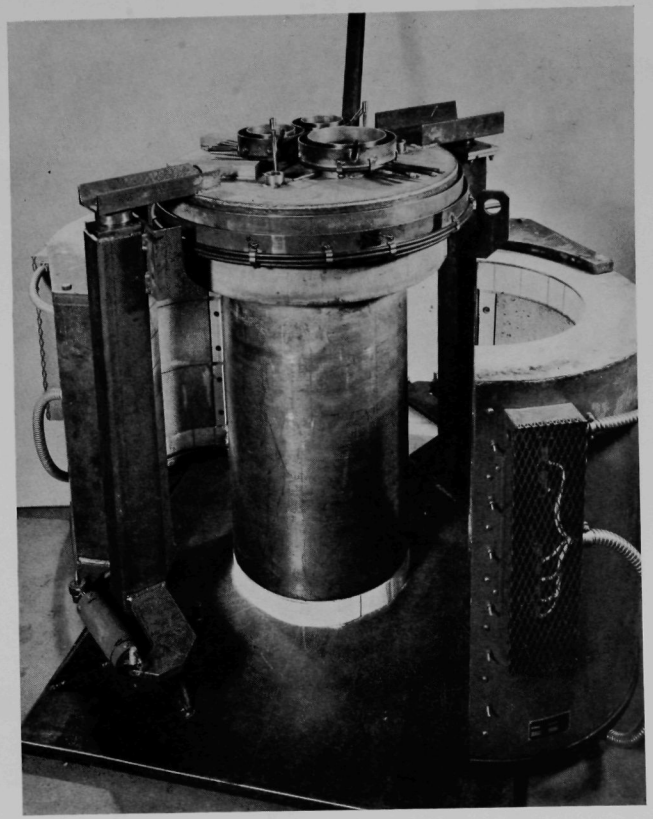

108-8136

b

FIG. I-28. Skull Oxide Reduction and Purification (M-2) Furnace Shown with Heater Halves in the Closed and Open Positions. Gas-operated, double-action cylinders hold the heaters around the furnace body during the heating cycles and open the heaters during the cooling cycles.

(a) Heater halves shown in the closed position. (The scale of the ruler is in inches.)

(b) Heater halves shown in the open position.

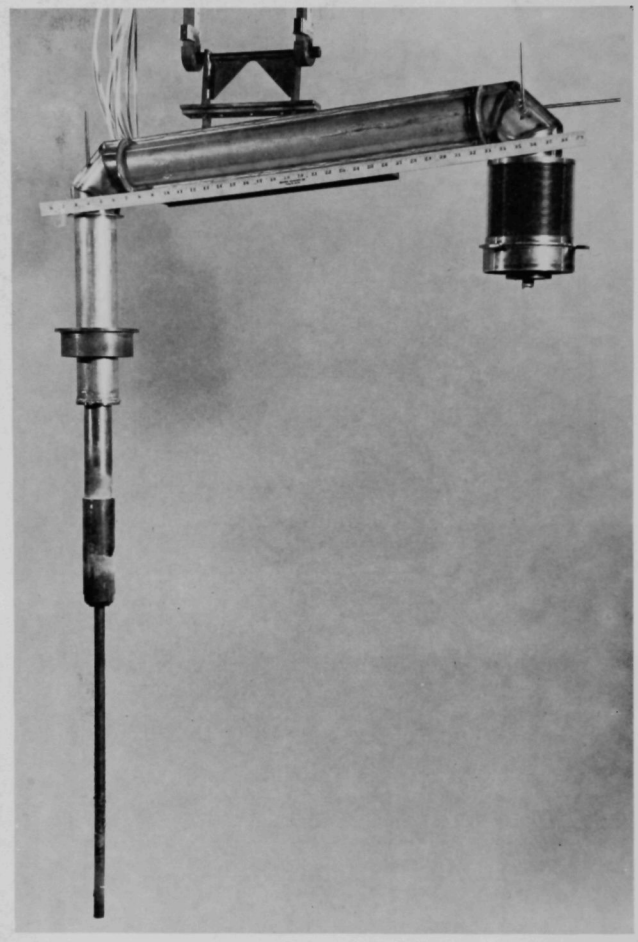

108-8170

FIG. I-29. Heated Transfer Line for M-2 Furnace.

The longer end of the transfer line dips into the furnace crucible, as shown in Fig. I-27. The bellows assembly located at the discharge end of the transfer line allows for thermal expansion when the transfer line is connected between the furnace and the transfer receiver equipment (see Figure I-30). The transfer of molten product and molten waste materials will be carried out by pressurizing the furnace to 14 to 15 psig argon. (The scale of the ruler is in inches.)

step, the major heat-producing fission products are concentrated in the flux layer. For the proper separation of solid flux and molten zinc, it is necessary for the fission product heat to be removed from the flux while it is below its freezing temperature (560–600°C) and the zinc remains above its freezing point (420°C). A heat transfer study in 1961 showed that the required condition could be achieved.

Since that time, the process and the furnace have undergone substantial changes. It was therefore de-

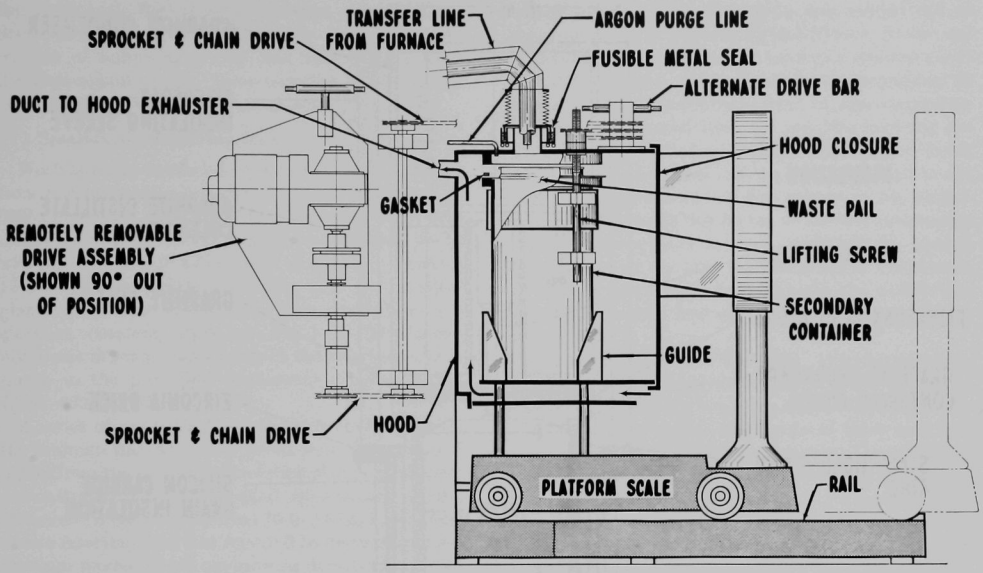

108-8568

FIG. I-30. Transfer Receiver for Skull Reclamation Process.

cided to re-examine the effects of fission product heating on the solidification of the flux at the end of the noble metal extraction step.

The new calculations are based upon a flux layer that is 4 in. thick and has an estimated thermal conductivity of 0.00338 cal/(sec) (cm) (°C). There are two primary routes for heat to escape from the flux. One route is through direct contact with the molten zinc and the crucible. The other route is by radiation and convection from the top surface of the flux to the exposed crucible wall surface. (Heat shields above the crucible prevent significant heat loss to the furnace cover.) On the assumption that the heat flow by the two routes is approximately equal, the maximum temperature of the flux will be at its center. The calculations show that this temperature will be about 310°C higher than the temperature of the zinc phase below the flux. Accordingly, all the flux cannot solidify while the zinc is still molten.

Nevertheless, separation of molten flux and zinc phases can be accomplished by the pressure-siphoning technique. However, the transfer of molten zinc from the crucible will have to be terminated before any molten flux enters the transfer line. This is accomplished by weighing the zinc as it is transferred and quickly venting the furnace when the required amount of zinc has been transferred. This technique has recently been demonstrated in semiworks runs. The elimination of the requirement for freezing the flux will result in a reduction in operating time for the process since the transfer can take place at temperatures higher than the formerly required temperature of 425°C. In addition, consideration is being given to a change in the flux composition which will lower its freezing point and reduce the possibility of accidentally plugging the transfer line with solid flux.

c. RECOVERY OF URANIUM PRODUCT (W. Miller, J. Lenc, M. Slawecki, J. Harast, A. Chandler, R. Paul)

The final material transferred from the skull oxide reduction and purification furnace consists of about 4 kg of uranium in approximately 36 kg (~8 liters) of Zn-12 w/o Mg-12 w/o U. Development work is being conducted on recovering uranium from this solution in a form suitable for use as supplementary make-up feed material for the melt refining process. Plant-scale equipment is under development to recover the uranium by distilling the volatile zinc-magnesium. Work during this reporting period has

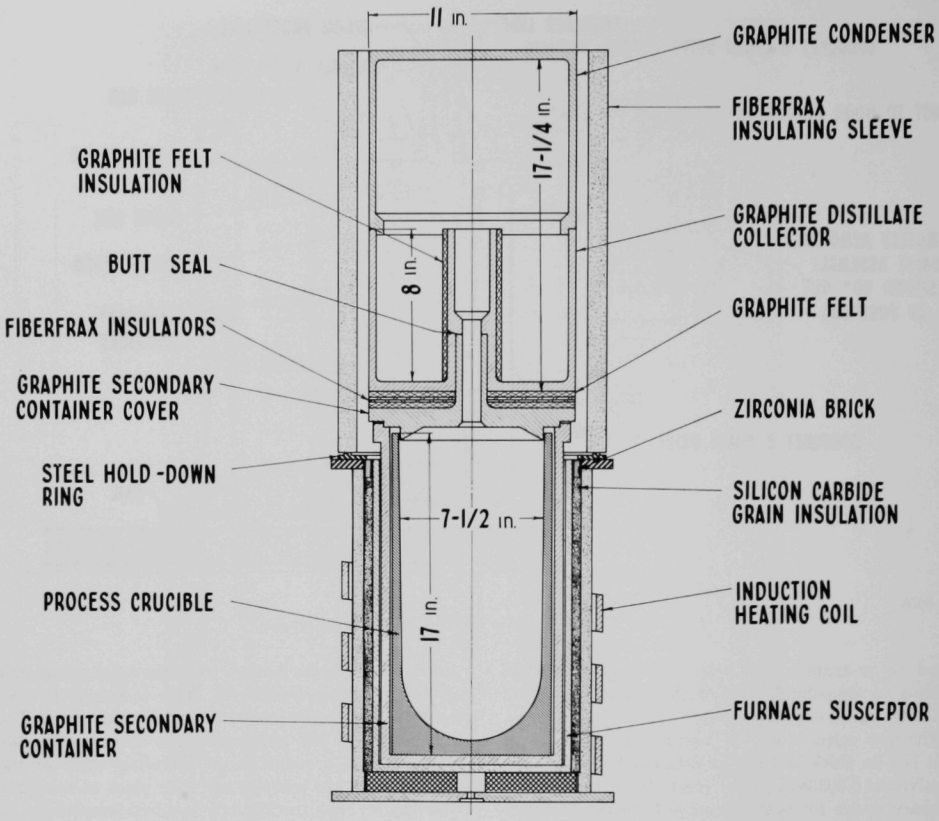

108-8736

FIG. I-31. Plant-Scale Apparatus for Retorting Zinc-Magnesium. (This apparatus is to be used in the EBR-II Fuel Cycle Facility and is sized for operation with the product reclaimed from about 5.8 kg of skull oxide.)

included distillation of Zn-Mg alloy from the uranium product, uranium-hydriding experiments, and use of uranium hydride as make-up material for melt refining (see ANL-6925, pp. 65–68). All runs were made with tungsten crucibles, which are being considered as an alternative to beryllia crucibles in the retorting step. [Small-scale BeO crucibles produced by different fabricating techniques have been tested and have shown variable performance (see ANL-6925, pp. 64–66).] However, tungsten crucibles cannot be substituted for beryllia crucibles without some modification of the final product recovery step of the skull reclamation process. The need for the modification is brought about by the fact that the uranium product remaining in the crucible (after zinc and magnesium have been distilled off at temperatures up to 950°C) adheres to the bottom of a tungsten crucible. Moreover, if the uranium product is consolidated by liquation (1150–1250°C), the tungsten crucible is severely attacked by the molten uranium.[54] A possible means for overcoming these difficulties is hydriding of the uranium product at 250 to 330°C, after distillation of zinc and magnesium has been completed, to convert the retorted uranium product to a free-flowing powder that can be transferred from the tungsten crucible.

Although hydriding of the retorted product would permit the use of tungsten crucibles, it would be desirable to avoid this additional processing step. Consequently, beryllia crucibles continue to be considered for use in the retorting operation. A thixotropically-

[54] Beryllia crucibles are not attacked or wetted by molten uranium.

cast plant-scale BeO crucible has been obtained from Brush Beryllium Co. A plant-scale isopressed BeO crucible of improved quality has been ordered from the same manufacturer. These crucibles will be tested in the plant-scale retorting apparatus.

(1) Small-Scale Retorting Runs

Work is being continued on the recovery of uranium from zinc-magnesium-uranium by retorting (see ANL-6925, pp. 62–64). The retorting experiments have been conducted with 5- to 7-kg charges of nominal Zn-12 w/o Mg-10 w/o U.[55] (This scale of operation is about 15% of the plant scale and about 45% of the pilot-plant scale.) The experiments were conducted in a glovebox containing argon (see Fig. I-25). The assembly of the internal components of the retorting unit is shown in the preceding semiannual progress report (ANL-6925, p. 62, Fig. I-25).

A series of retorting runs was conducted to recover the uranium present in the Zn-12 w/o Mg-10 w/o U ingots from the uranium dissolution step of pilot-scale demonstration runs of the skull reclamation process. Since each ingot weighed from 10 to 13 kg, a minimum of two retorting runs was required to recover the total uranium product from one process demonstration run in the pilot plant.

The same general experimental procedure was used in all the retorting runs. The Zn-12 w/o Mg-10 w/o U charge was placed in a pressed-and-sintered tungsten crucible. The crucible and other components of the retorting apparatus were then assembled. The distillations were carried out at temperatures up to 950°C and at argon pressures between 1 and 50 torr. Following the distillation step, the uranium was converted to uranium hydride (see following section on Uranium Hydriding Experiments).

Two retorting runs (GBD-23A and GBD-23B) were made with charges which simulated an incomplete transfer of the flux from the uranium reduction step (see ANL-6800, p. 61). The flux heel would be transferred along with the uranium product ingot (Zn-Mg-U) to the retorting crucible. The charges consisted of Zn-12 w/o Mg-10 w/o U (from skull reclamation demonstration run SKR-9) and unused, pretreated flux ($MgCl_2$-50 w/o $CaCl_2$)[56] containing added MgO and Ce_2O_3 to simulate the process flux heel. In the first run (GBD-23A), the feed was composed of about 4.6 kg of Zn-Mg-U ingot, 200 g of flux, 20 g of MgO and about 5 g of Ce_2O_3. (This quantity of flux heel would represent a very poor flux transfer after the uranium reduction step.) The distillation was carried out at argon pressures of between 32 and 50 torr. At the end of the run, the uranium retort product contained about 25 g of flux, oxide, and undistilled zinc-magnesium as impurities. An appreciable amount of zinc-magnesium and flux had escaped from the graphite retorting enclosure and condensed on the wall of the water-cooled bell jar enclosure. This leakage was attributed to the relatively large amount of flux present in the charge. The layer of molten flux on top of the zinc-magnesium metal phase appears to have inhibited the normal vaporization of the zinc and magnesium. Distillation of the zinc-magnesium from beneath the molten flux resulted in a great deal of spattering of the melt from the crucible.

In the second run (GBD-23B), two changes were made in the operating conditions in order to achieve more nearly complete retorting of the zinc-magnesium and flux and to reduce the escape of these materials from the graphite retorting enclosure. These changes were: (1) reducing the amount of flux heel in the feed, and (2) carrying out the distillation at a pressure lower than that in the first run in order to improve the distillation of the molten flux layer. The feed was composed of about 5 kg of Zn-Mg-U ingot, 88 g of flux, 9 g of MgO, and 2 g of Ce_2O_3. This feed was charged to the crucible containing the retort product from the first run. Except for a new graphite condenser, the distillation apparatus was the same as that used in the first run. The distillation was carried out at temperatures up to 950°C and at an argon pressure of less than 1 torr. At the end of the run, the retorted product was mainly in the form of a metallic, sponge-like mass which adhered to the crucible bottom; a small amount of the material adhered to the crucible sidewall. A considerable amount of zinc-magnesium and flux had escaped from the graphite retorting enclosure and condensed on the wall of the water-cooled bell jar enclosure. The graphite condenser, collector, and secondary container cap, which were bonded to each other by condensed metal and flux, could not be disassembled and were removed as one piece. They were readily lifted off the secondary container. The vapor opening above the retorting crucible was almost completely plugged with condensed material. [In previous retorting runs, the presence of very small amounts of flux (~10 g) which had been transferred along with the uranium product solution (Zn-Mg-U) did not result in bonding of the components of the distillation apparatus to each other.] On the basis of these observations, it is planned to examine each zinc-magnesium-uranium ingot before retorting it and to remove by mechanical means any visible flux layer.

Additional retorting runs (GBD-24A, GBD-24B,

[55] The uranium concentration in the product solution from pilot-scale runs was approximately 10 w/o rather than the 12 w/o stipulated in the process flow sheet.

[56] The flux was pretreated with magnesium to remove residual moisture.

and GBD-25A) were made in order to obtain uranium product for use in hydriding experiments.

Runs GBD-24A and GBD-24B were made with 7-kg charges of Zn-12 w/o Mg-10 w/o U (from skull reclamation demonstration run SKR-24). The distillations were carried out at argon pressures between 20 and 30 torr and were satisfactorily completed. However, after each of the runs, a metallic product (probably uranium) was found in the annulus between the tungsten crucible and the graphite secondary container. The tungsten crucible (the only crucible available for these runs) had been used previously in semiworks experiments and was known to have a crack running vertically downward from the top edge. Leakage of melt had not occurred in the semiworks experiments because the charge sizes were smaller and the liquid level consequently lower.

In retorting run GBD-25A, in which the same crucible was used, the charge was 6 kg of Zn-12 w/o Mg-10 w/o U from skull reclamation demonstration run SKR-26. Operation was terminated before completion of retorting when a short occurred in the induction coil owing to leakage of metal through the vapor seal between the graphite container and its graphite cap. The melt had leaked through the crack in the upper portion of the tungsten crucible into the annulus between the tungsten crucible and the graphite secondary container. After a new induction coil was installed, the remaining Mg-Zn was distilled from the uranium in the crucible.

(2) Uranium Hydriding Experiments

Hydriding experiments were carried out to determine if the hydriding technique could be used to remove (1) the uranium product from a tungsten crucible after the distillation step and (2) the product from the uranium-zinc intermetallic decomposition step (see ANL-6800, p. 61). Tests were also carried out to determine if the uranium hydride formed could be utilized as make-up fuel material in the EBR-II melt refining operation.

Following the distillation step in all the small-scale retorting runs described above, the material contained in the tungsten crucible was subjected to a hydriding procedure. The hydriding was carried out in a hydrogen atmosphere (1-atm pressure) at temperatures between 250°C and 330°C. In each case, the uranium product remaining in the crucible was completely hydrided and was easily dumped. The hydrided material (~970 g) from runs GBD-23A and GBD-23B was used as make-up material in one of the melt refining runs discussed in the following paragraph.

Two melt refining runs with unirradiated fuel material were carried out in a zirconia crucible. In both runs, the furnace atmosphere during melt refining was argon (1 atm), and the molten metal was held at 1400°C for 2 hr. In the first run, a charge of 10 kg chopped, depleted uranium-5 w/o fissium pins and 40 g sodium[57] was melt refined; the poured yield was 92.9 w/o. The surface of the ingot was bright and shiny. In the second run, the charge consisted of chopped, depleted uranium-5 w/o fissium pins (~9.1 kg), sodium (40 g) and the above-described hydrided material (~970 g). The crucible and contents were first heated at 400°C for 1 hr under reduced pressures (30 to 165 torr) in order to decompose the hydrided material. About 5 gram-moles of hydrogen was evolved and evacuated from the furnace. Following the decomposition step, the charge was melt refined; the poured yield was 93.0 w/o. The surface of the ingot was somewhat dull. The two runs demonstrated the following: (1) Uranium hydride can be decomposed and combined with fuel material. (2) The pouring yield is not affected by the presence of the material from the hydride step. (3) The quality of the ingot appears to be satisfactory. Additional runs will be made with the remaining hydrided materials to verify these results and to obtain analytical data to establish ingot quality.

Work was continued on determining whether the hydriding technique could be applied to removal of the uranium product material which remains in the tungsten crucible after the intermetallic decomposition step has been completed and the zinc-magnesium supernatant (Zn-50 w/o Mg) has been removed from the crucible (see ANL-6925, p. 67). This procedure would have the advantage of eliminating the dissolution step, which is now a means for transferring the uranium product from the crucible. The zinc-magnesium solvent required to carry out this step would also be eliminated. Thus the volume of material transferred to the retorting crucible would be decreased substantially. The load on the retorting apparatus would be reduced, and small-size beryllia crucibles could be utilized.

One additional hydriding experiment (UR-2) was carried out in a beryllia crucible. For this experiment, a charge was prepared by precipitating uranium from a zinc-50 w/o magnesium solution and decanting the supernatant metal. The precipitate, metallic uranium dispersed in the residual Zn-50 w/o Mg remaining in the crucible, was heated to 300°C for 3 hr in a hydrogen atmosphere. After hydriding, only 31% (~380 g) of the original material charged could be poured from the crucible; the poured material was in the form of powder. The remaining material was locked in the crucible and consisted of many interlocking pieces

[57] Approximately 40 g of sodium adheres to a 10-kg charge of irradiated fuel pins.

with some fines held in place by the interlocking structure.

The material remaining in the crucible was dehydrided by heating to 300°C at less than 1 torr pressure. It was then subjected to a second hydriding step similar to the first. Further breakup of the large pieces did not occur. In order to remove the material from the crucible, the interlocking structure was broken manually. The fines were then separated from the large pieces and were combined with the poured powdered material from the first hydriding step. The fines and powdered material were retorted and the uranium product recovered. The large pieces of material were retorted separately to recover the uranium. The weights and uranium content of the charge and of the material removed from the crucible are as follows:

	Weight (g)	Uranium Content (g)	Uranium Content (w/o)
Original Zn-Mg-U material	~1283	451	35
Large pieces recovered from crucible	~750	142	19.2
Fines and powder recovered from crucible	533	312	58.5

The results of this experiment and two similar experiments described previously (see ANL-6725, pp. 67–68) show that precipitated uranium enveloped in Zn-50 w/o Mg can be disintegrated by a hydriding technique. However, the degree of disintegration obtained is very dependent upon the uranium content and its distribution in the zinc-50 w/o magnesium matrix. In two of the three experiments, there was evidence that the Zn-Mg-U material was far from homogeneous; that is, considerable segregation of uranium had occurred. In these two experiments, it was not possible, with the hydriding technique, to disintegrate all of the Zn-Mg-U into fine material which would be free-flowing and therefore easily removable from the crucible. Since a high degree of segregation may occur in the plant-scale process, hydriding of the precipitate is not considered a practical way to achieve removal of the product. For this reason, the study of this method will not be pursued further.

(3) Plant-Scale Retorting Apparatus[58]

Prior to installation of the plant-scale retorting apparatus in the large argon-atmosphere enclosure, preliminary retorting tests were carried out. In these tests, charges of Zn-Mg (no uranium) were distilled from a graphite crucible at reduced pressures and at temperatures up to 950°C. The retorting apparatus (see Figure I-31) was operated in air; the atmosphere within the apparatus was argon. After the first of these tests, the design of the three-turn induction heating coil was modified in order to improve delivery of power to the retorting charge. The new induction coil, formed from ⅜-in. thick by 2-in. wide solid copper flat stock, replaced one formed from ⅝-in. dia. solid copper bar. With this new coil, distillation rates as high as 97 g/min were achieved in a run which was carried out with a 30-kg charge of Zn-14 w/o Mg at an argon pressure of 10 torr. (A 100 g/min distillation rate has been tentatively selected for plant operation in the EBR-II Fuel Cycle Facility.)

It was noted in these runs that the heat transfer rate into the Zn-Mg charge was affected by the liquid level in the crucible. This condition had not been observed in the experiments conducted in the small-scale (~5 kg of Zn-Mg) apparatus. In the plant-scale apparatus, the larger charge size of 30–40 kg of Zn-Mg resulted in a higher initial liquid level in the crucible. At the end of a distillation run with 30 kg Zn-Mg, the liquid level was 9 in. below the initial level. (The crucible was boiled dry at this point.) As the liquid level dropped, the power input to the apparatus had to be increased to maintain a constant heat input to the decreasing volume of boiling molten metal. This requirement was successfully met in these preliminary runs by increasing the power input incrementally. No operational difficulties were encountered.

After the preliminary tests, the retorting apparatus was installed in the large inert-atmosphere enclosure. The electrical circuit for inductively heating the retorting unit will be water-cooled outside the large enclosure. However, that part of the circuit inside the enclosure will not be water-cooled; it will be connected through a prototype EBR-II Fuel Cycle Facility induction heating feed-through. The feed-through is being used in the circuit in order to simulate the anticipated hook-up of the retorting apparatus in the EBR-II Argon Cell in Idaho. Data relative to transmission line losses can be obtained with this arrangement. These data should be directly applicable to the eventual operation of the retorting unit in Idaho. Tests of the induction heating system are being carried out.

[58] The apparatus to be used in the EBR-II Fuel Cycle Facility is sized for operation with the amount of product obtained by reclaiming ~5 kg U_3O_8.

C. EBR-II FUEL CYCLE FACILITY OPERATIONS (C. E. Stevenson, D. C. Hampson, M. J. Feldman, D. M. Paige)[59]

The first pyrochemical process being tested in the EBR-II Fuel Cycle Facility is melt refining. Equipment installed in the Facility for this process and for the refabrication of fuel elements is being operated with irradiated fuel. The first subassembly made from irradiated fuel processed and refabricated in the Facility has been returned to the EBR-II Reactor and is undergoing additional irradiation. Additional irradiated subassemblies have been received from the EBR-II Reactor and are being processed.

1. Operations with Equipment for Recovery of Irradiated Fuel (D. C. Hampson, R. M. Fryer, D. L. Mitchell)[59]

a. SUBASSEMBLY DISMANTLER

A subassembly dismantler serves to dismantle the fuel (and blanket) subassemblies to be processed (see ANL-6605, pp. 52–58). The dismantling machine is located in the Air Cell. To this dismantling machine, a fuel element removal machine (FERM) has been attached. The FERM provides a semi-automatic method for separating the individual fuel elements from the subassembly. (A master-slave manipulator was previously used to remove fuel elements individually from the cluster.) To separate one row of fuel elements from the grid and the remaining rows of fuel elements, wedges on the FERM are forced by pneumatic pressure first between the outermost and the adjacent row of fuel elements and then are moved forward. The fuel elements are then individually released from the wedges and allowed to fall into the inspection station. Reindexing of the wedges allows for removal of each of the remaining rows. The FERM was previously remotely installed on the dismantler to test its operability and then remotely removed and transferred to the mock-up area to allow personnel to be trained in its operation (see ANL-6925, p. 69). After completion of out-of-cell wiring and controls, the FERM was remotely reinstalled. It has been used on irradiated fuel subassemblies for the first time. The use of the FERM has reduced the time required to remove the fuel elements to ¾ hr per subassembly instead of the 2½ hr per subassembly required when master-slave manipulators were used.

When fuel subassemblies that had received a maximum burnup of 0.5 a/o were dismantled, the time required to cut the outer hexagonal stainless steel tube (ANL-6605, p. 22) was found to have increased, because of increased metal hardness, from the two minutes noted with unirradiated fuel to four minutes. It is not known whether this increase in hardness is a result of the higher irradiation that the subassembly received or of the prolonged period that the subassembly was in the hot (450°C) sodium in the EBR-II Reactor tank. The radiation level of this subassembly was 9×10^4 R/hr at one foot when it was introduced into the Air Cell.

b. FUEL ELEMENT DECANNING (AND PIN CHOPPING) MACHINE

The failure of the decanner tool bits discussed in the preceding semiannual report (ANL-6925, p. 69) has been successfully resolved by proper heat treatment of the tool bit by the supplier. One of these tool bits, currently being used, has decanned over 800 elements without difficulty.

Considerable difficulty has been encountered with irradiated fuel pins jamming in the scrap separator tube of the decanner (and pin chopper). This tube is used to guide the fuel pin from the tool bit to the fuel pin chopper and to support the fuel pin while it is being chopped. The tube diameter is about one and one-half times the pin diameter. About 6 to 7% of the decanned irradiated fuel pins have jammed in the tube. The jamming is caused by secondary breakage of the fuel pin inside the scrap separator tube as a result of the intentional breaking of the fuel pin by the fuel chopper. When the fuel pin breaks inside the separator tube, a wedge-shaped chip and tapered or nonsquare ends of the fuel pin may be formed at the break point. The forward rotational motion of the fuel pin then causes the tapered end to overlap either the wedge-shaped chip or the other portion of the fuel pin that is still in the tube. This phenomenon had not been observed when fuel pins not coated with sodium were decanned and was not as prevalent when unirradiated sodium coated fuel pins were decanned. The sodium presumably increases the jamming tendency by acting as an adhesive and thus prevents the chip or the broken end of the fuel pin from being pushed free from the tube by the advancing fuel pin. The increased breakage of the fuel pins received from the EBR-II Reactor may be a result of increased hardness owing to phase changes or irradiation effects.

In an effort to reduce the jamming in the scrap separator tube, the diameter of the exit portion of the

[59] Idaho Division.

tube was enlarged to 300 mils (more than twice the 144-mil dia. of the fuel pin). No change was made in the diameter of the entrance portion of the tube, which is 200 mils. This modification worked well as long as the sodium on the fuel pin remained in solid form; however, when the burnup of the fuel pins increased to about 0.5%, the sodium on the fuel pins liquefied, at least at the time of decanning, and the jamming reoccurred. Heating of the separator tube to about 150°C was then tried; this temperature was selected to ensure that the sodium was molten. This method appeared to work well. In one run, no jamming difficulties were encountered until the heater failed and the jams again occurred. No further tests or modifications are planned, unless trouble occurs.

The decanning unit was remotely removed from the machine and transferred from the Argon Cell to the Air Cell to determine the cause of an increasing and excessive power requirement. Examination showed that the cutting roll was badly chipped and that two of the graphite bearings were worn. The cutting roll holders were removed from the cell and decontaminated. New silver-impregnated graphite bearings were installed by hand and the shafts were lubricated with a thin film of radiation-resistant oil. Also, a new double drive-chain-and-sprocket assembly was installed to replace the single chain-and-sprocket assembly previously used. The decanner unit was reassembled in the Air Cell and run-in in the Argon Cell. Running-in was accomplished by operating with a cycle of 5 minutes on and 5 minutes off for a total running time of 30 minutes. The running time interval was then increased until a total running time of three hours was completed. At no-load, the wattage dropped from 95 watts initially to 75 watts at the end of the break-in period. During decanning, the wattage was 125 watts compared with the greater than 300 watts before the repairs were made.

Currently about 25% of the cladding scrap is failing to enter the chute of the scrap cutter and has to be removed with a master-slave manipulator. This scrap is set aside and later reintroduced to the cutter manually.

A change in the mechanical properties of the stainless steel spacer wire on the fuel elements was observed with increased burnup and residence time in the EBR-II Reactor. With fuel pins that had attained a 0.5 a/o burnup, the spacer wire on 10% of the fuel elements did not uncoil as expected when the ends of the fuel elements were sheared at decanning. When the spacer wire did not uncoil, the master-slave manipulator was used for the removal of the wire. Current plans are to continue the wire removal operation by this means.

TABLE I-10. Pouring Yields in Melt Refining Runs

No. of Runs	Purpose of Run	Average Pour Yield (w/o)
6	Unirradiated uranium-fissium alloy preparation	89.8
3	Melt refining of irradiated fuel	94.2
5	Scrap consolidation (2 irradiated, 3 unirradiated)	92.6

c. MELT REFINING AND SKULL OXIDATION

A total of fourteen melt refining runs in which 10 to 12 kg ingots of enriched uranium-fissium were produced has been made in the past reporting period. Nine of the runs have involved unirradiated fuel; six of them were made to prepare new fissium alloy and three of them were made to carry out scrap consolidation. Five of these runs have involved irradiated fuel; three of them were made with fuel not previously processed that had attained a maximum total burnup of 0.25–0.5 a/o, and two of them were made to consolidate scrap and heels from the three irradiated fuel runs. The lower burnup fuel had cooled for 4 months prior to melt refining, and the 0.5 a/o burnup fuel was out of the EBR-II Reactor for 18 days at the time of melt refining. The pouring yields obtained in these runs are shown in Table I-10. The average pouring yields for the irradiated fuel runs (94.2 w/o) and for the scrap consolidation runs (92.6 w/o) compare very favorably with the pour yields (90 to 97 w/o) obtained in pilot-scale work with unirradiated fuel.[60]

The differences in yields may be attributed to the surface condition or surface purity of the charge material. The uranium used in the fissium alloy preparation runs was in the form of thin plates that had a moderate layer of oxide on the surface. The scrap consolidation runs utilized shards and reject pins from pin processing and heels from injection casting. The heels appeared to have a heavy layer of dross on the top surface. The dross may have resulted from the graphite mold into which the ingot was cast, the thoria-coated graphite injection casting crucible, or the thoria-coated Vycor[61] injection casting molds. However, this metal is protected from contact with an air atmosphere. The irradiated fuel was handled in the inert atmosphere of the Argon Cell and should have experienced very little surface oxidation.

[60] G. A. Bennett, N. R. Chellew, and D. C. Hampson, The Melt Refining of Irradiated Uranium: Application to EBR-II Fast Reactor Fuel. V. Yields of Fissionable Material Upon Pouring, Nucl. Sci. Eng. 6(6), 511 (1961).

[61] A trade name for high-silica glass manufactured by the Corning Glass Company.

The chopped fuel pins from the approximately 0.5 a/o burnup subassemblies showed a tendency to agglomerate in the charging tray used to transfer the chopped pins from the decanner to the melt refining crucible. This is presumed to be a result of melting because of the internal fission product heat and later refreezing of the sodium on the pins as a result of enhanced heat transfer characteristics. However, they were able to be charged to the crucible.

Preliminary analytical results from melt refining runs MR-2 and MR-3 indicate that the fission product decontamination of the fuel was essentially as good as that obtained in the first melt refining run (MR-1) with irradiated fuel (ANL-6925, pp. 73–74). Data on the removal of iodine and barium-lanthanum was not obtained for these two runs owing to the long cooling time (4 months) that these subassemblies had received prior to melt refining.

All of the skulls from the 14 melt refining runs were oxidized in the skull oxidation furnace satisfactorily. A minor difficulty was occasionally encountered when the crucible was inverted in attempts to pour out the skull oxide in the crucible dumper. In about one-fourth of the oxidation runs, the crucible cracked approximately at the melt line during the oxidation operation. During the transfer of the crucible in its stainless steel container from the skull oxidation furnace to the dumper, shifting of the crucible takes place and results in an apparent increase in height of the crucible which interferes with the dumping operation. This problem of apparent height increase can be eliminated by the use of a slightly shorter stainless steel crucible container which would compensate for the displacement of the crucible in the container. This will be tried out.

Considerable radioactive contamination of Argon Cell equipment as a result of melt refining run MR-4 and skull oxidation run SO-4 was experienced. The irradiated fuel used in run MR-4 had attained a 0.5 a/o burnup and was cooled for 18 days prior to melt refining. The skull material from run MR-4 was used in run SO-4. The vacuum pump radiation level increased initially from 1 mR/hr to 9 mR/hr,[62] during the course of the melt refining run and then increased to 20 mR/hr when the melt was poured. The following morning, the gas in the furnace was pumped out to the delay tank. (The off-gas systems for the melt refining and skull oxidation furnaces are shown in ANL-6925, p. 70.) The pump oil readings surged to 3 R/hr for a short time during the pumpout and then decreased to 120 mR/hr. The reading at the refrigeration cooling coils associated with the Argon Cell cooling system increased from 120 mR/hr to 300 mR/hr when the melt refining furnace was opened after being pumped out and refilled with cell argon. This reading increased to 400 mR/hr when the fume trap was sampled and gradually to 2 R/hr over the next three days. No further increase in radiation level was recorded. The readings, taken with a Geiger-Müller tube, at the surface of the one-inch thick steel shielding of the off-gas delay tank increased from background (less than 0.1 mR/hr) to 45 mR/hr when the gas from the melt refining furnace was pumped into this tank.

After completion of the skull oxidation run, radiation intensity measurements of the following items were obtained: melt refining product ingot (run MR-4), melt refining furnace fume trap, skull oxide in a zinc storage can, and the empty crucible from skull oxidation run SO-4. The radiation levels were remotely measured inside the Argon Cell by means of a monitoring instrument having a maximum range of 500 R/hr. Distances from the instrument were estimated; the radiation levels listed below were corrected for these distances and are as follows:

Item	R/hr at 1 ft
Melt refining ingot (run MR-4) in storage container	4.5×10^2
Fume trap from Melt Refining Furnace	4.0×10^2
Skull oxide (run SO-4) in zinc can	3.6×10^4
Empty crucible after skull oxidation run	5.2×10^4

After the crucible, in its stainless steel container, was removed from the skull oxidation furnace, a red glow was observed inside the crucible at approximately the melt line. The photograph (Figure I-32) of this glow in the Argon Cell was taken through a five-foot thick shielding window.

The crucible had cracked at the melt line during the oxidation process; after the oxide was dumped, the top of the crucible (a 7-in. portion above the melt line) was removed from the container for examination. The examination showed that the glow was confined to the inside portion of the crucible from the melt line upward for approximately 1½ in. No glow was observed below the melt line or in the skull oxide removed from the crucible. The glow does not appear to be caused by a thermal effect; a small thermocouple junction touched to the glowing area registered less than 100°C. Samples of the crucible were taken from the glowing area and from below the melt line for analytical purposes to determine what fission products were present.

[62] Unless otherwise stated, the radiation levels indicated represent readings recorded from remote gamma detectors located in the vicinity (3 to 4 ft away) of the item being monitored and, as such, should be regarded as relative values rather than absolute values.

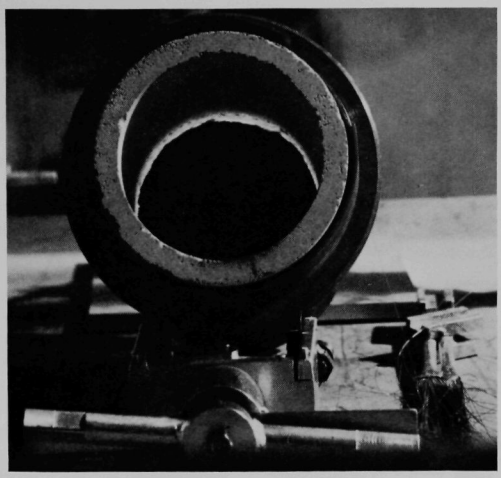

103-G5080

FIG. I-32. Glowing Melt Refining Crucible after Skull Oxidation Process.

2. Operations with Equipment for Fuel Fabrication (M. J. FELDMAN, J. P. BACCA, V. G. ESCHEN, D. E. MAHAGIN)[59]

a. INJECTION CASTING

Successful operation of the injection casting station, described in ANL-6925, pp. 76–79, has continued. Sixteen additional casting runs (about 11 kg each) have been completed. Of these, six were with irradiated fuel material and ten were with nonirradiated fuel material.

No significant difference was noted between the casting results obtained with unirradiated fuel and those obtained with irradiated fuel. The heel of metal remaining in the crucible after casting averaged about 30% of the charge weight. Approximately 73% of the metal cast resulted in pins 15 inches or longer in length; of these, about 70% were acceptable pins. Heels, short pins, sheared portions, and pins rejected for other reasons are all recycled, either to succeeding injection casting batches, or to melt refining for consolidation.

b. PIN PROCESSING

The demolder section of the pin processor (ANL-6605, pp. 85–92) was modified to facilitate the disassembly of the mold crusher blade. A pin was removed which secured the hold-down bolts, and a spacer plate was welded to the crusher plate, to enable remote disassembly. A number of castings were being processed which had an adhering ball of cast metal at the mold mouth. This oversize section periodically lodged in the crusher blade and jammed the machine. The modification has shortened the time necessary to clear the machine.

Fifteen additional pin processing runs have been made. Table I-11 shows the results of inspecting the castings from these runs. The data indicate that short castings and those castings having diameter defects account for two-thirds of the rejected pins.

An improvement in the eddy-current porosity detection system has resulted in significantly increased sensitivity and in simplification in the interpretation

TABLE I-11. RESULTS OF PIN PROCESSING OF INJECTION CAST FUEL
(15 runs—1518 castings)

	Percent
Acceptable Pins	51
Rejected Pins	49
Cause of Rejection	
Casting Length[a]	38
Shearing Length	12
Weight	0.4
Diameter (including surface defects)	30
Porosity	19

[a] Only molds that appear to contain fuel pins over 15 in. in length are processed. Of these, some are rejected as not being of full diameter for the 15-in. length required for shearing to the desired 14.22 ± 0.030 in. length.

of the detection signal. In the original design, the change in impedance of the coil as a fuel pin passed through it was recorded. With this system, it was difficult to differentiate between surface defects and internal defects. In the modified detection system, the phase angle of the coil voltage is recorded as well as the coil impedance change. Since the phase angle is different for surface and internal defects, the two types of defects can be differentiated by comparing the impedance trace with the direction of the deflection of the phase angle trace. The increased sensitivity of the system has been a large factor in the increased rejection rate for porosity. In the first eight runs with enriched fuel which were reported in ANL-6925, p. 82, porosity accounted for about 1% of the rejections. In the fifteen runs reported in Table I-11, porosity accounted for 19% of the rejections. A reappraisal of the specifications for porosity rejection is therefore being undertaken.

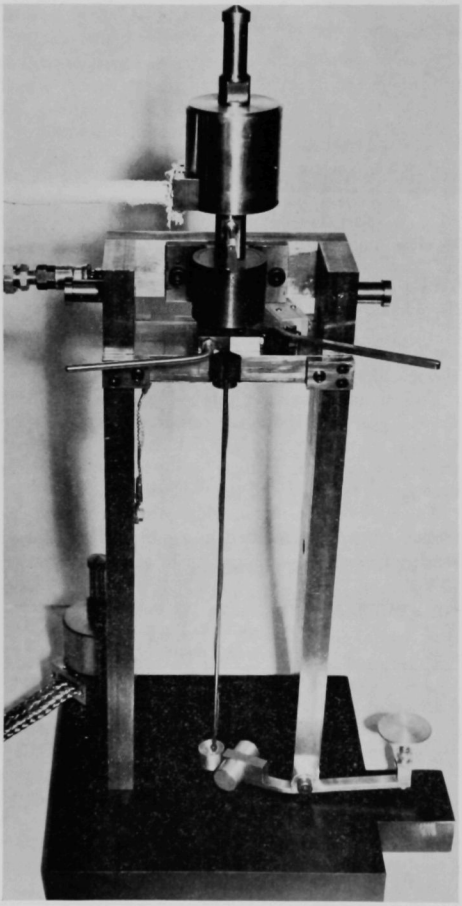

103-F5850

FIG. I-33. Single Element Master-Slave Operated Welding Station.

TABLE I-12. SUMMARY OF LEAK DETECTION TESTS OF FUEL ELEMENTS WELDED IN SINGLE-ELEMENT WELDING STATION

Number of fuel elements: 558

Operation	Acceptance (%)	Rejection (%)
Initial Welding	85	15
Rewelding[a]	45	55
Overall	89	11

[a] Those welds which exhibit a leak and do not have any sodium extruding through the leak are rewelded and retested for leakage.

c. FUEL ELEMENT ASSEMBLY, WELDING, AND LEAK DETECTING

Alignment difficulties with the 20-fuel element welding station[63] indicated that the modification or replacement of the welding machine might be advantageous. Misalignment of the machine was evident at the leak detection station. Two effects were noted: first, an increase in the number of leaking welds, and second, the formation of nonconcentric or "slumped" weld beads. This second effect requires that the weld bead be swaged before the welded element will fit into the leak detection station (see ANL-6925, p. 83). Examination of the machine indicated that the misalignment between the element and the welding electrode was due to the necessity to provide a shaft tolerance in order to accomplish rotation of the 20-fuel element basket (A-basket) under the weld electrode.

A single-element welding station, shown in Figure I-33, was designed, fabricated, and placed in operation. An immediate improvement in welding efficiency was noted. Not only did the number of leaking elements decrease, but also the number of welds that required swaging decreased from about 7% to essentially zero. Table I-12 summarizes the results of the welding and the leak detection of 558 fuel elements.

d. BONDING AND BOND AND LEVEL TESTING

The purpose of bonding and bond-testing operations is to insure the quality and quantity of the sodium heat

[63] T. C. Cameron and N. F. Hessler, Assembling, Sodium Bonding, and Bond Testing of EBR-II Fuel Rods, Nucl. Sci. Eng. **12**, 424–31 (1962).

transfer envelope. The bonding operation is a high-temperature (500°C) vibrating impaction step which removes voids in the sodium. The testing operation utilizes an eddy current detection system which measures the integrity of the bond and the sodium level.

Bonding and bond and level testing operations have continued to operate successfully. However, during a recent repair operation on the bond and level testing machine involving replacement of a broken retaining ring (Tru-arc ring), examination of the components of the machine showed indications of wear at a number of points. It is estimated that the bond tester has completed approximately 10,000 test operations and that component replacement is imminent. Minor modifications, based on experience to date, will be incorporated in the design of replacement parts. The machine has been returned to service, although design changes have not been completed.

A summary of data involving the testing of 470 fuel elements in recent operations of the bonding and bond and level testing machine is shown in Table I-13.

TABLE I-13. Summary of Bonding and Bond and Level Testing of Fuel Elements Manufactured in the Argon Cell

Number of Fuel Elements: 470

Operation	Acceptance (%)	Rejection (%)
Initial Bonding	58	42
Cause of Initial Rejection		
Sodium Level		11
Voids		56
Bubbles		33
Rebonding Operation	58	42
Cause of Rebonding Rejection		
Sodium Level		35
Voids		42
Bubbles		23
Overall	83	17

e. FINAL ASSEMBLY AND TESTING

The final assembly and testing machine has continued to operate satisfactorily. The straightness testing portion of the tensile and test machine has been replaced by a straightness testing and straightening machine incorporating six dial gauges and a pneumatic impactor. As noted previously (see ANL-6925, p. 85), the original straightness tester was difficult to maintain and produced data that were subject to question. The replacement machine now fulfills the original design criteria, assuring that the maximum bow of the subassembly is less than 0.080-in. T.I.R.[64] In addition to providing the necessary measurements, the new machine is capable of correcting out-of-tolerance subassemblies by applying a force at the point of maximum deflection.

In addition to the 22 subassemblies whose fabrication and testing were previously reported, the assembly and test machine has been used to manufacture thirteen additional subassemblies. One subassembly (C-162) was made of reprocessed and refabricated irradiated fuel. This subassembly has been returned to the EBR-II Reactor and is now undergoing additional irradiation. The radiation level of this subassembly was 10^3 R/hr at one foot when it was transferred from the Fuel Cycle Facility.

3. Fuel Surveillance Program (M. J. Feldman, D. C. Hampson, J. P. Bacca, E. R. Ebersole, V. G. Eschen, D. E. Mahagin, D. L. Mitchell)[59]

Thirteen subassemblies have been subjected to detailed fuel surveillance. Burnup (calculated) of core fuel elements observed has ranged from 0.10 a/o to 0.78 a/o.

The external observations and measurements carried out on the elements and the subassembly have disclosed no apparent changes (swelling or distortion). However, the results of measuring sodium level, internal pressure and void volume of fuel elements have indicated that the fuel is undergoing initial stages of expansion. The measurements on length and diameter of the fuel pin do not as yet clearly reflect the volume change, since the pre-irradiation data are in the form of tolerance ranges rather than individual specific measurements. A summary of pertinent data from the surveillance program is shown in Table I-14.

A method has been developed for determining the relative burnup of EBR-II fuel. The method involves the direct counting of the 1.6 Mev ^{140}La gamma through a 5-ft long collimated aperture in the Air Cell wall. The fuel element, complete with spacer wire, is counted at constant geometry through a 0.25-in. dia. collimator at 1.5-in. intervals along the fuel element length using a 1 by 1 in. thallium-activated sodium iodide crystal coupled to a 256-channel analyzer. The total counts summed under the photoelectric peak of the 1.6 Mev ^{140}La gamma are recorded as a function

[64] T.I.R. represents Total Indicator Reading upon rotation about a fixed axis.

TABLE I-14. EBR-II FUEL SURVEILLANCE PROGRAM DATA

Subassembly	Calculated Burnup (a/o)	Fuel Element Diameter	Average Increase[a] in Sodium Level (in.)	Gas Pressure in Void Space (atm)	Fuel Pin Diameter
C-115	0.12	No Change	0	~1	No Change
C-140	0.26	No Change	0	~1	No Change
C-112	0.44	No Change	0.14	~1	No Change
C-143	0.50	No Change	0.22	1–1.1	<1 mil increase
C-122	0.62	No Change	0.38	1–1.2	<1 mil increase
C-103	0.75	No Change	0.42	1–1.2	<1 mil increase

[a] Based on average initial sodium level for 1000 elements measured at Fuel Cycle Facility.

of distance from the spade end of the fuel element to give the relative axial burnup. This method was tested with irradiated fuel elements that had cooled for four months. Because of the long cooling time, the ^{140}Ba-^{140}La had completely decayed. The 0.72 to 0.77 Mev ^{95}Zr-^{95}Nb gamma was then counted to determine the precision of the method and the relative burnup of these particular pins. Future burnup measurements will be made by counting the ^{140}La gamma.

To determine the precision of counting, the precision of repositioning the pin, the effect of the spacer wire, and of realignment of the detector crystal, a fuel element was counted repetitively before and after changing each of the above variables. The maximum variation for any of the variables tested was a value of approximately 1.5% found for the effect of the spacer wire. This necessarily included repositioning of the pin.

Radiochemical analyses of a limited number of fuel pin samples are being carried out in order to obtain absolute values of burnup for comparison with the relative values obtained by the direct counting method.

4. Performance of Process Auxiliaries (D. M. PAIGE, W. F. HOLCOMB, J. O. KLEFFNER)[59]

a. ARGON CELL ATMOSPHERE CONTROL AND PURIFICATION

The Argon Cell pressure control system has continued to operate very satisfactorily during the past six months at a controlled pressure of three inches of water below atmospheric pressure.

After approximately 7400 hr of operation, the lower bearing in cell cooling fan "B" indicated a temperature of 295°F (150°F is normal). Although the contact microphones on the fan bearings did not indicate any abnormalities, the fan itself was observed to produce an abnormal oscillating noise. The fan was immediately turned off, and the isolation valves were closed. This bearing had twice previously given momentary indications of high temperature; the first occurred approximately one hour after the last periodic greasing, and the second took place approximately 16 days later. In each case, the temperature returned to normal before the cause of the trouble could be determined. However, on the third instance, about 18 days after the last periodic lubrication, the bearing temperature remained abnormally high until the fan was shut down.

The malfunctioning bearing was removed from the fan and inspected for damage. An external examination of the bearing indicated that it had ample grease and had no physical defects. The bearing was then destructively dismantled to facilitate inspection of the balls and raceways. The balls and raceways were in good condition with only minor pits noted. The lubricant (Dow Corning, Type 44 silicone grease) appeared to have hardened in the bearing and had the consistency of road tar. It is not known whether this hardening is a cause or result of the excessive temperatures. This bearing had been previously operated for 360 hr in an air atmosphere followed by 550 hr in a nitrogen atmosphere; the final 6500 hr of operation was in the dry argon atmosphere. The fan had been lubricated after every 1000 hr of operation in accordance with the manufacturer's recommendation; however, the belief is that none of the grease actually reached the bearing, since the lower bearing housing was only partially full.

All bearings on the assembly were replaced with new factory prepacked bearings containing a lithium grease. These bearings need not be greased, because they are sealed bearings and, according to the manufacturer, are "lifetime" lubricated. Cell cooling fan A has operated successfully for over 6000 hr with this type of lubricant.

Approximately 4½ hr were required by two men to remove the fan for repairs; the same time was required for reinstallation of the repaired fan. Each man received a total radiation exposure of less than 190 mR. However, future repairs of the fans will be more difficult to carry out because the radiation background in the sub-cell has increased by an order of magnitude in the past two months, and it will probably continue to increase as more irradiated fuel is processed in the Argon Cell. Table I-15 shows background radiation levels in the sub-cell areas. These readings are obtained by remote reading gamma detectors located

in the sub-cell areas. In general, the detectors are located close to the equipment that they are associated with; however, for the purposes of this table, they are used to indicate general cell background and as such, no distance figures are stated. These radiation levels indicate that the radiation background will limit any future contact maintenance time.

At the controlled Argon Cell pressure of minus 3 in. of water, the average leak rate of air into the cell was 0.3 SCFH, and typical values were normally in the range of 0.2 to 0.4 SCFH. Table I-16 shows the concentrations of impurities present in the Argon Cell atmosphere.

In order to maintain these levels of water and oxygen, the argon purification system was operated about 60% of the time. About 50,000 cu ft of argon was used in the normal course of transfer lock operations and pressure control of the Argon Cell; this is in the order of two-thirds of a cell volume. The nitrogen level reached 6.9 v/o owing to occasional high air inleakages (bad lock gaskets, etc.). This is about 1% higher than values observed in the first 6-month period; however, the nitrogen level appears to have reached an equilibrium value (6–7 v/o) for normal operating conditions. If it becomes desirable to reduce this nitrogen level, a nitrogen getter system (see ANL-6925, pp. 23–25) or an extensive fresh argon dilution program will be required.

TABLE I-15. Sub-Cell Background Radiation Levels

Area	Present Level (R/hr)	Highest Level in Past 6 Months (R/hr)
Sub-cell No. 5: High pressure argon compressor suction filters	0.004	—
Sub-cell No. 6: North cooling box	1	2
Sub-cell No. 6: Oil separator melt refining vacuum pumps	2	2
Sub-cell No. 7: South cooling box	1.1	5

TABLE I-16. Concentration of Impurities in the Argon Cell Atmosphere

Contaminant	Concentration of Contaminant (ppm)		
	High	Low	Average
H_2O	159	8	42
O_2	140	8	57
N_2	69,000	—	66,000
He	3,200	—	1,800
CO_2	37	26	—

b. CRANES AND ELECTROMECHANICAL MANIPULATORS

All cranes and electromechanical manipulators have operated very well over the past six months (November, 1964 through April, 1965) with only very minor difficulties. In Table I-17, the total hours of usage of motor drives for the cranes and manipulators are compiled. These data indicate a usage of 4 to 5 times over that observed for the previous 6-month period (see ANL-6925, p. 88).

Inspection of a set of manipulator grip drive brushes used about 14 hr in an argon atmosphere containing 20 to 100 ppm each of oxygen and water (Stackpole type 660 brushes containing molybdenum disulfide) indicated no measurable wear. This may be compared with the one-hour life in dry argon observed for the original brushes.

Slack-cable limit switches on the carriages of two Argon Cell manipulators were replaced. This was accomplished by removing the carriage to the Air Cell roof using the jib crane on the Facility roof. To minimize the radiation levels at the hatch opening, all fuel in the Air Cell was moved toward the end of the cell away from the hatch opening. Radiation levels varied from 20 mR/hr around the edge of the hatch to 1.5 R/hr at the center of the opening.

TABLE I-17. In-Cell Crane and Electromechanical Manipulator Usage

Type of Unit	No. of Units	Total Hours of Motor Operation for All Units of the Same Type									
		Grip		Rotate		Hoist		Carriage		Bridge	
		Past 6 Months[a]	Total To Date	Past 6 Months[a]	Total To Date	Past 6 Months[a]	Total To Date	Past 6 Months[a]	Total To Date	Past 6 Months[a]	Total To Date
Argon Cell Manipulators	5[b]	176	266	190	234	730	898	530	659	980	1190
Air Cell Manipulators	2	40	50	30	41	70	170	70	122	30	167
Argon Cell Cranes	2	—	—	—	—	280	327	85	103	100	159
Air Cell Cranes	1	—	—	—	—	290	227	60	70	55	69

[a] Period from November 1964 through April 1965.
[b] One unit out of service.

D. CHEMISTRY OF LIQUID METALS (I. Johnson, H. M. Feder)

The physical chemistry of liquid metals and alloys is being investigated to provide basic data for liquid alkali metal technology and for the testing of theories of liquid metal solutions. Special emphasis is being given to the chemistry of liquid sodium and its common contaminants—carbon, hydrogen, oxygen—because of the importance of sodium as a reactor coolant.

1. Fundamental Studies

Research is being directed toward the development of a theoretical basis for the understanding of the physicochemical properties of liquid metals and alloys. The following experimental studies are under way:

(a) An atomic absorption spectrophotometric method is being used to determine thermodynamic properties of binary alkali metal liquid solutions. These studies will yield data suitable for testing theoretical calculations (based on a free-electron model) of the properties of the simplest metallic systems.

(b) The Knudsen effusion method, supplemented in some cases by high-temperature galvanic cell measurements, is being used to determine thermodynamic properties of binary alloys of rare earth metals with cadmium. These studies will yield data suitable for the empirical correlation of alloy stability with parameters such as atomic radius and electronegativities. Such a correlation provides a valuable guide to the development of theory for alloy systems which are at present beyond the reach of purely theoretical investigation.

(c) The magnetic susceptibility of certain alloys is being studied. These studies yield information on the electronic configuration of the constituents in metallic systems and are therefore useful in the interpretation of thermodynamic properties.

(d) Studies of the solubilities of inert gases in liquid metals are being made to determine quantitatively the importance of the polarizability factor in metallic solutions. These studies are continuing on a part-time basis.

(e) A study is planned on the measurement of the velocity and the absorption of very high frequency sound in liquid metal solutions. It is hoped to determine whether distinct molecules exist in certain metallic solutions.

a. THERMODYNAMICS OF BINARY ALKALI METAL SOLUTIONS (F. Cafasso, V. Khanna[65])

Advances in theoretical methods for treating the properties of metallic solution have been made in recent years.[66] It seems likely that sophisticated treatments of the thermodynamic properties of metallic solution may be possible in the near future. A test of the calculations involved will require precise, experimentally measured thermodynamic quantities. It is believed that alkali metal solutions should be susceptible to such theoretical treatments, and accordingly, we are determining certain thermodynamic quantities of selected binary, liquid, alkali metal systems.

The thermodynamic activities of alkali metals in their binary liquid solutions are being determined by a method based on the principles of absorption spectrophotometry. (Details of this method have been given in ANL-6725, p. 107.) This method was shown to be highly effective in the measurement of the thermodynamic activity of sodium in sodium-potassium solutions (ANL-6925, p. 95). The versatility of the method has now been demonstrated by its use in the determination of the activity of potassium in the same binary solutions.

Absorption measurements were made for potassium as a function of composition between 69 and 75°C. No significant variation of potassium activity with temperature was observed. Therefore, the variation of potassium activity with composition is given in a single plot, Figure I-34, together with the previously obtained sodium data. Potassium behavior shows significant departures from ideality. This result is consistent with expectations based on the previous sodium activity determinations and the Gibbs-Duhem relation. Some of the thermodynamic properties of the sodium-potassium system derived from the present results are shown in Figure I-35. In this figure are given the Gibbs excess free energy of mixing, ΔG^{xs} (derived by Gibbs-Duhem integration), the heat of mixing ΔH^M (measured[67] at 111°C but assumed to be valid at 72°C), and the excess entropy of mixing (from $T\Delta S^{xs} = \Delta H^M - \Delta G^{xs}$). It is evident that the curves of ΔG^{xs} and ΔH^M *vs* atom fraction are asymmetric and that the system is not regular, i.e., $\Delta S^{xs} \neq 0$. These results are identical to those of the sodium activity measurements. The

[65] Postdoctoral Fellow.

[66] A. Bellemans and M. DeLeener, Phys. Rev. Letters, **6**, 603 (1961); Phys. Letters, **4**, 157 (1963).

[67] T. Yokokawa and O. J. Kleppa, J. Chem. Phys., **40**, 46 (1964).

tentative conclusions drawn from the sodium data (ANL-6925, p. 95), namely, that "the size effect may predominate over the electronic effect in this system, and that calculations involving both may be required to fit the data" appear to be supported by the potassium measurements.

b. THERMODYNAMIC PROPERTIES OF 1:1 COMPOUNDS IN LANTHANON-CADMIUM SYSTEMS (E. Veleckis, R. Murray)

When alloyed with cadmium, the rare earths (Ln) form numerous intermediate phases. The stability of these phases is being determined by measuring the partial pressure of cadmium over various two-phase alloys with a recording effusion balance.[68] At 450°C the partial pressure of cadmium varies from about 1 torr for the compounds richest in cadmium ($LnCd_{11}$) to about 10^{-4} torr for the compounds poorest in cadmium (LnCd). The largest relative decreases in pressure are observed on going from the $LnCd_2$-LnCd fields to the LnCd-Ln fields. Experimental conditions can be adjusted to allow a single-sweep measurement of decomposition pressures of all intermediate phases from $LnCd_{11}$ to $LnCd_2$. These conditions, however, are not suitable for the accurate determination of the cadmium partial pressures over the LnCd-Ln fields. To measure the thermodynamic properties of formation of selected LnCd compounds, the procedure described below was used.

Specimens of LnCd-Ln were prepared by heating mixtures of cadmium (45 a/o) and rare earth metals in a tantalum capsule which had been sealed in an inert atmosphere. The alloys were heated in a vacuum furnace at 1200°C for about one hour, cooled rapidly, and then dejacketed and powdered (60 to 200 mesh) in a helium-filled glovebox. X-ray examinations revealed the presence of both LnCd and free Ln metal in the specimens.

Two tantalum effusion cells were employed. The effective orifice area of both cells was determined by calibration with pure, solid zinc. (The calibration for one of the cells was verified independently by optical measurement of the orifice geometry.) The effusion cell, containing approximately 3 g of powdered alloy, was suspended from the beam of the recording balance.[68] The system was evacuated to 10^{-6} torr and the cell was brought to temperature by means of a salt-bath furnace. Isothermal effusion was continued for 2 to 10 hr, the longest periods being employed at the lowest temperatures. In order to assure the presence of solid alloys during effusion, the effusion temperatures were kept below the respective eutectic temperatures

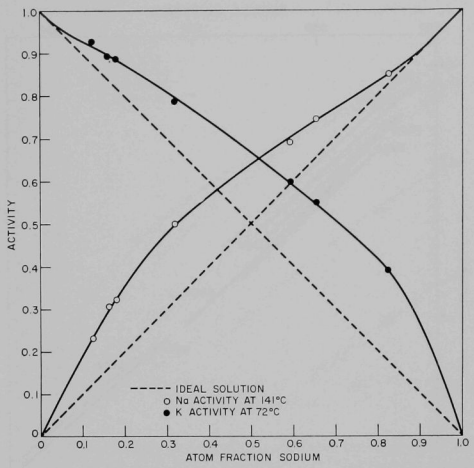

108-9069

Fig. I-34. Variation of Sodium and Potassium Activities with Composition in Sodium-Potassium Solutions.

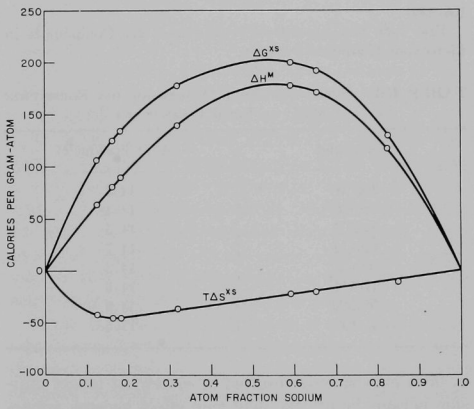

108-9068

Fig. I-35. Thermodynamic Functions for the Sodium-Potassium System at 72°C.

for each system (ANL-6925, p. 96). After each isothermal period, the temperature was adjusted to a new value without interrupting the effusion. When the initial effusion rate at a particular temperature was observed to decrease, the experiment was discontinued. Such decreases occurred in the final stages of each experiment and were probably due to depletion of the evaporating component, cadmium, from the sample surface. The use of finer powders (100 to 200 mesh)

[68] E. Veleckis, C. L. Rosen, and H. M. Feder, J. Phys. Chem., **65**, 2127 (1961).

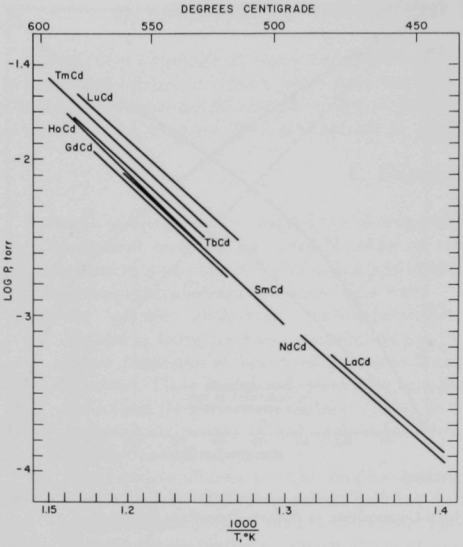

108-9066

FIG. I-36. Decomposition Pressures of 1:1 Compounds in Lanthanon-Cadmium Systems.

TABLE I-18. STANDARD FREE ENERGIES OF FORMATION AT 500°C OF LnCd COMPOUNDS

Compound	$-\Delta Gf^o$ (kcal/mole)
LaCd	14.3
NdCd	14.4
SmCd	14.5
GdCd	14.7
TbCd	14.2
HoCd	14.5
TmCd	13.9
LuCd	13.5

in later experiments resulted in somewhat longer effusion periods before the depletion effect became apparent. Typical effusion rates were 10^{-8} to 10^{-10} g/sec.

The decomposition pressures of LnCd compounds are proportional to the (constant) rates of effusion in the LnCd-Ln regions and can be calculated by means of the Knudsen equation. Decomposition pressure data have been obtained for eight LnCd compounds, and the results are shown in Figure I-36 as Clausius-Clapeyron plots. The standard (Gibbs) free energies of formation of the LnCd compounds at 500°C according to the reaction,

$$\mathrm{Ln}(s) + \mathrm{Cd}(\ell) = \mathrm{LnCd}(s),$$

were calculated (by extrapolation) using the relation,

$$\Delta Gf^o = RT \ln (P/P^o),$$

where P is the decomposition pressure at temperature T in °K, and P^o is the corresponding vapor pressure of pure liquid cadmium.[69] The results are given in Table I-18.

It is of interest to note the similarity of decomposition pressure values for the systems investigated: at 500°C, only 30% difference exists between the extremes of GdCd and LuCd decomposition pressures. This similarity is reflected in the standard free energies of formation. The trends in Table I-18, however, appear to be real. The decrease in $-Gf^o$ values from GdCd to LuCd is surprising. An increase in bond strength was expected owing to shortening of the Ln-Cd bond distances.

Decomposition pressure studies on CeCd and PrCd are currently being made. The decomposition pressures of the compounds DyCd and ErCd will be estimated by interpolation. Of the two atypical rare earth elements, Eu and Yb, only EuCd will be investigated; the high volatility of ytterbium precludes the accurate determination of YbCd decomposition pressures.

c. ULTRASONIC MEASUREMENTS IN LIQUID METAL SOLUTIONS (F. CAFASSO)

Spectroscopy has been a valuable tool in elucidating the nature of species in nonmetallic solutions. The usefulness of this tool with metallic solutions, however, is hampered by their opacity. Despite this limitation, a number of spectroscopic methods are currently being used to study metallic systems. Of these methods, ultrasonic absorption appears to offer the greatest potential for studies of liquid metal solutions. The value of this method as a spectroscopic tool arises largely from the fact that metal solutions are not opaque to sound.

Ultrasonic methods have come into prominence in recent years as a means for detecting complex species in nonmetallic solutions.[70-73] However, these methods have so far provided only suggestive evidence[74-76] for

[69] A. N. Nesmeyanov, "Vapor Pressure of the Elements," Academic Press, New York, 1963, p. 44.

[70] J. R. Saraf and P. N. Sharma, J. Sci. Res. Inst. (Tokyo), **49**, 236 (1955).

[71] P. C. Bose and L. N. Srivastava, Z. physik. Chem. (Leipzig), **205**, 96 (1955).

[72] T. Satyavati, P. J. Reddy, and S. V. Subrahmanyam, J. Phys. Soc. Japan, **17**, 1061 (1962).

[73] S. Prakash, F. M. Ichhaporia, and J. D. Panday, J. Phys. Chem., **68**, 3078 (1964).

[74] J. Jarzynski, Proc. Roy. Soc., **81**, 745 (1963).

[75] G. Abowitz and R. B. Gordon, Trans. AIME, **227**, 51 (1963).

the existence of association, but their potential with regard to metallic solutions has not yet been fully explored. For example, the method of continuous variations (method of Job[77]) has been used successfully with ultrasonic measurements[73] to detect aqueous complexes, but has not yet been tried with liquid metal solutions.

We are planning to study the existence of association in liquid metal solutions by using the method of continuous variations in conjunction with ultrasonic velocity measurements. Initially, several ternary liquid metal systems, formed by mixing dilute binary solutions which contain a common solvent, will be examined by ultrasonic velocity measurements. The systems which show some degree of ordering will then be studied more thoroughly by ultrasonic absorption methods. An amplified presentation of both the aims and methods of this research will be given at a later date.

d. MAGNETIC SUSCEPTIBILITIES OF URANIUM MONOSULFIDE-THORIUM MONOSULFIDE SOLID SOLUTIONS (F. Cafasso, D. Gruen,[78] C. Thalmayer[78])

Two band models have been proposed to describe the probable electronic configuration of ferromagnetic uranium monosulfide.[79] To choose between the models, information about the number of magnetic electrons per uranium atom and about the extent of quenching of angular momentum was needed. Such information can be obtained from magnetic susceptibility studies, provided that the technique of magnetic dilution[80, 81] can be used. The formation of a complete range of solid solutions between uranium monosulfide (US) and (weakly paramagnetic) thorium monosulfide (ThS) made this kind of study possible. Accordingly, the magnetic susceptibilities of a series of US-ThS solid solutions ranging from 100 to 27% US were measured.

The results of these measurements are shown in Figure I-37 where the reciprocal molar susceptibility of uranium[82] is plotted against temperature. The figure shows that the Curie temperature (intersection at the temperature axis) is progressively lowered as the US-ThS solutions become more dilute in uranium. Indeed, dilution is so effective that no ferromagnetic ordering was detected down to 4.2°K in a solid solution containing as much as 27% US. Furthermore, dilution to 27% US leads to a susceptibility curve which is typical of a paramagnetic system with a negative Weiss constant. It is apparent that dilution of US with ThS leads to a significant reduction of exchange interactions in this system. Another noteworthy feature of Figure I-37 is the pronounced curvature exhibited by the 27% US solution. It is believed that this curvature arises from the population of an excited low-lying energy level in this alloy. Calculations are now being made which may support this tentative conclusion.

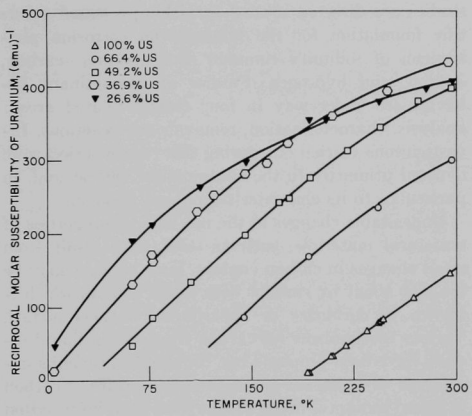

108-9067

Fig. I-37. Variation of Reciprocal Molar Susceptibility of Uranium in US-ThS Solid Solutions with Temperature and Composition.

These data have been reported at this time to present their salient features. When the interpretation of the data is completed, some comments on the probable electronic configuration of uranium in US will be made.

2. Liquid Sodium Chemistry: Behavior of Carbon

The objective of the liquid sodium studies is to obtain fundamental information concerning chemical reactions that can affect the use of sodium as a heat transfer medium in nuclear reactors. In particular, the

[76] J. Jarzynski and T. A. Litovitz, J. Chem. Phys., **41**, 1290 (1964).

[77] P. Job, Ann. Chim. (Paris), [10], **9**, 113 (1928).

[78] Cooperating Chemist, Chemistry Division.

[79] C. W. Kazmierowicz, "Galvanomagnetic Properties of Uranium Monosulfide," Master of Science thesis, Illinois Institute of Technology, June 1963.

[80] P. W. Selwood, J. Am. Chem. Soc., **55**, 3161 (1933).

[81] W. Trzebiatowski and P. W. Selwood, J. Am. Chem. Soc., **72**, 4504 (1950).

[82] These values have been corrected for the paramagnetism of both UOS and ThS and the diamagnetism of both ThOS and the core electrons of uranium. Impurity corrections were made on the assumption that all the solid solutions contained proportionately the same impurities found in the 27% US-ThS solution by electron probe microanalysis and chemical analysis.

studies are directed toward furnishing a sound scientific foundation for the influence on corrosion phenomena of sodium's common contaminants—carbon, oxygen, and hydrogen. Studies of contaminant behavior are under way in four closely related areas: analysis, characterization, removal, and reactions. Investigations carried out during this report period were devoted primarily to the contaminant carbon and, in particular, to its characterization and removal.

Undesirable changes in the mechanical properties of structural materials, such as steel, may result from small changes in carbon content. Such changes may be brought about by contact with liquid sodium which is known to carburize or decarburize various metals. Various mechanisms for carbon transport in liquid sodium have been proposed but the problem remains unresolved. Elucidation of the chemical nature of carbon in liquid sodium is being sought since such information would furnish a logical basis for the understanding of carbon transport. Our previous studies (ANL-6925, p. 92) have shown that a considerable quantity of carbon may be dispersed in sodium in the form of particles smaller than 5μ, and that the solubility of carbon in sodium is not readily measured. Additional information on the chemical forms in which carbon may exist in liquid sodium is being obtained by (a) dissolution of solid sodium and identification of the reaction products, (b) centrifugation of liquid sodium, (c) filtration of liquid and gaseous sodium, (d) mass spectrometric examination of the vapors above sodium, and (e) extraction of liquid sodium with an organic solvent. These studies will also furnish information concerning the ultrapurification of sodium from carbon. Ultrapure sodium is needed for research purposes and, possibly, will be needed to meet the more rigorous standards of future, high-performance reactors.

a. DISSOLUTION STUDIES (C. Luner, C. Clifton)

Information concerning the nature of carbon-containing species in sodium is being sought by experiments which involve hydrolysis of sodium and examination of the hydrolysis products. Information thus obtained is indirect in that changes in the original carbon-containing species are likely to occur during the hydrolysis; nevertheless, the reaction products may give some insight as to the nature of such species.

Preliminary dissolution experiments were made by hydrolyzing 1.5-g samples of sodium with excess 2 N sulfuric acid in an evacuated system. The evolved gases were pumped through a trap containing silica gel which was cooled with liquid nitrogen. After the sodium dissolved, the trap was detached from the system and the absorbed gases were analyzed by gas chromatography. Only carbon dioxide (6 ppm carbon) was detected although the sensitivity of the instrument was such that about 10 micrograms of carbon as carbon monoxide, methane, or acetylene would have been detected.

The dissolution of the sodium left a residue of dark particles in the acid solution. The particles were collected on a fine-porosity quartz frit and found to be 20 to 200μ in size. Their X-ray diffraction patterns showed the halos typical of amorphous materials. The carbon content of the particles was determined by heating the quartz frit in pure oxygen at 800°C and measuring the carbon dioxide formed. The results, given in Table I-19, show that 30 to 70% of the carbon in the sodium samples was recovered as particulates. These values may be considered as lower limits, since not all the particulate material was successfully transferred from the hydrolysis vessel to the filter.

Further work is in progress to determine more quantitatively the proportion of particulate carbon and the size of the crystallites from which the larger aggregates may be formed.

b. CENTRIFUGATION STUDIES (C. Luner, K. Anderson, C. Clifton)

Previous experience has shown that particulate matter containing carbon is present in sodium and that these particles can pass through a 5μ-porosity filter. Calculations indicate that for small density differences (about 0.2 g/ml) between the particles and liquid sodium, particles larger than 1μ dia. should be separable by centrifugation at reasonable speeds and temperatures. A number of experiments have been made to test the feasibility of centrifugal separation of particulate carbon from sodium, using a commercial centrifuge (International Equipment Co., Model C1) which was rebuilt to maintain sodium up to 500°C at a maximum speed of 2000 rpm.

TABLE I-19. Particulate Carbon Found after Dissolution of Sodium in Water

Samples, ~1.5 g

Sodium	Initial Carbon (μg)	Carbon Found as Particles[a]	
		(μg)	(%)
MSA[b]	400	110	28
MSA[b]	400	290	73
Distilled Reagent Grade	370	120	32

[a] Considered to be lower limits because of incomplete recovery.

[b] Mine Safety Appliance Research Corp. This sodium had been zirconium-gettered at 600°C and filtered through a 5-μ porosity stainless steel frit.

Stainless steel (SS) capsules were filled with sodium in an inert atmosphere glovebox, sealed, removed from the glovebox, and centrifuged at 2000 rpm (335 to 625 G) at about 200°C. In one experiment, after centrifuging for 30 minutes, the SS capsule was rapidly cooled by immersion in liquid nitrogen and the sodium was analyzed for carbon. No significant difference in the carbon content was found between the top, center, and bottom portions of the sodium. In another experiment, after centrifuging for one hour, the heating was discontinued and the sodium was allowed to solidify while being centrifuged. Analysis of the top and bottom portions of the sodium indicated no significant carbon displacement. These results indicate that if carbon-containing particles were present in the sodium, they were probably less than 1μ in diameter.

c. FILTRATION STUDIES (C. Luner, R. Blomquist, C. Clifton)

If a large fraction of the carbon present in sodium is in the form of particulate matter, then a partial removal should be possible by filtration. The ineffectiveness of centrifugation for the removal of carbon (see Part 2b of this section) suggests that an impingement-type filter, which depends to some extent on centrifugal action, will be ineffective with liquid sodium. If a filter is to act as a sieve, then a filter with very fine porosity must be used to remove carbon-containing particulates.

Preliminary experiments to test removal of carbon from liquid sodium at about 150°C have been made with various filter media using a pressure differential of about 3 atm. The results are given in Table I-20. The results obtained with the Millipore[83] filters (porous, cellulose plastic membranes) are interesting since this organic material was found to be unstable in liquid sodium; even so, significant carbon removals were achieved. The use of a layer of activated charcoal on a stainless steel frit was based on the assumption that active carbon might be effective in removing carbon particles from liquid sodium; some removal of carbon was effected. The 5μ-porosity nickel filter also appeared to be effective in removing carbon. Future studies will include the use of higher pressure differentials so that filters with smaller pore size may be used and the examination of other filtering materials.

Very effective removal of particles from gases may be achieved by filtration. Accordingly, an attempt was made to remove carbon-containing particles from sodium by filtration of sodium vapor. Reagent grade sodium was heated in a Pyrex tube to 350°C at a pressure maintained at 10^{-5} torr with an oil diffusion pump. The vapor passed through a coarse-porosity (20–40 μ) and a medium-porosity (10–15 μ) glass frit before condensing in a cool region of the tube. After about eight hours, sufficient sodium was collected to enable an analysis for carbon. The initial sodium contained 160 ppm carbon; the condensed sodium, 77 ppm carbon. During the long time required for this experiment, contamination of the condensed sodium by diffusion pump oil may have occurred despite the use of two liquid-nitrogen-cooled traps between the pump and the filtration apparatus. Further work on purification of sodium by vapor phase filtration is planned.

TABLE I-20. Carbon Removal from Liquid Sodium by Filtration

Temperature: ~150°C

Filter	Initial Carbon (ppm)	Final Carbon (ppm)
Millipore, 1.2μ porosity, supported on a glass frit	100–200	67, 70, 85
Stainless steel, 5μ porosity, with layer of activated charcoal	140	90, 125
Nickel, 5μ porosity	70	52, 53, 70

d. MASS SPECTROMETRIC STUDIES (I. Johnson, J. W. Reishus,[84] C. Luner)

Previous studies (ANL-6925, p. 92) have shown that distillation is not effective in removing the carbon normally found in sodium. A possible explanation is the presence in sodium of carbon compounds whose volatilities are similar to that of sodium. Accordingly, the vapor phases over various heated samples of sodium were examined by means of a Bendix Time-of-Flight mass spectrometer.

The experiments were performed in the following fashion. A 0.1- to 0.2-g sample of sodium was placed in a tungsten Knudsen effusion cell within a helium-filled glovebox. The effusion cell was quickly transferred from the glovebox to the effusion assembly chamber of the mass spectrometer (ANL-6800, p. 301, Fig. III-3), and the chamber was quickly evacuated. After the effusion assembly chamber reached a pressure of about 10^{-7} torr, mass spectra were recorded at room temperature to establish the background of the instrument. Next, the effusion cell was heated to about 300°C by means of a tungsten filament around the cell. After the cell attained a constant temperature, as indicated by a thermocouple attached to its base, mass spectra were again recorded. Mass spectra could be recorded with and without a shutter in the direct path between the orifice of the effusion cell and the ionization region of the mass spectrometer. Thus the mass

[83] Millipore Filter Corp.

[84] High Temperature Reactor Materials Group.

TABLE I-21. RESULTS OF MASS SPECTROMETRIC EXAMINATION OF VAPOR OVER SODIUM
Sodium at ~300°C when vapor sampled

No.	Description of Sample	Carbon Content (ppm)	Mass Peaks Observed[a]
1	Baker and Adamson Reagent Grade; sample from surface of ingot	75–150	23(Na^+), 46(Na_2^+); 28, 42, 56, 78, 92, and other light hydrocarbon peaks; 207, 278, 353
2	Distilled reagent-grade sodium; sample from surface of ingot	64	23(Na^+), 46(Na_2^+); light hydrocarbon peaks; 207, 272, 285, 298, 312
3	U.S. Industrial Chemicals Co. Reactor Grade; sample from surface of ingot	25	23(Na^+), 46(Na_2^+); light hydrocarbon peaks[b]
4	Baker and Adamson Reagent Grade; ingot remelted and sample taken from surface	69, 140	23(Na^+), 46(Na_2^+); light hydrocarbon peaks[b]
5	Filtered liquid sample from sodium in contact with graphite at ~250°C for four months	79	23(Na^+), 46(Na_2^+); light hydrocarbon peaks[b]
6	Same as No. 2; sample taken adjacent to sample 2	64	23(Na^+), 46(Na_2^+); 65, 78, 139, and other light hydrocarbon peaks; 207, 282

[a] The shutter was not used with samples 1 and 2. Thus the observations regarding light peaks (C_1, C_2, C_3, C_4, C_5 hydrocarbons) are not well established.

[b] The light hydrocarbon peaks were slightly more intense with shutter open.

peaks which were obtained could be attributed to vapors from within the effusion cell, or to residual gases in the mass spectrometer, or to both sources.

Six samples of sodium were examined. The samples are described in Table I-21 together with summaries of the mass spectrometric observations. Mass peaks of 207 and higher were observed with samples 1, 2, and 6. These high mass peaks were accompanied by a significant increase in the intensity of the low mass peaks. The latter can be ascribed to C_1, C_2, C_3, etc., hydrocarbon fragments, i.e., CH_3^+(15), CH_4^+(16), $C_2H_2^+$(26), $C_2H_3^+$(27), etc. In some cases, individual low mass peaks were very much more intense than the background and these are identified in the table. The sodium which had been distilled, samples 2 and 6, gave high mass peaks, whereas the sodium which had not been distilled, samples 3, 4, and 5, did not. Furthermore, sodium which had been in contact with graphite powder for four months at about 250°C, sample 5, did not show any high molecular weight compounds in the vapor phase.

These results suggest that:

(1) It is possible for high molecular weight, presumably organic, compounds to exist for extended periods of time in liquid sodium at moderate temperatures (300°C or 572°F). Some high mass peaks were still observed after 3 hr of heating.

(2) Samples of distilled sodium may contain significant quantities of volatile, high molecular weight, organic contaminants.

(3) Sodium samples that contain carbon do not necessarily contain significant quantities of volatile organic compounds. The high mass peaks observed with sample 1, which was taken from the surface of a sodium ingot, may be attributable to contamination by oils commonly used as mold lubricants in the casting of sodium. The same sodium after melting, sample 4, did not give high mass peaks. The results with sample 5 indicate that liquid sodium can remain in contact with graphite for extended periods of time and not become significantly contaminated with volatile, high molecular weight, organic compounds.

e. LIQUID-LIQUID EXTRACTION STUDIES (C. LUNER, K. ANDERSON)

The results of mass spectrometric experiments (see Part 2d of this section) suggested that some of the carbon in sodium may be in the form of high molecular weight organic compounds. If so, extraction of the compounds by a hydrocarbon solvent might be feasible.

A preliminary test of this concept was made by repetitive extractions of sodium (U.S.I., 25 ppm carbon) with high purity n-nonane (Phillips Research Grade) at 125°C in a Pyrex glass vessel contained in a helium-filled glovebox. N-nonane was chosen as the solvent because aromatic compounds which might be extracted could be characterized or identified by ultraviolet spectroscopy. The n-nonane extracts were filtered and examined with ultraviolet light in a Carey Recording Spectrophotometer using n-nonane for the reference cell. None of the fractions showed any absorption in the range 2200 to 4000Å. The sensitivity of the method of detection was estimated by using xylene (Fisher Certified Reagent) as a stand-in for aromatic com-

pounds which absorb strongly in the ultraviolet region. It was found that as little as 10 ppm of an extractable organic compound with an absorbancy similar to that of xylene could be detected. Apparently, the sodium used contained less than 10 ppm of carbon in the form of extractable organic compounds that absorb in the ultraviolet.

Further experiments to investigate other solvents and samples, and more sensitive methods of analysis are contemplated.

f. REACTIONS OF LIQUID SODIUM WITH CARBON COMPOUNDS (A. Cosgarea, P. Pelton)

Very little is known regarding the reactions of liquid sodium with carbon compounds, except for a few simple substances, such as CO_2, CO, and Na_2CO_3. Such information would be useful in deducing the possible origin of carbon species found in sodium. A series of experiments is planned to determine the fate of various carbon-14-labeled compounds after treatment with liquid sodium. It will be determined whether the compounds dissolve or undergo reaction and, in the latter case, what the reaction products are.

g. ULTRAPURIFICATION OF SODIUM (J. G. Schnizlein, R. Blomquist)

Ultrapurification of sodium from impurities such as oxygen, hydrogen, and carbon is of interest for several reasons. The study of reactions between liquid sodium and impurities would be greatly simplified if ultrapure sodium were available. The reliability and accuracy of analytical methods for impurities could also be tested if sodium requiring a negligible blank correction were available. Furthermore, the development of economical, on-line, ultrapurification methods would be of considerable interest for reactor loops.

With respect to carbon, there is no *a priori* way of knowing that a particular purification technique will be effective since the chemical nature of carbon in sodium is not understood. The tentative hypothesis is advanced in part 2b of this section that a considerable fraction of the carbon is sodium is present as submicron-sized particles. Thus an effective means of ridding sodium of such carbon might be one whereby sodium atoms or ions are made to migrate through an electrolyte. A study involving electromigration of sodium in fused salts is now under way and will be reported on subsequently.

E. PREPARATION OF FUELS FOR FAST REACTORS (A. D. Tevebaugh)

1. Solid Refractory Fuels

Refractory compounds of uranium and plutonium, such as carbides, nitrides, and sulfides, show promise as fast reactor fuels capable of withstanding high temperatures and high burnup. Methods are being investigated for the preparation of these fuel materials, and the more promising methods are being used to provide materials for fabricability evaluations and irradiation testing.

Recent work has focussed on carbide and nitride preparations; sulfide studies may be found in a previous report (ANL-6800, p. 147). The nitride preparations are discussed in the mobile blanket fuel section (I-E-2), while the carbide work is summarized below. The major emphasis in these studies is on obtaining control of stoichiometry and purity. In the case of the mixed uranium-plutonium carbide, a highly desirable fuel for fast reactors, an additional goal is that of obtaining a solid solution of uranium-plutonium monocarbide [(U-Pu)C].

a. PREPARATION OF URANIUM MONOCARBIDE BY A FLUIDIZED-BED PROCESS (E. J. Petkus, C. C. Payne)

The aim of the present studies on fluidized-bed synthesis of uranium monocarbide (UC) is to produce a finely divided, free flowing product of stoichiometric composition, which can be pressed into a fuel without intermediate processing such as grinding and blending. The apparatus and technique have been previously described (ANL-6925, p. 99). The process steps are the following:

(1) Formation of uranium hydride (UH_3) particles by reacting uranium metal with hydrogen at 10 psig for 2 to 5 hr at 250 to 300°C.

(2) Decomposition of the UH_3 particles to uranium metal particles by heating to the reaction temperature (600 to 750°C) while fluidizing with a mixture of hydrogen and propane gas at atmospheric pressure.

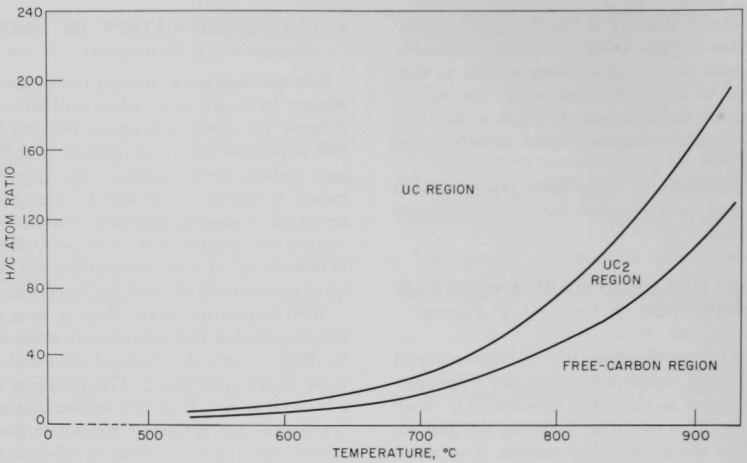

108-8882

FIG. I-38. Hydrogen-to-Carbon Ratios at Equilibrium in Uranium-Carbon Systems.

Typical Operating Temperatures (°C)	UC-UC_2 Boundary			UC_2-Free Carbon Boundary		
	H/C	v/o H_2	v/o C_3H_8	H/C	v/o H_2	v/o C_3H_8
600	15.2	94.5	5.5	9.8	91.4	8.6
700	34.6	98.0	2.0	20.6	96.4	3.6
750	49.0	98.6	1.4	28.9	97.5	2.5

(3) Continuation of the above fluidization step at 600 to 750°C for 3 to 20 hr to convert the uranium to uranium monocarbide.

The overall chemical reaction of uranium powder with propane can be represented by:

$$3\,U(s) + C_3H_8(g) \rightarrow 3\,UC(s) + 4\,H_2(g) \qquad (1)$$

However, in the temperature range of interest, propane, in the presence of excess hydrogen, decomposes into CH_4 and H_2,[85] so that the actual reaction is represented by:

$$U(s) + CH_4(g) \rightleftarrows UC(s) + 2\,H_2(g) \qquad (2)$$

(Propane has been used in the experiments thus far, chiefly because commercially available propane has a lower oxygen content than commercial methane.) Reaction 2 proceeds to completion to form UC at a very low methane partial pressure ($\sim 10^{-6}$ atm at one atm hydrogen pressure and 827°C). At much higher methane partial pressures, however, UC_2 or free carbon will form by the reactions:

$$UC(s) + CH_4(g) \rightleftarrows UC_2(s) + 2\,H_2(g) \qquad (3)$$

$$CH_4(g) \rightleftarrows C(s) + 2\,H_2(g) \qquad (4)$$

The equilibrium hydrogen-to-carbon ratios for these reactions are plotted in Fig. I-38 as a function of temperature. The presence of metallic uranium at the core of a fluidized particle may result in formation of UC (instead of UC_2) at lower hydrogen-to-carbon ratios than the equilibrium values, at least until nearly all of the uranium metal is converted to monocarbide. However, it is apparent that only a little of the carburizing potential is lost by raising the hydrogen-to-carbon ratio from the values at which methane decomposes to hydrogen and carbon (the lower curve in Fig. I-38) to values at which UC is the stable solid phase. The UC_2-stable region is narrow because the difference between the free energy of formation of UC_2 and that of UC is small, being approximately 1 kcal in the temperature range of interest.[86]

In the experiments performed to date, which are listed in Table I-22, the hydrogen-to-carbon atom

[85] Duff, R. E. and Bauer, S. H., The Equilibrium Composition of the C/H System at Elevated Temperatures, LA-2556, 1961.

[86] "The Uranium-Carbon and Plutonium-Carbon Systems, A Thermochemical Assessment," Technical Report Series No. 14, IAEA, Vienna, 1963.

TABLE I-22. PREPARATION OF URANIUM MONOCARBIDE (UC) BY FLUIDIZED-BED REACTION OF URANIUM POWDER AND PROPANE
100-g scale; uranium powder prepared by hydriding technique; 0.25 ft/sec fluidizing velocity

Run No.	Temp (°C)	Run Duration (hr)	Composition of Fluidizing Gas		Carbon Content (w/o) of Product at Indicated Time[b] (hr)					Final Oxygen Content (w/o)	X-ray Diffraction Analysis of Product	
			H/C Ratio	Propane[a] (v/o)	1	3	5	10	20		Major Phase	Minor Phase
UCF-35	600	5	4.2	30			4.3			0.46	UC	βUH_3
UCF-27	600	5	4.3	28.5	3.9	4.5	4.3			1.1	UC	Possibly βUH_3
UCF-29	600	5	5.3	20	3.2	4.1	4.3			1.1	UC	βUH_3
UCF-30	600	5	8.7	10		3.2	3.5			0.99	UC	βUH_3
UCF-37	600	10	15.3	5			2.8	4.1		1.24	UC	
UCF-34	700	5	5.3	20			5.4			0.84	UC	βUH_3
UCF-38	700	10	15.3	5			4.1	4.9		0.89	UC	
UCF-40[c]	750	20	31.0	2.3			3.6	4.7	4.6	0.81	UC	Possibly UC_2

[a] Balance hydrogen.
[b] The last analyses listed are of samples of the product after removal from the fluidized-bed reactor. The carbon content of stoichiometric UC is 4.80 w/o.
[c] Product partially sintered.

ratios were in the free-carbon region of Figure I-38, except for runs UCF-37 and UCF-40. However, the carbon content of the products was, in most cases, less than that of stoichiometric UC (carbon content, 4.80 w/o); X-ray analyses did not indicate the presence of UC_2 except in one case, run UCF-40. (A minor phase, βUH_3, was also found during X-ray analysis of the products. This phase probably resulted from the trapping of a small amount of uranium in a cool region near the bottom of the fluidized bed and subsequent hydriding of the uranium when the system was cooled under hydrogen.) In several runs the carbon content of the product appeared to have reached an equilibrium value. For instance, during the last ten hours of run UCF-40, the carbon content remained essentially constant at values (4.6 to 4.7 w/o) just below that of stoichiometric UC, even though the propane concentration of the gas corresponded to the UC_2 region of Fig. I-38. The reason why large amounts of UC_2 did not form in run UCF-40 is not immediately apparent.

The fact that the carbon content appeared to reach an equilibrium value in some of the runs at a level below that of stoichiometric UC is attributed to oxygen contamination. The oxygen content of these runs varied from 0.5 to 1.2 w/o (Table I-22). The oxygen contamination is probably in the form of UO_2 and UO dissolved in UC. Efforts to reduce the oxygen content of the UC powder will be made. Experiments on a larger scale, tighter equipment, improved control of the oxygen and water vapor content of the fluidizing gas, and a better glovebox atmosphere should reduce the oxygen content substantially.

The results of experiments given in Table I-22 indicate that a temperature of 750°C or higher will be necessary to complete the reaction leading to UC production in a reasonable time at the low propane concentrations represented by the UC region in Fig. I-38.

TABLE I-23. PARTICLE SIZE DISTRIBUTION OF UH_3 STARTING MATERIAL AND UC PRODUCT USING A FLUIDIZED-BED PROCESS

Run conditions: 5 hr at 700°C
Fluidizing gas: 85 v/o H_2, 15 v/o C_3H_8
Carbon content of product: 4.8 w/o

Particle Size (μ)	UH_3 (w/o)	UC (w/o)
>74	0.0	0.0
44–74	0.8	0.3
20–44	75.5	11.5
5–20	23.4	87.2
<5	0.3	1.2
	100.0	100.2

The particle size distribution of the UH_3 and UC produced in the fluidized-bed process has been determined by sieve analyses which employed two especially fine sieves[87] (5- and 20-μ hole sizes) in addition to standard sieves. Table I-23 shows the particle size distribution of the starting UH_3 particles (prepared under static conditions) and the size distribution of UC which had been prepared by fluidization of UH_3 with a C_3H_8-H_2 mixture at a linear gas velocity of 0.25 ft/sec for 5 hr at 700°C. As seen in Table I-23, there was some breakdown of particles, since the weight of particles in the 20- to 44-μ size range decreased from 75.7 w/o to 11.5 w/o. There was a corresponding increase of the amount of particles in the

[87] Buckbee Mears Company, St. Paul, Minnesota.

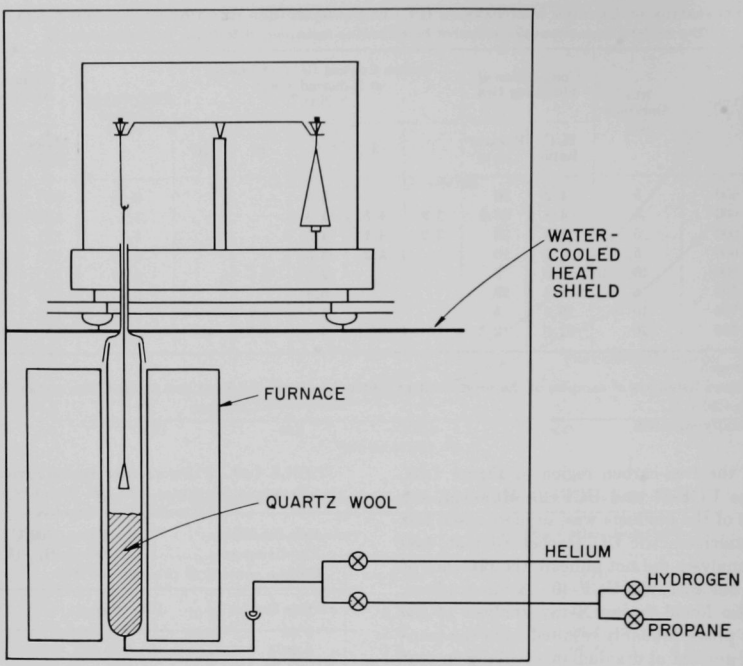

108-8886

FIG. I-39. Schematic of Thermobalance and Equipment for Preparation of (U-Pu)C.

5- to 20-μ size range of 23.4 w/o to 87.2 w/o. However, there was only a small increase (from 0.3 to 1.2 w/o) in the amount of the finest particles ($<5\ \mu$); this small increase has no significant effect on fluidization.

b. PREPARATION OF (U-Pu)C SOLID SOLUTION (S. VOGLER, J. PAVLIK)

Solid solutions of uranium-plutonium monocarbide, (U-Pu)C, are promising fuels for fast breeder reactors. Current methods of preparing the monocarbides involve either the carbothermic reduction of the mixed oxides with appropriate amounts of graphite or arc melting of the metals with graphite in the proper proportions. Both of these methods require grinding of the products in order to produce a powder for fabrication into fuel shapes. During the grinding step, the reactive carbide is susceptible to contamination by oxygen or nitrogen.

Because of the success with the preparation of uranium monocarbide by the fluidized-bed process, the feasibility of this technique for the preparation of (U-Pu)C solid solution was examined. Other workers[88] have demonstrated that the reaction of plutonium hydride with propane yields plutonium sesquicarbide (Pu_2C_3). When the reaction is stopped before the addition of a stoichiometric weight of carbon (based on PuC), the product consists of plutonium sesquicarbide and plutonium dihydride with a trace of plutonium monocarbide. The reaction of uranium with propane yields uranium monocarbide and uranium metal if the reaction is terminated before completion. With a uranium-15 w/o plutonium alloy, the reaction yields only the monocarbide phase (identified by X-ray diffraction techniques) if the reaction is stopped after addition of the stoichiometric weight of carbon.[89]

Prior to the preparation of (U-Pu)C in a fluidized bed, experiments were performed utilizing a thermobalance to measure the extent of reaction of a uranium-

[88] Brown, F., Dennard, F. S., Ellis, P., Good, P. J., and LaPage, Ruth, "The Preparation of Pu, U, and Mixed Pu-U Carbides by the Metal Hydrocarbon Gas Reaction," Conference on Carbides in Nuclear Energy, Harwell, 1963.

[89] Brown, F., Good, P. J., and LaPage, Ruth, "The Preparation of Mixed Pu-U Carbides by the Metal Hydrocarbon Gas Reaction," International Symposium, Compounds of Interest in Nuclear Reactor Technology, Boulder, Colorado, 1964 (AIME).

TABLE I-24. PREPARATION OF (U-Pu)C BY METAL-HYDROCARBON REACTION USING A THERMOBALANCE

Conditions: U-20 w/o Pu hydrided at room temperature, then reacted with propane-hydrogen mixtures at the indicated temperatures and flow rates

Run No.	17	18	19	20	21	22	23	24	25	26	27[a]	29	30
Temperature (°C)	650	650	600	650	700	650	700	670	750	750	650	750	750
Gas Flow Rate (liters/min)	2	2	2	3.1	3.1	3.1	3.1	3.1	3.1	3.0	3.0	1.4	1.4
Propane Conc. in Gas (v/o)	100	100	100	4.2	4.2	3.2	3.2	1.6	1.6	0.23	0.23	1.5	1.5
Time of Reaction[b] (min)	—	40	100	120	100	195	—	200	195	225	280	90[c]	210[d]
Weight Gain (g)													
Calc'd for (U-Pu)C	0.2144	0.1236	0.1484	0.1508	—	0.1582	0.1692	0.1459	0.1408	0.1444	0.1714	0.1704	0.1483
Det'd	0.2528	0.1735	0.1435	0.1750	—	0.1274	0.1532	0.1530	0.1411	0.1401	0.1118	0.1676	0.1587
X-ray Lattice Parameter (Å)	4.955 ±0.005	4.96	4.96	4.96	4.962 ±0.005	4.96	4.96	4.962 ±0.005	4.962 ±0.003	4.961 ±0.003	4.958 ±0.005	4.96	4.96[e]
Chemical Analysis (w/o)													
Carbon	5.40	5.68	5.57	4.83	4.62	4.64	4.80	4.72	4.88	4.47	2.82	4.07	4.88
Hydrogen	0.011	0.034	0.033	0.058	0.026	0.022	0.011	0.014	—	0.009	0.06	0.014	0.009
Oxygen	0.21	0.41	—	0.82	0.74	0.24	0.12	0.27	0.67	0.47	0.19	0.35	0.25
Nitrogen	0.084	0.10	—	0.16	0.16	0.13	0.022	0.09	0.094	0.69	0.20	0.12	0.10

[a] Reaction was incomplete for this experiment.
[b] Estimated time for completion of reaction, measured from time furnace reached 500°C.
[c] A second hydriding was performed, thereby reducing the particle size and resulting in a faster carbiding rate.
[d] Carbiding conditions maintained for more than 400 min after this estimated time (210 min) for completion of reaction.
[e] A minor component was observed with a bcc X_2C_3 structure. The diffraction pattern of the minor phase was too faint to obtain a lattice parameter.

plutonium alloy with propane-hydrogen mixtures. The primary purpose of these thermobalance experiments was to establish that a (U-Pu)C solid solution is formed by the reaction and secondly, that the use of the appropriate gas composition will limit the reaction to the formation of the monocarbide phase. A further aim was to identify and evaluate the variables in the reaction.

A schematic diagram of the equipment is indicated in Fig. I-39. An Ainsworth recording thermobalance installed in a plutonium facility was utilized for the study. A length of fine platinum wire, fastened to the left-hand balance pan, suspended a platinum dish holding the metallic sample in the furnace tube. The furnace was a 2½-in. dia. split Hevi-Duty furnace with a capacity of 1400 watts. The furnace shell was water-cooled in order to minimize heat dissipation to the glovebox.

Helium was used to sweep nitrogen from the system before beginning an experiment, and it was also used as a blanket gas in which the product was cooled after the reaction was completed. The hydrogen and propane reactant gas flow was regulated using calibrated rotameters in an external manifold. The gases were analyzed for oxygen and nitrogen impurities prior to use. The hydrogen usually contained less than 1 ppm oxygen and less than 10 ppm nitrogen. The helium contained approximately 2 ppm oxygen and the propane contained less than 10 ppm oxygen and 15–20 ppm nitrogen. Because of the low impurity level, the gases were used without further purification except for a trap of molecular sieve (4A) to remove moisture from the hydrogen-propane gas.

The first step in the procedure was to react uranium-20 w/o plutonium metal alloy with hydrogen at ambient temperatures to produce U-Pu hydride. When the thermobalance indicated the completion of this reaction (approximately 10 min), the proper hydrogen-propane gas mixture flow was started and the furnace heated to the carbide reaction temperature. The gas flow was continued until completion of reaction was indicated by unchanging sample weight. At that point the reactant gas flow was stopped and the sample allowed to cool under a helium atmosphere. After cooling, the reaction tube was removed and the sample transferred to the helium glovebox for weighing and sampling.

The results of the experiments are summarized in Table I-24. In those experiments in which 100% propane was used, the carbon content of the product was

TABLE I-25. ANALYTICAL DATA FOR PRESSED AND SINTERED (U-Pu)C

Samples were pressed in ¼-in. dia. dies and then sintered in argon at 1900°C for 2 hr.

Run No.	18	21	23	24
Wt. powder (g)	2.7063	1.8913	2.6682	2.2164
Wt. pellet (g)	2.4262	1.6784	2.4552	2.0045
% Recovery	89.7	88.7	92.0	90.4
Measured volume (cc)	0.1999	0.1336	0.1970	0.1604
Density (g/cc)	12.14	12.56	12.46	12.50
% Theoretical Density	89.5	92.4	91.6	92
Chemical Analysis of Pellet (w/o)				
Carbon (powder)	5.68	4.62	4.80	4.72
Carbon (pellet)	4.44	4.27	4.68	4.59
Hydrogen	0.0008	0.0004	0.0004	0.0009
Oxygen	—	—	0.18	0.19
Nitrogen	—	—	0.025	0.083

high, as was predicted by thermodynamic analysis. This was probably due to the deposition of free carbon on the (U-Pu)C particles, since dissolution of these products in nitric acid resulted in a residue and X-ray diffraction patterns gave no indication of the presence of higher carbides. For those experiments with hydrogen-propane mixtures, the carbon content was quite close to the stoichiometric value of 4.80 w/o.

The oxygen content is low for these small-scale (3 g/run) experiments. It is expected that products with oxygen contents of 0.1 w/o or less can be obtained by this reaction in a large-scale fluidized bed. The nitrogen and hydrogen contents appear to be at a satisfactorily low level.

In all cases, X-ray diffraction patterns have indicated that the major phase had a face centered cubic crystal symmetry with a lattice parameter of about 4.96 Å (see Table I-24). The lattice parameter is within the range of values that might be expected for a uranium-plutonium monocarbide solid solution.[90, 91] In one or two instances UO_2 was indicated to be a possible minor component. In those cases where incomplete reaction had occurred, the X-ray patterns indicated the presence of plutonium hydride. In all the X-ray patterns, no evidence was observed to indicate the presence of sesquicarbide phases, except for experiments 29 and 30, in which there was a faint indication of such a phase. (The operating conditions for these two experiments were extremely close to the UC-UC_2 equilibrium boundary, which might account for the appearance of higher carbides. However, experiment 25 under similar conditions did not indicate the presence of a sesquicarbide phase.) These results confirm the findings of Brown[89] who observed the presence of the monocarbide phase only, when reacting uranium-15 w/o plutonium powder with propane at 645–745°C until the stoichiometric weight increase for the monocarbide was attained.

Because of the rapid increase in temperature at the beginning of carbiding, a quantitative determination of the reaction rate at a given temperature cannot be made from the thermobalance charts (time *vs.* weight gain plots). However, estimates can be made. For example, in run 25 the average initial reaction rate was approximately 2 mg/min. Comparisons of the reaction rates between experiments are as expected; a higher partial pressure of propane and a higher temperature each result in an increased rate for the carbiding reaction. Of particular interest is the observation that even with a hydrogen-to-propane ratio of 428 as in run 26, carbiding proceeded at a reasonable rate at 750°C and

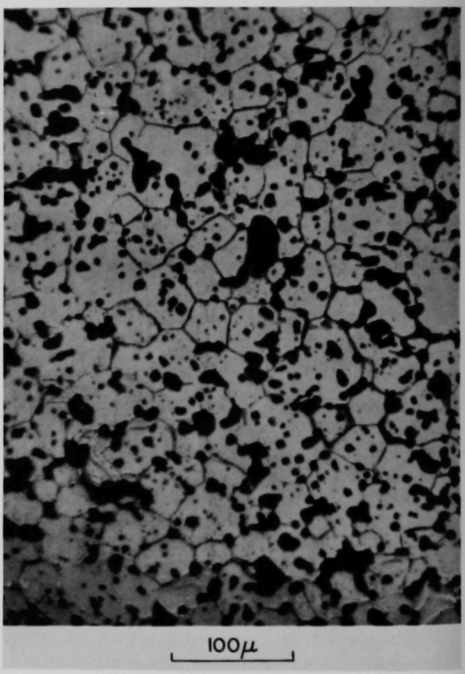

108-8899

FIG. I-40. Photomicrograph of Pressed and Sintered (U-Pu)C from Run 18. Polished specimen etched with equal volumes HNO_3, acetic acid, H_2O.

[90] Rosen, D., Nevitt, M. V., and Mitchell, A. W., J. Nucl. Mat. **9**, 137 (1963).

[91] Russell, L. E., The Structure and Properties of UC and (U-Pu)C Alloys, *Conference on New Nuclear Materials Including Non-Metallic Fuels*, Vienna, 1963, IAEA, Vol. 1, p. 409.

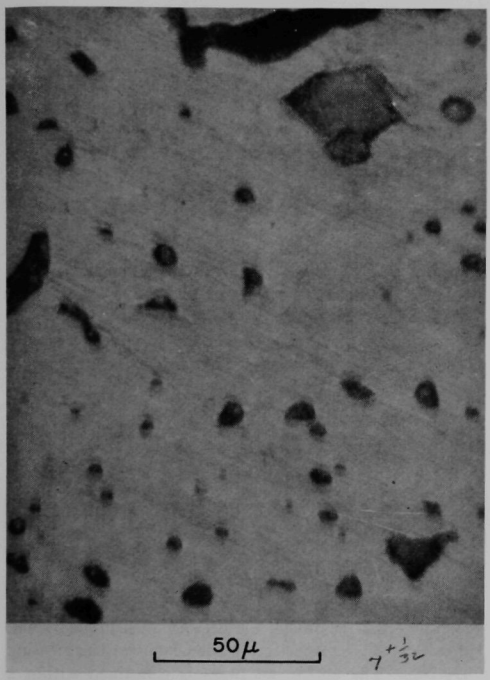

108-8900

FIG. I-41. Photomicrographs of Pressed and Sintered (U-Pu)C from Run 24.

A. As polished.

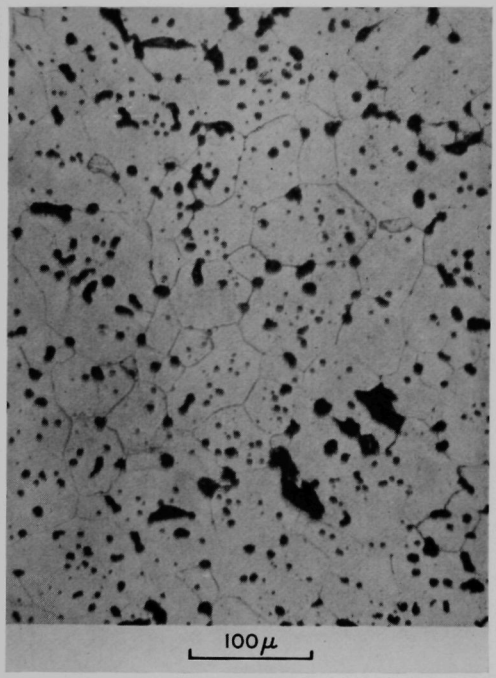

108-8756A

B. Polished specimen etched with equal volumes HNO_3, acetic acid, H_2O.

was completed within 3¾ hr. However, at 650°C under the same conditions, the reaction was sufficiently slow that carbiding was only ⅔ complete after 5 hr.

Run 30 was carried out for an extended period of time to demonstrate that higher carbides would not form if the proper gas composition were maintained. The carbiding conditions were maintained for approximately seven hours after the weight gain reached the calculated value. The final weight gain, which was approached slowly, was only 7% higher than the value calculated for formation of the monocarbide. The additional weight gain is attributed to reaction with oxygen and nitrogen impurities in the gas.

The products from four experiments were pressed and sintered into pellets,[92] primarily for metallographic examination. Before pelletizing, the powders were heated to approximately 1000°C in vacuum to remove gases, primarily hydrogen. The powders were then pressed into ¼-in. pellets with a pressure of 25,000 to 30,000 psi. The pellets were sintered for two hours at 1900°C in argon. The pellets were weighed and measured in order to determine the density and samples were also taken for chemical analysis. The results are summarized in Table I-25.

The densities of these first pellets appear satisfactory. In comparing the chemical analyses in Tables I-24 and I-25, it can be seen that there was no significant change in the nitrogen content of the product during the sintering step. However, there was a small loss in carbon during this step. In one case (run 24) there was a decrease in the oxygen content, but in run 23 there is an increase in the oxygen content. Additional results will be examined to further evaluate this anomaly.

As an additional aid in identifying the products, the microstructures of these materials were examined utilizing metallographic techniques. The material was mounted in a polyester resin. The carbide solid solu-

[92] The pelletizing and sintering were performed by the Metallurgy Division through the courtesy of Owen Krueger.

108-9126

FIG. I-42. Photomicrograph of Pressed and Sintered (U-Pu)C from Run 23. Polished specimen etched with equal volumes HNO_3, acetic acid, H_2O.
108-8901

tion was coarse ground on silicon carbide paper through 600 grit, followed by final polishing with 14μ and 3μ diamond paste. A swab etch of equal volumes of acetic acid, nitric acid, and water was used to bring out the microstructure of the pressed and sintered pellets.

The specimen from run 18 (Fig. I-40) shows a typical monocarbide structure, although there are few indications of possible impurities at the grain boundaries. The pellet from run 24 (Fig. I-41) is similar to that from run 18 although there are fewer voids and the grain size appears to be somewhat larger. The specimen from run 23 (Fig. I-42) also shows the same structure, but in addition there are small lines which probably are higher carbide impurity phases.

The results are encouraging and indicate that the basic objectives have been fulfilled. A uranium-plutonium monocarbide solid solution has been prepared from a uranium-20 w/o plutonium alloy; the product was limited to the monocarbide phase by the use of hydrogen-propane mixtures of suitable composition. Further analytical work will be performed to reinforce these preliminary conclusions. The preparation of uranium-plutonium monocarbide solid solutions will continue with the emphasis shifting to the use of fluidized beds.

c. PREPARATION OF CERAMIC FUEL SPECIMENS BY HOT PRESSING (E. J. PETKUS, C. C. PAYNE)

A hot press has been assembled to produce various ceramic fuel specimens for density measurement and metallographic inspection in the Chemical Engineering Division. The entire hot press is contained within a vacuum-helium glovebox in order to prevent oxidation of the powder material. The assembly is shown in Fig. I-43. The sample is loaded into the graphite die and pressure is applied through the graphite or 30 w/o W-Mo rods by a laboratory press. Heat is supplied by induction and temperature is measured by a Pt-Pt, 10% Rh thermocouple.

In preliminary pressing, UC specimens have been pressed to densities of 90% of theoretical by applying pressure of 5,000–10,000 psi at temperatures of 1250–1500°C for 1 hr.

2. Studies of Mobile Blanket Fuels for Fast Reactors (A. D. Tevebaugh)

Mobile blanket fuels for fast breeder reactors show promise of reducing reactor down-time for fuel shuffling, improving sodium coolant utilization and, thus, power conversion efficiency, and decreasing fuel processing and refabrication costs. Consideration of reactor requirements and the properties of various fuel materials has led to selection of a paste of finely ground uranium mononitride in sodium as, currently, the most attractive mobile blanket fuel. Therefore, experimental work is being conducted to prepare and test UN-sodium pastes.

a. PREPARATION OF URANIUM MONONITRIDE (P. A. NELSON, C. LEHMANN)

Uranium mononitride powder was prepared by reaction of nitrogen with uranium shot or turnings at 800 to 1350°C and subsequent grinding of the product (see ANL-6925, p. 105 for preliminary experiments).

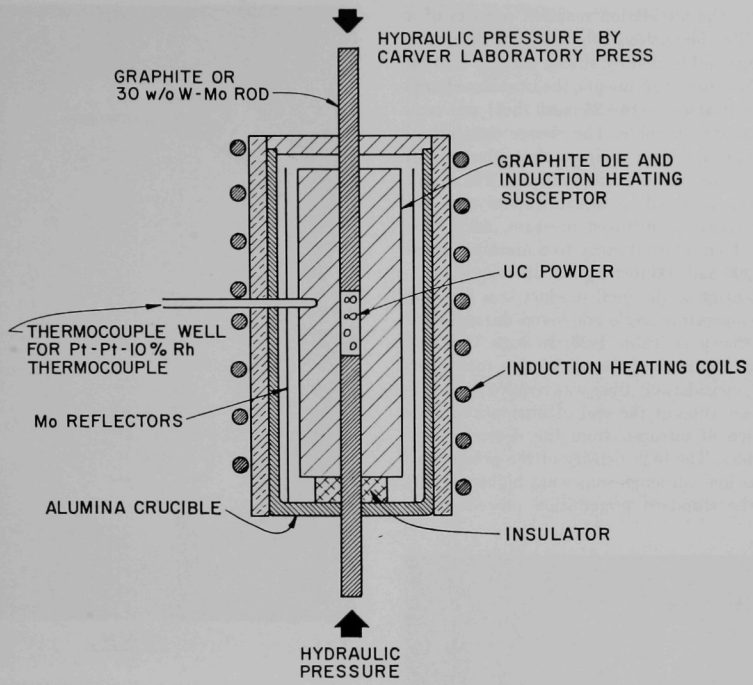

108 8909

FIG. I-43. Hot Press Assembly in Vacuum-Helium Glovebox.

TABLE I-26. NITRIDATION OF URANIUM SHOT

Uranium charge consisted of 300 to 1000 g of −14+25 mesh shot

Run No.	Time (hr) at indicated temperature (°C)				Time to Evacuate[b] to 0.05 torr (hr)	Chemical Analysis (w/o)		Bulk Density (g/cc)	Product Agglomeration (%)
	700–1100[a]	1100–1150	1150–1250	1250–1350		Nitrogen[c]	Oxygen		
UN-4[a]	0.5	0.1	0.6	7.0	0.3	5.50	0.10	7.1	70
UN-6	5.0	0.1	0.4	1.8	1.5	5.51	0.15	—	20
UN-7	9.0	0.1	2.0	0.3	2.7	5.35[d]	0.048	5.8	<5
UN-9	3.1	0.3	2.7	1.3	1.3	4.73[e]	0.04	6.5	30
UN-10	2.1	0.3	2.4	1.6	0.3	2.8[f]	0.6	7.3[f]	40
UN-11	1.3	0.7	1.0	2.5	0.3	—	—	—	0
UN-13	1.8	0.7	1.0	7.2	0.3	—	0.44	7.9	0
UN-14	1.3	0.6	1.8	1.3	0.3	5.31[e]	0.06	8.3	0

[a] Nitrogen added at 1080°C in UN-4; in other runs the nitrogen was added before heatup.
[b] The evacuation was done at 1350°C with the pressure eventually reaching about 10^{-4} torr.
[c] Stoichiometric UN contains 5.55 w/o nitrogen.
[d] Nitrogen analysis believed to be erroneously low.
[e] Nitrogen analysis of sample of ground material.
[f] The very low nitrogen analysis indicates that the product contains free uranium; if true, this would affect the bulk density of the powder.

The furnace for the nitridation reaction consists of a 6-in. dia. mullite combustion tube fitted with a vacuum-tight flange and heated by silicon carbide heating elements. In the latest experiments, the uranium charge (usually 300 to 1000 g of −14+25 mesh shot) was contained in a tungsten crucible. The charge was heated under nitrogen, rather than an inert atmosphere, from the beginning of the run to avoid sintering. The extent of reaction was followed semiquantitatively by recording the decrease in nitrogen pressure. Additional nitrogen was added intermittently to maintain a pressure between 200 and 500 torr during the reaction.

The bulk density of the final product is a function of the time-temperature cycle employed during nitridation, as is shown in Table I-26. In runs UN-6, 7, and 9, in which the bulk of the nitridation took place below 1100°C, considerable time was required to evacuate the furnace tube at the end of nitridation, indicating evolution of nitrogen from the decomposition of higher nitrides. The bulk density of the products of these runs was low, although somewhat higher than is obtained in the standard preparation procedure for UN. (In the standard procedure,[93] bulk uranium is nitrided at 800 to 900°C, followed by decomposition of the higher nitrides under vacuum at 1100 to 1400°C to obtain powdered UN with a bulk density of about 4 or 5 g/cc.)

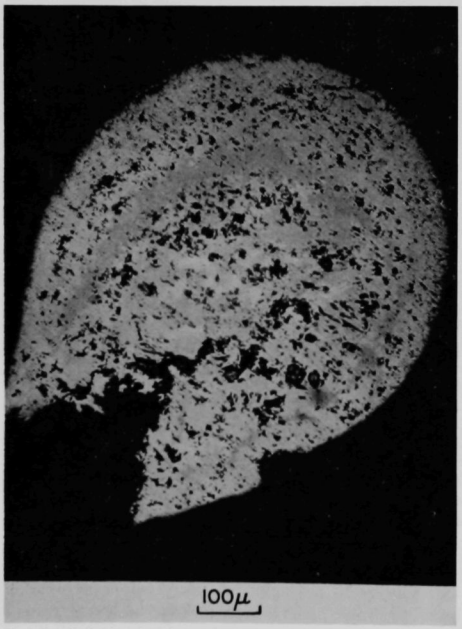

Fig. I-44. Photomicrograph of Uranium Mononitride from Run UN-4. See Table I-26 for conditions.
108-8898

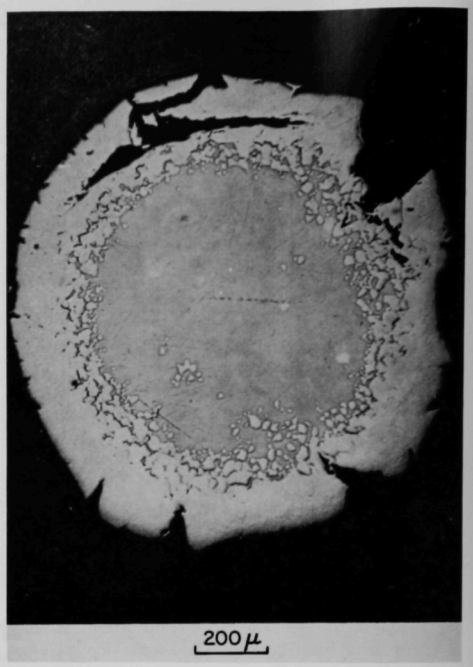

Fig. I-45. Photomicrograph of Uranium Mononitride from Run UN-14. See Table I-26 for conditions. Outer layer is UN; inner area is unreacted uranium.

In runs UN-4, 10, 11, 13, and 14 (see Table I-26), in which the bulk of the nitridation took place above 1150°C, the time required to evacuate the furnace tube at the end of a run was only 15 or 20 min, about the same as without a charge. This indicates that very little of the higher nitrides formed. The density of the products of these runs was comparatively high as indicated in the table. A photomicrograph of the product from run UN-4 is shown in Fig. I-44. As was typical of all of these runs, the spheres which had been charged were still intact although somewhat distorted.

It is postulated that in the procedure used in these experiments dense UN, rather than higher nitrides,

[93] Speidel, E. O. and Keller, D. L., Fabrication and Properties of Hot-Pressed Uranium Mononitride, BMI-1633, May 1963.

is produced initially because of the presence of metallic uranium. If the reaction continues at a temperature of less than 1200°C, the formation of higher nitrides causes disruption of the face centered cubic lattice structure of UN, thereby creating voids. On the other hand, if the temperature is raised to above 1200°C when the nitrogen-to-uranium ratio in the product is about 0.5 to 0.7, no higher nitrides are formed.

A problem which arises in this procedure is that the dense UN layer around the particles tends to inhibit further reaction of the uranium metal with nitrogen. This is shown in Fig. I-45, a photomicrograph of the product of run UN-14 which was not completely converted to UN. It is estimated that 10 to 15 hr of nitridation would be required for the complete conversion to UN of the uranium shot used in these experiments (−14+25 mesh).

In many of the earlier runs, a sizable fraction of the product was stitched together into a single agglomerate at the bottom of the crucible. Photomicrographs of the particles indicated that the stitching was caused by molten uranium leaking through the nitride skin formed on the particles. It was subsequently found that by raising the temperature slowly (~70°C/hr) from 1100 to 1150°C, through the melting point of uranium, agglomeration of the product was avoided. This method was successfully applied in runs UN-11, UN-13, and UN-14 (Table I-26). In run UN-7, nitridation was far advanced before the melting point of uranium was reached.

The nitrided product, which retained the form of the original shot, was ground in a ball mill, usually for 24 hr. The material was charged into a steel milling jar which was sealed with a rubber gasket. This loading was done in a helium glovebox so that the jar was filled with helium at the beginning of grinding.

Partial oxidation of UN during grinding has a marked effect on the bulk density of the ground product as shown in Table I-27. A high oxygen content in itself did not result in a low density product as evidenced by runs UN-10 and UN-11. The extent of oxidation during grinding (or, at least, oxidation taking place after nitridation) appears to be the important factor. In run UN-9A only a small amount of oxidation (from 0.04 w/o to 0.23 w/o oxygen) occurred during grinding. The ground product had the highest bulk density obtained thus far, although the unground material (the nitrided product of run UN-9) had a rather low bulk density. In run UN-9B the second half of the nitrided product of run UN-9 was ground in a different milling jar which was not gas tight. The oxidation to 0.8 w/o oxygen, which occurred during grinding, resulted in a bulk density for the ground product of only 3.0 g/cc or 37% of the bulk density obtained in run UN-9A, made with the same batch of feed material. The deleterious effect of oxidation during grinding on the bulk density of UN powder, which was noted in run UN-9B, is corroborated by the results for runs UN-10 and UN-13, although the effect was not as obvious.

TABLE I-27. Effect of Oxidation during Grinding on Bulk Density of Uranium Mononitride

UN formed by nitriding uranium shot was ground in a ball mill for 24 hr to 50–100 μ median size

Run No.	Oxygen Content (w/o)		Bulk Density (g/cc)	
	Not Ground	Ground	Not Ground	Ground
UN-7	0.05	0.39	5.8	7.4
UN-9A[a]	0.04	0.23	6.5	8.2
UN-9B[a]	0.04	0.8[c]	6.5	3.0
UN-10	0.6	1.9[c]	7.3	6.6
UN-13[b]	0.44	0.6[c]	7.9	7.9

[a] The product of UN-9 was ground in two separate batches. The second batch (UN-9B) was ground in a mill that was not gas tight.

[b] The product of UN-13 was ground for a total of 72 hr in three 24-hr periods. The extended grinding time was necessary to reduce the product to 50–100 μ size.

[c] The oxygen content varied considerably between different samples of the same batch of material.

It is apparent that grinding of dense UN, such as the product of UN-13, in a gas-tight ball mill would result in a product of higher bulk density than has been obtained thus far. As indicated in the following sections, a dense UN is a prerequisite for satisfactory sodium-UN paste preparation.

b. WETTING OF URANIUM MONONITRIDE BY LIQUID SODIUM (M. G. Chasanov, H. Griffin)

The wetting properties of liquid sodium for ceramic fuel materials are of importance in operation of a mobile blanket based on slurries or pastes of these materials. The sessile drop experiments reported previously in ANL-6925, p. 106, were inconclusive in demonstrating whether uranium nitride was readily wetted by liquid sodium. Since the objective of these wetting studies was to determine whether sodium-uranium ceramic pastes could be prepared easily, direct preparation of a paste was undertaken.

Experiments were conducted in a helium glovebox to examine the feasibility of preparation of UN-sodium pastes by direct mixing of the components. The UN powders employed were those prepared by either direct nitridation of uranium metal or by the more usual hydriding route.[94] The pastes were pre-

[94] Katz, J. J. and Rabinowitz, E., *Chemistry of Uranium*, Dover Publications, Inc., New York, 1961, p. 237.

pared by heating and stirring the UN powder in contact with liquid sodium at various temperatures in an alumina crucible; no differences were observed between the pastes prepared from the two powder sources. At 300°C, about ½ hr of intimate contact and stirring of −200+325 mesh powder in sodium (5 v/o solids content) was required for complete wetting of the solids; at 250°C, 1 hr was required.

Examination of the pastes indicated that the UN particles were well coated with sodium. The pastes did not separate on cooling; no instances of dewetting were observed. Treatment of the paste with ethanol resulted in liberation of black particles of UN from the dissolving sodium. The precipitated powder was found by X-ray diffraction analysis to be identical to the UN initially charged.

These results indicate that preparation of stable UN-sodium pastes can be readily achieved. The experimental observations that wetting will take place if the contact time is long enough implies that a surface reaction which promotes wetting takes place between the sodium and the UN powder; the exact nature of this reaction is not clear. It may be the removal of some interfering substance from the surface by sodium or the formation of some compound which in turn is readily wetted by molten sodium.

c. PREPARATION OF URANIUM MONONITRIDE-SODIUM PASTE (P. A. Nelson, C. Lehmann)

Following the preliminary wetting experiments described above, preparation of a UN-sodium paste of high uranium content was attempted. The UN powder of run UN-9A (Table I-27), which had a bulk density of 8.2 g/cc and a median diameter of about 100μ, was mixed with sodium at 300°C to obtain 346 g of paste containing 49 v/o solids (6.6 g of uranium/cc). The paste contained 8 v/o gas, as determined by difference from the amounts of sodium and UN added.

At 40 v/o solids, an intermediate stage in the preparation, the paste was judged to have good flow properties. However, at its final composition (49 v/o solids) the paste was quite viscous and probably not directly suitable for a flowing system. It is apparent that pastes with higher uranium densities or better flow characteristics could be prepared from denser UN powder.

II

Fuel Cycle Applications of Volatility and Fluidization Techniques[1]

(A. A. Jonke)

INTRODUCTION

The objective of the fluoride volatility program is to develop the technical data required for the design of an all-volatility commercial reprocessing plant for power reactor fuels. The process should also have the capability for operation with high enrichment fuels. To achieve this aim, the program is directed toward the development of a fluid-bed fluoride volatility process which is considered applicable to a wide variety of fuels. The following four types of fuel are under study:

(1) low-enrichment UO_2-PuO_2 clad in Zircaloy,
(2) low-enrichment UO_2-PuO_2 clad in stainless steel,
(3) high-enrichment uranium alloyed with Zircaloy, and
(4) high-enrichment uranium alloyed with aluminum.

Since the first of the above-listed fuels is most likely to be used in future water-cooled power reactors, major attention is being given to this fuel. A number of conceptual process flowsheets for this fuel were described in ANL-6925, pp. 107–108. In order to narrow the development program, attention is now being concentrated primarily on the two flowsheets described below. Although these flowsheets are not yet completely proven and are subject to change as more information is accumulated, they are based on a large body of knowledge which has been accumulated over a number of years. It is anticipated that eventually a single flowsheet will be selected for final development.

In Figure II-1 is shown the reference flowsheet on which most of the development planning has been based. This concept is described below for the case of Zircaloy-clad fuel.

Fuel assemblies which have been discharged from a nuclear reactor are charged to a fluid-bed reactor (primary reactor) where they are immersed in a bed of high-fired alumina. The Zircaloy cladding is removed by reaction with HCl gas at a temperature above the sublimation point of $ZrCl_4$ (331°C). The $ZrCl_4$ gas is pyrohydrolyzed to a solid oxide waste by reaction with steam in a second fluid-bed reactor (or pyrohydrolyzer).

The declad uranium dioxide and plutonium dioxide are unattacked and remain on the fuel support plate in the primary reactor in the form of pellets or pellet fragments. The fuel is next treated with diluted oxygen in the lower zone of the heated primary reactor in order to oxidize the UO_2 and thereby convert the fuel pieces to a finely powdered mixture of U_3O_8 and PuO_2. The mixing action of the fluid bed transports the fuel powder to the upper zone of the bed where fluorine is continuously injected. Fluorination reactions in the upper zone result in the formation of UF_6 and PuF_6, which are volatilized from the reactor and collected in refrigerated traps. Excess fluorine gas is recycled during the later stages of fluorination in order to conserve fluorine.

The mixture of hexafluorides, together with the fission products whose fluorides are volatile, is next revaporized and passed from the cold traps to a vessel (thermal decomposer) in which the less stable PuF_6 is thermally decomposed to the nonvolatile PuF_4. It is possible that the PuF_4 product from this step will require additional treatment to produce a fully decontaminated product. The UF_6 and the remainder of the fluorides pass into cold traps where they are again condensed, and are later fed to fractional distillation columns for separation of the fission product fluorides from the UF_6. The impurities, NpF_6 and TcF_6, which may not be separated by distillation, are removed from the UF_6 gas stream by sorption on solid MgF_2.

The bulk of the fission products are removed as solid waste in the alumina bed from the primary reactor. Other lower-level radioactive waste streams are removed from various process vessels.

The alternative flowsheet, which is called the interhalogen flowsheet, is shown in Figure II-2. In this

[1] A summary of this section is given on pages 7 to 13.

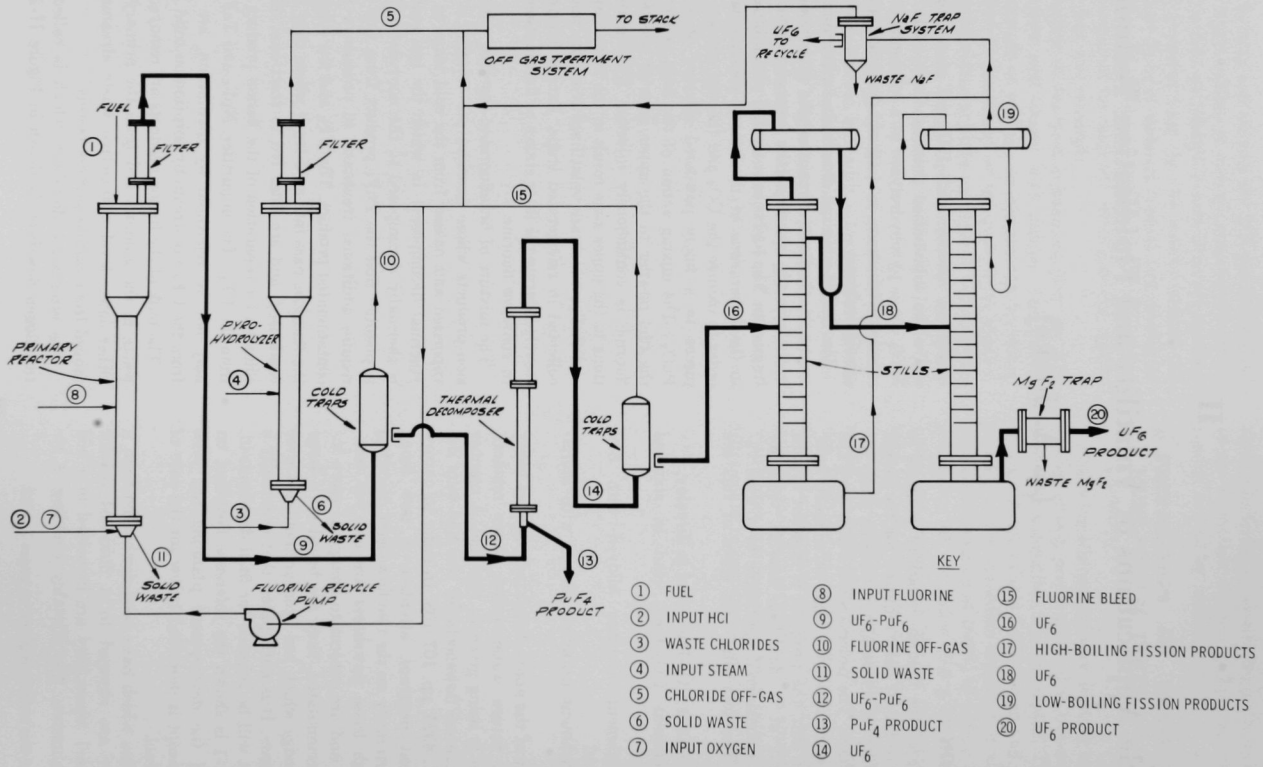

108-8171

FIG. II-1. Fluid-Bed Fluoride Volatility Process. (ANL Reference Flowsheet as of Jan. 1, 1965.)

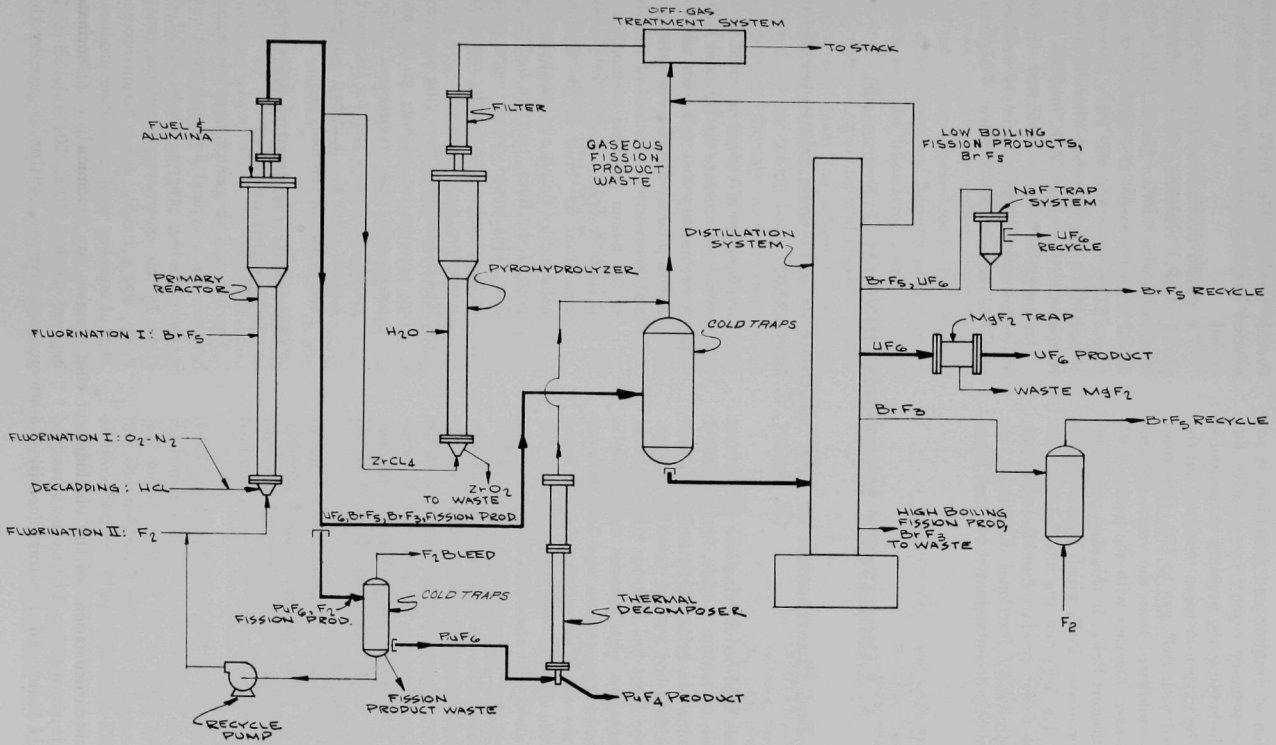

108-8381 Rev. 1

FIG. II-2. Fluid-Bed Volatility Process Interhalogen Reference Flowsheet. (Feb. 1, 1965.)

case the separation of uranium and plutonium is accomplished in the primary reactor by selective fluorination. After decladding, the uranium in the fuel is oxidized to U_3O_8 by oxygen-nitrogen mixtures and the U_3O_8 is fluorinated with BrF_5 gas to UF_6 (Fluorination I), which is volatilized from the vessel and collected in a condenser, together with the excess BrF_5 and the reaction product BrF_3. In this step, plutonium reacts to form nonvolatile PuF_4 which remains in the primary reactor. The UF_6 and the interhalogens, together with those fission product fluorides which are volatile, are separated by fractional distillation, resulting in a completely decontaminated uranium hexafluoride product. The BrF_3 in the bromine fluoride mixture is refluorinated to BrF_5 and the BrF_5 is recycled.

In a second fluorination step, the plutonium compound (PuF_4) remaining in the primary reactor is fluorinated with fluorine gas to PuF_6, which is volatilized from the vessel and collected in separate cold traps. After collection, the PuF_6 is revaporized and passed into a heated vessel where it is thermally decomposed to nonvolatile PuF_4 product.

Development work is underway on both of the above flowsheets, although primary emphasis has been placed on the reference flowsheet of Figure II-1.

A. LABORATORY INVESTIGATIONS (M. J. Steindler)

1. Fluid-Bed Fluorination of U_3O_8 Mixtures in a $1\frac{1}{2}$-Inch Diameter Reactor (R. Jarry, J. Stockbar)

Laboratory-scale fluid-bed fluorinations of mixtures of uranium oxides, plutonium dioxide, fission product oxides, and alumina are being performed in support of studies on the fluid-bed fluoride volatility process. In this process, the spent fuel element, after chemical decladding, is contacted with gaseous reagents in a fluid bed at elevated temperatures, and both uranium and plutonium are converted to the volatile hexafluorides. Since the alumina will be ultimately discarded as waste along with associated fission products, it is essential that very little uranium and plutonium be retained on the solids at the end of fluorination. Laboratory work is being performed to determine the conditions needed for removal of at least 99% of the uranium and plutonium from the fluid bed. In addition, laboratory experiments are designed to produce information useful to the operation of the fluid-bed fluoride volatility pilot plant.

Current work concerns the fluid-bed fluorination of mixtures of U_3O_8, PuO_2, fission products, alumina, and the product obtained by reacting stainless steel with an HF-O_2 mixture. Results have been obtained on the following topics:

(1) The distribution of iron and chromium, which is present in stainless steel, was determined for the various parts of the reaction system (reactor, disengaging chamber, filter chamber, and cold traps). This information is necessary to permit calculation of the buildup of cladding elements in the alumina used as inert material in the fluid bed. Further, volatile fluorides and oxyfluorides of chromium could be formed and would contaminate the UF_6 and PuF_6 product.

(2) A preliminary determination was made of the fission product distribution between the coarse and fine particle fractions of the alumina bed. If the fission products accumulate in the fine particle fraction, removal of the fission products from the bulk of the alumina may be achieved by simply sieving the bed or by transport of the fines from the bed in an inert gas flow. This would permit more extensive reuse of the alumina and thereby reduce the losses of plutonium and uranium.

(3) The possibility of removing plutonium retained on alumina by leaching of the alumina with nitric acid was investigated. This procedure could be used as a step for the recovery of plutonium from the fluid-bed material after several reuses of the fluid bed.

a. IRON AND CHROMIUM DISTRIBUTION IN FLUID-BED SYSTEM

The iron and chromium material balances reported here are for a typical fluid-bed experiment reported in the preceding progress report (ANL-6925, Table II-4). In this experiment, a mixture containing 1.6 g PuF_4, 300 g UO_2F_2, 2.3 g fission product fluorides, 33 g of stainless steel decladding product, and 430 g of alumina was fluorinated for 20 hr at temperatures between 450 and 550°C. The stainless steel decladding product, prepared by the HF-promoted oxidation of

type 304 stainless steel, was analyzed and shown to contain as major constituents, 47.6% iron and 12.8% chromium.

The distribution of iron and chromium in the reactor system for a typical experiment is shown in Figure II-3. Most of the iron (96%) remained in the alumina bed located in the reactor, and 3% was found in the disengaging chamber residue. However, only 35% of the chromium remained in the alumina bed, and 2% of the chromium appeared in the disengaging chamber residue. The weights of the alumina bed and the disengaging chamber residue were 467 and 1.9 g, respectively. A very small amount of the chromium (about 1%) was found in the outside filter chamber up-stream of the reactor. These data indicate that as much as 60% of the chromium initially present in the reaction system may be transferred along with the volatile UF_6 and PuF_6.

During the course of removing cold traps for weighing, a cinnamon-red vapor was noticed coming from the tubing above the cold trap valve. This material had accumulated in the tubing connection between the cold trap valve and the valve on the manifold. The only chromium compound which contains fluorine and corresponds in volatility and color to that observed is chromyl fluoride (CrO_2F_2). Attempts to identify this material by infrared absorption analysis failed, and hence the identity of this material is not yet known.

b. DISTRIBUTION OF FISSION PRODUCTS IN SOLID REACTION PRODUCT

Upon the fluorination of uranium and plutonium to the volatile hexafluorides, most of the fission product elements remain as solids in the alumina bed, their concentrations increasing as the bed is reused for additional fluorinations. The distribution of these fission products between the coarse and fine particle fractions of the alumina bed is of interest in the evaluation of means for separating the fission products from the bulk of the solid, bed material. If a substantial fraction of the fission products was in the fine particle fraction of the alumina bed, removal of the fine fraction would permit increased reuse of the alumina since limitations on reuse due to the heat generated by fission products would be reduced. In addition, the fluidizing quality of the alumina bed would be improved by the elimination of fine particles.

In this study on the measurement of the fission product distribution, the fine particle fraction was obtained from a disengaging chamber residue, and an alumina bed was used as the coarse particle fraction. The samples were taken from the fluorination experiment described in the preceding section. Zirconium was chosen as a typical fission product and the analyses for zirconium were made by X-ray fluorescence techniques. The results showed a 4:1 ratio between the concentrations of zirconium in the fine and the coarse particle fractions. The weight of the fine fraction was 22.5 g and that of the coarse fraction was about 646 g; the zirconium concentrations were 0.4 and 0.1 w/o, respectively. If stainless steel decladding products are also considered to be present in the fine fraction, about 50% of the fission products would be in the fine particle fraction. In view of these results, significant benefits may be obtained by removal of the fine particle of the bed material.

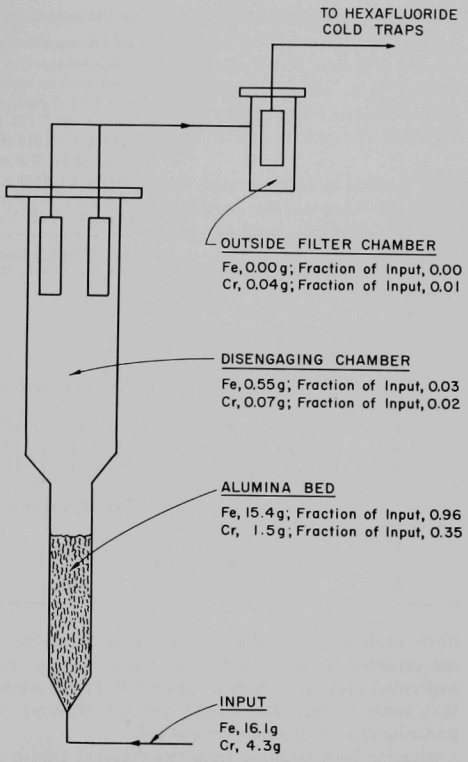

108-9102

FIG. II-3. Typical Distribution of Iron and Chromium in Fluid-Bed Reactor after Twenty Hours of Fluorination of a Mixture of PuF_4, UO_2F_2, Fission Product Fluorides, Stainless Steel Decladding Product, and Alumina.

c. LEACHING OF PLUTONIUM FROM ALUMINA USED IN FLUID BEDS

A brief study was made to determine the efficiency of leaching of plutonium from fluid-bed alumina with

TABLE II-1. Recovery of Plutonium from Alumina Beds by Leaching with Nitric Acid

Leaching acid composition: $6N$ HNO_3-$0.1M$ $Al(NO_3)_3$
Leaching temperature: 100°C
Weight of bed used in each test: 50 g
Fuel and cladding elements in bed:
Bed 1: 5.5 mg Pu (0.011 w/o); 7.0 mg U (0.014 w/o); 1650 mg Fe (3.3 w/o); 160 mg Cr (0.32 w/o)
Bed 2: 59 mg Pu (0.118 w/o); 12 mg U (0.024 w/o)

Leaching Time (hr)	Elements Found in Leach Solution (total weight, percentage of original quantity in alumina)								Pu Remaining in Alumina After Leach		
	Pu		U		Fe		Cr				
	(mg)	(%)	(mg)	(%)	(mg)	(%)	(mg)	(%)	(w/o)	(mg)	% of Original Pu
Part A. Experiments Using Alumina Bed 1											
1	3.3	60	4.1	59	1170	69	110	69	0.003	1.4	25
3	4.2	76	5.3	76	1360	83	134	84	0.002	0.8	15
5	4.7	86	—	—	1440	87	141	88	0.002	1.2	22
Part B. Experiments Using Alumina Bed 2											
1	48	81	15	125	—	—	—	—	0.012	5.9	10
3	51	86	14	116	—	—	—	—	0.007	3.3	6
5	51	86	15	125	—	—	—	—	0.008	3.9	7

nitric acid. Removal of plutonium in this manner is not expected to be a process operation, but was investigated only as a backup procedure in the event that some malfunction should prevent removal of plutonium by the fluorination method.

Alumina beds resulting from two different fluid-bed fluorination experiments were used in the leaching experiments. One of the alumina beds (alumina bed 1) contained 0.011 w/o plutonium, 0.014 w/o uranium, 3.3 w/o iron, and 0.32 w/o chromium (see ANL-6925, Table II-4). The second alumina bed (alumina bed 2) contained 0.118 w/o plutonium and 0.024 w/o uranium, but did not contain any iron or chromium.[2] The leaching solution used was $6N$ nitric acid-$0.1M$ aluminum nitrate. The aluminum nitrate was added to complex the fluoride ion and to aid in the dissolution.

Leaching experiments were performed for 1, 3, and 5 hr at 100°C for each of the alumina beds. In each experiment 50 g of the alumina bed was slurried with 100 ml of the nitric acid-aluminum nitrate solution. After the leaching period the solution was decanted from the solid, filtered, and then diluted to a known volume by the addition of the nitric acid-aluminum nitrate mixture used to rinse the solid residue. The solution was sampled and submitted for plutonium, uranium, iron, and chromium analyses. The solid residue was dried, ground, and submitted for the same analyses. The filter papers used were also submitted for plutonium analysis.

The data obtained from these two series of leaching tests are listed in Table II-1. For the series of experiments using alumina bed 1, which contained iron and chromium as well as plutonium and uranium (Part A, Table II-1), the leach solutions contained 60, 76, and 86% of the original plutonium contained in the alumina for the 1-, 3-, and 5-hr tests at 100°C, respectively. The corresponding solid residues contained 25, 15, and 22% of the original plutonium content of the alumina, corresponding to a reduction in the plutonium content of the alumina by about a factor of five, i.e., from 0.011 w/o to about 0.002 w/o. The solutions for the 1- and 3-hr tests contained 59 and 76% of the uranium originally present on the alumina. The uranium datum for the 5-hr test was anomalous (greater than 200% recovery) and was discarded. The leach solutions contained 69, 83, and 87% of the iron originally present and 69, 84, and 88% of the chromium originally present for the 1-, 3-, and 5-hr tests, respectively.

For the series of experiments using alumina bed 2 (Part B, Table II-1) in which the alumina did not con-

[2] The bed material was from experiments described in ANL-6900, p. 149, Table II-2 (last entry) and was reanalyzed for uranium and plutonium.

tain iron or chromium, the leach solutions contained 81, 86, and 86% of the plutonium originally present on the alumina for 1-, 3-, and 5-hr tests, respectively. The corresponding solid residues contained 10, 6, and 7% of the original plutonium content of the alumina, corresponding to a reduction in the plutonium content of the alumina by an order of magnitude, i.e., from the original value of 0.118 w/o to 0.01 w/o or less. Essentially all of the uranium contained on the alumina was removed in all three tests. Uranium recoveries shown in Table II-1 to be >100% can probably be attributed to variations in the uranium contents of the analytical samples.

The total plutonium recovered in the solutions and on the solid residues in all tests did not equal the amount considered to be present in the solid alumina at the start of the tests. This discrepancy may be attributed to variation in the plutonium contents of the various 50-g samples, or to sorption of plutonium on the surfaces of the glassware used in handling the solutions. The filter papers contained only microgram quantities of plutonium. If one normalizes the leaching recoveries to the quantities of plutonium actually found in the solutions and on the solid residues, recoveries in the solutions are 71, 84, and 80% for the alumina bed originally containing 0.011 w/o Pu, and 89, 94, and 93% for the alumina bed originally containing 0.118 w/o Pu for the 1-, 3-, and 5-hr tests, respectively.

These data indicate that a leaching process using nitric acid-aluminum nitrate solution under the rather mild reaction conditions of 100°C and 5-hr exposure or less would efficiently remove plutonium from alumina. For alumina beds containing approximately 0.1 w/o plutonium, the plutonium content can be lowered to 0.01 w/o or less. For an alumina bed containing about 0.01 w/o plutonium, the plutonium content would be reduced to 0.002 w/o. In those beds containing iron and chromium, about 85% of both of these elements would be removed together with about 75% of the uranium present. When no iron or chromium is present, essentially all of the uranium is removed from the alumina solids.

2. Fluorination of UO_2-PuO_2 (and F.P.) Pellets in a 2-Inch Diameter Fluidized-Bed Reactor (L. J. Anastasia, P. G, Alfredson,[3] J. G. Riha, G. W. Redding)

The 2-in. dia. fluidized-bed reactor is being used to determine fluorination conditions for UO_2-PuO_2 pellets which will ensure that a minimum of uranium and plutonium is retained by the alumina in the fluidized bed. The reactor has been equipped to study: (a) the fluorination of pellets by the two-zone oxidation and fluorination technique, and (b) the fluorination of fine particles of uranium and plutonium oxides and fluorides which are produced by the reaction of either clad or bare pellets with hydrogen fluoride-oxygen mixtures. This work is performed in support of the fluid-bed fluoride volatility pilot plant.

In the fluid-bed fluoride volatility process, chemical destruction of either stainless steel or Zircaloy cladding is possible by reaction with HF-oxygen mixtures at 550°C; pulverization of the fuel pellets occurs simultaneously.

Alternatively, Zircaloy cladding may be removed by reaction with HCl at 400°C; in this case, the pellets would not react with the decladding agent. Further processing of the pellets may be accomplished either by the two-zone oxidation-fluorination technique or by treatment with HF-O_2 mixtures followed by reaction with fluorine. In the two-zone oxidation-fluorination process,[4] pulverization of the pellets and fluorination of the resulting fines are carried out simultaneously by reaction of pellets with oxygen in the lower zone containing the packed bed of pellets and fluorination of the resulting fines with fluorine in the upper fluid-bed zone of the reactor. In the (HF-O_2)-F_2 cycle, the pellets may be initially pulverized by oxidation and hydrofluorination with HF-O_2 mixtures. The resulting fine particles of uranium and plutonium oxides and fluorides are then fluorinated to the volatile hexafluorides with fluorine. In both processing cycles, periods of recycle-fluorination with an enriched fluorine atmosphere are required to recover all the uranium and plutonium from the fluidized solids.

This report presents the results of the first three runs (Pure-1, Pure-2, and Pure-3) with UO_2-PuO_2-fission product pellets. These runs were carried out by the two-zone oxidation-fluorination process (see Figure II-1) followed by periods of recycle-fluorination. Prior to these runs, a series of eleven shakedown experiments (Sure 1 through Sure 11) with UO_2 pellets was

[3] Guest scientist from the Australian Atomic Energy Commission.

[4] L. J. Anastasia and W. J. Mecham, Oxidation-Fluorination of Uranium Dioxide Pellets in a Fluidized Bed, Ind. Eng. Chem., Process Design Develop., 4(3), 338–344 (July 1965).

made to provide checkout information on the operation of the reactor and its associated equipment and to develop satisfactory operating procedures for the fluorination of UO_2-PuO_2 pellets. Nine runs were made to study the pulverization of UO_2 pellet beds with HF-O_2 mixtures and the subsequent fluorination of the resultant fines (two shakedown runs, Sure-1 and Sure-2, have been reported previously in ANL-6925, pp. 118–120), and two runs (Sure-6 and Sure-8) were made to demonstrate the two-zone oxidation-fluorination cycle.

a. EQUIPMENT AND PROCEDURE

The equipment used in this work has been described in detail previously (ANL-6925, pp. 116–118). The major components in the system are the 2-in. dia. fluidized-bed reactor, a hydrogen fluoride disposal system, a hexafluoride collection system, a thermal conductivity cell for continuous fluorine analysis, a fluorine disposal system, and the remote-head diaphragm pump. These components, which are contained in an alpha glovebox, are shown schematically in Figure II-4.

When the pellets are reacted with HF-O_2 mixtures, volatile hexafluoride products are not formed and the reactor effluent gases are passed directly to the hydrogen fluoride disposal system. This system consists of four units in series: two traps containing soda lime, 10% $Ca(OH)_2$ in NaOH, which remove hydrogen fluoride from the gas stream by chemical reaction, a vessel which collects the moisture released by this reaction, and an activated alumina trap which removes trace quantities of hydrogen fluoride and moisture from the gas before release to the box atmosphere.

When fluorine is fed to the reactor, volatile hexafluoride products are formed and the reactor effluent gases are routed through the hexafluoride collection system. This system consists of three baffled cold traps and two NaF traps in series. The cold traps are maintained at −78°C by trichloroethylene-dry ice baths; the series of cold traps has a collection efficiency of ~97% for UF_6 under normal operating conditions.

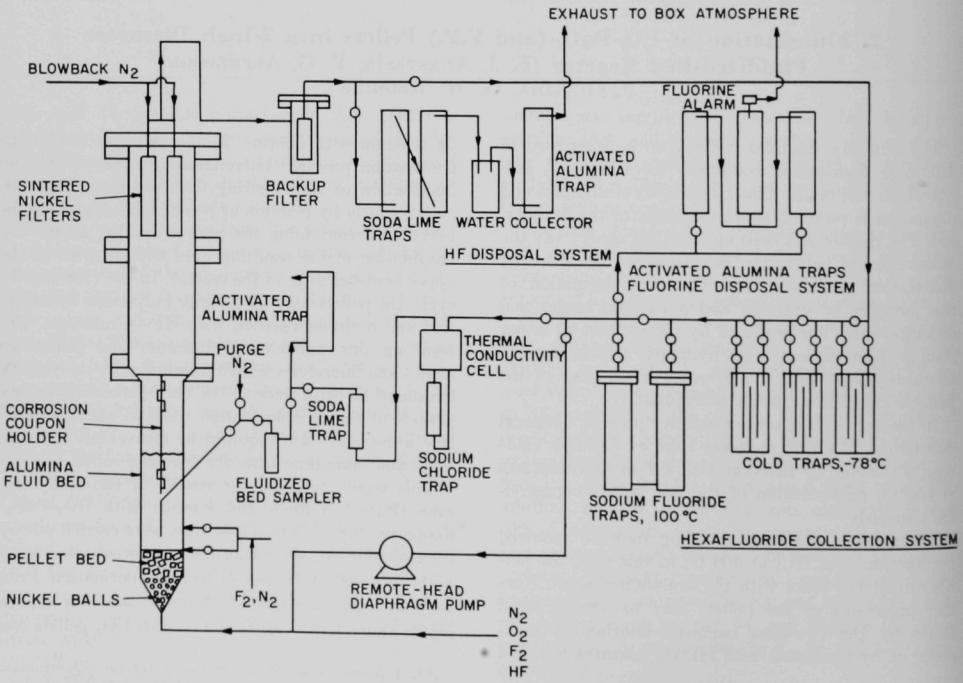

108-9113

FIG. II-4. Two-Inch Diameter Fluid-Bed Reactor System.

The remaining hexafluoride products are removed from the gas by sorption in two NaF traps at 100°C. Effluent gas from the hexafluoride collection system can be either recirculated to the fluidized-bed reactor with the remote-head diaphragm pump or passed through a series of activated alumina traps for fluorine disposal.

During two-zone oxidation-fluorination, the concentration of fluorine in the effluent gas is continuously measured by the thermal conductivity cell. The cell is used in the period of fluorination when most of the uranium and plutonium charge is present in the reactor. During this period, single-pass gas flow is used and the fluorine concentration to the reactor is normally less than 20 v/o. When more than 90% of the charge has been reacted, recycle-fluorination with a gas having a high fluorine concentration (80 to 95 v/o) is commenced. During this part of the fluorination, fluorine is circulated through the fluid-bed system by the remote-head diaphragm pump.

Samples of the fluidized alumina bed are taken through the bed sampler to monitor the fluorination of the uranium and plutonium in the reactor. The sampler consists of a ¼-in. OD tube which extends into the reactor such that the sampling point is 7 in. above the top of the bed support of nickel balls. In a typical sampling procedure, two bed samples were taken; the initial sample is taken to prevent cross-contamination from previous samples and is discarded, while the second sample is utilized for chemical analysis.

Hydrogen fluoride and fluorine were obtained from commercially available vendor's cylinders. High-purity refractory grain Alundum (Type RR, Norton Co., Worchester, Mass.) or T-61 tabular alumina (Alcoa, Pittsburgh, Pa.) was used as the fluidized-bed material. The UO_2 pellets used in these runs were hydrogen-fired, reactor grade pellets. The UO_2-PuO_2-fission product pellets used in runs Pure-1, Pure-2, and Pure-3 are described in a following section.

b. EQUIPMENT SHAKEDOWN RUNS

Eleven shakedown runs with UO_2 pellets were carried out to provide information on the operation of the fluid-bed reactor with its associated equipment and to develop operating procedures suitable for the fluorination of UO_2-PuO_2 pellets. Reaction of UO_2 pellets with HF-O_2 mixtures and fluorination of the resulting fine particles of uranium oxides and fluorides were investigated in nine runs; two runs were made to demonstrate the two-zone oxidation-fluorination cycle.

(1) Experiments Using HF-O_2-F_2 Cycle

The first two runs, Sure-1 and Sure-2, in which 2-in. deep fluidized-packed beds of UO_2 pellets were reacted with HF-O_2 mixtures at 550°C were reported previously (ANL-6925, pp. 118–120). In one of these runs (run Sure-2), caking of the pellet bed occurred. Further, it was considered that a packed bed of pellets is not representative of the conditions which exist during a decladding step at 550°C. For runs Sure-3 and Sure-4, UO_2 pellets were placed in open nickel baskets, $^9/_{16}$-in. dia. by 8 in. long, in order to provide an orientation of the pellets which simulated the conditions during a decladding step. The pellet charge of 590 g was immersed in 1000 g of alumina (static bed height of 10 in.) and reacted with approximately 40 v/o HF in oxygen at 550°C. In each run, the reactor was inspected after 3 hr of reaction and a layer of uranium-bearing fines, approximately 2 in. thick, was observed on top of the static alumina bed. In run Sure-3, the fines were successfully fluorinated with a reaction sequence of once-through gas flow for 6.5 hr with 4 to 20 v/o fluorine at 400 to 500°C and recycle-fluorination for 5 hr with 90 to 100 v/o fluorine at 500°C. In run Sure-4, fluorination with once-through gas flow was carried out with 12 to 21 v/o fluorine at 400 to 500°C. This fluorination step was limited to 2.5 hr in an attempt to reduce the overall fluorination time. Subsequently, about 30% of the alumina bed agglomerated during the next 3 hr of recycle-fluorination at 500°C with 50 to 100 v/o fluorine.

In runs Sure-5 and Sure-7, a 2-in. deep bed of UO_2 pellets (660 g) was immersed in 1100 g of alumina (12-in. static bed height), and pulverization of the pellets was attempted with approximately 40 v/o HF in oxygen at 400°C. Caking of the pellet bed was encountered in run Sure-5 after 1.5 hr of reaction and also in run Sure-7, after 2.4 hr of reaction. An additional 1.5 hr of exposure to the HF-oxygen mixture successfully removed the caking condition in run Sure-5, but a similar treatment was unsuccessful in run Sure-7. Fluorination of the resulting fines was carried out in run Sure-5 by a reaction sequence involving 3.5 hr of once-through gas flow, followed by recycle-fluorination periods of 5 hr at 450°C, 5 hr at 500°C, and 10 hr at 550°C. These recycle-fluorination conditions have been effective for plutonium removal from alumina in previous studies with a 1.5-in. dia. fluid-bed reactor (ANL-6925, pp. 110–116). Operating conditions for run Sure-5 are reported in Table II-2.

Three additional runs were completed to study the effects of reactant concentration and reaction temperature on the pulverization of pellets with HF-oxygen. Operating conditions were varied in an attempt to determine conditions which were less conducive to cake formation than the 40 v/o HF in oxygen mixtures

TABLE II-2. OPERATING CONDITIONS FOR RUNS SURE-5 AND SURE-11

Equipment:	2-in. dia. fluid-bed reactor
UO_2 Pellets:	
Size:	0.5-in. dia. by 0.5-in. right cylinders
Weight:	657 g
Bed Depth:	2 in.
Bed Support:	Nickel balls (¼-in. dia.)
Alumina Fluid Bed:	
Material:	Alcoa Type T-61 alumina
Size Limits:	Nominal 48 to 100 mesh[a]
Weight:	1100 g
Static Bed Depth:	12 in.

	Run Sure-5	Run Sure-11
Oxidation-Fluorination with HF-O_2:		
Cumulative process time (hr)	0–3.0	0–3.0
Reactor pressure (mm Hg)	910–975	1000–1060
Total gas flow to fluid bed (liters/min)[b]	15.3–16.6	16.9–19.7
Superficial velocity (ft/sec)[c]	0.7–0.8	0.8–0.9
Reactant gas concentration to pellet bed:		
HF (v/o)	40	19
O_2 (v/o)	60	29
N_2 (v/o)	—	52
Temperature (°C)	400	450
Fluorination with F_2, Once-through Flow:		
Cumulative process time (hr)	3.0–6.5	3.0–6.0
Reactor pressure (mm Hg)	1255–1340	1230–1460
Total gas flow to fluid bed (liters/min)[b]	14.2–16.4	15.8–20.4
Superficial velocity (ft/sec)[c]	0.5	0.6–0.7
Fluorine concentration to fluid bed (v/o)	5–20	3–15
Diluent	N_2	N_2
Temperature (°C)	400 (3.0–6.0 hr) 400–450 (6.0–6.5 hr)	450
Fluorination with F_2, Recycle:		
Cumulative process time (hr)	6.5–26.5	6.0–11.0
Reactor pressure (mm Hg)	1000–1160	1270–1360
Total gas flow to fluid bed (liters/min)[b]	9.2–11.6	13.2–16.2
Superficial velocity (ft/sec)[c]	0.4–0.6	0.5–0.6
Fluorine concentration to fluid bed (v/o)	80–95	80–95
Diluent	N_2	N_2
Temperature (°C)	450 (6.5–11.5 hr) 500 (11.5–16.5 hr) 550 (16.5–26.5 hr)	450

[a] The −170 mesh fraction was screened from the alumina for Run Sure-11. This fraction represents about 2% of the nominal 48 to 100 mesh material.

[b] Measured at 1 atm, 25°C.

[c] Based on cross-sectional area of the fluid-bed reactor and calculated for operating conditions.

previously used. In runs Sure-9, Sure-10, and Sure-11, 660 g of UO_2 pellets and 1100 g of alumina were used. In each case pulverization of the pellets was limited to 3 hr and the extent of reaction was determined by dismantling the reactor and visually observing the quantity of fines present. After exposure of the pellets to 21 v/o HF-10 v/o oxygen in nitrogen at 400°C in run Sure-9, no reaction was evident. At the same temperature, but with 19 v/o HF-28 v/o oxygen in nitrogen, about 50% of the pellet bed was reacted in run Sure-10. With similar reactant concentrations at 450°C, the pellet bed was completely pulverized in run Sure-11. In this run, fluorination of the fines was continued for 3 hr at 450°C with 3 to 15 v/o fluorine and for 5 hr of recycle-fluorination at 450°C with 80 to 95 v/o fluorine. Operating conditions for run Sure-11 are given in Table II-2. Subsequent recycle-fluorination periods at 500 and 550°C were not carried out because this step had been successfully demonstrated in previous runs.

TABLE II-3. Operating Conditions for Runs Sure-6 and Sure-8

Equipment:	2-in. dia. fluid-bed reactor
UO_2 Pellets:	
Size:	0.5-in. dia. by 0.5-in. right cylinders
Weight:	655 g
Depth:	2 in.
Bed Support:	Nickel balls (¼-in. dia.)
Alumina Fluid Bed:	
Material:	Alcoa T-61 alumina
Weight:	1100 g
Size Limits:	Nominal 48–100 mesh
Static Bed Depth:	12 in.

	Run Sure-6	Run Sure-8
Two-Zone Oxidation-Fluorination with O_2-F_2:		
Cumulative process time (hr)	0–3.0	0–3.0
Reactor pressure (mm Hg)	1315–1375	1480–1510
Total gas flow to fluid bed (liters/min)[a]	19.4–20.1	21.3–22.5
Superficial velocity (ft/sec)[b]	0.7–0.8	0.7
Oxygen concentration to pellet bed (v/o)	18	11
Fluorine concentration to fluid bed (v/o)	7	15
Diluent	N_2	N_2
Temperature (°C)	500	450
Fluorination with F_2-Recycle:		
Cumulative process time (hr)	3.0–18.0	3.0–23.0
Reactor pressure (mm Hg)	1010–1330	1220–1460
Total gas flow to fluid bed (liters/min)[a]	10.0–14.5	10.0–14.5
Superficial velocity (ft/sec)[b]	0.5–0.6	0.5–0.6
Fluorine concentration to fluid bed (v/o)	80–95	80–95
Diluent	N_2	N_2
Temperature (°C)	500 (3.0–8.0 hr) 550 (8.0–18.0 hr)	450 (3.0–8.0 hr) 500 (8.0–13.0 hr) 550 (13.0–23.0 hr)

[a] Measured at 1 atm, 25°C.
[b] Based on cross-sectional area of column and calculated for operating conditions.

(2) Two-Zone Oxidation-Fluorination Experiments

The two-zone method of oxidation and fluorination was successfully demonstrated in two experiments, runs Sure-6 and Sure-8. In these runs, 2-in. deep fluidized-packed beds of UO_2 pellets were reacted with either 18 v/o oxygen in nitrogen at 500°C or 11 v/o oxygen in nitrogen at 450°C. In each case, recycle-fluorination with 80 to 95 v/o fluorine was begun after 3 hr of two-zone operation. Operating conditions for these runs are given in Table II-3.

(3) Evaluation of Checkout Runs

In the series of checkout runs with 2-in. deep fluidized-packed beds of UO_2 pellets, the two-zone method of oxidation and fluorination has given smooth operation for the entire fluorination cycle, whereas operational difficulties were generally experienced when the pellets were reacted with mixtures of hydrogen fluoride and oxygen. In the latter runs, particular interest was focused on (a) establishing processing conditions for the reaction of UO_2 pellets with HF-O_2 mixtures which would avoid caking of the pellet bed, and (b) demonstrating fluorination of the fluidized alumina bed containing 40 w/o uranium fines produced by the reaction of UO_2 with HF-O_2 mixtures.

The results of shakedown runs concerning the reaction of UO_2 pellets with HF-O_2 mixtures are summarized in Table II-4. Caking of the pellet bed was encountered in runs which used approximately 40 v/o HF in oxygen (runs Sure-2, Sure-5, and Sure-7) at 400 or 550°C. In one case, run Sure-5, the caking condition was successfully removed by continuing the exposure to the HF-oxygen mixture, and the entire processing cycle was completed. In two runs, Sure-1 and Sure-9, in which the hydrogen fluoride concentration exceeded that of oxygen, UF_4 formation on the pellet surfaces inhibited further reaction at both 400 and 550°C.[5] Satisfactory conversion of the pellets to

[5] Visual examination of the pellets revealed a thin layer of green material which covered the surface of the pellets and is believed to be uranium tetrafluoride (UF_4).

fine powder was demonstrated at 550°C in runs Sure-3 and Sure-4 for which the pellets were stacked in open baskets. Satisfactory reaction of a 2-in. pellet bed was also obtained with 20 v/o HF-30 v/o O_2 in nitrogen at 450°C, as demonstrated in run Sure-11. In this run, a successful operating procedure for fluorination of the bed of uranium fines produced in the HF-O_2 step was also demonstrated. This procedure is outlined in Table II-5.

In the shakedown runs which were carried out for the complete recycle-fluorination periods (runs Sure-5, Sure-6, and Sure-8), uranium removal from the alumina was greater than 99.95%; the uranium removed was completely accounted for by UF_6 collected in the cold traps and NaF traps. The distribution of uranium as a function of alumina particle size was determined from a sample of the final alumina bed from run Sure-8. This distribution is given in Table II-6. Increased uranium retention with decreased particle size is clearly indicated.

TABLE II-4. Summary: Oxidation-Fluorination of UO_2 Pellets with HF-O_2 Mixtures

Equipment:	2-in. dia. fluid-bed reactor
UO_2 Pellets:	0.5-in. dia. by 0.5-in. right cylinders
Pellet Bed Depth:	2-in. (~660 g)
Bed Support:	Nickel balls
Alumina Fluid Bed	
Runs Sure-1, Sure-2, and Sure-4:	Norton RR Alundum, −40+170 mesh
Remaining Runs:	Alcoa Type T-61, nominal 48 to 100 mesh
UO_2/Al_2O_3:	0.6 g/g
Superficial Gas Velocity in Fluid Bed at Operating Conditions:	0.7 to 1.0 ft/sec
Duration:	3 hr
Reactant Gas Diluent:	Nitrogen

Run Sure-	Temp (°C)	Reactant Concentration to Pellet Bed		Comments
		HF (v/o)	O_2 (v/o)	
1[a]	550	47	12	No reaction
2[a,b]	550	42	58	Cake after 0.5-hr reaction
3	550	33	60	Pellets contained in basket—satisfactory reaction
4	550	46	46	
5	400	40	60	Satisfactory reaction—partial cake during run
7[c]	400	42	58	Cake after 2.4 hr of reaction
9[d]	400	21	10	No reaction
10[d]	400	19	28	Approximately 50% reaction
11[d]	450	19	29	Satisfactory reaction

[a] These runs were reported previously in ANL-6925, p. 119.
[b] Superficial gas velocity in the fluid bed at operating conditions was 1.4 to 1.7 ft/sec.
[c] Run duration was 3.5 hr.
[d] The −170 mesh fraction was screened from the alumina. This fraction represents about 2% of the nominal 48 to 100 mesh material.

TABLE II-5. Fluorination Conditions for Run Sure-11[a]
Temperature: 450°C

Cumulative Process Time (hr)	Fluorine		Gas Flow
	(v/o)	Inlet Location	
3.0–4.0	10	Lower side[b]	Once-through
4.0–4.5	3	Bottom	Once-through
4.5–5.0	8	Bottom	Once-through
5.0–6.0	15	Bottom	Once-through
6.0–11.0	80–95	Bottom	Recycle

[a] For other operating conditions, see Table II-2.
[b] Lower side inlet is 3 in. above the bed support of nickel balls.

TABLE II-6. Variation of Uranium Concentration with Particle Size in Final Alumina Bed, Run Sure-8

Mesh Size	Average Particle Size (μ)	Uranium Concentration (w/o)
−40+60	335	0.003
−60+80	214	0.002
−80+120	151	0.004
−120+170	107	0.006
−170+325	66	0.020

c. FLUORINATION OF UO_2-PuO_2-FISSION PRODUCT PELLETS

(1) Materials and Procedure

Several runs (Pure-1, Pure-2, and Pure-3) have been completed with UO_2-PuO_2 pellets containing nonradioactive fission products. In each of the runs, a 2-in. deep fluidized-packed bed of pellets was reacted in a sequence consisting of two-zone oxidation and fluorination, single-zone fluorination, and recycle-fluorination. The pellets, containing nominally 0.4 w/o plutonium (as PuO_2), 86 w/o uranium (as UO_2), and 1 w/o fission products (as the oxides), were made by the Numec Co., (Apollo, Pa.) from a solid solution UO_2-PuO_2 powder which was mixed with specified quantities of 19 nonradioactive fission product oxides. The pellets were pressed and then sintered in nitrogen-6 v/o hydrogen at 1600°C. The composition of the pellets is reported in Table II-7. Alcoa T-61, tabular alumina (nominal 48 to 100 mesh) was used as the fluidized bed material for runs Pure-1 and Pure-2, and Norton high-purity, refractory grain Alundum (type

RR, −40+170 mesh) was used in run Pure-3. Operating conditions for the three runs are shown in Table II-8.

In run Pure-1, the rate of reaction indicated by fluorine utilization was lower than in previous shakedown runs with UO_2 pellets. In subsequent runs with plutonium-bearing fuels, the oxygen concentration was increased from 11 v/o to 19 v/o during the oxidation-fluorination step and the reaction temperature was increased from 450 to 500°C in an attempt to increase the rate of oxidation of the pellets and thereby increase the fluorine utilization. Also, the duration of the oxidation-fluorination step (3 hr in runs Sure-6 and Sure-8) was prolonged to 4 hr to increase the extent of reaction. The lower oxidation rates observed for the UO_2-PuO_2-fission product pellets, compared with those found for UO_2 pellets, are attributed to the presence of 1% fission products (as oxides) and 0.4% plutonium (as PuO_2) in these pellets. Similar results have been observed by Schmets and coworkers.[6] During two-zone operation in runs Pure-2 and Pure-3, approximately 20 v/o oxygen in nitrogen was fed to the pellet zone and the fluid-bed temperature was maintained at 450°C for 3 hr. In all three runs, conversion of the pellets to hexafluorides was 80 to 90% complete at the end of the two-zone oxidation-fluorination step, and therefore only 1 hr of single-zone fluorination with 10 v/o fluorine was required to insure that the pellets were reacted before recycle-fluorination commenced. Recycle-fluorination for 5 hr at 450°C, 5 hr at 500°C, and 10 hr at 550°C was carried out in runs Pure-2 and Pure-3. The 450°C period was omitted in run Pure-1 because the two-zone operation had been concluded at 500°C.

Fluorine concentration during the recycle-fluorination periods (see Table II-8) varied because of the admission of nitrogen for filter blowback and as instrument purges. In run Pure-1, each filter was blown back hourly with 50 psig nitrogen during the recycle-fluorination period. This nitrogen, combined with that from instrument purges, gradually reduced the fluorine concentration from 95 v/o to 80 v/o; therefore, fluorine was admitted to the system at regular intervals to return the fluorine concentration to 95 v/o. In runs Pure-2 and Pure-3, each filter was blown back every 5 min with 50 psig nitrogen: fluorine was continuously fed to the reactor system to maintain a fluorine concentration of 90 v/o. Owing to malfunctioning of the remote-head diaphragm pump, the superficial gas velocity in the fluidized bed during recycle-fluorination was lower in run Pure-1 (0.3 to 0.5 ft/sec) than in runs Pure-2 and Pure-3 (approximately 0.6 ft/sec). Alcoa T-61, tabular alumina (nominal 48 to 100 mesh) was used as the fluidized bed material in runs Pure-1 and Pure-2, and Norton high-purity, refractory grain alundum (type RR, −40+170 mesh) was used in run Pure-3.

[6] J. Schmets *et al*, paper presented at the Third United Nations International Conference on the Peaceful Uses of Atomic Energy, Geneva, 1964, Paper A/Conf. 28/P/771.

TABLE II-7. Composition of the UO_2-PuO_2 (and F.P.) Pellets[a]

Used in Runs Pure-1, Pure-2, and Pure-3

Oxide	Concentration in Pellets (w/o)	S_{Rel}[b] (%)	
PuO_2	0.488	1.8	
UO_2	97.9	1.8	
BaO	0.063	3	This group of fission product oxides has been used in previous work on the fluid-bed fluorination of U_3O_8-PuO_2-F.P. oxide mixtures in a 1.5-in. dia. reactor. See ANL-6800, pp. 148–207, ANL-6900, pp. 144–155, ANL-6925, pp. 110–116.
Ce_2O_3	0.111	10	
Eu_2O_3	0.0019	15	
Gd_2O_3	0.0005	16	
La_2O_3	0.041	10	
Nd_2O_3	0.210	6	
Pr_6O_{11}	0.039	8	
Sm_2O_3	0.043	11	
Y_2O_3	0.022	5	
ZrO_2	0.183	6	
MoO_3	0.237	4	
Ag_2O	0.045	4	
CdO	0.0002	50	
In_2O_3	0.0002	50	
Nb_2O_5	0.0001	10	
PdO	0.014	9	
RhO_2	0.023	8	
RuO_2	0.210	8	
SrO	0.045	6	

[a] Representative of spent Dresden-type fuel after 10,000 Mwd/ton burnup, 4 yr in reactor, 30-day cooled.

[b] Percent standard deviation of the mean at the 95% confidence level (Pu and U analyses, Argonne; other analyses, Numec).

(2) Results and Discussion

The uranium and plutonium concentrations in the fluidized alumina bed at various intervals during the recycle-fluorination step are shown in Figures II-5, II-6, and II-7 for runs Pure-1, Pure-2, and Pure-3, respectively. These data were obtained from samples taken from the fluid bed using the sampling device described previously. As a test of the sampling procedure, three samples were collected at 11.5 hr in run Pure-2 (Figure II-6). The initial sample was taken to prevent cross-contamination from previous samples, and then two further samples were collected for chemical analysis. The second sample contained 0.0087 w/o uranium

TABLE II-8. OPERATING CONDITIONS FOR RUNS PURE-1, PURE-2, AND PURE-3

Equipment:	2-in. dia. fluid-bed reactor
UO_2-PuO_2 (and F.P.) Pellets:	0.5-in. dia. by 0.5 in. long right cylinders
Bed Depth:	2 in.
Bed Support:	Nickel balls (¼-in. dia.)
Alumina Fluid Bed:	
Weight:	1100 g
Static Bed Depth:	12 in.

	Pure-1	Pure-2	Pure-3
Materials Charged:			
Weight of UO_2-PuO_2 (and F.P.) pellets (g)	654.6	653.7	653.1
Alumina: Type	Alcoa T-61 alumina	Alcoa T-61 alumina	Norton RR Alundum
Size Range	Nominal 48–100 mesh[a]	Nominal 48–100 mesh[a]	−40+170
Two-Zone Oxidation-Fluorination:			
Cumulative process time (hr)	0–4.0	0–3.0	0–3.0
Reactor pressure (mm Hg)	1500–1540	1480–1530	1510–1550
Total gas flow to fluid bed (liters/min)[b]	20.5–22.5	22.4–23.8	22.0–22.6
Superficial velocity (ft/sec)[c]	0.7–0.8	0.7–0.8	0.7
Oxygen concentration to pellet bed (v/o)	11–19	20	16
Fluorine concentration to fluid bed (v/o)	11	10	8
Diluent	N_2	N_2	N_2
Temperature (°C)	450–500	450	450
Single-Zone Fluorination:			
Cumulative process time (hr)	4.0–5.0	3.0–4.0	3.0–4.0
Reactor pressure (mm Hg)	1230–1350	1390–1400	1405–1410
Total gas flow to fluid bed (liters/min)[b]	16.4–17.3	18.9–19.5	18.7
Superficial velocity (ft/sec)[c]	0.7	0.6–0.7	0.6
Fluorine concentration to fluid bed (v/o)	10	10	10
Diluent	N_2	N_2	N_2
Temperature (°C)	500	450	450
Recycle-Fluorination:			
Cumulative process time (hr)	5.0–20.0	4.0–24.0	4.0–24.0
Reactor pressure (mm Hg)	1380–1480	1380–1480	1370–1510
Total gas flow to fluid bed (liters/min)[b]	8.1–12.5	16.2–18.1	14.9–19.9
Superficial velocity (ft/sec)[c]	0.3–0.5	0.6–0.7	0.5–0.7
Fluorine concentration to fluid bed (v/o)	80–95	90	90
Diluent	N_2	N_2	N_2
Temperature (°C)	500 (5.0–10.0 hr) 550 (10.0–20.0 hr)	450 (4.0–9.0 hr) 500 (9.0–14.0 hr) 550 (14.0–24.0 hr)	450 (4.0–9.0 hr) 500 (9.0–14.0 hr) 550 (14.0–24.0 hr)

[a] The −170 mesh fraction was removed.
[b] Measured at 1 atm, 25°C.
[c] Based on cross-sectional area of column and calculated for operating conditions.

and 0.032 w/o plutonium, while the third sample contained 0.0080 w/o uranium and 0.029 w/o plutonium. These results are in good agreement and indicate the effectiveness of the method used to sample the fluidized bed.

The final uranium and plutonium concentrations in the fluidized beds of alumina were about 0.004 w/o and 0.007 w/o, respectively; these results are listed in Table II-9. In each run, the uranium removal was virtually complete (>99.99%) and the plutonium removal was 97% complete. These results are in good agreement with previous experiments in a 1.5-in. dia. fluidized bed reactor which utilized (1) U_3O_8-PuO_2-fission product feed mixture containing the selected fission products shown in Table II-7, (2) a recycle-fluorination sequence of 5 hr at 450°C, 5 hr at 500°C, and 10 hr at 550°C, and (3) a single use of the alumina bed. In the previous experiments the final bed of alumina contained 0.003 to 0.015 w/o uranium and 0.003 to 0.008 w/o plutonium (ANL-6800, p. 207; ANL-6900, p. 149; ANL-6925, p. 113, Table II-1, entry B.1 and p. 116). Extrapolation of the data in Table II-9 indicates that

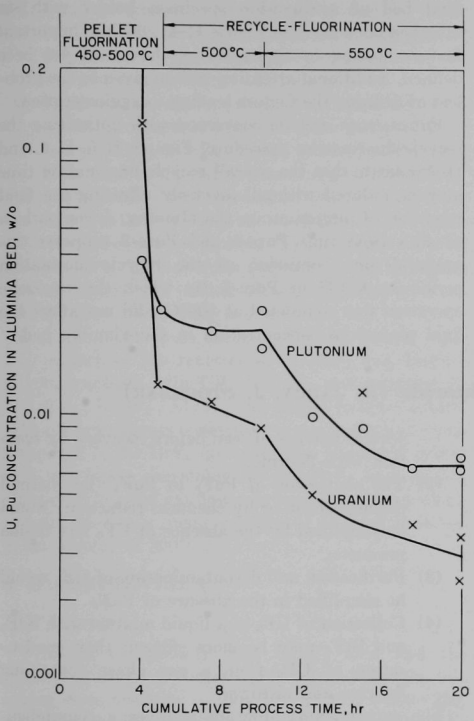

108-8908

FIG. II-5. Uranium and Plutonium Concentrations in Alumina Fluidized Bed, Run Pure-1.

if the plutonium concentration in the alumina can be held to a level of 0.007 w/o, plutonium losses associated with the final alumina bed may be reduced to less than 1% by reusing the alumina to process three batches of fuel.

The final uranium and plutonium concentrations in the alumina beds for the three runs were apparently independent of variations in the operating conditions among the runs. No significant effects were observed as a result of changes in the fluorine concentration, the filter blowback frequency, the superficial gas velocity in the fluidized bed during the recycle-fluorination, and the type of alumina used as fluid bed material.

In each run, agglomeration of a small amount of the alumina bed was observed. In run Pure-1, the weight of the agglomerate was 34 g; in each of the subsequent runs the weight was approximately 100 g. Agglomeration may have been aggravated by the presence in the

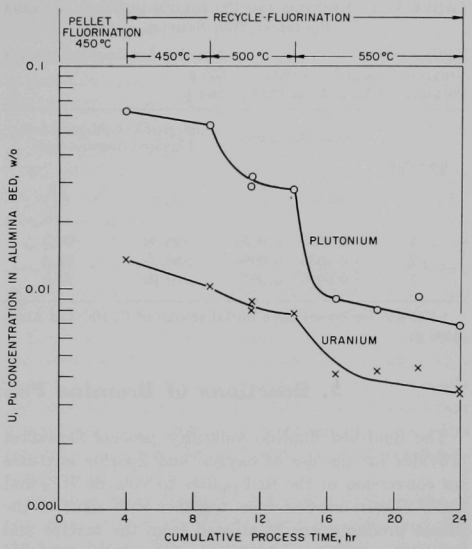

108-8915

FIG. II-6. Uranium and Plutonium Concentrations in Alumina Fluidized Bed, Run Pure-2.

108-8912

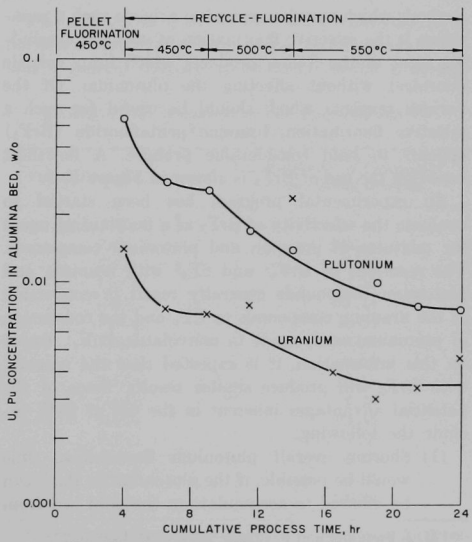

FIG. II-7. Uranium and Plutonium Concentrations in Alumina Fluidized Bed, Run Pure-3.

TABLE II-9. URANIUM AND PLUTONIUM IN FINAL ALUMINA FLUIDIZED BED SAMPLES

Equipment: 2-in. dia. fluidized bed reactor
Uranium Charged (as UO_2): 565 g
Plutonium Charged (as PuO_2): 2.81 g

Run Pure-	Final Bed Sample		Indicated Volatilization from Fluidized Alumina Bed[a]	
	U (w/o)	Pu (w/o)	U (%)	Pu (%)
1	0.0035	0.0070	>99.99	97.3
2	0.0035	0.0068	>99.99	97.3
3	0.0046	0.0076	>99.99	97.0

[a] Calculation based upon initial charge of U, Pu, and Al_2O_3 (1100 g).

fluid bed of a corrosion specimen holder with six attached coupons (see Figure II-4), but the important factors leading to agglomeration have not yet been defined. Additional attention will be given to the problem of defining the factors leading to agglomeration.

Future runs will be concerned with optimizing the recycle-fluorination procedure. Figures II-5, II-6, and II-7 indicate that the overall recycle-fluorination time may be reduced without adversely affecting the final retention of plutonium on the alumina. A comparison of data from runs Pure-1 and Pure-2 supports this proposal since omission of the recycle-fluorination period at 450°C in Pure-1 (in which the two-zone operation was completed at 500°C) did not affect the final plutonium concentration in the alumina bed.

3. Reactions of Bromine Pentafluoride (R. JARRY. J. STOCKBAR)

The fluid-bed fluoride volatility process flowsheet provides for the use of oxygen and fluorine mixtures for conversion of the fuel pellets to volatile UF_6 and PuF_6. These hexafluorides, together with some of the fission products, are volatilized from the reactor and are subsequently separated from each other by thermal decomposition of PuF_6 and distillation of UF_6 in order to obtain purified products. Considerable advantage may be gained, however, if the separation of uranium and plutonium can be accomplished prior to volatilization from the fluorination reactor. One of the methods which may be applied to achieve such a separation is the selective fluorination of uranium (including most of the fission products which form volatile fluorides) without affecting the plutonium. Of the various reagents which should be useful for such a selective fluorination, bromine pentafluoride (BrF_5) appears to hold considerable promise. A flowsheet based on the use of BrF_5 is shown in Figure II-2.

An experimental program has been started to evaluate the selectivity of BrF_5 as a fluorinating agent for mixtures of uranium and plutonium compounds. The reactions of BrF_3[7] and SF_4[8] with uranium and plutonium compounds generally result in conversion of the uranium compounds to UF_6 and the conversion of plutonium compounds to nonvolatile PuF_4. Based on this information, it is expected that the reaction with BrF_5 will produce similar results. Some of the potential advantages inherent in the use of BrF_5 include the following:

(1) Shorter overall plutonium fluorination time would be possible, if the plutonium as PuF_4 can be allowed to accumulate in the fluid bed from several batches of feed before recovery by reaction with fluorine.
(2) The conversion of PuF_6 to PuF_4 (by thermal decomposition or by chemical reduction) would be simplified by the absence of UF_6 and fission products.
(3) Purification and decontamination of UF_6 would be simplified in the absence of PuF_6.
(4) Collection of UF_6 in a liquid mixture with BrF_5 and BrF_3 may be more efficient than condensation of UF_6 from a gas phase containing fluorine and nitrogen.

The experimental program involves a comprehensive study of the fluorination of BrF_5 with solid reaction mixtures containing uranium and plutonium compounds, fission product element compounds, alumina, and stainless steel or Zircaloy decladding product. In particular, rate data for the reactions between BrF_5 and uranium compounds such as UF_4, UO_2F_2, U_3O_8, UO_2, and UO_3 are of practical interest. The initial experimental work is concerned with the reaction of BrF_5 with various uranium compounds and with solid mixtures containing uranium compounds, fission products, alumina, and decladding products. These experiments are performed to determine reaction conditions adequate to result in the removal of greater than 99% of the uranium. In addition, a method for the safe disposal of BrF_5 is being developed using a solid reactant such as activated alumina or soda lime.

This report presents experimental results for the following types of investigations:

1. The reactions between activated alumina and BrF_5 and between soda lime and BrF_5 were investigated to develop a method for transforming waste BrF_5 to an inert solid reaction product for disposal.

[7] M. J. Steindler and F. Linzer, ANL-5633, 1956, p. 27.
[8] C. E. Johnson, J. Fischer, and M. J. Steindler, J. Am. Chem. Soc., **83**, 1620 (1961).

2. Reaction kinetics were measured for the UF_4-BrF_5 reaction over the temperature range 175 to 275°C, and for the UO_2F_2-BrF_5 reaction over the the temperature range 175 to 300°C.
3. Experiments were performed to determine the extent of uranium removal from mixtures containing UF_4, UO_2F_2, fission product oxides, and alumina over the temperature range 175 to 250°C.
4. Experiments were performed to determine the ultimate removal of uranium at 300°C from reaction mixtures containing UF_4, UO_2F_2, fission products, and alumina and from such mixtures to which was added either stainless steel or Zircaloy decladding products.
5. Experiments were performed which permit comparison of the reactivities of BrF_5 and fluorine in reactions with UF_4, UO_2F_2, and mixtures of UF_4, UO_2F_2, Al_2O_3, and fission product oxides.

In all experiments concerning investigations of items 2 through 5, the BrF_5 flow rate was about 0.5 g/min in a gas phase containing 26 v/o BrF_5 and 74 v/o nitrogen. The total gas flow rate was 250 ml/min which corresponded to a linear velocity of about 0.04 ft/sec in the reactor at 300°C.

a. EXPERIMENTAL

(1) Materials

Uranium Compounds. The UO_2F_2 used had the theoretical uranium content (77.3%) and had the following sieve analysis: −180+200, 17.2%; −200+230, 8.4%; −230+325, 32.7%; and −325, 41.7%. The UF_4 used contained 75.6% uranium and 23.8% fluorine (theor. 75.8% U, 24.2% F) by analysis and had the following sieve analysis: +60, 5.8%; −60+140, 16.5%; −140+230, 12.6%; −230+325, 4.7%; and −325, 60.4%.

Bromine Pentafluoride. The BrF_5 used was material which had been purified by distillation for previous work done in this Division. A check of the vapor pressure at 0°C and at room temperature did not show evidence of contamination by volatile substances. An infrared scan of the BrF_5 was made. The very strong peak at 644 cm^{-1} and the weak peak at 580 cm^{-1} reported by Stein[9] were found; peaks at 1192 and 1226 cm^{-1} were noted, but not in the strength reported. Inspection of the scan did not show the very strong peak at 613 cm^{-1} for BrF_3 reported by Claassen[10] *et al.*

Fission Product Compounds. The fission product mixture, designated F.P. VI, contained the following compounds: Y_2O_3, ZrO_2, BaO, La_2O_3, CeO_2, Pr_6O_{11}, Nd_2O_3, Sm_2O_3, Eu_2O_3, Gd_2O_3, MoO_2, SrF_2, CsF, Nb_2O_5, and RuO_2. The concentrations of the compounds, which are the amounts calculated to be present in partially spent Dresden-type fuel elements of specified burnup and cooling period, are given in Table II-10. All of the compounds used to make up the fission product mixture had purities of 99% or greater.

Alumina. Alcoa T-61 tabular alumina was used. This material had a median particle size of 150μ and a particle size range of 80 to 250μ.

Diluent Gas. Nitrogen was used as the diluting medium. The source of the nitrogen was the house supply and the gas was passed through Linde Type 4A Molecular Sieve to remove water prior to use.

Zircaloy Decladding Product. This material was prepared by HF-O_2 reaction with Zircaloy-clad UO_2 pellets, and X-ray analysis indicated that the principal component was ZrF_4. The decladding product was ground and the −200 mesh fraction was used. The uranium content of the decladding product was determined to be 0.3 w/o.

Stainless Steel Decladding Product. This material was produced by the HF-O_2 reaction with type 304 stainless steel. The decladding product contained 47.6% iron and 12.8% chromium as determined by chemical analysis. The material was ground, and the −200 mesh fraction was used in the experiments.

(2) Apparatus

The apparatus used in this work consisted of a horizontal tubular reactor, a gas metering manifold, and a general purpose manifold to which a system

TABLE II-10. Composition of Fission Product Mixture VI

Fission Product Compound	Weight (g) of Compound[a] per 100 kg Uranium
Y_2O_3	26.46
ZrO_2	209.10
BaO	66.54
La_2O_3	57.00
CeO_2	108.34
Pr_6O_{11}	50.26
Nd_2O_3	198.28
Sm_2O_3	45.69
Eu_2O_3	1.99
Gd_2O_3	0.46
MoO_3	214.84
SrF_2	47.25
CsF	149.73
Nb_2O_5	0.23
RuO_2	106.22

[a] Based on fission product distribution calculated for Dresden-type, low-enrichment UO_2 fuel, 10,000 MWd/ton burn-up, 4-yr exposure, 30-day cooled.

[9] L. Stein, J. Am. Chem. Soc., **81**, 1273 (1959).
[10] H. H. Claassen *et al*, J. Chem. Phys. **28**, 285 (1958).

of cold traps and vacuum services were attached. The manifolds were constructed of nickel tubing and fittings. The valves were Hoke 413 Series Monel with nickel diaphragms. The tubular reactor was constructed from a 1-ft length of 1½-in. dia. nickel pipe flanged at one end. A hemicylindrical nickel bar, with a cross section half that of the reactor, was placed in the reactor to act as a support for the nickel reaction boat and to distribute heat evenly to the bottom of the boat. A nickel boat (4 in. long, 1⅜ in. wide, and 3/16 in. deep) contained the solid reactants. The temperature of the boat was sensed by a chromel-alumel thermocouple placed in a well within the bar at the midpoint of the boat and approximately 1/16 in. from the top surface of the bar.

The gas metering manifold contained three rotameters for metering fluorine, nitrogen, and BrF_5. The nitrogen flowmeter was a conventional glass rotameter; the flow meters for fluorine and BrF_5 were constructed of Kel-F. Bromine pentafluoride was supplied to the flow meter at an absolute pressure of 900 mm Hg from a liquid storage vessel heated to about 50°C. The tubing between the storage vessel and the flow meter, as well as the flow meter itself, were heated to about 60 to 70°C to prevent condensation of BrF_5 (the boiling point of BrF_5 is 40.7°C).[11] The BrF_5 line from the flow meter to the reactor and the reaction-product line from the reactor to a general purpose manifold were heated to 60 to 70°C to prevent condensation of BrF_5, BrF_3 (reaction product), and UF_6.

(3) Procedure

A weighed sample of solid reactant was carefully placed in the reaction boat to form a uniform layer of material in the boat. The boat was then placed in the reactor, and the reactor was closed and then evacuated for leak testing. A flow of about 200 ml/min of nitrogen was then started through the reactor and the heating started. When the system reached the specified reaction temperature, flow of BrF_5 was started. The exit gases from the reactor were passed through a trap containing soda lime to remove bromine fluorides and UF_6 before exhaust to the ventilation system. After the reaction was completed, the BrF_5 flow was stopped and the reactor was cooled to room temperature under an atmosphere of flowing nitrogen. During this period the BrF_5 container was cooled, the material in the feed lines was recondensed, and the BrF_5 container was weighed to determine the quantity of BrF_5 used in the reaction. The reaction boat was removed from the reactor and weighed to determine the weight loss due to the reaction. For experiments in which pure UO_2F_2 or pure UF_4 were fluorinated, the weight loss was sufficient for the calculation of extent of reaction. For the experiments using alumina-uranium mixtures, the residue was ground to ensure homogeneous sampling, and a sample was submitted for uranium analysis.

[11] M. T. Rogers and J. L. Spiers, J. Phys. Chem., **60**, 1462 (1956).

b. DISPOSAL OF BrF_5

Several tests were performed to evaluate suitable methods for disposal of excess BrF_5 from the laboratory experiments. Two solid materials were evaluated: commercial grade activated alumina (4 to 8 mesh) and reagent grade soda lime (4 to 8 mesh) which contained 7% water. The disposal experiments were performed by passing a BrF_5-N_2 mixture through a 2-in. dia., 6-in. long trap containing a weighed amount of the solid disposal agent. Thermocouples to monitor the temperature of the disposal reaction were placed on the outside surface of the reaction vessel near the bottom, top, and center, and in a re-entrant well. The thermocouple in the well could be positioned from near the bottom of the solid bed to a point midway up the reaction vessel. A sodium hydroxide solution bubbler was placed downstream of the disposal reaction vessel to indicate the break-through of bromine or BrF_5.

In one experiment using activated alumina as the disposal agent, a feed stream consisting of 33 v/o BrF_5 and 67 v/o nitrogen was passed through a 4-in. deep bed at a flow of about 0.4 g/min of BrF_5. The reaction front was at 120°C and after 14 g of BrF_5 had been passed through the reaction vessel, bromine was noted in the effluent gas stream. At this point in the reaction, the upper part of the reaction vessel was at 100°C. The alumina removed from the reactor showed a narrow white band (AlF_3) at the bottom of the bed, indicating that reaction with the fluorine component of the BrF_5 had occurred. There was no evidence of reaction in the upper portion of the alumina bed; instead it was found that bromine was adsorbed on the alumina. This experiment showed that 14 g of activated alumina would be needed as a disposal agent for 1 g of BrF_5. However, the fact that the bromine is adsorbed on alumina rather than reacting with alumina suggests that activated alumina is unsuitable for use as a disposal agent.

Two experiments were performed to evaluate soda lime as a disposal agent. In one experiment the bed was 4 in. deep, while in the other experiment the bed was approximately 6 in. deep. The BrF_5 flow was 1.2 g/min in a gas phase containing 50 v/o BrF_5 and 50 v/o nitrogen. Bromine was noted in the effluent gas stream after 28 g and 52 g of BrF_5 had been passed through the 4-in. (120 g) and 6-in. (220 g) beds, re-

spectively. At this point in the reaction, the temperature of the upper portion of the soda lime bed was 100°C.[12] Just prior to the time when bromine was noted in the effluent gas, water was observed in the effluent gas stream. These experiments showed that about 4.3 g of soda lime is required per gram of BrF_5 reacted. Examination of the soda lime bed after the reactions indicated that BrF_5 reacted completely with the soda lime. On the basis of these tests, soda lime appears to be a suitable disposal agent.

c. KINETICS OF THE UF_4-BrF_5 AND UO_2F_2-BrF_5 REACTIONS

Reaction rates were measured for the $UF_4 + BrF_5$ reaction over the temperature range 175 to 275°C, and for the $UO_2F_2 + BrF_5$ reaction over the temperature range 175 to 300°C. The data were treated using the "diminishing sphere model." In this kinetic model, developed by Anderson,[13] the reaction rate is related to the changing surface area available for reaction due to the reduction in diameter of the reacting particles with reaction time. The final equation developed is:

$$(1 - F)^{1/3} = 1 - k't \qquad (1)$$

in which F is the fraction of the solid reacted, k' is a reaction constant related to the true reaction constant by the expression $k' = k/r_0\rho_0$ (r_0 = initial radius, ρ_0 = bulk density), and t is the reaction time.

The reaction between UF_4 and BrF_5 is complicated by the formation of intermediate fluorides as a result of the reaction between UF_4 and UF_6. The reaction sequence can be depicted by the following set of equations:

1. $UF_4 + BrF_5 \rightarrow UF_6 + BrF_3$
2. $UF_4 + UF_6 \rightarrow 2UF_5$ and/or
   $2UF_4 + BrF_5 \rightarrow 2UF_5 + BrF_3$,
   $2UF_5 + BrF_5 \rightarrow 2UF_6 + BrF_3$

in which UF_5 is an intermediate compound and BrF_3 is a volatile product. The intermediate compound might be designated more properly as UF_{4+x}, with x having values of 0.25, 0.5 and 1.0 corresponding to the intermediates U_4F_{17}, U_2F_9, and UF_5. In view of the reaction temperatures, 175 to 275°C, employed in this study, and the partial pressure of UF_6 in the gas phase (1 to 60 mm Hg), the intermediate compounds most probably formed,[14] either directly or as the result of disproportionation of UF_5, were U_4F_{17} and U_2F_9. The reaction residues were brown or black, indicating the presence of these intermediate fluorides. These materials are probably formed at the reaction interface on the surface of the particles and probably exist only at the reaction interface. In treating the experimental data, i.e., the fraction of solid reacted, the assumption is therefore made that the contribution of the direct reaction, $UF_4 + BrF_5 \rightarrow UF_6 + BrF_3$, predominates.

The reaction between UO_2F_2 and BrF_5 is considered to proceed through a single step as shown in the following equation:

$$UO_2F_2 + 2BrF_5 \rightarrow UF_6 + 2BrF_3 + O_2$$

In this reaction, as is indicated for the UF_4-BrF_5 reaction above, BrF_3 is given as the reaction product of the BrF_5 component of the reaction. It is also possible that BrF and bromine are products of the reaction. Identification of the gaseous products has not yet been made. Although the stoichiometry of the reactions involving BrF_5 and oxygen-containing compounds of uranium has not been fully established, it is likely that fluorination of the uranium compounds proceeds with the formation of BrF_3 and elemental oxygen. However, the possibility of forming small quantities of Br_2 and BrF cannot be neglected. The instability of bromine oxides at temperatures above 0°C[15] makes their presence all but impossible. The equilibria between Br_2, BrF, BrF_3 and BrF_5 are sufficiently complex so that experimental determination of the stoichiometry of the reaction is required.

The experimental data for the UF_4-BrF_5 and UO_2F_2-BrF_5 reactions consisted of values expressing the fraction of solid reacted for various reaction times at several temperatures. The general rate equation, $(1 - F)^{1/3} = A - k't$, was fitted to the experimental data by the method of least squares to obtain a solution for the reaction rate constant, k'. These values of k' and values of $1/T$ derived from the reaction temperatures were subsequently used in a least squares fit of the integrated form of the Arrhenius equation:

$$\log k' = C - [E/2.303R]\cdot 1/T \qquad (2)$$

From this equation, values of the reaction rate constant, k', and the apparent activation energy, E, could be calculated.

The values of the reaction rate constant, k', for the UF_4-BrF_5 reaction varied from 0.0005 min^{-1} at 175°C to 0.0331 min^{-1} at 275°C. For the UO_2F_2-BrF_5 re-

[12] In subsequent use of a large soda lime trap, it was found that a temperature of 100°C is necessary for the bromine to react with the soda lime. If the bed temperature is not raised to this value by the heat of the fluorine reaction, the disposal trap must be heated externally.

[13] J. S. Anderson, Bull. Soc. Chim. France, **20**, 781 (1953).

[14] J. Katz and E. Rabinowitch, *The Chemistry of Uranium*, Dover, 1961, p. 385.

[15] See, for example, N. V. Sidgwick, *The Chemical Elements and Their Compounds*, Vol. II, Oxford, London, 1950, p. 1207.

action, the reaction rate constant k' varied from 0.0040 min^{-1} at 175°C to 0.0276 min^{-1} at 300°C. The values of $(1 - F)^{1/3}$ calculated from the experimentally determined fraction reacted and the theoretical plots from the least squares solution of the equation $(1 - F)^{1/3} = A - k't$, are shown in Figure II-8 for the UF_4-BrF_5 reaction and in Figure II-9 for the UO_2F_2-BrF_5 reaction. The individual equations are listed in Table II-11.

The least squares fit of the Arrhenius equation to the experimental values of k' resulted in the following equations relating the dependence of the reaction rate constant on temperature:

For the UF_4-BrF_5 reaction:

$$\log k' \ (\pm 0.00049) = 5.71942 \ (\pm 0.00024) - 3948.3 \ (\pm 2.3) \cdot 1/T \quad (3)$$

For the UO_2F_2-BrF_5 reaction:

$$\log k' \ (\pm 0.00174) = 1.49312 \ (\pm 0.00071) - 1747.1 \ (\pm 3.7) \cdot 1/T \quad (4)$$

The experimental and calculated values of the reaction rate constants are listed in Table II-12, and plotted as values of log k' *versus* $1/T$ in Figure II-10. Values for the apparent activation energy of 18.1 kcal/mole for the UF_4 reaction and 8.0 kcal/mole for the UO_2F_2 reaction were calculated from the appropriate constants of the two equations.

The activation energy values obtained from this study using BrF_5 as the fluorinating agent are compared in Table II-13 with those obtained for reactions in which fluorine, ClF_3, or SF_4 were used as fluorinating agents. The activation energy for the UF_4-BrF_5 reaction is similar to that found for the UF_4-fluorine reaction rather than that found for the UF_4-ClF_3 reaction. However, the activation energy for the UO_2F_2-BrF_5 reaction is similar to the activation energy for the UO_2F_2-ClF_3 reaction rather than that found for either the UO_2F_2-fluorine or UO_2F_2-SF_4 reactions.

d. REACTIONS OF BrF_5 WITH MIXTURES OF ALUMINA, UO_2F_2, UF_4, AND FISSION PRODUCT OXIDES

A series of experiments were performed using solid reaction mixtures simulating those used in fluid-bed experiments. The reaction mixtures contained 10 g of T-61 alumina (48 to 100 mesh, nominal), 4.2 g of UO_2F_2, 2.2 g of UF_4, and 0.07 g of fission product mixture VI (Table II-10). The alumina to uranium weight ratio in these solid mixtures was 2:1 and the

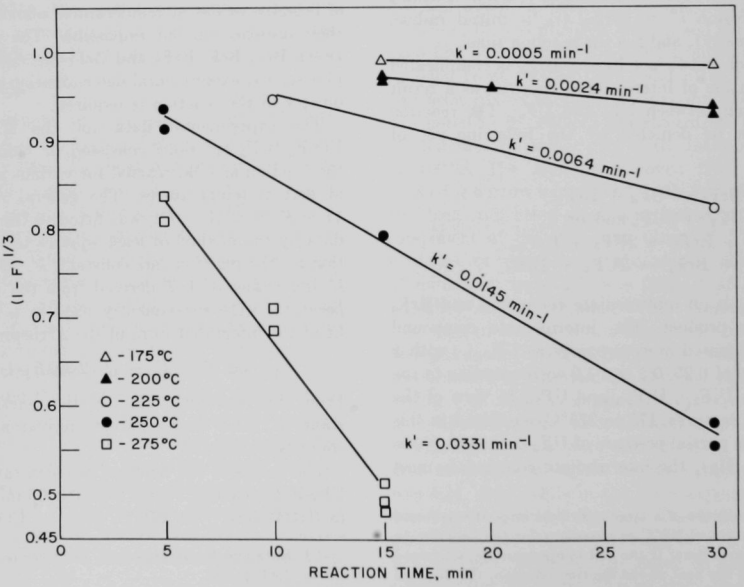

108-9109

FIG. II-8. The $UF_4 + BrF_5$ Reaction: Plots of $(1 - F)^{1/3}$ Versus Reaction Time, t. Temperature Range, 175 to 275°C.

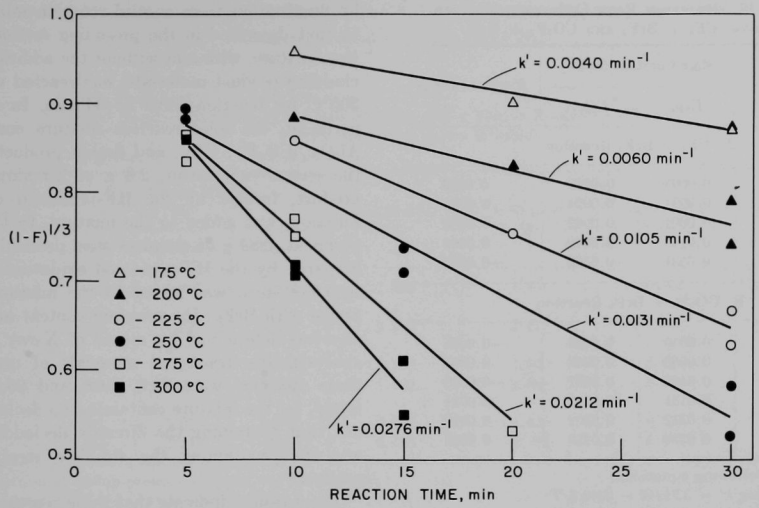

108-8910

FIG. II-9. The UO_2F_2 + BrF_5 Reaction: Plots of $(1 - F)^{1/3}$ Versus Reaction Time, t. Temperature Range, 175 to 300°C.

weight ratio of UO_2F_2 to UF_4 was also 2:1. The experiments were performed using a flow rate of BrF_5 of about 0.5 g/min in a gas phase containing 26 v/o BrF_5 and 74 v/o nitrogen. The total flow rate was 250 ml/min which was equivalent to a linear velocity in the reactor of 0.04 ft/sec. The experiments were performed at four temperature levels in the range 175 to 250°C with reaction times of 30 min.

The results obtained from these experiments together with the experimental conditions used are listed in Table II-14. The values of the fraction of uranium reacted varied from 0.3 at 175°C to 0.9 at 250°C. Values of the reaction rate constant, k', calculated from these data varied from 0.0038 min^{-1} at 175°C to 0.017 min^{-1} at 250°C. The logarithms of the rate constants are plotted in Figure II-11 against $1/T$ together with calculated data for a mixture composed of UO_2F_2 and UF_4 in the ratio of 2:1. The calculated data are obtained from the rate constants listed in Table II-12. The line through the experimental points was derived from the experimental data by a least squares solution which resulted in the following equation:

$$\log k' = 2.01969 - 1970.3/T \qquad (5)$$

Comparison of the experimental and calculated rate constants show reasonably good agreement; the experimental values are about 20% higher than the calculated values. The apparent activation energy calculated by means of Equation 5 is 9.0 kcal/mole, while the apparent activation energy calculated for a mixture of ⅔ UO_2F_2-⅓ UF_4 is 10.0 kcal/mole.

TABLE II-11. VALUES OF CONSTANTS FOR THE EQUATION $(1 - F)^{1/3} = A - k't$ FOR THE UF_4-BrF_5 AND UO_2F_2-BrF_5 REACTIONS. TEMPERATURE RANGE, 175 TO 300°C

Temp (°C)	Equation
	A. UF_4 + BrF_5 Reaction:
175	$(1 - F)^{1/3} \pm 0.002 = 0.998 \pm 0.001 - (0.0005 \pm 0.0002)\,t$
200	$(1 - F)^{1/3} \pm 0.005 = 1.004 \pm 0.002 - (0.0024 \pm 0.0004)\,t$
225	$(1 - F)^{1/3} \pm 0.012 = 1.017 \pm 0.006 - (0.0064 \pm 0.0007)\,t$
250	$(1 - F)^{1/3} \pm 0.012 = 1.003 \pm 0.005 - (0.0145 \pm 0.0005)\,t$
275	$(1 - F)^{1/3} \pm 0.026 = 1.001 \pm 0.021 - (0.0331 \pm 0.0052)\,t$
	B. UO_2F_2 + BrF_5 Reaction:
175	$(1 - F)^{1/3} \pm 0.008 = 0.995 \pm 0.004 - (0.0040 \pm 0.0005)\,t$
200	$(1 - F)^{1/3} \pm 0.026 = 0.948 \pm 0.013 - (0.0060 \pm 0.0016)\,t$
225	$(1 - F)^{1/3} \pm 0.019 = 0.965 \pm 0.009 - (0.0105 \pm 0.0011)\,t$
250	$(1 - F)^{1/3} \pm 0.029 = 0.942 \pm 0.012 - (0.0131 \pm 0.0011)\,t$
275	$(1 - F)^{1/3} \pm 0.018 = 0.968 \pm 0.008 - (0.0212 \pm 0.0015)\,t$
300	$(1 - F)^{1/3} \pm 0.026 = 0.994 \pm 0.012 - (0.0276 \pm 0.0031)\,t$

e. EFFECT OF ZIRCALOY AND STAINLESS STEEL DECLADDING PRODUCT ON URANIUM REMOVAL

Extrapolation of the experimental rate data given above for the reaction of BrF_5 with Al_2O_3-UO_2F_2-

TABLE II-12. REACTION RATE CONSTANTS FOR THE REACTIONS, $UF_4 + BrF_5$ AND $UO_2F_2 + BrF_5$

Temp (°C)	Rate Constant (min^{-1}) Exp.	Rate Constant (min^{-1}) Calc.[a]	k' calc − k' exp
A. $UF_4 + BrF_5$ Reaction			
175	0.0005[b]	0.0008	0.0003
200	0.0024	0.0024	0.0000
225	0.0064	0.0062	−0.0002
250	0.0145	0.0149	0.0004
275	0.0331	0.0329	−0.0002
B. $UO_2F_2 + BrF_5$ Reaction			
175	0.0040	0.0039	−0.0001
200	0.0060	0.0063	0.0003
225	0.0105	0.0097	−0.0008
250	0.0131	0.0142	0.0011
275	0.0212	0.0202	−0.0010
300	0.0276	0.0279	0.0003

[a] Using the following equations:

UF_4 : $\log k' = 5.71942 - 3948.3/T$

UO_2F_2 : $\log k' = 1.49312 - 1747.1/T$.

[b] This value not used in least squares calculation.

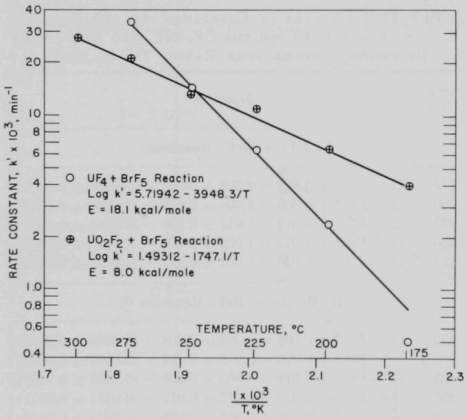

108-9104

FIG. II-10. Variation of Rate Constant for the $UF_4 + BrF_5$ and $UO_2F_2 + BrF_5$ Reactions over the Temperature Range 175 to 300°C.

UF_4-fission product oxides, indicates that a reaction time of about 30 min at 300°C would be adequate to convert the uranium contained in the solid reaction mixture completely to UF_6.

A series of three experiments was performed to evaluate the effect of the addition of decladding product materials on the extent of uranium removal by fluorination from a solid reaction mixture similar to that described in the preceding section. The reaction mixture, with and without the addition of the decladding product materials, was reacted with BrF_5 at 300°C for reaction times of 60 min. In the first experiment, the solid reaction mixture contained only Al_2O_3, UO_2F_2, UF_4, and fission products oxides. In the second experiment, 2.6 g of Zircaloy decladding product, formed by the HF-promoted oxidation of Zircaloy, was added to the mixture. In the third experiment, 0.89 g of stainless steel decladding product, prepared by the HF-promoted oxidation of type 304 stainless steel, was added to the mixture. After reaction with BrF_5, the uranium content of these samples was determined by means of X-ray fluorescence analysis. The fractional removals of uranium from these mixtures were 99.8, 99.2, and 99.6%, respectively, for the mixture containing no decladding product, that containing the Zircaloy decladding product, and that containing the stainless steel decladding product.

These results indicate that these reaction conditions (300°C and a reaction time of 60 min) are adequate to remove more than 99% of the uranium from such solid reaction mixtures. Further, the results show that the presence of Zircaloy or stainless steel decladding

TABLE II-13. ACTIVATION ENERGIES FOR THE REACTIONS BETWEEN UF_4 AND UO_2F_2 AND VARIOUS FLUORINATING AGENTS

Fluorinating Agent	Activation Energy, E (kcal/mole)	Temp. Range (°C)	Reference
Reaction with UF_4			
BrF_5	18.1	175–275	This study
ClF_3	3–6	17–194	*
ClF_3	2.6	40–80	**
F_2	15–20	265–348	***
F_2	14–16	100–375	†
Reaction with UO_2F_2			
BrF_5	8.0	175–300	This study
ClF_3	8.9	104–165	††
F_2	19.5	200–375	‡
SF_4	32	250–340	‡‡

* V. Y. Labaton, J. Inorg. Nucl. Chem., **10**, 86 (1959).

** W. Davis and R. L. Jarry, K-849, December 1953.

*** V. Y. Labaton and K. D. B. Johnson, J. Inorg. Nucl. Chem., **10**, 74 (1959).

† M. J. Steindler, ANL-5896, October 1958.

†† R. C. Shrewsberry and E. L. Williamson, KY-L-362, Part 1, 1964.

‡ M. J. Steindler, ANL-5959, March 1959.

‡‡ C. E. Johnson and J. Fischer, J. Phys. Chem., **65**, 1849 (1961).

TABLE II-14. FLUORINATION OF Al_2O_3-UO_2F_2-UF_4-FISSION PRODUCT MIXTURES USING BrF_5

Total Flow Rate: 250 ml/min (26 v/o BrF_5, 74 v/o N_2)
Linear Velocity: 0.04 ft/sec
Total Pressure: 1 atm
BrF_5 Flow Rate: 0.5 g/min
Solid Reaction Mixture: 10.0 g T-61 Alumina, 0.07 g Fission Products,[a] UF_4 and UO_2F_2 (quantities shown in table)
Reaction Time: 30 min

Reaction Temp. (°C)	U in Original Mixture (g)			U in Residue (g)	U Reacted (g)	Fraction of U Reacted	Rate Constant, k' (min^{-1})
	as UF_4[b]	as UO_2F_2[c]	Total				
175	1.650	3.217	4.867	3.395	1.472	0.302	0.0038
200	1.832	3.223	5.055	2.276	2.779	0.550	0.0078
225	1.833	3.217	5.050	1.360	3.690	0.731	0.0118
	1.652	3.215	4.867	1.169	3.698	0.760	0.0126
250	1.831	3.216	5.047	0.628	4.419	0.876	0.0167
	1.649	3.219	4.868	0.575	4.293	0.882	0.0170

[a] For composition of fission product mixture, see Table II-10.
[b] UF_4 used contained 75.6% U (theoretical, 75.8%).
[c] UO_2F_2 used contained 77.3% U (theoretical, 77.3%).

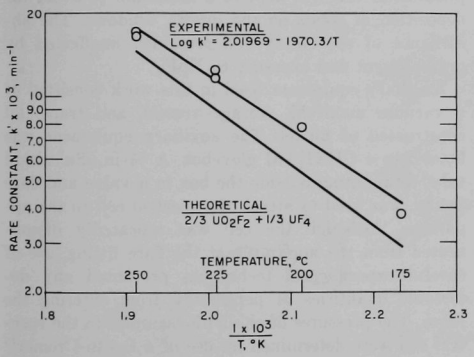

108-9107

FIG. II-11. Variation of Rate Constants for the Reaction Between Mixtures of UF_4 and UO_2F_2 with BrF_5 over the Temperature Range, 175 to 250°C.

product in the solid mixtures will not hinder uranium removal, and that tin is the only component of the decladding products that is removed during fluorination.

f. COMPARISON OF REACTIVITY OF BrF_5 AND FLUORINE

A series of experiments were performed in which UF_4 or UO_2F_2 or mixtures containing UF_4, UO_2F_2, alumina, and fission product oxides were reacted with fluorine to obtain reaction rate data suitable for comparison with similar rate data obtained with BrF_5 (Table II-15). The reactions with fluorine were carried out using the same reaction conditions previously listed (Table II-14) for the reactions with BrF_5.

TABLE II-15. REACTION RATE CONSTANTS FOR REACTIONS USING BrF_5 OR FLUORINE AS THE FLUORINATING AGENT

Temp (°C)	Reaction Rate Constant, k' (min^{-1})					
	UO_2F_2		UF_4		UF_4-UO_2F_2-Al_2O_3-F.P. Mixtures	
	BrF_5	F_2	BrF_5	F_2	BrF_5	F_2
200	0.0064	0.0005	—	—	—	—
250	—	—	0.0145	0.0010	0.0169	0.0013
275	—	—	0.0344	0.0040	—	—
300	0.0276	0.0008	—	—	—	—

The data show that the rate constants for reactions with fluorine are an order of magnitude lower than those for the reactions using BrF_5 as the fluorinating agent. For example, considering a 30-min reaction period: for UO_2F_2 at 300°C the fractions reacted would be 0.995 for BrF_5 and 0.070 for fluorine; for UF_4 at 250°C the fractions reacted would be 0.820 for BrF_5 and 0.087 for fluorine; and for the UF_4-UO_2F_2-alumina-fission product mixtures at 250°C, the fractions reacted would be 0.873 for BrF_5 and 0.112 for fluorine. It can be anticipated that the increased reaction rates when BrF_5 is employed as the fluorinating agent for uranium would result in shortening the time required to process a batch of oxide fuel.

Future work will be concerned with determining the stoichiometry of the reactions of BrF_5 with selected uranium compounds and examining the effect of BrF_5 on plutonium compounds.

4. Chemistry of Neptunium Hexafluoride (T. Gerding)

a. INTRODUCTION

Neptunium-237 can be expected to be a significant contaminant in highly irradiated low-enrichment fuels.[16] A knowledge of the pertinent physical and chemical properties of neptunium hexafluoride is necessary in order to achieve a complete separation of uranium and plutonium from neptunium by the fluoride volatility process. Little information on the chemistry of neptunium hexafluoride is available and hence, a study of the properties of neptunium hexafluoride has been initiated. A detailed determination of the spectrum of gaseous NpF_6 was carried out in the ultraviolet, visible, and near-infrared regions. These data are expected to be useful as an analytical tool for the detection and determination of NpF_6.

b. EXPERIMENTAL

Neptunium-237 in the form of the dioxide (NpO_2) was obtained from Oak Ridge National Laboratory. Analysis of the dioxide indicated the presence of 0.13% plutonium and 0.04% uranium in the sample. Spectrographic analysis showed only minor metallic impurities.

The neptunium hexafluoride used for the spectral determination was prepared by the reaction of NpO_2 and elemental fluorine at 500°C. A sample of NpO_2, contained in a nickel reaction boat, was placed in a nickel reaction tube which was heated by a furnace. Elemental fluorine was passed over the heated sample and the gaseous reaction product, together with unreacted fluorine, was passed through traps cooled to −78°C to condense the neptunium hexafluoride. Fluorine was circulated through the system by means of a remote head connected to a Lapp Pulsafeeder pump. Fluorine was added periodically to maintain the system pressure near 1 atm. The rate of reaction of NpO_2 and fluorine was greater than 2 g NpO_2/hr. The NpF_6 was purified by trap-to-trap distillation under vacuum.

Purity of the NpF_6 was ascertained by vapor pressure measurements and infrared scan of the vapor. Prior to each spectral determination, the purity of the sample was determined by vapor pressure measurement. In all cases, the measured vapor pressure agreed with that reported in the literature.[17]

Spectral cells were constructed of 1¼-in. dia. Monel tube, threaded at each end to receive a brass retaining ring which contained a Teflon washer, a 3-mm thick quartz window, and a Teflon gasket. Cell lengths of 1 and 10 cm were used. A small valve containing a flare fitting was silver-soldered into the body of the cell. Figure II-12 shows the construction of the spectral cells.

Prior to use, each cell was thoroughly cleaned and checked for leaks with a helium mass-spectrometer leak detector. In addition, each cell was treated with elemental fluorine at room temperature for 30 min, followed by treatment with NpF_6 for 15 min before the sample of NpF_6 was introduced.

Samples were introduced by expansion of the gas into the evacuated cells. In all instances the length of time that NpF_6 was in contact with the spectrophotometer cell was kept to a minimum to avoid the deposition of solids on the quartz windows. The absorbance of the empty cell remained unaffected by pretreatment and exposure to NpF_6.

Auxiliary equipment used in this work consisted of a vacuum manifold, storage vessels, and traps, all constructed of nickel. The auxiliary equipment was housed in a CENHAM glovebox. A ¼-in. dia. nickel tube, terminating outside the box in a valve and flare fitting, was used to attach the spectral cell to the apparatus. Although the cell was repeatedly disconnected from the apparatus at the flare fitting, use of careful experimental techniques prevented any detectable quantities of neptunium from entering the room. The pressures of the NpF_6 samples in the spectral cell were determined by use of a Booth-Cromer[18] pressure transmitter and self-balancing relay connected to a mercury manometer and a Taylor absolute pressure transmitter connected to an Ashcroft gauge calibrated to read 0 to 200 mm Hg absolute.

The absorption spectra were determined using a Cary Model 14 double beam, recording spectrophotometer. The wavelength calibration of the instrument was checked against a mercury arc and was found to deviate only very slightly from the literature values for the mercury arc.[19] The spectrophotometer recorded the value of absorbance ($\log I_0/I$) directly.

The concentration of neptunium hexafluoride in the cell in units of moles per liter was calculated from the

[16] D. R. Vondy, J. A. Lane, and A. T. Gresky, Ind. Eng. Chem. Process Design Develop., **3**, 293 (1964)

[17] B. Weinstock, E. Weaver, and J. Malm, J. Inorg. Nucl. Chem., **11**, 104 (1959).

[18] S. Cromer, USAEC Report MDDC-803, 1944.

[19] K. S. Gibson, NBS Circular 484, 1949, p. 12.

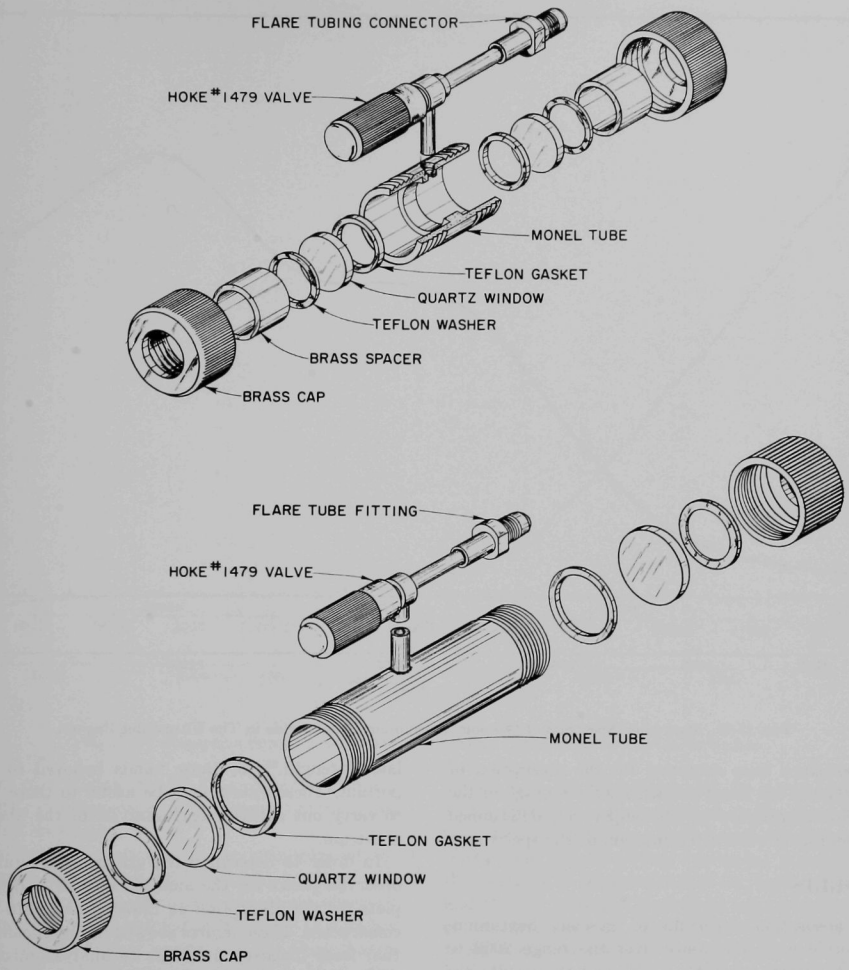

108-6826

FIG. II-12. Spectral Cells for Use with Corrosive Gases.
Top: 1-cm cell
Bottom: 10-cm cell

observed pressure and temperature. All spectral determinations were carried out at ambient laboratory temperatures. Molar absorptivities (molar extinction coefficients) were calculated from the measured absorbance and the calculated concentrations of NpF_6 in the samples, according to the equation:

$$\log \frac{I_0}{I} = \epsilon \ell c, \quad \text{or} \quad \epsilon = \frac{1}{\ell c} \log \frac{I_0}{I},$$

where $\log I_0/I$ is the absorbance, ϵ is the molar absorptivity in liters mole^{-1} cm^{-1}, c is the concentration in moles liter^{-1}, and ℓ is the thickness of the absorbing medium or the length of the light path in the sample. The length of the light path was obtained from a knowledge of the dimensions of the nickel cell and the thickness of the compressed gaskets sealing the quartz windows to the body of the cell. Values for

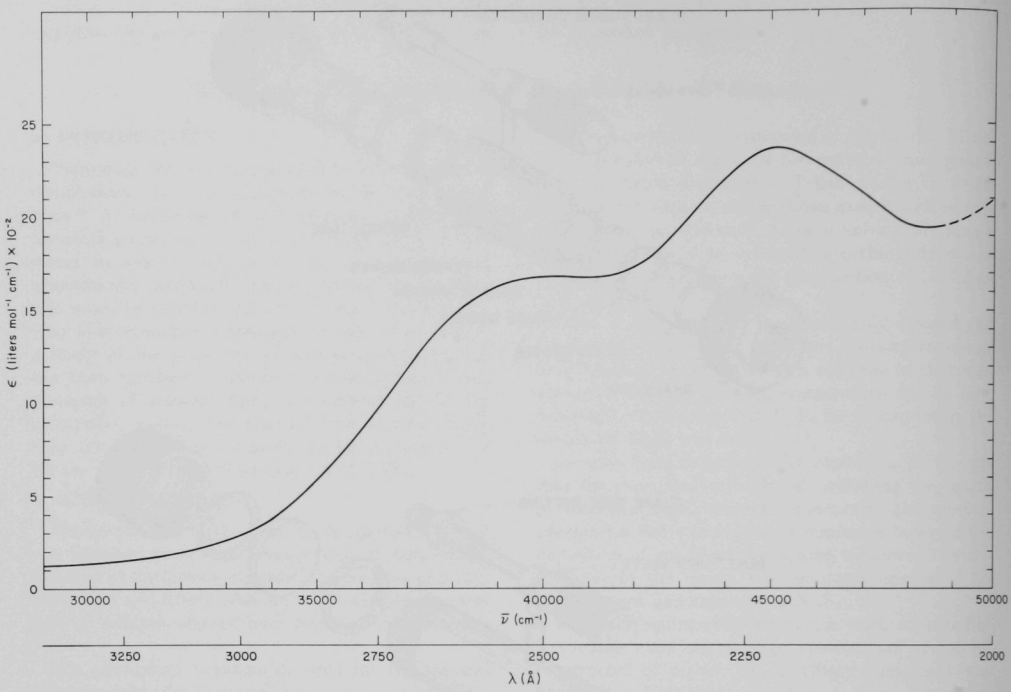

108-8611

FIG. II-13. Absorption Spectrum of Gaseous Neptunium Hexafluoride in The Ultraviolet Region.

the absorbance were corrected for the absorption of the empty cell by using the arithmetic average of the values for absorbance of the empty cell determined before and after each determination of the spectrum.

c. RESULTS

The absorption spectrum of gaseous neptunium hexafluoride was determined over the range 2000 to 25,000 Å (50,000 to 4,000 cm^{-1}), and the results are shown in Figures II-13, II-14, and II-15. The figures illustrate the variation of molar absorptivity, ϵ, with wave number over the indicated range. All values of the molar absorptivity, shown in the three figures, represent averages of at least two determinations, and in most instances, of three or more determinations. The molar absorptivity value of each peak (the peak height) is based on four or more determinations. The position of the principal peaks and their molar absorptivities are tabulated in Table II-16.

Included in Table II-16 are values of f, the oscillator strength,[20] for those bands believed to be important. These values may be useful to those wishing to carry out a theoretical analysis of the absorption spectrum.

In order to determine the utility of several of the observed peaks for the analysis of NpF_6, Beer's law plots for the absorption at 12970 Å and 2210 Å were constructed. These figures showed no significant deviation from linearity. In order to analyze mixtures of NpF_6 and other gases, the Beer's law relation in the presence of the other gases should be determined.

Decomposition of NpF_6 under the action of light, with a resultant change in the absorption curve, was observed while the absorption spectrum in the near-infrared region was being determined. The samples of NpF_6 were exposed to the full light intensity of the source during this time, owing to the characteristics of the optics of the spectrophotometer. It was found necessary to isolate the near-infrared spectral region

[20] G. H. Beavan *et al*, *Molecular Spectroscopy*, Heywood and Company Limited, London, 1961, p. 14.

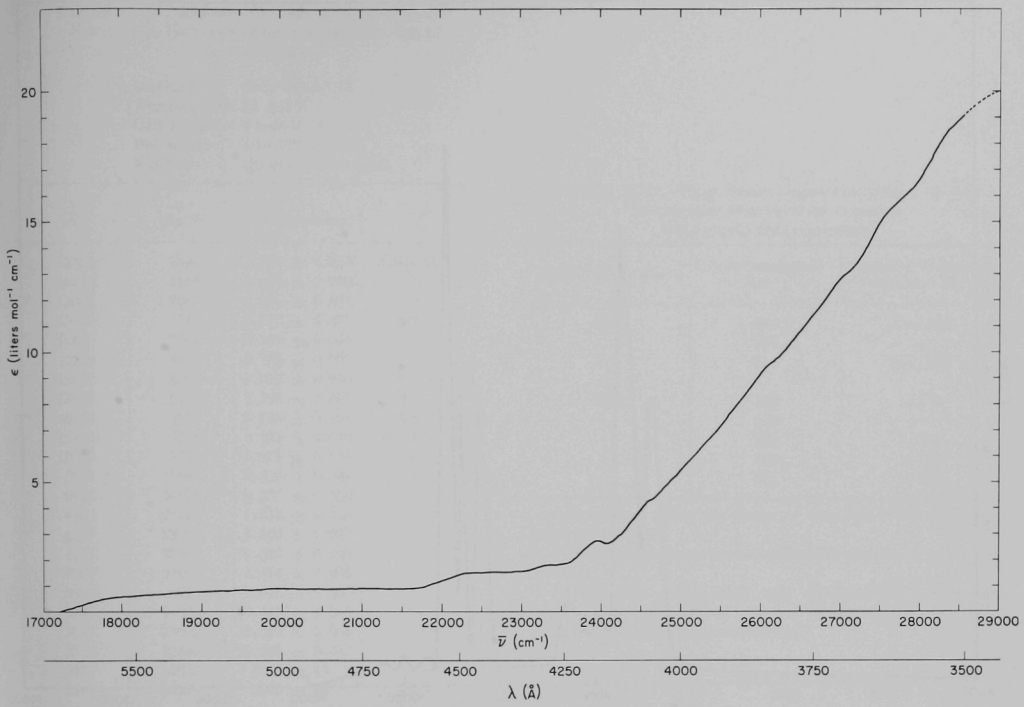

108-8615

FIG. II-14. Absorption Spectrum of Gaseous Neptunium Hexafluoride in the Visible Region.

by means of a Kodak No. 87 filter in order to minimize NpF_6 decomposition and thereby obtain a reproducible spectrum.

The absorption spectrum in the near-infrared region showed two prominent bands which exhibit observable fine structure. The peak separations observed in the spectrum are tabulated in Table II-17 together with the observed peak separations for those bands which permit such calculations. Since it is likely that the observed fine structure represents the vibrational energy levels of NpF_6, a list of the fundamental vibrational frequencies observed in the infrared region[21] has been included in Table II-17.

d. DISCUSSION

Goodman[22] shows a tracing of the absorption spectrum of neptunium hexafluoride. His results do not extend into the ultraviolet and do not contain data which permit the evaluation of molar absorptivities. Goodman developed a discussion of the spectrum of NpF_6 from the theoretical viewpoint and calculated the energies of peaks expected for NpF_6. Eisenstein and Pryce[23] present a theoretical interpretation based on measurements of the magnetic and spectroscopic properties of neptunium hexafluoride.

Malm and associates[24] indicate that NpF_6 is photosensitive. This contention was substantiated in the present work when operating in the near-infrared region; it was observed that samples of NpF_6 exposed to high-intensity white light exhibited tendencies toward decomposition. However, decomposition of NpF_6 by light does not occur at a significant rate when the material is exposed to light of narrow wavelength

[21] J. G. Malm, B. Weinstock, and H. Claassen, J. Chem. Phys., **23**, 2192 (1955).

[22] G. Goodman, Thesis, Harvard University, 1959.

[23] J. C. Eisenstein and M. H. L. Pryce, Proc. Roy. Soc. (London) **A255**, 181 (1960).

[24] J. G. Malm, B. Weinstock, and E. E. Weaver, J. Phys. Chem., **62**, 1506 (1958).

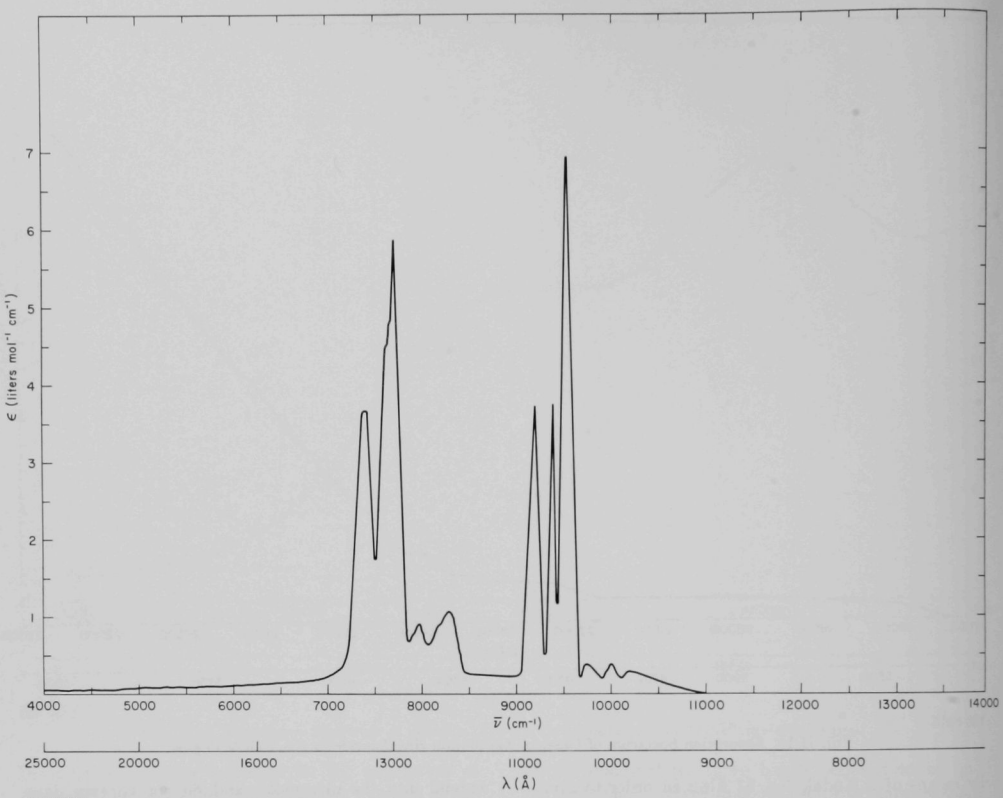

108-8613

FIG. II-15. Absorption Spectrum of Gaseous Neptunium Hexafluoride in the Near Infrared Region.

spread in the visible and ultraviolet regions. No attempt was made to elucidate the rate or mechanism of the photodecomposition.

Spectra of compounds in the isoelectronic series Pa(IV), U(V) and Np(VI) should show similarity if the electronic environment of the central ions is nearly the same. Although direct comparison of the spectra is made difficult by the absence of data taken from similar compounds, certain similarities can be pointed out. Several of the peaks observed in the absorption spectrum of cesium uranium (V) hexafluoride[25] ($CsUF_6$) can be correlated with those observed for NpF_6. Specifically, the absorption band at 7350 to 8250 cm^{-1} in NpF_6 corresponds to a similar band in $CsUF_6$ with the strong peak of $CsUF_6$ at 7399 cm^{-1} corresponding to the peak at 7396 cm^{-1} in NpF_6. The spectrum of Pa(IV) in aqueous solution[26] shows peaks at 44,643 cm^{-1}, 39,216 cm^{-1}, and 36,232 cm^{-1}, the first two corresponding to the peaks observed at 45,249 cm^{-1} and 38,835 cm^{-1} for gaseous NpF_6. It has also been observed that Pa(IV)[27] and U(V)[25] are, like NpF_6, sensitive to light and undergo photodecomposition.

The absorption spectra data obtained for NpF_6 should have direct application to the analysis of NpF_6 in gaseous mixtures once the Beer's law relation has been established for the mixtures.

Future work will entail study of the chemistry of NpF_6 and examination of the rates of fluorination of NpF_4 to form NpF_6.

[25] M. Reisfeld and G. Crosby, Inorg. Chem., **4**, 65 (1965).

[26] S. Fried and J. C. Hindman, J. Am. Chem. Soc., **76**, 4863 (1954).

[27] C. F. Miranda and R. Muxart, Bull. Soc. Chim. France, **9**, 2174 (1964).

TABLE II-16. ABSORPTION SPECTRUM OF GASEOUS NEPTUNIUM HEXAFLUORIDE. SIGNIFICANT PEAKS AND SHOULDERS

Instrument: Cary Model 14
Temperature: 22 ± 1°C
Cell Lengths: 1 and 10 cm
Pressures: 4 to 100 mm Hg
Window: Quartz, 3 mm thick

λ (Å)	$\bar{\nu}$ (cm^{-1})	ϵ[a] (liters/mole-cm)	f[b]
13520	7396	3.674 ± 0.035	3.634×10^{-6}
13099	7634	4.488 ± 0.062	—
13050	7663	4.823 ± 0.031	—
12970	7710	5.877 ± 0.015	6.083×10^{-6}
12540	7974	0.904 ± 0.064	—
12215	8187	0.882 ± 0.071	—
12040	8306	1.077 ± 0.058	0.693×10^{-6}
10875	9195	3.726 ± 0.055	2.314×10^{-6}
10665	9376	3.738 ± 0.046	1.290×10^{-6}
10495	9528	6.924 ± 0.049	4.141×10^{-6}
10250	9756	0.379 ± 0.065	—
9982	10018	0.359 ± 0.064	—
9825	10178	0.267 ± 0.059	—
4400	22727	1.553 ± 0.103	—
4275	23392	1.790 ± 0.077	—
4175	23952	2.695 ± 0.093	—
4065	24600	4.214 ± 0.058	—
3835	26075	9.607 ± 0.066	—
3700	27027	12.863 ± 0.046	—
3615	27662	15.362 ± 0.045	—
3510	28490	18.505 ± 0.087	—
2575	38835	1675 ± 49	—
2210	45249	2360 ± 54	9.66×10^{-2}

[a] Based on at least four determinations at each peak. The error is the average deviation.

[b] $f = (4.60 \times 10^{-9})\ \epsilon_{max}\ \Delta\nu_{1/2}$. See G. H. Beavan *et al.*, *Molecular Spectroscopy*, Heywood and Company, Ltd., 1961, p. 14.

TABLE II-17. PEAK SEPARATIONS FOR BANDS IN THE ABSORPTION SPECTRUM OF GASEOUS NEPTUNIUM HEXAFLUORIDE

Band Center[a] (cm^{-1})	Peak Separation[b] (cm^{-1})	Pertinent Vibrational Frequency[c] (cm^{-1})
7710	332	ν_2-ν_4 324
	264	—
	314	ν_2-ν_4 324
9376	160	ν_6 164
	262	—
	228	ν_5 208
	152	ν_6 164
	181	ν_4 200

[a] Position of either the center of the band or the principal peak in the band.

[b] Determined from a plot of molar absorptivity versus wave number.

[c] Correlation made using only fundamental frequencies (ν_1 to ν_6) or combinations observed in the infrared spectrum of gaseous neptunium hexafluoride.

5. Solid-Liquid Equilibria (L. E. TREVORROW, J. SAVAGE)

Experimental studies of the solid-liquid equilibria in the system UF_6-PuF_6 are being made. The results of these studies will be useful in the choice of process conditions for the separation of PuF_6 from UF_6 in the fluid-bed fluoride volatility process and will contribute to the understanding of the fundamental chemistry of this system (see ANL-6925, p. 120). Extensive preliminary testing of the apparatus with UF_6-MoF_6 mixtures has been carried out before final closure of the apparatus in the glovebox. The purpose of the preliminary tests was to discover any need for modifications of the apparatus, and to effect the modifications before the apparatus was contaminated with plutonium. Although the temperature-composition diagrams of the systems UF_6-PuF_6 and UF_6-MoF_6 may differ, the latter binary is considered to be a suitable test system since the physical properties of the compounds are sufficiently similar that the same measurement techniques may be applied to both systems. Since there are no literature references to solid-liquid equilibria in the system UF_6-MoF_6, this work has been expanded to complete the temperature-composition diagram.

a. DESCRIPTION OF THERMAL ANALYSIS APPARATUS

The apparatus used in the determination of the liquid-solid equilibria for the MoF_6-UF_6 system is

shown in Figure II-16. Mixtures of the volatile fluorides to be examined by thermal analysis are contained in a sample tube constructed of ½ in. dia. nickel tubing with a 20-mil wall thickness. The tube is 1¾ in. long, and has a well in the bottom which extends a distance of ¼ in. along its central axis. The inside diameter of the well is slightly greater than $^1/_{16}$ in. which is sufficient to admit the tip of an Inconel-sheathed thermocouple with a diameter of $^1/_{16}$ in. The sample tube is bolted through a Teflon-gasketed flange to a brass valve body. Closure of the valve body and containment of the fluoride samples is effected by

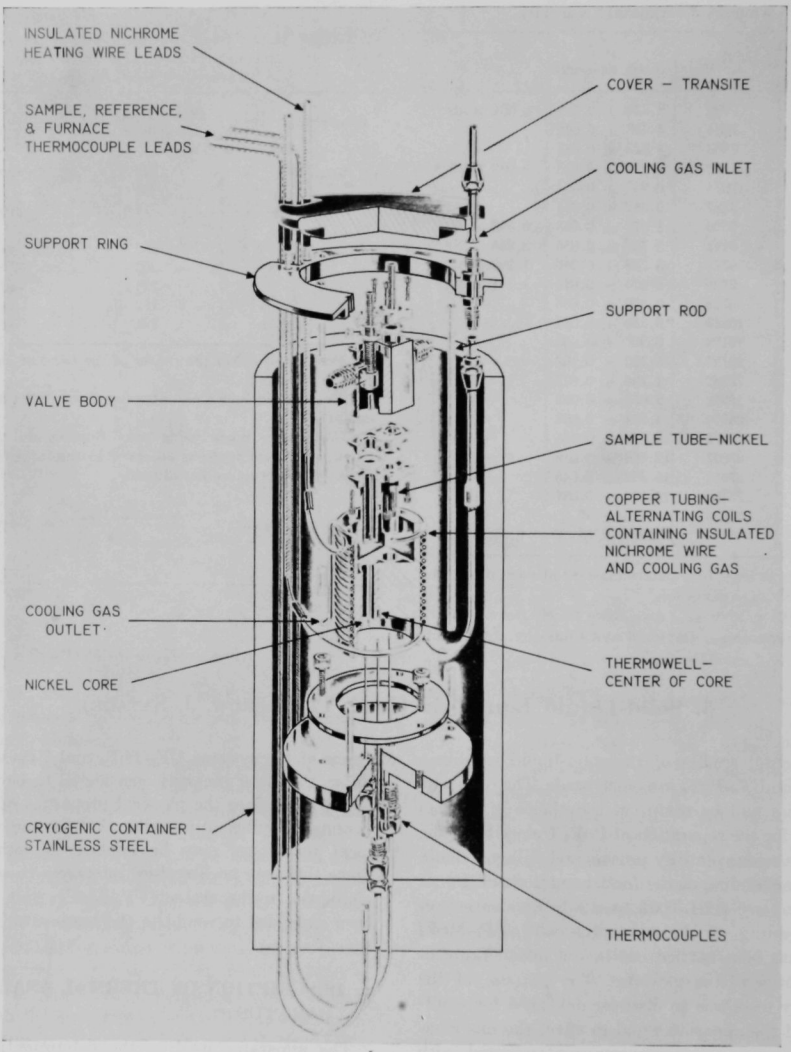

108-8917

FIG. II-16. Nickel Furnace Block and Sample Tube Assembly for Thermal Analysis of MoF_6-UF_6 Mixtures.

means of a ½-in. bellows assembly (Veeco Vacuum Corp.) with a Teflon seat. The sample tube assembly can be attached to a vacuum manifold by means of a ⅜-in. male flare fitting soldered to an opening of the brass valve body. The volume of the sample tube is about 4 ml when the valve is closed. The sample tube-valve assembly is shown in Figure II-17. Sample tubes are loaded by condensing volatile fluorides in the bottom of the tubes, using a vacuum distillation technique. The amount of each charge component added to the tube is determined by weight difference on a 1-kg capacity Mettler balance.

A mixture contained in the sample tube is subjected to thermal analysis while the tube is positioned in a cavity in a cylindrical nickel block which is heated or cooled. For differential thermal analysis, two tubes are positioned side by side in the nickel block. One tube contains the mixture to be examined by thermal analysis; the other contains air at 1 atm as a reference material. The nickel block is wound with a double helix of $^{3}/_{16}$-in. OD copper tubing. Cooled gas may be blown through one helix. Asbestos-covered Nichrome wire, threaded through the other helix, serves as the source of heat. The coolant gas is nitrogen which is cooled by passing it through a copper coil immersed in a trichloroethylene-dry ice slush. The nickel block is bolted to a flange attached to a tripod which hangs within a stainless steel Dewar flask fitted with a transite cover. The nickel block and tripod assembly are shown in Figure II-18.

The temperature of the nickel block can be increased or decreased as a linear function of time. The time-temperature program of the block is determined by a Minneapolis-Honeywell strip chart proportioning program controller incorporating a set point driven by a clock motor. A timer can be set to interrupt the clock motor at intervals to determine the driving rate of the set point. The electrical imbalance between the set point and a thermocouple positioned centrally in the nickel block is used to control the power input to the heating wire around the block. A Honeywell Electro-volt Control Unit and a silicon-controlled rectifier are used in conjunction with the programmer to provide a proportioned, d-c source of electrical power for the heating wire.

Figure II-19 is a schematic diagram of the thermocouple circuit. The thermocouple wires are iron and Constantan imbedded in magnesia and covered with an Inconel sheath. The thermocouple wires are electrically insulated from the sheath. The signal of the thermocouple in the sample tube can be determined either by a recording potentiometer (1 mv span, 0 to 50 mv suppression) or by a Leeds and Northrup type K-3 potentiometer. The sample thermocouple

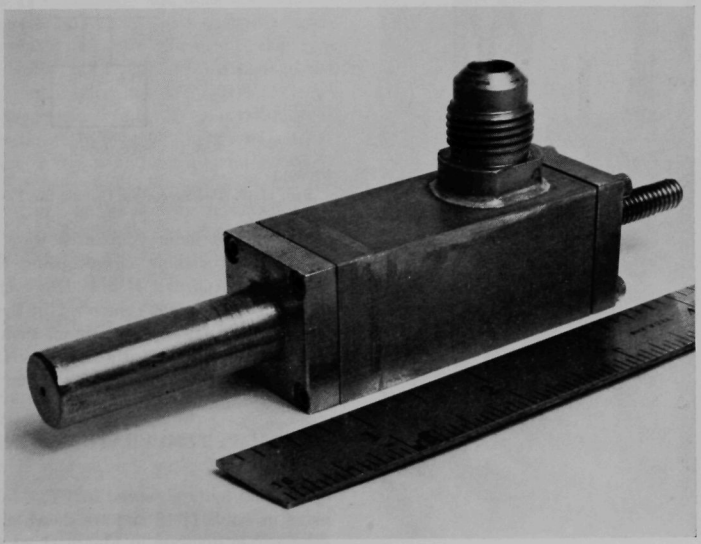

108-7538

Fig. II-17. Sample Tube and Valve Assembly for Thermal Analysis.

had been calibrated against four other thermocouples which had been previously calibrated against an NBS-standardized platinum resistance thermometer. For differential thermal analysis, the difference between the temperatures of the sample and reference tubes is registered by the electrically opposed thermocouples. The difference signal is put into a Leeds and Northrup d-c amplifier (No. 9835-B) where it is amplified and fed into a Minneapolis-Honeywell Electronik 18 stripchart recorder with a zero center and a span of −5 to +5 mv. With these instruments, the record of the difference signal can be increased by factors varying from 2½ to 100.

It has not been possible to obtain sharp melting points for UF_6-MoF_6 mixtures from heating curves, probably because the mixtures were not stirred. Thermal halts in UF_6-MoF_6 mixtures have therefore been determined from cooling curves although uranium hexafluoride has a tendency to supercool extensively. Vibration of the apparatus with an electric core box vibrator did not eliminate supercooling. Freezing points of the binary mixtures were determined by extrapolating cooling curves using the method developed by Andrews *et al.*[28] However, the extent of supercooling was not controlled in these experiments, but depended on random stimuli such as chance mechanical vibration of the apparatus. Andrews,[28] in his work, used a seeding technique to control the extent of supercooling.

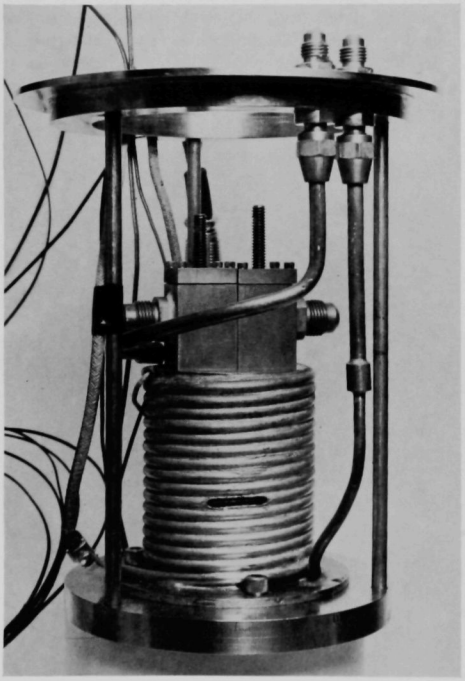

108-7537

Fig. II-18. Nickel Block and Tripod Assembly for Thermal Analysis.

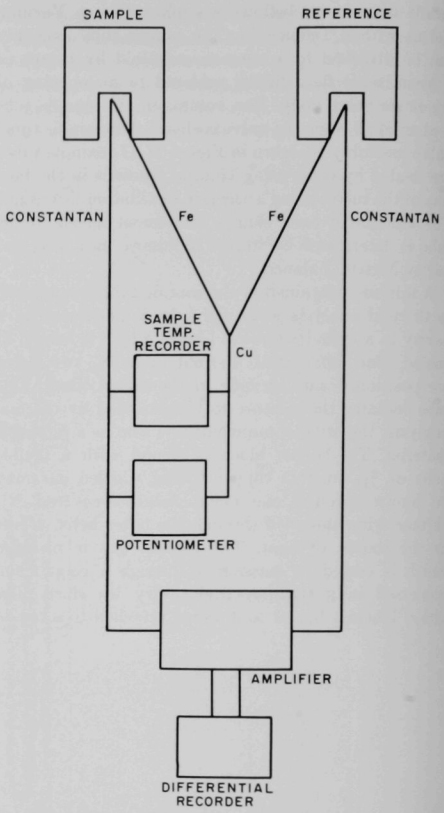

108-8913

Fig. II-19. Thermocouple Circuit for Thermal Analysis.

b. UF_6-MoF_6 TEMPERATURE-COMPOSITION DIAGRAM

Thermal halts observed in UF_6-MoF_6 mixtures are listed in Table II-18 and are shown as a temperature-composition diagram in Figure II-20. The solid-liquid

[28] D. H. Andrews, G. I. Kohman, and J. Johnston, J. Phys. Chem., **29**, 914 (1925).

TABLE II-18. TEMPERATURE HALTS IN UF_6-MoF_6 MIXTURES

Mole Fraction UF_6	Freezing Point (°C)	Eutectic (°C)	Solid Transition (°C)	Solid Transition (°C)
0.873	60.8	13.4 ± 0.4		
0.729	52.1	13.8 ± 0.3		−8.2 ± 0.2
0.583	46.4	13.7 ± 0.2		−8.4 ± 0.5
0.490	40.0	13.7 ± 0.2		−8.5 ± 0.3
0.404	31.4	14.0 ± 0.2	4.4 ± 0.4[a]	−8.4 ± 0.3
0.337	23.9 ± 1.4	13.6 ± 0.6	4.1 ± 0.4[a]	−9.1 ± 0.3
0.331	29.2	13.8 ± 0.3	4.3 ± 0.5[a]	−9.2 ± 0.2
0.276	21.9 ± 0.4	13.9 ± 0.4	3.6 ± 0.8[a]	−9.1 ± 1.0
0.231	16.0	13.4 ± 0.3		−8.8 ± 1.1
0.200	13.0 ± 0.5		6.7 ± 0.9	−8.9 ± 0.3
0.146	14.3 ± 0.1		0.3 ± 0.6	−8.8 ± 0.5
0.0972	15.2 ± 0.1	13.4 ± 0.6	−4.5 ± 0.4	−8.8 ± 0.5
0.0554	16.3 ± 0.1			−7.9 ± 0.4
0.0296	16.7 ± 0.2	14.5 ± 0.1		−9.2 ± 0.2

[a] Thermal effect very small; the existence of a temperature halt is questionable.

equilibria data show that the UF_6-MoF_6 is essentially a simple eutectic system with the eutectic point at a temperature of 13.7 ± 0.3°C and a composition of 0.2 mole fraction UF_6. The system is a eutectic rather than a series of solid solutions because the crystal structure of solid UF_6 and solid MoF_6 above −8.7°C are probably different. Uranium hexafluoride has an orthorhombic crystal structure,[29] and does not undergo transformations in the solid phase with changes in temperature.[30] There is no literature reference to the crystal structure of MoF_6, but the solid transitions of the 5d transition series hexafluorides, WF_6, ReF_6, OsF_6, IrF_6, and PtF_6 are reported to involve a crystal structure change from the orthorhombic form below the transition temperature to the cubic form above the transition temperature.[31] It is probable that MoF_6 has the same crystal structure as WF_6. Thus if solid UF_6 is orthorhombic and if solid MoF_6 has a cubic structure above the transition point, the components can be expected to form a eutectic rather than a series of solid solutions.

The eutectic temperature is well-established on the UF_6-rich side of the eutectic. There is, however, a difference of no more than 3.5°C between the freezing point and the eutectic temperature on the MoF_6-rich side of the eutectic. It was difficult to obtain separate thermal halts for freezing and eutectic crystallization on the MoF_6-rich side of the eutectic and, consequently, the presence of the eutectic is not well-established in this part of the diagram.

c. COMPARISON OF OBSERVED WITH THEORETICAL BEHAVIOR IN UF_6-MoF_6 SYSTEM

It is assumed that the solid-liquid equilibria involve the crystallization of pure UF_6 on the UF_6-rich side of the eutectic and the crystallization of pure MoF_6 on the MoF_6-rich side of the eutectic. The curves representing solid-liquid equilibria are compared with the respective ideal solubility curves for UF_6 and MoF_6 in Figure II-21. The ideal solubility of UF_6 was calculated from the equation:

$$\ln \frac{1}{X^i} = \frac{\Delta H^F_{UF_6}}{RT}\left(\frac{Tm - T}{T\,Tm}\right),$$

where

R = gas constant
X^i = mole fraction of UF_6 in ideal saturated solution at temperature T
$\Delta H^F_{UF_6}$ = heat of fusion of pure UF_6 at temperature T
T = freezing point of the mixture
Tm = melting point of pure UF_6,[32] 337.17°K or 64.05°C.

The heats of fusion of UF_6 at various temperatures were calculated by differences of the enthalpies of solid UF_6 and liquid UF_6 using the equations listed by Katz and Rabinowitch.[33]

The ideal solubility of MoF_6 was calculated by the equation,

$$\log_{10}\left(\frac{1}{X^i}\right) = \frac{\Delta H^F_{MoF_6}}{4.575}\left(\frac{Tm - T}{T\,Tm}\right) - \frac{\Delta Cp}{4.575}\left(\frac{Tm - T}{T}\right) + \frac{\Delta Cp}{1.987}\log\frac{Tm}{T}$$

where

X^i = mole fraction of MoF_6 in ideal saturated solution at temperature T
$\Delta H^F_{MoF_6}$ = heat of fusion of pure MoF_6
T = freezing point of the mixture
Tm = melting point of pure MoF_6,[34] 290.7°K or 17.5°C.
ΔCp = difference between the heat capacities of solid and liquid MoF_6.

It is assumed that the solid designated by Brady *et al*[34] as solid MoF_6(I) (see Figure II-20) is involved in

[29] J. L. Hoard and J. D. Stroupe, in Chemistry of Uranium, Collected Papers, U.S. Atomic Energy Commission Report TID-5290, Book 1, 1958, p. 325.

[30] B. Weinstock, Record Chem. Progr., **23**, 23 (1962).

[31] B. Weinstock, J. Phys. Chem. Solids, **18**, 86–89 (1961).

[32] B. Weinstock, E. E. Weaver, and J. G. Malm, J. Inorg. Nucl. Chem., **11**, 104 (1959).

[33] J. J. Katz and E. Rabinowitch, *The Chemistry of Uranium*, National Nuclear Energy Series, Division VIII, Vol. 5, Dover Publications, Inc., New York, N.Y., 1961, pp. 412–413.

[34] A. P. Brady, O. E. Myers, and J. K. Clauss, J. Phys. Chem., **64**, 588 (1960).

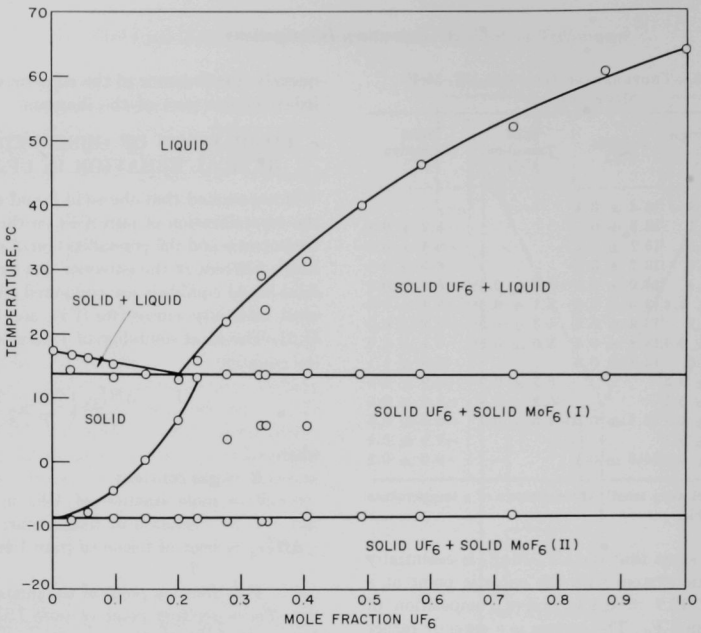

108-8914

FIG. II-20. Temperature-Composition Diagram for the System UF_6-MoF_6.

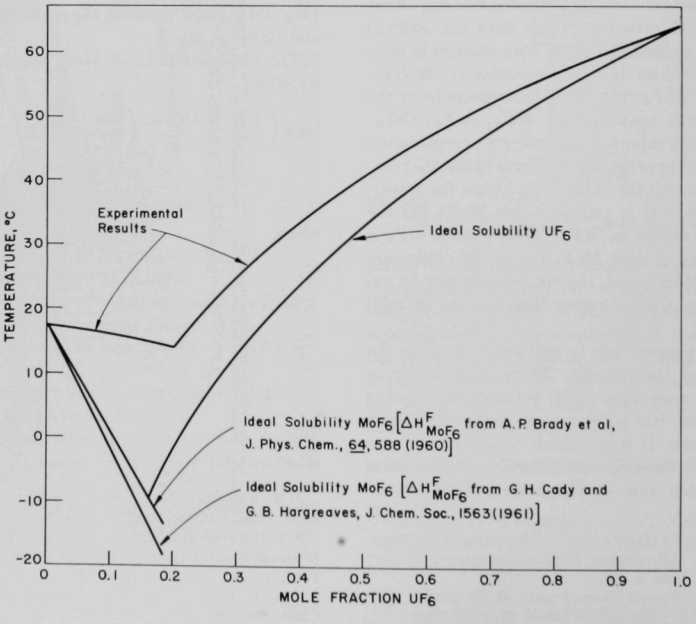

108-9103

FIG. II-21. Solubility Diagram for UF_6-MoF_6.

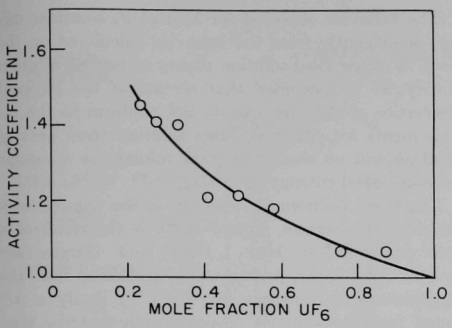

108-8907

FIG. II-22. Activity Coefficient of UF_6 in UF_6-Saturated Solutions Containing MoF_6.

the solid-liquid equilibria, since $MoF_6(I)$ is the stable form at these temperatures. Since the data of Brady *et al*[34] on the heat capacity of liquid MoF_6 do not permit expressing heat capacity as a function of temperature, ΔCp was assumed to be a constant 3 cal mole^{-1} deg^{-1}. The ideal solubility of MoF_6 was calculated from the heat of fusion determined calorimetrically by Brady *et al*[34] and also by the difference of ΔH vaporization and ΔH sublimation determined from the vapor pressures of MoF_6 reported by Cady and Hargreaves.[35]

Activity coefficients for UF_6 in saturated solutions of UF_6 in MoF_6 were calculated by means of the equation,

$$\ln \frac{1}{\gamma_{UF_6}} = \ln X + \frac{\Delta H^F_{UF_6}}{RT}\left(\frac{Tm - T}{T\,Tm}\right)$$

in which,

γ_{UF_6} = activity coefficient of UF_6
X = observed mole fraction of UF_6
T = observed freezing point of mixture
$\Delta H^F_{UF_6}$ = heat of fusion of UF_6 at temperature T
Tm = melting point of pure UF_6.

The activity coefficient of UF_6 is plotted as a function of composition of the mixture in Figure II-22.

Smoothed values of the observed solubility of UF_6 in UF_6-MoF_6 mixtures are compared with the solubility predicted by regular solution theory in Table II-19. The regular solution solubility was calculated using the equation,[36]

$$\log \frac{1}{X_{UF_6}} = \log \frac{1}{X^i_{UF_6}} + \frac{V_{UF_6}}{4.575T}\left(\delta_{MoF_6} - \delta_{UF_6}\right)^2 \phi^2_{MoF_6}$$

TABLE II-19. SOLUBILITY OF UF_6 IN UF_6-MoF_6 MIXTURES: A COMPARISON OF EXPERIMENTAL AND THEORETICAL VALUES

Temp (°C)	Mole Fraction UF_6 in Saturated Solution		
	Experimental[a]	Regular Solution	Ideal Solution
61.8	0.932	0.9560	0.9560
51.8	0.690	0.7746	0.7746
41.8	0.518	0.6215	0.6215
31.8	0.382	0.4933	0.4936
21.8	0.271	0.3879	0.3880
16.8	0.224	0.3426	0.3429

[a] Values taken from smooth curve drawn through experimental points.

where

X_{UF_6} = mole fraction of UF_6 in saturated, regular solution
$X^i_{UF_6}$ = mole fraction of UF_6 in saturated, ideal solution
V_{UF_6} = molar volume of liquid UF_6
δ_{MF_6} = solubility parameter

$$= \left(\frac{\Delta E_{MF_6}\ \text{vaporization}}{V_{MF_6}}\right)^{1/2},$$

where M = Mo or U,

ϕ_{MoF_6} = volume fraction

$$= \frac{V_{MoF_6}X^i_{MoF_6}}{V_{MoF_6}X^i_{MoF_6} + V_{UF_6}X^i_{UF_6}}$$

For the calculation of regular solution solubility, the molar volume of liquid UF_6 was calculated from the equation for the density of liquid UF_6 given by Wertz and Hedge.[37] The energy of vaporization of UF_6 was calculated from the equation developed by Kirshenbaum.[38] The energy of vaporization of MoF_6 was calculated from the heat of vaporization of MoF_6 given by Cady and Hargreaves[35] and corrected for the difference in vapor and liquid volumes as suggested by Hildebrand,[39] using the assumption that the vapor behaves as an ideal gas. The liquid volume of MoF_6 was obtained by extrapolating the data of Ruff and Ascher on the density of liquid MoF_6.[40] The values of regular solution solubility expressed as mole fraction UF_6 differ very little from the values for the ideal solubility of UF_6; the regular solution solubility is about

[35] G. H. Cady and G. B. Hargreaves, J. Chem. Soc., 1563–1568 (1961).

[36] J. H. Hildebrand and R. L. Scott, *The Solubility of Nonelectrolytes*, Third Ed., Reinhold, New York (1950), p. 270.

[37] R. J. Wertz and W. D. Hedge, Density of Liquid Uranium Hexafluoride, U.S.A.E.C. Report K-1466, Feb. 1, 1965.

[38] J. J. Katz and E. Rabinowitch, *The Chemistry of Uranium*, National Nuclear Energy Series, Division VIII, Vol. 5, Dover Publications, Inc., New York, N.Y., 1961, pp. 422–423.

[39] J. H. Hildebrand and R. L. Scott, op. cit., pp. 424–425.

[40] O. Ruff and E. Ascher, Z. Anorg. Chem., **196**, 413 (1931).

TABLE II-20. ACTIVITY COEFFICIENT OF UF_6 IN UF_6-SATURATED SOLUTIONS CONTAINING MoF_6

Mole Fraction UF_6	γ_{UF_6}, Experimental	γ_{UF_6}, Calculated[a]
0.873	1.07	1.000
0.729	1.07	1.000
0.583	1.18	1.000
0.490	1.22	1.000
0.404	1.21	1.001
0.331	1.40	1.002
0.276	1.41	1.003
0.231	1.46	1.004

[a] Calculated on the basis of regular solution theory.

0.9 % less than the ideal solubility for the largest deviation calculated.

Activity coefficients for UF_6 were calculated on the basis of regular solution theory from the equation,[41]

$$\log \gamma_{UF_6} = \frac{1}{RT} V_{UF_6} \phi^2_{MoF_6} (\delta_{MoF_6} - \delta_{UF_6})^2,$$

and are compared with experimental activity coefficients in Table II-20. The regular solution activity coefficients do not differ significantly from unity, i.e., regular solution theory predicts that UF_6-MoF_6 mixtures should be nearly ideal. Regular solution activity coefficients calculated using the added correction for difference of molal volumes of the two components[42] differ even less from unity.

[41] J. H. Hildebrand and R. L. Scott, op. cit., p. 131, equation 46.

[42] Ibid., p. 131, equation 47.

The behavior observed for MoF_6-UF_6 solutions differs significantly from the behavior calculated on the basis of either ideal solution theory or regular solution theory. It is concluded that certain of the physical properties of the mixtures do not conform to the requirements for either an ideal solution (zero heat of solution and no change in total volume) or a regular solution (ideal entropy of mixing).

The lower isothermal boundary in the temperature-composition diagram, Figure II-20, is the result of a solid transition in MoF_6. Cady and Hargreaves[35] found, from vapor pressure measurements, that the temperature of transition was −8.7°C; Brady *et al*[34] found from calorimetric measurements that the temperature of transition was −9.6°C. In the present work, the average temperature of the solid transition in mixtures, determined from the position of the peaks in the records of the differential thermocouple signal, is −8.7 ± 0.4°C.

An additional thermal halt observed in MoF_6-UF_6 mixtures occurs at temperatures between the eutectic temperature and that of the solid transition of pure MoF_6. The temperature of the halt increases as the mole fraction of UF_6 in the mixture increases, generating a boundary which extends from the temperature of the solid transition in pure MoF_6 to the temperature of the eutectic at a composition of about 0.23 mole fraction UF_6. The process which causes the variable temperature halt has not been determined from the experiments carried out thus far. X-ray analysis of solid mixtures is being planned to determine whether there is a crystal structure change involved in the variable thermal halt.

B. ENGINEERING-SCALE INVESTIGATIONS OF FLUID-BED FLUORIDE VOLATILITY PROCESSES (A. A. JONKE)

1. The Engineering-Scale Alpha Facility (N. LEVITZ, G. J. VOGEL, I. KNUDSEN, E. L. CARLS, R. LAMBERT,[43] L. YOUNGBLOOD,[44] W. A. MURPHY, R. KINZLER, B. KULLEN, A. RASHINSKAS, J. HEPPERLY, M. DEERWESTER)

The engineering-scale high-alpha facility has been constructed to study steps in the processing of ceramic UO_2-PuO_2 fuels by the fluid-bed volatility process (see Fig. II-23). These studies will be performed with unirradiated fuel materials in three separate process systems in the facility: (1) a fluorination pilot plant for processing batches of UO_2-PuO_2 pellets (containing fission products) to hexafluorides, (2) a distillation column for studies with UF_6-PuF_6 mixtures, and (3) a dual-purpose converter for transforming UF_6-PuF_6 to a stable, dense mixed UO_2-PuO_2 particulate solid and for studies on thermal decomposition as a means of separating plutonium as PuF_4 from UF_6-PuF_6 mixtures. The major equipment items, shown in the layout in Figure II-23, are in the larger of the two alpha boxes that comprise the facility. The smaller alpha box contains auxiliary items such as inlet gas distribution manifolds and off-gas scrubbers. A complete description of the alpha facility and the fluorinator and converter systems is given in a topical report.[45]

[43] Industrial trainee from the General Electric Company.

[44] Temporary staff appointee from ORNL.

[45] G. J. Vogel, E. L. Carls, and W. J. Mecham, Engineering Development of Fluid-bed Fluoride Volatility Processes, Part 5. Description of a Pilot-Scale Facility for Uranium Dioxide-Plutonium Dioxide Processing Studies, ANL-6901, December 1964.

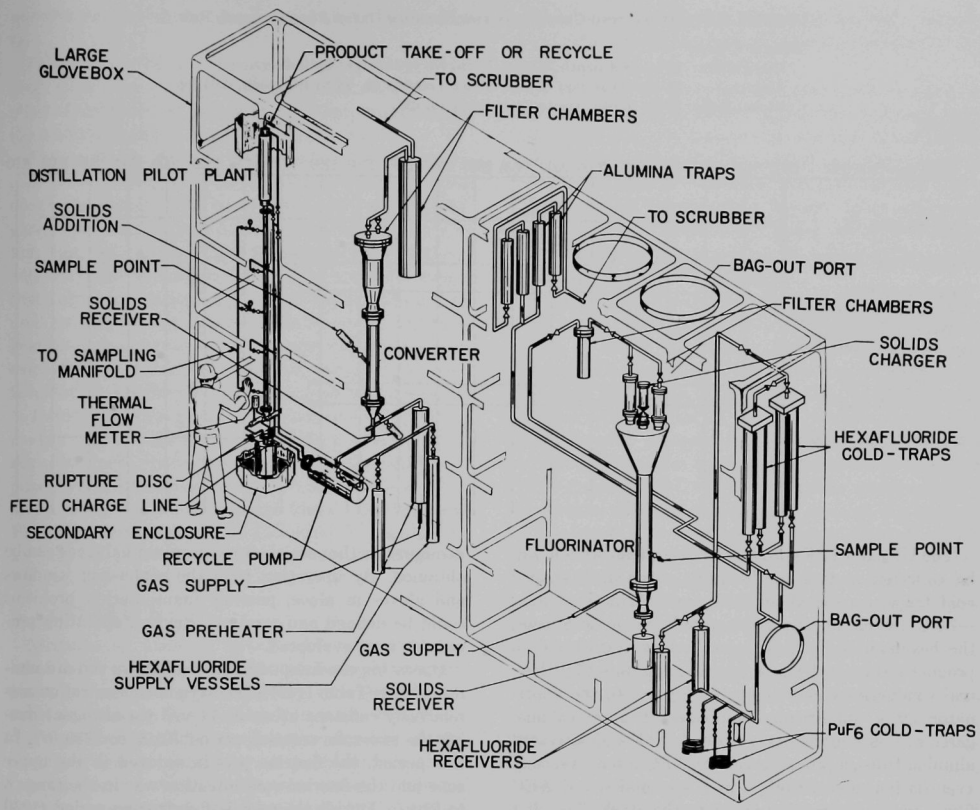

108-8791T

FIG. II-23. Engineering-Scale Alpha Facility.

The distillation column for studying the separation of UF_6-PuF_6 mixtures has been fabricated. This unit will be tested in a mock-up area before being installed in the alpha facility. Bagging-in procedures for the components of the distillation unit will be required because operations with plutonium-bearing materials will have started in the facility during this period. The design of the distillation column permits disassembly into the three main components: still pot, column, and condenser, thereby facilitating the bagging operation.

The process systems utilized in the fluorinator and converter are described below, along with recent shakedown experiments. After successful completion of shakedown experiments under simulated alpha conditions, plutonium-bearing feeds such as UO_2-PuO_2 will be used in subsequent runs. Work of a mechanical and electrical nature, suggested mainly by the results of recent experiments, was continued in the facility. Windows are now being sealed in preparation for a final check of all facility systems.

a. THE FLUORINATION PILOT PLANT

The fluorinator is constructed of welded nickel and consists of a 3-in. dia. reaction zone, a disengaging zone with a maximum diameter of 15 in., and two 4-in. dia. sections containing sintered metal filter elements. Batch charges of about 8.8 kg of UO_2-PuO_2 pellets (12-in. depth) will be processed in this unit by the two-zone oxidation-fluorination method (ANL-6687, pp. 112–124). The reactions will be conducted in a fluidized bed of high-fired alumina which will serve as a heat-transfer medium.

TABLE II-21. Operating Conditions for Uranium Oxide Fluorination Run

Reactor Charge:

UO_2 Pellets: 12-in. bed depth, 8.8 kg, ½-in. by ½-in. right cylinders.
Alumina: 24-in. static bed depth, Alcoa Tabular 61, 48 to 100 mesh, 6.04 kg
Nickel Balls: 10-in. depth, approximately ¼-in. dia.

108-9125

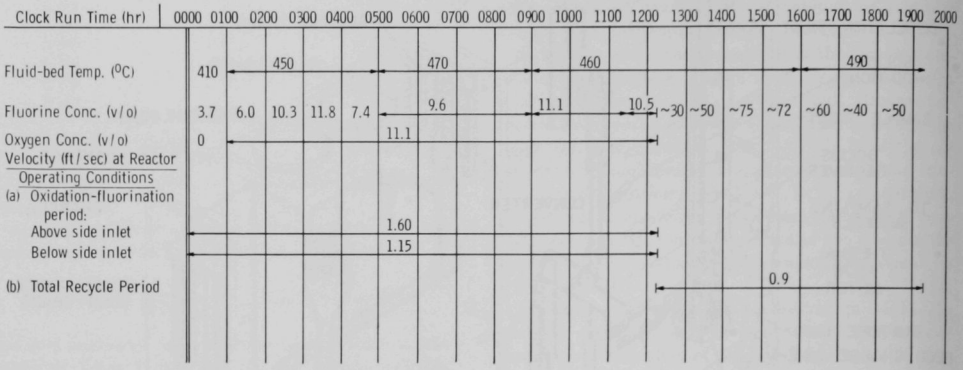

The UF_6 and PuF_6 produced during fluorination will be collected in two continuously weighed, U-shaped cold traps, connected in series, and maintained near −70°C by circulating refrigerated trichloroethylene; the hexafluorides will be subsequently transferred to product receivers. Unused fluorine, monitored by thermal conductivity cells, may be recycled to the fluorinator by a diaphragm compressor. Process exhaust gases will pass successively through NaF and activated alumina traps, a process scrubber, AEC filters, a second (ventilation gas) scrubber, and a second set of AEC filters before being discharged to the stack. The first shakedown experiment, run UO-1, is described in ANL-6925, pp. 133–136.

The two-zone oxidation-fluorination run described in this report was made under simulated alpha conditions. The charge consisted of 8.8 kg of UO_2 pellets (½ in. by ½-in. right cylinders) and 6.04 kg of sintered alumina (Alcoa, Tabular 61, nominal 48 to 100 mesh), equivalent to a static bed depth of ~24 in. A 10-in. deep bed of nickel balls (¼-in. dia.) served as a fuel support. A temperature gradient of about 150°C (300°C at the bottom to 450°C at the top) was maintained across the pellet bed (the lower or oxidation zone). The temperature of the upper (fluorination) zone was maintained in the range 450 to 470°C during most (16 hr) of the run, and was raised to 490°C for the final 3.5 hr.

The objectives of this run were: to investigate the performance of all equipment, to provide training for the operating personnel, to determine the level of UF_6 production for a given set of input conditions, and to demonstrate that satisfactory uranium balances can be obtained. By operating with the alpha-box windows and gloves in place, possible manipulation problems could be defined and resolved. Revised operating procedures were evaluated.

Operating conditions for the shakedown run are summarized in Table II-21. The oxygen concentration was relatively constant at about 11 v/o (in nitrogen) during the two-zone reaction period (0100 to 1230 hr). In this period, the fluorine was introduced in the upper zone and the fluorine concentration was in the range 6 to 12 v/o. During the recycle-fluorination period (1230 to 1930 hr), the fluorine was introduced at the bottom of the reactor; fluorine concentrations were relatively high (in the range 30 to 75 v/o).

Although peak UF_6 production rates of 2.20 kg/hr were attained during the run, the production rates were widely variable, and values as low as 300 g/hr were observed. About 95% of the UF_6 was collected during the 11.5-hr two-zone reaction period at an average rate of about 1.0 kg/hr [43 lb UF_6/(hr)(sq ft reactor cross section)]. An objective of subsequent work will be to operate with high, uniform UF_6 production rates.

Nearly complete recovery of the UF_6 product in the cold traps was achieved; approximately 98% of the UF_6 was collected in the first cold trap, about 1.3% in the second cold trap, and about 0.7% in a NaF trap downstream of the second cold trap. Only 6 g out of a total of 11,478 g of UF_6 (equivalent to the UO_2 charge) remained unaccounted for after the transfer of UF_6 from the cold traps to the 4-in. dia. product receivers Less than 0.1 w/o of the uranium in the initial charge

was associated with the alumina bed after the fluorination.

Performance of all operating units was generally good. Operations carried out with gloves, such as sampling of the fluid bed during fluorination, proved feasible with no apparent interferences present.

Future Work. To gain additional operating experience, another two-zone fluorination run will be made under simulated alpha conditions—with all windows, gloves, and bags in place and with the required ventilation flow through the alpha box. Operating conditions will be similar to those in the run just described, except that only 3 in. instead of 10 in. of nickel balls will be used to support the pellets. The lowest of the three heating-cooling zones of the reactor can therefore be employed to achieve more uniform control of the reaction. Several modifications in processing techniques will be tested. These modifications include the use of higher oxygen concentrations in the gas stream to the pellet zone, and more precise programming of the pellet temperatures and the time at which the fluorine is introduced to the pellet zone through lower side feed ports. Fluorine utilization will be increased, if possible, by keeping the fluorine concentration in the process off-gas at a fixed low value (3 to 5 v/o).

b. CONVERTER

Mixtures of uranium hexafluoride and plutonium hexafluoride are produced in the processing of uranium-plutonium ceramic oxide fuels by fluoride volatility methods. Because PuF_6 suffers from alpha decomposition[46] producing solid plutonium tetrafluoride and fluorine gas, long-term storage of the plutonium as the hexafluoride is undesirable. For this reason a fluid-bed reactor for converting the mixed UF_6-PuF_6 products of the fluorination step to a stable oxide powder form has been installed in the alpha facility. The unit and associated equipment were described in the preceding semiannual report, ANL-6925, pp. 136–138. As a converter, this unit will also be used to investigate the effects of process variables in the production of high-density mixed-oxide particles for compacted fuels, investigations similar to those carried out with UF_6 alone.[47] Recycling of the converter product to the fluorinator is being considered in the program. Studies of the thermal decomposition[48] of PuF_6 to PuF_4 as a means of separating the plutonium fraction from the bulk uranium stream will also be carried out in this unit.

The converter process equipment includes gas supply sources, a gas preheater, a 2-in. dia. fluid-bed reactor with a 4-in. dia. integral filter section, a backup filter in a separate 4-in. dia. section, an off-gas analysis system, an exit gas scrubber, and dry chemical traps. The reactor is fabricated of Inconel; other equipment and lines are of nickel and Monel. Associated equipment includes feed systems for the hexafluorides, steam, hydrogen, oxygen, and nitrogen.

The procedure involves periods of feeding hexafluoride, steam, and hydrogen into a fluid bed of oxide particles at 650°C, alternating with periods of product cleanup. The formation of UO_2, in general, follows the equation $UF_6 + H_2 + 2H_2O \rightarrow UO_2 + 6HF$. Newly formed solids deposit on the bed particles during feed periods, with consequent particle growth. The converter is designed to operate at a hexafluoride feed rate of 22 g/min [84 lb U/(hr) (sq ft reactor cross section)], equivalent to the 50 g/min rate in the 3-in. dia. reactor. A low steam rate (steam/UF_6 mole ratio of 2), which favors the production of dense oxide, is used during the hexafluoride feed period. The hydrogen rate is maintained at a high value (hydrogen/steam mole ratio near 3) to give the desired superficial fluidizing gas velocity (~1 ft/sec). The product density was found to be unaffected by variations in the hydrogen feed rate.

Periods of hexafluoride feed and fluoride cleanup each have a 30-min duration. During the fluoride cleanup period, the steam rate is increased, giving a hydrogen/steam mole ratio of one; a high steam rate enhances the rate of fluoride removal. Product is usually withdrawn at the end of each cleanup period through a line provided near the bottom of the reactor. Product withdrawal is effected through the operation of an electrically operated plug valve.

A shakedown test of the converter was made with UF_6 under conditions established in the previous studies[47] in the 3-in. dia. unit. The shakedown test, run CU-1, was made with a starting bed of 2.5 kg of UO_2 (static bed height, 9 in.). The average particle size (volume-surface, $D_{v/s}$) for this bed was 239μ. The run consisted of hexafluoride feed periods at rates of 12 g/min and 16 g/min (the feed cylinder was weighed between feed periods to obtain data points for calibration of the hexafluoride feed system). The actual steam/UF_6 mole ratios for these periods were 4.4/1 and 3.5/1, respectively.

Approximately 1.3 kg of UF_6 was processed in the

[46] M. J. Steindler, D. V. Steidl, and J. Fischer, Laboratory Investigations in Support of Fluid Bed Fluoride Volatility Processes. Part V. The Radiation Chemistry of Plutonium Hexafluoride, ANL-6812, December 1963.

[47] I. Knudsen and N. M. Levitz, Engineering Development of Fluid-Bed Fluoride Volatility Processes. Part 6: The Fluid-Bed Conversion of Uranium Hexafluoride to High-Density Uranium Dioxide, ANL-6902, December 1964.

[48] L. Trevorrow, J. Fischer, and J. Riha, Laboratory Investigations in Support of Fluid-Bed Fluoride Volatility Processes. Part III. Separation of Gaseous Mixtures of Uranium Hexafluoride and Plutonium Hexafluoride by Thermal Decomposition, ANL-6762, August 1963.

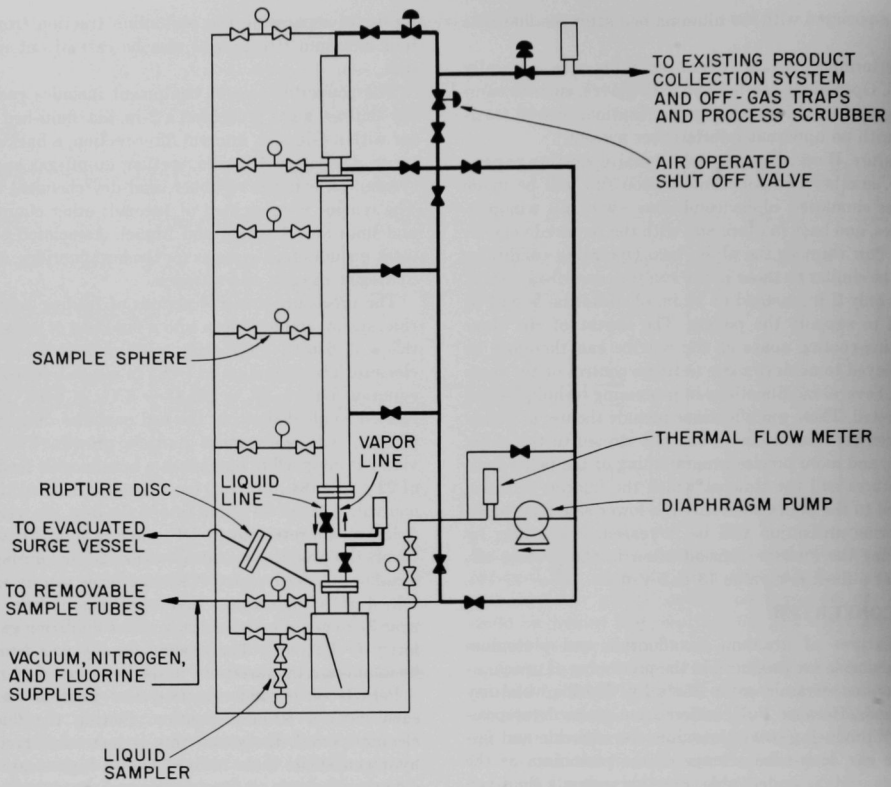

108-9110

FIG. II-24. Piping Layout of Distillation Pilot Plant.

converter in the 3-hr run period. The average particle size of the bed increased from 239μ to 278μ. A calculated estimate of the final average particle diameter was 281μ. Product density, based on tapped bulk density measurements of individual sieve fractions, was essentially the same as the starting bed density (8.4 g/cc).

Equipment performance was generally good, although some refinement of the UF_6 feed system is needed to eliminate surging of the UF_6 at the start of the feed periods. The converter off-gas scrubber proved to be quite efficient; only traces of fluoride passed to the fluorinator scrubber. Uranium retention in the reactor by the filters was essentially complete; the trace quantity of uranium detected in the converter off-gas scrubber represented less than 0.001% of the quantity fed.

An extensive review of the performance of all parts of the converter installation is being made to improve the effectiveness and workability of the unit for closed box (alpha) conditions. In subsequent tests of the converter, an oxidation treatment (see ANL-6900, pp. 175–181) for particle size reduction will be included.

c. DISTILLATION PILOT PLANT

A distillation system for processing UF_6-PuF_6 mixtures is being installed in a mock-up area for testing prior to installation in the alpha facility.

(1) Piping Schematic and General Design Considerations

The basic distillation unit consists of a still pot, a packed tower, and a condenser, which are shown schematically in Figure II-24. The unit is installed within a secondary, heated enclosure, which facilitates operations under adiabatic conditions. Batch operations at

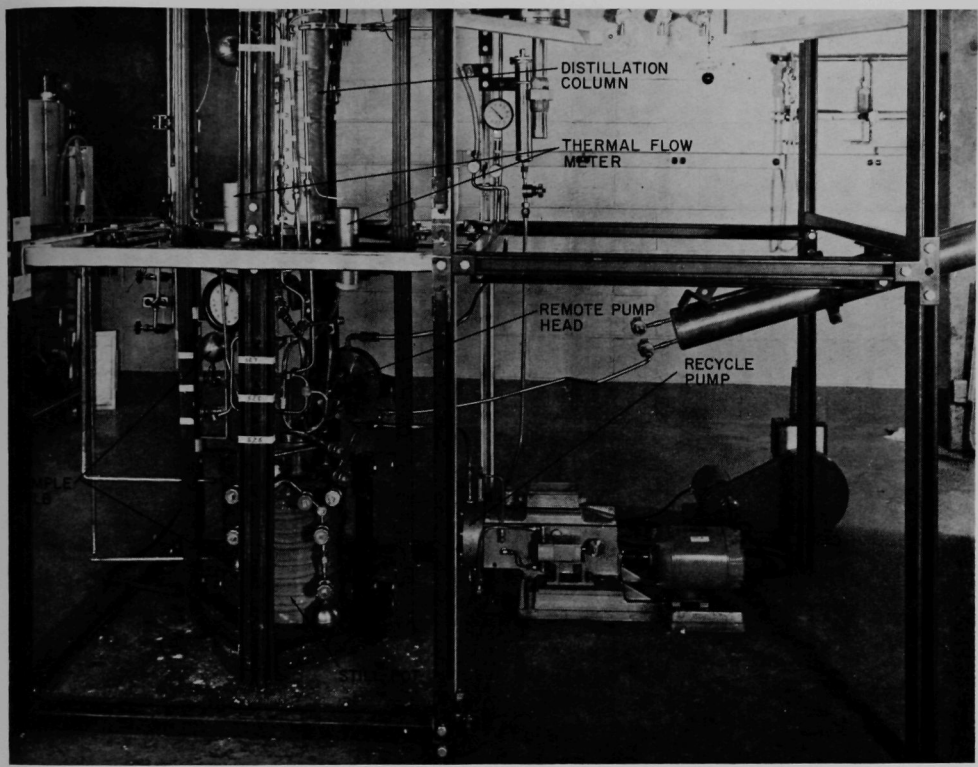

108-8863A

FIG. II-25. Distillation Pilot Plant: Still Pot and Recirculating Pump.

total reflux or operations with product take-off, as vapor, from either the bottom or the top of the condenser can be accommodated. When installed in the alpha box, the product take-off lines are connected to existing alpha-box equipment so that the product can be collected in either the coiled cold traps, the fluorinator product receivers, or the main large cold traps. All uncondensed off-gases will be processed in the NaF and activated alumina traps before entering the process exhaust gas scrubber system.

Continuous operation with no product take-off will be simulated in this unit. By recycling vapor from either the top or the bottom of the column to one of several feed points along the column, portions of the column can be operated under rectifying or stripping conditions. A diaphragm pump is provided for vapor recycle. The performance of the equipment will be evaluated on the basis of the separations obtained. Initial tests with the unit will be performed with mixtures of methylcyclohexane and n-heptane.

Vapor sample points are provided at several points along the column, and also at the still pot and condenser, and in the piping used for the recirculating stream (see Figures II-25 and II-26). Vapor samples are collected in evacuated 3-in. dia. spheres, each of which is between two valves. The trapped vapor is transferred through a manifold to sample tubes for weighing, hydrolysis, and subsequent analysis. In addition, provisions are made to sample the still pot liquid. Column holdup is measured by isolating the still pot from the column.

Extensive use of electrical control systems has been made in the design of the unit. Measurement of gas flows will be accomplished with thermal flow meters. Pressures are measured with pneumatic pressure transmitters coupled to transducers to obtain a millivolt sig-

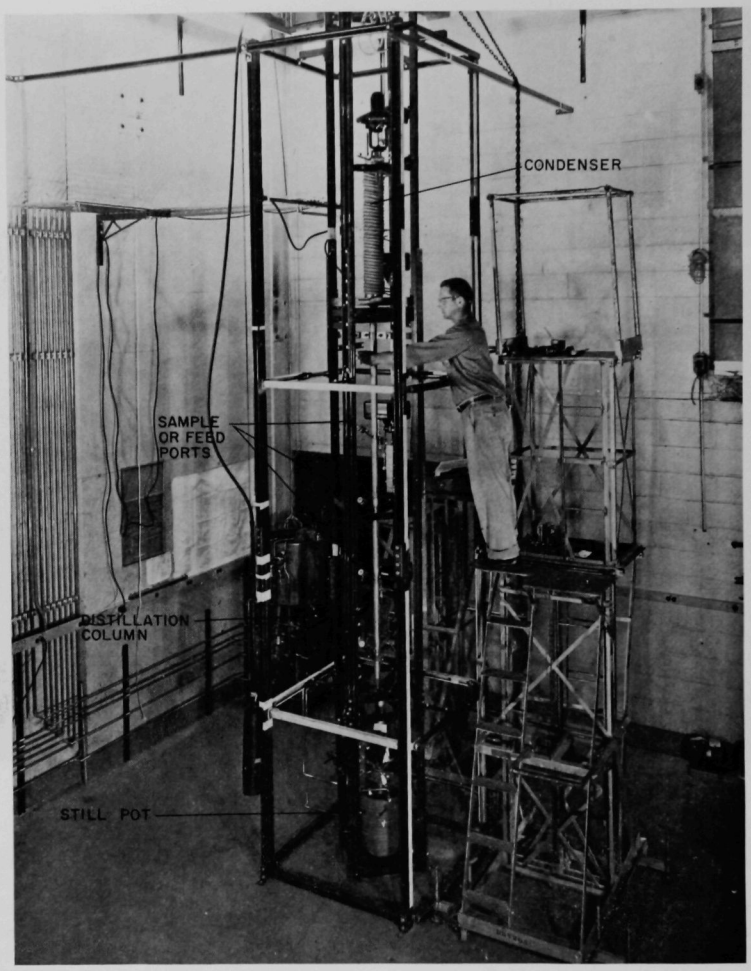

108-8792A

FIG. II-26. Distillation Pilot Plant: Distillation Column Assembly.

nal. Multipoint electrical converters mounted in the alpha-box end plate and in the wall of the heated enclosure are used for the power and thermocouple runouts from the column. Electrical jumper connections are used inside the heated enclosure. With only electrical connections between the equipment and the panelboard area, overall installation and maintenance are simplified.

The distillation unit is designed for operation at two temperature levels. The nominal operating temperature during distilling operations will be 80°C. At this temperature UF_6 has a vapor pressure of 35 psia. The piping for the vapor recirculation system will be heated approximately 10°C higher than the column temperature to insure against condensation.

During cleanup operations, in which PuF_4, formed as a result of decomposition of PuF_6, will be recovered by fluorination, the portions of the equipment that normally contain liquid will be heated to 350°C. Understandably, the liquid contents of the system will be re-

moved prior to this operation. Refluorination of PuF_4 deposited in the part of the equipment that normally contains only vapor will be at a temperature of about 150 to 200°C because of the limitations of various equipment components. These lower temperatures should be adequate since decomposition rates in the vapor phase are low and the quantities of residual plutonium in this part of the system should therefore be small.

(2) EQUIPMENT COMPONENTS

Column. The column consists of an 8-ft section of 1¼-in. schedule 80 nickel pipe flanged at both ends. The packing material is ⅛-in. dia. nickel wire helices (24-gauge thickness). Cone-shaped packing retainers are used to support the packing and to prevent shifting of the packing at high boilup rates. In order to prevent packing from entering the sample and feed lines, each opening contains a perforated plate with $^3/_{32}$-in. dia. holes.

Two types of heating elements are used. Clamshell resistance heaters, applied directly on the column wall, are used during refluorination (cleanup) operations at ~350°C. These heaters are wrapped with a layer of insulation, a layer of aluminum sheet, and finally with a row of mantle heaters. Adiabatic operation of the column is achieved by heating the column with the mantle heaters, which are controlled by differential thermocouples located at the column wall and the outer side of the first layer of insulation. The air inside the secondary enclosure will also be heated to the proper temperature to maintain adiabatic conditions.

Still Pot. The still pot is fabricated from 8-in. schedule 80 nickel pipe and is 13½ in. tall (Figure II-25). It is sized to accommodate a 13-kg charge of UF_6 (or a mixture of UF_6 and PuF_6). Internal fins on the bottom of the still pot provide sufficient heat transfer area to maintain boilup rates of 2500 lb/(hr)(sq ft) in the column even after only 1.3 kg of the charge remains in the still pot. A down line for taking liquid samples, as well as two vapor take-off points, are provided. The top of the still pot is flanged and is connected to the column through two bellows-sealed valves. The vapor line to the column has an in-line thermal flow meter to measure boilup rates. A U-bend in the liquid return line to the still pot provides a seal and prevents the vapor from bypassing the flow meter. An alternative method for determining boilup rate involves measuring the input power to the still pot heaters. Heaters for the distillation operations are mounted on the bottom of the still pot. Side heaters on the still pot are used only during cleanup refluorination periods. Emergency cooling water coils are copper-spray-bonded to the sides of the still pot.

Condenser. The condenser consists of a bundle of seven ½-in. dia. nickel tubes manifolded at both ends. The overall height of the unit is 40 in. Cooling coils and calrod heaters are wrapped over the exterior, and the entire assembly was copper-sprayed. Internal thermocouples are provided at both ends of the condenser. Axial thermocouples can be installed in one of the tubes that comprise the tube bundle. Temperature differences between the upper and lower ends of the condenser are used to detect the presence of noncondensables. Vapor can be removed from either the top or the bottom of this unit. Water is circulated in a closed loop through the external coils and through a constant-temperature bath located in the cell area. A measure of the heat pickup by the coolant will serve as an additional check on boilup rates. Provisions are made to drain the water from this coil during periods of refluorination of the condenser.

Valves. The majority of valves are the manual, packless, metal diaphragm type. These are operated through extension handles mounted on the face of the secondary enclosure. Several air-operated or solenoid valves are also used.

(3) Safety Features

The column is equipped with several automatic safety devices which shut off all heat to the still pot and actuate emergency cooling water to the still pot cooling coils. The safety actions are initiated by: (1) excessive still pot temperature, or (2) excessive still pot pressure, or (3) excessive column pressure. In addition to the above safety features, the still pot is connected to an evacuated surge vessel (located in an adjoining module) by a line containing a rupture disc designed for 150-psig release. Calculations indicate that, in the event of release of still pot contents into the surge vessel, the heat transfer from this surge vessel to the glovebox air would be sufficient to dissipate the heat being applied by the heaters to the still pot and prevent any further pressure buildup. As an added safety feature, cooling water is admitted to coils of the surge vessel upon a pressure rise in this vessel.

Where applicable, the equipment will be pressure- and vacuum-checked before a run. Also being considered is the installation of a smoke or halogen-detecting device in the secondary enclosure, which would initiate shutdown of the still pot in the event of a leak.

(4) Status of Unit

The three major components (the column, the still pot, and the condenser) have been received and have been installed in a Unistrut enclosure in a mock-up area where preliminary tests will be made. Placement of auxiliaries such as valves, the remote head of the pump, and instrumentation inside of the enclosure is

underway. Major piping and electrical work has been completed. Test operations with organic or fluorocarbon mixtures (as a substitute for UF_6 and PuF_6) will proceed as soon as installation work is completed.

2. Decladding and Fluorination of Uranium Dioxide Fuels

(D. Ramaswami, J. Gabor, D. Raue, J. Strand)

Development studies on the decladding and fluorination of low-enriched uranium dioxide fuels were continued. These studies are being made to establish processing conditions for recovery of fissionable values from spent power reactor fuels using fluidization techniques.

Previous work (ANL-6925, pp. 139–141) indicated the feasibility of disintegrating stainless steel-clad fuel with gas mixtures of HF and oxygen in a fluid-bed reactor, and subsequently recovering uranium by reaction with fluorine. The disintegration of the fuel was conducted at ~550°C with 40 v/o HF in oxygen diluted with nitrogen. Next, the fluorination was conducted by introducing fluorine into the reactor through several side ports. The location of the fluorine inlet port and the fluorine concentration were programmed to provide high fluorination rates and absence of bed caking by sintering of the uranium particles. Applicability of this method for processing UO_2-stainless steel (SS) cermet fuels was demonstrated.

The objectives of the current work are (1) to establish more firmly the conditions for processing the UO_2-SS cermet fuel by the above method, (2) to explore the use of this processing method for Zircaloy-2 clad UO_2 fuel bundles, and (3) to determine the feasibility of converting UO_2 pellets to fines in a separate step after the decladding step.

a. PROCESSING OF UO_2-SS CERMET FUELS

A miniature fuel element subassembly, simulating those used in stationary medium power plants,[49] was processed (run HF-16) in the bench-scale fluid-bed unit (ANL-6829, pp. 18 to 24) by the method discussed above. The conditions for this run are presented in Table II-22. The subassembly consisted of 4 plates, $^{11}/_{16}$ in. by 0.5 in. by $8^{3}/_{8}$ in. long, and weighed 90 g. Each plate was composed of 18 w/o UO_2-SS (type 304) clad in stainless steel. The destructive oxidation was performed in fluid beds of alumina maintained at 550°C. The fluorination was conducted in the temperature range of 250 to 550°C with 5 to 95 v/o fluorine in the feed.

The progress of uranium removal during the fluorination of residues from the destructive oxidation step of run HF-16 is illustrated in Figure II-27. The concentration of uranium in the reaction bed, composed of sintered alumina and nonvolatile compounds of iron and chromium, was reduced from 0.16 w/o to 0.005 w/o in 8 hr. The results suggest that shorter fluorination periods of approximately 6 hr may be sufficient.

Uranium distribution in the process streams is given in Table II-23. The residual uranium on the alumina bed was 0.8% of the uranium in the fuel charge. The residual uranium can be partially recovered by recycle of the alumina bed.

The recommended reprocessing conditions for the UO_2-SS cermet fuel subassemblies are:

Fluid-Bed Material: High-fired alumina (sintered or fused): sufficient quantity of nominal 40 mesh size to cover the fuel element.

Destructive Oxidation: Temperature of the fluid bed: 550°C.
Temperature of off-gas filter: 50 to 100°C.
Gas Velocity: 0.5 to 0.7 ft/sec in the fluid bed.
Feed Gas Composition: 40 v/o HF, 40 to 60 v/o oxygen, 0 to 20 v/o nitrogen.

Fluorination: Temperature: 250°C at the beginning and 550°C at the end; the fluorine concentration in nitrogen is gradually increased from 5 to 95 v/o while the bed is maintained at 250°C; the bed temperature is then slowly raised to 550°C while the fluorine concentration is maintained at 95 v/o; the fluorination may be completed using either fluidized-bed or static-bed conditions. The total time for fluorination may be 6 to 10 hr, depending on the quantity of uranium to be processed.

No further development work on the reprocessing of stainless steel-UO_2 cermet fuel materials will be done.

b. PROCESSING OF ZIRCALOY-2-CLAD UO_2 FUELS

Current plans are to declad Zircaloy-2-clad UO_2 fuels by treatment with HCl to form volatile $ZrCl_4$. An alternative method is the destructive oxidation procedure, in which the zirconium alloy is converted to oxide by treatment with an HF-oxygen mixture. During decladding, the zirconium alloy is converted to flakes of ZrO_2, $ZrOF_2$, or both, and the UO_2 pellets are converted to UO_2F_2 and UF_4 powder. Two bench-

[49] Directory of Nuclear Reactors, Vol. IV, Power Reactors (Revised and Supplemented Edition of Vol. I), International Atomic Energy Agency, Vienna, 1962, pp. 9 to 14.

TABLE II-22. CONDITIONS FOR DECLADDING AND FLUORINATION OF URANIUM DIOXIDE FUELS

Reactor System	Run No.							
	HF-16	HF-15	HF-14	SSOX-6	HF-18	HF-19	SSOX-4	SSOX-5
	Bench-scale			Pilot-scale	Bench-scale		Pilot-scale	
UO_2 charge (kg)	0.0053	none	0.513	3.2	0.274	0.273	4.5	6.8
Cladding type	stainless steel cermet	Zircaloy-2	Zircaloy-2	Zircaloy-2	none	none	none	none
Cladding charge (kg)	0.087	0.176	0.113	0.92	—	—	—	—
Alumina charge (kg)	0.48	0.64	0.64	5.5	0.47	0.47	7.7	5.2
DESTRUCTIVE OXIDATION								
Temperature (°C)	550	550	550	550–300[a]	400–600[b]	400–600[b]	400	370
Time (hr)	6.0	3.0	3.0	6.5	1.83	1.83	3	3
Feed gas composition (v/o)								
HF	40	40	40	45	38	—	43	51
O_2	40	40	40	55	51	31	57	49
N_2	20	20	20	—	11	69	—	—
Gas velocity (ft/sec)	0.75			0.9	0.8	0.5	0.8	1.2
FLUORINATION								
Initial Period		none	none		none	none		
Temperature (°C)	250			300–600[c]			400	380
Time (hr)	5.0			7.67			6.5	4.75
Fluorine conc. in nitrogen (v/o)	5–40			16.7			9.1	9.1
Gas velocity (ft/sec)	0.7			0.8			0.8	0.8
Final Period		none	none		none	none		
Temperature (°C)	250–550			600			550	[d]
Time (hr)	6.0			1.33			3	
Fluorine conc. in nitrogen (v/o)	95			90			90	

[a] Bed temperature was 550°C for first 3 hr, and dropped to 300°C for final 3.5 hr.
[b] Reaction was conducted at 400°C; then the bed temperature was raised to 600°C.
[c] Bed temperature was 300°C for first 4.5 hr, and increased to 600°C for final 4.5 hr. Owing to poor fluidization a portion of the bed attained a temperature of 850°C.
[d] No final cleanup period.

scale tests were made to determine the destructive oxidation rates, and a pilot-scale run was made to demonstrate both decladding by the destructive oxidation method and the uranium oxide fluorination step.

In the two bench-scale tests (runs HF-14 and HF-15), Zircaloy-2 specimens, immersed in a fluidized bed of alumina, were contacted with 40 v/o HF-40 v/o oxygen-20 v/o nitrogen for 3 hr at 550°C (Table II-22). The penetration rates ranged from 12 to 18 mils/hr, suggesting that Zircaloy-2-clad fuel bundles may be declad satisfactorily under these conditions.

A simulated fuel bundle, comprising six 2-ft long Zircaloy-2 tubes packed with cylindrical UO_2 pellets (0.43 by 0.43 in.), was processed in the pilot-scale reactor (ANL-6725, pp. 134–137). The quantities of uranium dioxide and alumina in the charge (see Table II-22, run SSOX-6) were proportioned to produce a fluid bed containing 40 w/o uranium fluoride fines after the destructive oxidation step.

The decladding conditions employed in this pilot-scale run were similar to those used in the bench-scale tests. Decladding was conducted for 6½ hr at a nominal temperature of 550°C. Operation during the initial 3 hr proceeded smoothly. Although the reactor wall temperatures remained constant at ~590°C throughout the 6½-hr period, during the final 3½ hr the temperature in the center of the bed decreased to 300°C because of poor heat transfer. Apparently, disintegration of the Zircaloy tubing produced a scaly oxidation product which restricted movement of the fluidized-bed particles and thus caused a marked reduction in heat transfer from the reactor wall to the center of the bed.

Fluorination was conducted using a fluorine feed procedure (ANL-6925, p. 141) that facilitates the fluorination of large quantities of uranium fluoride fines in deep fluid beds. During the initial fluorination period (2.5 hr), fluorine and recycle gas were introduced into the side of the reactor at approximately the middle of the fluid bed, and nitrogen as the fluidizing gas was fed at the bottom of the reactor. During the subsequent 0.5-hr period, the fluorine and recycle gas were introduced through a side inlet located 10 in. below the first

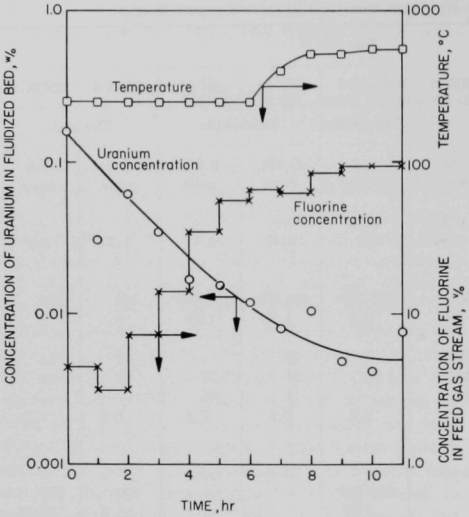

108-9123

FIG. II-27. Progress of Uranium Recovery During Fluorination Step of Run HF-16. (For run operating conditions, see Table II-22.)

TABLE II-23. URANIUM DISTRIBUTION IN PROCESS STREAMS

For run operating conditions, see Table II-22

	Run HF-16
Type of Fuel Subassembly	UO_2-SS cermet
Fuel Charge (g)	90
Uranium in the fuel charge (g)	5.3[a]
Uranium Recovered (% of total U found in all streams)	
1. UF_6 product recovered from cold traps	80.9
2. UF_6 recovered from activated alumina traps	17.4
3. Uranium in bed samples	0.9
Total Uranium Recovered	99.2
Uranium Lost (% of total U found in all streams)	
Uranium retained in alumina fluid bed	0.8

[a] Total uranium found in the various process streams. This method of accounting for uranium was proved to be satisfactory previously (ANL-6829, p. 42).

inlet. The fluorination step was completed by introducing fluorine and recycle gas at the bottom of the reactor for 6 hr. Throughout the entire fluorination step, the temperature of the fluid bed varied widely (between 300 and 850°C) due to poor fluidization properties of the bed. High UF_6 production rates [50 lb/(hr)(sq ft)] were achieved during the initial 2 hr of fluorination, wherein 56% of the uranium was recovered as UF_6.

At the end of the fluorination step, large cakes containing ZrF_4, AlF_3, and Al_2O_3 were found in the reactor. No uranium compounds were detected in the cakes. A factor which may have contributed to the formation of the cakes was that the fuel bundle was not completely oxidized at the time the fluorination was begun. A radiograph taken at the start of the fluorination step showed the presence of unreacted UO_2 pellets. Gamma-ray radiographs were taken at intervals throughout the run.

Further development work on the destructive oxidation method for decladding Zircaloy-2-clad UO_2 fuel will be conducted at other laboratories, and no additional work will be done at Argonne.

c. PULVERIZATION AND FLUORINATION OF URANIUM DIOXIDE PELLETS

Two runs were performed in the pilot-scale reactor and two runs in the bench-scale reactor to determine the feasibility of pulverizing UO_2 pellets in a HF-oxygen atmosphere and subsequently fluorinating the uranium fines to recover the uranium as UF_6. These tests represented the processing of UO_2 pellets which would follow the removal of Zircaloy cladding as volatile chlorides in a hydrochlorination step.

In the pilot-scale runs (SSOX-4 and SSOX-5), the operating conditions (see Table II-22) were similar except for the concentration of uranium fines in the alumina fluid bed after the pulverization (destructive oxidation) step. The pulverization step was conducted at ~400°C with 43 to 51 v/o HF in oxygen as the feed gas. The fluorination procedure for the uranium fines was similar to that discussed earlier and was conducted in the temperature range of 400 to 550°C with 9 to 90 v/o fluorine. The operation of both the pulverization and fluorination steps was satisfactory for the run with the lower concentration (40 w/o) of uranium fines, whereas minor operational problems occurred in the run with the higher concentration (60 w/o) of fines.

The two bench-scale tests (runs HF-18 and HF-19) were performed to compare the sintering characteristics of the uranium fines produced by HF and oxygen mixture with the characteristics of fines produced by oxygen alone. Pulverization of UO_2 pellets was conducted under similar conditions (see Table II-22). After the reaction was conducted at 400°C, the fines were maintained in an atmosphere of nitrogen as the temperature was increased to 600°C. The surface area of uranium fines produced by HF-oxygen gas mixtures decreased during the heating cycle from 12.2 to 1.5 m^2/g

whereas the surface area of the fines produced by oxygen alone decreased from 0.8 to 0.5 m^2/g. Apparently, uranium fines produced by the reaction of HF-oxygen mixtures with UO_2 sinter more readily than do fines produced by the oxidation of UO_2 with oxygen. No additional work on the use of HF-oxygen mixtures for pulverizing UO_2 will be done at Argonne. Further work in this area will be done at other laboratories.

d. FUTURE WORK

In order to provide additional flexibility in the application of the fluid-bed fluoride volatility process to low-enriched uranium dioxide fuels, further development work is being directed toward establishing operating conditions for a process scheme which involves pulverization of the UO_2 fuel with oxygen, followed by fluorination of the uranium fines.

3. Cleanup of Cell Exhaust Air Contaminated with Plutonium Hexafluoride

(R. Kessie, D. Ramaswami, L. Marek)

The investigation of the cleanup of cell exhaust air contaminated by the release of PuF_6 is continuing. This investigation concerns the evaluation of high-efficiency filters and the determination of the effects of the concentrations of moisture and PuF_6 on the extent of plutonium removal from gas streams.

The initial experiments in this program (ANL-6725, p. 157) indicated that the release of pure PuF_6 (or UF_6) into an atmosphere containing moisture resulted in the instantaneous reaction:

$$PuF_6(g) + 2H_2O(g) \rightarrow PuO_2F_2(s) + 4HF(g).$$

This reaction is completed in the gas phase and results in the production of a fume of plutonyl fluoride (PuO_2F_2) with a particle size $<0.1\mu$. Two AEC-type filters in series at 40% of rated flow (1 cm/sec) reduced the plutonium concentration of the fume in the gas stream by 10^{-6} to 10^{-9}.

Studies of the hydrolysis and filtration of dilute PuF_6 and UF_6 indicated that the reaction does not proceed at a detectable rate in the gas phase, but occurs on any solid surface exposed to the reactants. The rate of hydrolysis has been measured on packed beds of glass spheres for dilute UF_6 (ANL-6900, p. 170). The data were correlated by the rate equation:

$$r = \frac{191.5 p_{UF_6} p_{H_2O}}{1 + 597 p_{UF_6} + 95.5 p_{HF}}$$

where

r = reaction rate, mg U/(hr) (cm^2), and

p = partial pressure of subscripted component, mm Hg.

The relative error between the rates from the correlation and the measured rates was ±26% (root mean square) for individual bed segments.

Measurements of hydrolysis rates of dilute PuF_6 and dilute mixtures of PuF_6-UF_6 are reported.

a. APPARATUS FOR MEASURING PuF_6 HYDROLYSIS RATES

The PuF_6 hydrolysis rate experiments were performed in equipment similar to that used with UF_6. Briefly, the equipment, which has been described in detail in ANL-6925, pp. 144–147, consisted of a magnetically coupled stirrer for mixing the nitrogen-diluted PuF_6 and moist air streams. The mixed gases were passed through the packed bed of glass spheres which were 3.2 mm in diameter. The bed was 1.5 in. in diameter and was divided into ½- and 1-in. segments by stainless steel screens so that each of the segments could be removed separately. The gases leaving the packed bed were filtered by three AEC type filter media disks, 1.5 in. in diameter, mounted in series. The filters could be removed from the apparatus separately.

After each experimental run, the plutonium that had been deposited on the bed segments, filters, mixer, etc. was dissolved by submerging each of the separated units in a measured volume of 10% nitric acid plus 0.01% wetting agent (Aerosol) for 24 hr. The solution was then mixed and sampled for analysis of plutonium or for analysis of uranium.

b. HYDROLYSIS RATES OF PLUTONIUM HEXAFLUORIDE

All of the experimental conditions and results for runs involving PuF_6 are reported in Table II-24. The partial pressures in the initial mixed gas ranged from 0.06 to 5.6 mm Hg of water vapor and from 0.00001 to 0.02 mm Hg of PuF_6.

Results and Discussion. The average hydrolysis rates computed for the individual bed segments ranged from 0.0000004 to 0.1 mg plutonium/(cm^2) (hr). These data were treated by the same computer program that had been used for calculating the constants in the rate equation for the UF_6 hydrolysis. The best constants in this form of the rate equation are:

$$r = \frac{53.5 p_{PuF_6} p_{H_2O}}{1 + 142 p_{PuF_6} + 1.9 p_{HF}}$$

The relative error between the rates from the correlation and the measured rates was ±81%. This form of the rate equation does not correlate the PuF_6 data as well as it did the UF_6 data but, considering the wide

TABLE II-24. SURFACE REACTION DATA FOR PLUTONIUM-URANIUM HEXAFLUORIDES HYDROLYSIS KINETICS

Column diameter: 1.5 in.
Linear velocity: 9.8 cm/sec
Temperature: 22–25°C
Run time: 60.0 min

Run	$p^o_{H_2O}$ (mm Hg)	M[a]	$p^o_{MF_6}$ (mm Hg)	Feed Rate (mg M/hr)	mg M Collected in Bed Segment[b]				mg M Collected in Filter			mg M Collected in Mixer	mg M Collected on Cylinder and Screens
					0–½ in.	½–1 in.	1–2 in.	2–3 in.	1st	2nd	3rd		
Plutonium Hexafluoride Experiments													
PM-4	5.6	Pu	0.00098	5.06	1.067	0.0619	0.0863	0.0604	0.231	0.00123	0.00215	3.07	0.483
PM-1	0.54	Pu	0.00150	7.84	2.31	0.506	0.139	0.0438	0.0515	0.00152	0.00237	3.72	1.068
PM-6	0.060	Pu	0.00217	11.29	1.98	1.30	1.49	1.037	0.878	0.00088	0.00059	3.23	1.37
PM-5	0.49	Pu	0.0221	114.4	16.6	12.2	22.0	14.9	13.8	0.394	0.0364	20.7	13.8
PM-8	0.45	Pu	0.000303	1.56	0.316	0.0301	0.0317	0.0198	0.0531	—	—	0.963	0.148
PM-9	0.46	Pu	0.000181	0.938	0.192	0.0209	0.0219	0.0133	0.0186	0.000135	0.000246	0.578	0.0933
PM-7	0.45	Pu	0.0000115	0.059	0.00313	0.00102	0.0012	0.00212	0.00101	0.000073	0.000073	0.0471	0.00317
Mixed Hexafluoride Experiments													
PM-11	5.3	Pu	0.00078	3.97	0.875	0.0550	0.0406	0.0339	0.229	0.0001	0.000098	2.35	0.387
		U	0.00108	5.52	0.694	0.086	0.124	0.114	0.945	0.0001	0.00022	3.14	0.412
PM-10	0.43	Pu	0.00090	4.63	1.24	0.1215	0.184	0.0350	0.1004	0.00020	0.00022	2.42	0.529
		U	0.00113	5.80	0.94	0.769	1.37	0.512	0.056	0.00019	0.00019	1.49	0.665
PM-12	0.052	Pu	0.00049	2.51	0.699	0.1022	0.0368	0.0151	0.0362	0.000024	0.000110	1.32	0.300
		U	0.00094	4.82	0.481	0.358	0.736	0.748	0.499	0.355	0.325	0.918	0.404

[a] Hexafluoride (MF_6).
[b] Bed area = 332 cm²/in., wall area = 30.4 cm²/in., area of screen between beds = 20.7 cm².

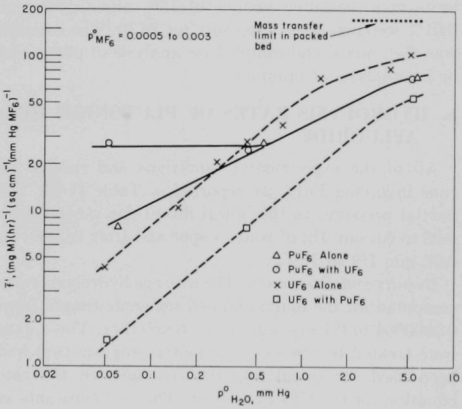

108-9124

FIG. II-28. Pseudo First Order Rate Constant for PuF_6 or UF_6 (MF_6) Hydrolysis.

range of the partial pressures used in the experimental program, the equation is regarded as a reasonable empirical correlation.

The ratio of PuF_6 to UF_6 reaction rates at similar concentrations of reactants, as indicated by the correlations, ranges from 0.28 to 2.4. The extent of departure of this ratio from unity is not highly significant when one considers the average error of the PuF_6 results from the correlation.

c. HYDROLYSIS RATES OF THE MIXED HEXAFLUORIDES

Three experiments (Table II-24) were made with approximately equimolar mixtures of PuF_6-UF_6 to determine more accurately the relative reaction rates of PuF_6 and UF_6.

Similar hydrolysis rates of PuF_6 were expected in experiments with mixed and unmixed hexafluorides; a similar effect was also expected for experiments with UF_6. Instead, an entirely new effect is indicated by the data in Table II-24. The hydrolysis rates for PuF_6 in the mixtures are higher than the rates obtained in experiments in which PuF_6 alone was hydrolyzed in air with low moisture concentrations. The UF_6 hydrolysis rates in the mixture are lower than the hydrolysis rates for unmixed UF_6. Further, in the experiments with mixtures, PuF_6 hydrolysis rates were uniformly higher than the UF_6 hydrolysis rates. These comparisons are substantiated by the following approach.

The hydrolysis rate, r, may be represented by the equation

$$r = f\, p_{MF_6} \tag{1}$$

where f is a function of the reactant and product partial pressures and p_{MF_6} is the partial pressure of the hexafluoride. For the data reported in Table II-24, in any single experimental run, f changes more slowly than r or p_{MF_6}. Assuming that f is not widely variant, an average value of f between any two sections of the packed bed can be computed by integrating the rate equation. The fraction, x, of unreacted PuF_6 or UF_6, designated as MF_6, is defined by:

$$p_{MF_6} = x\, p^0_{MF_6} \tag{2}$$

where $p^0_{MF_6}$ is the initial value of p_{MF_6} before any reaction occurs. Material balance gives:

$$r\, dS = -F\, dx \tag{3}$$

where S is surface area in the packed bed, cm²; F is the feed rate of M (plutonium or uranium), mg M/hr. Solving the above equations for f and integrating gives:

$$\bar{f} = \frac{F \ln \dfrac{x_1}{x_2}}{p^0_{MF_6}(S_2 - S_1)}$$

Using Equations 1 and 2 gives

$$\frac{x_1}{x_2} = \frac{r_1 f_2}{r_2 f_1} \quad \text{or} \quad \bar{f} = \frac{F \ln \dfrac{r_1 f_2}{r_2 f_1}}{p^0_{MF_6}(S_2 - S_1)}$$

The plutonium or uranium concentrations deposited on the packed bed surfaces give the average value of r in each bed section. $S_2 - S_1$ is the total surface area between the bed midpoints where r_1 and r_2 are determined. A first approximation ($\bar{f}'$) to $\bar{f}$ is obtained by setting $f_1 = f_2$. It can be proved that

$$f_{\text{minimum}} \leq \bar{f}' \left(1 - \frac{\ln f_2/f_1}{\ln r_2/r_1}\right) \leq f_{\text{maximum}}$$

As an example, if f decreases by 10% and r decreases by a factor of 100,

$$1 - \frac{\ln f_2/f_1}{\ln r_2/r_1} = 0.98$$

Thus the difference between $\bar{f}$ and $\bar{f}'$ is only 2% in an interval where f is decreasing by 10%.

The first approximation to $\bar{f}$ computed from the data of Table II-24 is plotted as a function of $p^0_{H_2O}$ in Figure II-28. For values of $\bar{f}$ less than 40 or $p^0_{H_2O}$ less than 1.0 mm Hg, r_1 and r_2 were determined for the first and last bed segments in calculating $\bar{f}$. For $\bar{f}$ greater than 40 or $p^0_{H_2O}$ greater than 1.0 mm Hg, the first and second bed segments were used because the rapid decrease in concentration present in the first two beds was masked in the last bed by even small collection of product from the gas phase reaction. The curves in Figure II-28 illustrate the statements, made earlier, about the relative hydrolysis rates.

As a general approach to data correlation, the use of the pseudo first order rate constant f may be of continuing value in the correlation and application of the hydrolysis rate data.

The penetration of AEC filters resulting from gas phase reaction, estimated from the results of packed-bed experiments, is much less than would be expected from penetration of particulate material. This estimation involves an extrapolation of the data to concentrations of plutonium that are lower than those used in the packed bed experiments.

d. FUTURE WORK

Experiments are planned in which filter penetration will be measured at typical media gas velocities of 0.2 to 2 cm/sec instead of 9.8 cm/sec used in the work just completed. Filter units containing about 100 cm² of media can be assembled into a series of units and substituted for the packed bed section in the existing equipment. In order to avoid contamination of the filters and thereby measure plutonium penetration rates to less than 10^{-9}, the filter units will be assembled outside the plutonium box, and after completion of the experiment the lower level units will be disassembled in open-faced hoods.

There is some uncertainty about the uniformity of filter media, and any variations in filter efficiency may affect the reproducibility of the experimental results. It is possible that small sections of the media will have much wider variations in efficiency than would exist in large commercial units. If normal AEC type filter media contain local statistical variations in efficiency, the variation of the average efficiency of a section of media will be inversely proportional to the area of the section tested. To answer this question, and also to compensate for the effect in small-scale tests, a DOP (dioctylphthalate) test will be made on individual filter units. Fabrication of the DOP test equipment is nearly complete.

4. Process Studies on the Recovery of Uranium from Highly Enriched Uranium Alloy Fuels (A. A. Jonke)

Development studies were continued on a fluid-bed fluoride volatility process for recovering highly enriched uranium from uranium-alloy fuels. The overall objectives of these studies are to develop and demonstrate an economical, high-decontamination, high uranium recovery (99%) process that is applicable to a variety of fuels. Presently, tests are being conducted with uranium-aluminum and uranium-Zircaloy alloy fuels.

The process involves hydrochlorination of the fuel

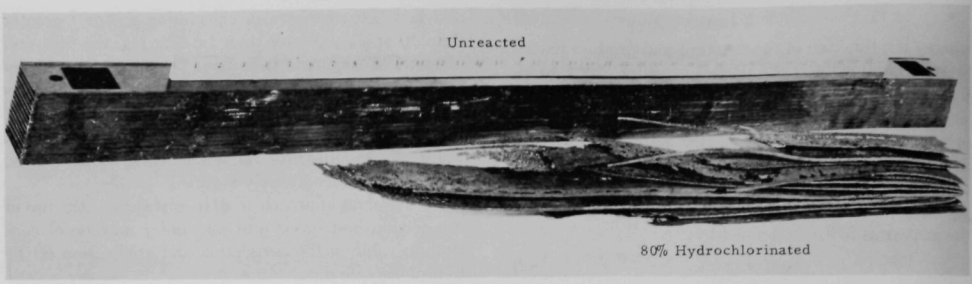

108-8004T

FIG. II-29. Uranium-Zircaloy Simulated Fuel Subassemblies.

subassemblies to separate the bulk of the alloying material as a volatile chloride,[50] followed by a hydrofluorination step and a fluorination step to recover the uranium as the hexafluoride; both reactions are conducted in the same vessel. These reactions are highly exothermic. Through the use of fluidized beds with their excellent heat transfer characteristics, it is possible to conduct and control the highly exothermic reactions under nearly isothermal conditions. The progress of the reactions is monitored continuously by measuring the concentrations of key components in the off-gas stream by in-line thermal conductivity cells.

Hydrochlorination is carried out at temperatures greater than the sublimation point of the chloride of the alloying element (sublimation points at 1 atm for $ZrCl_4$ and $AlCl_3$ are 331°C and 180°C, respectively), thereby providing the means for separating the main fuel constituents. During hydrochlorination, uranium is converted to solid uranium trichloride (UCl_3). The uranium chloride remains, for the most part, associated with the fluid-bed material; however, a portion of the uranium chloride is entrained in the gas stream and is collected on a packed bed of alumina which serves as a high-temperature filter. After the fuel charge has been completely reacted, the bulk of the solid chlorides are converted to fluorides by reaction with HF at 350°C. This step was adopted for use in process studies to avoid the production of gaseous chlorine and chlorine fluorides that would occur in the direct fluorination of UCl_3. However, it may not be necessary to prescribe this processing step in the commercial application of the process. Uranium is recovered as the volatile hexafluoride (sublimation point for UF_6 at 1 atm is 56.6°C) in the final step by fluorination by fluorine gas.

Experimental work was continued in two facilities. In the pilot-scale facility, a demonstration of the process on a practical engineering level was made with multiplate unirradiated fuel assemblies. Studies with irradiated fuel materials were made in a bench-scale (1½-in. dia.) unit. Conditions for the process steps were established in studies on unirradiated materials performed earlier[51] in a separate bench-scale unit. In addition, in-plant and tube-furnace corrosion studies in support of the fluid-bed fluoride volatility program are in progress. One phase of the corrosion work has been completed and reported in a recent topical report.[52]

a. PILOT-PLANT DEMONSTRATION OF THE FLUID-BED VOLATILITY PROCESS FOR ENRICHED URANIUM-ALLOY FUELS (J. T. HOLMES, H. STETHERS, C. SCHOFFSTOLL, W. KREMSNER)

The pilot-plant facility includes a 6-in. dia. halogenation reactor coupled to a 9-in. dia. packed-bed filter section, a second 6-in. dia. fluid-bed reactor for pyrohydrolyzing the volatile waste metal chlorides to a particulate solid (oxide), and NaF traps for collection of the UF_6 product. The facility was operated with unirradiated, normal uranium fuel subassemblies (Fig. II-29) which simulate those used as seed assemblies in the Shippingport PWR Core I [uranium-Zircaloy (U-Zr) alloy], and those used in the MTR or ETR [uranium-aluminum (U-Al) alloy]. The processing capacity of the pilot plant was about 30 kg per batch of Zircaloy fuel and 14 kg per batch of aluminum fuel. The current work, a concluding series of six experiments, completes the 18-run pilot-plant program.

[50] The volatile chloride is converted to a solid oxide in a pyrohydrolysis reactor.

[51] D. Ramaswami *et al*, Engineering Development of Fluid-bed Fluoride Volatility Processes, Part 1. Bench-scale Investigation of a Process for Zirconium-Uranium Alloy Fuel, ANL-6829, December 1964.

[52] A. A. Chilenskas and G. E. Gunderson, Engineering Development of Fluid-bed Fluoride Volatility Processes, Part 7. The Corrosion of Nickel in Process Environments, ANL-6979, March 1965.

Prior experiments (ANL-6925, p. 149, ANL-6900, p. 194 and ANL-6800, p. 282) with both aluminum and zirconium fuel subassemblies demonstrated: (1) excellent control over the highly exothermic hydrochlorination reaction was achieved in a fluidized bed of alumina, (2) High processing rates of 3.0 kg/hr for uranium-Zircaloy fuel and 2.0 kg/hr for uranium-aluminum fuel were obtained, (3) High HCl utilization (40 to 50%) was achieved without recycle, and (4) Conversion of the waste metal chlorides to solid oxides in the fluid-bed pyrohydrolysis reactor was completely satisfactory.

The overall aims of this final series of experiments were to demonstrate: (1) multiple reuse of the alumina bed material to effect further reduction in uranium losses and (2) improved processing rates and HCl utilizations by the use of multiple hydrochlorinations followed by a single fluorination. Solutions to the filter-bed caking problems that had been encountered while processing uranium-aluminum fuels were to be obtained, and the minimum amount of time required for the hydrofluorination reaction was to be determined.

(1) Experimental Procedure and Conditions

Of the final experiments, three each were made with uranium-Zircaloy and uranium-aluminum fuel subassemblies. One of the uranium-Zircaloy runs involved a multiple hydrochlorination (three subassemblies successively were reacted with HCl and HF followed by a single fluorination) while the other five runs were each made with single fuel subassembly charges.

Prefluorinated alumina from previous runs was used as bed material in the halogenation reactor in all instances except one run in which a fresh bed was used. The filter beds, on the other hand, were fresh prefluorinated alumina except for one case in which the bed from the previous run was reused. The reactor bed was Alcoa type T-61, nominal 48 to 100 mesh alumina; nominal 14 to 48 mesh alumina was used as the filter bed. The quantities of alumina for the fluid and filter beds were 40 kg (~48-in. static height) and 13 to 15 kg (10 to 12-in. depth), respectively. The filter bed was supported on coarse (⅛ to ¼-in. dia.) nickel balls.

The hydrochlorination steps were conducted using conditions prescribed in earlier pilot-plant experiments. The reactor wall temperature was controlled between 330 and 350°C in each run. The packed-bed filter was maintained in the range 340 to 355°C for the uranium-Zircaloy runs and between 250 and 355°C in the uranium-aluminum runs. The input concentration of HCl in nitrogen was about 80 to 85 v/o in all experiments. For the multiple hydrochlorination of uranium-Zircaloy fuel, three fuel elements were reacted one at a time. When about 60 to 80% of a fuel element has been hydrochlorinated, the reaction rate diminishes and the HCl utilization decreases markedly. At this point, a new fuel element is charged to the reactor. By use of the successive charging technique, operation for extended periods of low reaction rate and low HCl utilization, as was the case of batch hydrochlorination of single elements, was avoided.

The hydrofluorination step was carried out using 10 to 30 v/o HF in nitrogen for 2 hr at about 350°C. The fluorination step employed a scheme developed in the bench-scale work (ANL-6900, p. 193).

Fluorination was initiated using 1 to 5 v/o fluorine in nitrogen while the fluid bed and packed beds were heated from 250 to 500°C. When 500°C was attained, the fluorine concentration was raised to 30 v/o and then to 80 v/o by reducing the flow of nitrogen diluent. The reactor bed became static as the total flow was reduced. Fluorine was not recycled. The process times for the 250 to 500°C part of fluorination ranged from 2.0 to 6.2 hr, and the process times at 500°C ranged from 2.0 to 4.1 hr.

Two NaF traps in series, each containing 7 kg of ⅛-in. pellets, were used to collect the UF_6 product. The NaF pellets were activated by desorbing HF at 300°C from a bed of sodium bifluoride[53] pellets, thereby producing NaF pellets of high surface area. For collection of UF_6, the traps were operated at a temperature of 100 to 125°C at the inlet to the first trap and at 30 to 60°C at the outlet of the second trap. At the end of a run, both beds of pellets were ground in a disk mill and sampled for analyses.

(2) Results and Discussion

In general, the operation of the pilot-plant facility was highly satisfactory. The conditions and results for the current six runs are summarized on Table II-25. Detailed discussion of the results of the process steps follows.

Hydrochlorination. The temperatures were well controlled in all runs; the reactor bed temperatures averaged about 380°C, while the maximum bed temperature was only 410°C. The maximum temperature measured in the channels between the fuel plates was about 480°C in the case of the uranium-Zircaloy runs and 580°C for the uranium-aluminum runs. The average HCl utilization was about 25% when single uranium-Zircaloy fuel elements were processed; average HCl utilization increased to about 35% in the multicharge run in which three fuel elements were reacted using the successive charging technique. A corresponding increase in the average reaction rate (and therefore a decrease in the hydrochlorination time per element) resulted from the use of the multicharge procedure.

Inspection of partially hydrochlorinated fuel charges

[53] Sodium bifluoride (NaF·HF) pellets were obtained from the Harshaw Chemical Company, Cleveland, Ohio.

TABLE II-25. PROCESS CONDITIONS AND RESULTS OF PILOT-PLANT EXPERIMENTS

	Uranium-Zircaloy Alloy Runs			Uranium-Aluminum Alloy Runs		
	Run 13	Run 14	Run 15	Run 16	Run 17	Run 18
Alloy Charge						
Fuel Subassembly (kg)	12.720 (9 plates)	~21.0	20.380 (15 plates) 20.972 (16 plates) 15.038 (11 plates) 56.390	6.025	6.127	5.965
Uranium (g)	117 ± 4	~160	546 ± 10	273.6	289.0	280.0
Hydrochlorination						
Av. Rate (kg/hr)	1.39	~2.8	2.06	0.88	0.90	0.94
Max. Rate (kg/hr)	3.0		3.3	1.4	1.4	1.5
Reaction Time (hr)	9.2	7.5	27.4 (9.1/sub-assembly)	6.9	6.8	6.3
Av. HCl Utilization (%)	22.1		33.5	43.2	45.5	45.4
Max. HCl Utilization (%)	53.0		59.0	66.6	72.0	69.1
Temperatures (°C)						
A. Hydrochlorination						
Reactor Bed Av.	360	~395	372	364	365	383
Max.	388	408	403	408	402	407
Fuel Element Channel Av.	370	~415	377	380	380	393
Max.	424	480	428	520	578	564
Reactor Wall	347	340	355	351	346	348
Packed-bed Filter	346	360	365	335	255	250
Pyrohydrolyzer Bed	333	363	355	355	349	349
B. Hydrofluorination of 2 hr						
Reactor Bed	357	—	360	349	356	330
Filter Bed	354	—	353	362	352	250
C. Fluorination						
Reactor Bed and Filter Bed						
(1) Reactor Fluidized	250–500 (6.2 hr)	250–500 (3.3 hr)	250–500 (2.5 hr)	250–500 (2.8 hr)	250–500 (2.2 hr)	250–500 (3.3 hr)
(2) Reactor Static	500 (2.1 hr)	500 (3.8 hr)	500 (2.1 hr)	500 (3.0 hr)	500 (4.1 hr)	500 (2.7 hr)
Reactant Concentrations (*v/o*)						
A. HCl in N_2	85	~80	79	83	85	83
B. HF in N_2	35	—	17.5	~20	~20	~20
C. F_2 in N_2						
(1) Reactor Fluidized	4.6	~5	4.6	4.6	4.6	4.6
(2) Reactor Static	68	~70	68	68	68	68
Gas Velocity in Reactor (*ft/sec*)						
A. Hydrochlorination	0.44	~0.4	0.42	0.40	0.38	0.36
B. Hydrofluorination	0.38	—	0.49	0.50	0.50	0.50
C. Fluorination						
(1) Reactor Fluidized	0.40	~0.4	0.40	0.40	0.40	0.40
(2) Reactor Static	0.04	~0.04	0.04	0.04	0.04	0.04

showed that greater reaction had occurred in the vicinity of the reagent gas inlet. This is well illustrated in Figure II-29, which shows a uranium-Zircaloy fuel subassembly about 80% reacted, and an unreacted fuel subassembly for comparison. The uranium-aluminum subassemblies reacted in a similar manner.

Problems associated with caking of the packed bed filter during the hydrochlorination step and with temperature excursions within the filter during the fluorination step were reported in work with uranium-aluminum fuels (see ANL-6925, p. 151). These problems have been attributed to the presence of iron chlorides ($FeCl_3$[54] or $FeCl_3$-$AlCl_3$[55]) that condensed on and in

[54] Boiling point of $FeCl_3$ is 319°C at 1 atm.

TABLE II-26. Typical Bulk Densities of Fluid-Bed Materials after Pyrohydrolysis

Fuel: uranium-aluminum, 6.0-kg batch Starting bed: nominal 48 to 100 mesh alumina (Alcoa type T-61)			Fuel: uranium-Zircaloy, 13-kg batch Starting bed: nominal 48 to 100 mesh alumina (Alcoa type T-61)		
	Untapped Bulk Density (g/cc)	Tapped Bulk Density (g/cc)		Untapped Bulk Density (g/cc)	Tapped Bulk Density (g/cc)
Starting Bed	1.62	1.86	Starting Bed	1.75	1.90
Product	1.1	1.5	Product	2.3	2.7
Final Fluid Bed	1.8	2.1	Final Fluid Bed	1.7	2.4

the packed-bed filter when low filter-bed temperatures (180 to 200°C) were used. In the current three runs with uranium-aluminum subassemblies, the packed-bed filter temperature was maintained at 335°C, 255°C, and 250°C. Caking problems were encountered only in the run at 250°C (run 18), and an analysis of the deposited material on the filter surface indicated the presence of iron chlorides. Temperatures above 250°C apparently allow the iron chlorides to pass through the filter, but at the higher temperatures high uranium losses (up to 6.6% at 355°C) by passage of uranium through the filter to the pyrohydrolysis reactor were also sustained. The higher uranium loss may be related to the formation of highly volatile UCl_5 or UCl_6 from the lower chloride (UCl_3) as a result of oxidation by $AlCl_3$.[56] A solution to the overall problem may be to condense the iron chlorides on the particles in the fluid bed while reacting the alloy at relatively low temperature (<250°C); with the filter bed at a similarly low temperature, acceptably low uranium losses should be obtained. If this new procedure is successful in causing the chlorides to be deposited on the fluid bed particles, its use should also result in the elimination of temperature excursions in the filter which were encountered in the fluorination step of some earlier runs as a result of the reaction between fluorine and the deposited chlorides; the chlorides would now be reacted in the fluid-bed reactor where heat removal is efficient. Previous work in a 1½-in. dia. reactor (ANL-6800, pp. 271–282) has shown that hydrochlorination of uranium-aluminum fuels proceeds at satisfactory rates at temperatures as low as 200°C. Even though the uranium-Zircaloy and uranium-aluminum fuels contain similar amounts of iron, caking problems are not encountered for the former alloy because the iron chlorides are transported from the system as a volatile material through the packed-bed filter at the higher operating temperatures (~350°C). Uranium losses during the hydrochlorination of uranium-Zircaloy fuels remained low, indicating that uranium behavior varies with fuel type.

The pyrohydrolysis reactor for converting the zirconium and aluminum chlorides to their respective solid oxides operated smoothly in all experiments. A steam rate of about three times the stoichiometric requirement for conversion of the chloride to oxide was sufficient. Chemical analyses of the solid products indicated that the residual chloride content ranged from 0.3 to 3.0 w/o in the uranium-Zircaloy runs and from 4 to 10 w/o in the uranium-aluminum runs. This quantity of chlorides in the waste oxide (probably present as oxychlorides) is not expected to affect the storage properties of the solid. Approximately 1 to 2 w/o of the product is soluble in boiling water (1-hr test).

The tapped and untapped bulk density of the pyrohydrolysis product and samples from typical beds are shown on Table II-26. The density of the product from the aluminum fuel was as much as 40% less than the density of the starting alumina fluid-bed material. The density of the product from the Zircaloy fuels was as much as 40% greater than the density of the starting alumina bed. In both cases, the product was a relatively dense material that was suitable for disposal or storage as radioactive waste.

The oxide product produced by pyrohydrolysis was primarily in the form of fine particles (−200 mesh). Also, there was little if any indication that the oxide deposited on the particles constituting the starting bed. The large proportion of fines in the resulting fluidized bed (up to 60% −230 mesh) did not hamper the operation of the reactor; bed temperatures remained uniform, and no significant increase in pressure drop across the sintered metal filters because of fines loading was noted. The sieve analysis of typical pyrohydrolyzed material, presented in Table II-27, suggests that coarse particles may have to be added to the pyrohydrolyzer fluid bed during continuous plant operation in order to maintain a fluidizable particle size distribution since part of the starting bed containing coarse particles is removed continuously with the product.

A number of generalizations can be made, based on

[55] The phase diagram for $FeCl_3$-$AlCl_3$ was presented by K. N. Semenenko *et al*, Proc. Acad. Sci. USSR, Chem. Sect. (English Transl.) **154**(1–6), 42–43 (Jan.-Feb. 1964).

[56] Personal communication, T. Gens (ORNL) March 29, 1965.

TABLE II-27. Typical Sieve Analysis of Typical Fluid Bed and Product Material from the Pyrohydrolysis Reactor

Screen Size	Weight Percent of Bed on Sieve					
	Batch Uranium-Aluminum Fuel Charge			Batch Uranium-Zircaloy Fuel Charge		
	Starting Fluid Bed	Final Fluid Bed	Product	Starting Fluid Bed	Final Fluid Bed	Product
+60	5	3	2	5	2	2
+80	47	23	19	47	17	13
+120	40	25	20	40	18	14
+170	6	4	2	6	3	2
+230	1	1	3	1	1	1
+325	1	10	12	1	14	16
−325	—	34	42	—	45	52
Average Particle Size	183μ	114μ	97μ	183μ	91μ	78μ

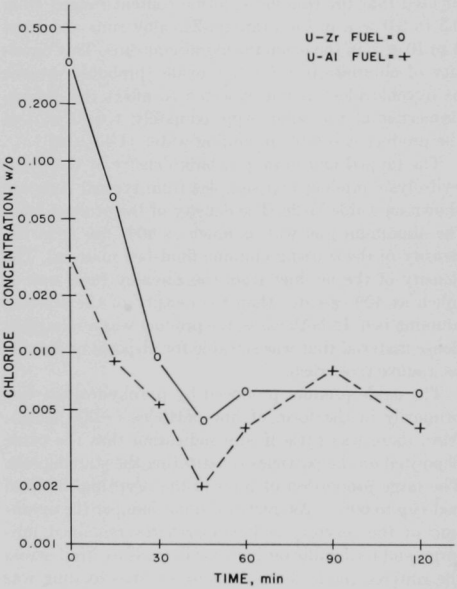

108-8401 T Rev.

Fig. II-30. Typical Chloride Concentration of the Halogenation Reactor Bed During Hydrofluorination.

results from all pilot-plant runs (see also ANL-6925), concerning the hydrochlorination reaction characteristics when processing aluminum-uranium and zirconium-uranium fuels:

(a) The reaction rate is nearly independent of bed temperature in the range of 330 to 400°C during the part of the run when HCl utilization is high.

(b) Gas velocities in the fluid-bed reactor of about 0.6 ft/sec, give higher reaction rates with little or no decrease in HCl utilization efficiency than did velocities of about 0.4 ft/sec.

(c) A satisfactory combination of high reaction rate and high HCl utilization can be achieved using about 80 v/o HCl in nitrogen as the feed gas to the reactor.

(d) An increase in both the overall HCl utilization and the reaction rate can be realized by charging additional fuel after the previous charge has reacted to a point where the reaction rate and HCl utilization begin to decrease. This procedure may be important in reducing the total processing time for multiple-subassembly batches, thereby increasing the capacity of the process equipment.

(e) The packed-bed filter operated satisfactorily even though a caked surface layer was formed during the hydrochlorination step of the runs with uranium-aluminum fuels. Means of avoiding the caked layer by minor changes in process conditions and equipment design appear to be readily available.

(f) The operation of the pyrohydrolysis reactor in series with the halogenation reactor and packed-bed filter was satisfactory. The pyrohydrolyzer product has a relatively high density (~2.0 g/cc) and should be a satisfactory material for waste disposal.

Hydrofluorination. The residual chloride content of the reactor and filter bed after the HF treatment was satisfactorily low (0.004 to 0.01 w/o), a level which corresponds to only about 2 to 6 g of chlorine in the entire reactor and filter-bed system. Figure II-30 illustrates that the minimum residual chloride value is obtained in about 45 min, confirming previous data obtained in a 1½-in. dia. reactor (ANL-6829, p. 36). The recommended hydrofluorination period would probably be of 1- to 2-hr duration.

Fluorination. The fluorination step proceeded without difficulty in all runs except the one uranium-aluminum run (run 18) in which chlorides had condensed on the packed-bed filter. In this one case, some caked material remained on the filter bed after fluorination; also, uranium retention by the filter bed was relatively high.

The overall fluorine requirement was about 8 g per gram of uranium recovered. The minimum fluorine requirement for one run was 2.7 g per gram of uranium; this gives a fluorine reagent cost as low as a few cents per gram of uranium. These low fluorine requirements

TABLE II-28. SUMMARY OF URANIUM LOSS DATA

Run No.	U Content of Charge (g)	Uranium Content						Final Concentration of U in Reactor and Filter Beds (w/o)
		Pyrohydrolysis Reactor Product		Halogenation Reactor Bed		Packed-bed Filter		
		(g)	(%)[a]	(g)	(%)[a]	(g)	(%)[a]	
13	117 ± 4	0.3	0.2	5.7	1.9[b]	1.5	1.3	
14	~160	0.25	0.2	3.8	0.8[b]	1.6	0.6[b]	0.01
15	546 ± 10	4.4	0.8	4.3	0.8	2.9	0.5	
16	275.9	18.0	6.6[c]	3.3	0.13[b]	1.1	0.4	
17	292.3	4.9	1.7[c]	3.5	0.08[b]	0.9	0.16[b]	0.005
18	283.5	4.2	1.5[c]	0.9	0.03[b]	4.2	1.5[d]	

[a] Percent of uranium in alloy charge.

[b] Bed reused from the previous run with the same type of fuel; percentage is calculated from the uranium remaining in the bed at the end of the run and the total uranium on U charged to that bed during all runs.

[c] High packed-bed filter temperature caused large uranium losses.

[d] Cake found at surface of packed-bed filter; uranium level might be reduced by fluorination of the packed-bed material as a fluidized bed.

suggest that no fluorine recycle procedure may be required for plant-scale operation.

Uranium Disposition and Material Balance. The demonstration that less than 1% of the uranium in the fuel charge was lost was of prime importance in the overall pilot-plant program. A summary of the uranium loss data for the current runs is given in Table II-28. It is apparent from these data that reuse of the alumina beds effects a reduction in the overall loss of uranium. For example, a twofold improvement (1.9 to 0.8% loss to the reactor bed and 1.3 to 0.6% loss to the filter bed) was achieved by reuse of the beds in runs 13 and 14 with the uranium-Zircaloy fuel subassemblies. The total loss to the halogenation reactor bed was only 0.03% in a series of seven runs (includes runs 16, 17, 18) with uranium-aluminum fuel subassemblies. The number of times the bed material can be reused will probably be limited by the heat load generated by the buildup of fission products. Lower residual uranium concentrations than those obtained, 0.01 w/o and 0.005 w/o uranium in alumina for the uranium-Zircaloy and uranium-aluminum runs, respectively, would be expected from optimization of the fluorination conditions.

Uranium losses to the pyrohydrolysis reactor were relatively high in the uranium-aluminum runs made with filter-bed temperatures >200°C during the HCl step. Lower temperatures should give lower losses for the reasons discussed previously. The loss to the pyrohydrolysis reactor was in the range 0.2 to 0.8% in uranium-Zircaloy runs. It is expected that these losses for both types of fuel could be further reduced by increasing the filter-bed depth to greater than 12 in. This was the maximum depth available in the existing equipment.

Conditions and techniques recommended to assure >99% uranium recovery and smooth operation of the process are:

1) Employ a packed-bed filter depth of over 12 in. and filter temperatures of 180 to 200°C for the uranium-aluminum fuels and 335 to 350°C for the uranium-Zircaloy fuels during the hydrochlorination step.
2) Use lower (<250°C) fluid-bed temperatures during the HCl step for uranium-aluminum fuels to prevent transport of volatile iron chlorides to the packed-bed filter.
3) Employ the two-temperature fluorination procedure outlined in the experimental procedure section of this report.
4) Reuse the alumina bed material for a number of reaction cycles.

Corrosion. Corrosion rates have been measured for coupons mounted at various locations in the pilot plant. The test exposures ranged from 2 to 9 days and included up to 16 processing cycles. Welded and unwelded corrosion coupons of nickel-200 and -201 were exposed to process environments in the halogenation reactor. Corrosion rates ranging from 0.08 to 0.12 mil/day for samples exposed in the fluidized bed region and from 0.03 to 0.09 mil/day for samples suspended above the fluidized bed were obtained from defilmed coupons, using weight loss data.[57] In an independent study[52] of corrosion in simulated fluid-bed volatility process gas environments, it was observed that the corrosion rate of nickel was less than the rate observed for specimens

[57] Specimens were defilmed by immersion for 0.5 hr in a salt bath containing equimolar potassium nitrate-sodium nitrate at 500°C.

TABLE II-29. RECOMMENDED MATERIALS OF CONSTRUCTION FOR THE FLUID-BED FLUORIDE VOLATILITY PROCESSING OF URANIUM-ALLOY FUELS

	Corrosive Environment	Recommended Material	Maximum Corrosion Rate (mil/day)
Halogenation Reactor and Packed-bed Filter	HCl, $ZrCl_4$, $AlCl_3$, H_2, HF, F_2, UF_6	Nickel-200 or -201	0.12
Pyrohydrolyzer	HCl, $ZrCl_4$, $AlCl_3$, H_2, H_2O	Stainless steel or Inconel	0.04
Pyrohydrolyzer Filters	HCl, H_2O, H_2	Nickel or Inconel	—
Process Piping	Dry HCl	Stainless steel	—
	HF, F_2	Monel or nickel	—
	HCl, $ZrCl_4$, $AlCl_3$, H_2, HF, F_2, UF_6	Nickel-200 or -201	0.09
	Wet HCl above condensation point	Stainless steel or Inconel	0.04

immersed in the pilot plant fluid-bed material. This has been attributed to the removal of the protective fluoride film by the abrasive action of the fluid-bed particles.

Types 304 and 347 stainless steel coupons mounted in the pyrohydrolysis reactor exhibited corrosion rates of less than 0.04 mil/day from exposure in both the fluidized bed region and in the gas space above the fluidized bed. Corrosion rates of Inconel-600 exposed in the pyrohydrolyzer bed were about 25% lower than those of the stainless steel.

Both Inconel and nickel sintered metal filters (pore size 10μ) were satisfactory for use in the pyrohydrolyzer off-gas (HCl-H_2O-H_2). After a final cleaning with steam, the filters exhibited pressure drops corresponding to new filters. Stainless steel filters were not tested.

In general, the corrosion coupons did not undergo intergranular attack. In isolated cases, however, specimens of nickel-200 and -201 exhibited a few areas where apparent intergranular modifications had occurred near the surface, ranging in depth from 1 to 2 mils.

There was no evidence of gross dimensional changes in the reaction vessels from corrosion. However, thermal cycling will cause permanent distortion of the equipment if the strength-temperature limits of the material are exceeded. Variance in the diameter measurements of up to ⅛ in. were measured for the 6-in. dia. nickel halogenation reactor in the vicinity of the heaters. Slight distortion was also noted on the pyrohydrolyzer. Two final measurements of the ID of the stainless steel pyrohydrolyzer were 6.077 in. and 6.026 in.; the corresponding as-installed measurements were 6.061 in. and 6.089 in. Recommended materials of construction are presented in Table II-29.

(3) Conclusions

The fluid bed volatility process for uranium-Zircaloy and uranium-aluminum fuels has been successfully demonstrated on a pilot-plant scale. High hydrochlorination rates and HCl utilization efficiencies were achieved in the fluid-bed halogenation reactor using 80 v/o HCl in nitrogen. By the use of two-temperature fluorination procedures developed in bench-scale work, over 99% of the uranium was removed from the reactor and filter beds and recoveries of over 99% of the input uranium as UF_6 on beds of NaF were demonstrated. Recommendations for scale-up work in addition to those suggested from the bench-scale work are the advisability of providing (1) a means for submerging the uranium-aluminum fuel elements in the fluid bed during the hydrochlorination step, as discussed in an earlier report (ANL-6925, p. 152) and (2) a method for preventing $FeCl_3$ or $AlCl_3$-$FeCl_3$ condensation on the packed-bed filter during uranium-aluminum fuel processing.

The fluid-bed volatility process offers the advantages of (1) simplified reprocessing of a variety of fuels, (2) high uranium recovery, (3) a uranium product (UF_6) in a form amenable both to isotope enrichment and to conversion schemes for production of fuel materials, and (4) relatively small volumes of solid radioactive waste products.

(4) Topical Reports

The pilot-plant development work is being reported in detail in ANL-6973, Engineering Development of Fluid-bed Fluoride Volatility Processes, Part 8. Pilot Plant Development of a Process for Uranium-Alloy Fuels, and in a paper accepted for publication by *Nuclear Applications*, Engineering Development of a Fluid-bed Fluoride Volatility Process for High-Enriched Uranium-Alloy Fuels, Part II—Pilot-Scale Studies. The automatic data processing techniques used in the course of this work and in bench-scale work are summarized in ANL-6992, Engineering Development of Fluid-Bed Fluoride Volatility Processes, Part 9. Computer Programs for Alloy-Fuel Process Calculations.

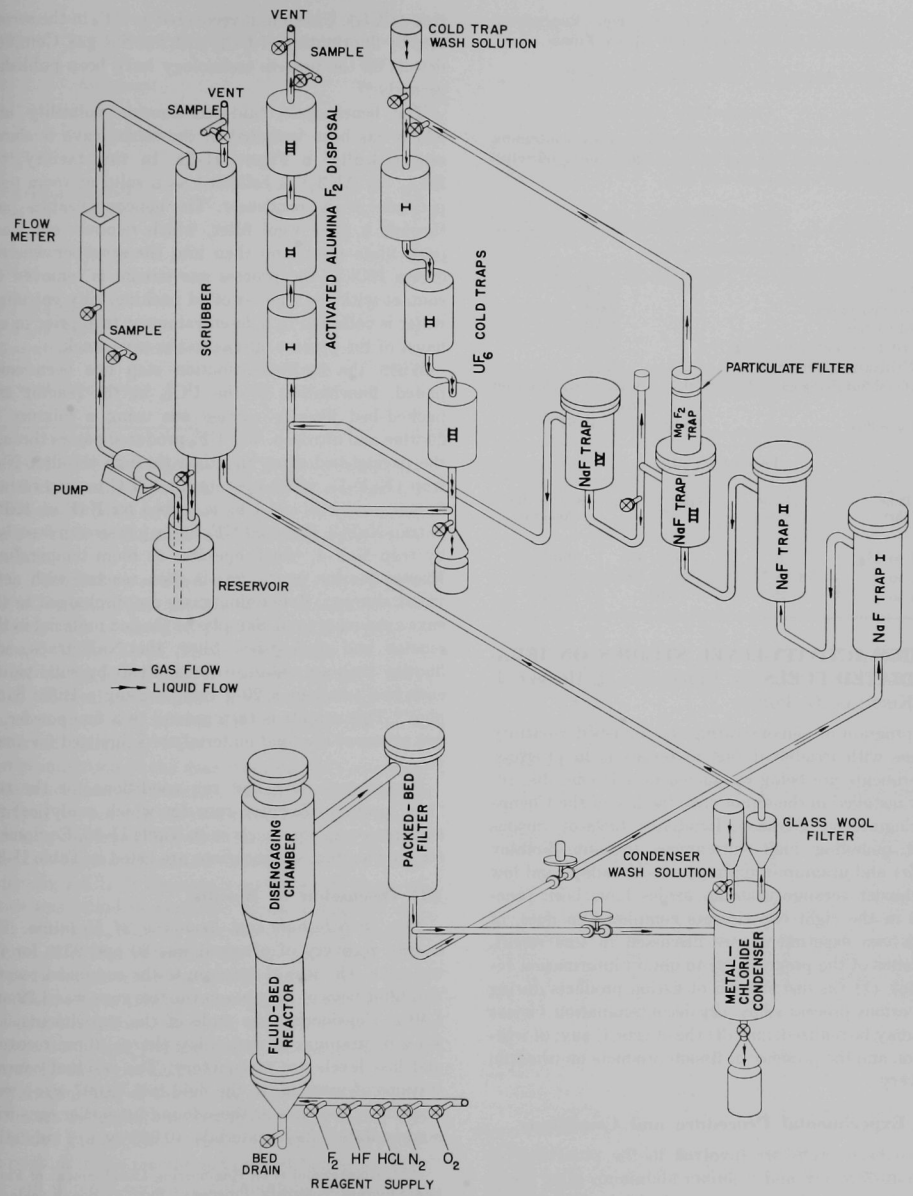

108-8452 Rev. 2

FIG. II-31. Bench-Scale Fluid-Bed Fluoride Volatility Unit Installed in the Senior Cave.

TABLE II-30. OPERATING CONDITIONS FOR PROCESSING IRRADIATED URANIUM-ZIRCALOY ALLOY FUELS

Run 1 (typical for uranium-Zircaloy run 2)

Charge Data

269 g of 5-yr-cooled uranium-Zircaloy-2 alloy containing 4.92 g of uranium and 3.28 g of fission products (41% burnup). Original uranium enrichment was 93%.

Run Conditions

Hydrochlorination Step

Duration	6¼ hr
Reactor-bed temp	400°C
Filter-bed temp	350°C
Inlet HCl concentration (avg.)	40 v/o
HCl Utilization efficiency	32%
Superficial fluidizing gas velocity	0.54 ft/sec (at reaction conditions)
Total gas flow	5 liters/min at STP

Fluorination Step

Time (hr)	F_2 Conc. (v/o)	Reactor Temp (°C)	Reactor Bed Condition
0 to 1½	8	250 to 475	fluidized
1½ to 2	8 to 75	475 to 500	fluidized
2 to 4	75	500	static

b. HIGH-ACTIVITY-LEVEL STUDIES ON IRRADIATED FUELS (A. CHILENSKAS, J. HOLMES, J. KINCINAS, G. POTTS)

A program of demonstrating the fluid-bed volatility process with irradiated fuel materials is in progress. Experiments are being conducted in a 1½-in. dia. reactor installed in the senior cave facility of the Chemical Engineering Division. Irradiated fuels of various types including high enrichment uranium-Zircaloy (U-Zr) and uranium-aluminum (U-Al) alloys and low enrichment ceramic uranium oxides have been processed in the eight experiments completed to date, of which two experiments are discussed in this report. The aims of the program are to obtain information regarding (1) the distribution of fission products during the various process steps, (2) decontamination factors that may be realized, and (3) the effects, if any, of irradiation and the presence of fission products on uranium recovery.

(1) Experimental Procedure and Conditions

Two basic steps are involved in the processing of uranium-Zircaloy and uranium-aluminum alloy fuels. In the first step, the fuel is reacted with hydrogen chloride gas to form volatile chlorides of zirconium or aluminum which separate from nonvolatile uranium chloride (UCl_3). Uranium is recovered as UF_6 in the second step by fluorination of UCl_3 with fluorine gas. Complete details on the process technology have been published recently.[58]

The bench-scale fluid-bed fluoride volatility unit which has been installed in the senior cave is shown schematically in Figure II-31. In this facility, the $ZrCl_4$ (or $AlCl_3$) is collected as a solid at room temperature in the condenser. The noncondensables pass through a glass wool filter, which removes entrained particulate fines, and then into the scrubber wherein excess HCl in the process gas stream is removed by contact with the water-wetted packing. Any entrained water is collected in a de-entrainment trap prior to exhaust of the process off-gas to the cave stack.

When the hydrochlorination step has been completed, fluorination of the UCl_3 in the reactor and packed-bed filter is carried out using a mixture of fluorine and nitrogen. The UF_6 produced passes through the packed-bed filter and then through the first NaF trap (NaF-1), which operates at 400°C to trap certain fission products; the UF_6 is sorbed on NaF at 100°C in trap NaF-3. Residual UF_6 in the gas stream is sorbed by trap NaF-4, which operates at room temperature. Excess fluorine in the gas is then reacted with activated alumina. Remaining gases are discharged to the cave exhaust system. Samples of the bed material in the reactor and packed-bed filter, the NaF traps, and fluorine trap are obtained for analysis by subdividing each bed to about a 20-g sample using a Riffle Sampler.[59] This sample is then ground to a fine powder. A few grams of the final material are submitted for analysis.

Fuel charge data and run conditions for the two "hot" uranium-Zircaloy runs for which analytical results are complete are given in Table II-30. Equipment size and loading specifications are listed in Table II-31.

(2) Discussion of Results

The Distribution and Recovery of Uranium. The overall recovery of uranium was 80 and 93% for the two runs. The loss of uranium to the combined reactor and filter beds of alumina in the two runs was 1.22 and 1.40%. Considering the scale of the experiments, i.e., 4.5 g of uranium in each alloy charge, these recovery and loss levels are satisfactory. The residual concentrations of uranium in the fluid bed (0.007 w/o) were essentially the same as those found for earlier runs with nonirradiated fuel materials (0.006 w/o), indicating

[58] D. Ramaswami *et al*, Engineering Development of Fluid-bed Fluoride Volatility Processes, Part 1. Bench-Scale Investigation of a Process for Zirconium-Uranium Alloy Fuel, ANL-6829, December 1964.

[59] Conforming to standards ASTM D 271.

TABLE II-31. EQUIPMENT SIZE AND LOADING SPECIFICATIONS

Component	Size		Charge Material	
	ID (in.)	Length (in.)	Description	Weight or Volume
Reactor	1.5	14	Alcoa T-61 alumina (nominal 28 to 100 mesh)	700 g
Disengaging chamber	4.5	12	—	—
Packed-bed filter section	2.5	6.5	Alcoa T-61 alumina (nominal 41 to 48 mesh)	900 g
Metal chloride condenser	5.0	16	Empty	
Scrubber	4.0	5 ft	3-ft depth, ½-in. Raschig rings	10–15 liters (reservoir capacity)
NaF-1 and NaF-2	2.5	26	⅛-in. NaF pellets	1000 g
NaF-3 and NaF-4	2.5	14	⅛-in. NaF pellets	500 g
F_2 absorption tower (three sections in series)	3.0	12/section	¼-in. dia. activated alumina pellets	1000 g/section
Glass wool filter section	3.0	3	Pyrex wool filtering fiber (Owens-Corning No. 3950)	22 g

that irradiation or the presence of fission products does not affect uranium retention. Identical uranium concentrations of 0.002 w/o were found in the packed-bed filter for runs with irradiated and nonirradiated fuel materials.

The Distribution of Fission Products. The distributions of uranium and the important fission products following each of the two process steps are given in Tables II-32 and II-33. The major gamma activity in the fuel charge is due to ^{137}Cs, which represents about 90% of the total gamma; next important is ^{144}Ce which comprises about 7% of the total (mainly due to its short-lived daughter ^{144}Pr).

An examination of the data from the HCl step leads to the conclusion that cesium, cerium, ruthenium, and strontium are nonvolatile under the hydrochlorination conditions employed. However, small amounts of these elements were entrained and deposited along with the condensing $ZrCl_4$ in the condenser. None of these activities was found downstream of the condenser (i.e., in the scrubber). This is believed due to the removal of these entrained activities by the glass wool filter interposed between the condenser and scrubber. Since technetium and antimony were found in the scrubber indicating that their movement was not restricted by the glass wool filter, the transport of these activities is apparently due to volatilization.

An examination of the fission product and activity distribution following the fluorination step shows that the bulk of the cesium, cerium, ruthenium, and strontium remains in the reactor and packed-bed filter. That some entrainment occurs is apparent by the presence of cesium and cerium activities in all of the NaF traps. Antimony appeared in the 400°C NaF trap in quantities which are too large to account for by an entrainment mechanism. Of the antimony found, about one-half remained in the reactor and packed-bed filter; the

TABLE II-32. DISTRIBUTION OF URANIUM AND FISSION PRODUCTS FOLLOWING THE HYDROCHLORINATION OF URANIUM-ZIRCALOY FUEL

Analysis for Run 1[a] Fuel Charge

Isotope	Weight of Element (g)	% of Total Gamma Activity
U	4.9	—
^{137}Cs	—	88.5
^{125}Sb	—	1.1
^{106}Ru	—	0.9
^{144}Ce	—	9.5
Mo[b]	0.455	—
Tc	0.089	—

Isotope or Activity	Percent Retained in Reactor and Filter[c]	Volatilized or Entrained in Gas			
		% of Charge in Chloride Condenser		% of Charge in Scrubber	
		Run 1	Run 2	Run 1	Run 2
Uranium	>99	0.40	0.37	0.02	0.25
Gross γ	>99	0.05	0.05	0.001	0.13
Gross β	>99	0.05	0.01	0.0008	0.02
Cs, Ce	>99.9	[d]	[d]	nil	nil
^{125}Sb	>95	2.7	[e]	0.1	[e]
Tc	>95	0.9	[d]	1.05	2.6
^{106}Ru	>99.9	nil	nil	nil	nil

[a] Analysis for Run 2 charge is similar.

[b] Molybdenum was not analyzed in process streams after hydrochlorination step.

[c] By difference from gross gamma analysis.

[d] Trace amounts of beta and gamma activities found.

[e] Not analyzed.

TABLE II-33. DISTRIBUTION OF URANIUM AND FISSION PRODUCTS FOLLOWING THE FLUORINATION STEP

Isotope or Activity	Retained in Reactor and Filter (% of Charge)		Collected in 400°C NaF Trap (% of Charge)		Collected in 100°C NaF Trap				Collected in 25°C NaF Trap (% of Charge)	
					(% of Charge)		(D.F.)[a]			
	Run 1	Run 2	Run 1	Run 2	Run 1	Run 2	Run 1	Run 2	Run 1	Run 2
Uranium	1.22	1.40	0.37	0.49	89.0	75.2	—	—	0.80	1.29
Gross γ	43.9	48.2	0.61	0.70	0.002	0.006	5×10^4	1.7×10^4	0.09	0.002
Gross β	50.5	52.0	0.95	0.13	0.003	0.017	4×10^4	6×10^3	0.23	0.008
^{137}Cs	45.5	48.9	[b]	nil	0.002	0.006	5×10^4	1.7×10^4	[b]	[b]
^{125}Sb	20.1	10.7	25.2	50.0	0.035	0.005	3×10^3	2×10^4	nil	nil
^{106}Ru	56.0	54.2	0.59	0.31	0.006	0.013	1.6×10^4	8×10^3	nil	[b]
Mo	[c]	[c]	[c]	[c]	26.0	12.3	3.8	8	37.3	11.7
Tc	[c]	[c]	[c]	[c]	76.0	78.5	1.3	1.3	[c]	[c]
Other non-vol. fission products	^{144}Ce[b]	^{144}Ce[b]	^{144}Ce[b]	nil	^{144}Ce[b]	^{144}Ce[b]	—	—	^{144}Ce[b]	^{144}Ce[b]

[a] $\text{D.F.} = \dfrac{\text{activity per gram uranium in charge}}{\text{activity per gram uranium in trap NaF-3 (100°C)}}$.

[b] Detected by gamma ray spectrometry.

[c] Not analyzed.

remainder volatilized and was sorbed by the 400°C NaF trap (NaF-1). The removal of molybdenum and technetium from the reactor and filter beds during the fluorination step was high and appeared to be complete. Analytical confirmation of the degree of removal of these two elements was not obtained. Large amounts of the molybdenum fluoride and technetium fluoride were collected with the UF_6 in the 100°C and 25°C NaF traps. Separation of UF_6 from MoF_6 and TcF_6 can be readily accomplished by the use of sorption-desorption techniques.[60]

Decontamination factors for uranium were calculated on the basis of (1) the fuel charge analysis and (2) the uranium content and the fission product activities found on the UF_6 product NaF trap (trap NaF-3). Average decontamination factors of about 3×10^4 were obtained for gross gamma, gross beta, and ^{137}Cs activities, and about 1×10^4 for ^{125}Sb and ^{106}Ru. Additional decontamination can be achieved by incorporating a step in which UF_6 is desorbed from the sodium fluoride traps, passed through a sintered metal filter and collected in cold traps. This step has been demonstrated in subsequent tests.

[60] Chemical Technology Division Annual Progress Report for Period Ending May 31, 1964, USAEC Report ORNL-3627, pp. 30–32, Oak Ridge National Laboratory.

The contaminants contributing most of the gamma to the uranium product were found to be ^{137}Cs and ^{144}Ce. These activities were entrained by the process gas and deposited with the UF_6 in the NaF product trap. It is expected that better gamma decontamination could be obtained by increasing the depth of the alumina packed-bed filter and/or decreasing the particle size of the bed material. The filter-bed depth is 6½ in. (fixed by equipment design) while other laboratory experience[61] suggests that a filter depth of 8 to 10 in. is needed for high efficiencies.

Balances on fission product activities in the various process streams ranged between 44 and 81%. Some loss of activity is known to occur as the filter bed is withdrawn (by vacuum) out of the filter housing prior to sampling. An accumulation of activity within the equipment, as deposited particulate material, has also been noted during various cleanup operations. Work is under way to estimate the activity deposition within the equipment following a run.

Future work involves demonstration runs with Zircaloy-clad UO_2 pellets and irradiated PuO_2-UO_2 fuels and results of these runs will be reported later.

[61] D. Ramaswami *et al*, Engineering Development of a Fluid-Bed Fluoride Volatility Process, Part I. Bench-Scale Studies, to be published in *Nuclear Applications*, 1965.

5. Basic Studies of Fluidized-Bed Behavior Related to Process Operations

(J. Gabor, D. Ramaswami, J. Phelps, D. Raue)

Basic studies in support of fluidized-bed processing of fine particles were continued. Fluidization of fine particles is encountered in the fluorination of PuO_2-U_3O_8 fines and in the preparation of particulate nuclear fuel.

Previous studies (ANL-6687, pp. 128–139, ANL-6900, pp. 181–187) established that, by the addition of coarse particles to a bed of fine particles, fluidization of fine particles was improved, and hence better heat transfer was achieved. Beds containing 15 to 20 w/o U_3O_8 fines exhibited maximum heat transfer coefficients at superficial gas velocities of 0.6 to 1.4 ft/sec. However, fine particles were readily elutriated from the fluidized bed, and methods for removing them from the gas stream and returning them to the fluidized bed are required in process operations.

Current studies are aimed at the determination of the optimum size distribution of coarse alumina particles which, when mixed with fine particles, would maximize the residence time of the fine particles in the fluidized bed and would provide high rates of heat and mass transfer. In order to clearly define the effect of fine particles on fluidized-bed behavior, these studies will include investigation on the following topics:

(a) elutriation of fines from the fluidized bed
(b) solids mixing and segregation of fines
(c) gas-solid contacting
(d) heat transfer from the bed to the column walls

a. CURRENT WORK

Tests were made to determine the rate of fine particle elutriation from a fluidized bed, the concentration distribution of fines within the bed, and the effect of fines on bed expansion. Sintered alumina, Alcoa Type T-61, nominal 48 to 100 mesh with particle size distribution as shown in Figure II-32, was used as the coarse bed material. Humidified air or nitrogen was used as the fluidizing gas.

(1) Elutriation Tests

Several tests were conducted to determine the effect of various concentrations of nickel fines in the fluidized bed on the rate of elutriation. These tests were performed with a 3-in. ID brass column, 6 ft long. To minimize effects of static electricity, the fluidizing air was humidified and the brass column was grounded. The air was distributed by a porous metal plate. The elutriated fines were filtered from the off-gas and col-

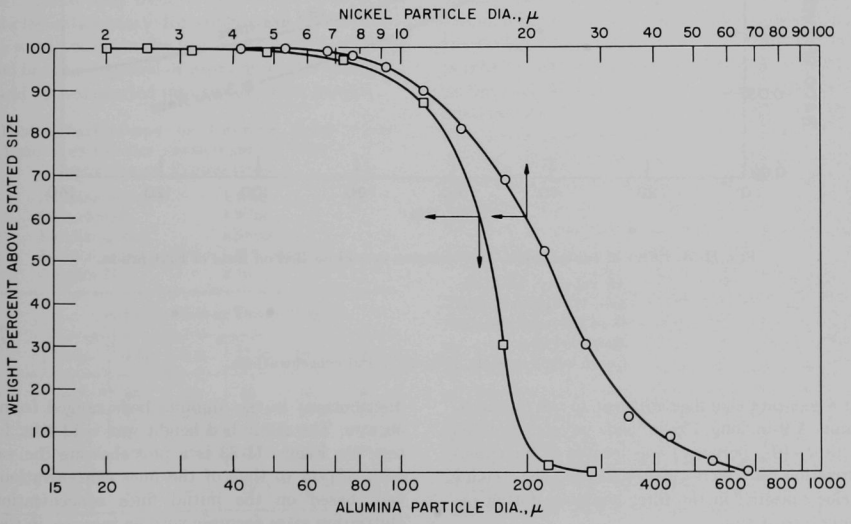

108-8911

Fig. II-32. Size Distribution of Granular Alumina and Nickel Fines. (Type T-61 alumina, nominal 48 to 100 mesh, manufactured by Alcoa.)

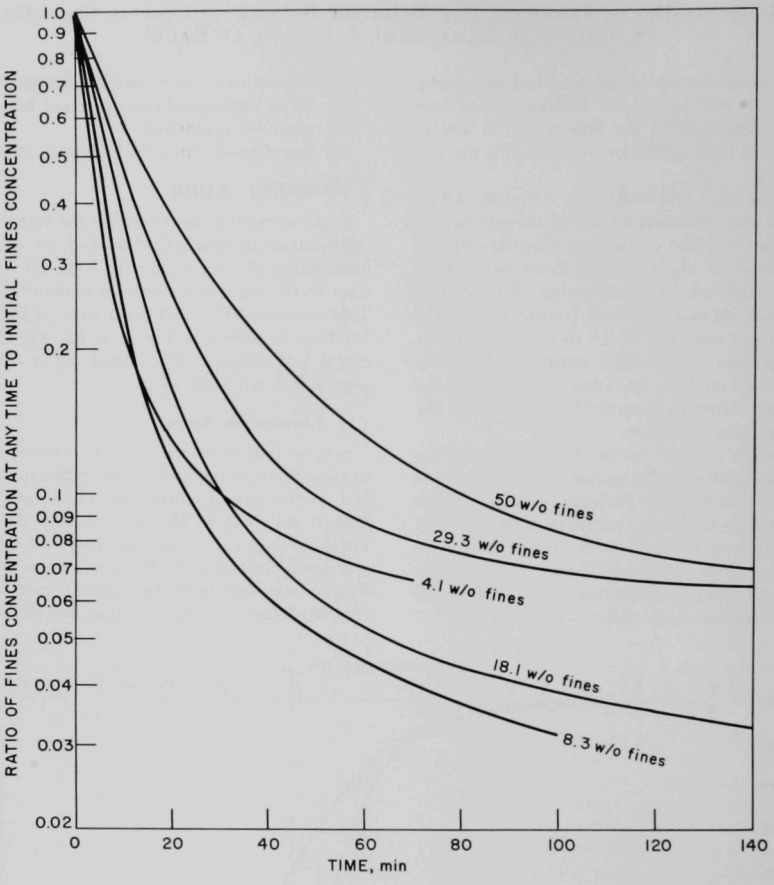

108-9105

FIG. II-33. Effect of Initial Fines Concentration in a Fluid Bed on Rate of Elutriation.

Air velocity: 1.5 ft/sec
3-in. ID brass column
48 to 100 mesh alumina
22μ nickel fines
Curve labels indicate different initial concentrations.

lected in a separate chamber adjacent to the fluidized-bed column. A 9-in. long, 1¾-in. wide bayonet sintered Inconel filter (10-μ porosity) was located in the chamber. Elutriation rates were calculated from the weights of particles collected in the filter chamber during periodic intervals of time.

The superficial velocity of the fluidizing gas in these studies was 1.5 ft/sec (25°C, 1 atm). The initial concentrations of nickel fines (see Figure II-34 for size distribution) in the alumina beds ranged from 4.1 to 50 w/o. The static bed height was ~13.5 in. for each test. On Figure II-33 is a plot showing the variation with respect to time of the fines concentration in the bed, based on the initial fines concentration. The elutriation rates decrease with an increase in the quantity of fines initially present in the bed. However, when there is only a small residue of fines present (as for the test with 4.1 w/o fines after 80% of the fines were

elutriated), the generalized behavior no longer holds because of losses of material that adhere to the column walls and off-gas line.

(2) Segregation Studies

A series of tests was made to determine the manner in which fines are distributed in a fluidized bed of alumina. These tests were made in a 2-in. ID, 6-ft long Lucite column with sampling ports at 4-in. intervals. The fluidizing gas was humidified nitrogen. The superficial gas velocity was 1.0 ft/sec. A porous metal plate served as the fluidized bed support and gas distributor. The fine particles used in the studies of particle segregation were −325 mesh particles of U_3O_8 containing a small quantity of UO_2F_2. A weighed portion of the fine particles was thoroughly blended with the alumina bed material prior to the test to give a mixture containing 40 w/o fines. The static height of the bed was about 22 in. The bed was fluidized, and bed samples were taken from ports at various elevations after 5, 10, 15, and 60 min of fluidization. The samples were analyzed by leaching the uranium fines with nitric acid and weighing the dried alumina residue. The results of the tests are given in Table II-34. These data reveal no distinct separation of fines and coarser alumina, although there was a variation in fines concentration with height. Fine particles were more concentrated at the top and at the bottom portions of the bed than at the center. These tests indicate that a distribution of fine particles satisfactory for conducting fluorination reactions would occur in the bed, and that if a portion of the bed became depleted of uranium by fluorination, fines would be transported into the depleted portion.

TABLE II-34. Distribution of Uranium Fines along Height of Column after Various Time Intervals of Fluidization

Alumina charge: 1.5 kg
U_3O_8 charge: 1.0 kg
Fluidizing gas: nitrogen
Fluidizing gas velocity: 1.0 ft/sec
Column ID: 2 in.

Time (min)	w/o U_3O_8 Fines at Various Heights					
	0 in.	4 in.	8 in.	12 in.	16 in.	20 in.
0[a]	40	40	40	40	40	40
5	12.4	47.0	27.4	65.4	27.8	41.9
10	19.2	24.6	25.6	71.9	25.5	27.3
15	No sample	42.5	26.8	28.7	26.4	59.6
60	43.4	43.5	16.5	18.2	19.7	[b]

[a] Bed concentrations of various levels were based on the initial charge.

[b] No sample could be taken because of reduction of bed height due to frequent sampling.

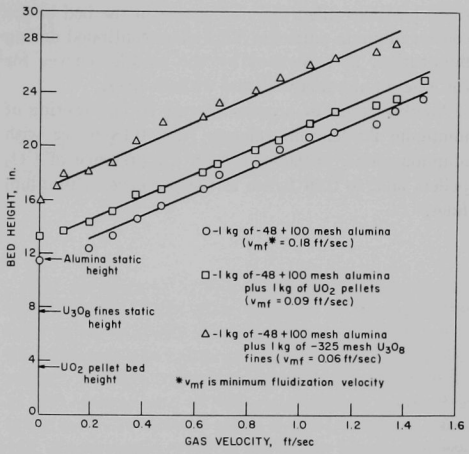

108-9097

Fig. II-34. The Effects on Fluidized Bed Expansion of Addition of U_3O_8 Fines and UO_2 Pellets to Alumina. (Fluid-bed column: 2-in. ID Lucite column.)

(3) Bed Expansion Studies

The effect of the addition of fine particles to a bed of coarser particles on the expansion of the fluidized bed was studied in the 2-in. dia. Lucite column. Accurate knowledge of this property of the fluidized bed is of practical interest since in process applications it is required that the fluidized bed be confined to the reaction zone and not be expanded into the disengaging chamber. Three tests were performed to measure bed expansion, using the fine and coarse particles employed in the studies on particle segregation. The tests involved measurements on (1) alumina alone, (2) alumina mixed with uranium fines, and (3) alumina in which UO_2 pellets were immersed.

The tests consisted of measuring bed heights of the three different types of beds at various gas flow rates. Figure II-34 shows the relationship of bed expansion as a function of gas velocity. The bed expansion was described fairly well by a straight line within the range of data obtained, although bed expansion is not generally considered a linear function of gas velocity. The data indicate that the bed expansion increases uniformly in a linear manner from the point of incipient fluidization in all three cases (minimum fluidization velocities are shown in the figure). The static height (16 in.) of the mixture of uranium fines and alumina was less than the additive static heights (total of 19.2 in.) of the separate fines and alumina because the

small particles filled the void spaces in the bed of the coarser alumina particles. This effect continued during fluidization, as evidenced by the parallel curves for the cases of alumina with and without fines.

Another result of process interest is the lowering of minimum fluidization velocity from 0.18 ft/sec with alumina alone, to 0.09 ft/sec in the presence of UO_2 pellets and, to 0.06 ft/sec in the presence of uranium fines.

b. FUTURE WORK

Work will continue in the areas outlined in the introduction. Future studies will concern the effect of alumina particle sizes other than the nominal 48 to 100 mesh used for the current work on the processing of fines. Tests will also be made to determine those conditions for operating a blowback filter that would maximize the residence time of the fine particles in the fluidized bed.

III

High Temperature Reactor Materials Development[1] (R. K. Edwards, H. M. Feder)

A program directed toward the development of reactor materials for use at high temperatures (1500 to 3000°C) is under way. The objective is to build up a reservoir of basic data which may be used for screening and evaluation. The study will be concerned with the chemical stability of potential high temperature fuels, i.e., oxides, phosphides, sulfides, arsenides, and nitrides of uranium and their solid solutions; and with the reactions of these fuels with hydrogen, its contaminants, and supporting structural materials such as tungsten, rhenium, molybdenum, tantalum, and certain alloys. These studies will be done quantitatively to yield thermodynamic and phase-diagram information. Each selected fuel-refractory metal-gas system is to be studied in an integrated way, using several methods of investigation that are mutually supporting.

[1] A summary of this section is given on page 13.

The emphasis of current experimentation is on the determination of the phase diagram of the condensed state of the uranium-urania[2] system and on the equilibria between the vapor and condensed phases of this system. A detailed discussion of the expected behavior in this system and of the experimental approaches being used for study is given in ANL-6925, pp. 165–173. Experimental work to determine phase relations in the tungsten-uranium-urania triangle is being initiated. The study initiated earlier of the uranium-uranium monosulfide phase diagram has been set aside temporarily.

[2] The term urania will be used in Section III to denote a phase of fluorite structure with composition unspecified; the symbol UO_2 will be used to denote stoichiometric uranium dioxide. The terms hyperstoichiometric and hypostoichiometric refer to the oxygen in UO_2; the symbols UO_{2-x} and UO_{2+x} denote hypostoichiometric and hyperstoichiometric urania, respectively.

A. PHASE DIAGRAM STUDIES

1. The Uranium-Urania System (A. E. Martin, F. C. Mrazek)

Additional work on the uranium-urania phase diagram has added better definition to the uranium liquidus and has confirmed the urania solidus previously reported (ANL-6925, p. 166, Fig. III-1), but no important changes in the phase diagram[3] are required. The essential features of the phase diagram are best represented as follows:

A wide liquid miscibility gap exists at temperatures above 2500 ± 30°C, which represents a monotectic temperature. At the monotectic temperature, the compositions in O/U atom ratio units of the three condensed phases in mutual equilibrium are liquid uranium, 0.06 ± 0.02; monotectic liquid, 1.30 ± 0.10; and hypostoichiometric urania solid, 1.64 ± 0.02.

Analysis of the hypostoichiometric urania phase boundary data shows that between 1600 and 2300°C the phase boundary compositions can be expressed by the equation

$$\log x = 1.854 - 6066/T, \qquad (1)$$

where x is the oxygen deficiency in the formula UO_{2-x}, and T is temperature in °K. Equation 1 reproduces the data to within 5.8% standard deviation in x. Above 2300°C, the data reported in ANL-6925, p. 166 deviate from Equation 1 giving higher O/U ratios; additional measurements have con-

[3] A preliminary publication of the uranium-urania phase diagram has been published in J. Phys. Chem., **69**, 1788 (1965).

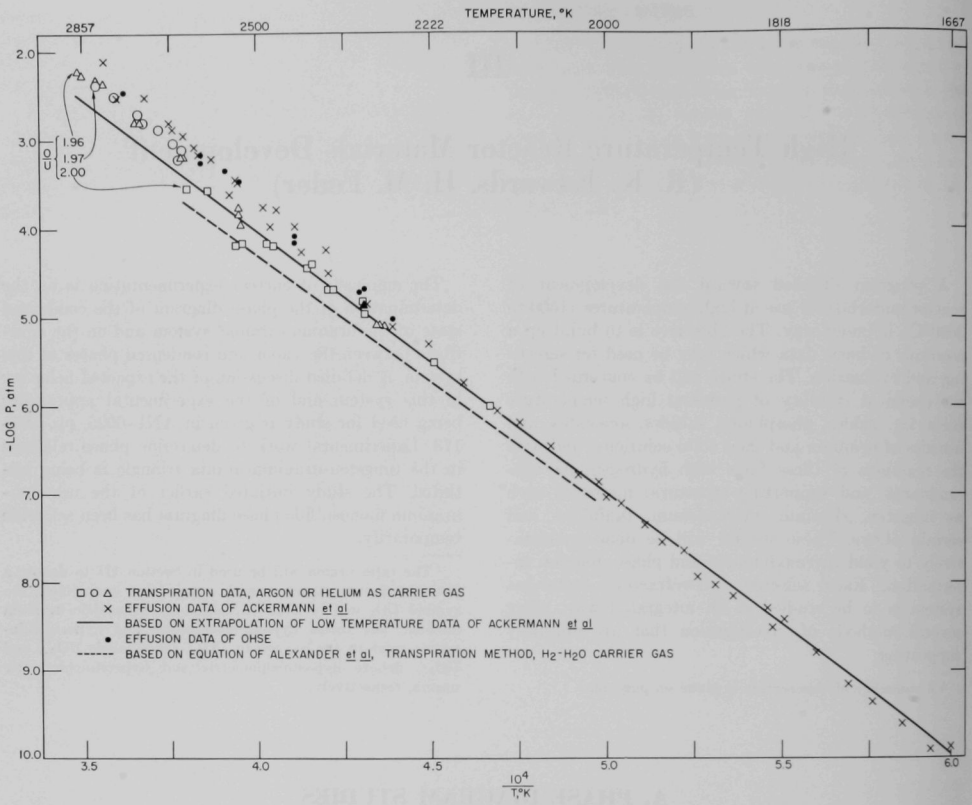

08-8877

FIG. III-1. Total Pressure of Uranium-Bearing Species over Urania as a Function of Temperature.

firmed this deviation. This strong upturn of the curvature of the hypostoichiometric phase boundary possibly implies that additional phase transformations occur in hypostoichiometric urania between 2300 and 2500°C. Further study on this point will be conducted.

2. Hypostoichiometric Phase Boundary of Urania: Isopiestic Measurements

(M. S. CHANDRASEKHARAIAH, R. J. ACKERMANN,[4] AND R. J. THORN[4])

The determination of the hypostoichiometric phase boundary of urania by a method independent of that used in the work reported in Part A-1 is nearing completion. The isopiestic equilibration technique being used has been discussed in ANL-6925, p. 170. The results between 1600 and 2100°C are in very good agreement with those obtained by use of Equation 1 in Part A-1; between 2100 and 2250°C, the isopiestic results seem to yield O/U atom ratios higher by as much as 0.1. Some further checks will be carried out for the latter temperature range.

[4] Members of the Chemistry Division.

3. The Uranium-Urania-Tungsten System (A. E. Martin, F. C. Mrazek)

The study of the uranium-urania-tungsten system is being initiated because of its relevance to the use of tungsten as a cladding for urania fuels. The work will be primarily limited to the three-phase field expected at mutual saturation of the three listed components and to the four-phase field expected when the ternary monotectic liquid is additionally present.

B. VAPOR PRESSURE STUDIES

1. Transpiration Studies of the Total Vapor Pressure of Uranium-Bearing Species over Urania (M. Tetenbaum, P. D. Hunt)

Measurements of the total pressure of uranium-bearing species over nearly stoichiometric uranium dioxide have been made between 1850 and 2600°C by the transpiration method using inert carrier gases. The prime purpose of these initial measurements was to check the reliability of the apparatus and procedures by comparing the results with those from effusion measurements reported in the literature.

The results are given in Figure III-1. The figure also includes the results of effusion measurements by Ackermann, Gilles, and Thorn[5] (AGT) and by Ohse,[6] and the results of transpiration measurements by Alexander, Ogden, and Cunningham[7] (AOC). The AOC work is shown as a dashed line which is based on their equation for a solid urania whose composition was held in the range O/U = 1.98 to 1.99 by buffering with a H_2-H_2O carrier gas. The solid line given in the figure is based on a least squares analysis of the AGT results between 1600 and 2000°K and extrapolation to higher temperatures. At the higher temperatures, the AGT measurements deviate from this line toward higher pressures. This deviation has been attributed by Ackermann and Thorn[8] to the possibilities of "exceeding the upper limit of the effusion method" (i.e., pressures too high for molecular flow conditions), or changes in the solid composition to "a substoichiometric dioxide phase."

In our study, no significantly different results were found between the use of helium or argon (both of ionization grade purity) as the carrier gases. Most of our results given in Figure III-1 were obtained with argon as the carrier gas. The square data points in the figure were obtained in a series of measurements with a urania charge whose O/U ratio was found to be 2.00 after completion of the final (highest temperature) measurement. These points conform very well with the AGT line. The empty circle data points were obtained in a series of measurements with a urania charge whose

TABLE III-1. Total Pressure of Uranium-Bearing Species over Urania

Carrier gas: ionization grade argon

Temperature (°C)	Argon Flow Rate (cc/min)	Vapor Density (mg/liter)	Pressure (atm)
2255	65	1.5	1.5×10^{-4}
2260	60	1.1	1.2×10^{-4}
2260	119	1.7	1.8×10^{-4}
2025	114	0.079	8.1×10^{-6}
2370	115	6.4	6.5×10^{-4}
2370	61	6.4	6.5×10^{-4}
2370	60	5.9	6.0×10^{-4}
2030	118	0.080	8.2×10^{-6}
2460	61	14.9	1.5×10^{-3}
2465	60	16.2	1.6×10^{-3}
2460	59	15.6	1.6×10^{-3}
2025	59	0.081	8.2×10^{-6}
2540	124	44.0	4.5×10^{-3}
2550	58	46.8	4.8×10^{-3}
2050	119	0.14	1.4×10^{-5}
2590	129	62.3	6.3×10^{-3}
2585	59	52.9	5.4×10^{-3}

[5] R. J. Ackermann, P. W. Gilles, and R. J. Thorn, J. Chem. Phys., **25**, 1089 (1956).

[6] R. W. Ohse, EUR-2166.e, (1964).

[7] C. A. Alexander, J. S. Ogden, and G. W. Cunningham, BMI-1707, pp. B8, B9 (1964).

[8] R. J. Ackermann and R. J. Thorn, *Thermodynamics of Nuclear Materials, Proceedings of the Symposium on Thermodynamics of Nuclear Materials*, International Atomic Energy Agency, Vienna, 1962, pp. 445–464.

initial and final O/U ratios were 2.00 and 1.97, respectively. The triangle data points were obtained in a series of measurements with a urania charge whose initial and final O/U ratios were 2.01 and 1.96, respectively. The data for the last series is given in Table III-1 in chronological sequence. It is to be noted that following measurements in each new temperature interval a repeat run at 2025 to 2050°C was made. The reproducibility observed for these repeat runs indicates that thermodynamic reversibility prevailed.

The deviation of our higher temperature data from the AGT line appears to result from hypostoichiometry in the uranium dioxide. It seems reasonable to suppose that the same deviation seen in the work of AGT and of Ohse partially arises from the same cause. The reason for the lower vapor pressures obtained by AOC is not obvious at present.

Transpiration measurements are currently being conducted with H_2-H_2O buffering carrier gas mixtures in order to fix the oxygen partial pressures at known values and thereby control the composition of the solid urania phases.

2. Effusion Studies of the Total Vapor Pressure of Uranium-Bearing Species over the Uranium-Urania Two-Phase System (M. S. Chandrasekharaiah, R. J. Ackerman,[4] and R. J. Thorn[4])

Additional measurements of the total vapor pressure of uranium-bearing species over the two-phase system, uranium (liquid, saturated with UO_{2-x}) in equilibrium with UO_{2-x} (solid, saturated with uranium), have been made by the Knudsen effusion method in the range 1300 to 2000°C. The effusion apparatus and procedures being used have been described in previous reports (ANL-6900, p. 203 and ANL-6925, p. 170). The curve previously presented (ANL-6925, p. 167, Fig. III-2) adequately represents both the earlier and the more recent data. The study for the temperature range noted is considered complete, and an ANL topical report on the work is being prepared. Beyond 2000°C, pressures are too high to permit the application of the effusion method. In a future study measurements up to 2500°C will be made by the transpiration method.

3. Mass Spectrometric-Effusion Studies of the Partial Pressures of Uranium-Bearing Species over the Uranium-Urania Two-Phase System (J. W. Reishus, J. E. Battles, G. E. Gundersen)

Measurements of the partial pressures of the principal gaseous species, U, UO, and UO_2, in equilibrium with the same uranium-urania two-phase system defined in Part B-2 of this section are being made by a mass spectrometric-effusion method.

Five sets of measurements made between 1650 and 2050°C have yielded straight line relationships between log pressure and $1/T$. However, the slopes of the lines, i.e., the apparent heats of vaporization, do not agree satisfactorily among the sets. It was suspected that temperature gradients within the effusion cells might be responsible for the disagreements. Investigation revealed that temperature gradients as large as 50°C could exist between the top and bottom of the effusion cells. Redesign of the electron-bombardment heating filament has reduced the gradient to about 5°C. Further work to reduce the uneven heating is being carried out.

IV

Calorimetry[1] (W. N. Hubbard, H. M. Feder)

For many compounds of interest in high temperature chemistry and nuclear technology, thermochemical data are either completely lacking or lack acceptable accuracy. This may be due to experimental difficulty in making the necessary measurements or to the difficulty of obtaining well-characterized samples. The present thermochemical program places equal emphasis on the procurement of well-characterized samples and the development of adequate experimental techniques.

The determination of standard enthalpies of formation of compounds is an essential foundation for further thermodynamic studies. Part of the program has been devoted to determinations of these enthalpies by oxygen bomb calorimetry. Many of the compounds of interest are difficult to burn in oxygen, however, and can not be studied by this method. To study the compounds not amenable to oxygen bomb calorimetry, the techniques of the bomb calorimetric method, which has been developed to a high degree of precision and accuracy, have been modified so that fluorine can be used as the oxidant.

[1] A summary of this section is given on pages 13 to 14.

The accumulation of enthalpy-of-formation data for elemental fluorides is both a necessary preliminary to the general use of fluorine bomb calorimetry for various compounds (especially those of uranium, thorium, etc.) and a valuable program on its own merit. To date, enthalpy-of-formation values have been determined for 22 elemental fluorides. The enthalpies of formation of the following compounds have been determined by fluorine bomb calorimetry: boron nitride, quartz and vitreous silica, α- and β-silicon carbide, and the diborides of zirconium, hafnium, niobium, and tantalum.

To determine thermodynamic properties at high temperatures, one combines values of enthalpies of formation at 25°C with values of the enthalpy increments up to the higher temperatures. A drop calorimeter for making enthalpy increment measurements up to 1500°C has been assembled and is being tested by measurements on a standard sample of synthetic sapphire. A calorimeter for making enthalpy increment measurements up to 2500°C has also been designed and is being constructed.

A. THE ENTHALPIES OF FORMATION OF THE HEXAFLUORIDES OF SULFUR, SELENIUM, AND TELLURIUM (P. A. G. O'Hare,[2] J. L. Settle)

A technique similar to that previously described (ANL-6925, p. 175) for the measurement of the enthalpy of formation of phosphorus pentafluoride, $\Delta Hf^{\circ}(PF_5)$, was used to study the enthalpy of reaction of fluorine with the Group VIB elements. High-purity, crystalline samples of rhombic sulfur, hexagonal selenium, and tellurium were treated with fluorine at about 5 atm. pressure in the two-chambered combustion apparatus described in detail elsewhere.[3] Sulfur and selenium, which were supported on nickel dishes, combined spontaneously with fluorine and were converted (>99.59%) to the respective gaseous hexafluorides. Tellurium, however, when treated in this way underwent superficial fluorination only; the temperature attained was insufficient to kindle the sample. This difficulty was circumvented by the substitution of a 50-g. disc of boron carbide (B_4C), which is an excellent thermal insulator, for the nickel dish and by the addition of a fuse of sulfur (3 to 7 mg.) under the sample. The instantaneous heat liberated when the fluorine first contacted the sample was dissipated slowly,

[2] Postdoctoral Fellow.

[3] R. L. Nuttall, S. Wise, and W. N. Hubbard, Rev. Sci. Instr., **32**, 1402 (1961).

TABLE IV-1. Results of Sulfur Combustion Experiments

Experiment No.	RS-1	RS-2	RS-4	RS-5	RS-6	RS-7
1. m', g.	0.53386	0.49542	0.46120	0.36066	0.61185	0.62415
2. Δt_c, °C	1.43742	1.33398	1.24029	0.97347	1.64851	1.68018
3. $\mathcal{E}$(calor.) $(-\Delta t_c)$, cal.	−4838.79	−4490.58	−4173.34	−3275.54	−5546.92	−5653.49
4. ΔE(contents), cal.	−3.83	−3.51	−4.70	−2.64	−4.54	−6.41
5. ΔE(gas), cal.	−0.35	−0.27	−0.36	−0.29	−0.46	−0.47
6. ΔE(impurities), cal.	−0.21	−0.20	−0.19	−0.14	−0.24	−0.25
7. ΔE(blank), cal.	4.54	4.54	5.45	5.45	5.45	5.45
8. $\Delta Ec^o/M$, cal. g.$^{-1}$	−9063.4	−9063.0	−9048.4	−9075.4	−9065.4	−9060.5

Mean $\Delta Ec^o/M$ = −9062.7 cal. g.$^{-1}$
Std. dev. of mean = ±3.5 cal. g.$^{-1}$

TABLE IV-2. Results of Selenium Combustion Experiments

Experiment No.	SE-1	SE-2	SE-3	SE-4	SE-5	SE-6
1. m', g.	1.47330	1.49955	1.45805	1.14187	1.65239	1.27158
2. Δt_c, °C	1.47278	1.49896	1.45889	1.14264	1.65285	1.27267
3. $\mathcal{E}$(calor.)$(-\Delta t_c)$, cal.	−4955.61	−5043.70	−4908.87	−3844.76	−5561.51	−4282.28
4. ΔE(contents), cal.	−6.82	−6.95	−6.75	−5.27	−7.66	−5.88
5. ΔE(gas), cal.	0.09	0.09	0.09	0.06	0.10	0.07
6. ΔE(impurities), cal.	−1.43	−1.46	−1.43	−1.12	−1.61	−1.23
7. ΔE(blank), cal.	7.52	7.52	7.52	7.52	7.52	7.52
8. $\Delta Ec^o/M$, cal. g.$^{-1}$	−3364.05	−3364.01	−3367.13	−3366.03	−3366.74	−3367.31

Mean $\Delta Ec^o/M$ = −3365.88 cal. g.$^{-1}$
Std. dev. of mean = $\pm 0.6_1$ cal. g.$^{-1}$

TABLE IV-3. Results of Tellurium Combustion Experiments

Experiment No.	TE-1	TE-2	TE- 3	TE-4	TE-5
1. m', g.	1.33774	1.34462	1.25750	1.18773	1.20758
2. Δt_c, °C	1.04473	1.05416	0.97609	0.92171	0.93943
3. $\mathcal{E}$(calor.)$(-\Delta t_c)$, cal.	−3513.58	−3545.30	−3282.74	−3099.85	−3159.44
4. ΔE(contents), cal.	−12.94	−13.17	−12.19	−11.52	−11.74
5. ΔE(gas), cal.	−0.10	−0.13	−0.12	−0.12	−0.12
6. ΔE(impurities), cal.	0.52	0.52	0.49	0.46	0.47
7. ΔE(blank), cal.	18.60	22.73	19.51	16.68	16.68
8. ΔE(S fuse), cal.	44.68	61.81	34.62	25.74	42.96
9. ΔE(B_4C), cal.	49.63	39.80	23.88	37.69	29.03
10. $\Delta Ec^o/M$, cal. g.$^{-1}$	−2551.46	−2553.69	−2557.89	−2551.86	−2552.34

Mean $\Delta Ec^o/M$ = −2553.45 cal. g.$^{-1}$
Std. dev. of mean = $\pm 0.9_6$ cal. g.$^{-1}$

thereby allowing the tellurium to attain its kindling temperature. Using these modifications, more than 99.59% conversion to TeF_6 was achieved with very little attack (1 to 2 mg.) of the B_4C support disc.

Calorimetric data are presented in Tables IV-1, -2, and -3. Entries in the tables are as follows:

1. m' is the mass of sample burned in the experiment.
2. Δt_c is the observed increase in calorimeter temperature corrected for heat exchanged between the calorimeter and its surroundings.
3. $\mathcal{E}$(calor.)$(-\Delta t_c)$ is the energy equivalent of the calorimetric system minus the contents of the bomb, multiplied by the negative of the temperature increase.
4. ΔE(contents) is the correction for the energy absorbed by the contents of the bomb during the hypothetical isothermal bomb process at 25°C $(= \mathcal{E}^i[\text{contents}]\ [t_i - 25] + \mathcal{E}^f[\text{contents}]\ [25 - t_f + \Delta t_{\text{corr.}}])$.
5. ΔE(gas) is the net correction for reducing the pressures of the bomb gases to standard state conditions $(= \Delta E^i(\text{gas})]_0^{P^i(\text{gas})} + \Delta E^f(\text{gas})]_{P^f(\text{gas})}^0)$.
6. ΔE(impurities) is the net correction for impurities in the sample.

TABLE IV-4. DERIVED DATA AT 25°C

	SF_6	SeF_6	TeF_6
Energy of Formation $\Delta Ef^o = \Delta Ec^o$, kcal. mole^{-1}	$-290.5_9 \pm 0.2_3$	$-265.7_7 \pm 0.1_2$	$-325.8_2 \pm 0.2_6$
Enthalpy of Formation $\Delta Hf^o = \Delta Ef^o - 2\ RT$, kcal. mole^{-1}	$-291.7_7 \pm 0.2_3$	$-266.9_5 \pm 0.1_2$	$-327.0_0 \pm 0.2_6$
Entropy of Formation ΔSf^o, cal. deg.$^{-1}$ mole^{-1}	-83.29	-80.47	-76.94
Gibbs Energy of Formation $\Delta Gf^o = \Delta Hf^o - T\Delta Sf^o$, kcal. mole^{-1}	$-266.9_4 \pm 0.2_3$	$-242.9_2 \pm 0.1_2$	$-304.0_6 \pm 0.2_6$

7. ΔE(blank) is the net correction for the heat of expansion of fluorine into the combustion chamber (Joule-Thomson effect) and the reaction of fluorine with small amounts of water adsorbed on the combustion chamber walls.
8. ΔE(S fuse) is the correction for the energy of combustion of the sulfur fuse (9.063 cal. mg.$^{-1}$).
9. $\Delta E(B_4C)$ is the correction for the energy of combustion of the B_4C support disc (23.41 cal. mg.$^{-1}$).
10. $\Delta Ec^o/M$, the energy of combustion per gram, is the energy evolved for the reaction with fluorine according to the equation,

$$M(c) + 3\ F_2(g) \rightarrow MF_6(g) \qquad (1)$$

where M = S, Se, or Te, and all the reactants and products are in their respective standard states at 298.15°K and 1 atm pressure. $\Delta Ec^o/M$ is obtained by summing the heat terms (cal.) in each column and dividing by the mass (g.) of sample burned.

The mean value of $\Delta Ec^o/M$ for each series was used to calculate the standard energy of formation, ΔEf^o, and the standard enthalpy of formation, ΔHf^o, for each of the hexafluorides. These results are summarized in Table IV-4 together with the standard entropies of formation, ΔSf^o, and the standard Gibbs energies of formation, ΔGf^o, for the reactions of Equation 1. The uncertainties quoted are equal to twice the overall standard deviations contributed by the variations of the observed mean reaction energy and by the uncertainties in ΔE(blank), weighings, impurity levels, and calibrations.

The enthalpies of formation of SF_6, SeF_6, and TeF_6 obtained by previous investigators[4, 5] are compared in Table IV-5 with our values. The measurement of Gross[4] was carried out in 1958; he has recently repeated this work and has informed us that his new value for $\Delta Hf^o(SF_6)$ is in good agreement with ours. It is not immediately obvious why the results of Yost and Claussen[5] are about 10% lower than ours. It should be pointed out, however, that their experiments were carried out in a fluorine flow calorimeter, and that their conclusions were based on the assumption that the reactants were converted exclusively to the hexafluoride. Recent experiments using a similar flow system were carried out in this laboratory and it was found that considerable quantities of S_2F_{10} were formed when fluorine at low pressure was passed over sulfur.

TABLE IV-5. ENTHALPIES OF FORMATION OF SF_6, SeF_6, AND TeF_6

	$-\Delta Hf^o_{298}$, kcal. mole^{-1}		
	SF_6	SeF_6	TeF_6
Yost and Claussen[5]	262 ± 5	246 ± 5	315 ± 6
Gross[3]	289.7 ± 1.4		
This Work	291.8 ± 0.2	266.9 ± 0.1	327.0 ± 0.3

Combustion of arsenic in fluorine by a technique similar to that used for sulfur, selenium, and tellurium is being employed to determine $\Delta Hf^o(AsF_5)$.

[4] P. Gross, Fulmer Research Institute, Stoke Poges, Bucks., England, private communication.

[5] D. M. Yost and W. H. Claussen, J. Am. Chem. Soc., **55**, 886 (1933).

B. THE ENTHALPIES OF FORMATION OF THE TRIFLUORIDES OF ALUMINUM, YTTRIUM, GADOLINIUM, AND HOLMIUM

(E. Rudzitis, E. Van Deventer)

Combustions in fluorine of metals that form nonvolatile fluorides present special problems. To overcome these problems a combustion technique has been developed in which a suspended metal sample is burned in a bomb lined with the fluoride of the metal. The technique is described in ANL-6900, p. 227 and in ANL-6925, p. 179.

Results for the enthalpy of formation of magnesium

TABLE IV-6. Results of Aluminum Combustion Experiments

Experiment No.	3	5	6	7	8	9
1. m', g.	0.30078	0.42743	0.52101	0.49376	0.37882	0.50717
(%)	(92.3)	(92.8)	(93.7)	(83.4)	(88.7)	(89.7)
2. Δt_c, °C	1.21176	1.68917	2.04937	1.95157	1.51632	2.01678
3. $\mathcal{E}$(calor.)$(-\Delta t_c)$, cal.	−4163.0	−5803.2	−7040.6	−6704.7	−5209.3	−6928.7
4. ΔE(contents), cal.	−128.0	−175.0	−214.0	−196.3	−150.5	−193.0
5. ΔE(ignition), cal.	1.8	1.6	1.5	1.7	1.6	1.4
6. ΔE(gas), cal.	−1.1	−1.7	−1.8	−1.7	−1.3	−1.9
7. ΔE(impurities), cal.	−2.4	−3.4	−4.1	−3.9	−3.0	−4.0
8. ΔE(Cd fuse), cal.	279.7	277.4	303.9	303.5	314.0	358.9
9. $\Delta Ec^o/M$, cal. g.$^{-1}$	−13,342	−13,346	−13,349	−13,370	−13,327	−13,343

Mean $\Delta Ec^o/M$ = −13,346 cal. g.$^{-1}$
Std. dev. of mean = ±6 cal. g.$^{-1}$ or 0.04%

TABLE IV-7. Results of Yttrium Combustion Experiments

Experiment No.	1	2	3	4	5	6	7
1. m', g.	1.3332_2	1.0415_1	0.8387_8	1.0800_3	0.9187_5	0.8188_0	1.0861_8
(%)	(99.8)	(99.5)	(97.6)	(99.8)	(99.9)	(99.7)	(99.8)
2. Δt_c, °C	1.75540	1.36663	1.09937	1.42287	1.21214	1.07710	1.43267
3. $\mathcal{E}$(calor.)$(-\Delta t_c)$, cal.	−6027.1	−4692.3	−3774.6	−4885.4	−4161.8	−3698.2	−4919.1
4. ΔE(contents), cal.	−102.5	−76.4	−62.0	−75.2	−51.3	−54.4	−70.2
5. ΔE(ignition), cal.	0.1	0.1	0.1	0.1	0.1	0.1	0.1
6. ΔE(gas), cal.	−0.7	−0.5	−0.4	−0.5	−0.4	−0.4	−0.5
7. ΔE(impurities), cal.	−30.4	−23.8	−19.1	−24.6	−21.0	−18.7	−24.8
8. $\Delta Ec^o/M$, cal. g.$^{-1}$	−4620.9	−4601.9	−4597.1	−4616.2	−4608.9	−4606.2	−4616.6

Mean $\Delta Ec^o/M$ = −4609.7 cal. g.$^{-1}$
Std. dev. of mean = ±3.2 cal. g.$^{-1}$ or 0.07%

TABLE IV-8. Results of Gadolinium Combustion Experiments

Experiment No.	2	3	4	5
1. m', g.	1.79468	2.23639	1.60620	2.06767
(%)	(99.0)	(98.8)	(98.8)	(98.4)
2. Δt_c, °C	1.31764	1.64275	1.18017	1.52030
3. $\mathcal{E}$(calor.)$(-\Delta t_c)$, cal.	−4529.2	−5646.8	−4056.7	−5225.8
4. ΔE(contents), cal.	−84.5	−100.3	−68.6	−85.0
5. ΔE(ignition), cal.	0.2	0.2	0.2	0.2
6. ΔE(gas), cal.	−0.3	−0.4	−0.3	−0.4
7. ΔE(impurities), cal.	−17.8	−22.1	−15.9	−20.4
8. $\Delta Ec^o/M$, cal. g.$^{-1}$	−2580.7	−2579.8	−2578.3	−2578.5

Mean $\Delta Ec^o/M$ = −2579.3 cal. g.$^{-1}$
Std. dev. of mean = ±0.6 cal. g.$^{-1}$ or 0.02%

TABLE IV-9. Results of Holmium Combustion Experiments

Experiment No.	3	4	5	6	7	8
1. m', g.	1.70134	1.63385	2.10819	2.28254	2.00921	1.64240
(%)	(99.4)	(98.3)	(96.0)	(89.8)	(98.8)	(97.6)
2. Δt_c, °C	1.19466	1.14698	1.48028	1.61076	1.41557	1.15110
3. $\mathcal{E}$(calor.)$(-\Delta t_c)$, cal.	−4102.8	−3939.0	−5083.7	−5531.8	−4861.4	−3953.2
4. ΔE(contents), cal.	−72.8	−67.4	−83.7	−86.4	−73.0	−56.6
5. ΔE(ignition), cal.	0.3	0.3	0.2	0.2	0.4	0.3
6. ΔE(gas), cal.	−0.3	−0.4	−0.4	−0.4	−0.4	−0.3
7. ΔE(ignition), cal.	−12.7	−12.1	−15.8	−17.0	−15.0	−12.3
8. $\Delta Ec^o/M$, cal. g.$^{-1}$	−2461.8	−2459.6	−2458.7	−2468.9	−2463.4	−2448.9

Mean $\Delta Ec^o/M$ = −2460.2 cal. g.$^{-1}$
Std. dev. of mean = ±2.6 cal. g.$^{-1}$ or 0.11%

difluoride have recently been published;[6] ΔHf^o_{298} = −268.7 ± 0.3 kcal. mole^{-1}.

Tables IV-6 to IV-9 list experimental data for fluorine combustions of aluminum, yttrium, gadolinium, and holmium. The results for aluminum are redeterminations which were made to improve on earlier work (ANL-6648, p. 179). Most of the entries in the tables have been explained earlier in this section. Additional entries are: (%) under m' is the percentage of combustion of the sample introduced into the bomb; ΔE(ignition) is the correction for the electrical energy used to ignite the fuse; and ΔE(Cd fuse) is the correction for the energy of combustion of the cadmium fuse. The ΔHf^0_{298} values derived for the trifluorides of aluminum, yttrium, gadolinium, and holmium are presented in Table IV-10. The results of the combustions of gadolinium and holmium are tentative. The uncertainty intervals equal twice the combined standard deviations arising from known sources.

Similar techniques are being used for combustions of nickel and lanthanum in fluorine.

[6] E. Rudzitis, H. M. Feder, and W. N. Hubbard, J. Phys. Chem., **68**, 2978 (1964).

TABLE IV-10. Enthalpies of Formation

Reaction	$-\Delta Hf^o_{298}$, kcal. mole^{-1}
Al(c) + 1.5 F_2(g) → AlF_3(c)	361.0 ± 0.4
Y(c) + 1.5 F_2(g) → YF_3(c)	410.7 ± 0.8
Gd(c) + 1.5 F_2(g) → GdF_3(c)	406.5 ± 0.3
Ho(c) + 1.5 F_2(g) → HoF_3(c)	406.5 ± 1.0

C. COMBUSTION OF SILICON CARBIDE IN FLUORINE (E. Greenberg)

Data for combustions in fluorine of beta silicon carbide (β-SiC) and for preliminary combustions of alpha silicon carbide (α-SiC) were presented in ANL-6925, p. 177. The combustion results obtained with two β-SiC specimens for the reaction,

$$SiC(c) + 4\ F_2(g) \rightarrow SiF_4(g) + CF_4(g), \quad (2)$$

were quite satisfactory and no further experiments with β-SiC are planned. Two α-SiC specimens yielded discordant results which were ascribed to their combustion behavior. The α-SiC specimens did not burn as completely as the β-SiC specimens and also yielded a greater proportion of higher fluorocarbons (C_2F_6 and C_3F_8) as side-products of combustion.

It was suspected that the difference in combustion behavior was due to particle size, the α-SiC specimens being much coarser than the β-SiC specimens. A new specimen of α-SiC with particle size distribution similar to that of the β-SiC specimens was obtained from the Carborundum Co.; it was indeed found that the combustion yields (99.1 to 99.8%) and the extent of higher fluorocarbon formation were similar to those obtained with the β-SiC specimens.

The preliminary results of the new α-SiC combustion experiments are given in Table IV-11. The entries in the table are the same as those used previously (ANL-6925, p. 178). The mean $\Delta Ec^o/M$ value was found to be −14,732.6 cal. g.$^{-1}$ with a standard deviation of the mean of ±7.0 cal. g.$^{-1}$ (or 0.05%). Combining the $\Delta Ec^o/M$ value with the values of $\Delta Hf^o(SiF_4)$[7] of

[7] S. S. Wise, J. L. Margrave, H. M. Feder, and W. N. Hubbard, J. Phys. Chem., **67**, 815 (1963).

TABLE IV-11. Results of Alpha Silicon Carbide Combustion Experiments

Experiment No.	20	21	22	23	24	26	27
1. m', g.	0.49747	0.49899	0.48449	0.49630	0.29908	0.30024	0.69508
2. Δt_c, °C	2.06378	2.07372	2.01034	2.06569	1.24187	1.24893	2.87460
3. $\mathcal{E}$(calor.)$(-\Delta t_c)$, cal.	−7304.75	−7339.93	−7115.60	−7311.51	−4395.60	−4420.59	−10,174.64
4. ΔE(contents), cal.	−8.72	−8.72	−8.72	−8.72	−5.14	−5.14	−12.29
5. ΔE(ignition), cal.	0.18	0.13	0.24	0.19	0.18	0.18	0.13
6. ΔE(Mo fuse), cal.	6.31	13.50	9.55	9.17	13.42	9.86	11.53
7. ΔE(gas), cal.	0.26	0.26	0.26	0.26	0.18	0.18	0.33
8. $\Delta E(C_2F_6)$, cal.	−10.27	−8.40	−10.52	−9.40	−8.24	−4.60	−29.11
9. $\Delta E(C_3F_8)$, cal.	−4.59	−5.24	−3.91	−5.13	−5.44	−2.32	−14.19
10. ΔE(impurities), cal.	−4.70	−4.72	−4.58	−4.69	−2.83	−2.84	−6.57
11. $\Delta Ec^o/M$, cal. g.$^{-1}$	−14,727.1	−14,736.0	−14,723.3	−14,769.0	−14,723.4	−14,739.4	−14,710.3

Mean $\Delta Ec^o/M$ = −14,732.6 cal. g.$^{-1}$
Std. dev. of mean = ±7.0 cal. g.$^{-1}$ or 0.04$_8$%

−386.0 kcal. mole^{-1} and $\Delta Hf^o(CF_4)$[8] of −221 kcal. mole^{-1} yields a value of ΔHf^o_{298} (α-SiC) of −15.1 kcal. mole^{-1}. The latter value is 0.4 kcal. mole^{-1} less negative than that obtained for β-SiC (ANL-6925, p. 179). This difference in the enthalpies of formation lies between the 0.2 kcal. mole^{-1} calculated by d'Entremont and Chipman[9] from the data of Grieveson and Alcock[10] and the 1.1 kcal. mole^{-1} found by Humphrey *et al.*[11]

[8] This is the value currently suggested by the National Bureau of Standards, Washington, D. C.

[9] J. C. d'Entremont and J. Chipman, J. Phys. Chem., **67**, 499 (1963).

[10] P. Grieveson and C. B. Alcock, in "Special Ceramics," Heywood and Co., Ltd., London, 1961, p. 183.

[11] G. L. Humphrey, S. S. Todd, J. P. Coughlin, and E. G. King, U. S. Bureau of Mines Report of Investigations 4888, 1952.

D. COMBUSTION OF BORON IN FLUORINE (G. K. Johnson)

The values of ΔHf^o_{298} determined in this laboratory for BF_3, BN, and zirconium diboride have been found on re-examination to show a consistent low bias when compared to literature values determined by methods other than fluorine bomb calorimetry. Three possible explanations for this discrepancy were postulated. (1) The boron combustion results previously obtained by Wise[12] in this laboratory were incorrect. (2) The previous boron combustion results were correct but insufficient account was taken of the impurities in the specimen. (3) The use of different techniques, i.e., single-chambered bomb for the boron combustion and two-chambered vessel for the BN and zirconium diboride combustions, introduced significant error. The following steps were therefore taken.

1. Two samples of the specimen used in Wise's work were burned in argon-diluted fluorine in the single-chambered bomb. The results obtained for the energy of combustion per gram of sample uncorrected for impurities ($\Delta Ec^o/M$(sample) = −24,857 and −24,825 cal. g.$^{-1}$) were in good agreement with that observed by Wise (−24,837 ± 9 cal. g.$^{-1}$).

2. Wise's sample was completely re-analyzed and the following additional impurities were found (in percent): N, 0.234; Ca, 0.27; Zr, 0.29; Cr, 0.013; and Al, Cu, Ni, Ti (each) 0.01. Wise's original result, $\Delta Hf^o(BF_3)$ = −269.88 ± 0.29 kcal. mole^{-1}, when corrected for these additional impurities becomes −271.7 ± 0.8. The more negative value for $\Delta Hf^o(BF_3)$ removes the low bias from the calculated ΔHf^o values for BN and zirconium diboride. However, the uncertainty associated with the large impurity content of Wise's sample made a redetermination with a purer sample imperative.

A specimen of zone-refined boron was obtained in the form of a 10-g. bar which was broken into 0.01- to 0.15-g. pieces for the calorimetric combustions. Analysis showed the following impurities (in ppm): O, 580; C, 450; N, 260; H, 7. No metallic impurities were detected by spectrography.

The two-chambered vessel[3] was used for the combustions. Eight calibration experiments (combustions of benzoic acid in oxygen) prior to the calorimetric

[12] S. S. Wise, J. L. Margrave, H. M. Feder, and W. N. Hubbard, J. Phys. Chem., **65**, 2157 (1961).

series yielded a mean value of $\mathcal{E}$(calor.), the energy equivalent of the calorimetric system, of 3399.63 ± 0.10 cal. deg^{-1}. Six blank experiments were made to determine ΔE(blank), the net energy correction for the expansion of fluorine from the storage chamber into the combustion chamber and for its reaction with the combustion chamber's walls and/or surface contaminants. The mean value of the correction was 3.97 ± 0.77 cal. For the calorimetric experiments with the two-chambered vessel, the storage chamber was charged with fluorine to a pressure of 7250 torr. The combustion chamber was pretreated for one hour with BF_3 at 2 atm. pressure prior to being evacuated overnight. (The BF_3 pretreatment was used because prior experience had shown that ΔE(blank) was thereby made smaller and more reproducible.) The boron samples were supported on small nickel dishes which showed evidence of slight but measurable fluorination after the combustions. Because the boron samples did not ignite spontaneously on exposure to fluorine, the combustions were initiated by electrical ignition of molybdenum wire and foil positioned over the samples.

The results of five acceptable combustions are presented in Table IV-12. The mean value of $\Delta Ec^o/M$ was −25,112 cal. g.$^{-1}$ and the derived value of $\Delta Hf^o(BF_3)$ was −271.79 ± 0.18 kcal. mole^{-1}. This value appears to be the appropriate one to use in connection with the combustions of BN and zirconium diboride, which were performed in a similar setup.

3. A comparison of the single-chambered and two-chambered techniques was made in the following way. A Teflon plug was inserted into the line connecting the two chambers, thus isolating the storage tank, and fluorine was introduced into the combustion chamber via a direct line after overnight evacuation. The fluorine, at 5000 torr, was diluted by the addition of 8000 torr of argon. (The dilution with argon was found to moderate the reaction so that fluorination of the nickel dish did not take place.) Other details of the experiments were the same as in the two-chambered vessel.

The results of nine acceptable calorimetric experiments are presented in Table IV-13. The apparent mean value of $\Delta Ec^o/M$ was −25,133 cal. g.$^{-1}$ and the derived value $\Delta Hf^o(BF_3)$ was −272.01 ± 0.17 kcal. mole^{-1}. This result was close enough to that obtained in the two-chambered vessel to establish that the cause of the original discrepancy (about 200 cal. g.$^{-1}$) was, in fact, due to impurities rather than to differences in

TABLE IV-12. Results of Boron Combustions in Two-Chambered Vessel

Experiment No.	1	2	3	5	6
1. m', B reacted, g.	0.24955	0.29523	0.24776	0.23484	0.31235
2. Δt_c, °C	1.89882	2.23869	1.88743	1.79126	2.35423
3. $\mathcal{E}$(calor.)$(-\Delta t_c)$, cal.	−6455.29	−7610.72	−6416.56	−6089.62	−8003.51
4. ΔE(contents), cal.	−9.02	−10.66	−8.96	−8.50	−11.22
5. ΔE(ignition), cal.	0.31	0.31	0.30	0.28	0.29
6. ΔE(Mo fuse), cal.	199.47	211.66	204.31	203.69	175.87
7. ΔE(gas), cal.	0.05	0.06	0.05	0.05	0.06
8. ΔE(blank), cal.	3.97	3.97	3.97	3.97	3.97
9. ΔE(Ni reacted), cal.	1.32	0.55	0.55	0.30	0.41
10. $\Delta Ec^o/M$(sample), cal. g.$^{-1}$	−25,081.91	−25,081.56	−25,090.17	−25,080.18	−25,081.26

Mean $\Delta Ec^o/M$(sample) = −25,083.0 cal. g.$^{-1}$
Std. dev. of mean = ±1.8 cal. g.$^{-1}$
Impurity correction = −29.0 cal. g.$^{-1}$
$\Delta Ec^o/M$ (B,c) = −25,112.0 cal. g.$^{-1}$

Table IV–13. Results of Boron Combustions in Single-Chambered Bomb

Experiment No.	1	2	3	4	5	6	7	8	9
1. m', B reacted, g.	0.25301	0.17739	0.26778	0.25392	0.34796	0.34021	0.18481	0.34288	0.24999
2. Δt_c, °C	1.91426	1.35699	2.02869	1.92501	2.61700	2.56679	1.42315	2.61755	1.93005
3. $\mathcal{E}$(calor.)$(-\Delta t_c)$, cal.	−6507.78	−4613.26	−6896.80	−6544.32	−8896.83	−8726.14	−4838.18	−8898.70	−6561.46
4. ΔE(contents), cal.	−8.13	−6.89	−10.27	−9.76	−13.33	−13.07	−7.19	−13.33	−9.78
5. ΔE(ignition), cal.	0.33	0.50	0.36	0.36	0.40	0.44	0.36	0.37	0.40
6. ΔE(Mo fuse), cal.	161.28	167.47	183.76	178.93	176.76	198.35	203.65	307.20	294.31
7. ΔE(gas), cal.	0.17	0.13	0.19	0.18	0.24	0.24	0.13	0.23	0.17
8. $\Delta Ec^o/M$(sample), cal. g.$^{-1}$	−25,114.15	−25,097.53	−25,105.53	−25,104.80	−25,096.97	−25,102.67	−25,113.52	−25,094.00	−25,106.44

Mean $\Delta Ec^o/M$(sample) = −25,104.0 cal. g.$^{-1}$
Std. dev. of mean = ±2.3 cal. g.$^{-1}$
Impurity correction = −29.0 cal. g.$^{-1}$
$\Delta Ec^o/M$ (B, c) = −25,133.0 cal. g.$^{-1}$

techniques. On the other hand, the 21 cal. g.$^{-1}$ difference between the single-chambered and two-chambered combustions was significantly larger than the estimated combined uncertainties. A closer examination of the results in Table IV-13 revealed that despite their apparent precision they exhibited a trend with sample mass. A least squares fit of the results to a linear regression of the form

$$\text{(Corrected) Energy evolved per run} = am' + b$$

yielded the following parameters: $a = -25{,}115.5 \pm 9.79$ cal. g.$^{-1}$ and $b = -4.48 \pm 2.70$ cal. The significance of these parameters is that the value of $\Delta Ec^o/M$ $(=a)$ derived from the regression is in good accord with the value obtained in the two-chambered combustions; and that a significant, constant, extraneous source of energy, of the order of 4 cal. per combustion $(=b)$, is the probable source of the 21 cal. g.$^{-1}$ discrepancy. Attempts to account for the extraneous energy have been unfruitful. A small number of additional combustions were made in the two-chambered vessel after variations in the method of surface pretreatment but the results were inconclusive. Exhaustion of the specimen precluded further investigations.

E. FLUORINE FLOW CALORIMETER (J. L. Settle)

The considerations leading to the construction of a trial apparatus for testing the combustion behavior of fluorine-sensitive substances, e.g., uranium compounds, in a fluorine flow calorimeter were discussed in ANL-6925, p. 182. Satisfactory combustions of uranium monosulfide, US, were obtained without encountering the problems associated with similar combustions in a bomb calorimeter. During the present report period, work has proceeded on the construction, assembly, and testing of a flow calorimeter in which the enthalpy of reaction of uranium compounds with fluorine will be determined.

F. 1500°C DROP CALORIMETER (J. E. Brugger, A. T. Hu,[13] A. Chaudhuri[14])

Much of the effort during this report period has involved the training of personnel in the use of the 1500°C drop calorimeter equipment. The Calorimetry Conference heat capacity standard, synthetic sapphire (aluminum oxide, prepared by the National Bureau of Standards), has been used in a series of enthalpy increment measurements between 850 and 1150°C. The preliminary data obtained for drops of filled and empty (tantalum) capsules indicate that the measured enthalpy differences, $H_T - H_{298}$, are slightly higher than those reported by Kelley.[15] Electrical calibrations of the copper-block calorimeter have been made to match the temperature rises produced by the capsule drops and, in many instances, the calibrations were made immediately following a drop. It is planned to follow this procedure routinely.

In the current series of measurements, the mass of the aluminum oxide sample is 3 g. and that of the heavy-walled tantalum capsule is 53 g. The ratio of heat stored in the sample to that stored in the capsule is about 0.4. On the face of it, the capsule design may appear faulty since drop calorimetrists generally maximize this ratio by the use of thin-walled capsules. In any drop, it is desirable that the heat loss from the capsule be the same for empty and filled capsules. For drops at low temperatures, conventional thin-walled capsules are satisfactory. At high temperatures, the temperature distribution—and hence the radiation-controlled heat loss—may differ significantly between empty and filled capsules. (To minimize the difference in heat loss between empty and filled capsules, one should select a capsule material with a low thermal diffusivity, resort to installing radiation shields on the capsule, or fabricate a double-walled capsule of thin stock and fill the annular space with a powder of low thermal diffusivity.) Thickening the walls of a capsule reduces the effect of temperature distribution but decreases the sample-to-capsule heat storage ratio. Based on assumptions concerning both the absolute and the relative precision and accuracy of the drop calorimeter data, an attempt is being made to optimize the sample-to-capsule heat storage ratio and the material and geometrical aspects of capsule design. It is conceivable that capsules of different design will be used for low and for high temperature drops.

[13] Postdoctoral Fellow.

[14] Graduate Student, Rice University.

[15] K. K. Kelley, Bureau of Mines Bulletin 584, U. S. Government Printing Office, Washington, D. C., 1960.

The apparatus is not in its final form and a shutdown for replacement of the furnace heater elements and/or thermocouples may be necessary. Assembly of the adiabatic calorimeter to replace the copper-block test receiver in current use is under way. After the program of testing and calibration with aluminum oxide has been completed, the determination of enthalpy increments for uranium monophosphide will be started.

G. 2500°C CALORIMETER SYSTEM (D. R. Fredrickson, R. Kleb[16])

Work has been resumed on the calorimetric system for determining enthalpy increments up to 2500°C. The 2500°C system differs from the 1500°C system basically in (1) the mode of heating (electron bom-

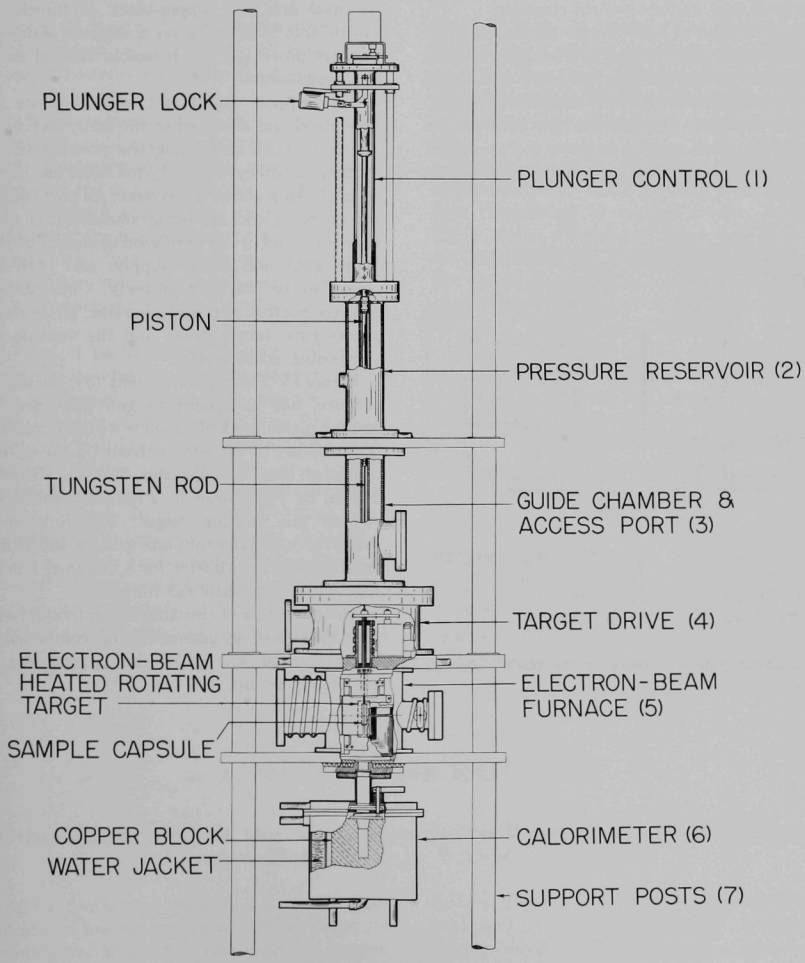

Fig. IV-1. 2500°C Calorimeter System.

108-8377 T Rev.

[16] Central Shops.

bardment versus resistance windings) and (2) the method of transfer of the capsule from the furance to the calorimeter proper (pneumatic versus free fall).

Figure IV-1 shows the overall 2500°C calorimeter system. The main components starting from the top are (1) plunger control, (2) pressure reservoir, (3) guide chamber and access port, (4) target drive, (5) electron beam furnace, (6) copper-block calorimeter, and (7) support posts. Completing the system (but not shown in the figure) are two electron beam guns and their associated power supply, a 4-in. dia. and a 2-in. dia. vacuum system, and various control circuits.

The plunger control (1) accelerates the sample capsule to several times gravitational acceleration, thereby minimizing the time that the capsule spends in the cold region between the furnace and the calorimeter proper. The pressure reservoir (2) provides gas pressure for forcing down the piston and the tungsten rod connected thereto. The guide chamber and access port (3) provide alignment of and access to the tungsten rod. The sample capsule is attached to the bottom of the rod. The target drive (4) rotates a cylindrical tantalum furnace core within the furnace (5). The core is heated by electron bombardment from two diametrically opposed electron guns. Longitudinal temperature uniformity is obtained by programmed sweeping of the electron beams along the length of the furnace core. Circumferential temperature uniformity is obtained by rotating the furnace core around its axis. The sample capsule is suspended within the furnace core and, when uniformly heated, is dropped into the copper-block calorimeter (6). The entire unit is built up on a support stand containing support posts (7) which enable vertical movement of the components.

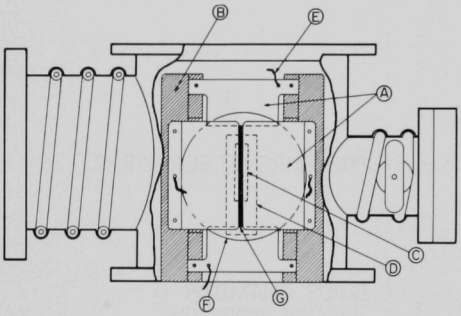

Ⓐ BEAM LOCATOR PLATES
Ⓑ LAVITE SUPPORT POST
Ⓒ SAMPLE CAPSULE
Ⓓ ROTATING TARGET
Ⓔ WIRE TO MILLIAMMETER
Ⓕ GUN OUTLINE
Ⓖ BEAM SLOT

108-8789

FIG. IV-2. Electron Beam Furnace for the 2500°C Calorimeter System.

The support stand and support posts have been assembled and attached to the floor, thereby providing the framework and fixing the position for the entire system. A trolley with a $\frac{1}{4}$-ton hoist has been installed on an I-beam above the system. All parts of the furnace are on hand and are being assembled. A test vacuum furnace chamber has been used to check out the electron beam guns and power supply, and both have been found to be working properly. Construction of the plunger control, pressure reservoir, guide chamber and access port, target drive, and the vacuum systems is proceeding satisfactorily.

Figure IV-2 shows component (5), the electron beam furnace. For each electron gun there are four beam locator plates, each of which is wired to a milliammeter. The absence of emission current on the milliammeters indicates that the electron beam is directed into a $2\frac{3}{4}$-in. by $\frac{3}{32}$-in. slot in a radiation shield which surrounds the rotating target. The furnace has been mounted on an adaptor plate to allow substitution of the copper-block calorimeter for a designed but not as yet constructed adiabatic calorimeter.

The procedure of checking out individual components and then testing assemblies of components on the support stand will be continued until the system is completely set up.

V

Reactor Safety[1] (L. Baker, Jr., A. D. Tevebaugh)

The program on reactor safety is concentrated in two areas of research: (1) the study of metal-water reactions, and (2) studies relating to the safety of fast reactors.

In water-cooled reactors, coolant failure or a severe nuclear excursion could cause the reactor core metals to melt and disperse rapidly in the water. Chemical reactions between the metals and water could result in the release of energy approaching or exceeding the energy released by the fission process during a nuclear excursion. Studies of these reactions are being carried out so that realistic estimates can be made of the rates and extents of reactions during hypothetical reactor accidents.

The reactions of the metals of interest with water are being studied in several ways. Experimental methods include isothermal reaction rate determinations, nonisothermal studies of the reactions with fine metal particles, in-pile meltdown experiments with specimens of typical reactor fuel materials, and heating experiments designed to simulate the conditions experienced by fuel elements during a loss-of-coolant accident. An additional research area consists of calculational studies in which experimental results obtained by several methods are correlated and methods of accident analysis are developed.

Studies relating to the safety of fast reactors include a survey study of chemical and physical interactions of fuel and cladding materials at high temperature with molten sodium. Emphasis is given to detecting and evaluating exothermic alloying reactions and interactions which result in extensive break-up or frothing.

Another study involves the transient boiling of molten sodium or water resulting from sudden contact with fragmented or molten reactor core materials. These studies are designed to provide data needed for the analyses of the transient pressures generated by the violent disruption of reactor cores in nuclear excursion accidents. Initial experiments are being performed in water.

A third study, still in the apparatus development stage, is the determination of the extent of fuel migration and segregation in mixed uranium-plutonium fuels. A fourth study which has recently been initiated is the measurement of the high temperature physical properties of fast reactor materials.

In addition, the sodium-air reaction, which is important in judging the safety of fast reactor installations, is under investigation. Although no experimental work is presently planned, some theoretical calculations have been performed to serve as a guide to the prediction of maximum pressures and temperatures that can be obtained when molten sodium, in the form of a spray, burns in an air-filled enclosure.

[1] A summary of this section is given on pages 14 to 16.

A. METAL-WATER REACTIONS

1. Isothermal Studies of the Aluminum-Steam Reaction by the High Pressure Furnace Method (R. E. Wilson, C. Barnes)

Studies of the isothermal reaction between molten metals and steam are being carried out in order to provide kinetic rate data. These rate data are needed for predicting, by means of mathematical models, the chemical behavior of core materials during reactor incidents. The reaction of molten aluminum with steam is of particular interest because of the large number of reactors which use aluminum-base alloys as the fuel matrix or cladding.

The reactions of pure aluminum and aluminum-5

w/o uranium alloys with steam were studied by means of the pressure-pulse method over the temperature range 800 to 1200°C (see ANL-6413, p. 178). These experiments showed that, for both pure aluminum and the uranium alloy, the reaction followed a cubic rate law. The pressure-pulse method was not satisfactory at temperatures greater than 1200°C because of the volatility of aluminum, which produced a reactive film of aluminum deposited on the cooler surfaces of its reaction vessel during the initial heating period.

In order to circumvent the difficulties associated with the pressure-pulse method, the levitation method was developed. By means of this method, the reactions with steam of pure aluminum, aluminum alloy 6061 (1.0 w/o magnesium, 0.6 w/o silicon, 0.25 w/o copper, 0.25 w/o chromium), and aluminum-based SL-1 fuel material (17 w/o uranium, 2 w/o nickel, 0.5 w/o iron) were studied at temperatures from 1200 to 1600°C (see ANL-6900, p. 233). The results of these experiments showed that the data for pure aluminum could best be described by a cubilinear rate law (an initial cubic rate law which later transforms into a linear rate law). The data for the SL-1 fuel material followed, for extended periods of time, the initial cubic part of the rate law representative of pure aluminum; no transformation to linear kinetics was observed. The 6061 alloy exhibited behavior similar to that of pure aluminum at temperatures of 1200 and 1300°C; but, in general, showed anomalous behavior from 1400 to 1600°C, the experimental points being higher than those for pure aluminum. Studies of the reaction of water with aluminum-bearing fuel materials (SPERT 1-D and SL-1 plate fuel) in the Transient Reactor Test Facility (TREAT) indicated that there was a marked effect of water vapor pressure on the extent of the aluminum-water reaction (see ANL-6725, p. 212).

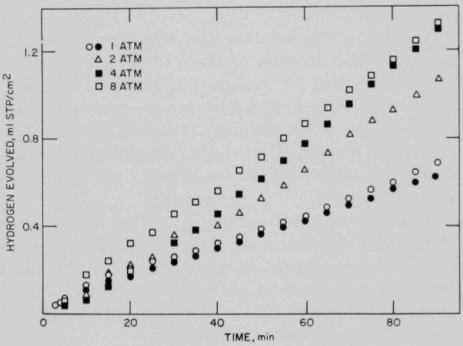

108-8739 T 2

FIG. V-1. Hydrogen Evolved by the Aluminum-Steam Reaction at 1200°C.

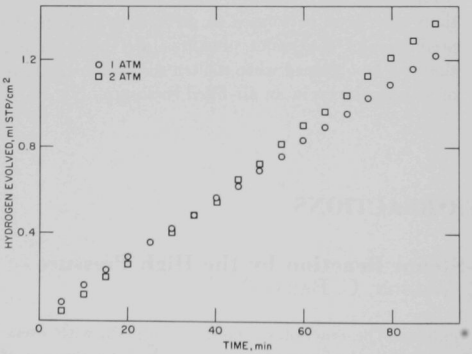

108-9082 T

FIG. V-2. Hydrogen Evolved by the Aluminum-Steam Reaction at 1300°C.

TABLE V-1. HYDROGEN GENERATED BY THE ALUMINUM-STEAM REACTION IN THE HIGH PRESSURE FURNACE EXPERIMENTS

Temperature (°C)	Pressure (atm)	Hydrogen from Aluminum-Steam Reaction (% of total gas evolved)
1200	1	7.3
1200	1	19.1
1200	2	24.9
1200	4	28.3
1200	8	36.2
1300	1	9.3
1300	2	8.9

Because of the effect of pressure found in the TREAT studies, it was considered necessary to perform isothermal studies of the aluminum-steam reaction by a method in which the steam pressure could be varied over a wide range. A high pressure furnace, which was described in a previous report (ANL-6900, p. 242), was developed for this purpose. The furnace, which is contained in a steel pressure vessel, consists of two zones: an internal, steam-filled zone that is surrounded by an alumina tube, and an external zone that is argon-filled. The argon-filled zone contains molybdenum heater windings and insulation. The pressures in the two zones are automatically matched to avoid stresses on the alumina tube. Water is introduced into the lower part of the steam zone by a positive displacement pump and is converted to steam. Some unreacted steam and the hydrogen produced by metal-steam reaction are continuously removed from the upper part of the steam zone (high temperature

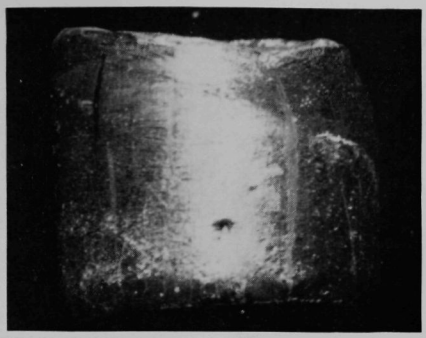

700°C—11 atm

1200°C—1 atm

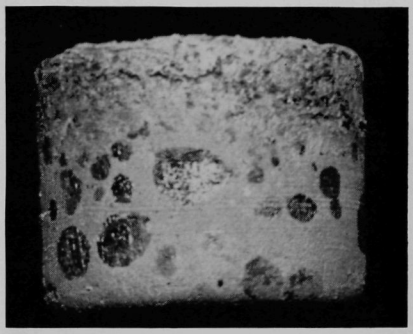

1200°C—2 atm

1200°C—4 atm

1200°C—8 atm

108-9075 T

FIG. V-3. Appearance of Aluminum Samples Exposed to Flowing Steam for 90 Minutes in the High-Pressure Furnace. (Nominal sample size: ¾-in. dia. by ½ in. long.)

section) through an outlet valve. The extent of reaction is determined by the amount of hydrogen collected. The pressure is controlled by a pressure regulator operating the outlet valve. The apparatus is designed for a maximum pressure of 1000 psig and sample temperatures as high as 1700°C. During the start-up period of an experiment, the sample is introduced into the lower (cooler) part of the steam-filled zone, the air is flushed out, and the furnace (already at the operating temperature) is brought up to the operating pressure. After conditions have stabilized, the sample is raised into the upper (hottest) part of the steam zone by an external crank mechanism. After exposure to the high temperature for the desired length of time, the sample is lowered into the original position in the cooler area.

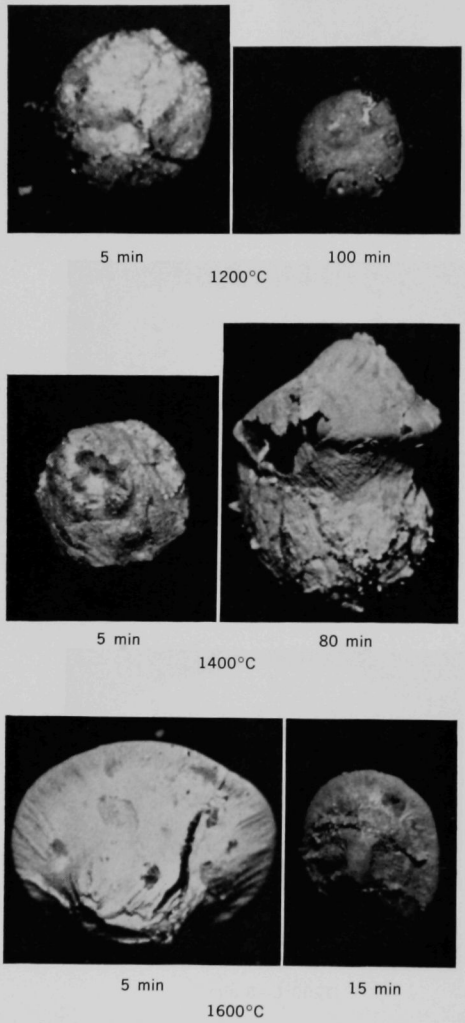

108-9072 T

FIG. V-4. Appearance of Aluminum Pellets Exposed to Flowing Steam at One Atmosphere Pressure by the Levitation Method. (Nominal pellet diameter: ¼ in.)

The aluminum used in the experiments was Alcoa 99.99+% aluminum which was originally in the form of ¾ in. rod cut into nominal ½ in. lengths.

Preliminary experiments with aluminum samples in the high pressure furnace showed the presence of extraneous gases in the effluent steam. These gases consisted mostly of hydrogen and oxygen (which were produced by the decomposition of steam) and a small quantity of air and helium. An effort was made to decrease the gas content by degassing the inlet water to reduce the amount of air and by contacting the mixture with platinum at about 500°C to promote the recombination of the hydrogen and oxygen to steam. These measures lowered the evolution of extraneous gas from 1.7 ml/min to 0.6 ml/min. Methods for further reduction of the gas content are under study.

Preliminary data for the aluminum-steam reaction at 1200°C are shown in Figure V-1, and for the reaction at 1300°C in Figure V-2. These data are corrected for the presence of extraneous gases. The corrections were made by applying the following formula to each experimental datum:

$$R = H - 2\ (X - 0.268N) \qquad (1)$$

where

R = hydrogen generated by aluminum-steam reaction (%),

H = total hydrogen in the gas sample (%),

X = total oxygen in the gas sample (%), and

N = total nitrogen[2] in the gas sample (%).

The percentage of each of the above gases was determined by a mass spectrometric analysis of the gas evolved during the experiment. It is apparent from Table V-1 that the corrections were, unfortunately, rather large in these preliminary experiments.

Figure V-3 shows representative samples of aluminum exposed to flowing steam for 90 minutes in the high pressure furnace under various conditions of

[2] This corrects the oxygen value by eliminating the contribution of any air impurity.

steam pressure and temperature. These samples have been broken free from the alumina crucibles that were used to contain the molten samples. A portion of the crucible can be seen adhering to the side of one of the samples. Figure V-4 shows, for comparison purposes, representative samples obtained from earlier levitation experiments (ANL-6900, p. 233). In the levitation experiments, nominal ¼-in. aluminum pellets were exposed to flowing steam at 1 atm for various times and temperatures. Some of the samples from both experimental methods show signs of gas bubbles, probably hydrogen, which were evolved during solidification. The amount of this gas is negligible (about 1%) in comparison with the total amount of gas evolved during the reaction. In all cases, the samples show evidence of greater reaction with increasing severity of exposure, in agreement with the increasing extent of reaction reported.

Representative specimens from the various experiments were sampled for X-ray diffraction analysis by mechanically scraping some of the oxide coating free from the metal. The results of these analyses are shown in Table V-2. In all cases the major phase present in the oxide film was alpha alumina. Some aluminum metal was scraped off along with alumina during sampling when the oxide film was very thin and adhered tenaciously to the sample. This accounts for the report of aluminum metal in the X-ray diffraction results in Table V-2.

Because of the preliminary nature of the data, it is not possible to make a quantitative analysis of the effect of pressure on the extent of reaction. However, from the data gathered thus far, it is clear that increasing pressure causes an increase in the reaction rate. The temperature and pressure will be further increased in future experiments.

TABLE V-2. Results of X-Ray Diffraction Analysis of Representative Samples of the Reaction Products from the Aluminum-Steam Reaction

Temperature (°C)	Pressure (atm)	Time (min)	Major Phase	Minor Phase
High Pressure Furnace Experiments				
700	11	90	Al	α-Al_2O_3[a]
1200	1	90	Al and α-Al_2O_3	—
1200	2	90	α-Al_2O_3	Al
1200	4	90	α-Al_2O_3	Al
1200	8	90	Al and α-Al_2O_3	—
Levitation Experiments				
1200	1	5	Al	α-Al_2O_3[a]
1200	1	100	Al and α-Al_2O_3	possible ZrO_2
1400	1	5	Al	α-Al_2O_3[a,b]
1400	1	80	Al and α-Al_2O_3	—
1600	1	5	Al and α-Al_2O_3	—
1600	1	15	Al and α-Al_2O_3	—

[a] Unidentified phase(s) also present.
[b] Possible β-Al_2O_3 also present.

2. Studies of Metal-Water Reactions by the Laser Heating Method
(L. Leibowitz, L. W. Mishler)

Laser beam heating has proven useful in the study of rates of chemical reaction and heat transfer between individual metal particles and water (see, for example, ANL-6925, p. 198). Using a simple lens, the beam from a ruby laser is focused on a small particle of metal submerged in water. Since the pulse duration is about one millisecond, this technique simulates the rapid contacting of water with heated metal that would occur during a violent excursion in a water-cooled nuclear reactor. Analysis of such reactor incidents requires information on the rate of exchange of both chemical and thermal energy between the metal and water. The laser heating technique was developed to allow the study of both single metal particles of known size and materials which cannot readily be examined by other methods.

The procedure followed for the aluminum-water reaction studies has already been described in detail (ANL-6800, p. 327) and consists simply of sealing a small square of aluminum foil (usually 1 by 1 by 0.025 mm) with degassed water in a cell bearing optically flat quartz windows. Following heating of the metal by the focused laser pulse, the cell contents are analyzed for hydrogen and the particle residue is examined microscopically. High speed (5000 frames/sec) motion pictures are usually taken through the top window of the cell without external lighting. From these films, it is possible to measure the time of luminosity of the sample. The concluding phases of this study of the aluminum-water reaction are summarized below.

a. EFFECT OF INERT GAS OVERPRESSURE

It was reported in ANL-6925, p. 199 that the variation of extent of reaction with laser energy changed markedly when the water temperature was increased

from 25°C to 100°C. At 25°C the extent of reaction was constant, about 8%, in the range of laser output energy between 10 and 49 joules. At 100°C, however, reaction was negligible for energies below 40 joules, while above 45 joules essentially complete metal-water reaction occurred. Thus, at water vapor pressures between 0.03 atm (25°C) and 1 atm (100°C), a change apparently takes place in the reaction mechanism.

In order to obtain further insight into the reaction mechanism, a series of experiments was carried out in cells at 25°C with 1 atm overpressure of argon gas. Analyses of the cell contents in these cases were performed by gas chromatography. The results are summarized in Table V-3. The values of extent of reaction for these runs are significantly lower than those in 25°C water with no argon overpressures and indicate that the results in 100°C water must be attributable to increased water vapor pressure and not to increased total pressure.

TABLE V-3. Results of Aluminum-Water Reaction Experiments by the Laser Heating Method

Water at 25°C with one atmosphere argon overpressure

Run Number	Laser Output (joules)	Metal-Water Reaction (%)
123	24	<0.5
126	26	1.6
124	45	3.5
125	45	2.7

b. EFFECT OF INCREASED STEAM OVERPRESSURE

In order to increase the pressure range studied by the laser method, a reaction cell suitable for use with pressures up to ten atmospheres was constructed.

The reaction cell is shown in Figure V-5. The cell is constructed of stainless steel with ½-in. thick quartz optical flats as windows.

Modifications of the laser beam-directing prism and its mount were required. Water to be used in an experiment is initially degassed in a separate metal vessel and transferred under vacuum to the reaction cell containing the aluminum foil sample. The entire cell is wrapped with heating tape and allowed to reach thermal equilibrium at the desired temperature before beginning an experiment. Studies were performed in the reaction cell with water at 100°C (1 atm steam overpressure) or 181°C (10 atm steam overpressure). Temperatures were measured by a thermocouple in a well inside the body of the cell or by a thermocouple attached to the outside of the reaction cell. Following each experiment, the cell contents were analyzed as before. The results of these studies with increased steam overpressure are summarized in Figure V-6. Although the value of the threshold laser beam energy for significant reaction changed from that found in the quartz cell (probably due to a slightly changed optical system), the threshold energy was not significantly affected by changes in pressure. Thus it is apparent that once the water pressure reaches a certain level (be-

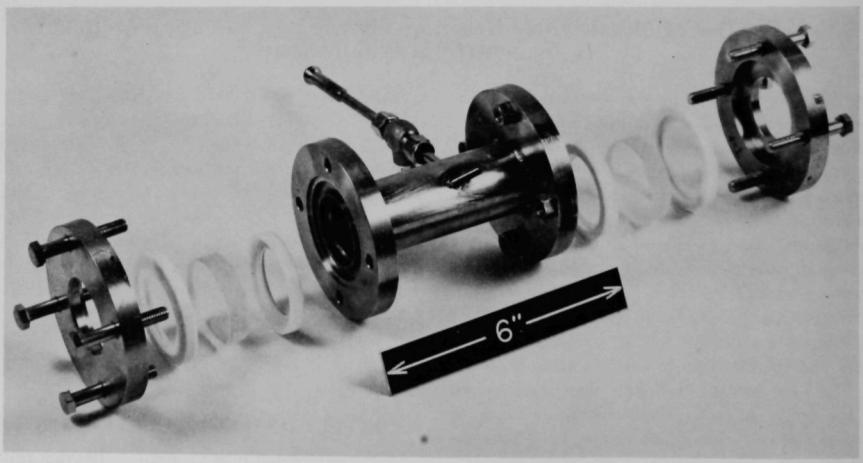

108-8697 T

Fig. V-5. High Pressure Reaction Cell for Studies of Metal-Water Reactions by the Laser Heating Method.

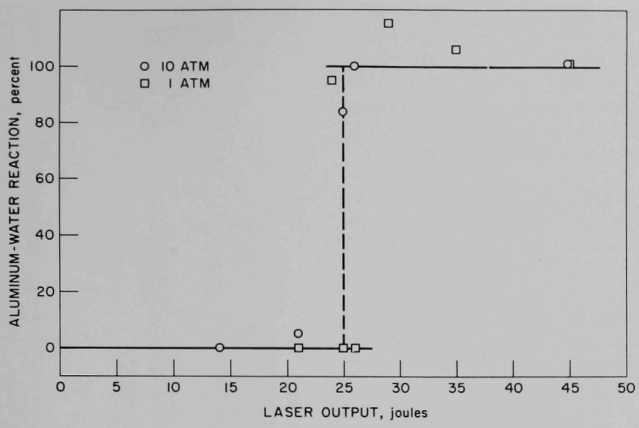

108-9083 T

FIG. V-6. Effect of Laser Beam Energy on the Extent of Aluminum-Water Reaction. (High pressure cell. Nominal particle diameter: 360μ.)

tween 0.03 and 1 atm), the course of the reaction is independent of water pressure up to at least 10 atm and is controlled by processes involving the aluminum. Below 1 atm, the water vapor pressure becomes important.

c. X-RAY STUDIES OF OXIDE

Three samples of reacted aluminum particles were selected for examination by X-ray diffraction.[3] These samples had been reacted under different conditions and were entirely transformed to oxide or to oxide-covered metal spheres. To prepare these samples for examination, a glass rod was drawn down to a fine tip, and the spheres ($\sim$360μ in diameter) were fastened in place on the end of the tip by means of a small quantity of Duco cement. The results of the examinations are summarized in Table V-4. The principal oxide observed was α-Al_2O_3.

TABLE V-4. RESULTS OF X-RAY DIFFRACTION EXAMINATION OF ALUMINUM PARTICLES HEATED IN WATER BY THE LASER METHOD

Run Number	Laser Energy (joules)	Aluminum-Water Reaction (%)	Cell Used	Water Pressure (atm)	Phases Determined, by X-ray Diffraction
141	45	38	Steel	1	Al, α-Al_2O_3, possibly another unidentified phase.
148	25	84	Steel	10	α-Al_2O_3, possibly very minor κ-Al_2O_3.
87	46	97	Quartz	1	α-Al_2O_3.

d. CONCLUSIONS

The results of the laser experiments have shown that the reaction of small aluminum particles rapidly heated in water is considerably different from that of larger aluminum specimens in steam. While a complete understanding of the aluminum-water reaction has not been achieved through use of the laser heating technique, it is believed that the information gained has significantly contributed to this understanding. A literature report summarizing in detail the various aspects of the investigation is now being prepared.

[3] These examinations were carried out by R. Schablaske.

3. Short-Period Transient Irradiation[4] (R. C. LIIMATAINEN, R. O. IVINS, F. J. TESTA)

The recent power excursion of the Kiwi-TNT reactor at the Nuclear Rocket Development Station at Jackass Flats, Nevada offered a unique opportunity to obtain data on metal-water reactions of typical reactor fuel-element materials during a short-period (0.6

[4] The cooperation of personnel of the Los Alamos Scientific Laboratory, who conducted the reactor transient at the Nevada Test Site, is gratefully acknowledged.

msec) transient. Previous experiments in the in-pile, metal-water reaction program have been carried out during transients in TREAT, with reactor periods ranging from about 50 to 500 msec (see ANL-6250). The Kiwi-TNT transient allowed fission heating of the fuel material under conditions more closely approximating those achieved during a short-period nuclear-reactor excursion.

Prior to the test, twenty-four stainless steel autoclaves (see Figures V-7 and V-8) containing various fuel samples in water were each placed within an outer stainless steel capsule (2-in. schedule 40 pipe) and positioned at distances of from 8 in. to 12 ft from the Kiwi-TNT reactor vessel (Figure V-9). Each autoclave contained a flux-monitor wire and a fuel pin immersed in water. Six samples of each of the following

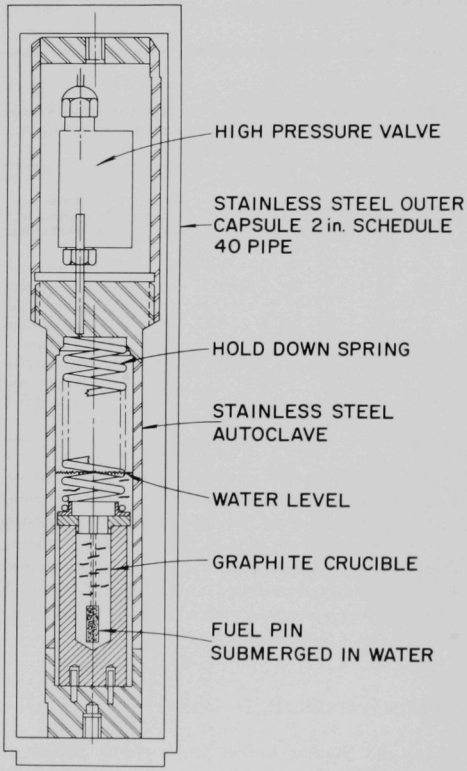

108-8664 T Rev.

FIG. V-7. Double Capsule Assembly for Kiwi-TNT, Metal-Water Irradiation Test.

108-8657 T 2

FIG. V-8. Inner Autoclave and Outer Capsule No. 24 for Kiwi-TNT Test.

enriched fuel materials were used: (1) uranium alloy (5 w/o Zr, 1.5 w/o Nb) pin, unclad; (2) UO_2 core, Zircaloy-2-clad pin; (3) UO_2 core, 304 stainless steel-clad pin; and (4) aluminum alloy (17 w/o U, 2 w/o Ni) plate, unclad.

Twenty-three of the autoclaves were recovered at distances from 30 to 500 ft from the reactor following the transient of January 12, 1965 and returned to Argonne. All were intact except one, which was almost completely crushed, most likely by impact with a por-

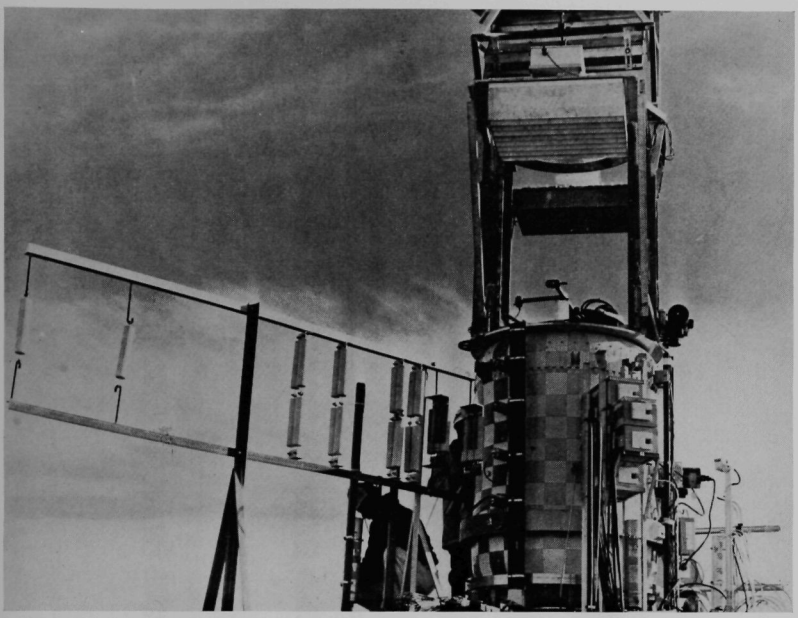

108-8629 T

FIG. V-9. Placement of Autoclaves Adjacent to Kiwi-TNT Reactor for Short Period Power Excursion.

tion of the reactor itself. However, the containment capsules all underwent various degrees of deformation (see Figure V-10) except the one that was farthest (12 ft) from the reactor; in addition, in each case the side of the outer capsule facing the reactor was darkened.

A test conducted on a double-capsule assembly indicated that a static load of 15 tons (30,000 lb) was required to cause the observed deformations of the wall of the outer capsule. The double-capsule assembly weighed 7.5 lb. For those that flew 500 ft from the reactor, an initial velocity of 125 ft/sec (86 miles/hr) was computed, assuming that they left at a trajectory of 45° with respect to the horizontal.

Post-irradiation observations and analyses of the fuel samples have included measurement of the hydrogen evolved from the metal-water reaction, particle size distribution of the fuels which were fragmented, and determination of energy input (from burnup analyses). Some of the hydrogen sampling valves of the autoclaves were damaged in the transient and the hydrogen evolved in the metal-water reaction was lost; for these, the amount of unreacted metal will be determined by chemical methods.

The results are summarized in Table V-5. The condition of the fuel specimens after the transient was dependent both on the distance of the specimen from the reactor and on the composition of the fuel. All of the uranium alloy pins and two of the aluminum alloy plates melted and apparently underwent substantial metal-water reaction. Only one of each type of metal-clad, UO_2 core specimens (the one nearest the reactor) was fragmented. Figures V-11, V-12, V-13, and V-14 compare the appearances of the residues and the particle size distribution plots for one specimen (the one which was nearest to the reactor) of each of the four types of fuel samples.

The relative energy input (proportional to fissions/mg ^{235}U in the unperturbed sample) as a function of distance between the sample and the reactor is plotted in Figure V-15. The relative energy input data were obtained by counting the jacketed natural uranium neutron flux-monitor wires and integrating over the 1.60 Mev barium-lanthanum-140 photopeak. The counting was done on a multichannel gamma analyzer.

An estimate of the absolute energy inputs can be obtained by noting that the uranium alloy fuel pin in Capsule 6, which was 6 ft from the face of the reactor, was at the point of incipient melting. To accomplish

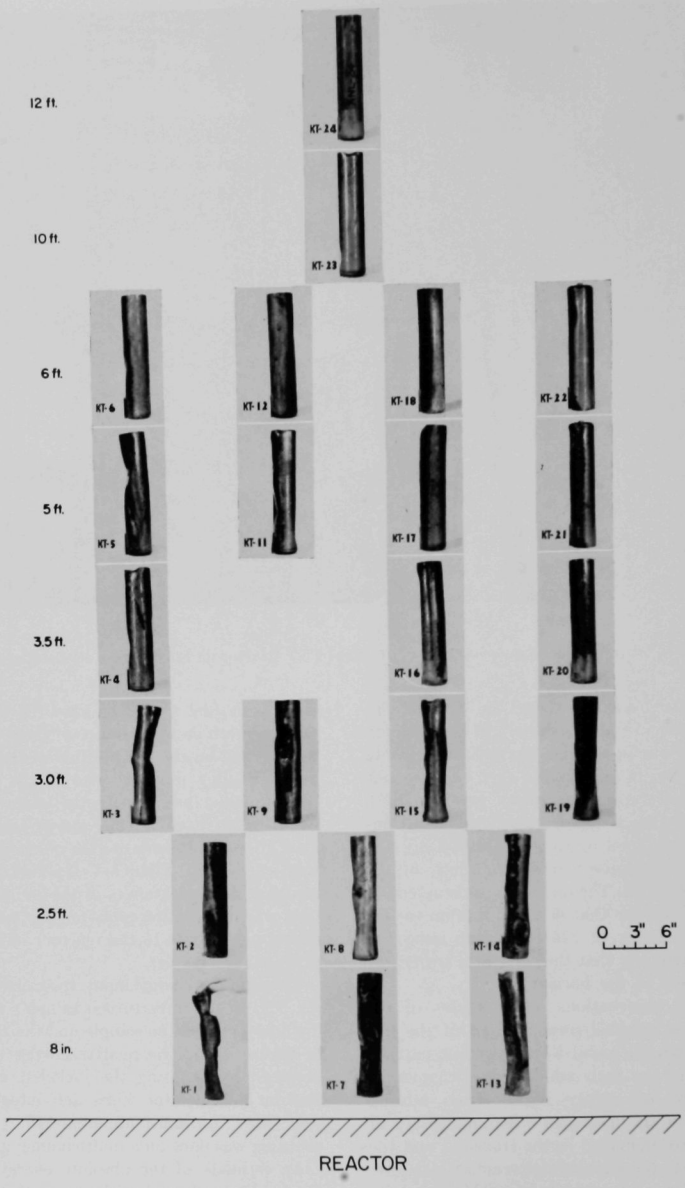

108-8415 T Rev.

Fig. V-10. Metal-Water Experimental Capsules Recovered from Kiwi-TNT Reactor Transient.

TABLE V-5. OBSERVATIONS AND DATA FROM KIWI-TNT SHORT-PERIOD TEST

Autoclave			Fuel Sample				
No.	Dist.[a] (ft)	Condition of Outer Capsule after Transient	Est. Fission Energy Input (cal/g)	Est. Peak Adiabatic Core Temp (°C)	Condition of Fuel after Transient	Metal-Water Reaction (%)	d_{av}^{c} (mil)
			Uranium alloy[b]				
1	⅔	Completely crushed	420	3800	Fragments and fine particles		6
2	2	Dented severely	200	3800	Completely melted into fine particles		3
3	3	Distorted	125	2800	Particles		6
4	3.5	Dented	100	2200	Melted into globules and fines		21
5	5	Dented	63	1133	Globule and particles		19
6	6	Dented mildly	50	1133	Partially melted	3.4	98
			304 Stainless steel-clad UO_2[b]				
7	⅔	Dented severely	400	3300	Completely melted, globules and particles		32
8	2	Dented severely	190	2400	Intact, slight swelling		—
9	3	Dented	120	1600	Intact		—
10	3.5	Not recovered	96	1300	—	—	—
11	5	Dented	60	900	Intact	0	—
12	6	Dented mildly	48	700	Intact	0	—
			Zircaloy-2-clad UO_2[b]				
13	⅔	Distorted	400	3300	Cladding ruptured, core converted into particles		6
14	2	Dented severely	190	2400	Intact (swelled)		—
15	3	Dented severely	120	1600	Intact (slight oxidation)		—
16	3.5	Dented severely	96	1300	Intact (slight darkening)		—
17	5	Dented mildly	60	900	Intact	0.03	—
18	6	Dented mildly	48	700	Intact	0.03	—
			Aluminum alloy[b]				
19	3	Dented severely	180	660	Completely fragmented, particles and fines		150
20	3.5	Dented	144	660	⅓ melted, some particles		196
21	5	Dented	90	400	Intact (darkened)		—
22	6	Dented mildly	72	300	Intact	0.01	—
23	10	Dented mildly	31	170	Intact	0.01	—
24	12	No change	22	100	Intact	0.01	—

[a] Distance between autoclave and reactor vessel.
[b] Uranium alloy: 93.5 w/o U, 5.0 w/o Zr, 1.5 w/o Nb, 20% enriched, 0.2-in. dia by 0.5-in. long.
304 Stainless steel clad UO_2: single UO_2 pellet, 11.2% enriched, 20 mil cladding, 0.375-in. dia by 0.5-in. long.
Zircaloy-2 clad UO_2: single UO_2 pellet, 11.2% enriched, 20 mil cladding, 0.375-in. dia by 0.5-in. long.
Aluminum alloy: 81 w/o Al, 17 w/o U, 2 w/o Ni, 93% enriched, 0.5-in. long plate sample.
[c] Mean volume-to-surface particle size of fragmented fuel sample.

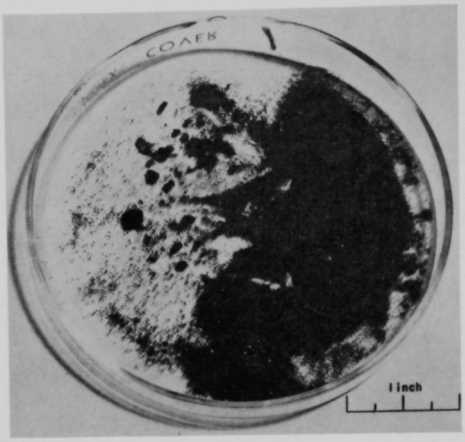

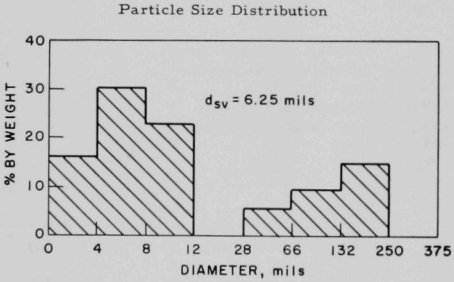

108-8660 T 2

Fig. V-11. Uranium Alloy Fuel Pin, Autoclave 1, after Kiwi-TNT Transient. (Capsule located 8 in. from reactor.)

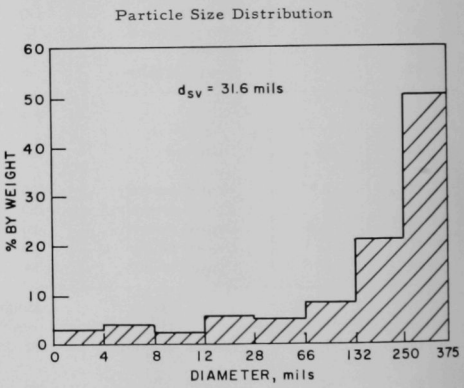

108-8663 T 2

Fig. V-12. SS 304-Clad, UO_2-Core Pin, Autoclave 7, after Kiwi-TNT Transient. (Capsule located 8 in. from reactor.)

this, with no heat loss, would require an energy input of 50 cal/g of uranium. Thus, taking this value as a point of reference, the arbitrary energy scale of the ordinate in Figure V-15 is such that the value of 6 units is equivalent to a fission energy input of 50 cal/g of uranium; this corresponds to a peak uranium fuel temperature of 1133°C. From this relationship, or calibration, it can be shown that the uranium alloy sample nearest the reactor (⅔ ft) attained a temperature of 3800°C, the vaporization temperature of uranium at one atmosphere pressure.

A comparison of Kiwi-TNT results with the previously published TREAT correlation of the average particle size with energy input is shown in Figure V-16. For a given energy, the shorter reactor period (0.6 msec vs ~100 msec) gives a smaller fuel particle size, and thus more fragmentation and surface area relative to the "slower" transient. It seems probable, therefore,

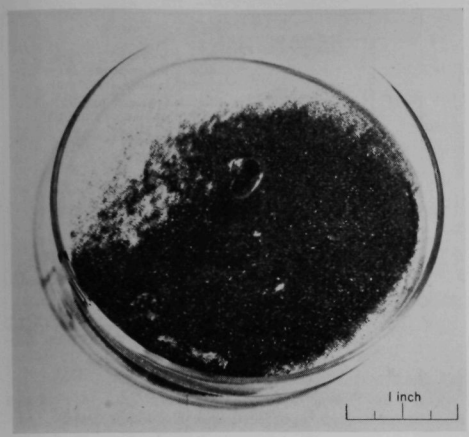

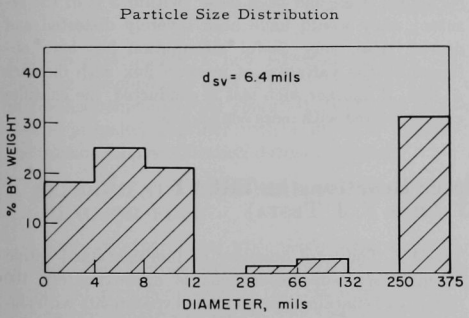

108-8659 T 2

FIG. V-13. Zircaloy-2-Clad, UO_2-Core Pin, Autoclave 13, after Kiwi-TNT Transient. (Capsule located 8 in. from reactor.)

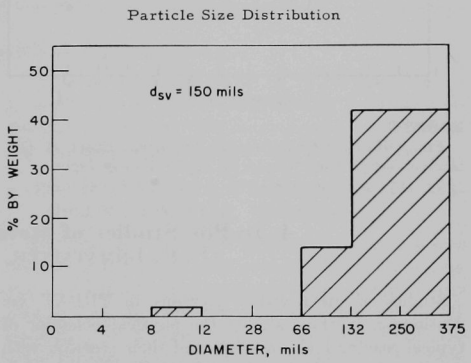

108-8661 T 2

FIG. V-14. Aluminum-Uranium Alloy (SL-1) Plate, Autoclave 19, after Kiwi-TNT Transient. (Capsule located 3 ft from reactor.)

that there will be somewhat more metal-water reaction at a comparable energy for the Kiwi-TNT experiment. This is also indicated by the observation that, in the 0.6 msec period test, an energy input of 50 cal/g of uranium gave 3.4% uranium-water reaction, whereas TREAT (~100 msec period) data suggest that only about 0.5% reaction would occur at this energy level. To get 3.4% metal-water reaction in TREAT requires an energy input of 120 cal/g U.

Some additional background information concerning the transient itself is of interest, since the test is pertinent to work in nuclear reactor safety. The total yield of the test was 3×10^{20} fissions, corresponding to an integrated power of 10,000 MW-sec. The anticipated yield was 10^{21} fissions; thus, the total energy of the excursion was somewhat less than that predicted. Since the capsules were placed in positions based on a yield of 10^{21} fissions, a few more of the fuel pins remained

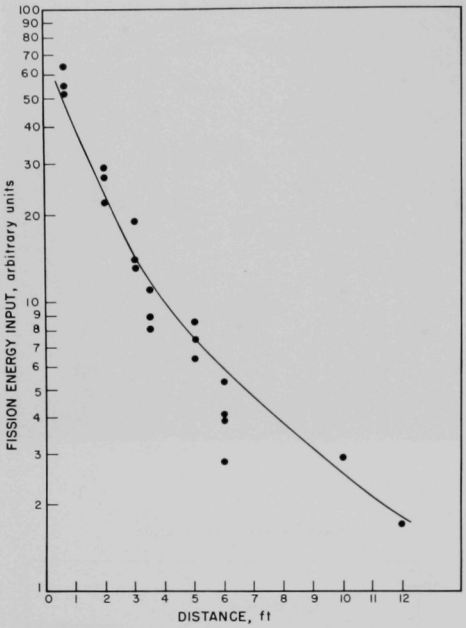

108-8460 T

FIG. V-15. Kiwi-TNT Reactor Transient: Effect of Distance of Sample from Reactor on Fission Energy Input.

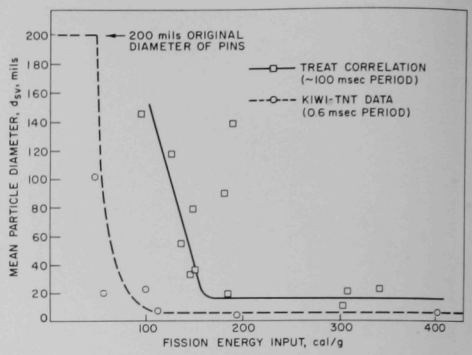

108-8666 T 2

FIG. V-16. Degree of Fragmentation of Uranium Fuel as a Function of Energy Input in Reactor Excursion Tests.

intact (i.e., the heating was not sufficient to melt them) than would have otherwise been the case. However, on the whole, the placement of the capsules was about optimum; if all had been close (within 3 ft of the reactor), they would have been severely distorted and dented. Also, very useful information has been obtained on the variation of neutron flux with distance so that, if another such test is conducted, the capsules can be located with more confidence.

4. In-Pile Studies of Metal-Water Reactions in TREAT

(R. C. LIIMATAINEN, R. O. IVINS F. J. TESTA)

Studies of metal-water reactions in TREAT are continuing. In these studies the physical behavior of typical reactor fuel materials and their reaction with water under conditions directly simulating a nuclear excursion accident in a water-cooled reactor are determined. The objectives of the program are:

(a) to determine the extent of reaction between the fuel materials and water,
(b) to determine the fuel temperature and pressure history during the excursion, and
(c) to determine the physical damage that occurs as a result of the transient.

Experimental work is progressing along three lines. Progress in each area is briefly summarized in the following paragraphs.

a. SCALE-UP EXPERIMENTS

In the scale-up experiments, subassemblies of 9 fuel pins, each 5⅝ in. long, are subjected to transients in TREAT. The total quantity of fuel contained within a single scale-up experiment is approximately 100 times that contained in previous experiments with single fuel pins.

Two scale-up experiments were performed with 9-pin fuel subassemblies of unclad uranium alloy fuel. The equipment and results were described in the previous report, ANL-6925, p. 209. Experiments with 9-pin subassemblies of Zircaloy-2-clad and 304 stainless steel-clad UO_2 pellet fuel are in progress. The initial series of four transient experiments include two experiments each with the Zircaloy-clad fuel and with the stainless steel-clad fuel. Fission energy input in two of the experiments (one each of the two cladding materials) will result in temperatures close to the cladding failure threshold. The energy in the other two transients will be greater and should cause extensive destruction of the fuel.

Because of the greater quantities of fuel involved in

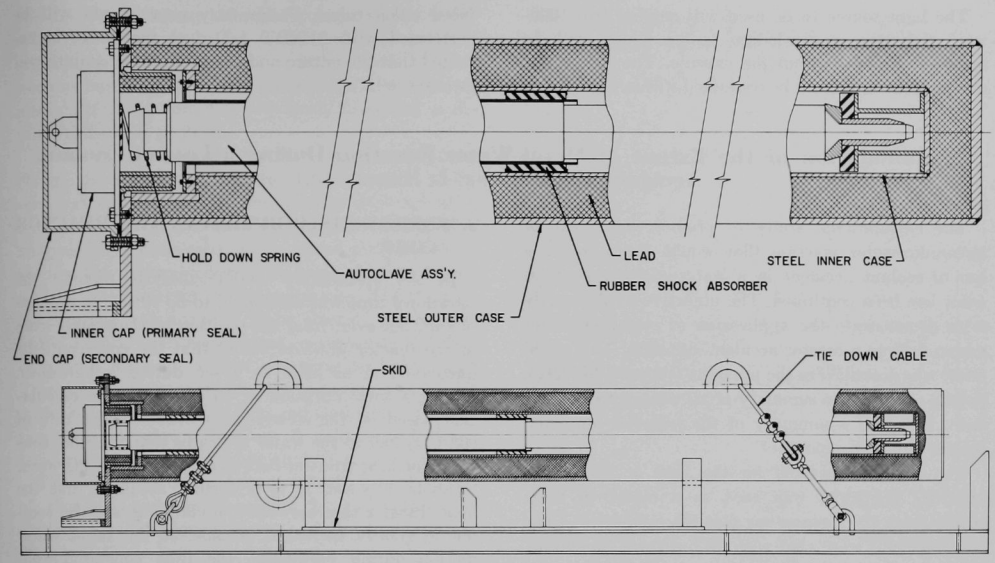

108-8949 T2

FIG. V-17. Shielding-Shipping Cask for TREAT Scale-Up Experiments.

scale-up experiments, a new shielded shipping cask has been designed and built. Figure V-17 is a drawing of the lead-shielded steel container. A double gasket seal is provided, together with a liner, to minimize the transmission of vibration during transport.

b. EXPERIMENTS WITH HIGH FLUX ISOTOPE REACTOR FUEL

A series of experiments with single plate specimens of High Flux Isotope Reactor (HFIR) fuel is being performed in cooperation with the Oak Ridge National Laboratory, builders of HFIR. The fuel plates are 0.5 by 1.0 by 0.050 in. in size. The center fuel core section is 0.030 in. thick and is a cermet containing 41.45 w/o U_3O_8 (93.17% enriched) in aluminum. The plates are clad on both sides with 0.010-in. 6061 aluminum alloy. The first series of experiments, which is in progress, consists of six experiments in 25°C water with a 20 psia overpressure of helium and two experiments in 285°C water with 1000 psia steam overpressure. Fission energy input will vary from an amount insufficient to melt the aluminum to an amount which will bring the temperature of the aluminum above 2000°C. Results will be compared with previous data obtained with SPERT 1-D fuel and SL-1 fuel (aluminum-uranium alloys) as reported in ANL-6725, p. 212. A succeeding series of approximately four experiments will be performed in water at 120°C with a steam overpressure of 600 psia. The latter conditions will simulate the proposed operating conditions of HFIR.

c. PHOTOGRAPHIC EXPERIMENTS WITH ALUMINUM-BASE FUEL MATERIALS

Attempts are underway to take high-speed motion pictures of fuel plate meltdowns in TREAT. The original development of photographic capsules for in-pile photography in TREAT was achieved by G. H. Golden, C. Dickerman, and L. E. Robinson of the Reactor Physics Division and is reported in ANL-6457. High-speed photography of fuel meltdowns in TREAT have also been performed by several other investigators at Argonne (ANL-6572, ANL-6873). Two new problems, however, have been encountered in attempts to photograph metal-water reaction experiments. These are (1) the necessity of including a high-powered light source within the capsule and (2) the presence of water surrounding the specimen. Previous photography has employed the luminescence of the heated sample as the only light source. This is unsatisfactory for studies of aluminum-base fuel because of negligible luminescence at the aluminum melting point, 660°C. The inclusion of water in the experiment requires a transparent container that does not darken because of the transient flux.

The light source to be used will employ two 1000-watt Sylvania quartz-iodine lamps which will be mounted directly within the capsule. The fuel specimen and the water will be contained within high purity fused silica tubes. Preliminary experiments will be performed with SPERT 1-D fuel plates. It is expected that the nature and the time of fuel failure will be observed.

5. Calculation of the Extent of Metal-Water Reaction During a Loss-of-Coolant Accident (R. O. Ivins, L. Baker, Jr.)

The calculational study to predict the extent of zirconium-water reaction that would occur during a loss-of-coolant accident in a water-cooled power reactor has been continued. The objective of this study is to demonstrate the application of metal-water reaction data to a reactor accident situation. The initial effort was described in the previous report (ANL-6925, p. 215). A complete summary of all work performed to date, including a summary of the material presented herein, has been reported.[5]

The reactor conceived for the Loss of Fluid Test (LOFT) facility[6, 7] was used as a model in these studies with the assumption that the cylindrical UO_2-core fuel pins were clad with 25-mil thick zirconium. The analysis of the bottom inlet pipe break (i.e., below the core) described by J. M. Waage *et al* of Phillips Petroleum[6] was used as far as possible as the basis for the metal-water reaction calculations. In this analysis, the core temperature rises owing to decay heating after a 10-sec blowdown due to the pipe break which completely uncovers the reactor core. The core eventually collapses as a result of clad melting.

In the analysis described in ANL-6925, p. 215, the assumption was made that the entire reactor core (cladding and fuel) had a temperature of 544°F (285°C) following the 10-sec blowdown. In making this assumption, it was tacitly assumed that the heat stored in the UO_2 fuel during full power operation was transferred completely to the coolant during the blowdown. This assumption is reexamined in the following paragraphs and the accident calculations are repeated for the opposite assumption that none of the heat stored in the UO_2 fuel during full power operation is lost to the coolant during the blowdown. Other assumptions given in ANL-6925 were retained.

a. ENERGY DISTRIBUTION IN THE REACTOR CORE

In the preliminary LOFT analysis report,[7] the blowdown time was calculated to be 10 sec. It was apparent, however, from the position of the reactor core in the reactor pressure vessel that the core could be uncovered in as little as 4 sec during a blowdown having a total duration of 10 sec. A simple calculation based on the steady-state heat transfer rate of the UO_2 fuel to the water indicates that the time constant for heat transfer between the UO_2 and the water is about 7½ sec. If it is further assumed that the heat transfer rate between the cladding and the coolant is greatly increased because of the rapid water motion during blowdown, the time constant probably decreases to a minimum of about 5 sec. The principal resistance to heat transfer in this case is conduction through the UO_2 and across the fuel-cladding gap.

If 7.5 sec is a typical time-constant for heat transfer during blowdown, then only about 30% of the stored energy in the fuel would be removed during the 4 sec available. The average fuel temperature in this case would be reduced from 816°C to about 650°C. A slower blowdown would result in the removal of nearly all of the stored energy in the fuel. Because of the wide range of coolant voiding rates possible in loss-of-coolant accidents, only two extreme cases were considered.

Case A: The reactor core is cooled during blowdown to a uniform temperature of 544°F (285°C), the coolant operating temperature. (These calculations are described in ANL-6925, p. 215.)

Case B: The energy stored in the fuel during full power operation is fully retained by the fuel.

In order to facilitate the calculations, the core was segmented and each segment was ascribed a volumetric power ratio. This was accomplished by segmenting the core into thirteen radial zones of equal volume. Eight of these zones were of low enrichment and five were of high enrichment. Each radial zone was further divided into twelve axial segments, which were also of equal

[5] L. Baker, Jr. and R. O. Ivins, Analyzing the Effects of a Zirconium-Water Reaction, Nucleonics **23**(7), 70 (July 1965).

[6] J. M. Waage *et al*, Preliminary Safety Analysis Report, LOFT Facility, Report IDO-16981, Phillips Petroleum Co., April 1964.

[7] T. R. Wilson *et al*, An Engineering Test Program to Investigate a Loss-of-Coolant Accident, Report IDO-17049, Phillips Petroleum Co., October 1964.

volume. The resulting 156 equal-volume segments (12 cylindrical segments in the center and 144 surrounding doughnut-like segments) were grouped into ten sections based on their average power ratio. The segmentation of the core was previously discussed in detail (ANL-6925, p. 215).

In the calculations of Case B, which are discussed herein, the initial temperature of each section of the core was calculated from the average fuel operating temperature of 1500°F (816°C) reported in the LOFT analysis.[6] For each section, the initial temperature of the fuel was determined from the ratio of power in that section to the average power in the core. The cladding temperature was assumed to be that of the coolant, 544°F (285°C). An equilibrium temperature was then calculated for each section assuming no heat losses. This equilibrium temperature was assumed to be the initial temperature of the UO_2 and cladding in the section after blowdown for Case B calculations. These temperatures are tabulated in Table V-6.

The method of calculation of extent of reaction and of chemical and decay energy for individual core sections was previously developed in detail (ANL-6925, p. 216).

Initial calculations were performed neglecting the chemical energy in order to generate reference temperature-time curves for each power section. The results are plotted in Figure V-18 for the Case B situation; Case A was previously reported. It is apparent from the figure that melting of the cladding begins after 115 sec and that one-half of the cladding (end of melting in the 6th section) in the reactor is melted after 790 sec for the calculations in which chemical heating is not included.

TABLE V-6. Calculated Equilibrium Temperatures of Core Sections after Blowdown

Case B: The energy stored in the fuel during full power operation is fully retained by the fuel.

Percent of Core in Section	Ratio of Power in Section to Average Power in Core	UO_2 Average Temperature at 50 MW Operation (°C)	Equilibrium Temperature of Cladding and UO_2 (°C)
2.56	2.28	1495	1289
7.69	2.04	1368	1184
5.13	1.80	1241	1078
10.26	1.56	1113	972
14.10	1.32	986	867
10.26	1.08	858	761
11.54	0.84	731	655
11.54	0.60	603	550
16.67	0.36	476	444
10.26	0.12	349	337

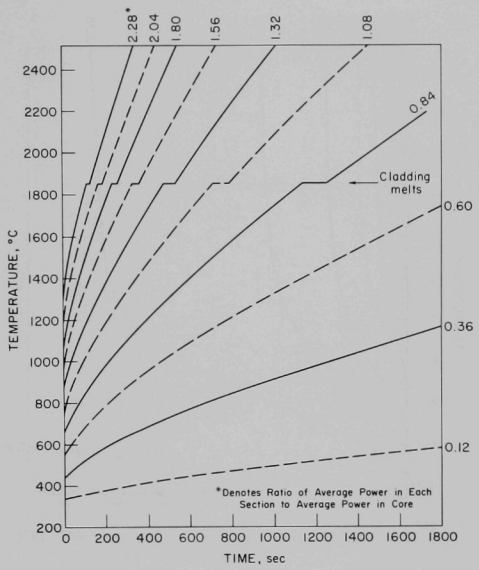

108-9085 T

Fig. V-18. Calculated Temperature-Time Curves for Each Power Section for No Metal-Water Reaction in Loss-of Coolant Accident. (Case B. Initial section temperatures are those at operating power.)

b. TEMPERATURE AND REACTION HISTORY OF INDIVIDUAL SECTIONS WITH UNLIMITED STEAM SUPPLY TO THE REACTOR CORE

The calculation of the temperature and reaction of the individual core sections with an unlimited supply of steam was performed using the parabolic rate law and the energy balance previously developed (ANL-6925, p. 218). The results for Case B are plotted as temperature-time histories in Figure V-19 and percent metal-steam reaction-time histories in Figure V-20. At first, the temperatures of those sections of the core initially below 800°C follow a course identical with the curves for which chemical heat was neglected (shown in Figure V-18) and the extent of metal-steam reaction is very small. As the temperature of each section reaches about 800°C, both the rate of temperature rise and the reaction rate increase rapidly, indicating ignition. At the melting temperature of the cladding (1852°C), the extent of reaction varies from 18% for the most energetic reactor section (relative power, 2.28) to 24% for the ninth section (relative power, 0.36), as indicated in Figure V-20. The lowest energy

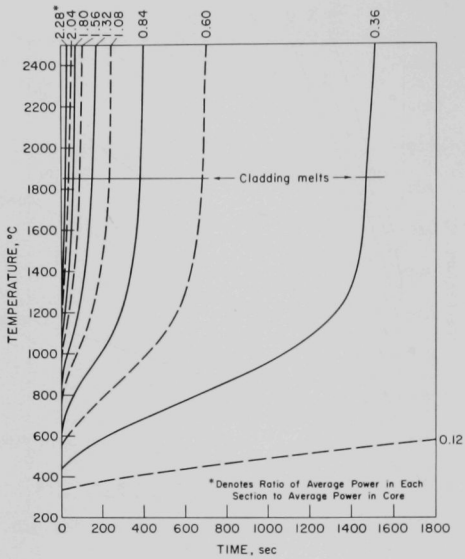

108-9088 T

FIG. V-19. Calculated Temperature-Time Curves for Each Power Section for Metal Reacting with an Unlimited Quantity of Steam in Loss-of-Coolant Accident. (Case B. Initial section temperatures are those at operating power.)

core section does not ignite within 2000 sec; however, it is clear that the calculations would predict eventual ignition since no provision was made in the calculations for the effect of heat losses.

In the several sections initially at temperatures greater than 800°C, significant reaction occurs immediately. In the five sections with the highest initial temperatures (see Figure V-20), the cladding-steam reaction causes the temperatures to rise rapidly and these sections ignite within a period of 200 seconds.

c. TEMPERATURE AND REACTION HISTORY OF INDIVIDUAL SECTIONS WITH A LIMITED STEAM SUPPLY TO THE REACTOR CORE

The calculation described above (Subsection b) employed the parabolic rate law as the only factor limiting the reaction rate. It is clear, however, that as the temperature becomes high, the parabolic rate law allows a very rapid reaction. Such a rapid reaction requires that steam be provided at a very rapid rate. A realistic appraisal of a loss-of-coolant accident, therefore, requires a determination of the rate of steam supply to the reactor core. Rather than attempt to specify steam flow rates resulting from various accident conditions at this time, calculations were performed for two reasonable flow rates.

In the LOFT analysis report,[6] it is estimated that 10% of the decay energy is lost from the core by heat convection during the first fifteen minutes after blowdown. By equating ten percent of the decay heat generated during this 15 min period to a mass of steam flowing through the core, entering at 540°F (282°C) and leaving at an assumed temperature of 1800°F (982°C), the rate of steam flow was calculated to be 510 lb/hr. The rate of 1000 lb/hr was chosen as an order-of-magnitude estimate for free heat convection through the core. Calculations for a rate of steam flow of 100 lb/hr, which was assumed to be representative of more restricted flow, were also performed. These rates were also used in the previous calculations (ANL-6925, p. 221) for Case A.

In order to relate the steam flow rate to the reaction rate, it was assumed that the maximum reaction rate of any unit of cladding surface was equal to the steam flow rate through the entire core divided by the total surface area of cladding. Accordingly, the maximum reaction (penetration) rate for the case of 1000 lb steam/hr was 5.7×10^{-5} cm/sec and for the case

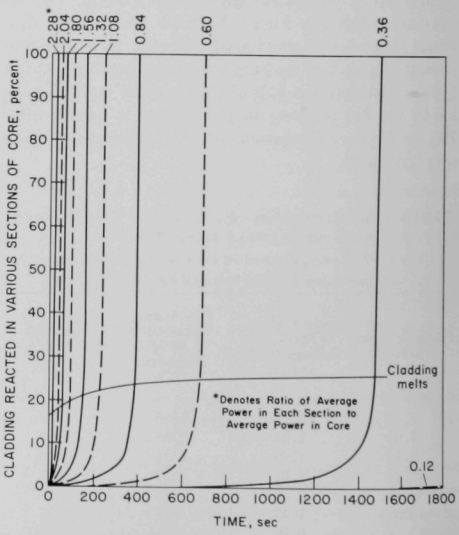

108-9087 T

FIG. V-20. Calculated Percent Reaction-Time Curves for Each Power Section for Metal Reacting with an Unlimited Quantity of Steam in Loss-of-Coolant Accident. (Case B. Initial section temperatures are those at operating power.)

of 100 lb/hr, it was 5.7×10^{-6} cm/sec. The calculations were performed by examining the results for the unlimited-steam case and determining the time at which the reaction rate, limited by the parabolic rate law, reached the steam-limited rates. At this point, calculations were continued for each section of the reactor on the basis that the reaction rate could not increase further.

The results of the calculations of the temperature histories of the individual sections for Case B are given in Figures V-21 and V-22. In both cases the temperature curves were identical with those calculated for an unlimited steam supply (Figure V-19) until they reached about 1300°C for a flow rate of 1000 lb/hr and 900°C for a flow rate of 100 lb/hr. At these temperatures the reaction was limited by the steam supply and the temperature rises were less rapid than those calculated for unlimited steam. The temperatures and times at which this change in controlling mechanism occurred are indicated on the figures.

The cladding-steam reaction histories of the individual sections are shown in Figures V-23 and V-24 for the two assumed steam flow rates.

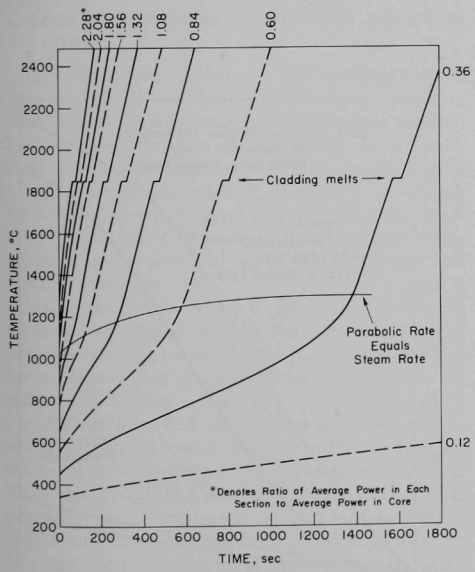

108-9086 T

FIG. V-21. Calculated Temperature-Time Curves for Each Power Section for Metal Reacting with Limited Quantities of Steam in Loss-of-Coolant Accident: Steam Flow Rate 1000 lb/hr. (Case B. Initial section temperatures are those at operating power.)

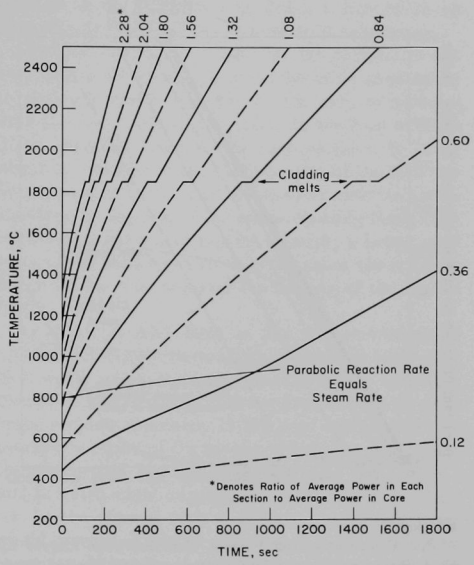

108-9084 T

FIG. V-22. Calculated Temperature-Time Curves for Each Power Section for Metal Reacting with Limited Quantities of Steam in Loss-of-Coolant Accident: Steam Flow Rate 100 lb/hr. (Case B. Initial section temperatures are those at operating power.)

d. COMPARISON OF THE EXTENT OF REACTION OF THE CLADDING IN THE LOFT CORE FOR THE VARIOUS ASSUMED QUANTITIES OF AVAILABLE STEAM

The extent of reaction for the entire core was obtained by summing the reactions of each section for the various calculations. In Figure V-25 the percent of cladding reacted versus time is plotted for an unlimited supply of steam. Both cases of assumed initial section temperatures are shown, those previously reported (Case A) and those reported herein (Case B). The stepwise character of the curves is a result of the use of only ten rather large power sections in the calculations. Actually, ignition would progress continuously through the core.

The results of the calculations for the two assumed flow rates are plotted in Figure V-26. Curves for both cases of initial section temperature are again included in the figure. Comparison of the curves points out the marked effects of both steam flow rate and initial section temperature on the amount of cladding that reacts in the core considered as a whole.

The extent of metal-water reaction, and hence the

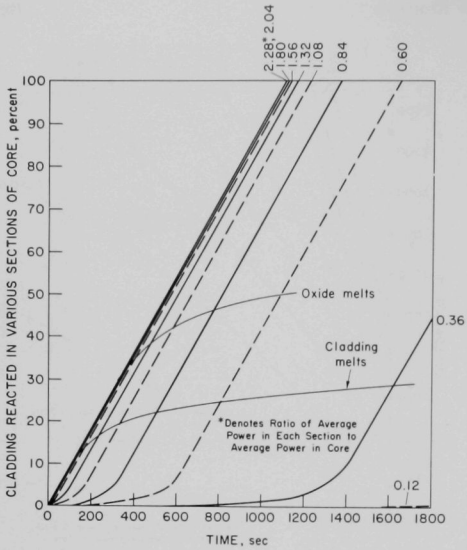

108-9080 T

FIG. V-23. Calculated Percent Reaction-Time Curves for Each Power Section for Metal Reacting with Limited Quantities of Steam in Loss-of-Coolant Accident: Steam Flow Rate 1000 lb/hr. (Case B. Initial section temperatures are those at operating power.)

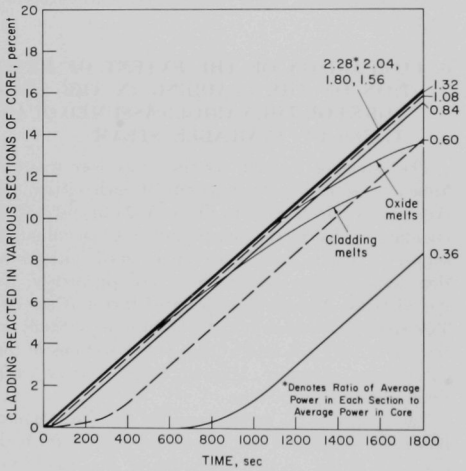

108-9079 T

FIG. V-24. Calculated Percent Reaction-Time Curves for Each Power Section for Metal Reacting with Limited Quantities of Steam in Loss-of-Coolant Accident: Steam Flow Rate 100 lb/hr. (Case B. Initial section temperatures are those at operating power.)

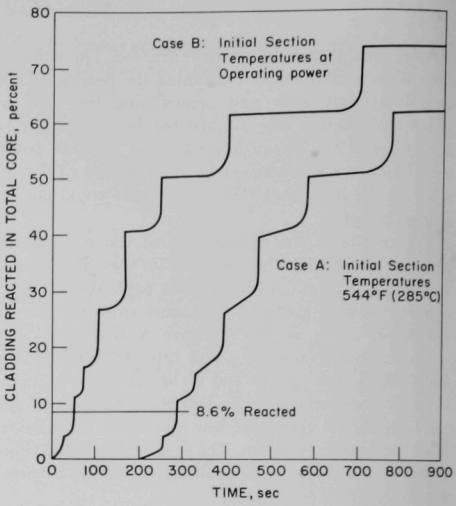

108-9078 T

FIG. V-25. Calculated Percent Reaction Curves for Entire Reactor Core with an Unlimited Quantity of Steam in Loss-of-Coolant Accident.

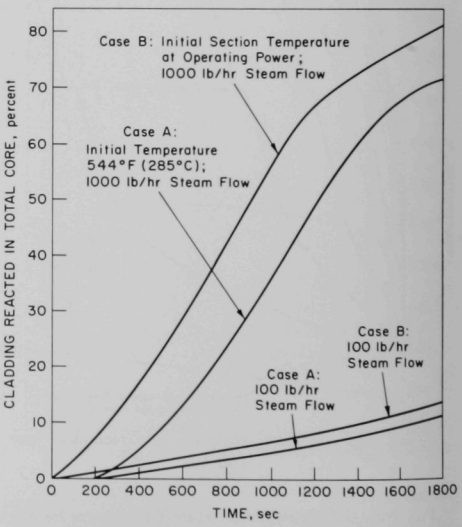

108-9081 T

FIG. V-26. Calculated Percent Reaction-Time Curves for Entire Reactor Core with Limited Quantities of Steam in Loss-of-Coolant Accident.

TABLE V-7. COMPARISON OF THE TIME REQUIRED TO MELT THE CLADDING FOR VARIOUS STEAM FLOW RATES

Steam Flow	Time at which Melting of Cladding Begins[a] (sec)		Time to Melt One-half of Cladding[a] (sec)	
	Case A	Case B	Case A	Case B
Unlimited	240	20	560	230
1000 lb/hr	300	70	680	330
100 lb/hr	390	110	1050	630
No flow (no metal-water reaction)	430	115	1250	790

[a] Case A: initial section temperatures 544°F (285°C).
Case B: initial section temperatures are those at operating power (see Table V-6).

steam flow rate and initial section temperatures, has a marked effect on the meltdown history of the cladding. This is shown in Table V-7 where the times corresponding to the beginning of melting of the cladding and the point where one-half of the cladding is melted (end of melting of the 6th section) are tabulated for all of the cases considered.

e. LOSS OF INTEGRITY OF THE REACTOR CORE

The calculations presented in the previous sections have ignored the loss of integrity of the core resulting from excessively high temperatures and have assumed that the core structure remains intact. As a result, these calculations eventually predict complete reaction of either the core cladding or the available steam, depending upon which factor limits the reaction. However, the extreme temperatures reached make it apparent that the core will suffer severe damage and eventually collapse.

It is of major importance to determine the time at which the core melts through the support structures and falls into the bottom of the reactor vessel, since this occurrence will bring to an end the reaction regimes discussed above.

In ANL-6925, p. 222, an extensive discussion is presented on both the loss of integrity of the reactor core and metal-water reaction following total core collapse. While this presentation was based on the Case A situation only, the calculations are similar for Case B. Table V-8 summarizes the times calculated to be required for either complete melting of the cladding or incipient melting of the fuel for both cases. The extent of metal-steam reaction for the total core at each of these times is also included in Table V-8. Calculation of these times is based on an average energy accumulated throughout the core, i.e., complete heat transfer, in contrast to the times given in Table V-7 in which no heat transfer between power sections is assumed.

Since no satisfactory model for the collapse of the core exists, the times shown in the table were taken to represent those required for the core to collapse onto the lower support structure. In the case of little or no chemical reaction, the time required to bring about the collapse of the major portion of the core can be assumed to be the time required to melt the metal cladding. In the case of the metal cladding being converted extensively and rapidly to oxide, a better estimate of the time required to bring about the collapse would be the time required for melting of the urania fuel.

As stated in ANL-6925, p. 224, the course of the accident subsequent to core collapse depends both upon how much water is in the reactor vessel following blowdown and upon the time required to melt through lower support structures. If the core collapses into a nearly dry region of the reactor vessel, it is likely that the core would form a random pile of UO_2, ZrO_2, and Zr which might or might not melt through the vessel. In the case of such a collapse, further reaction would proceed slowly by diffusion of steam or air into the mass. However, if the hot core material were to collapse into a large quantity of water, then a rapid quenching reaction should occur. If a major portion of the core falls at one time, a violent steam explosion might occur. This seems unlikely, since the energy generated at the center of the reactor is greatest and the supporting structures in this region will probably be the first to fail. The failure would then spread radi-

TABLE V-8. TIME REQUIRED FOR COLLAPSE OF CORE AND EXTENT OF REACTION BASED ON THE AVERAGE NUCLEAR DECAY AND CHEMICAL ENERGY CONTENT

Steam Flow	Average Core Energy Sufficient To Melt Cladding Completely (1852°C)				Average Core Energy Sufficient To Begin to Melt Fuel (2800°C)			
	Collapse Time[a] (sec)		Metal Reacted[a] (%)		Collapse Time[a] (sec)		Metal Reacted[a] (%)	
	Case A	Case B	Case A	Case B	Case A	Case B	Case A	Case B
Unlimited	465	105	40	27	765	240	62	50
1000 lb/hr	740	390	21	16	1080	685	41	34
100 lb/hr	1200	700	6.0	4.0	2090	1500	13	10
No flow (no metal-water reaction)	1400	1100	—	—	2600	2300	—	—

[a] Case A: initial section temperatures 544°F (285°C).
Case B: initial section temperatures are those at operating power (see Table V-6).

ally with the core debris entering the water over a period of time, minimizing the chance of a serious explosion.

The extent of the chemical reaction during quenching can probably be estimated from results of condenser-discharge experiments and meltdown experiments in TREAT. Results of zirconium-water reaction studies by both methods indicate that the extent of reaction would be quite limited (<15%) unless the temperature of the debris was above 2600°C, the melting point of ZrO_2. In this case, the ZrO_2 would be molten, and extensive particle subdivision and increased metal-water reaction could occur.

f. DISCUSSION

In the analysis of the loss-of-coolant accident presented above and in ANL-6925, a preliminary attempt has been made to predict the general features of such an accident in order to disclose gaps in the knowledge required for a precise analysis. Accurate estimates of the UO_2 and cladding temperatures throughout the core would be necessary to carry out a more refined analysis. Such an analysis would include in the calculation the temperature gradients through the UO_2 and cladding, as well as the effects of initial steam cooling of the core and the heat capacity of support structures within the core. As core melting and collapse begin, it is clear that uncertainties multiply. It is also clear, however, that an increasing quantity of zirconium is reaching temperatures at which it will react with all of the steam that can enter central regions of the core.

The principal uncertainties in the analysis were discussed in ANL-6925, p. 225 and bear repeating at this point. They are related to the lack of a meltdown model from which to estimate the failure times of the lower core supporting plates and the temperature of debris falling into the bottom of the reactor vessel. Ultimate analysis of the accident requires calculations of the steam flow through the core following blowdown and the quantity of water remaining in the lower part of the reactor vessel. In the LOFT analysis, the quantity of water remaining ranged from 0 to about 2000 lb, whereas only 320 lb are required to react with the entire cladding.

One of the uncertainties in the analysis is the relation between the steam flow rate and the limiting reaction rate. Questions concerning the efficiency of reaction of steam flowing upward along individual fuel rods were ignored. In reality, reaction would be greater at lower positions in the core.

One case which was not considered in the analysis presented was that of no net steam flow through the core (i.e., where no rupture in the reactor vessel exists above the core). In this case, there might be some convective circulation of steam, and eventually hydrogen, through the core. Although a detailed calculation of the convective circulation of gases has not been performed, some guide to the extent of metal-water reaction might be gained by noting that the steam present in the entire reactor pressure vessel after the blowdown is sufficient to react with about 8.6% of the cladding (see Figure V-25).

Two additional uncertainties in the analysis involve chemical phenomena which have not been investigated in sufficient detail to allow assessment of their possible roles in the meltdown accident. These are the reaction of zirconium with hydrogen and the reaction of UO_2 with steam. For a severely steam-limited case, the former reaction could provide a steam-pumping action which would bring steam into the lower portion of the core and form zirconium hydrides in the upper portion of the core. For unoxidized zirconium[8] the hydriding reaction is sufficiently rapid at temperatures of around 1000°C to merit consideration; however, the retarding effect of oxide films on the hydriding reaction at higher temperatures has not been studied extensively. In destructive tests in TREAT (ANL-6925, p. 204), it has been shown that UO_2 will react with water to form $UO_{2.2}$ and hydrogen. The reaction rate, however, has not been evaluated under conditions of high temperature for the case in which no violent fragmentation occurs. Although hydrogen is produced in the UO_2-steam reaction, little or no heat is evolved.

[8] R. B. Bernstein and D. Cubicciotti, The Permeability of Zirconium to Hydrogen, J. Phys. and Colloid Chem. **55**, 238 (1951).

B. FAST REACTOR SAFETY STUDIES

1. Fuel-Coolant and Cladding-Coolant Interaction Studies (D. Swift, P. Krause)

The high temperature interactions between sodium coolant and fast reactor materials are currently being investigated. In order to simulate the contact of coolant and reactor materials in a fast reactor meltdown accident, a technique has been developed in which a small sample (~0.3 cc) of the material to be investigated is inductively heated and dropped into a pool of liquid sodium.

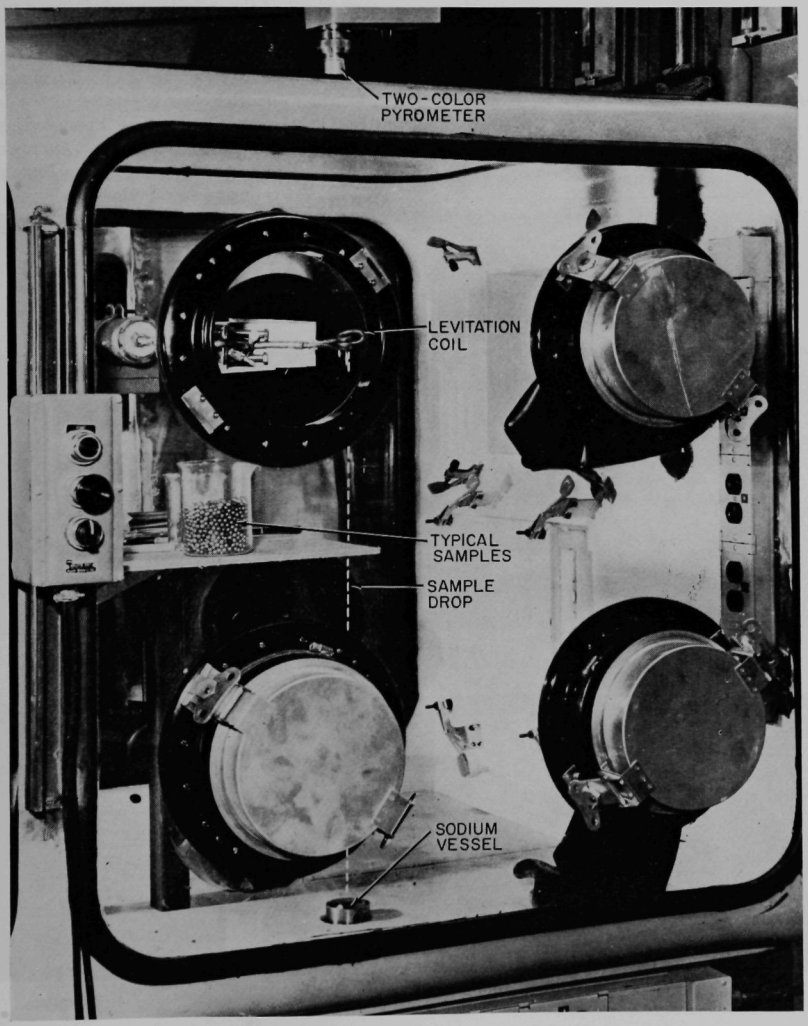

108-8352 T

Fig. V-27. Glovebox for Studies of Interaction of Molten Fuel and Cladding Materials with Molten Sodium.

These experiments are being carried out in a two-module argon-filled glovebox. The glovebox modifications, apparatus assembly, and operation of the argon purification system have been described in a previous report (ANL-6925, p. 226). Figure V-27 shows the apparatus used for the experiments conducted with metallic samples; the apparatus includes a copper levitation heating coil which is powered by a 15 KW, 250 kc induction generator, a two-color pyrometer to determine sample temperature, and a sodium container. The drop path in this arrangement is approximately 60 cm, but the container can be raised for shorter drop distances. All of the experiments performed to date have been with metallic samples. Provision has been made to replace the levitation coil with an induction coil and a tantalum susceptor to heat nonmetallic samples. The impurity concentrations in the box atmosphere during experiments were 5 ppm oxygen, 20 to 30 ppm water, and <0.5% nitrogen. Approximately 1.5 liters of reagent grade sodium were contained in the sodium vessel during an experiment.

TABLE V-9. Melting Points and Maximum Drop Temperatures of Samples Used in the Sodium Interaction Studies

Sample	Melting Point (°C)	Maximum Drop Temperature (°C)
High Melting		
Tantalum	2980	2200
Molybdenum	2600	2200
Niobium	2470	2300
Niobium-1 w/o Zirconium	~2450	2200
Low Melting		
Vanadium	1890	2200
Zirconium	1852	2350
Nickel	1453	2100
Mild Steel	~1450	2400
304 Stainless Steel	~1425	2400

a. RESULTS WITH SOLID REFRACTORY METALS

In experiments with niobium, molybdenum, tantalum, and niobium-1 w/o zirconium alloy, sample

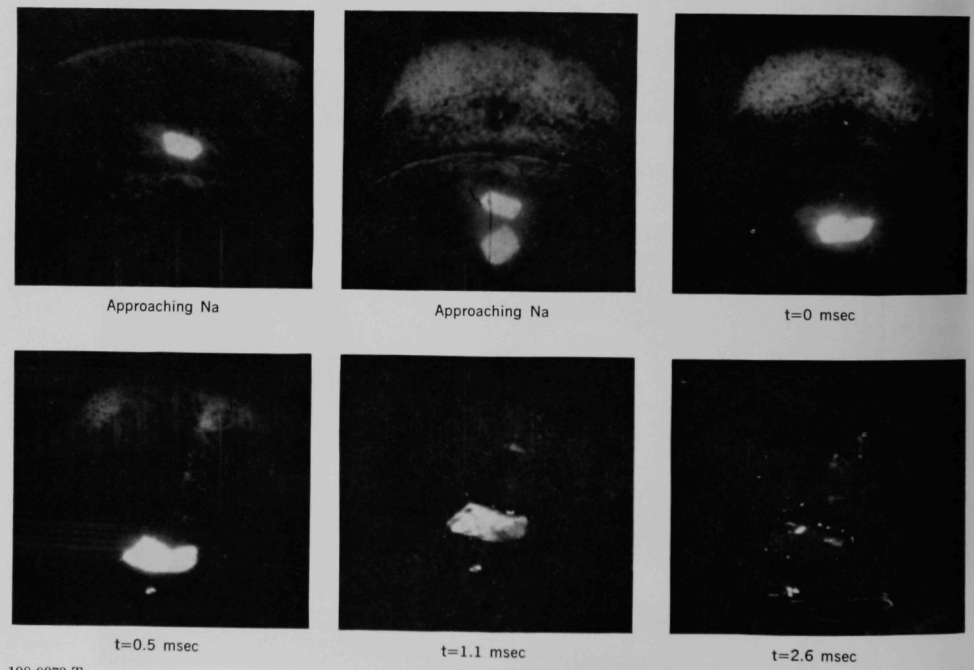

108-9073 T

Fig. V-28. Selected Fastax Frames of Niobium Sample dropped into Molten Sodium. (T_{Nb} = 2300°C; T_{Na} = 250°C.)

melting could not be achieved because of the high melting points of these materials, which are shown in Table V-9. Table V-9 also lists the maximum temperatures of the samples at the moment of dropping (drop temperatures) as recorded by the Pyro-Eye two-color pyrometer. The maximum temperature decrease by radiative heat transfer as the particle falls from the coil into the molten sodium was calculated to be approximately 100°C (assuming unit emissivity). As the solid particles enter the liquid sodium (at 250°C), a brief period of bubbling is observed, but the samples immediately disappear from view. Fastax movie films of the niobium experiment reveal considerable surface turbulence of the sodium following sample immersion: several frames (not adjacent) illustrating the sequence of events are shown in Figure V-28. The quenched samples of the various refractory materials were recovered from the sodium and examined visually; there was no evidence of any chemical or physical interaction. The samples were removed from the box for sectioning and metallographic mounting. Photomicrographs of these samples are shown in Figure V-29 and provide further evidence that no chemical interaction occurred.

b. RESULTS WITH MOLTEN METALS AND ALLOYS

In experiments with nickel, zirconium, vanadium, mild steel, and type 304 stainless steel, all of which have melting points below 2000°C, it was possible to drop molten samples into the sodium. The melting points and maximum drop temperatures obtained for these materials are also included in Table V-9. Each material at its maximum drop temperature suffered some degree of

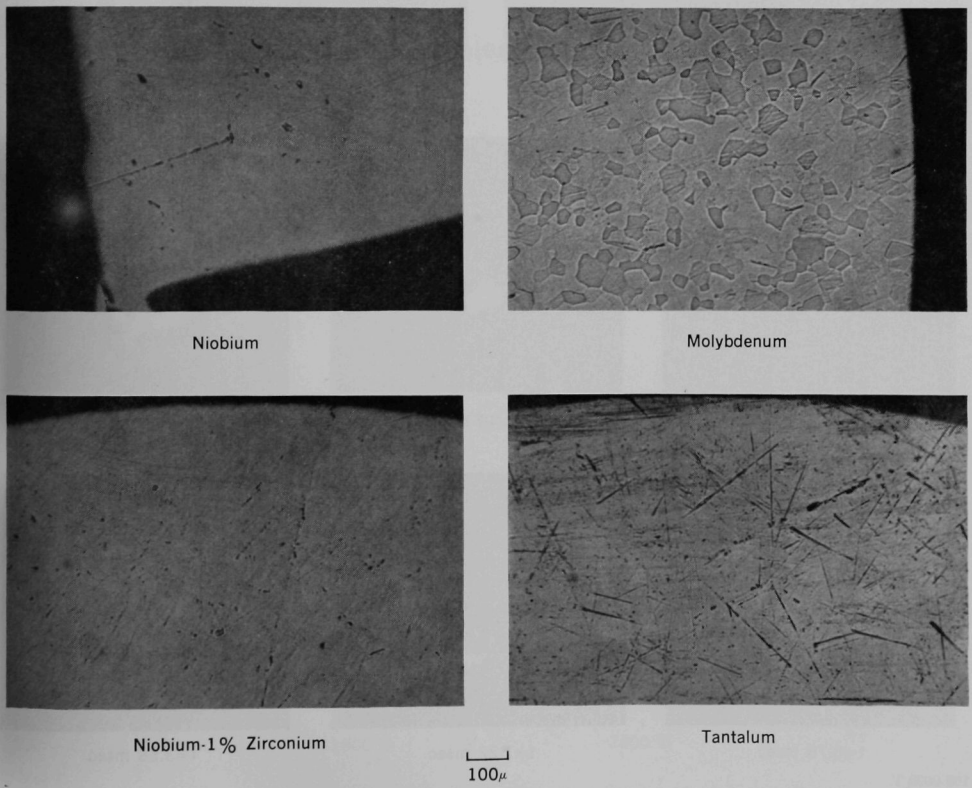

108-9071 T

Fig. V-29. Metallographs of Refractory Metal Residues.

drop fragmentation upon contact with the liquid sodium. At the same time, the contact brought about an explosive expulsion of a small fraction of the sodium; in one case the sodium was expelled with such force that sodium droplets were found on the ceiling and walls of the glovebox.

The most violent interaction was observed when type 304 stainless steel initially at 2400°C was dropped into sodium at 250°C. This is the experiment alluded to earlier in which many small droplets of sodium (0.2 to 0.3 cm in dia.) were found on the walls and ceiling of the glovebox, which were at a maximum distance of 4 ft from the sodium container. Fastax motion pictures of the event showed that some of the fragments of the stainless steel also were thrown from the container. The formation of a vapor cloud, assumed to be sodium

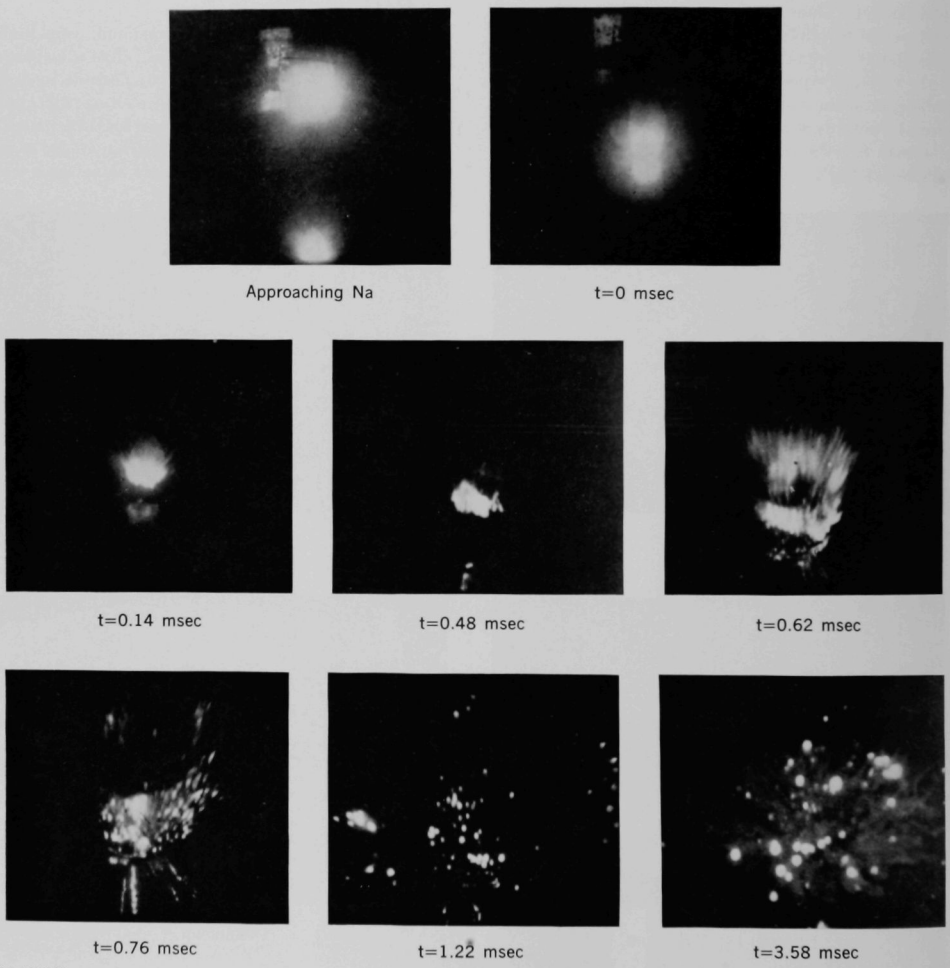

108-9070 T

FIG. V-30. Selected Fastax Frames of Type 304 Stainless Steel Sample dropped into Molten Sodium. (T_{SS} = 2400°C; T_{Na} = 250°C.)

vapor, was observed immediately following the contact. This vapor cloud had a maximum diameter of about 1 ft and condensed into small particles. Figure V-30 shows several selected frames of the Fastax film of this event; the particle fragmentation and droplet expulsion can be seen.

That portion of the stainless steel residue which remained in the sodium was recovered and is shown in Figure V-31. Examination of this residue gave no evidence of chemical interaction with sodium; furthermore, the shiny, compact appearance of the individual particles indicated that foaming (as is observed in the case of high temperature stainless steel-water interactions, see ANL-6925, p. 189) had not occurred during cooling. Nevertheless, if such particle fragmentation were to occur in a fast reactor meltdown incident, coolant channel blockage and expulsion of coolant from the core could result.

In order to better understand the fragmentation process, experiments with type 304 stainless steel and cold-rolled mild steel were performed at several different drop temperatures. The residues from these experiments are also shown in Figure V-31. A most interesting residue was observed for the stainless steel sample dropped at 2100°C. In this case, the molten sample flattened out into a rather thin sheet, a section of which is shown in Figure V-31. In this experiment there was a small amount of sodium thrown from the container and some vapor formation, but the interaction was much less violent than that which occurred with the stainless steel initially at 2400°C. The fragmentation of the mild steel sample at 2400°C was as complete as that of the stainless steel, as seen in Figure V-31, but the observed interaction was not as vigorous.

A series of experiments using samples of crystal bar zirconium gave somewhat different results from the stainless steel, as can be seen in Figure V-32. At the highest temperature obtained (2350°C), drop frag-

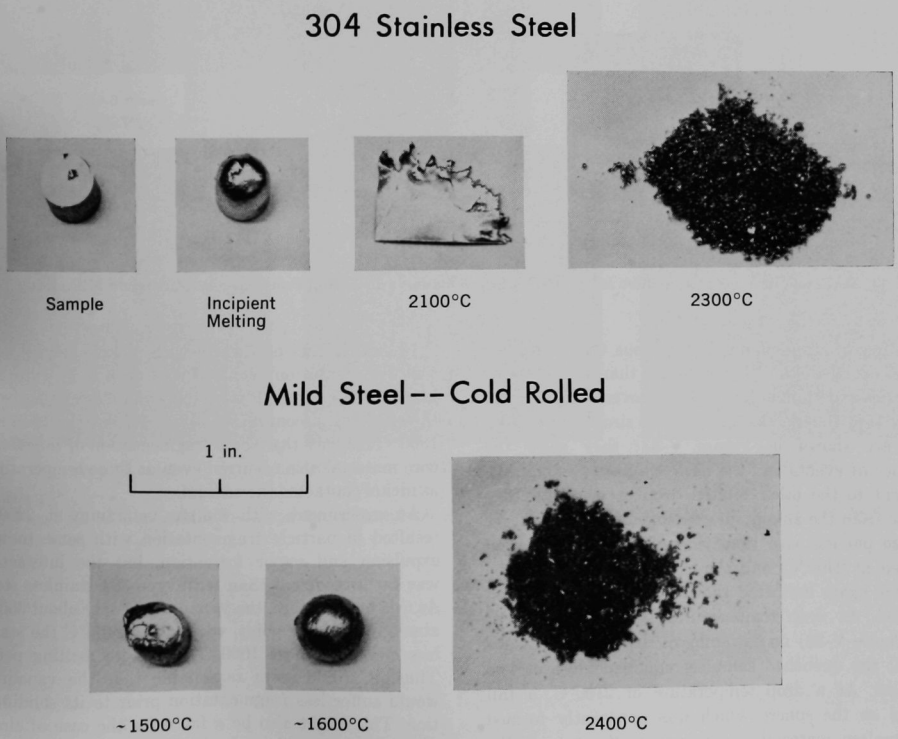

108-8655 T

Fig. V-31. Stainless Steel and Mild Steel Residues from Sodium Interaction Experiments at Various Drop Temperatures.

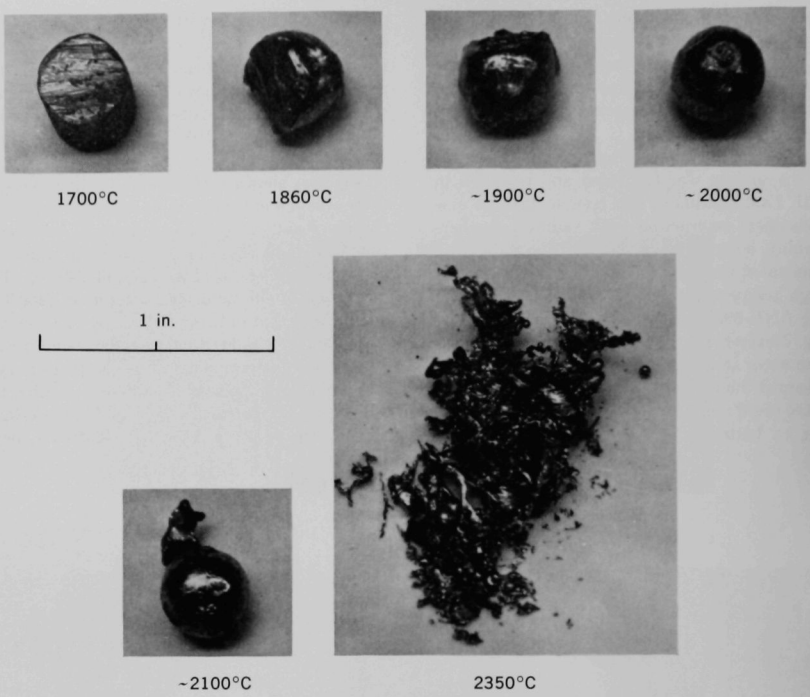

108-8654 T
FIG. V-32. Zirconium Residues from Sodium Interaction Experiments at Various Drop Temperatures. (Zirconium M.P., 1860°C.)

mentation occurred upon contact, but there was less sodium expelled from the container than in the stainless steel experiment at 2400°C. Several frames selected from the Fastax film of the zirconium experiment are shown in Figure V-33; they show the sequence of events and the basic similarity of this experiment to the other molten drop experiments. The residue from the zirconium experiment was of a larger average particle size than that of the stainless steel dropped at 2400°C, and the shiny appearance of the particles again indicated that no chemical interaction occurred. At drop temperatures lower than 2350°C (see Figure V-32) no flattening of the particle was observed; the quenched samples remained more or less spherical. At a drop temperature of 2100°C, a tail formed on the sphere which was apparently formed from molten material escaping from the core of the particle.

In experiments performed with nickel samples, particle fragmentation occurred at a drop temperature of 2100°C (see Figure V-34), somewhat lower than with the steels or zirconium. It appears from the 1600 and 1800°C residues that some fragmentation of the molten core material also occurred even at these temperatures as nickel contacted the sodium.

An experiment with molten vanadium at 2200°C resulted in particle fragmentation with some sodium expulsion and vapor formation, but the interaction was far less violent than with type 304 stainless steel. At this temperature, the vanadium is only about 300°C above its melting point, whereas at 2400°C the stainless steel is almost 1000°C above its melting point. Thus, it would seem reasonable that the vanadium would suffer less fragmentation prior to its solidification. This might also be a factor in the case of zirconium; however, other physical properties such as surface tension, viscosity, and thermal conductivity are

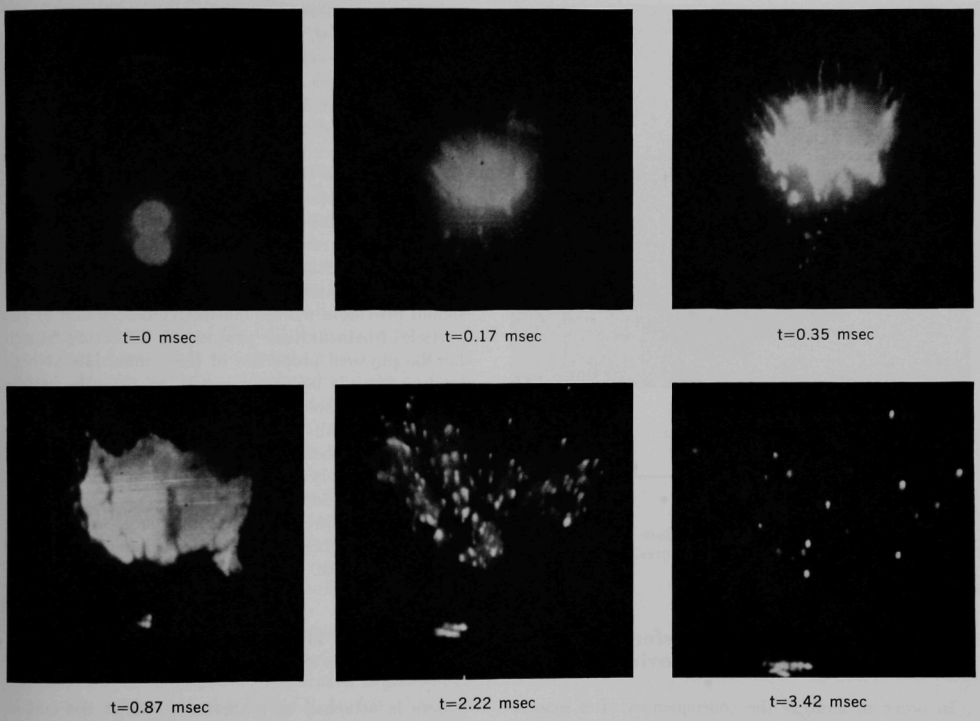

108-9074 T

FIG. V-33. Selected Fastax Frames of Zirconium Sample Dropped into Molten Sodium. (T_{Zr} = 2300°C; T_{Na} = 250°C.)

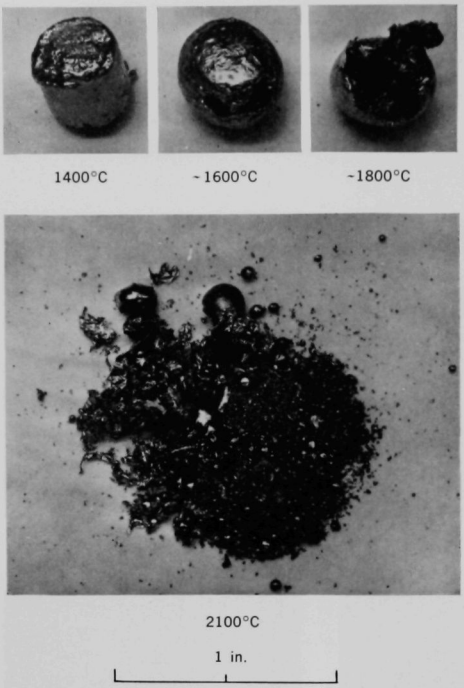

108-8653 T

FIG. V-34. Nickel Residues from Sodium Interaction Experiments at Various Drop Temperatures. (Nickel M.P., 1453°C)

also likely to be important determinants in the extent of particle fragmentation.

It was not possible to reach a temperature above the melting point of 1130°C for uranium samples; at this temperature the sample dropped out of the coil. Examination of the residue from this experiment gave no indication of chemical interaction. Similar difficulties were encountered with samples of Armco iron in an attempt to make a comparison of results with stainless steel; temperatures above the melting point of 1540°C were not obtained.

In order to evaluate the effect of impact velocity upon the stainless steel-sodium interaction, an experiment was performed in which type 304 stainless steel at 2400°C was dropped only 15 cm into the sodium. This gave a calculated impact velocity of 168 cm/sec, which is one-half the velocity for the 60 cm drops. The observed interaction in terms of particle fragmentation and sodium expulsion was not diminished.

Most of the results of these experiments thus far have been qualitative in nature. Future experiments with molten metallic samples are being planned which should provide a more quantitative description of the particle fragmentation process. A literature search for the physical properties of these materials at high temperatures is being conducted, so that the results of the experiments may be interpreted. Interaction experiments with nonmetallic reactor materials are also planned; these will include UO_2, UN, and UC, and as previously mentioned, these experiments will involve the development of the susceptor heating technique. Experiments with uranium metal will also be extended to higher temperatures using the susceptor heating technique.

2. Transient Heat Transfer Studies: Measurement of Heat Flux from a Heated Metal Sphere Moving Through Water (R. O. IVINS, L. BAKER, JR.)

In order to analyze the consequences of a reactor incident in which hot fuel materials may be dispersed into a liquid coolant, knowledge of the rate and quantity of energy transfer that occurs between the fuel particles and the coolant is necessary. Neither theoretical nor experimental information is available for the calculation of the heat transfer that occurs when small particles at high temperatures are rapidly dispersed in either water or a liquid metal such as sodium.

An experimental effort to study transient heat transfer from small hot particles moving through a liquid coolant has been initiated. The apparatus (see Figure V-35) consists of a swinging arm (or pendulum) with a knife blade attached to the arm. A small metal sphere is attached to a thermocouple at the end of the blade. The metal sphere is heated to the desired temperature in an electrically heated tube furnace prior to release of the arm. A vessel filled with water (sodium will be used in later experiments) is placed below the pivot of the arm. As the arm swings freely, the knife blade and metal ball pass through the water. The arm is stopped after the ball has once passed through the water; the sphere is then allowed to cool in the air. Nickel spheres, ¼ in. in dia., were used in the first experiments.

Two methods were used to attach the nickel spheres to the Pt/Pt, 10% Rh thermocouples. In one, a thermocouple junction was imbedded in a ceramic cement contained in a hole that was drilled through the center

of the sphere. In the other, the thermocouple was welded to the surface of the ball, the thermocouple leads being welded to opposite sides of the ball so that the ball was suspended between the two lead wires.

The water was maintained at room temperature, and no attempt was made to deaerate the water. High speed motion pictures were taken of the ball moving through the water. The time of immersion of the knife blade was measured electronically. The angular velocity calculated from these measurements was used to obtain the linear ball velocity; the average linear velocity was determined to be about 10 ft/sec.

The distance of travel through the water can be varied by changing the depth of water in the vessel. Path lengths of from 21.3 to 30.6 in. have been employed.

A record is made of millivolt output of the thermocouple on a Brown pen recorder. The relatively slow cooling in air compared with the very rapid cooling in the water allows determination of the temperature of the ball as it enters and leaves the water (see Figure V-36). The temperature drop during the pass through the water and the weight of the ball are used to calculate the energy loss of the ball from enthalpy data.[9] An average heat flux is calculated for each experiment by dividing the energy loss by the area of the ball and the time of passage through the water.

The data from several series of experiments, in which both methods of attaching the thermocouple to the ball and four different path lengths were employed, are shown in Figure V-37. The heat flux is plotted vs the initial ball temperature as it enters the water. The measured heat fluxes generally decreased with initial ball temperature and were relatively unaffected by the slight variations of velocity and path length through the water.

No attempt to fit the data to a curve was attempted since the proper shape of the correlation is masked by the scatter of the data points. The scatter is greatest at high temperatures of the balls. It is felt that the largest contribution to the scatter, i.e., the largest error in the measurements, is due to spattering of water as the ball and knife blade exit from the vessel. Any small drops of water that strike the ball after it has left the vessel lower the measured temperature and thus tend to yield high heat fluxes. Modifications of the knife blade should reduce this problem considerably.

The heat fluxes shown in Figure V-37 vary from about 80 cal/(cm^2) (sec) at an initial ball temperature of 300°C to between 150 and 210 cal/(cm^2) (sec) at an initial ball temperature of 1000°C. These values

[9] R. Hultgren *et al*, *Selected Values of Thermodynamic Properties of Metals and Alloys*, J. Wiley & Sons, New York, 1963.

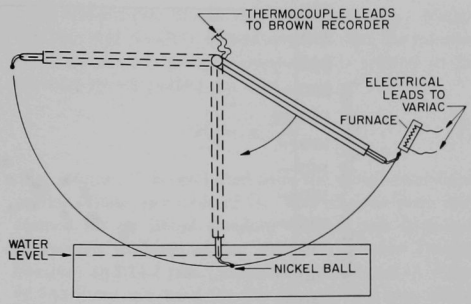

108-8740 T 2

FIG. V-35. Diagram of Pendulum (Swinging Arm) Apparatus Used in Study of Heat Transfer from Moving Spheres to Water.

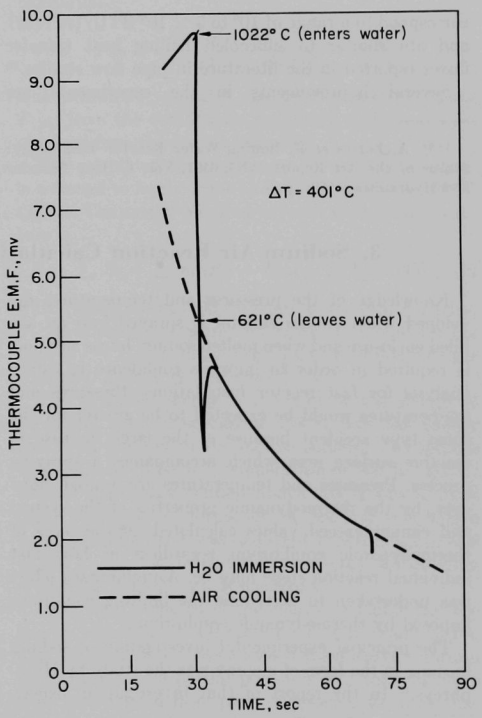

108-8738 T Rev. 1

FIG. V-36. Chart Record of Thermocouple EMF in a Typical Experiment by the Swinging Arm Method. (Air cooling curve superimposed.)

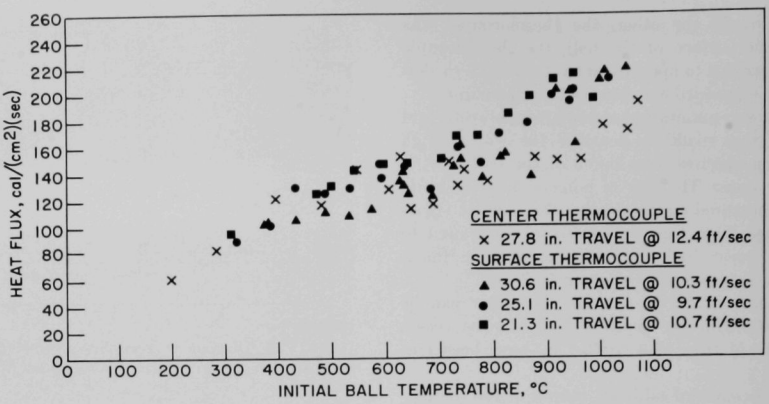

108-8741 T Rev. 1

FIG. V-37. Heat Flux from a ¼-in. Nickel Ball to Water at 23°C by the Swinging Arm Method.

correspond to a range of 10^6 to 3×10^6 BTU/(ft^2) (hr) and are similar to subcooled boiling heat transfer fluxes reported in the literature in pipe flow studies.[10]

Several improvements in the experiments are planned. Platinum balls will be used in order to increase the initial ball temperatures and also to prevent possible oxidation of the ball. The water will be deaerated and its temperature will be varied. In addition, the knife blade-ball attachment scheme will be modified so that the ball is pushed through the water, thus avoiding any spatter of droplets thrown by the blade as it exits from the water.

[10] P. A. Lottes *et al*, Boiling Water Reactor Technology: Status of the Art Report, ANL-6561, Vol. 1, Heat Transfer and Hydraulics (1962), p. 9.

3. Sodium-Air Reaction Calculations (L. BAKER, JR., A. D. TEVEBAUGH)

Knowledge of the pressures and temperatures developed when molten sodium is sprayed into an air-filled enclosure and when molten sodium burns as a pool is required in order to improve confidence in safety analysis for fast reactor installations. Pressures and temperatures would be expected to be greater for the spray-type accident because of the large increase in reactive surface area which accompanies a spraying process. Pressures and temperatures are limited, however, by the thermodynamic properties of the system and cannot exceed values calculated on the basis of thermodynamic equilibrium regardless of how fast individual reaction steps may be. A preliminary effort was undertaken to determine the limiting conditions imposed by thermodynamic equilibrium.

The principal experimental investigation of sodium burning in the form of a spray was the study by Humphreys.[11] In the report of that investigation, experimental pressures were compared with theoretical maximum pressures. It was concluded from this comparison that measured pressures were no more than about ⅔ of the theoretical maximum. Theoretical maximum temperatures were also reported and were as high as 3500°C. The high values of the reported theoretical temperatures necessitated a review of these calculations. It was readily apparent, after looking into the thermodynamics of the sodium-oxygen system, that theoretical temperatures are, in fact, much lower than the values given by Humphreys. It was also likely, therefore, that the theoretical pressures are lower than his values. A brief hand calculation of the temperatures and pressures was undertaken. The method employed and the results obtained are reported in the following paragraphs.

Support for the idea that limiting temperatures are much lower than 3500°C is given in a paper by Grosse and Conway.[12] It is pointed out therein that metal burning temperatures are often limited by the decom-

[11] J. R. Humphreys, Jr., Sodium-Air Reactions as They Pertain to Reactor Safety and Containment, *Proc. of the Second Intern. Conf. on the Peaceful Uses of Atomic Energy*, Geneva (1958) Vol. 11, p. 177.

[12] A. V. Grosse and J. B. Conway, Combustion of Metals in Oxygen, Ind. and Eng. Chem. **50**, 663 (1958).

position temperature of the oxide. The reason for the temperature limitation derives from the fact that the energy source is the formation of an oxide. When temperatures are reached at which oxide decomposition occurs, the energy must be reabsorbed and the attainment of higher temperatures is prevented. The limiting temperature for sodium is given as being about 2000°K (1727°C) by Grosse and Conway.

The most recent compilation of thermodynamic data is the JANAF[13] tables. These data were used for our calculations.

The first step in the calculation is to establish the chemical species present. The tables for free energy of formation indicate that, above 1200°K (927°C), $Na_2O(\ell)$ is the most stable condensed phase. From 1200°K down to room temperature, the most stable condensed phase is $Na_2O_2(s)$, if excess sodium metal is not present. Since it is expected that temperatures of interest will exceed 1200°K, the only condensed phase considered was $Na_2O(\ell)$. The gaseous species considered in the calculations were N_2, O_2, Na(g), and NaO(g). Data for the species $Na_2(g)$ indicated that the concentration of the dimer is only a few percent of the Na(g) concentration; since the energy of formation of the dimer is not great, this species was ignored. Species such as NO, O, and N were expected to be negligible so long as temperatures did not greatly exceed 2000°K (1727°C).

The second step in the calculation requires the determination of the equilibrium composition at trial temperatures. The initial composition of the mixtures considered was 4 moles of N_2, 1 mole of O_2 (2 gram atoms of O), and Z gram atoms of Na. This leads to three atomic balance equations which must be satisfied:

nitrogen
balance: $n_{(N_2)} = 4$ (2)

oxygen
balance: $2n_{(O_2)} + n_{(NaO)} + n_{[Na_2O(\ell)]} = 2$ (3)

sodium
balance: $n_{[Na(g)]} + n_{(NaO)} + 2n_{[Na_2O(\ell)]} = Z$ (4)

where n is the number of moles of each species present at equilibrium. There are also two equilibrium equations:

$$Na_2O(\ell) \text{ equilibrium: } P^2_{[Na(g)]}P^{1/2}_{(O_2)} = K_1 \quad (5)$$

$$NaO(g) \text{ equilibrium: } \frac{P_{[Na(g)]}P^{1/2}_{(O_2)}}{P_{[NaO(g)]}} = K_2 \quad (6)$$

These five equations are sufficient to define the equilibrium composition of the five species N_2, O_2, Na(g), NaO(g), and $Na_2O(\ell)$. It was assumed that the number of moles of each gaseous component is related to its pressure by the perfect gas law:

$$P_i = n_i \frac{RT}{V} \quad (7)$$

The volume, V, is computed from the initial conditions as the volume per mole of O_2. Calculations were performed for an initial pressure of 12.2 psia (nominal barometric pressure at the National Reactor Testing Station) and 14.7 psia (standard atmosphere). A value of 143 liters was used for the case of 12.2 psia initial pressure and a value of 122 liters was used for the case of 14.7 psia. The gas constant, R, is 0.08206 liter-atm/(mole)(°K). Equilibrium constants K_1 and K_2 are taken from JANAF tables at the trial temperature. In practice, the following equation derived by simultaneous solution of the above expressions was used for the calculations:

$$P_{Na} + \frac{4 - Z}{(RT/V)} = \frac{K_1}{K_2}\frac{1}{P_{(Na)}} + \frac{4K_1^2}{P^4_{(Na)}} \quad (8)$$

The pressures $P_{(O_2)}$ and $P_{(NaO)}$ are then obtained, using $P_{(Na)}$ from the equilibrium equations, and $n_{[Na_2O(\ell)]}$ is obtained from the atomic balances.

The calculated composition at several temperatures is assumed to be the same as the composition at 298°K (25°C). The energy required to reach the trial temperature is

$$E = \sum E_i = \sum n_i\,[H_T - H_{298} - R(T - 298)] \quad (9)$$

which is equivalent to the integral of the heat capacity, C_V, over the temperature difference. The value for the term $H_T - H_{298}$ is taken from JANAF tables. The gas constant, R, is 1.987 cal/(mole)(°K).

The available energy is the sum of the energy of formation of each species at 298°K plus the energy contained initially in the molten sodium. The sodium was assumed to be at a temperature of 700°K (427°C) so that the energy content above 298°K was 3,524 Z cal. The energy of formation of $Na_2O(\ell)$ was 93,996 $n_{[Na_2O(\ell)]}$. From this was deducted 12,904 $n_{[NaO(g)]}$ and 25,164 $n_{[Na(g)]}$ for the endothermic energy of formation of NaO(g) and Na(g), respectively.

Plots were prepared of the energy available and the energy required as a function of trial temperature. The intersection of these curves defined the equilibrium temperature. The partial pressures and total pressure were interpolated from plots of pressure vs. trial temperature. The results are given in Table V-10 and Figure V-38.

The results indicated that the maximum temperature was 1950°C for a mixture consisting of 5 gram

[13] JANAF Thermochemical Tables, The Dow Chemical Co. Midland, Michigan, 1965.

TABLE V-10. CALCULATED ADIABATIC PRESSURES AND TEMPERATURES FOR SODIUM-AIR REACTION

Initial conditions: air, 12.2 psia, 25°C; sodium, 427°C, liquid

Sodium-Oxygen Ratio (gram atoms Na/mole O_2)	Adiabatic Temp. (°C)	Total Pressure		Partial Pressure (atm)			
		(psig)	(atm)	N_2	O_2	NaO(g)	Na(g)
1	1257	49.2	4.18	3.52	0.66	0.002	0.0018
2	1707	67.3	5.40	4.55	0.60	0.08	0.17
4	1902	81.1	6.35	5.00	0.17	0.18	1.00
5	1947	91.6	7.05	5.05	0.07	0.20	1.73
6	1877	97.8	7.49	4.93	0.002	0.02	2.54
7	1660	101.9	7.77	4.44	0.000	0.000	3.33
7.74	1427	98.6	7.54	3.90	0.000	0.000	3.64
8.37	1227	93.8	7.22	3.45	0.000	0.000	3.77
4[a]	1930	97.5	7.47	5.91	0.22	0.22	1.12

[a] Air initially at 14.7 psia.

atoms Na/mole O_2 whereas the peak pressure was 102 psig for a mixture of 7 gram atoms Na/mole O_2. The location of the peak pressure at such a sodium-rich mixture was unexpected. It appears to be due to the effect of oxide dissociation, which suppresses the temperature and pressure in sodium-lean mixtures. Above a sodium content of about 6 gram atoms Na/mole O_2, the calculations are very simple since there are no dissociation products. The mixtures consist of 2 moles $Na_2O(\ell)$, 4 moles N_2, and Z minus 4 gram atoms Na(g). It is only necessary to calculate the energy balance in order to find the adiabatic temperature. The nitrogen pressure is then $4/(V/RT)$, the sodium pressure is $(Z - 4)/(V/RT)$, and the total pressure is $Z/(V/RT)$. Above a sodium content of about 9 gram atoms Na/mole O_2, it is evident that a new equilibrium phase would form, namely $Na(\ell)$. Sodium has a vapor pressure of 6 atm at 1125°C and 2.6 atm at 1000°C,

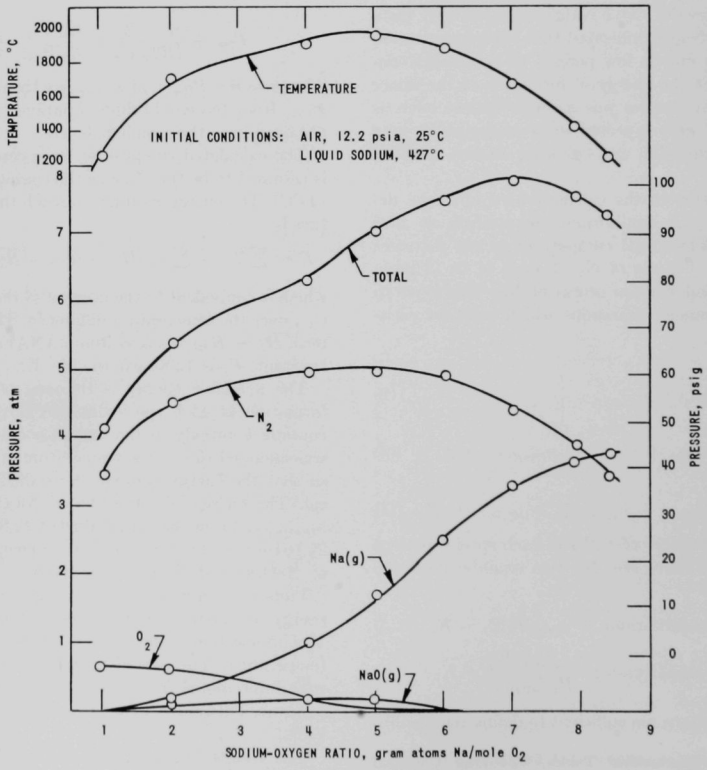

108-9076 T

FIG. V-38. Calculated Adiabatic Pressures and Temperatures for Sodium-Air Reaction.

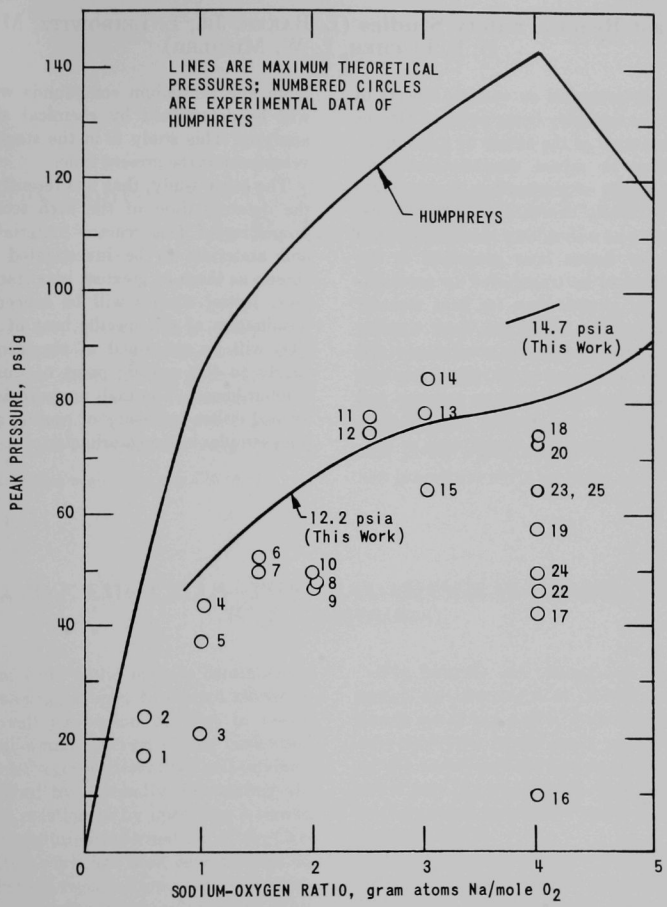

108-9077 T

FIG. V-39. Comparison of Maximum Theoretical Pressures for Sodium-Air Reaction with Data of Humphreys.[11]

so that it is evident that liquid sodium will be present when the temperature approaches 1000°C.

The calculated results are compared with experimental pressures determined by Humphreys[11] in Figure V-39. His experimental pressures exceed our calculated pressures in some cases. However, our calculated curve refers to an initial pressure of less than one atmosphere. A single point calculated for 14.7 psia initial pressure shows a considerably increased pressure which is high enough to encompass the experimental points. In general, it appears that Humphreys' experimental pressures were very nearly the theoretical maximum values. More study of the situation is required since the energy content of the hydrogen-oxygen mixture and the water vapor content of Humphreys' system were not considered in our calculations. The calculated curve should be directly applicable to show maximum theoretical values for a spray-type accident such as might be considered in safety analysis for the Fast Reactor Test facility (FARET). A computer program is under development in order to extend and refine these calculations.

4. Other Fast Reactor Safety Studies (L. Baker, Jr., L. Leibowitz, M. Chasanov, D. F. Fischer, L. W. Mishler)

Two other research programs on various aspects of fast reactor safety are currently being pursued. One of these is the determination of the extent of fuel migration and segregation in mixed uranium-plutonium fuels. A significant degree of segregation in an operating reactor might seriously decrease the effectiveness of Doppler broadening as a shutdown mechanism since the time required for fission heat generated in the plutonium-rich regions to be transferred to uranium-rich regions would be greater than for heat transfer in unsegregated fuel. This additional heat transfer time would delay increased neutron absorption (and decreased reactivity) in a reactor. In this investigation, the behavior of mixed fuels such as uranium and plutonium oxides, carbides, and nitrides under a thermal gradient will be investigated. Segregation of uranium and plutonium compounds within fuel samples will be determined by chemical and metallographic analyses. This study is in the stage of apparatus development at the present time.

The other study, that has recently been initiated, is the determination of the high temperature physical properties of fast reactor materials. The properties and materials to be investigated will be carefully chosen as those of greatest importance in safety analyses. Initial studies will be concerned with the determination of the specific heat of molten UO_2. The UO_2 will be contained in tungsten crucibles heated nearly to the melting point of tungsten by electron bombardment. Thermal measurements will be performed either by means of cooling curves or by dropping samples into a calorimeter.

VI

Energy Conversion[1] (C. E. Crouthamel, J. C. Hesson, A. D. Tevebaugh)

A regenerative emf cell operating in a closed cycle to convert heat to electricity is an attractive energy conversion device. The studies being undertaken at Argonne are concerned with devising regenerative cell systems which can be coupled eventually to a reactor heat source. The principal advantages of these systems are the elimination of most of the moving parts that are found in conventional systems, compactness (a low weight per unit of power output), and a long, maintenance-free life. The applications of such systems might be for remote terrestrial and extraterrestrial power units, energy depots for armed services, and propulsion units for ships and large vehicles.

[1] A summary of this section is given on pages 16 to 17.

A. REGENERATIVE EMF CELLS—PHYSICAL-CHEMICAL LABORATORY STUDIES (C. E. Crouthamel)

Regenerative emf cells would operate continuously in a closed Carnot cycle, subject to Carnot efficiency limits for the overall conversion of heat to useful energy. An emf cell would function in one isothermal leg of a Carnot cycle; regeneration of the cell products could be accomplished by thermally dissociating the products of the cell reaction or by operating a second cell in the high temperature isothermal leg of the Carnot cycle. The initial work has been concentrated on the spontaneous thermal regeneration of the cell products in the systems currently under consideration. This type of regeneration requires the physical separation at high temperature of the anode and cathode reactants. These considerations have led to the study of two types of emf cell for possible application in a regenerative cycle. These are the hydride cell and the bimetallic concentration cells.

The hydride cell consists of an anode of molten metal, an electrolyte of molten salts containing the anode metal ion, and a hydrogen gas cathode. In cell operation, the liquid anode metal is oxidized to ions of the metal and the hydrogen gas is reduced to hydride ions. At the present time, only lithium hydride is of practical interest for application in a regenerative hydride cell.

The bimetallic cells have two liquid metal electrodes in contact with a molten salt electrolyte which contains only the salts of the anode metal. The metals currently under consideration are lithium and sodium for the anode and bismuth, tin, and lead for the cathode. The overall cell reaction is the oxidation of the metallic anode to produce metal ions in the electrolyte, and the reduction of the metal ions in the electrolyte at the cathode to produce an alloy.

1. Lithium Hydride Cell Studies (C. E. Johnson, R. R. Heinrich)

In the lithium hydride cell studies utilizing a lithium anode and a cathode of active metal, the main interest has centered on the cathode because the reaction taking place there is complex. Considerable effort has been directed toward developing a reversible cathode so that the standard emf for the lithium hydride cell,

$$Li(\ell)/LiCl \text{ sat'd with } LiH(s)/H_2(g)\ 1\text{ atm, Fe}$$

could be obtained. The early experimental cells uti-

lized a metal diaphragm cathode (see ANL-6687, p. 196), the diaphragm being submerged beneath the surface of the fused salt electrolyte. As hydrogen diffused through this diaphragm, the electrode functioned and the cell followed the expected Nernst relation. In these cells, hydrogen gas was present above the electrolyte to suppress the thermal dissociation of the lithium hydride in the system. With hydrogen above the electrolyte and in contact with the diaphragm tube, it was noted that the cathode reaction was occurring preferentially at the liquid-gas interface where the metal diaphragm tube penetrated the surface of the melt. (There is no known insulator which will function in this melt without reacting or dissolving.)

As a result of this development, a metal flag cathode at the electrolyte liquid-gas interface was utilized in subsequent work.

Reproducible emf measurements were obtained from cells using the metal flag electrode (ANL-6900, p. 320), and calculations of the standard thermodynamic functions (ΔH_f^o, ΔF_f^o, ΔS_f^o, for lithium hydride formation from emf data compared well with the literature data on lithium hydride obtained calorimetrically.

For a lithium hydride cell using the standard states of pure solid lithium hydride, pure liquid lithium metal, and hydrogen gas at one atmosphere, thermodynamics require that the activity of lithium hydride be less than unity when the electrolyte solution is no longer saturated with lithium hydride. Thus, when the temperature coefficient of the cell emf is obtained over the region where the electrolyte is not saturated with lithium hydride, the slope of a plot of emf *vs.* temperature is less than the slope obtained over the region in which the electrolyte is saturated with lithium hydride. In the first experiments, using a static iron flag electrode, the slope of the emf-temperature curve for the nonsaturated solution was greater than the slope of the saturated solution. With the above thermodynamic analysis, it was recognized that the emf data must be in error.

In searching for an adequate explanation of the difficulty, two hypotheses were considered. First was the possible existence of two immiscible layers of electrolyte in the system, the lighter phase rich in lithium hydride and the heavier phase rich in lithium chloride. A second hypothesis held that the cell emf was lowered by either polarization of the cathode by dissolved lithium metal or electronic conduction due to high concentrations of lithium metal in the electrolyte.

The postulate concerning immiscible liquids was tested by setting up a cell with a flat-type cathode, a lithium anode, and an electrolyte [LiH(sat.)-LiCl] which could be stirred at a variety of speeds. A comparison of the cell voltage with rate of speed of the stirrer indicated that the greater the rate of stirring, the lower the cell emf. The general characteristics of the emf-temperature data remained unchanged. From this experiment, it became evident that immiscibility was not a problem in this system. However, it was noted that the consumption of lithium metal was abnormally high during the course of the stirring, so that the lower cell voltage could be due to dissolved lithium metal leading to polarization of the cathode, to electronic conduction, or to a combination of both effects.

Since the flat type cathode did not given satisfactory results, the design of the cathode was changed. In a new cell, the cathode was an Armco iron cap welded to a stainless steel tube, enabling pure hydrogen gas to bubble over the catalytic iron surface. In actual operation, the bubble cap is located beneath the surface of the electrolyte. This design permits a clean active surface to be present at all times and eliminates questions about miniscus or surface effects associated with the flag electrode. Emf-temperature data for a cell using a 50 m/o LiH-50 m/o LiCl electrolyte are given in Figure VI-1. This electrolyte is not saturated with lithium hydride above a temperature of 564°C. The broken line on the figure represents an extrapolation of the data obtained for the saturated region.

As can be seen from these data, the new cathode arrangement does give emf-temperature slopes which have the proper relationship between the lithium hydride-saturated and -unsaturated electrolytes. Additional experiments with electrolytes of 45 m/o and 60 m/o LiH in LiCl gave similar results.

For the cells with the higher lithium hydride compositions (50 to 60 m/o LiH), it was noted that after the cell had been cycled through the high temperature unsaturated region, the previous emf data obtained in the LiH-saturated region could not be reproduced. These subsequent measurements always yielded emf values which were 6 to 10 mv lower than the initial values. It was assumed that this was caused by the increased solubility of lithium metal in electrolytes containing high concentrations of lithium hydride. The electrolyte was then scavenged for approximately 16 hr with pure hydrogen gas to convert the dissolved lithium metal to lithium hydride. After such treatment, the cell emf in the LiH-saturated region agreed well with the initial data.

Another problem caused by the presence of excess lithium metal in the electrolyte was discovered on examination of the emf-temperature data for each individual cell. The examination revealed that the temperature coefficient, $(\partial E/\partial T)_P$, became progressively more negative as the lithium hydride concentration in

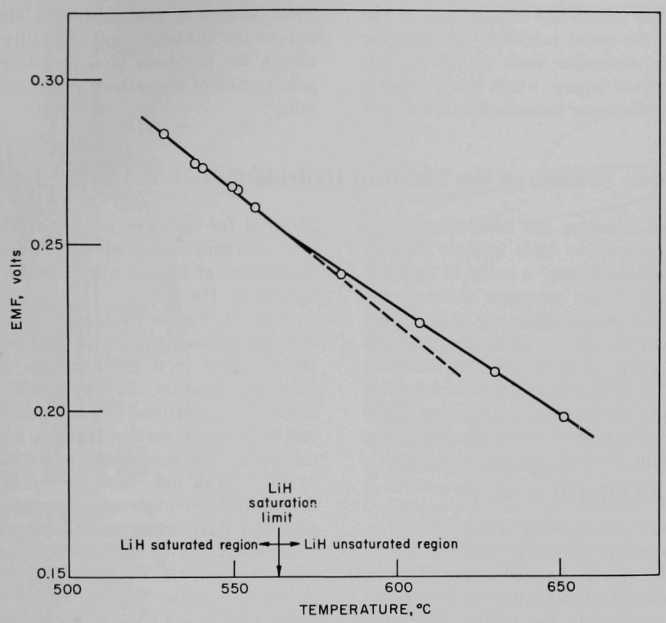

108-9108

FIG. VI-1. Lithium Hydride Cell: Emf vs. Temperature.

Open lithium anode
Bubbling iron flag cathode (H_2 = 760 mm)
Electrolyte, 50 m/o LiH-50 m/o LiCl

the electrolyte was increased. This type of behavior would be expected if the lithium metal solubility in the electrolyte increases as the operating temperature of the cell is increased.

Experiments designed to restrict the rate at which lithium metal could diffuse into the electrolyte were carried out on cells in which a cover with a small (1/32 in. dia.) hole was placed over the lithium metal anode. Diffusion of dissolved lithium metal out of the anode into the electrolyte was now severely restricted and the temperature coefficient for this cell was more negative than before, but quite reproducible. This result is consistent with the hypothesis that a diffusion potential was superimposed on the cell emf by the use of the covered anode. Experiments in which the potential of the covered lithium electrode was measured with reference to an open lithium electrode in a LiH(sat.)-LiCl electrolyte resulted in measured diffusion potentials varying from 1 mv at 520°C to 22 mv at 600°C. These diffusion potentials were used to correct the emf data of cells with covered anodes. Calculations of the standard thermodynamic functions (ΔF_f^o, ΔH_f^o, ΔS_f^o) made from these corrected emf data compare favorably with existing literature values[2, 3] obtained calorimetrically.

In reviewing the data and results thus far, it appears that further experimental work will have to proceed along one or both of the following paths. The first alternative is to extend the data to regions of higher lithium hydride compositions using cells with covered anodes. This approach suffers somewhat from the fact that the lithium diffusion potential at a given temperature becomes larger as the lithium hydride composition is increased. It also appears that with increasing temperature, the problems associated with lithium metal solubility rapidly become more pronounced. The second alternative is to continue using

[2] C. E. Messer and L. G. Fasolino, Report NYO-3956, March 1954.

[3] S. R. Gunn and L. G. Green, J. Am. Chem. Soc. **80**, 4782 (1958).

an open anode but to reduce the temperature of the cell and, therefore, the metal solubility by changing to a lower melting electrolyte such as the lithium bromide-lithium hydride binary, which has a eutectic melting at 453.3°C. The lower temperatures associated with the use of this electrolyte should considerably reduce the lithium metal solubility and thereby diminish the problems of electronic conduction and/or polarization of the cathode associated with metal solubility.

2. Voltammetric Studies of the Lithium Hydride Cell (J. P. Elder,[4] J. A. Plambeck[5])

Since considerable attention has been directed towards thermally regenerative ionic hydride cells as direct energy conversion devices,[6] a study of the electrochemistry involved in the operation of these cells is of interest. Such an investigation has been carried out on a lithium hydride cell by employing the solid microelectrode voltammetric technique. The resulting data not only yield current-voltage characteristics for an operating cell but may be discussed in terms of the modern concepts of electrode kinetics. The configuration of the cell used in these studies was as follows:

$$Li^{o}(\ell)/LiCl\text{-}KCl,\ LiH/H_2(g),\ Fe$$

The experiments were carried out at 375°C.

A diagram of the cell employed is shown in Figure VI-2. The two lithium cup electrodes and the two stainless steel-sheathed thermocouples are symmetrically located with respect to the central indicating microelectrode of pure iron, which is supported by the pin vise. The magnitude of the disparity between the area of the microelectrode and that of the lithium cup electrode is such that, for the minute currents which pass through the cell, the latter electrode remains completely unpolarized. Thus, a single cup electrode may be employed in a dual capacity for voltammetric studies, namely, as a second working electrode and a reference electrode.

The LiCl-KCl eutectic served as the electrolyte and in some studies was saturated at 375°C with lithium by immersing a fiber metal sponge soaked with lithium metal in the melt for several days prior to use.

Curves A and B in Figure VI-3 show the current-potential relationships for experiments with pure electrolyte and lithium metal-saturated electrolyte, respectively. A helium atmosphere of high purity was used in both experiments.

The section of curve B, Figure VI-3, from zero to +0.6 volt is interpreted as characteristic of the oxidation of soluble lithium metal. The succeeding step appears to be characteristic of the oxidation of soluble magnesium metal used in the salt purification.

Curve C, Figure VI-3, shows the polarization data obtained for the same sample of lithium metal-saturated electrolyte, but which had been held under one atmosphere of hydrogen for two days to form lithium hydride in the salt.

Curve B, Figure VI-4, is the current-voltage relationship for an unsaturated lithium hydride solution (8.1×10^{-2} m/o LiH) in the LiCl-KCl eutectic fused salt mixture. As the applied voltage is made increasingly positive (forward polarization), at +0.40 volt the cathodic current begins to approach zero fairly rapidly and becomes anodic at +0.42 volt as indicated by the broken line. Between +0.48 and +0.52 volt, the anodic current becomes unstable, slowly falls to zero, and then reverses, attaining the cathodic value commensurate with the extrapolation of the pre-peak curve. Beyond this region steady currents are again observed until the limiting anodic region is reached. From +0.7 to +2.1 volt, random current fluctuations are observed, indicating random variation of the active electrode area as a result of bubble formation during hydrogen gas evolution. On the return excursion (reverse polarization), curve B is retraced until the unstable region is reached. Behavior analogous to that observed during forward polarization but in a cathodic direction is now observed in this region. If sufficient time is allowed for a steady state condition to be attained at each potential setting during reverse polarization, this cathodic dip disappears. However, the anodic peak is always in evidence. Finally, at +0.34 volt, the curve merges with that obtained during forward polarization.

Curve A, Figure VI-4, is the current-voltage relationship for a saturated lithium hydride solution (about 5.0 m/o LiH). Stable currents are observed throughout except for the random fluctuations in the anodic hydrogen evolution region. As the concentration of LiH in the electrolyte is increased, curve B approaches curve A. The unstable peaking effect is observed until the electrolyte is saturated with LiH. In the unstable region, for both forward and reverse polarization, the value of the potential at the point of maximum current increase remains constant at +0.42 volt. Similar behavior was observed when the iron microelectrode was replaced by a tungsten microelectrode of about the same size.

The shape and position of curve C, Figure VI-3, is

[4] Post-doctoral Fellow.

[5] Graduate student, University of Illinois.

[6] R. C. Werner and T. A. Ciarlariello, U.N. Geneva Conference on New Sources of Energy, 35/Gen/14 (May 23, 1961).

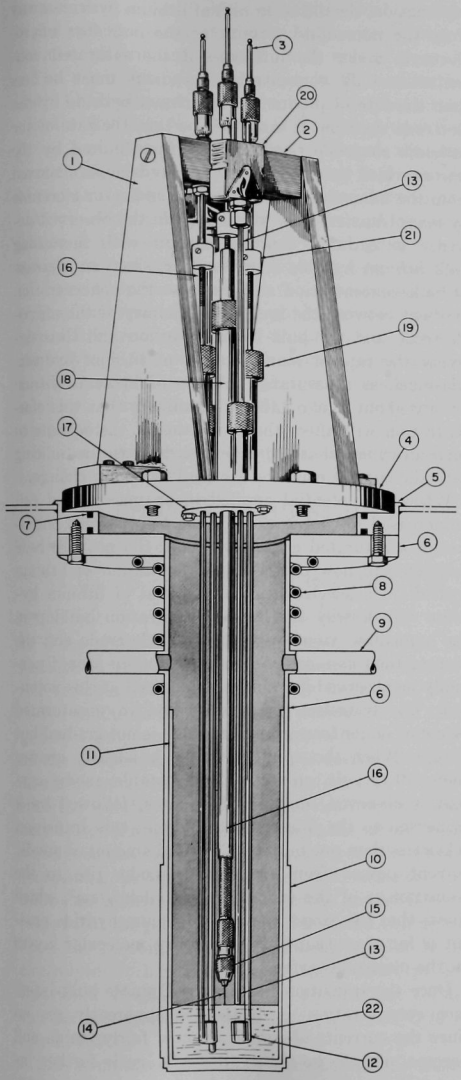

108-8966

FIG. VI-2. Schematic Diagram of Molten Salt Cell. (1. Aluminum depth gauge support; 2. Micarta insulating bar; 3. Micrometer depth gauge; 4. Cell head base; 5. Base of dry-box; 6. Furnace well; 7. "O" ring seal; 8. Water cooling coils; 9. Gas inlet; 10. Copper sheath; 11. Crucible; 12. Lithium cup electrode; 13. Thermocouple; 14. Wire microelectrode; 15. Pin vise; 16. Electrode lead rod; 17. Insulating disk; 18. Nylon-lined brass tube; 19. Insulating vacuum coupling; 20. Thermocouple connector block; 21. Nylon insulating connector; 22. Electrolyte.)

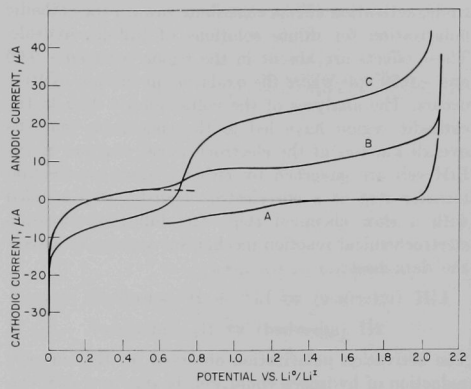

108-8968

FIG. VI-3. Voltammetric Data for the Lithium Hydride Cell. (LiCl-KCl eutectic, 375°C, iron microelectrode.)

A. Electrolyte alone, helium atmosphere
B. Lithium-saturated electrolyte, helium atmosphere
C. Lithium-saturated electrolyte with hydrogen atmosphere, 760 mm Hg

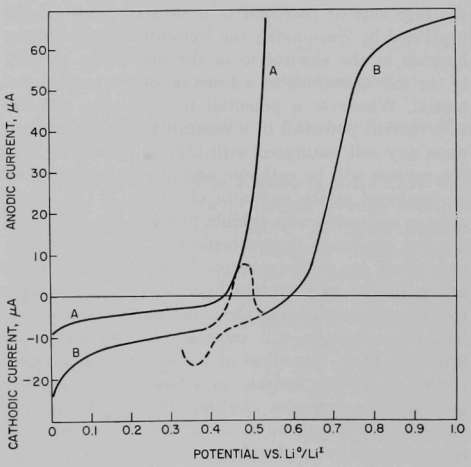

108-8967

FIG. VI-4. Voltammetric Data for the Lithium Hydride Cell. (LiCl-KCl eutectic, 375°C, iron microelectrode.)

A. Lithium hydride-saturated electrolyte, hydrogen atmosphere, 760 mm Hg.
B. Unsaturated electrolyte 8×10^{-2} m/o LiH, hydrogen atmosphere, 760 mm Hg.

characteristic of the lithium hydride-hydrogen system, as can be seen by a comparison of this curve with curve B, Figure VI-4. In the region between zero and +0.66 volt vs. the lithium-lithium ion reference elec-

trode, activation effects contribute toward the cathodic polarization for dilute solutions of lithium hydride. These effects are absent in the region between +0.66 and +0.70 volt where the oxidation of lithium hydride occurs. The analyses of the voltammetric data in the cathodic region have led to the conclusion that the overall kinetics of the electrochemical reaction of the LiH cell are governed by either a slow one-electron transfer step or a one-electron transfer step coupled with a slow chemical step. The following two-step electrochemical reaction mechanism appears to satisfy the data best:

$$\text{LiH (interface)} \rightleftarrows \text{Li}^+ + \text{H (adsorbed)} + e^-$$

$$2\text{H (adsorbed)} \rightleftarrows \text{H}_2 \text{ (interface)}$$

The activation polarization observed for the cathodic reduction of hydrogen could well be due to a slow dissociation of molecular hydrogen to atomic hydrogen adsorbed on the electrode surface, which would necessarily precede the electrochemical reduction and thus govern its rate. The nature of the adsorbed species is not known.

The peaking behavior of the current in unsaturated lithium hydride cells at the potential corresponding to the zero current potential of a saturated cell can be explained by considering the concentration of lithium hydride in the electrolyte in the immediate vicinity of the microelectrode as a function of the applied potential. Whenever a potential between zero and the zero current potential of a saturated cell is impressed upon any cell, saturated with lithium hydride or not, the current will be cathodic and lithium hydride will be produced at the indicator electrode. If the cell is already saturated with lithium hydride, the additional amount produced electrochemically will presumably precipitate out of the solution. If, however, the cell is not saturated with lithium hydride, then the lithium hydride concentration in the immediate vicinity of the indicator electrode will increase until saturation is attained. Thus, regardless of the actual bulk concentration of lithium hydride, over this range of applied potential the indicator electrode of any lithium hydride cell will respond as if it were immersed in a saturated solution and will produce polarization curves characteristic of a saturated cell.

In order to postulate such a local buildup in the lithium hydride concentration as is required by this explanation, the diffusion rate of lithium hydride away from the immediate vicinity of the indicator microelectrode under the influence of the saturated concentration-bulk concentration gradient must be less than the rate of production of lithium hydride by the electrode reaction. It may well be that the rate of the cathodic electrode reaction is in fact limited by the rate at which the product, lithium hydride, is removed from the immediate vicinity of the indicator electrode by mass transfer. This would explain the observed decrease in cathodic limiting current with increasing bulk lithium hydride concentration, since an increase in bulk concentration will decrease the concentration gradient between the immediate vicinity of the microelectrode and the bulk of the solution and thus decrease the rate of mass transfer of lithium hydride. Inasmuch as a saturated solution of lithium hydride is only about 5 m/o LiH, it is unlikely that this concentration will affect the properties of the solvent to such an extent that the observed decrease in limiting cathodic current could be ascribed to such a change.

When the potential applied to an unsaturated cell is increased so that it exceeds the zero current potential of a saturated cell, +0.42 volt, the net electrode reaction will now be the anodic oxidation of lithium hydride. The electrochemical removal of lithium hydride will destroy the local concentration buildup in the immediate vicinity of the microelectrode and the current then assumes a cathodic value as would normally be observed in an unsaturated cell at this potential. The transition from saturated to unsaturated behavior under forward polarization is not gradual but abrupt. When the applied voltage is slightly greater than +0.42 volt, an initial fairly stable anodic current is observed for several minutes, followed by a transition to the final cathodic value; this transition takes less than one minute. The total amount of anodic current passed from the initial anodic rise to the transition is of the order of one coulomb/cm^2, which shows that the excess amount of lithium hydride present is far more than just one or two molecular layers on the electrode surface.

Once the transition has occurred, stable bulk-interface concentration gradients are apparently set up since the currents observed are now fairly stable and become more so as the applied voltage is further increased.

3. Intermetallic Systems

a. SODIUM-BISMUTH SOLUBILITY STUDIES

(M. S. Foster, R. Eppley)

The first regenerative emf cell chosen for engineering evaluation is the sodium-bismuth bimetallic concentration cell. The bimetallic concentration cell, in general, consists of two liquid metal electrodes in

contact with a fused salt electrolyte which is stable in the cell environment, particularly with respect to the more electropositive metal in the anode.

The electrolyte chosen for use in the sodium-bismuth bimetallic concentration cell was the ternary eutectic 53.2 m/o NaI-31.6 m/o NaCl-15.2 m/o NaF. It has a melting point of 530°C which sets the lower limit for the cell operating temperature. It is desirable to maintain a liquid electrolyte and liquid metal electrodes to achieve high current densities and low polarization in the cell. Solid electrolytes, in general, have a high internal impedance to current flow, especially at lower temperatures. Since the temperature coefficient of the emf is usually negative, higher cell voltages will be realized at lower temperatures. The ideal electrolyte is one with a low melting point and one which is compatible with the cell environment at the minimum temperature necessary to liquify the cell components.

The sodium-bismuth bimetallic concentration cell may be represented as:

$$Na(\ell)/NaI\text{-}NaCl\text{-}NaF(\ell)/Na \text{ in } Bi(\ell)$$

and the overall cell reaction is:

$$Na \text{ (liquid)} \rightarrow Na \text{ dissolved in cathode alloy of Na and Bi (liquid)}.$$

It is the unusually strong interaction of sodium and bismuth in the cathode alloy which produces useful cell voltages. The strength of the interaction is reflected in the formation of solid stoichiometric intermetallic compounds in the cathode alloy, e.g., Na_3Bi, as the concentration of sodium is increased. In the operation of a bimetallic concentration cell, it is possible that soluble sodium metal species from the anode may diffuse through the electrolyte to the cathode. Conversely, soluble intermetallic species from the cathode (containing in this case sodium and bismuth) may diffuse through the electrolyte to the anode. It is expected that the rate of transfer of material will depend upon the solubility of the diffusing species in the electrolyte. It has been shown (ANL-6925, p. 239) that solid Na_3Bi solubility in the molten ternary eutectic mixture ranges from 1.2 m/o at 552°C to 8.5 m/o at 839°C.

The solubilities of sodium-bismuth species from a 55 a/o Na-Bi alloy in the molten ternary eutectic mixture have been measured. According to the phase diagram given by Hansen,[7] this alloy consists of solid Na_3Bi and a liquid phase in the temperature region from 550 to 600°C and a single liquid phase at higher temperatures.

[7] M. Hansen and K. Anderko, *Constitution of Binary Alloys*, McGraw-Hill Book Co., New York, N.Y., 1958, p. 322.

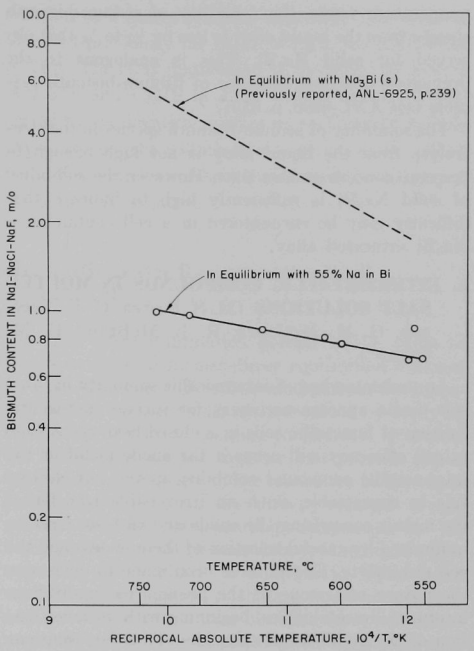

108-9111

FIG. VI-5. Relative Solubility of Bismuth in Eutectic Mixture of NaI-NaCl-NaF.

Samples of the eutectic mixture in equilibrium with the liquid metal alloy were filtered through tantalum frits at temperatures up to 600°C. At higher temperatures, samples were taken directly in sampling buckets. The results of the analyses (methods of analysis were described in ANL-6925, p. 239) are shown in Figure VI-5 and indicate solubilities of bismuth ranging from 0.7 m/o at 550°C to ~1.0 m/o at 750°C. The observed Na:Bi ratio was 2.71 ± 0.19 at temperatures up to 600°C and 2.89 ± 0.41 at higher temperatures. Also shown in Figure VI-5, for purposes of comparison, are the previously reported data for the case of $Na_3Bi(s)$ in equilibrium with the same ternary eutectic mixture.

It is interesting to note that the solubilities of bismuth from 55 a/o Na-Bi below 600°C are approximately 50% of the values observed previously for pure solid Na_3Bi. It was anticipated that these solubilities would be equal, since the 55 a/o Na-Bi alloy should be saturated with solid Na_3Bi at these temperatures. These data indicate that the solubility data given by Hansen for Na_3Bi in $Bi(\ell)$ may be somewhat high.

It also appears from these data that for the entire

temperature range, the solubility of sodium-bismuth species from the liquid alloy is less by ½ to ⅙ that observed for solid Na_3Bi. This is analogous to the previously observed behavior of lithium-bismuth systems (see ANL-6900, p. 310).

The solubility of sodium-bismuth species in the electrolyte from the liquid alloy is not high enough to warrant concern at this time. However the solubility of solid Na_3Bi is sufficiently high to indicate that difficulty may be encountered in a cell containing a Na_3Bi saturated alloy.

b. INTERMETALLIC COMPOUNDS IN MOLTEN SALT SOLUTIONS (M. S. Foster, C. E. Johnson, G. H. McCloud, R. L. McBeth,[8] D. M. Gruen[8])

An understanding of intermetallic solubility in fused salt media appears necessary for success in the utilization of bimetallic cells in a closed heat cycle. Loss in cell efficiency will occur if the anode metal or the intermetallic compound solubility in the cell electrolyte is appreciable. Such an irreversible transfer of the metals comprising the anode and cathode must be minimized by careful selection of these metals and the cell electrolyte. Efforts have been made to determine the nature and scope of the phenomena involved in intermetallic solubilities, beginning with an investigation of the alkali metal tellurides. Thus far, solutions of the tellurides in molten salt solvents have been studied by means of absorption spectra. Further spectral work has revealed anomalies in the results reported previously for solutions of the alkali tellurides in fused cesium chloride.

The following absorption spectra in the range 300 to 2500 mμ were previously reported: (a) a solution of Li_2Te in CsCl at 700°C exhibited peaks at ~465 mμ and ~635 mμ (see ANL-6900, p. 312), (b) a solution of Cs_2Te in CsCl at 700°C exhibited two peaks at these same wavelengths (see ANL-6900, p. 313), and (c) a solution of Na_2Te in CsCl exhibited shoulders at ~500 mμ and ~570 mμ (see ANL-6925, p. 240). The molar extinction coefficients reported for Li_2Te, Na_2Te, and Cs_2Te in CsCl were 605, 602, and 838, respectively (see ANL-6925, p. 240). In all of the preceding work, the CsCl salt originated from Penn Rare Metals, Inc., and was labeled "99% CsCl." When the concentration of Cs_2Te in the CsCl (Penn) was varied, it was discovered that a concentrated solution exhibited only one peak (at ~550 mμ) in contrast to the two peaks previously observed (at 465 and 635 mμ). Furthermore, solutions of tellurium metal in CsCl (Penn) exhibited the same spectrum as Li_2Te and Cs_2Te in this salt.

[8] Chemistry Division, ANL.

Because of these anomalous results, a check was made of some of the physical and chemical properties of this CsCl.

Emission spectra analyses on samples from two lots of CsCl (Penn) showed no unusual quantities of impurities. A portion of each lot of CsCl was purified by treating the molten salt with chlorine gas and then flushing with helium. Thermal analysis curves were obtained for material from both lots before and after purification. Material from the first lot froze at 638°C before purification and 640°C after purification (freezing point of CsCl = 645°C).[9] The thermal analysis curves for this sample were typical of curves usually obtained for single component systems. Material from the second lot yielded cooling curves typical of a two-component mixture. Before purification, the curve showed a break at 628°C and after purification, a break at 630°C. In both cases, a eutectic halt was noted at 456°C.

Cesium chloride of 99.9% purity was obtained from Atomergic Chemetals, Inc. Emission spectra analysis of this material showed no significant quantity of impurities. Thermal analysis of the material without purification yielded a freezing point of 644°C.

The spectra of both dilute and concentrated Cs_2Te solutions in the 99.9% CsCl at 675°C exhibited a single peak at 555 mμ in addition to the charge transfer band edge. The molar extinction coefficient of Cs_2Te based on an analysis of the more concentrated sample (1.57×10^{-2} w/o tellurium) was calculated to be 579.

The spectrum of Li_2Te in CsCl (Atomergic) at 675°C exhibited a single peak at 550 mμ in addition to a charge transfer band edge. The molar extinction coefficient for a dilute solution (4.3×10^{-3} w/o Te) was calculated to be 591, whereas a more concentrated solution (2.6×10^{-2} w/o Te) yielded a value of 613.

Tellurium was dissolved in molten CsCl (Atomergic) at 671°C. The resulting solution (1.28×10^{-2} w/o Te) was examined spectrophotometrically and the spectrum of tellurium in CsCl solution observed. This spectrum exhibits prominent peaks at 645 and 470 mμ, a minor peak at 1050 mμ, and a charge transfer band edge.

The absorption spectrum of Na_2Te dissolved in CsCl has not yet been reexamined with the pure CsCl from Atomergic.

It seems reasonable to postulate that the CsCl (Penn) previously used contained an impurity which oxidized the alkali metal tellurides to free tellurium. The spectra observed for Cs_2Te, Li_2Te, and Te in CsCl (Penn) were essentially identical.

[9] L. Brewer, "Fusion and Vaporization Data of the Halides," *Chemistry and Metallurgy of Miscellaneous Materials: Thermodynamics*, L. L. Quill, ed., National Nuclear Energy Series IV-19B, McGraw-Hill Book Co., New York, N.Y., 1950, pp. 196–197.

Additional spectral work has been done on solutions of tellurides in salts other than CsCl. Tellurium was dissolved in purified LiCl at 627°C. The resulting solution ($<5 \times 10^{-4}$ w/o Te) was not colored and yielded no absorption spectrum. Thus, the solubility of tellurium in LiCl is very low when compared with that observed for tellurium in CsCl, as given above.

Cs_2Te dissolved in purified LiCl yielded a spectrum at 650°C with an absorption peak at ~470 mμ in addition to a charge transfer band edge (the same as observed previously for Li_2Te in LiCl, see ANL-6925, p. 240). The clear implication of the identical spectra of Li_2Te and Cs_2Te in LiCl (which is further suggested by the identical spectra of Li_2Te and Cs_2Te in CsCl) is that the metathetical reaction of the alkali metal associated with the tellurium and the alkali ion in the melt is complete.

4. Liquid-Vapor Equilibria in the Sodium-Bismuth Regenerative Cell

(A. K. Fischer, S. Johnson)

Knowledge of the temperature-pressure-composition relationships in the liquid-vapor equilibria is necessary to optimize working conditions in the regeneration portion of the operating cycle of the sodium-bismuth bimetallic cell. The data required to delineate these relationships are total pressure (P) and the vapor composition (y) over a liquid phase of composition (x) at temperature (T). Complementary techniques are being used to provide this information; both ebulliometry (boiling point measurements) and the Rodebush-Dixion procedure[10] yield data for P, x, and T; transpiration experiments provide data for P, y, and x. These data are sufficient for constructing a phase diagram and for calculating activities of the components in the liquid phase.

Theoretical treatments of liquid-vapor equilibria by methods based on the Gibbs-Duhem relationship have resulted in computational techniques whereby P-x data for the system, along with knowledge of the heat of vaporization and vapor pressure of a reference substance, suffice for the calculation of y for the system. The treatment devised by Othmer[11] is one such computational technique. For a system as nonideal as the sodium-bismuth system, it is desirable to measure y as well as P and x (which permits construction of a phase diagram) and to use the Othmer calculations as a test of consistency.

By combining the results of the ebulliometric and transpiration experiments, it is possible to calculate partial pressures for the vapor species. It can be shown that for two component systems in which the vapor species are monomers and dimers, as in the sodium-bismuth system, data from total pressure and transpiration measurements may be combined to yield partial pressures for each of the four vapor species.[12] The only extra information needed is the value of the vapor phase monomer-dimer equilibrium constant for each component. This is available from the literature or may be independently determined by applying this dual procedure to the pure components. Thus, the two techniques applied together can provide values for the partial pressures of the monomers in the vapor phase; these, in turn, are directly related to the activity of the corresponding component in the liquid phase. Thermodynamic data for the liquid phase may thus be obtained, in addition to liquid-vapor equilibrium information. Such data would complement and extend the information obtained from emf measurements in the liquid phase at lower temperatures.

a. EBULLIOMETER

A diagram of the ebulliometer appears in Figure VI-6. Because of the reactivity of sodium, operations are performed in a helium-filled glovebox. A heating well is bolted to the floor of the box; inside the well, there is a sample container of sufficient length so that the open end extends up into the cool region of the well. The heart of the system is the Cottrell pump, which operates on the same principle as the coffee percolator. Bubbles of vapor generated in the funnel rise in the tube and carry slugs of liquid between them. These are squirted through the orifice against the thermocouple well, thereby allowing liquid-vapor equilibrium temperature to be established at a particular pressure. The system pressure is maintained by a Cartesian diver manostat inside the glovebox.

A measurement is made by setting the system pressure and adjusting the furnace heat input so that the boiling point of the liquid may be reached. When the temperature in the thermocouple well becomes steady while the furnace temperature is rising, this is taken as the first indication that a boiling point has been reached. The furnace temperature is stabilized at this point, and then the system pressure is increased slightly. A rapid rise of the thermocouple reading at

[10] W. H. Rodebush and A. L. Dixon, Phys. Rev. **26**, 851 (1925).

[11] D. F. Othmer, H. G. Ricciardi, and M. S. Thakar, Ind. Eng. Chem., **45**, 1815 (1953).

[12] C. Beusman, Activities in the KCl-$FeCl_2$ and $LiCl$-$FeCl_2$ Systems, ORNL-2323, 1957.

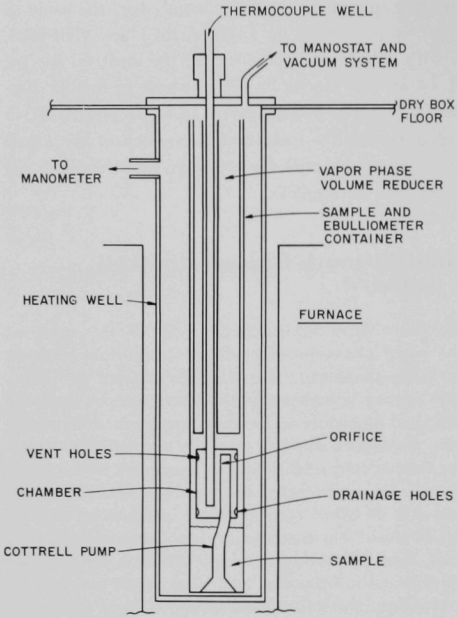

108-9098

Fig. VI-6. Ebulliometer Apparatus.

this point is taken as confirmation that a boiling point was being observed prior to the pressure change.

b. TRANSPIRATION APPARATUS

Figure VI-7 depicts the transpiration apparatus. Four tubes extend down into the large sample container. One of these, not shown, is closed at the lower end and is a thermocouple well for measuring the temperature of the gas phase. Tube 1 is a thermocouple well and stirrer. It also has a sampling cup, 6, attached to a splash shield, 5. Tube 2 is the inert gas carrier inlet, and tube 3 is the vapor sample condensing and collecting tube. During a run, tube 1 is rotated occasionally to stir the melt with the paddle, 4. While the apparatus and sample are coming to temperature, a slow stream of the argon carrier gas is passed into tube 3 and out tube 2, a direction of flow opposite to that in effect during a run. At time zero, when the run starts, the flow direction is reversed so that argon passes into tube 2 and out tube 3. In its passage through the vapor region, the carrier gas picks up vapor and carries it up tube 3 into the cool zone where the vapors condense and the carrier gas passes on. After leaving tube 3 the carrier gas volume is accu-

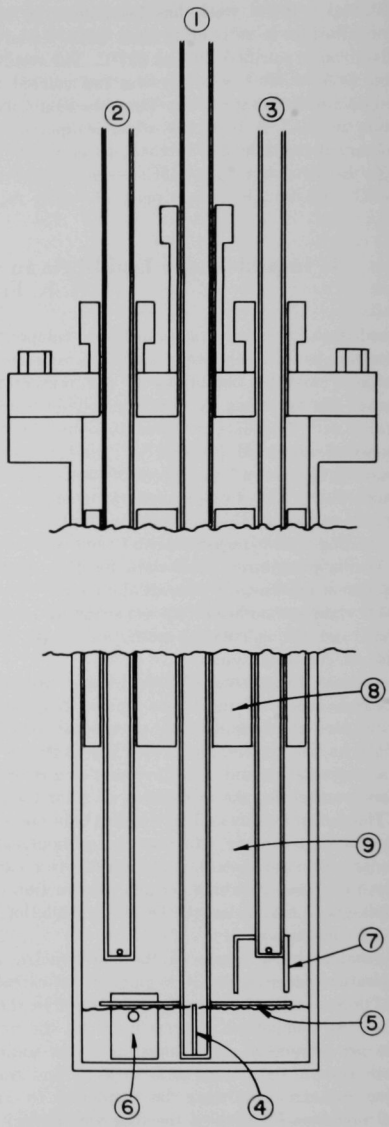

108-9112

Fig. VI-7. Transpiration Apparatus. (1. Thermowell; 2. Carrier gas inlet tube; 3. Condensation tube; 4. Paddle blade; 5. Splash shield; 6. Liquid phase sampling cup; 7. Drip deflector; 8. Channeled can; 9. Vapor region.)

rately measured with a wet test meter. At the end of a run, all tubes are raised in order to raise cup 6 out of the melt, thereby sampling the liquid phase at temperature. The entire assembly is then quenched. The condensate in tube 3 is analyzed to determine the masses of sodium and bismuth transported. These results represent the vapor composition. The transpiration technique requires that several experiments be done at different carrier gas flow rates in order to insure that an equilibrium vapor sample is being collected. The so-called plateau test provides this assurance: if over a range of flow rates the calculated partial pressure remains constant, then equilibrium vapor has been sampled.

TABLE VI-1. Results of Ebulliometric Measurements on Sodium-Bismuth Alloys

Alloy Composition (a/o Bi)	Temperature (°K)	Vapor Pressure of Pure Sodium (mm)	Observed Total Pressure over Alloy (mm)
9.98	958.2	86.25	85.25
	1014.8	174.52	175.80
	1037.9	227.94	230.60
	989.2	128.06	128.50
	1023.9	194.25	194.00
	1076.4	347.82	348.10
	1114.8	516.10	514.30
14.96	1079.2	358.2	367.70
	1085.4	382.4	392.95
	1089.7	399.8	414.75
	1103.2	459.4	471.75
	1041.9	238.5	244.20
	1049.2	258.8	265.65
	1057.7	284.4	291.85
	1064.4	305.7	313.10
	1020.7	187.1	189.45
	1027.0	201.2	204.55
	1035.4	221.6	225.85
	1041.7	237.9	242.80
	1116.7	525.8	541.90
	1122.4	553.9	569.35
	1129.6	596.6	611.30
	1141.4	668.7	684.55
18.75	973.7	105.6	105.55
	978.9	112.6	113.45
	985.2	121.8	122.85
	990.9	130.7	132.40
20.11	1097.7	434.1	446.2
	1115.2	518.0	530.6
	1118.7	536.3	547.5
	1084.9	380.5	389.7
	1090.9	404.7	414.6
	1098.2	436.3	444.4
	1105.5	469.9	479.6

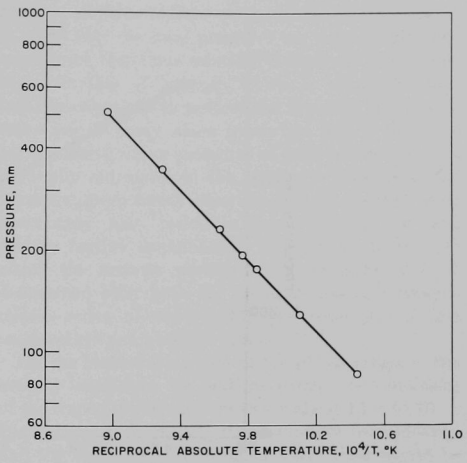

108-9114

Fig. VI-8. Total Vapor Pressure over Sodium-9.98 a/o Bismuth Alloy.

Partial pressures, p_v, are calculated from the equation

$$p_v = \frac{n_v}{n_v + n_g} P_{tr}$$

where n_v and n_g are the measured moles of vapor and carrier gas, respectively, and P_{tr} is the pressure inside the transpiration apparatus, which is essentially atmospheric pressure. The value of n_v is based on a knowledge of the molecular weight of the vapor in question. To apply the plateau test, an assumed molecular weight suffices. To get partial pressures for the actual species, the combined transpiration-total pressure method discussed earlier must be applied.

c. RESULTS

The ebulliometer was used to measure the vapor pressure of pure sodium in the temperature range 913 to 1152°K. A computer least squares fit of the data yielded the equation

$$\log p^{o}_{\mathrm{Na}}\ (\mathrm{mm}) = -4394.92/T + 0.50693.$$

The agreement with the Ditchburn-Gilmour equation in the literature[13] was excellent. The normal boiling point of sodium calculated from our equation is 1154.8°K whereas the value 1154°K was selected by Dunning (ANL-6246) as the "best" literature value.

[13] R. W. Ditchburn and J. C. Gilmour, Rev. Mod. Phys. **13**, 310 (1941).

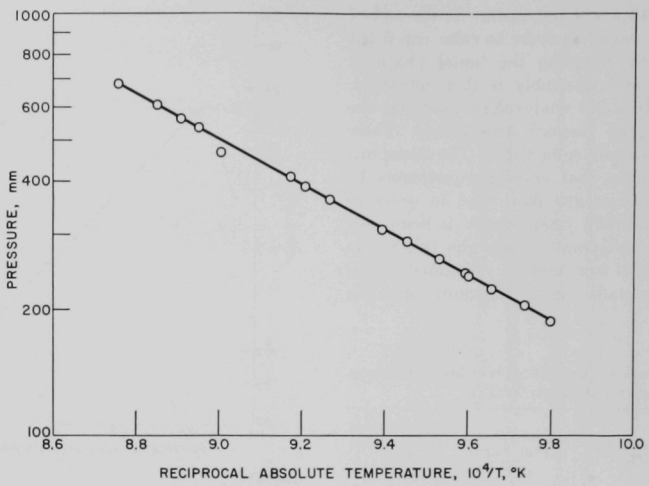

108-9099

FIG. VI-9. Total Vapor Pressure over Sodium 14.96 a/o Bismuth Alloy.

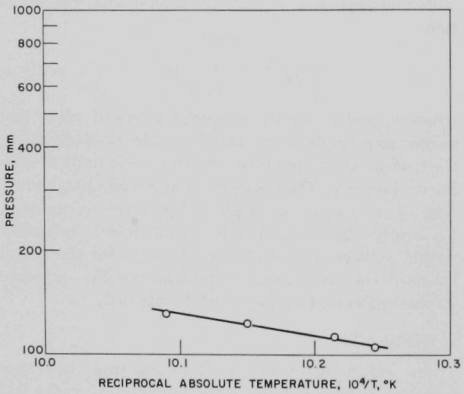

108-9100

FIG. VI-10. Total Vapor Pressure over Sodium-18.75 a/o Bismuth Alloy.

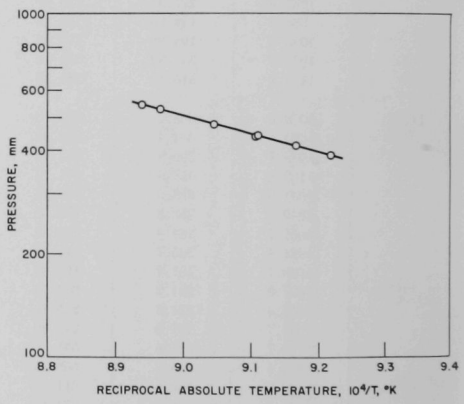

108-9106

FIG. VI-11. Total Vapor Pressure over Sodium-20.11 a/o Bismuth Alloy.

Total pressure measurements were made ebulliometrically on alloys of nominal 10, 15, 18.75, and 20 a/o bismuth in sodium. The results appear in Table VI-1 and are plotted in Figures VI-8, VI-9, VI-10, and VI-11.

Results for transpiration experiments with 60 and 80 a/o bismuth in sodium systems at 1175°K are tabulated in Table VI-2.

Since the pressure and temperature conditions for ebulliometer and transpiration experiments have not yet overlapped, it has not been possible to calculate activities with the available data. The ebulliometer design imposes a lower pressure limit of operation because of the hydrostatic head of the sample; this lower limit has been estimated to be about 50 mm. The compositions studied with the transpiration technique so far at 1173°K have generated pressures up to about 5 mm. Application of the Rodebush-Dixon technique will fill the pressure gap down to about 5 mm. Nevertheless, certain features of the phase diagrams for the

TABLE VI-2. TRANSPIRATION MEASUREMENTS ON THE SODIUM-BISMUTH SYSTEM AT 1175°K

Composition of Liquid Phase (a/o Bi)	Sodium Partial Pressure[a] (mm)	Bismuth Partial Pressure[a] (mm)	Composition of Vapor Phase (a/o Bi)
80	0.87 ± 0.06	0.59 ± 0.02	40.4 ± 2.1
60	4.76 ± 0.25	0.24 ± 0.03	4.90 ± 0.70

[a] These partial pressures are calculated on the assumption that only monatomic species are present in the vapor. The assumption is probably valid for sodium at the low pressure involved. Bismuth vapor, however, is probably composed of equal numbers of monatomic and diatomic particles. If this is the case, the listed numbers for bismuth partial pressures should be multiplied by 0.67.

sodium-bismuth system may be deduced tentatively from the results which are available.

One of these features is apparent from the ebulliometric measurements reported in Table VI-1. By comparing the observed total pressures with the vapor pressure of pure sodium at the same temperature, it is noted that the total pressures are surprisingly high considering that these solutions contain an appreciable atom fraction of bismuth which is relatively nonvolatile compared to sodium. In fact, the total pressures are in many cases somewhat higher than the corresponding vapor pressures of pure sodium. This is especially noticeable in the 14.96 a/o bismuth series. However, more recent experiments indicate that some uncertainty may reside in these results; this will require further examination. The extent, if any, to which the activity coefficient exceed unity will be determined after both the transpiration and ebulliometric series of experiments are complete in this temperature and pressure region.

On the bismuth-rich side of the phase diagram, the activity coefficient for sodium under the conditions of the transpiration experiments is about 10^{-3} to 10^{-4}. Here, there are strong negative deviations from ideality and the total pressure is much lower than would be expected for an ideal solution.

B. REGENERATIVE EMF CELLS—ENGINEERING STUDIES (J. C. HESSON)

Engineering studies are being continued to investigate the feasibility of developing a practical thermally regenerative emf cell, ultimately capable of being coupled to a reactor or other heat source. Both bimetallic and lithium hydride cells are being studied. Preliminary thermodynamic studies for both systems were reported (ANL-6925, pp. 243-245).

1. Physical Properties of Electrolytes and Bimetallic Mixtures (H. SHIMOTAKE, J. TRALMER)

The densities, viscosities, and surface tensions of electrolytes and bimetallic mixtures are needed in order to determine volumes, liquid levels, flow rates, and surface effects for the engineering design of bimetallic cell and regeneration apparatus. Although many physical properties are available in the literature for pure salts and metals, very little information on these properties is available for mixtures of salts or metals. In many cases, the actual deviations of properties of mixtures from computed values based on additive volumes of the components are considerable. Measurements of these physical properties of various electrolytes containing sodium ions and of sodium-bismuth and sodium-lead alloys have been started.

Determinations of liquid densities are being made by measuring the volume of a known weight of the materials in a calibrated crucible. An apparatus which utilizes a sensitive balance to weigh a calibrated plumb weight suspended in the liquid is also being set up. Viscosity determinations are being made by measuring the time required for the liquid between two measuring electrode levels in a calibrated cup to flow out through a capillary tube at the bottom of the cup. Surface tension determinations are made by measuring the force required to detach a calibrated annulus ring from the surface of the liquid.

The density of an electrolyte consisting of 17.7 w/o NaCl, 6.1 w/o NaF, and 76.2 w/o NaI (31.6 m/o NaCl, 15.2 m/o NaF, and 53.2 m/o NaI), having a melting point of about 535°C, was found to vary as follows over the temperature range of 540 to 800°C:

$$d = 3.05 - 0.0009\ T$$

where d = density, g/cc, and T = temperature, °C.

A preliminary experiment indicated that the kine-

matic viscosity of this electrolyte at 600°C is about 0.65 centistokes.

The density of a lead-30 m/o sodium alloy was also measured; the indicated value was 8.0 g/cc at 436°C.

2. Experimental Sodium-Bismuth Bimetallic Cell (J. Hesson, G. Rogers)

As a part of the engineering effort being directed toward developing a practical bimetallic emf cell, a closed cell apparatus with 3-in. dia. electrode sections but without a thermally operated regenerator was constructed of stainless steel (see Figure VI-12). This cell uses a combination of silicone rubber and frozen electrolyte to serve as both an electrical insulator and pressure seal. The cell body proper is heated by ⅛-in. dia. stainless steel sheathed electrical heating elements.

The cell was charged with 313.6 grams of salt electrolyte (31.6 m/o NaCl, 53.2 m/o NaI, and 15.2 m/o NaF) and 400 grams of bismuth. The cell was heated to an operating temperature of about 550°C, and a total of 15.5 grams of sodium was added to the cell anode. At this time the cell developed a potential of 1.22 volts, a voltage which agrees with the previously determined open-circuit cell data (see ANL-6900, p. 329). A load was placed on the cell, and the cell voltage gradually decreased as the sodium was transferred to the cathode.

In order to continue to operate the cell electrically, it was periodically recharged by reversing the current. The cell was completely discharged a number of times and recharged to voltages as high as 2¼ volts. The highest voltage observed on initially adding sodium to the cell was 1.22 volts, which indicates that, on charging the cell to 2¼ volts, decomposition of the sodium halide electrolyte may occur and after the recharging operation the recombination may be the driving force for the high voltage.

The cell has been charged and discharged at currents as high as 10 amp. The cell resistance is of the order of 0.1 to 0.025 ohm depending upon the temperature. At 0.05 ohm, cell resistance voltages of about 0.5 have been obtained at 4 amp discharge current under conditions where the open circuit potential was about 0.7 volt.

The cell has been at an operating temperature of from 535 to 650°C for over 200 days (as of June 30, 1965). The objectives of continued operation are to determine (1) the effects of operation on the freeze seal-insulator and stainless steel cell and (2) the effects of operating variables, such as temperature and current, on cell behavior. At present the freeze seal insulator and stainless steel cell show no evidence of deterioration.

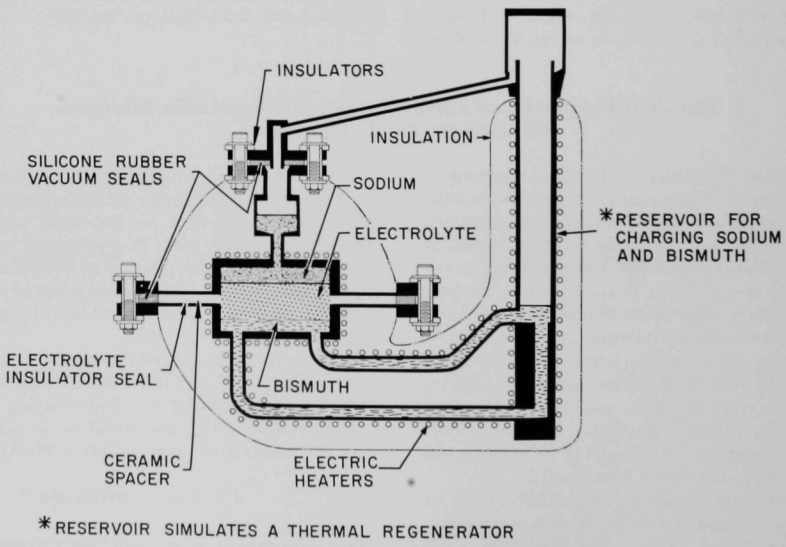

108-8378 Rev. 1

Fig. VI-12. Experimental Sodium-Bismuth Bimetallic Cell.

3. Experimental Sodium-Cathode Metal Thermal Regenerator (J. Hesson, G. Rogers, J. Tralmer)

An experimental apparatus for the study of regeneration of bimetallic emf cells has been constructed. The regenerator, which was constructed of stainless steel, is being used to study some of the engineering aspects associated with the separation of sodium from cathode metals by distillation. Among the parameters being investigated are distillation and circulation rates; temperatures of the still, column, condenser, and reservoir; mole fraction of sodium in the cathode metal; and distillation pressure.

The apparatus, shown in Figure VI-13, consists of a vertical cylindrical reservoir for containing the cathode metal (a 30 m/o sodium-70 m/o lead alloy for the initial studies) and a vertical cylindrical still with a sodium condenser at its upper end. The reservoir is connected to the still by two tubes through which the bimetallic alloy is thermally circulated back and forth between the reservoir and the still. The sodium vapor distilled from the sodium-lead alloy is condensed at the upper end of the still and returned to the reservoir where it mixes with the sodium-lead alloy for continuous circulatory operation. During a test run a cup can be positioned under the sodium return tube to catch the distilled sodium for a predetermined period of time (usually, 15–20 min). This allows measurement of the distillation rate and provides a sample of

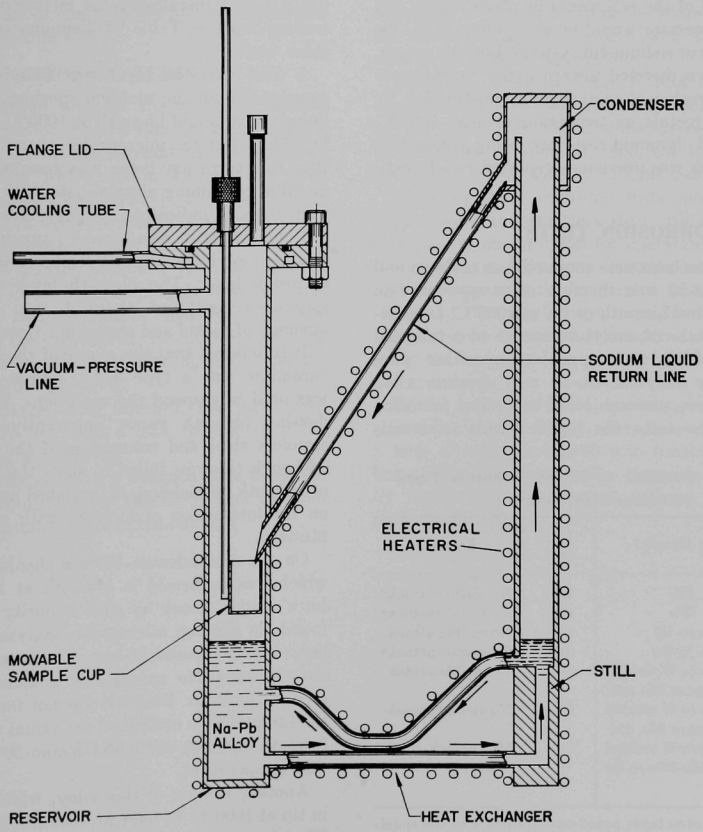

108-8605 Rev.
Fig. VI-13. Experimental Apparatus for Regeneration of Sodium from Cathode Metals of Bimetallic Emf Cells by Distillation.

the distilled sodium (up to 5 g) for analyses. A test run must be terminated to remove the sample; for the subsequent run an amount of sodium equal to the sample removed is added to the reservoir to maintain the alloy composition.

To date 28 test runs have been made under various operating conditions for a total operating time of 91 hr for the regenerator. Still temperatures of about 750 to 800°C and distillation pressures of from 3 to 7.5 mm Hg have been used. Total distillation rates of about 14 g of Na/hr or specific distillation rates of about 4.8 g of Na/(hr) (cm^2 of still evaporating surface) have been attained. Distilled sodium with less than 0.5 m/o lead has been obtained; this would be suitable for use in the anode of a sodium-lead cell. In a bimetallic cell, current densities of about 500 ma/(cm^2 of electrode area), which are high values, would require only about 0.5 g of Na/(hr) (cm^2 of electrode area). Thus, the distillation surface area of a regenerator such as the one described above could be considerably less than the electrode area of an associated cell.

4. Corrosion Studies (H. Shimotake, J. Hesson, J. Allen, G. Rogers)

In the thermally regenerative bimetallic emf cell systems described in the foregoing sections, the operating temperature of the cell would be about 550°C and that of the regenerator would be well above 800°C for sodium-bismuth or sodium-tin systems. For this reason, studies have been directed toward gathering information on the corrosion of materials of construction by liquid cathode metals at temperatures near 1000°C. Both static and dynamic tests are being conducted; preliminary work was previously reported (ANL-6925, p. 246).

a. STATIC CORROSION TESTS

Static corrosion tests were conducted on niobium and on molybdenum-50 w/o rhenium alloy specimens in contact with either bismuth or tin at 1000°C. In addition, welded joints of molybdenum-30 w/o tungsten alloy tubes, which were made using either pure molybdenum or molybdenum-50 w/o rhenium alloy welding rods, were also subjected to similar corrosion tests. During the tests, the liquid metals were contained in molybdenum-30 w/o tungsten crucibles. Following the tests, the various specimens were examined using both a metallographic microscope and an electron microprobe. Table VI-3 summarizes the results of these tests.

TABLE VI-3. Summary of Static Corrosion Tests
Test temperature, 1000°C

Liquid Metal	Test Material	Time (hr)	Remarks
Bi	Nb	17¾	No visible attack[a]
Bi	Nb	41¾	No visible attack[a]
Sn	Mo-50 w/o Re	63½	No visible attack
Bi	Mo-50 w/o Re	91¼	No visible attack[a]
Sn	Mo-30 w/o W welded with pure Mo rod	67	No visible attack
Bi	Mo-30 w/o W welded with pure Mo rod	96½	No visible attack
Sn	Mo-30 w/o W welded with Mo-50 w/o Re rod	24	Microcrack in the weld

[a] The thin corrosion layer noted on the surface of the specimen was the result of interaction with a stainless steel impurity in the bismuth (see discussion in text).

A thin corrosion layer was found by microscopic examination on the niobium specimens that had been immersed in liquid bismuth at 1000°C for 17¾ or 41¾ hr. The electron microprobe examination disclosed that this corrosion layer was composed of an intermetallic containing approximately 35 w/o niobium in iron, thereby indicating $NbFe_3$. This corrosion layer did not contain measureable amounts of bismuth. Neither molybdenum nor tungsten was detected in the corrosion layer. The bismuth layer adhering to the specimens contained about 1 w/o iron and trace amounts of nickel and chromium (less than 0.5 w/o).

It is believed that the source of the iron, nickel, and chromium was a type 304 stainless steel rod which was used to suspend the specimens. Reflux from condensing bismuth vapor apparently dissolved some stainless steel and contaminated the liquid bismuth. Although this run failed to show the corrosive effects of bismuth on niobium, it furnished useful information on the interaction of niobium with iron dissolved in bismuth.

On the molybdenum-50 w/o rhenium alloy sample which was immersed in bismuth at 1000°C for 91¼ hr, a similar attack by steel impurity in bismuth was found by electron microprobe analysis. The corrosion layer was composed of iron, chromium, rhenium, and molybdenum. No appreciable amount of nickel was seen in the layer. Bismuth was not found anywhere in the sample. This confirmed the visual observation that bismuth does not wet molybdenum-50 w/o rhenium at this temperature.

Another sample of this alloy, which was immersed in tin at 1000°C for 63½ hr, revealed no visible attack. The electron microprobe analysis of this sample has not yet been received.

The molybdenum-30 w/o tungsten alloy specimen welded with molybdenum-50 w/o rhenium rod and immersed in tin at 1000°C for 24 hr exhibited a microcrack along the grain boundary in the weld section. This crack was probably caused by thermal stress. The weld section showed no chemical attack. Two similar molybdenum-30 w/o tungsten alloy specimens were welded with pure molybdenum rod. One of the specimens was immersed in tin and the other in bismuth at 1000°C for over 60 hr. No corrosion effects were found. The specimen in liquid bismuth was not wet whereas the one immersed in tin was completely wet.

The above tests indicate that these various metals are not seriously corroded by bismuth and tin at 1000°C under static corrosion conditions. Dynamic corrosion tests are warranted to establish their suitability as materials of construction for the regenerator portion of a bimetallic cell.

b. DYNAMIC CORROSION TESTS

Dynamic corrosion tests of the effects of molten metals on materials of construction are continuing. A detailed description of the thermal convection loops (10-in. high by 6-in. wide) used in the tests was given in a previous report (ANL-6925, p. 246). Also given in the earlier report were the results of tests on Loops 1 to 4, which were made of mild steel.

Loops 5 and 6 utilized standard ¼-in. low carbon steel pipe. Both loops were thoroughly descaled with molten sodium hydride-sodium hydroxide mixture before beginning the experiment. During operation the hot leg temperature was maintained at 850°C and the cold leg temperature at 450°C.

Loop 5 was charged with bismuth. The experiment continued for 279 hr, when a leak developed in the bottom section of the hot leg.

Loop 6 was charged with a bismuth-20 a/o sodium alloy. The run continued for 125 hr. A leak also developed in the bottom section of the hot leg.

In both experiments extensive mass transfer and corrosion were observed, particularly at the entrance section of the hot leg. The internal cross-sectional area increased as much as 50%; the resulting reduction in the wall thickness was sufficient to cause leaks in both cases. The mass transferred materials were accumulated at the cold leg section as aggregates.

Loop 7, made of ¼-in. type 316 stainless steel tube, was charged with liquid bismuth. The temperature in the hot leg was kept at 850°C while the temperature in the cold leg was 450°C. The run was terminated after approximately 300 hr when a plug formed. Various cross sections of the loop were examined under the microscope. A thick corrosion layer and severe intergranular corrosion were found. The loop pipe became magnetic during the experiment. Further analysis by electron microprobe showed a high degree of migration of chromium from the center of the pipe to the corrosion layer. The iron and nickel, however, showed no evident segregation.

Loop 8, similar to Loop 7, was charged with a bismuth-30 a/o sodium alloy. The temperature of the hot leg was held at 650°C while the cold leg was kept at 550°C. As of June 30, 1965, the loop has been in operation for over 3000 hr without leaking.

These dynamic corrosion tests indicate that low carbon steel and stainless steel will not be suitable materials of construction for operation with bismuth-sodium alloys at hot zone temperatures of 850°C and higher such as would be present in the regeneration portion of the bimetallic system. However, they may be suitable for operation at temperatures of 650°C and lower such as would be present in the cell portion of the system.

Three loops each of niobium, niobium-1 w/o zirconium, and tantalum have been fabricated, and a loop of molybdenum-30 w/o tungsten is currently being fabricated for further dynamic corrosion tests by liquid bismuth, bismuth-sodium alloys, and tin under thermal gradients.

VII

Nuclear Constants[1] (D. C. Stupegia, A. D. Tevebaugh)

The fast neutron cross section program can be described in terms of the use of cross sections in the calculation of the breeding ratio of a fast reactor.[2] Detailed information is required on the nuclear properties of the fuels, fertile species, and reactor structural materials in order to make more efficient use of the fission reaction.

[1] A summary of this section is given on pages 17 to 18.

[2] A more detailed discussion of the breeding ratio and its relationship to nuclear cross sections can be found in a previous report (ANL-6800, p. 424).

Specifically, the following data are needed:

(1) radiative capture cross sections of structural and control materials,

(2) cross sections of the primary fissionable and fertile species for capture and for fission, and

(3) cross sections for reactions which degrade the neutron energy spectrum of the reactor.

In the present program, several of the above types of reactions are being studied; current progress is reported below.

A. RADIATIVE CAPTURE (D. C. Stupegia, C. R. Keedy, M. Schmidt, A. Madson)

One of the nuclear reactions which absorbs neutrons unproductively in a reactor is radiative capture. The cross sections for radiative capture as a function of neutron energy are needed in order to make proper use of materials proposed for structural and control use in reactors. Further, the study of neutron capture allows one to test theories of nuclear reactions and to derive information on the spacings and widths of nuclear energy levels. From such information one can then predict other neutron cross sections in the absence of experimental data.

The neutron energy range of interest in fast reactors lies between about 0.1 keV and several MeV. In the present program, radiative capture has been studied between 4 keV and 3 MeV, covering most of the fast reactor region.

The basic experimental technique used in the capture work is the activation method, wherein the nucleus to be studied is exposed to a monoenergetic neutron beam, and the radioactive species produced thereby are counted with either a beta counter or a gamma-ray analyzer. The counting rate of the activation product is then converted to a capture cross section by suitable calibrations which yield the absolute neutron flux and the absolute disintegration rate of the capture product. The monoenergetic neutron beam is produced by the reaction $^{7}Li(p,n)^{7}Be$ and $T(p,n)^{3}He$, when lithium and tritium targets are bombarded by protons from the Van de Graaff accelerator. The neutron flux is measured with a fission chamber, which counts fissions in a thin deposit of uranium.

In previous reports (ANL-6800, p. 425 and ANL-6900, p. 332), data were given for fast neutron capture in rhenium. The results of this work are being published.[3] The final data, consisting of the radiative capture cross sections of ^{185}Re and ^{187}Re, previously reported, and the cross section for the production of the 18.7-min state of ^{188}Re are shown in Figure VII-1. The cross sections are given as a function of neutron energy between 4 keV and 2.6 MeV. Also shown in Figure VII-1 are earlier data of other investigators.[4, 5]

In more recent work, measurements have been made on the capture cross sections of praseodymium. In Figure VII-2 are shown the relative cross sections of ^{141}Pr as a function of neutron energy between 0.2 and 2.5 MeV. Absolute cross sections will be calculated when the required calibrations are completed.

[3] D. C. Stupegia, M. Schmidt, A. A. Madson, Fast Neutron Capture in Rhenium, J. Nucl. Energy, in press.

[4] D. J. Hughes, R. C. Garth, and J. S. Levin, Phys. Rev., **91**, 1423 (1953).

[5] R. L. Macklin, N. H. Lazar, and W. S. Lyon, Phys. Rev. **107**, 504 (1957).

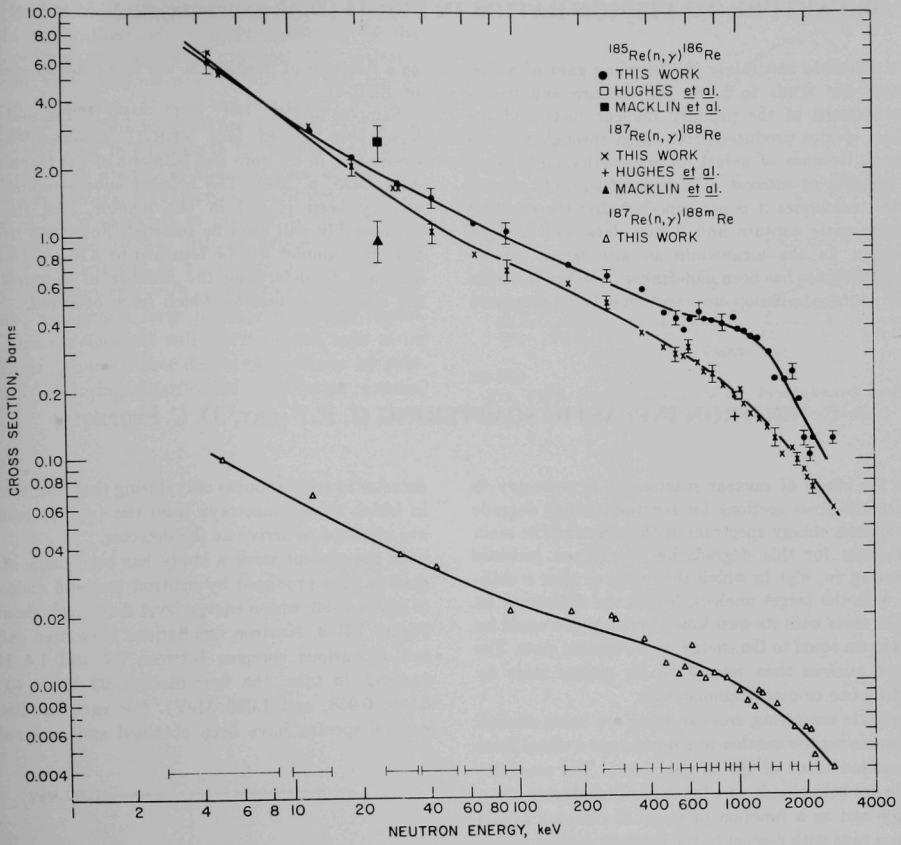

108-8527 Rev.

FIG. VII-1. Radiative Capture in Rhenium.

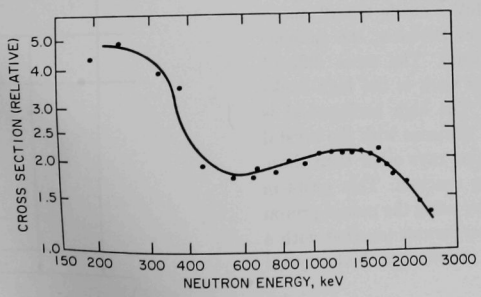

108-8788

FIG. VII-2. Praseodymium-141 Neutron Capture Cross Section.

B. CAPTURE-TO-FISSION RATIOS IN EBR-II (D. C. Stupegia, A. A. Madson)

To calculate accurately the breeding gain of a fast reactor, one needs to know the capture and fission cross sections of the primary nuclear fuels and the various species produced from them through neutron capture. Because of a lack of sufficient quantities of the isotopes of interest or a lack of suitable experimental techniques it is not expected that the required monoenergetic capture and fission data will soon be available. In the meanwhile an alternative experimental program has been undertaken, wherein the ratio of the capture to fission cross section is being measured as a function of position in the fast neutron spectrum of EBR-II.

Samples of ^{233}U, ^{235}U, ^{238}U, ^{239}Pu, ^{240}Pu, and ^{242}Pu have been placed into EBR-II subassemblies for irradiation in the core and blankets of the reactor (see ANL-6925, p. 251). The blanket subassemblies have already been placed in the reactor, and the core subassembly will soon be inserted. Following irradiation, the samples will be returned to ANL and will be analyzed to determine the number of captures and the number of fissions which have occurred.

C. NEUTRON INELASTIC SCATTERING (J. F. Barry,[6] D. C. Stupegia)

In the study of nuclear reactors, it is necessary to known the cross sections for reactions which degrade the neutron energy spectrum of the reactor. The main mechanism for this degradation is neutron inelastic scattering $(n, n'\gamma)$ in which the neutron, after a collision with the target nucleus, leaves the nucleus in an excited state with its own kinetic energy decreased by an amount equal to the energy of the excited state. The excited nucleus then returns to its ground state by emitting one or more gamma rays.

Inelastic scattering cross sections are being studied by measuring the number of gamma rays emitted from the excited state of the target nuclei. The measurements are being made as a function of incident neutron energy and as a function of angle of emission of the gamma rays with respect to the incident neutron direction.

The neutron source is a lithium target bombarded with protons from the 3-MeV Van de Graaff accelerator of the Reactor Physics Division; the gamma-ray detector is a NaI crystal. The most difficult experimental problem in this work is the high background in the NaI crystal. The high background is caused by the interaction of neutrons with the crystal and by the detection of gamma rays other than those from the inelastic scattering reaction. This problem is, to a large part, overcome by using the pulsed proton beam of the Van de Graaff accelerator together with a time-of-flight system which allows the NaI crystal detector to record counts only during that time interval in which the gamma rays from the $(n, n'\gamma)$ reaction are expected to arrive at the detector.

In the present work a study has been made of the gamma rays produced by neutron inelastic scattering in niobium-93, whose energy level diagram is shown in Figure VII-3. Neutron irradiations have been carried out at various energies between 0.7 and 1.4 MeV, exciting, in turn, the four niobium-93 levels (0.741, 0.809, 0.958, and 1.080 MeV). For each irradiation, gamma spectra have been obtained and analyzed at

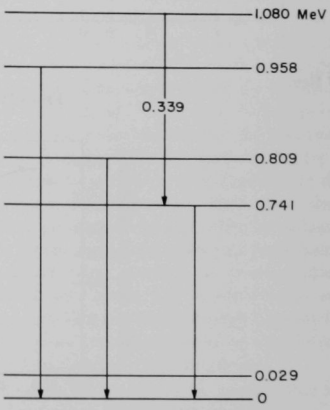

108-8541

Fig. VII-3. Energy Levels of Niobium-93.

[6] Present address, A.W.R.E., Aldermaston, England.

an angle of 90° with respect to the proton beam. After suitable calibrations of counting efficiency of the detectors and neutron flux monitor, the inelastic scattering cross sections were calculated. The results are shown in Figure VII-4 for the four energy levels.

A major problem in studying gamma rays from nuclear reactions, in addition to the background problem mentioned above, is the analysis of complex gamma-ray spectra. Development work now in progress at ANL is expected to produce a new type of gamma-ray detector, the lithium drifted germanium crystal. This detector, at a sacrifice in counting efficiency as compared with the presently used NaI crystals, will give a large increase in energy resolution. This development will allow gamma rays to be studied to a much higher degree of accuracy by substantially reducing interference from other gamma rays.

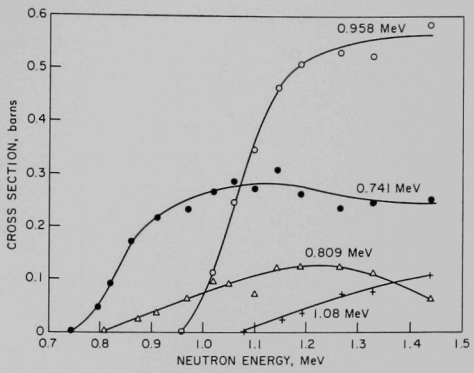

108-8790

FIG. VII-4. Cross Sections for the Production of Excited States of Niobium-93 by Neutron Inelastic Scattering.

ARGONNE NATIONAL LAB WEST
3 4444 00007711 5